# TECHNICAL DEVELOPMENT FOR AUTOMATIC AERIAL TRIANGULATION OF HIGH RESOLUTION SATELLITE IMAGERY

**ZHEN XIONG**

**May 2009**

**TECHNICAL REPORT NO. 268**

# TECHNICAL DEVELOPMENT FOR AUTOMATIC AERIAL TRIANGULATION OF HIGH RESOLUTION SATELLITE IMAGERY

Zhen Xiong

Department of Geodesy and Geomatics Engineering
University of New Brunswick
P.O. Box 4400
Fredericton, N.B.
Canada
E3B 5A3

May 2009

# PREFACE

This technical report is a reproduction of a dissertation submitted in partial fulfillment of the requirements for the degree of Doctor of Philosophy in the Department of Geodesy and Geomatics Engineering, May 2009. The research was supervised by Dr. Yun Zhang, and funding was provided by the Natural Sciences and Engineering Research Council of Canada and by the Canada Research Chairs Program.

 The citation to this work should appear as follows:

Xiong, Zhen (2009). *Technical Development for Automatic Aerial Triangulation of High Resolution Satellite Imagery*. Ph.D. dissertation, Department of Geodesy and Geomatics Engineering, Technical Report No. 268, University of New Brunswick, Fredericton, New Brunswick, Canada, 302 pp.

# ABSTRACT

Because they contain abundant spatial information, high resolution satellite images are widely used in a variety of applications. Aerial triangulation is one of the most important technologies to obtain accurate spatial information from those images. Thus aerial triangulation is always an important research topic in the photogrammetric community and automatic aerial triangulation is a common goal of such PhD research activities. To date, many techniques have been developed to improve the efficiency and accuracy of aerial triangulation. However, for processing high resolution satellite images, automatic aerial triangulation still faces many challenges, including tie point extraction and sensor model refinement. The main purpose of this research is to develop and test new tie point extraction, sensor model refinement and bundle block adjustment methods for improving the automation and accuracy of aerial triangulation.

The accuracy of tie points directly determines the success of aerial triangulation. Generally both the corner point and the gravity center point of a rectangular or circular object can be used as tie points, but the resulting outcomes can vary greatly in aerial triangulation. However, this difference has not drawn much attention from researchers yet. Thus, most of the tie point extraction algorithms only extract various corners. In order to quantify the difference between corner and center tie points for image registration, this research analyzed the error introduced by using corner or center tie points in different cases. Through quantitative analysis and experiments, the author

reached the conclusion that the 'center' points, when used as tie points, can improve the accuracy of image registration by at least 40 percent over that for the 'corner' points.

Extracting a large number of tie points is the prerequisite of automatic aerial triangulation. Interest point matching can extract tie points automatically. To date numerous interest point matching algorithms have been investigated. Those algorithms can be grouped into two categories: area based and feature based. However, both area based and feature based algorithms share a common limitation: ambiguity in a homogeneous area. Neither of the methods could efficiently extract tie points from the low texture area. In this research, a robust interest point matching algorithm has been developed. This algorithm incorporates spatial information through constructing a control network from 'super' interest points. Experiments show that the proposed algorithm almost solved the ambiguity problem in a "poorly textured" area.

Sensor model refinement is the core of aerial triangulation. The challenge is the use of the Rational Polynomial Camera (RPC) model in some high resolution satellites, such as IKONOS and QuickBird. Although some direct methods and indirect methods have been investigated, they either require excessive information concerning the RPC which is unavailable to the public (direct methods), or has rigorous conditions which seriously limits its applications (indirect methods). In this research, a generic method was developed for RPC refinement. The proposed method does not need any information about the RPC itself, and is not restrained by any conditions. Theoretically, the proposed generic method can be used in any kind of camera in which RPC is used as a sensor model.

Based on the proposed generic method for RPC refinement, a robust bundle block adjustment model is developed. This bundle block adjustment algorithm can efficiently process the high resolution satellite images and can reach sub-pixel accuracy in image space and sub-meter accuracy in object space. Experiments were conducted to verify this application.

# ACKNOWLEDGEMENTS

In the past several years, numerous people gave me strong support and encouragement. First of all, I would like to thank my supervisor, Dr. Yun Zhang, for his all-around support and guidance throughout my Ph.D program. During my program of study, he gave me many opportunities for growth by allowing me to be involved in projects, conferences, and other academic activities. For my technical reports, journal papers, and other presentations, he always gave me valuable comments and suggestions. Thank you, Dr. Zhang.

I am very grateful to Dr. David J. Coleman and Dr. Susan E. Nichols for their help in my minor examination, for their review of my Ph.D research proposal and dissertation, and for their valuable comments and suggestions. I thank Dr. Julian Meng for reviewing my Ph.D research proposal and providing helpful comments. I thank Dr. Costas Amenakis for reviewing my thesis and giving me valuable comments and suggestions. Thanks are also extended to the staff and faculty of the Department of Geodesy and Geomatics Engineering, in particular David Fraser, Terry Arsenault, Jay Woodyer, Sylvia Whitaker, Kim Delorey, Lorry Hunt and Michelle Ryan for their secretarial, advisory and technical support.

I want to thank my friends David Whyte for reviewing my papers, Dale Bray, Clark Hamilton, and Dennis Muehlhauser for helping me with my English. Special thanks must go to many friends and colleagues for their valuable advice, comments, support, encouragement, and friendship at various stages of the long journey towards completing this Ph.D program. They are Dr. Gong Hong, Shen Gao, Jianfeng Zhao, Gensheng Liang, Xiaolun Yi, Saili Tang, Tristan Goulden, Yongdae Gweon, and Robert Kingdon.

Finally I would like to thank my wife, Ying Ding, and my daughter Katherine, for their unconditional love, support, and understanding. I am truly grateful to my father, Youcai Xiong, my mother Qiaozhi Zhang, my father-in-law Chaoming Ding, and my mother-in-law Meijuan Dong for standing with me during my Ph.D program study.

# TABLE OF CONTENTS

# LIST OF TABLES

# LIST OF FIGURES

# LIST OF SYMBOLS, NOMENCLATURE, OR ABBREVIATIONS

BILS – Batch Iterative Least-Squares

GCP – Ground Control Point

CE90 – Circular Error 90%

CHK – Check Point

EP – Exterior Parameters

FOV – Field of View

GPS – Global Positioning System

HRSI – High Resolution Satellite Image

ICP – Iterative Closest Point

IDKF – Incremental Discrete Kalman Filtering

LE90 – Linear Error 90%

PG – Pseudo GCP

M – Meters

RMSE – Root Mean Square Error

MS – Multi-Spectral

PAN – Panchromatic

RES – Resolution

RPC – Rational Polynomial Coefficient

SLSS – Sequential Least Square Solution

SIFT – Scale Invariant Feature Transform

TPS – Thin Plate Spline

# Chapter 1 INTRODUCTION

This PhD research includes four parts: interest point extraction, interest point matching, geometric sensor model refinement, and bundle block adjustment, which are four important components for aerial triangulation. The dissertation is presented through following papers:

Paper 1 (peer reviewed):

Xiong, Z. and Y. Zhang (2009), Error Analysis of Corner and Center Points for Image, *Journal of Photogrammetric Engineering & Remote Sensing* (under review).

Paper 2 (peer reviewed):

Xiong, Z. and Y. Zhang (2009), A Novel Interest Point Matching Algorithm for Remote Sensing Images, *IEEE Transaction on Geoscience and Remote Sensing* (under review).

Paper 3 (peer reviewed):

Xiong, Z. and Y. Zhang (2009), A Generic Method for RPC Refinement, *Journal of Photogrammetric Engineering & Remote Sensing* (in press).

Paper 4 (peer reviewed):

Xiong, Z. and Y. Zhang (2009), Bundle Block Adjustment with Rational Polynomial Camera Models Based on Generic Method, *ISPRS Journal of Photogrammetry & Remote Sensing* (under review).

## 1.1 Dissertation Structure

This research is an articles-based dissertation. Four journal papers (one published, and three submitted for peer review) are incorporated in the work. The dissertation includes six chapters: introduction, four journal papers (each as one chapter), and conclusions. **Figure 1.1** illustrates the organization of this dissertation.

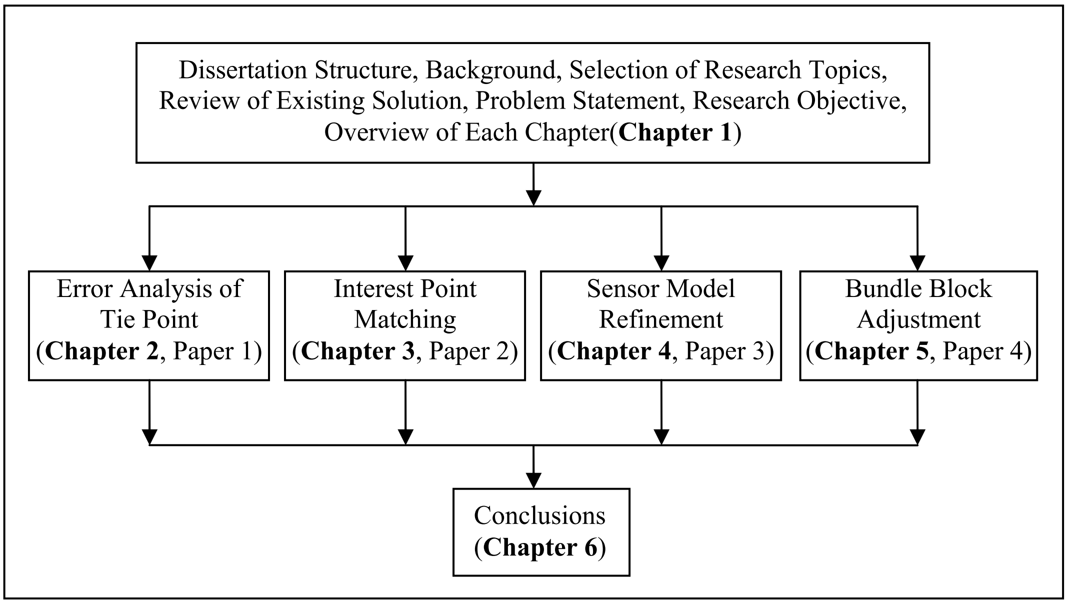


**Figure 1.1 Organization of this dissertation**

## 1.2 Background

When Landsat 5 was successfully launched on March 1$^{st}$, 1984 a new era of earth observation began with 30 m resolution images. With the subsequent technological advancements in computers, electronics, communications and mechanics, the resolution of satellite images has been continuously increasing. To date, at least 64 high resolution satellites (better than 30 m) have been launched by 23 countries (**Table 1.1**). At the same time, High Resolution Satellite Images (HRSI) have become widely used in various fields, including agriculture, forestry, ecology, environmental protection, land administration, resources management, and mapping. These applications take advantage of the large amount of information contained in HRSIs, especially geospatial information, such as position, elevation, and orientation. However, raw satellite images usually contain various distortions due to camera lens configuration, ground relief variation, the curvature of the earth, and atmospheric refraction, resulting in inaccurate geometric positions which are unsuitable for geospatial analysis and other applications. Therefore, effective technologies are required to remove the geometric distortions and improve the accuracy of geospatial information.

Aerial triangulation (aerotriangulation) is the best way to obtain accurate geospatial information from raw images, and refers to the process of determining the x, y, and z ground coordinates of individual ground points based on photo coordinate measurements on the raw image. Currently, automated aerial triangulation of high resolution satellite imagery still faces some significant technical problems in both tie point selection and bundle adjustment. This is the motivation behind this research.

**Table 1.1 High Resolution Satellites[1]**

| Satellite | Country | Launch | PAN RES. M | MS RES. M | Satellite | Country | Launch | PAN RES. M | MS RES. M |
|---|---|---|---|---|---|---|---|---|---|
| Landsat 5 | US | 03/01/84 | | 30.0 | VinSat-1 | Vietnam | 11/01/06 | 4.0 | 32 |
| SPOT-2 | France | 01/22/90 | 10.0 | 20.0 | Sumbandilasat | South Africa | 12/12/06 | | 6.5 |
| ERS-2 | ESA | 04/21/95 | 30.0 | | RadarSat 2 | Canada | 12/15/06 | 3.0 | |
| RadarSat 1 | Canada | 11/04/95 | 8.5 | | *RISAT* | India | 01/30/07 | 3.0 | |
| IRS 1C | India | 12/28/95 | 6.0 | 23.0 | IRS Cartosat 2 | India | 03/15/07 | 1.0 | |
| IRS 1D | India | 09/29/97 | 10.0 | 20.0 | GeoEye-1 | US | 03/16/07 | 0.41 | 1.64 |
| SPOT-4 | France | 03/24/98 | 10.0 | 20 | RapidEye-A | Germany | 06/01/07 | | 6.5 |
| Landsat 7 | US | 04/15/99 | 15.0 | 30.0 | RapidEye-B | Germany | 06/01/07 | | 6.5 |
| Ikonos-2 | US | 09/24/99 | 1.0 | 4.0 | RapidEye-C | Germany | 06/01/07 | | 6.5 |
| ASTER | Japan/US | 12/15/99 | | 15, 30, 90 | RapidEye-D | Germany | 06/01/07 | | 6.5 |
| KOMPSAT-1 | Korea | 12/20/99 | 6.6 | | RapidEye-E | Germany | 06/01/07 | | 6.5 |
| EO-1 | US | 11/21/00 | 10 | 30 | CBERS-2B | China/Brazil | 06/15/07 | 20 | 20 |
| EROS A1 | Israel | 12/05/00 | 1.8 | | THOES | Thailand | 06/30/07 | 2.0 | 15 |
| QuickBird-2 | US | 10/18/01 | 0.6 | 2.05 | HJ-1-A | China | 07/01/07 | | 30, 100 |
| Proba | ESA | 10/22/01 | 8.0 | 18, 36 | HJ-1-B | China | 07/01/07 | | 30, 150, 300 |
| *ENVISAT* | ESA | 03/01/02 | 30 | | WorldView-1 | US | 07/01/07 | 0.5 | |
| SPOT-5 | France | 05/04/02 | 2.5 | 10 | Skymed-1 | Italy | 11/12/07 | 1.0 | |
| DMC AISat-1 | Algeria | 11/28/02 | | 32 | HJ-1-C | China | 03/01/08 | | 5, 20 |
| OrbView 3 | US | 06/26/03 | 1.0 | 4 | EROS C | Israel | 03/21/08 | 0.7 | 2.5 |
| DMC-1 | Nigeria | 09/27/03 | | 32 | X-sat | Singapore | 04/16/08 | | 10 |
| DMC BilSat | Turkey | 09/27/03 | 12.0 | 26 | CBERS-3 | China/Brazil | 05/01/08 | 5.0 | 20 |
| DMC UK | UK | 09/27/03 | | 32 | Skymed-2 | Italy | 05/01/08 | 1.0 | |
| IRS 1 | India | 10/17/03 | 6.0 | 6, 23, 56 | WorldView-2 | US | 07/01/08 | 0.5 | 1.8 |
| CBERS-2 | China/ Brazil | 10/21/03 | 20.0 | 20.0 | Venus | Israel/France | 08/01/08 | | 5.3 |
| FormoSat | Taiwan | 04/20/04 | 2.0 | 8.0 | TerraSAR L | Germany | 08/15/08 | 1.0 | |
| ThaiPhat | Thailand | 12/01/04 | | 36 | Skymed-3 | Italy | 11/01/08 | 1.0 | |
| IRS CartoSat 1 | India | 05/04/05 | 2.5 | | Alsat-2A | Algeria | 12/01/08 | 2.5 | 10 |
| MONITOR-E-1 | Russia | 08/26/05 | 8.0 | 20 | IRS -2 | India | 12/15/08 | 6.0 | 6, 23, 56 |
| Beijing-1 | China | 10/27/05 | 4.0 | 32 | Pleiades-1 | France | 03/01/09 | 0.7 | 2.8 |
| TopSat | UK | 10/27/05 | 2.5 | 5 | Skymed-4 | Italy | 05/01/09 | 1.0 | |
| ALOS | Japan | 01/24/06 | 2.5 | 10 | TanDem-X | Germany | 06/30/09 | 1.0 | |
| *ALOS* | Japan | 01/24/06 | 10.0 | | Alsat-2B | Algeria | 12/01/09 | 2.5 | 10 |
| EROS B1 | Israel | 04/25/06 | 0.7 | | CBERS-4 | China/Brazil | 07/01/10 | 5.0 | 20 |
| Resurs DK-1 | Russia | 06/15/06 | 1.0 | 3 | Spain Sat | Spain | 07/01/10 | 2.5 | |
| KOMPSAT-2 | Korea | 07/28/06 | 1.0 | 4 | Pleiades-2 | France | 09/01/10 | 0.7 | 2.8 |
| *TerraSAR X* | Germany | 10/31/06 | 1.0 | | LDCM | US | 07/01/11 | 10.0 | 30 |
| RazakSat | Malaysia | 11/01/06 | 2.5 | 5 | | | | | |

PAN = Panchromatic, MS = Multi-Spectral, RES = Resolution, M = Meters

[1] Stoney, W.E., Mitretek Systems, 2008-2-12, http://www.asprs.org/news/satellites/

## 1.3 Selection of Research Topics

Aerial triangulation is the key technology for image rectification and extraction of geospatial information. Automated aerial triangulation involves four main steps: interest point extraction; interest point matching; sensor model refinement (space resection); and bundle adjustment (space intersection). The first two are used to extract tie points, while the latter two form the basis of aerial triangulation. The PhD thesis research topic covers all these four components. Therefore, it was decided to focus research attention on each of the above four components. The scope and importance of the research with respect to each component is briefly described in Sections from 1.1.1 to 1.1.4 below.

### 1.3.1 Interest Point Extraction

Bundle block adjustment typically requires a large number of tie points; however manual tie point selection is both time consuming and tedious. In addition it is sometimes very difficult for the human eye to identify a feature point (interest point) in images of homogeneous areas such grassland or forests. Furthermore, interest point extraction is a problem common to many fields, including computer vision systems, pattern recognition, and medical image diagnosis. Methods that allow automated interest point extraction are therefore of great significance, and numerous algorithms for interest point extraction have been developed [Rosenfeld and Johnston, 1973; Rosenfeld and Weszka, 1975; Freeman and Davis, 1977; Moravec, 1977; Beus and Tiu, 1987; Forstner and Gulch, 1987; Harris, 1988; Forstner, 1994]. These algorithms are capable of extracting large numbers of interest points. However, the quantity of points is not the main issue. Instead, attention must be paid to the <u>type</u> of interest point being selected, because this can have a significant impact on the effectiveness of the resultant bundle block adjustment. In light of the foregoing, this research will not focus on how to extract interest points, but rather on what <u>kind</u> of interest points can provide the most accurate control for bundle block adjustment.

Corners and gravity centers (referred to as centers in this dissertation) are two typical kinds of interest points. Research completed as part of this dissertation revealed that most interest point extraction algorithms are only capable of extracting corner points. This limitation is significant because corners sometimes fail to give satisfactory results for multi-modal or multi-resolution image registration, but gravity center points can provide precise positions for accurate image registration. This portion of the research was therefore directed toward an error analysis of corners and gravity centers, with a view to characterizing their differences for bundle block adjustment.

### 1.3.2 Interest Point Matching

Interest point matching is widely used for 3D object reconstruction, pattern recognition, and medical image registration [Brown, 1992; Zitova and Flusser, 2003]. Moreover, interest point matching is the core of computer vision systems. For photogrammetry, interest point matching is used for automated tie point extraction. The quality of tie points can determine the degree of success of the bundle block adjustment. Accurate tie points can speed up the convergence of bundle block adjustment, whereas low accuracy of tie points may result in no convergence at all.

To date, many algorithms have been developed for interest point matching [Booksten, 1989; Besl and McKay, 1992; Gold and Rangarajan, 1996; Gold, et al., 1997; Mount, et al., 1997; Cross and Hancock, 1998; Williams and Bennamoun, 2001; Rexilius, et al., 2001; Belongie, et al., 2002; Kybic and Unser, 2003; Chui and Rangarajan, 2003; Kaplan, et al., 2004; Demirci, et al., 2004; Caetano, et al., 2004; Terasawa, et al., 2005; Lepetit, et al., 2005; Auer, et al., 2005; Shokoufandeh, et al., 2006; Yang, et al., 2007; Tu, et al., 2008; Zhao, et al., 2006; Lepetit, et al., 2008; Boffy, et al., 2008]. These algorithms can be grouped into two categories: area based methods and feature based methods. Both groups face the same problem: ambiguity in homogeneous areas (areas without prominent texture) [Zitova and Flusser, 2003]. For most high resolution satellite images, the location of at least some interest points in smooth areas is unavoidable. Therefore, a more robust interest point matching method is necessary to overcome the location ambiguity in smooth areas. The research therefore focuses on finding such a method.

### 1.3.3 Sensor Model Refinement

The geometric model of satellite sensors (referred to ‘sensor model’ in this thesis) always contains some errors. These are caused by a number of factors, including ephemeris error, satellite attitude error, atmospheric refraction error, etc. The sensor model error can be found from the corresponding location error in the ground or object space. For example, according to our experiments, SPOT 4’s location error is about 500 m, SPOT 5’s is about 300 m, and the location error for the IKONOS’ sensor model is around 20 m. In order to obtain more accurate spatial information from the HRSIs of these sensors, the satellite’s sensor model must be improved.

The sensor model is at the core of satellite photogrammetry, so sensor models have long been a popular research topic within the photogrammetric community. Many methods for sensor model refinement have been developed for the various cameras in use, which include analog frame cameras, optical-mechanical scanning sensors, linear push broom sensors, among others. For many of these, the camera's physical parameters and operational data (position, attitude, etc.) can normally be obtained and can be used for sensor model refinement. However, vendors of some high resolution satellite images, such as IKONOS, do not release details of the sensor's physical parameters. In this case, conventional model refinement methods cannot be applied. Although many new model refinement methods have been developed in response to this issue [Grodecki and Dial, 2003; Gong et al., 2005; Hu et al., 2004; Hu and Tao, 2002; Bang et al., 2003], they all have limitations. For example, the direct methods need the sensor model's information which is unavailable to public, and the indirect methods are only suited for sensors with narrow field of view. A more robust algorithm for sensor model refinement is, therefore, necessary and the development of such a model is one of the goals of this research.

### 1.3.4 Bundle Block Adjustment

Bundle adjustment is the last step in determining ground coordinates from image coordinates. As previously noted, many sensor model refinement algorithms have been developed for high resolution satellite images [Grodecki and Dial, 2003; Gong et al., 2005; Hu et al., 2004; Hu and Tao, 2002; Bang et al., 2003]. These can be grouped into two categories: direct methods and indirect methods. Only the indirect methods have been used successfully for bundle block adjustment [Hu et al., 2004; Grodecki and Dial, 2003; Fraser and Hanley, 2003]. Unfortunately, the indirect methods can only be used under very rigorous conditions, such as narrow field of view, and when small positional & attitude errors of camera are present, which limit their utility [Grodecki and Dial, 2003]. This research is therefore directed toward the development of a generic bundle block adjustment algorithm that can be used for images that do not meet the above conditions.

## 1.4 Review of Existing Solution

### 1.4.1 Interest Point Extraction

Interest points are also referred to as salient image points, key points, or feature points. Corners, junctions, high curvature gradients, gravity centers, and line ends are examples interest points. A wide variety of interest point detectors exist in the literature. They can be grouped into three classes: contour based, intensity based and parametric model based methods [Cordelia, et al., 2000].

- Contour based methods first extract contours and then search for maximal curvature or inflection points along the contour chains, or perform some polygonal approximation and then search for intersection points.
- Intensity based methods compute a measure that indicates the presence of an interest point directly from grey values.
- Parametric model methods fit a parametric intensity model to the signal. They often provide sub-pixel accuracy, but are limited to specific types of interest points, e.g., L-corners (Cordelia, et al., 2000). Parametric Model Based

methods normally use a mathematical model to fit the signal and determine the "L" corner by a least square solution. Rohr (1992), Deriche and Blaszka (1993), Baker et al (1998), and Parida et al (1998) are typical parametric model based methods. Because they are limited to specific types of interest points, they normally cannot provide dense enough set of interest point for bundle block adjustment.

Contour based methods have a long history. A variety of contour based algorithms have been developed to date, including (Rosenfeld and Johnston (1973); Rosenfeld and Weszka (1975); Freeman and Davis (1977); and Beus and Tiu (1987); Liu et al., 1990). Contour based methods are normally applied to images that contain a large number of linear features. They are not suitable for use in extracting interest points for 3D reconstruction or aerotriangulation.

Intensity based methods are the most common ones used for interest point extraction. There are two different direct corner detection approaches described in the literature. Both are based on differential geometric concepts. The first approach measures isophote curvature, weighted with the gradient magnitude. The second group of detectors measures the Gaussian curvature of the intensity surface (Tobias, et al., 2004). Some methods use the first derivative of the signal to detect the interest point (Moravec, 1977), but most use the second derivative of the signal (Beaudet, 1978; Kitchen and Rosenfeld, 1982; Dreschler and Nagel, 1982; Nagel, 1983; Forstner and Gulch, 1987; Harris and Stephens, 1988; Tomasi and Kanade, 1991; Forstner, 1994; Lowe 2004).

Each of the above methods detects different kinds of “corners”, including geometric ‘L’ corners, or gradient corners. Obviously, a gravity center is neither a geometric corner, nor a gradient corner, so none of the above algorithms can be used to extract gravity centers.

### 1.4.2 Interest Point Matching

Interest point matching algorithms can be grouped into two main categories: area-based algorithms and feature based algorithms.

Area-based methods are normally stable and reliable, but still have many limitations. They have been widely used in remote sensing for interest point matching. However, photogrammetric scientists are still attempting to improve the stability and reliability of interest point matching techniques [Lu, et al., 1997; Zhang, et al., 2004]. Hierarchical matching and relaxation algorithms are typical examples of such attempts. At the same time, great efforts are also being made to reduce the search area and increase the matching speed. The use of epipolar geometry is one of the most important achievements of such work [Masry, 1972; Helava, et al., 1973; Dowman, 1977; Gupta, 1997; Kim, 2000]. The main limitations of area-based methods can be summarized as follows: 1) The rectangular image window is only suitable for image distortion caused by translation (in theory); 2) These methods cannot process smooth areas (areas without prominent texture); and 3) The methods are sensitive to image intensity changes which are caused by noise, varying illumination and the use of different sensors [Zitova and Flusser, 2003].

Feature-based algorithms can be further categorized into rigid and non-rigid (according to the transformation between images), global and local (according to the image distortions), or corrected and uncorrected (according to the image variations). Feature-based algorithms can also be grouped into three additional categories (Chui and Rangarajan, 2003). They either: solve the correspondence only, solve the transformation only, or solve both the correspondence and the transformation.

Every method must take into account the specific geometric image deformation (Zitova and Flusser, 2003). Some algorithms process global distortions. The ICP (Iterative Closest Point) algorithm is a classical global algorithm (Besl and McKay, 1992; Yang, etc., 2007). Because it requires the assumption that one surface is a subset of the other, this algorithm is only suitable for global distortion image registration (Williams and Bennamoun, 2001). For medical image registration and pattern recognition, many rigid global transformations are used (Besl and McKay, 1992; Mount, etc., 1997; Tu, etc., 2008). The B-Spline and TPS (Thin Plate Spline) deformation models are commonly used for global distortion in medical image registration (Booksten, 1989, Kybic and Unser, 2003).

Other algorithms deal with the local distortions. For non-rigid local distortions, more complicated transformations are developed. The TPS model was proposed initially for global transformations, but it was improved for smooth local distortions for medical image registration (Gold, etc., 1997; Chui and Rangarajan, 2003; Auer, etc., 2005). Another common local distortion model is the elastic deformation model (Auer, etc., 2005; Rexilius, etc., 2001).

Some algorithms do not need a transformation function. In computer vision systems and pattern recognition, feature descriptors extracted from an image's gray values are usually used (Belongie, etc., 2002; Kaplan, etc., 2004; Terasawa, etc., 2005; Lepetit, etc., 2005; Zhao, etc., 2006). SIFT (Scale Invariant Feature Transform) is one of the best descriptors for interest point matching (Lowe, 2004). In graph matching algorithms, topological relationship is the key feature and is widely used in pattern recognition (Gold and Rangarajan, 1996; Cross and Hancock, 1998; Demirci, etc., 2004; Caetano, etc., 2004; Shokoufandeh, etc., 2006). Another idea is to consider interest point matching as a classification problem. Features from a reference image are used to train the classifier (Lepetit, etc., 2008; Boffy, etc., 2008).

### 1.4.3 Sensor Model Refinement

Rational Polynomial Coefficients (RPCs) are used as sensor models of high resolution satellite cameras, such as IKONOS and QuickBird. The RPC may be refined directly or indirectly. Direct refining methods modify the original RPCs themselves, while indirect refining methods introduce complementary or concatenated transformations in image or object space, and do not change the original RPCs directly (Hu et al., 2004).

The first direct method is to compute the new rational polynomial coefficients (RPCs) using vendor-provided RPC coefficients as initial values. This method is not stable enough to provide sufficient accuracy in operational environments, unless a large number of densely distributed ground control points (GCPs) (about twice the number of unknowns) are available (Toutin, 2004; Tao and Hu, 2001; Di et al., 2003). Therefore, this method is not feasible for RPC refinement (Grodecki et al., 2003; Hu et al., 2004). A Batch Iterative Least-Squares (BILS) method and an Incremental Discrete Kalman Filtering (IDKF) method have been proposed to modify RPCs (Hu and Tao, 2002). The covariance matrices for the RPCs and the image measurements (provided by the data vendor who calculated the RPC initially) are needed for these methods. Moreover, significant numbers of new GCPs are also required (Hu and Tao, 2002). Bang et al., proposed three methods to modify RPCs: the Pseudo GCP (PG) method, the Using Parameters Observation Equation (UPOE) method, and the Sequential Least Square Solution (SLSS) method (Bang et al., 2003). For the PG method, the RPCs are imported as initial values. The additional GCPs are assigned a large enough weight (compared with the pseudo GCPs) to modify the original RPC. For the UPOE method, 59 RPC parameter observations are used instead of the pseudo GCPs.

Indirect methods use a polynomial to fit the error either in image space (Fraser and Hanley, 2003; Grodecki and Dial, 2003) or in object space (Grodecki and Dial, 2003). For high resolution satellite images such as IKONOS and QuickBird, such methods normally can provide satisfactory results for sensor model refinement. However, indirect methods can only be used under rigorous conditions: the sensor's attitude error is small and its field of view is narrow.

### 1.4.4 Bundle Adjustment

To date, four RPC-based block adjustment models defined in both image and object space have been proposed by other researchers:

(1) Image-Space Adjustment Models Defined in the Domain of Image Coordinates (Commonly known as the Image-Space Bias Compensation Adjustment Models). In this model, compensations are added to the rational functions to capture the discrepancies between the nominal and the measured image space coordinates [Fraser and Hanley, 2003; Fraser and Hanley, 2005; Grodecki and Dial, 2003; Fraser et al., 2006].

(2) Image-Space Adjustment Models Defined in the Domain of Object Space Coordinates [Grodecki and Dial, 2003]. This type of model accomplishes image-space compensation using a polynomial function that is defined in object space.

(3) Object-Space Adjustment Models Defined in the Domain of Object Space.

(4) Object-Space Adjustment Models Defined in the Domain of Image Space.
In both (3) and (4), the object-space RPC block adjustment model is nonlinear in the adjustment parameters and is unrelated to imaging geometry [Grodecki and Dial, 2003]. This model is therefore rarely used.

## 1.5 Problem Statement

Automatic aerial triangulation includes four major steps: interest point extraction; interest point matching; sensor model refinement; and bundle adjustment. Even though much research has been done for aerial triangulation, in this research, it is regarded that each step still contains certain limitations and that there is potential for improvement.

**Limitations in interest point extraction**

Although numerous algorithms have been developed for interest point extraction [Rosenfeld and Johnston, 1973; Rosenfeld and Weszka, 1975; Freeman and Davis, 1977; Moravec, 1977; Beus and Tiu, 1987; Forstner and Gulch, 1987; Harris, 1988; Forstner, 1994], they are all based on gray values and can only extract corners (either geometric 'L' corners, or gradient corners). Corners, however, do not always provide accurate control and sometimes are not suitable for image registration and bundle block adjustment; whereas centers can serve as more accurate controls than corners in most situations. Unfortunately, the difference in accuracy between centers and corners for bundle block adjustment is poorly understood, and the situations in which centers can provide more accurate control than corners is not well known yet.

**Limitations in interest point matching**

After a sufficient number of interest points have been extracted, interest point matching can generate tie points. Although many area-based methods and feature based methods have been developed for interest point matching, they all share the same limitation: ambiguity in smooth areas [Zitova and Flusser, 2003]. For high resolution satellite images containing smooth (low texture) areas such as grassland, forests, snow- or ice-cover, and deserts, neither of the existing types of algorithms can overcome local minimal problems and find correct correspondences.

**Limitations in sensor model refinement**

Vendors of high resolution images from satellites such as IKONOS and QuickBird use RPCs as sensor models instead of releasing the camera's physical parameters. This poses a new challenge for members of the photogrammetric community seeking to refine the sensor model. Many scientists have been working on this topic for a long time and have developed numerous methods for sensor model refinement, including direct methods and indirect methods. However, these methods either need supporting information that is unavailable to the public (direct methods), or have many rigorous conditions that limit their utility (indirect methods) [Grodecki and Dial, 2003; Gong et al., 2005; Hu et al., 2004; Hu and Tao, 2002; Bang et al., 2003].

**Limitations in bundle block adjustment**

There are direct and indirect methods for RPC sensor model refinement. Because the former are not based on an explicit mathematical model, only the latter have been successfully applied in bundle block adjustment. Based on the indirect methods, four bundle block adjustment models which are defined in image space and object space have been developed. Among these models, the bias compensation model defined in image space is most accurate, because the image coordinates reflect the satellite's imaging geometry. However, as an indirect refinement method, its utility is affected by the drawbacks (rigorous conditions with its utility) associated with all such methods as noted above.

## 1.6 Research Objectives

The objectives of this research are fourfold to solve the problems identified in the above four areas or steps.

### Interest point extraction

This portion of the research focuses on determining which type of interest point (centers or corners) can provide more accurate control for bundle block adjustment. Quantitative analysis of the errors of corners and centers with respect to image sampling will be performed. Experiments were designed to verify the quantitative analysis of errors for bundle block adjustment. The relative performance of corners and centers for bundle block adjustment has been quantified.

### Interest point matching

Area based and feature based methods face a common problem: ambiguity in smooth areas. This research focuses on solving this problem. A robust interest point matching algorithm will be developed that incorporates spatial information to overcome the aforementioned ambiguity.

### Sensor model refinement

Direct methods of sensor model refinement require a lot of supplementary information that is unavailable to the public, whereas the indirect methods have rigorous conditions which seriously limit their applications. This research has developed a generic method to overcome all such limitations.

### Bundle block adjustment

To date, four bundle block adjustment models which are defined in image space and object space have been developed; however, these models are based on the indirect methods of sensor model refinement, and therefore have the same limitations as all other indirect methods. Specifically, they can be only used for satellites with narrow field of view and small ephemeris error. This research has developed a robust bundle block adjustment model which can deal with these limitations.

The data and metrics used to evaluate the algorithms developed in this research are summarized in **Table 1.2**.

**Table 1.2 Data and Metrics Used for Evaluation**

| No | Data | Metric Description | Chapter |
|---|---|---|---|
| 1 | (1) A pair of QuickBird Images acquired on July 26, 2002 near Gagetown, New Brunswick, Canada. The QuickBird PAN image resolution is 0.61 m and the QuickBird MS image resolution is 2.44 m.<br>(2) A stereo pair of IKONOS images, acquired in February of 2003 in Hobart, Tasmania, Australia. The incidence angles are forward 75° and backward 69° respectively. | After image registration by using corners and centers respectively, The standard deviation of check points is used to evaluate the accuracy of image registration. | Chapter 2 [Xiong and Zhang, 2009] |
| 2 | (1) A stereo pair of level 1A IKONOS images acquired on June 25, 2004 over Penang, Malaysia. The incidence angles are 30° and 3.5° respectively.<br>(2) A stereo pair of IKONOS images which was acquired on February, 2003 in Hobart, Australia. The incidence angles are forward 75° and backward 69° respectively.<br>(3) Three pairs of QuickBird Images acquired in 2002 near Fredericton, New Brunswick, Canada. | Visual survey is used to evaluate the result of interest point matching. | Chapter 3 [Xiong and Zhang, 2009] |
| 3 | (1) A stereo triplet of IKONOS images which was acquired on February, 2003 in Hobart, Australia. The incidence angles are 69°, 75°, 69° respectively. There are 113 ground control points.<br>(2) A pair of QuickBird Images acquired in July, 2003 in Melbourne, Australia. The incidence angles are forward 65° and backward 65° respectively. There are 81 ground control points. | Standard deviation in image space and object space are used to evaluate the accuracy of bundle block adjustment. | Chapter 4 [Xiong and Zhang, 2009] |
| 4 | (1) A stereo triplet of IKONOS images which was acquired on February, 2003 in Hobart, Australia. The incidence angles are 69°, 75°, 69° respectively. There are 113 ground control points.<br>(2) A pair of QuickBird Images acquired in July, 2003 in Melbourne, Australia. The incidence angles are forward 65° and backward 65° respectively. There are 81 ground control points. | Standard deviation in image space is used to evaluate the accuracy of sensor model refinement. | Chapter 5 [Xiong and Zhang, 2009] |

The topics selected for this research are important not only for photogrammetry but also for other uses. For example, interest point matching is widely used in computer vision systems, pattern recognition, and medical image processing. The sensor model refinement is also widely used in a variety of applications, such as change detection, 3D reconstruction, robotics, and security surveillance.

## 1.7 Overview of Each Chapter

**Chapter 1** is the introduction. It includes the topic selection, research background, problem statement, research objectives, and dissertation outline.

**Chapters 2 to 5** contain the four journal papers, comprising the main contributions to this PhD research.

- Through quantitative error analysis of corners and centers, and experiments verification, **chapter 2** characterizes the performance of corners and centers in image registration and bundle block adjustment in a quantitative way.
- **Chapter 3** presents a robust interest point matching algorithm which incorporates spatial information and can overcome the limitation of ambiguity in smooth areas.
- **Chapter 4** presents a generic RPC refinement method which can be effectively used for different sensors without any limitations.
- **Chapter 5** presents a robust bundle block adjustment model which is based on the generic RPC refinement method. It can adjust large ephemeris and

attitude errors and can be used in images acquired by sensors with wide fields of view.

**Chapter 6** presents the conclusions. It summarizes the achievements of this research and outlines its drawbacks and limitations. It also presents some recomendations for future research.

## REFERENCES


Auer, Matin, Peter Regitnig, and Gerhard A. Holzapfel. (2005). "An Automatic Nonrigid Registration for Stained Histological Sections." *IEEE Transactions on Image Processing*, Vol. 14, No. 4.

Baker, S., Nayar, S.K., and Murase, H. (1998). "Parametric feature detection." *International Journal of Computer Vision*, 27(1):27–50.

Bang Ki In, Soo Jeong, Kyung-Ok Kim. (2003). "Modification of sensor model parameters with a few GCP." *Proceedings of the 2003 Annual Conference of the American Society of Photogrammetry and Remote Sensing (ASPRS)*, May 2003, Anchorage, Alaska.

Beaudet, P.R. (1978). "Rotationally invariant image operators." In *Proceedings of the 4th International Joint Conference on Pattern Recognition*, Tokyo, pp. 579–583.

Belongie, Serge, Jitendra Malik, and Jan Puzicha. (2002). "Shape matching and object recognition using shape contexts." *IEEE Transactions on Pattern Analysis and Machine Intelligence*, Vol. 24.

Besl, Paul J., and Neil D. McKay. (1992). "A Method for Registration of 3-D Shapes." *IEEE Transactions on Pattern Analysis and Machine Intelligence*, Vol. 14, No. 2.

Beus H.L. and Tiu S.S.H. (1987). "An improved corner detection algorithm based on chain-coded plane curves." *Pattern Recognition*, 20:291-296.

Boffy, Aurelien, Yanghai Tsin, and Yakup Genc. (2008). "Real-Time Feature Matching Using Adaptive and Spatially Distributed Classification Trees." http://www.macs.hw.ac.uk/bmvc2006/papers/397.pdf. Accessed: August, 14, 2008.

Booksten, Fred L. (1989). “Principal Warps: Thin-Plate Splines and the Decomposition of Deformations.” *IEEE Transactions on Pattern Analysis and Machine Intelligence*, Vol. 11, No. 6.

Brown, Lisa Gottesfeld. (1992). “A survey of image registration techniques.” *ACM Computing Surveys.* Vol. 24, No. 4.

Caetano, Tiberio S., Terry Caelli, and Dante A.C. Barone. (2004). “A Comparison of Junction Tree and Relaxation Algorithms for Point Matching Using Different Distance Metrics.” *Technical Report TR 04-04*, February 2004, Department of Computer Science, University of Alberta.

Chui, Haili and Anand Rangarajan. (2003). “A New Point Matching Algorithm for Non-Rigid Registration.” *Computer Vision and Image Understanding* 89 (2003) 114-141.

Cordelia Schmid, Roger Mohr and Christian Bauckhage. (2000). “Evaluation of Interest Point Detectors.” *International Journal of Computer Vision* 37(2), 151–172.

Cross, Andrew D.J. and Edwin R. Hancock. (1998). “Graph Matching With a Dual-Step EM Algorithm.” *IEEE Transactions on Pattern Analysis and Machine Intelligence*, Vol. 20, No. 11.

Demirci, M. Fatih, Ali Shokoufandeh, Sven Dickinson, Yakov Keselman, and Lars Bretzner. (2004). “Many-to-Many Feature Matching Using Spherical Coding of Directed Graphs.” *T. Pajdla and J. Matas (Eds.): ECCV 2004, LNCS 3021*, pp. 322-335, 2004.

Di Kaichang, Ruijin Ma, and Rong Xing Li. (2003). “Rational functions and potential for rigorous sensor model recovery.” *Photogrammetric Engineering & Remote Sensing,* Vol. 69, No. 1, pp. 33-41.

Dowman I. J. (1977). “Developments in Online Techniques for Photogrammetry and Digital Mapping.” *Photogrammetric Record*, 9(49): 41-54.

Dreschler, L. and Nagel, H.H. (1982). “Volumetric model and 3D trajectory of a moving car derived from monocular TV frame sequences of a street scene.” *Computer Graphics and Image Processing*, 20:199–228.

Förstner, W. (1994). “A framework for low level feature extraction.” *Proceedings of the 3rd European Conference on Computer Vision*, Stockholm, Sweden, pp. 383–394.

Förstner, W. and Gülch, E. (1987). “A fast operator for detection and precise location of distinct points, corners and centres of circular features.” *Intercommission Conference on Fast Processing of Photogrammetric Data*, Interlaken, Switzerland, pp. 281–305.

Fraser, Clive S., G. Dial, J. Grodecki. (2006). “Sensor orientation via RPCs.” *ISPRS Journal of Photogrammetry & Remote Sensing*, 60(2006) 182-194.

Fraser, Clive S. and Harry B. Hanley. (2003). “Bias Compensation in Rational Functions for Ikonos Satellite Imagery.” *Photogrammetric Engineering & Remote Sensing,* Vol. 69, No. 1, pp. 53 – 57.

Fraser, Clive S. and Harry B. Hanley. (2005). “Bias-compensated RPCs for Sensor Orientation of High-resolution Satellite Imagery.” *Photogrammetric Engineering & Remote Sensing,* Vol. 71, No. 8, pp. 909–915.

Freeman H. and Davis L.S. (1977). “A corner finding algorithm for chain-coded curves.” *IEEE Trans. Computers*, 26:297-303.

Gold, Steven and Anand Rangarajan. (1996). “A Graduated Assignment Algorithm for Graph Matching.” *IEEE Transactions on Pattern Analysis and Machine Intelligence*, Vol. 18, No. 4.

Gold, Steven, Anand Rangarajan, Chien-Ping Lu, Suguna Pappu, and Eric Mjolsness. (1997). “New Algorithms for 2D and 3D Point Matching: Pose Estimation and Correspondence.” URL: http://citeseerx.ist.psu.edu/legacymapper?did=88372, Accessed: August, 14, 2008.

Gong Jianming, Yang Xiaomei, Zhou Chenghu, Sun Xiaoyu, and Xue Cunjin. (2005). “Refinement and evaluation of Beijing-1 orthorectification based on RFM.” *ISPRS conference 2005, Commission VI, WG VI/4.*

Grodecki Jacek and Gene Dial. (2003). “Block adjustment of high resolution satellite images described by rational polynomials.” *Photogrammetric Engineering & Remote Sensing,* Vol. 69, No. 1, pp. 59-68.

Gupta, Rajiv. (1997). “Linear Pushbroom Cameras.” *IEEE Transactions on Pattern Analysis and Intelligence, VOL. 19, NO. 9, 1997.*

Harris C. and Stephens M. (1988). “A combined corner and edge detector.” *Alvey Vision Conference*, pages 147-151.

Helava, Uuno V., Chapelle, Walter E., Hornbuckle, John A. (1973). “Stereoplotting apparatus for correlating image points disposed along epipolar lines.” U.S.Patent No. 3726591, Apr. 10, 1973.

Hu Yong and C. Vincent Tao. (2002). “Updating solutions of the rational function model using additional control information.” *Photogrammetric Engineering & Remote Sensing,* Vol. 68, No. 7, pp. 715-723.

Hu Yong, Tao Vincent, Arie Croitoru. (2004). “Understanding the rational function model: methods and applications.” URL: http://www.geoict.net/Resources/Publications/IAPRS2004_RFM2394.pdf, last date accessed 31 December 2007.

Kaplan, Alexander, Ehud Rivlin, and Ilan Shimshoni. (2004). “Robust Feature Matching Across Widely Separated Color Images.” *Proceedings of the 17th International Conference on Pattern Recognition* (ICPR’04).

Kim, Taejung. (2000). “A Study on the Epipolarity of Linear Pushbroom Images.” *Photogrammetric Engineering & Remote Sensing*, VOL. 66, NO. 8, August 2000, 961-966.

Kybic, Jan, and Michael Unser. (2003). “Fast Parametric Elastic Image Registration.” *IEEE Transactions on Image Processing*, Vol. 12, No. 11.

Liu H.-C. and Srinath M.D. (1990). “Corner detection from chain-code.” *Pattern Recognition*, 23:51-68.

Lepetit, Vincent, Julien Pilet, and Pascal Fua. (2004). “Point Matching as a Classification Problem for Fast and Robust Object Pose Estimation.” http://cvlab.epfl.ch/~vlepetit/papers/lepetit_cvpr04.pdf. Accessed: August 14, 2008.

Lepetit, Vincent, Pascal Lagger, and Pascal Fua. (2005). “Randomized Trees for Real-Time Keypoint Recognition.” *Computer Vision and Pattern Recognition*, 2005. Volume: 2, 775- 781 vol. 2.

Lowe, David G. (2004). “Distinctive Image Features from Scale-Invariant Keypoints.” *International Journal of Computer Vision* 60(2), 91–110.

Lu Yihui, Kurt Kubik and Mohammed Bennamoun. (1997). “Stereo Image Matching Based on Probability Relaxation.” *IEEE 1997 TENCON-Speech and Image Technologies for computing and Telecommunications*.

Masry, S. E. (1972). “An Automatic Method for Height Profile Determination.” *The Photogrammetric Record*, Volume 7 Issue 42, Pages 728 – 730.

Moravec, H.P. (1977). “Towards automatic visual obstacle avoidance.” *Proceedings of the 5th International Joint Conference on Artificial Intelligence*, Cambridge, Massachusetts, USA, p. 584.

Mount, David M., Nathan S. Netanyahu, and Jacqueline Le Moigne. (1997). “Efficient Algorithms for Robust Feature Matching.” *Proceedings of the CESDIS Image Registration Workshop*, NASA Goddard Space Flight Center, Greenbelt, MD, 1997.

Nagel, H.H. (1983). “Displacement vectors derived from second order intensity variations in image sequences.” *Computer Vision, Graphics and Image Processing*, 21:85–117.

Parida, L., Geiger, D., and Hummel, R. (1998). “Junctions: Detection, classification, and reconstruction.” *IEEE Transactions on Pattern Analysis and Machine Intelligence*, 20(7):687–698.

Rexilius, J., S.K. Warfield, C.R.G. Guttmann, X. Wei, R. Benson, L. Wolfson, M. Shenton, H. Handels, and R. Kikinis. (2001). “A Novel Nonrigid Registration Algorithm and Applications.” *W. Niessen and M. Viergever (Eds.): MICCAI 2001*, LNCS 2208, pp. 923-931.

Rohr, K. (1992). “Recognizing corners by fitting parametric models.” *International Journal of Computer Vision*, 9(3):213–230.

Rosenfeld and E. Johnston. (1973). “Angle detection on digital curves.” *IEEE Trans. Computers*, 22:875-878.

Rosenfeld and J.S. Weszka. (1975). “An improved method of angle detection on digital curves.” *IEEE Trans. Computers*, 24:940-941.

Shokoufandeh, Ali, Yakov Keselman, Faith Demirci, Diego Macrini, and Sven Dickinson. (2006). “Many-to-Many Feature Matching in Object Recognition.” *H.I. Christensen and H.-H. Nagel (Eds.): Cognitive Vision Systems*, LNCS 3948, pp. 107-125.

Tao C. Vincent and Yong Hu. (2001). “A comprehensive study of the rational function model for photogrammetric processing.” *Photogrammetric Engineering & Remote Sensing,* Vol. 67, No. 12, pp. 1347-1357.

Terasawa, Kengo, Takeshi Nagasaki, and Toshio Kawashima. (2005). “Robust Matching Method for Scale and Rotation Invariant Local Descriptors and Its Application to Image Indexing.” *G.G. Lee et al. (Eds.): AIRS 2005*, LNCS 3689, pp. 601-615.

Toutin, T., and P. Cheng. (2000). “Demystification of IKONOS.” *Earth Observation Magazine*, 9(7):17-21.

Tu, Zhuowen, Songfeng Zheng, and Alan Yuille. (2008). “Shape Matching and Registration by Data-Driven EM.” *Computer Vision and Image Understanding,* 109 (2008) 290-304.

Williams, John and Mohammed Bennamoun. (2001). “Simultaneous Registration of Multiple Corresponding Point Sets.” *Computer Vision and Image Understanding* 81, 117-142.

Yang, Gehua, Charles V. Steward, Michal Sofka, and Chia-Ling Tsai. (2007). “Registration of Challenging Image Pairs: Initialization, Estimation, and Decision.” *IEEE Transactions on Pattern Analysis and Machine Intelligence*, Vol. 29, No. 11.

Zhang, Li, Maria Pateraki, Emmanuel Baltsavias. (2004). “Matching of Ikonos Stereo and Multitemporal GEO Images for DSM Generation.” *Commission III, WG III/2*, 2004.

Zhao, Wanlei, Yugang Jiang, and Chong-Wah Ngo. (2006). “Keyframe Retrieval by Keypoints: Can Point-to-Point Matching Help?” *H. Sundaram et al. (Eds.): CIVR* 2006, LNCS 4071, pp. 72-81.

Zitova, Barbara, Jan Flusser. (2003). “Image Registration Methods: a Survey.” *Image and Vision Computing* 21 (2003)977-1000.

# Chapter 2 ERROR ANALYSIS OF CORNER AND CENTER POINTS FOR IMAGE REGISTRATION[2]

## ABSTRACT

Image registration is a popular research topic in the fields of remote sensing, photogrammetry, computer vision, pattern recognition, and medical image processing. Both corner and center points are used for image registration, but the differences in performance of image registration depending on which points are used, has not drawn much attention. Such performance differences have the potential to directly affect the success of multi-resolution or multi-modal image registration.

The goal of this paper is to compare the characteristics of corner and center points in image registration and to quantify the differences in their performance. Corners and gravity centers were compared in two cases: 1) registration of images with the same resolution; and 2) registration of images with different resolution. The results showed that gravity centers provide more accurate results for image registration in both cases. Quantitative analysis revealed that the position error of the centers is only about 60% or less of the position error of the corners. Experiments are presented that confirm this finding.

**KEY WORDS:** Error Analysis, Gravity Centers, Corners, Image Registration

[2] This chapter has been submitted to the journal *Photogrammetric Engineering and Remote Sensing* (*PE&RS*) as a research paper for peer review and publication.
Xiong Z. and Y. Zhang, "Error Analysis of Corner and Center Points for Image Registration", *Photogrammetric Engineering and Remote Sensing,* 2009.

## 2.1. Introduction

Image registration normally requires conjugate points. Corners and gravity centers (referred to as "centers" in this paper) are the most typical and common interest points used as tie points for image registration. For example, both corners and centers are used to register images having the same resolution such as stereo pairs of IKONOS and QuickBird images [Fraser et al., 2005]. They are also used for registration of images having different resolutions [Xiong and Zhang, 2008]. When using photogrammetric systems, operators usually collect both corners and centers as tie points for image registration, but for automatic image registration, it is more common to use only corners. For example, corners are used for automatic medical image registration [Gold, etc., 1997; Chui and Rangarajan, 2003; Auer, etc., 2005], for automatic image registration in computer vision systems [Belongie, etc., 2002; Kaplan, etc., 2004; Terasawa, etc., 2005; Lepetit, etc., 2005; Zhao, etc., 2006], and for pattern recognition [Besl, etc., 1992; Lowe, 2004; Lepetit, etc., 2008; Boffy, etc., 2008].

One might ask why centers cannot be used in the foregoing automatic image registration systems. The major reason is that most interest point detection algorithms can only extract ‘corners’, i.e. the maximum gradient points. There are many examples. Well known algorithms that are based on auto-correlation matrices, such as Moravec [1977], Forstner and Gulch [1987], Harris [1988], and Forstner [1994], can only determine points with local maximum gradients. Similarly, contour based methods that extract maximal curvature or inflection points along the contour chains, or do some polygonal approximation and then search for intersection points, can only extract corners. Examples include Rosenfeld and Johnston [1973], Rosenfeld and Weszka [1975], Freeman and Davis [1977], Beus and Tiu [1987], and the IPAN99 algorithm [Dmitry and Zsolt, 1999].

To date, centers are mostly excluded from use in image registration except for manually selected tie points that include centers. This is a concern because gravity center points can provide precise image registration. Furthermore, corners sometimes fail to give satisfactory results for multi-modal or multi-resolution image registration.

In this paper we use error analysis and experiments to attempt to quantify the difference in accuracy between corners and centers for image registration. In the first section, we analyze the position error of corners and centers, both in images having the same resolution and in images having different resolutions. In the second section, we present three experiments using these different types of images. Finally, we analyze the results and present our conclusions.

## 2.2. Position Errors of Corners and Gravity Centers for Image Registration

In this research, the position errors of corners and gravity centers for image registration were studied in two cases: registration of images with different resolutions and registration of images with the same resolution. In **Figure 2.1**, the shaded area represents an object. The dot in **Figure 2.1** (a) represents a corner and the dot in **Figure 2.1** (b) represents a gravity center.

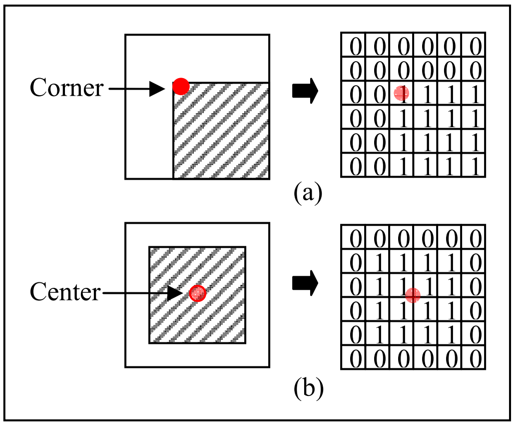


**Figure 2.1 Corner (a) and Center (b). The upper figures illustrate an object and a corner in the analog image and digital image (a); the lower figures illustrate an object and a center in the analog image and digital image (b).**

In a digital image, an object is represented by discrete pixels. Some pixels are completely filled by an object and some pixels are partially filled. In **Figure 2.2**, there are three pixels which are partially filled by an object. In **Figure 2.2** (1), (2), and (3) the object coverage is 50%, 75%, and 25% respectively. For the purposes of this research we assumed that: a)  when the object coverage is 50% (**Figure 2.2** (1)), the probability that such pixel is recognized as an object pixel is 50%; b) when the object coverage is above 50% (**Figure 2.2** (2)), the probability that such pixel is recognized as object pixel is 100%; and c) when the object coverage is below 50%, the probability that such pixel is recognized as object pixel is 0%.

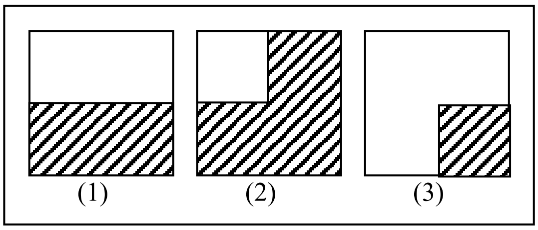


**Figure 2.2 Object Coverage in a Pixel. (1) Object covers 50% of a pixel, (2) Object covers 75%, (3) 25%.**

### 2.2.1 Corners and Gravity Centers Used for Registration of Images with Different Resolutions

This is a case study. So the conclusion from this study is only a result of an insufficient statistics. In order to determine the difference in accuracy between corners and gravity centers when they are used for the registration of different resolution images, the position errors of corners and centers were examined. The MS and PAN images were used as samples for this purpose (**Figure 2.3**). Only integer sampling (as opposed to continuous sampling) was considered. One MS image pixel covers the same area as 16 PAN image pixels, so 16 relative positions between the MS and PAN images were studied (**Figures 2.4** and **2.5**). In these sixteen cases, the corners and centers may have different positions on the MS and PAN images respectively. We know, for image registration, the positions of a tie point, no matter corner or center, on both images should be at the same position. Otherwise, any position difference of tie points between the MS and PAN images will result in registration error. From these sixteen cases, from the view of image sampling, the author attempted to perform an insufficient statistics computation and tried to study the position error of corners and centers between the MS and PAN images.

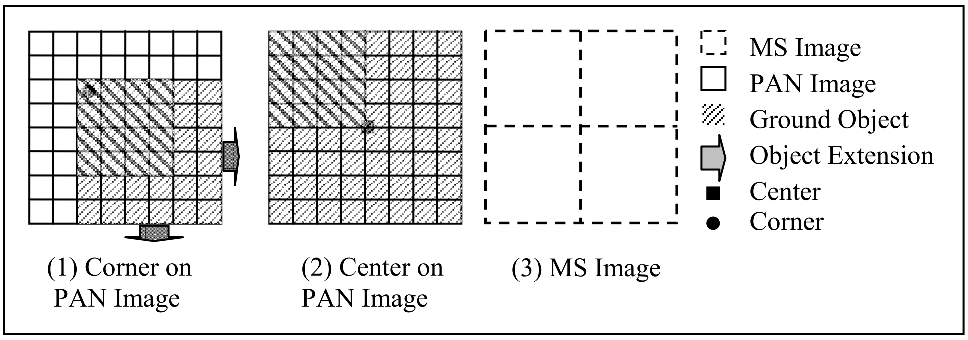


**Figure 2.3 Sampling of the Pan and MS Images with a resolution ratio of 1/4. In this case, 16 pixels in the PAN image cover the same area of 1 pixel in the MS image. The shaded area represents an object. (1) An object with its corner. This object extends in east and south. (2) An object with its center. This is a symmetric object with 8 by 8 pixels.**

**Figure 2.4** shows the corner positions on the MS and PAN images in sixteen cases. In each of these cases, the object corner is on the upper left. The object extends in south and east. Because of the different resolutions, the corner positions on the MS and PAN images may differ. The distances between the corners on the two types of images are summarized in **Table 2.1**.

**Figure 2.5** shows the center positions on the MS and PAN images in sixteen cases. In each of these cases, the object is an 8 by 8 pixel square (on the PAN image). In the 16 cases, the center positions on the MS and PAN images may be different because of the different relative positions between the PAN and the MS images. The distances between the centers on each image type are shown in **Table 2.1**.

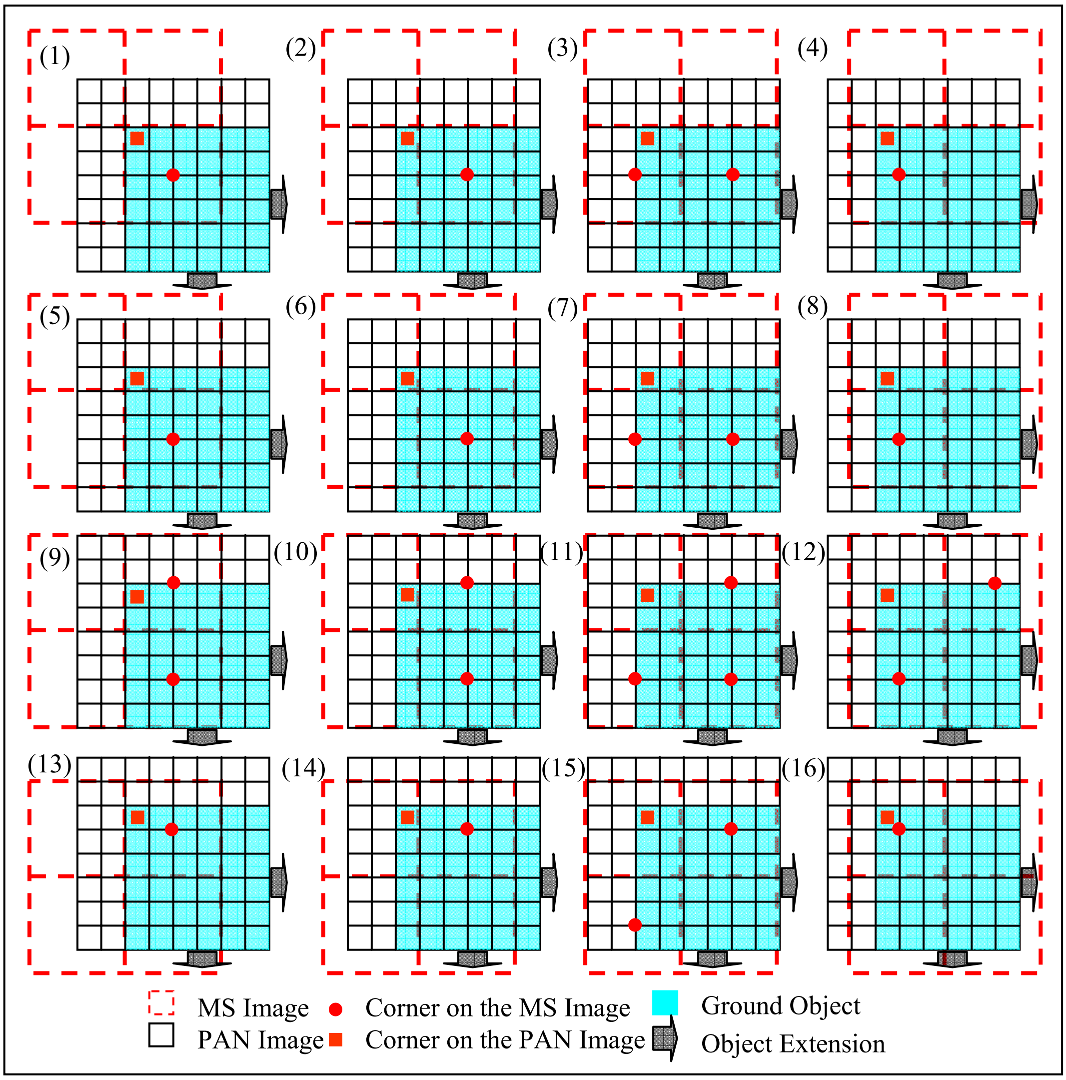


**Figure 2.4 Corner Positions of an Object on the PAN and MS Images (Cases 1 – 16). Due to the sampling error, the corner position on the MS image may change case by case. In these cases, the object extends in south and east. Therefore, the corner pixel of such object is in the upper left corner. According to the assumption in Figure 2.2, the MS pixel on the upper left corner which the object coverage equals or greater than 50% could be recognized as the corner pixel of the object on the MS image. So there may be more than one possible corner on the MS image. The PAN pixel on the upper left of the object is directly recognized as the corner pixel of the object on the PAN image.**

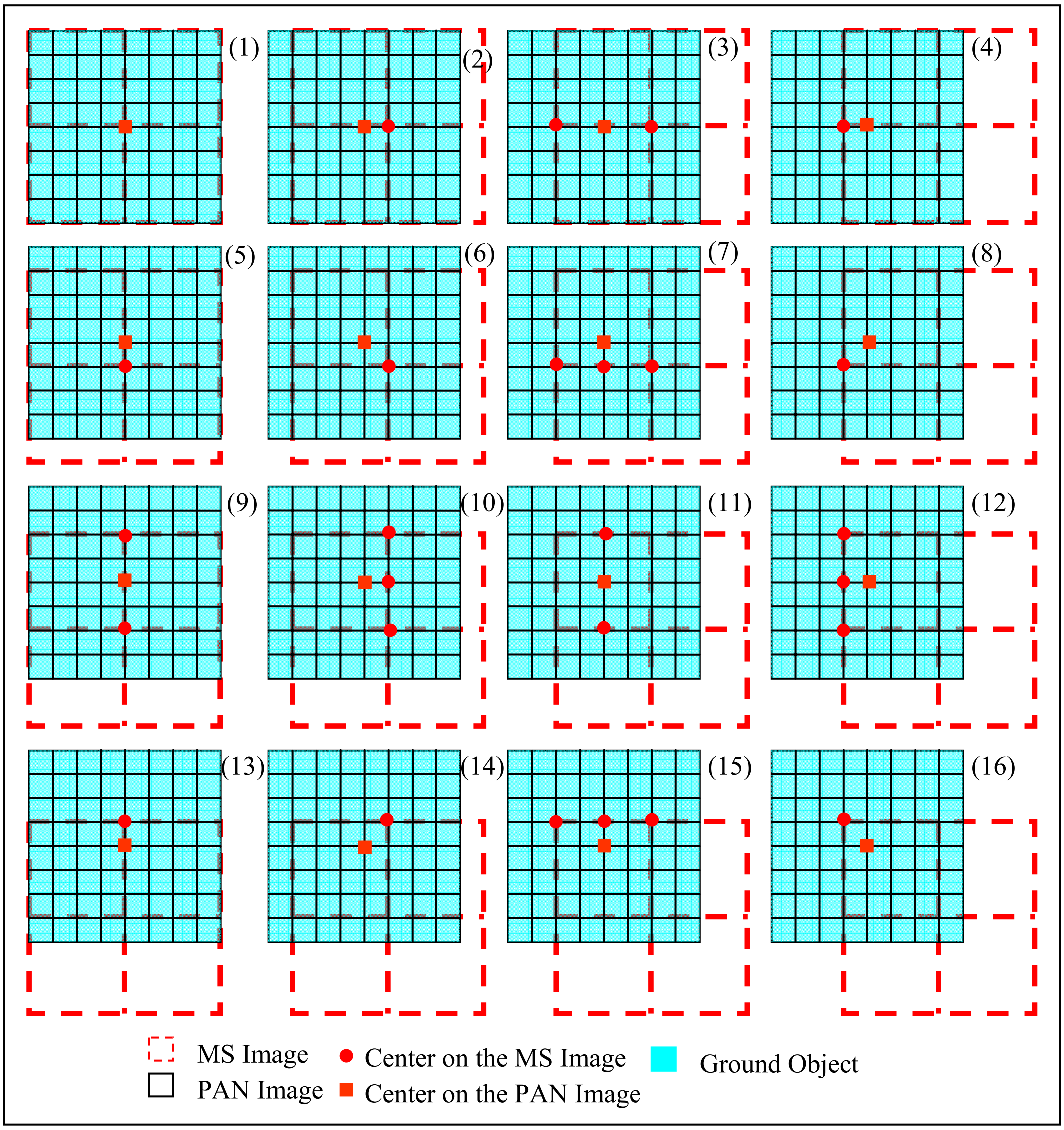


**Figure 2.5 Center Positions on the PAN and MS Images (Cases 1 – 16). In cases 1, 3, 9, 11, the center on the PAN image covers the center of the MS image. Due to sampling error, the center position on the MS image may change case by case. In these cases, the symmetric object covers 8 by 8 pixels on the PAN image. According to the assumption in Figure 2.2, the MS pixel which the object coverage equals or greater than 50% could be recognized as object pixel. The center position on the MS image is estimated based on the possible object pixels on the MS image. So there may be more than one possible center on the MS image. The center position on the PAN image is estimated based on 8 × 8 PAN image pixels.**

**Table 2.1 Deviation Between Corners/Centers on the PAN and MS Images.**

| Case | Deviation Between Corners on the PAN and MS Images (PAN pixels) | Average Deviation (PAN pixels) | Deviation Between Centers on the PAN and MS Images (PAN pixels) | Average Deviation (PAN pixels) |
|---|---|---|---|---|
| 1 | 2.12 | 2.12 | 0 | 0 |
| 2 | 2.91 | 2.91 | 1 | 1 |
| 3 | 1.58; 3.81 | 2.25 | 2; 0; 2 | 1.33 |
| 4 | 1.58 | 1.58 | 1 | 1 |
| 5 | 2.91 | 2.91 | 1 | 1 |
| 6 | 3.53 | 3.53 | 1.41 | 1.41 |
| 7 | 2.55;4.30 | 3.43 | 2.24; 1; 2.24 | 1.83 |
| 8 | 2.55 | 2.55 | 1.41 | 1.41 |
| 9 | 1.58; 3.81 | 2.70 | 2; 0; 2 | 1.33 |
| 10 | 2.55; 4.30 | 3.43 | 2.24; 1; 2.24 | 1.83 |
| 11 | 3.53; 3.53; 4.95 | 4.00 | 2; 0; 2 | 1.33 |
| 12 | 4.53; 3.53 | 4.03 | 2.24; 1; 2.24 | 1.83 |
| 13 | 1.58 | 1.58 | 1 | 1 |
| 14 | 2.55 | 2.55 | 1.41 | 1.41 |
| 15 | 3.53; 4.53 | 4.03 | 2.24; 1; 2.24 | 1.83 |
| 16 | 0.71 | 0.71 | 1.41 | 1.41 |
| Average Deviation (PAN pixels) | | 2.77 | | 1.31 |

**Table 2.1** shows that the average deviation of the corners is 2.77 pixels (PAN) and the average deviation of centers is 1.31 pixels (PAN). The position error of the gravity centers is only about 47.3% of the corner errors. For registration of images of different resolutions (e.g. PAN and MS images), use of gravity centers rather than corners therefore has the potential to reduce position error by about 50%.

### 2.2.2 Corners and Gravity Centers Used for Registration of Images Having the Same Resolution

This is a case study for registration of images with the same resolution. So the conclusion from this study is only a result of an insufficient statistics. In the registration of same resolution images, the position errors of corners and centers were examined for two objects. The first object exactly covers a 6 by 6 square of image pixels (**Figure 2.6**(1), (2), (3)) and the second object exactly covers a 5.5 by 5.5 square of image pixels (**Figure 2.6**(4), (5), (6)). In order to include as many situations as possible for statistical analysis, all possible object positions on the image should be considered. For the first object, there are two situations which may possibly cause the ambiguity of both corner position and center position (**Table 2.2**). The same situation is applicable to the second object. The possible corner positions and center positions are listed in **Table 2.2**.

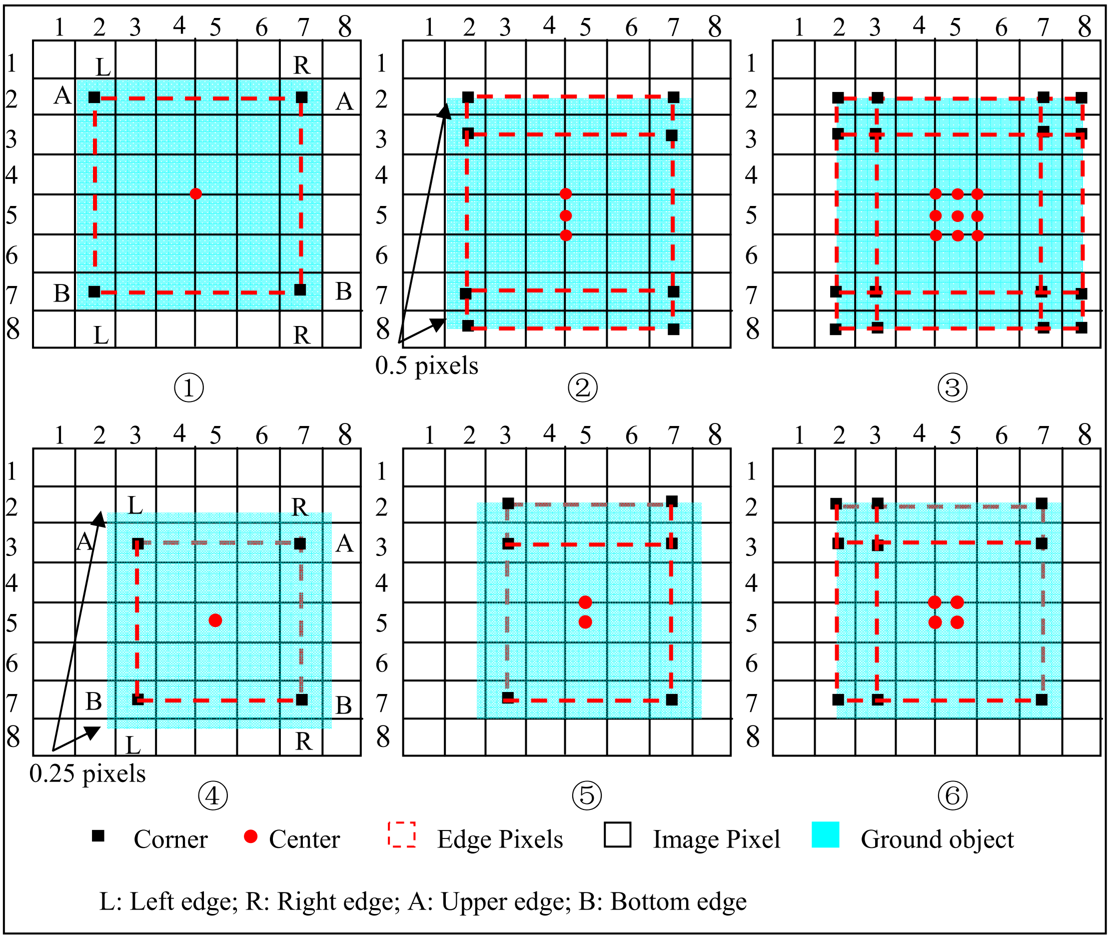


**Figure 2.6 Possible Corner Positions and Center Positions on the Square Object. The dot represents a possible center. The solid square represents a possible corner.**

According to the assumption in **Figure 2.2**, the pixel in which the object coverage equals or is greater than 50% could be recognized as an object pixel. The corner position is the possible object corner pixel. The center position of the object is estimated using the possible edge pixels.

**Table 2.2 Possible Positions of Corners and Centers, and their Corresponding Standard Deviation.**

| Case | Corner | | | Center | | |
|---|---|---|---|---|---|---|
| | Corner Position | σ1 column (pixels) | σ2 row (pixels) | Center Position | σ1 column (pixels) | σ2 row (pixels) |
| 2 | (2, 2), (2,3); | 0 | 0.71 | (4.5, 4.5), (4.5, 5), (4.5, 5.5) | 0 | 0.50 |
| | (7, 2), (7, 3); | 0 | 0.71 | | | |
| | (7, 7), (7, 8); | 0 | 0.71 | | | |
| | (2, 7), (2, 8) | 0 | 0.71 | | | |
| 3 | (2, 2), (2,3), (3, 2), (3, 3); | 0.58 | 0.58 | (4.5, 4.5), (4.5, 5), (4.5, 5.5); (5, 4.5), (5, 5), (5, 5.5); (5.5, 4.5), (5.5, 5), (5.5, 5.5) | 0.43 | 0.43 |
| | (7, 2), (7, 3), (8, 2), (8, 3); | 0.58 | 0.58 | | | |
| | (7, 7), (7, 8), (8, 7), (8, 8); | 0.58 | 0.58 | | | |
| | (2, 7), (2, 8), (3, 7), (3, 8); | 0.58 | 0.58 | | | |
| 5 | (3, 2), (3, 3); | 0 | 0.71 | (5, 4.5), (5, 5); | 0 | 0.35 |
| | (7, 2), (7, 3); | 0 | 0.71 | | | |
| | (7, 7); | 0 | 0 | | | |
| | (3, 7); | 0 | 0 | | | |
| 6 | (2, 2), (2, 3), (3, 2), (3, 3); | 0.58 | 0.58 | (4.5, 4.5), (5, 4.5), (4.5, 5), (5, 5); | 0.29 | 0.29 |
| | (7, 2), (7, 3); | 0 | 0.71 | | | |
| | (7, 7); | 0 | 0 | | | |
| | (2, 7), (3, 7); | 0.71 | 0 | | | |
| Average σ (pixels) | | 0.60 | 0.66 | | 0.36 | 0.39 |
| $\sigma_s$ (pixels) | | 0.89 | | | 0.53 | |

σ: Standard Deviation

In **Table 2.2**, $\sigma_1$ refers to the column standard deviation and $\sigma_2$ refers to the row standard deviation; $\sigma_s$ refers to distance standard deviation which can be defined as follows:

$$\sigma_s = \sqrt{(\sigma_1^2 + \sigma_2^2)} \qquad (2.1)$$

In **Figure 2.6**, the corner and the center could have several possible positions because of different sampling situations. We can consider these possible positions as a range of observations and we can use the standard deviation to evaluate the quality of the observations. For example, for a group of observations: $a_1$, $a_2$, $a_3$, …, $a_n$, the mean value can be calculated as follows:

$$m = \frac{a_1 + a_2 + ... + a_n}{n} \tag{2.2}$$

The deviation of each observation could then be expressed as

$$v_i = a_i - m \tag{2.3}$$

Therefore, the standard deviation of this group of observations can be calculated as follows:

$$\sigma = \sqrt{\frac{[vv]}{n-1}} \tag{2.4}$$

For example, in case 3, the upper left corner could be (2, 2), (2, 3), (3, 2), (3, 3). So there are totally 4 different columns 2, 2, 3, 3, and 4 different rows 2, 3, 2, 3. For columns, the mean column could be:

(2+2+3+3)/4=2.5

The residuals of columns are:

0.5, 0.5, -0.5, -0.5

So the column standard deviation of the upper left corner could be,

$$\sigma = \sqrt{\frac{[vv]}{n-1}} = \sqrt{\frac{0.5^2 + 0.5^2 + (-0.5)^2 + (-0.5)^2}{4-1}}$$

=0.58

Similarly, the row standard deviation of the upper left corner is 0.58 [**Table 2.2**]. The gravity center is determined based on the edge points and the corner is determined by edge intersections. In this research, we assumed that the center position is determined based on the corners' position. For example, in **Figure 2.6②**, the row of the gravity center can be calculated as follows:

$$Row_{Center} = \frac{Row_{Corner1} + Row_{Corner2} + Row_{corner3} + Row_{corner4}}{4} \quad (2.5)$$

Therefore, once the accuracy of the four corners has been determined, the accuracy of the gravity center can be determined according to the error propagation:

$$\sigma_{Center\_Row} = \sqrt{\frac{\sigma^2_{row\_corner1} + \sigma^2_{row\_corner2} + \sigma^2_{row\_corner3} + \sigma^2_{row\_corner4}}{4^2}} \quad (2.6)$$

For case 2 in Figure **2.6②,** according to the error propagation, the row standard deviation of the center could be:

$$\sigma_{Center\_Row} = \sqrt{\frac{0.71^2 + 0.71^2 + 0.71^2 + 0.71^2}{4^2}} = \frac{0.71}{\sqrt{4}} = 0.35$$

From the possible center positions, the row standard deviation of the center is estimated to be 0.50. So the accuracy of center position estimated by error propagation is a little bit different from the accuracy estimated by the distribution of centers.

We do believe that the probability that the position error of corners and centers is zero is extremely small. In order to estimate the position accuracy of corners and centers, and compare the position accuracy of corners and centers, only the cases where the position error is not zero are considered. In **Table 2.2**, the standard deviations of centers and corners are estimated by the distribution of centers and corners. It is obvious that the standard deviation of centers (0.53 pixels) is much smaller than that of the corners (0.89 pixels). In other words, the average standard deviation of centers is only about 60% of the corner deviations. This means that use of the center points may improve the accuracy of image registration by 40% in the registration of images having the same resolution.

To summarize our results, the average deviation of corners and centers (in the registration of different resolution images) and the standard deviation of corners and centers (in registration of same resolution images) are shown in **Table 2.3**.

**Table 2.3 Standard Deviation in 2 Cases**

| | 1. Different Resolution (MS/PAN) | 2. Same Resolution |
|---|---|---|
| Corner $\sigma_s$/Average deviation (pixels) | 2.77 | 0.89 |
| Center $\sigma_s$/Average deviation (pixels) | 1.31 | 0.53 |
| Center/Corner | 47.3% | 59.6% |

**Figure 2.7** shows a comparison of average deviation of corners and centers (in the registration of different resolution images) and the standard deviations of corners and centers (in registration of same resolution images) corresponding to **Table 2.3**.

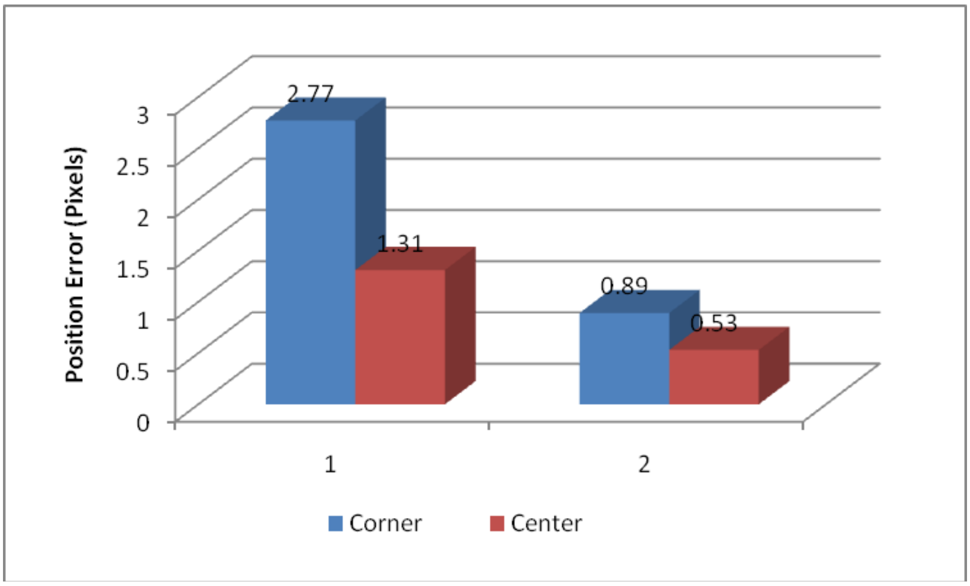


**Figure 2.7 Position Error of Corners and Centers in 2 Cases. The position error of centers is much smaller than that of corners in both cases.**

In conclusion, for registration of images having different resolutions (e.g. PAN and MS), gravity centers may reduce position error by 55% compared to the corners and for registration of images having the same resolution, the centers may improve the accuracy of image registration by 40%. In both cases the centers yielded better results.

## 2.3. Experiment

We designed three experiments for this research which correspond to the above analyses. The first experiment uses a pair of QuickBird images which consists of one MS image and one PAN image, having different resolutions. In the second and third experiments, a pair of IKONOS MS images is used to check the accuracy of registration of images having the same resolution.

**Experiment 1**

In this experiment, a pair of QuickBird images acquired on July 26, 2002 near Gagetown, New Brunswick, Canada is used **(Figure 2.8)** . The QuickBird PAN image resolution is 0.61 m and the QuickBird MS image resolution is 2.44 m. This image pair covers an area of 35.84 $km^2$ with length of 7.8 km and width of 4.8 km.

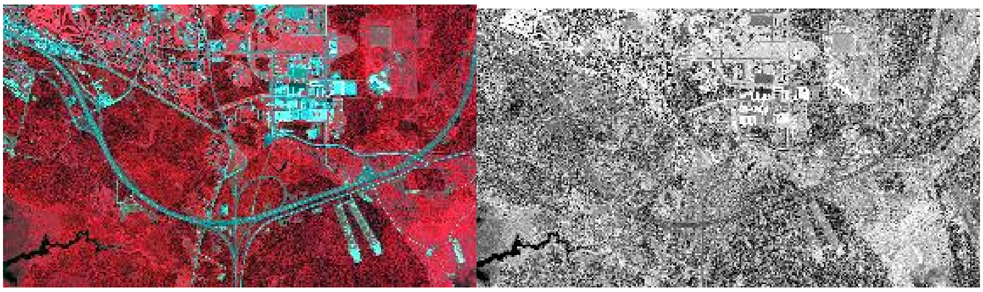

**Figure 2.8 QuickBird MS (left) image and PAN image (right).**

Tie points were used for image registration. The corner points and center points were measured manually (**Figure 2.9**). **Figure 2.11** shows part of corners and **Figure 2.12** illustrates some centers.

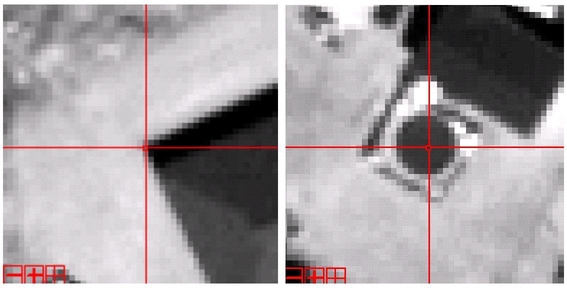

(a) (b)

**Figure 2.9 Corner (a) and Center (b) were measured manually.**

From the two images, 26 corners and 26 centers were selected as tie points. **Table 2.4** shows the image coordinates of corners and centers. These tie points were used to register the images. The ground position was calculated from the tie points' image position using the Direct Location Algorithm [Xiong and Zhang, 2008]. From the MS image position and PAN image position, two different sets of ground coordinates were independently obtained. In an ideal case, the two ground positions should be the same for image registration, but actually they are not because of position error caused by sampling. In order to eliminate such error, the weighted average ground position for each tie point was used to refine the image sensor model. Next, the ground positions of the tie points were calculated again. The deviation of the ground positions was used to evaluate the accuracy of image registration in object space. In order to calculate the ground position from the image position using the Direct Location Model, a DEM is needed (**Figure 2.10**).

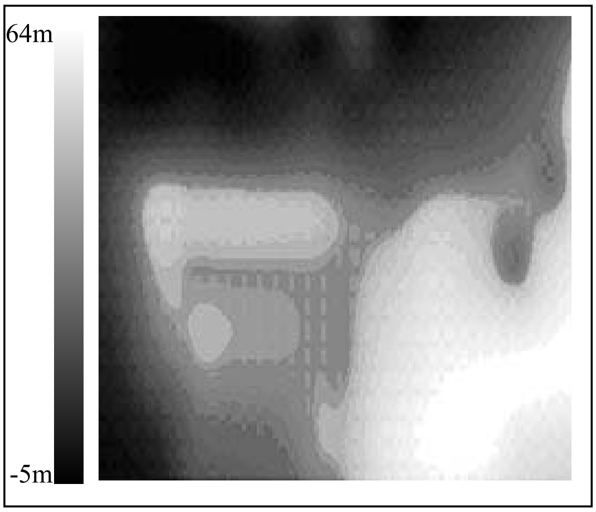


**Figure 2.10 Digital Elevation Model in Test Area (the minimum height is -5m and the maximum height is 64m) (from Global DEM)**

**Table 2.4 Image Coordinates of 34 Gravity Centers and 26 Corners**

| No | Gravity Center | | | | Corner | | | |
|---|---|---|---|---|---|---|---|---|
| | MS | | PAN | | MS | | PAN | |
| | Column | Row | Column | Row | Column | Row | Column | Row |
| 1 | 93 | 506 | 655 | 738 | 334 | 612 | 1616 | 1162 |
| 2 | 101 | 503 | 689 | 726 | 2730 | 570 | 11186 | 999 |
| 3 | 106 | 496 | 707 | 696 | 1887 | 503 | 7817 | 730 |
| 4 | 1704 | 815 | 7088 | 1978 | 93 | 506 | 655 | 738 |
| 5 | 1639 | 830 | 6827 | 2037 | 99 | 509 | 681 | 750 |
| 6 | 1673 | 843 | 6965 | 2088 | 91 | 497 | 648 | 702 |
| 7 | 1819 | 456 | 7547 | 539 | 96 | 500 | 669 | 714 |
| 8 | 2705 | 553 | 11084 | 930 | 101 | 503 | 689 | 726 |
| 9 | 2730 | 570 | 11186 | 999 | 94 | 493 | 659 | 687 |
| 10 | 2752 | 1243 | 11272 | 3691 | 95 | 490 | 665 | 672 |
| 11 | 2561 | 1690 | 10509 | 5477 | 101 | 493 | 687 | 685 |
| 12 | 1335 | 1778 | 5614 | 5827 | 106 | 496 | 707 | 696 |
| 13 | 1134 | 1771 | 4812 | 5800 | 2741 | 559 | 11232 | 957 |
| 14 | 1130 | 1799 | 4797 | 5911 | 2739 | 1144 | 11222 | 3297 |
| 15 | 1091 | 1747 | 4639 | 5706 | 3058 | 1764 | 12496 | 5775 |
| 16 | 106 | 793 | 707 | 1886 | 1333 | 1777 | 5610 | 5827 |
| 17 | 98 | 787 | 676 | 1859 | 1216 | 1223 | 5143 | 3609 |
| 18 | 152 | 776 | 892 | 1817 | 1361 | 572 | 5723 | 1008 |
| 19 | 135 | 770 | 822 | 1796 | 1475 | 459 | 6177 | 557 |
| 20 | 239 | 515 | 1237 | 772 | 1717 | 819 | 7147 | 2001 |
| 21 | 651 | 557 | 2884 | 943 | 1653 | 841 | 6890 | 2088 |
| 22 | 632 | 553 | 2807 | 926 | 584 | 876 | 2620 | 2222 |
| 23 | 1423 | 460 | 5966 | 555 | 345 | 542 | 1666 | 886 |
| 24 | 1414 | 461 | 5930 | 562 | 511 | 611 | 2326 | 1165 |
| 25 | 1397 | 454 | 5861 | 533 | 245 | 1675 | 1268 | 5418 |
| 26 | 2905 | 933 | 11882 | 2453 | 1737 | 829 | 7223 | 2038 |

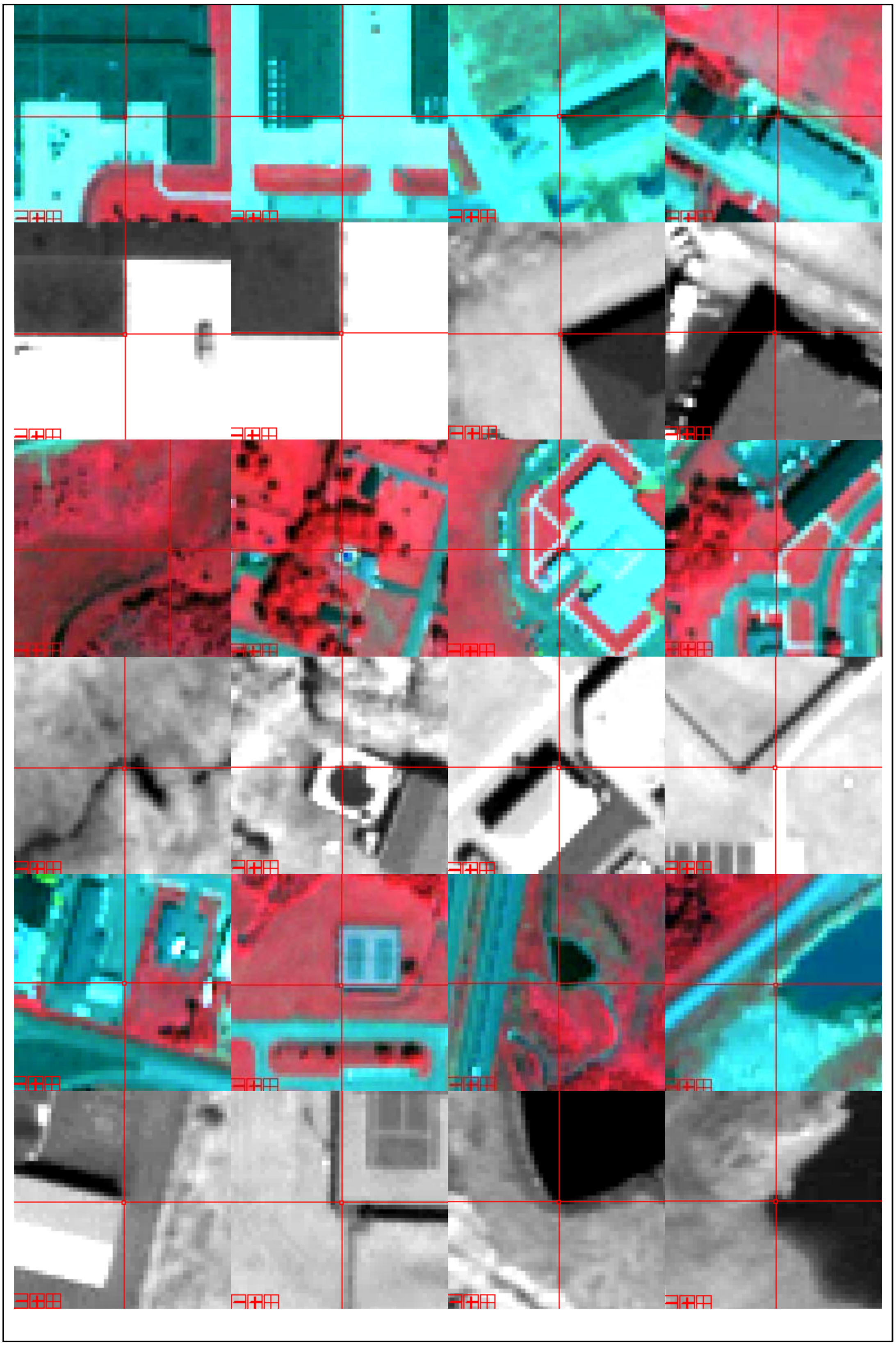

**Figure 2.11 Part of Corners.**

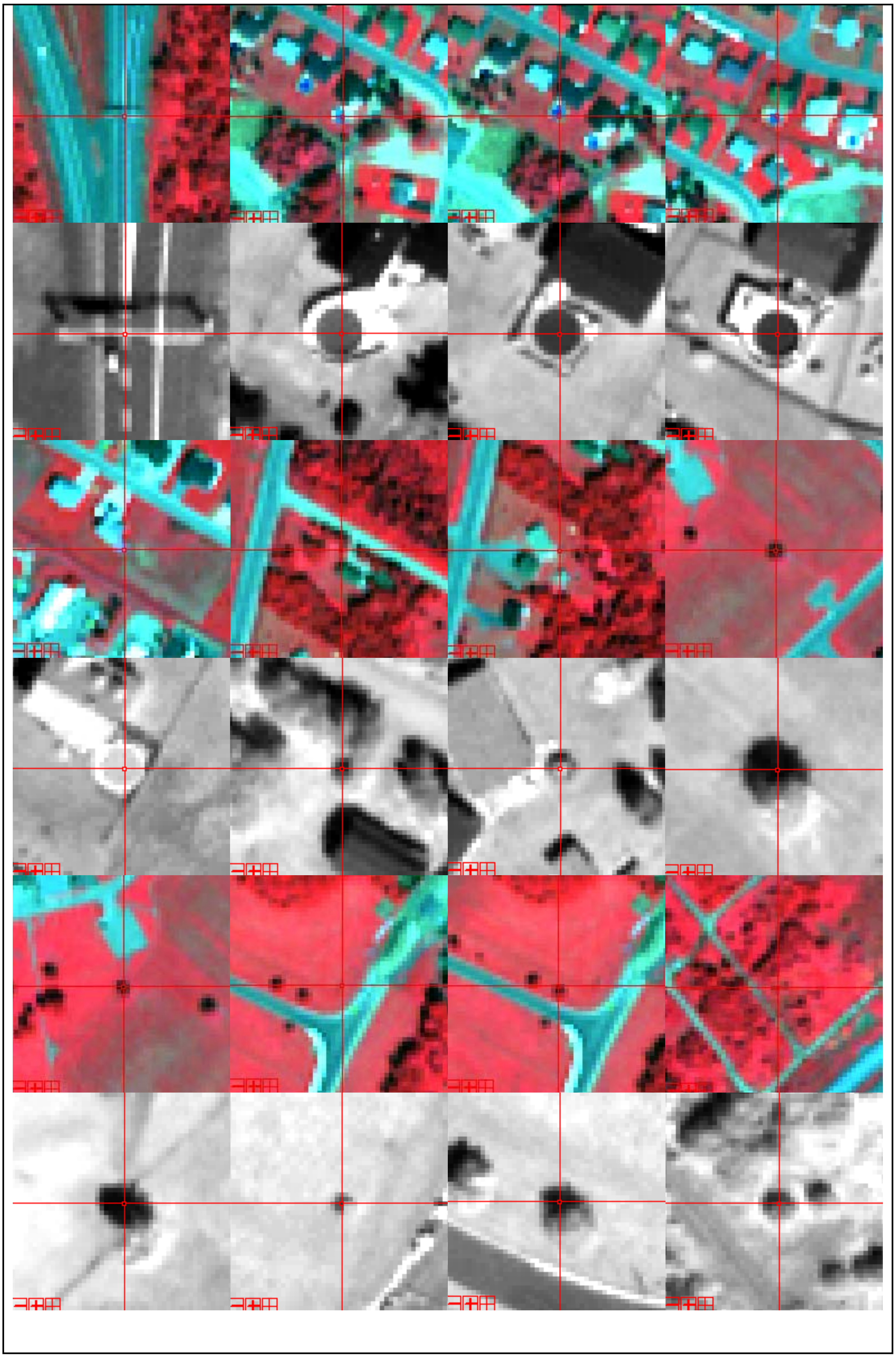

**Figure 2.12 Part of Centers.**

The residuals of the corner and center points are shown **Figures 2.13, and 2.14** respectively. For corners, the mean absolute residual is 1.83 m in x axis and 2.50 m in y axis. The standard deviation is 2.15 m in x axis and 3.04 m in y axis. The distance error is 3.72 m; For centers, the mean absolute residual is 0.68 m in x axis and 0.78 m in y axis. The standard deviation is 0.82 m in x axis and 0.94 m in y axis. The distance error is 1.25 m.

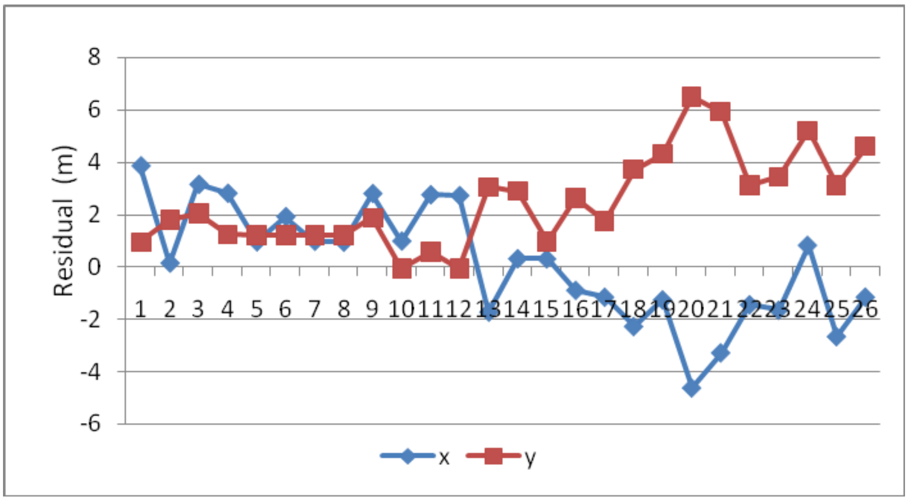


**Figure 2.13 Residuals of Corner Points after Image Registration by Using 26 Corner Points.**

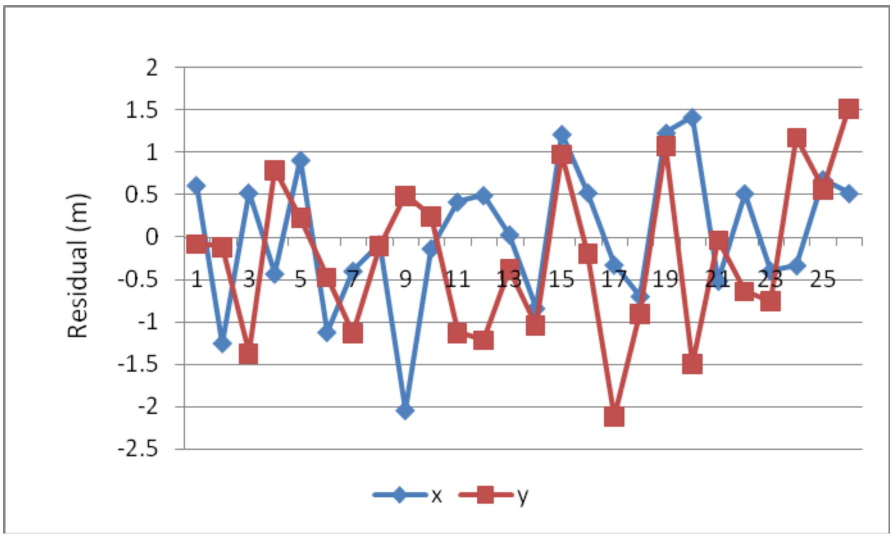


**Figure 2.14 Residuals of Center Points after Image Registration by Using 26 Center Points.**

**Experiment 2**

A stereo pair of IKONOS images, acquired in February of 2003 in Hobart, Tasmania, Australia was used for this experiment (**Figure 2.15**) (for detail please see **Appendix IV**). The incidence angles are forward 75° and backward 69° respectively [Fraser and Hanley, 2005]. **Table 2.5** lists the main characteristics of images in Hobart test field.

**Figure 2.15 Stereo pair of IKONOS images in Hobart (From the University of Melbourne)**

**Table 2.5 Characteristics of the IKONOS Imagery in Hobart Test Field (Fraser and Hanley, 2005)**

| | IKONOS, Hobart |
|---|---|
| Area | 120 km2 (11×11 km) |
| Elevation Range | Sea level to 1280 m |
| Image Coverage (elevation angles) | Stereo triplet (69˚, 75˚, 69˚) |
| Number of GCPs | 113 |
| Notable Features | Full scene; mountainous terrain |
| Base-to-height ratio | 0.8 |
| Date of acquirement | February, 2003 |
| GCP measurement on image | Sub-pixel accuracy for roundabout features; pixel accuracy for other features. |
| Scan model | Reverse model for 69˚ images; Forward model for 75˚ image |

Thirty corners and 30 gravity centers were selected as tie points (**Appendix V, VI**). In order to achieve sub-pixel accuracy, each corner was determined by linear intersection and each line was fitted to three or more edge points (**Figure 2.16 (a)**). Each center of the highway roundabouts was determined by a best-fitting ellipse to six or more edge points around the circumference of the feature, in both object and image space [Fraser and Hanley, 2005] (**Figure 2.16 (b)**).

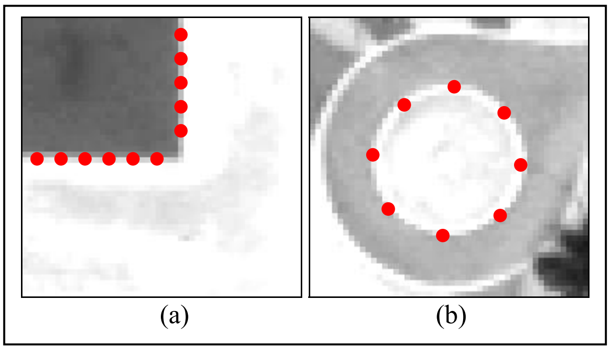


**Figure 2.16 Corner is determined by linear intersection (a) and Centre is determined by ellipse fitting (b)**

In the Hobart test field, "in order to insure high-accuracy GCPs and image coordinate data, multiple GPS and image measurements were made for each GCP with the centroids of roundabouts being determined by a best-fitting ellipse to six or more edge points around the circumference of the feature, in both object and image space. The estimated accuracy of this procedure is 0.2 pixels (Fraser and Hanley, 2005)." Corners on image were determined by linear fitting to three or more edge points and linear intersection. The coordinates of corners were measured by using GPS.

The image coordinates of corner and center points are listed in **Table 2.6**. The corners and centers were used to register the images independently. All these corners and centers are also ground control points (GCPs), so these GCPs were used to refine the sensor models. After the refinement of the sensor models, the refined sensor models and the image positions of the tie points were used to calculate tie points' ground coordinates by space intersection. The deviation between the ground coordinates calculated by space intersection and the ground coordinates obtained by GPS survey were used to evaluate the accuracy of image registration. The residuals of corners and centers are shown in **Figure 2.17, 2.18** respectively. The standard deviation of corners is 1.48 m. The standard deviation of centers is 0.55 m.

**Table 2.6 Image Coordinates of 30 Gravity Centers and 30 Corners**

| No | Gravity Center | | | | Corner | | | |
|---|---|---|---|---|---|---|---|---|
| | Column | Row | Column | Row | Column | Row | Column | Row |
| 1 | 3205.466 | 943.8452 | 3197.449 | 979.1123 | 131.1875 | 3881.802 | 136.8521 | 3855.142 |
| 2 | 2502.918 | 1117.83 | 2496.794 | 1144.931 | 3641.771 | 3262.286 | 3635.192 | 3288.175 |
| 3 | 5584.96 | 3845.874 | 5573.826 | 3891.996 | 917.6471 | 2384 | 923.7692 | 2354 |
| 4 | 5364.74 | 3333.832 | 5353.107 | 3382.78 | 8917.969 | 4086.271 | 8906.66 | 4131.909 |
| 5 | 4739.003 | 494.9105 | 4725.09 | 553.1594 | 11719.09 | 3545.31 | 11706.81 | 3600.65 |
| 6 | 7204.019 | 2524.417 | 7191.331 | 2579.148 | 12078.96 | 3582.764 | 12067.18 | 3636.468 |
| 7 | 6165.197 | 3297.199 | 6153.118 | 3349.02 | 12099.97 | 3579.298 | 12088.27 | 3632.32 |
| 8 | 7610.432 | 2576.011 | 7597.346 | 2632.208 | 5702.124 | 5044.487 | 5693.726 | 5076.962 |
| 9 | 10978.97 | 662.6056 | 10966.09 | 718.6864 | 9305.566 | 5373.866 | 9292.694 | 5426.79 |
| 10 | 8468.87 | 2927.04 | 8456.052 | 2981.898 | 9358.286 | 5381.928 | 9345.25 | 5435.037 |
| 11 | 9824.563 | 3245.225 | 9812.341 | 3297.39 | 9364.627 | 5338.448 | 9352.758 | 5391.224 |
| 12 | 11862.83 | 1466.89 | 11855.89 | 1499.25 | 9373.231 | 5294.246 | 9360.765 | 5347.106 |
| 13 | 3980.57 | 5177.107 | 3973.27 | 5205.688 | 9319.986 | 5285.286 | 9308.06 | 5338.904 |
| 14 | 7972.115 | 4341.714 | 7961.058 | 4392.152 | 9312.84 | 5329.762 | 9301.186 | 5382.867 |
| 15 | 7541.144 | 6338.449 | 7532.149 | 6378.38 | 9258.985 | 5292.607 | 9247.493 | 5346.666 |
| 16 | 7481.07 | 4529.91 | 7470.039 | 4579.2 | 9268.51 | 5239.991 | 9256.383 | 5293.991 |
| 17 | 7950.089 | 7562.403 | 7947.32 | 7574.377 | 9223.371 | 5233.149 | 9211.716 | 5286.729 |
| 18 | 6311.047 | 6208.249 | 6305.646 | 6230.287 | 9180.008 | 5226.156 | 9167.326 | 5279.719 |
| 19 | 6802.807 | 5269.853 | 6798.322 | 5288.811 | 9170.458 | 5278.377 | 9159.319 | 5331.765 |
| 20 | 8115.413 | 5815.098 | 8104.034 | 5861.54 | 9214.97 | 5285.509 | 9203.091 | 5339.332 |
| 21 | 8847.632 | 5952.455 | 8837.676 | 5993.797 | 10153.44 | 6912.51 | 10145.12 | 6946.547 |
| 22 | 8498.563 | 7248.658 | 8492.345 | 7273.738 | 3968.108 | 12343.59 | 3987.47 | 12253.39 |
| 23 | 9657.294 | 7010.835 | 9646.662 | 7056.817 | 3080.614 | 10428.1 | 3126.509 | 10217.84 |
| 24 | 11992.17 | 4870.161 | 11979.96 | 4924.785 | 3093.875 | 10257.56 | 3140.22 | 10046.99 |
| 25 | 9292.591 | 7713.623 | 9283.154 | 7753.984 | 3174 | 10338.71 | 3221.635 | 10127.37 |
| 26 | 11020.64 | 7979.273 | 11009.61 | 8027.79 | 3091.429 | 10415.93 | 3138.587 | 10205.41 |
| 27 | 7409.837 | 11754.13 | 7409.996 | 11751.96 | 4850.947 | 13054.84 | 4859.053 | 13017.82 |
| 28 | 7500.968 | 12224.78 | 7502.635 | 12215.12 | 11983.3 | 12369 | 11977.39 | 12398 |
| 29 | 10153.35 | 10314.73 | 10142.87 | 10360.56 | 10764.35 | 9832.306 | 10753.19 | 9882.394 |
| 30 | 9443.028 | 10288.03 | 9433.505 | 10326.64 | 9184.28 | 11867.95 | 9184.727 | 11864.96 |

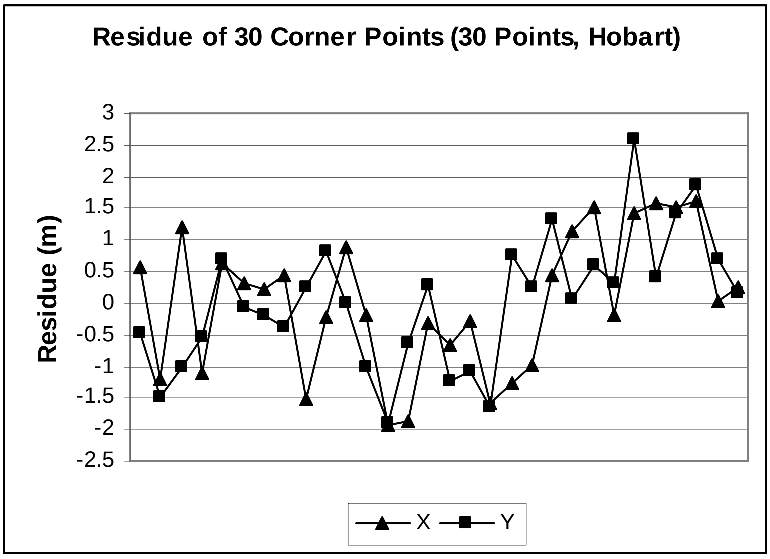


**Figure 2.17 Residuals of Corner Points after Image Registration by Using 30 Corner Points.**

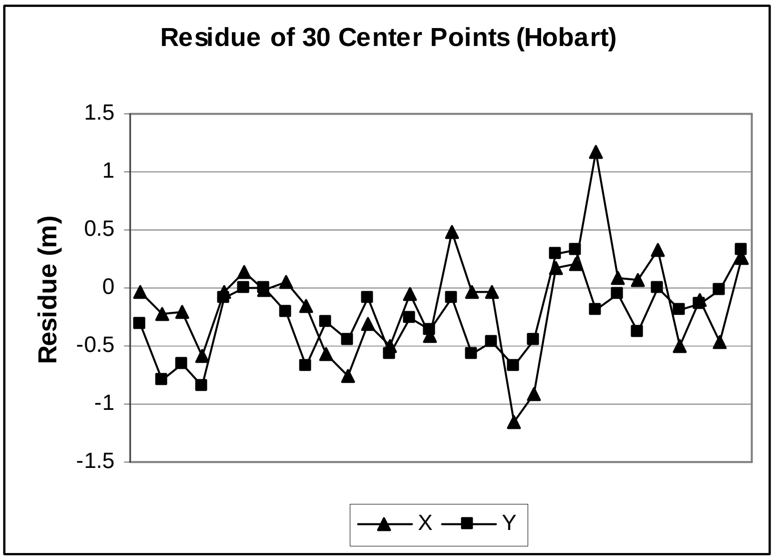


**Figure 2.18 Residuals of Center Points after Image Registration by Using 30 Center Points.**

### Experiment 3

In this experiment, the 30 center points and 30 corner points from the Hobart imagery were used together for image registration. The accuracies of center points and corner points respectively were then checked. The residuals of the corner points are shown in **Figure 2.19** and the residuals of center points are shown in **Figure**

**2.20**. The standard deviation of center points is 0.64 m and the standard deviation of corner points is 1.51 m.

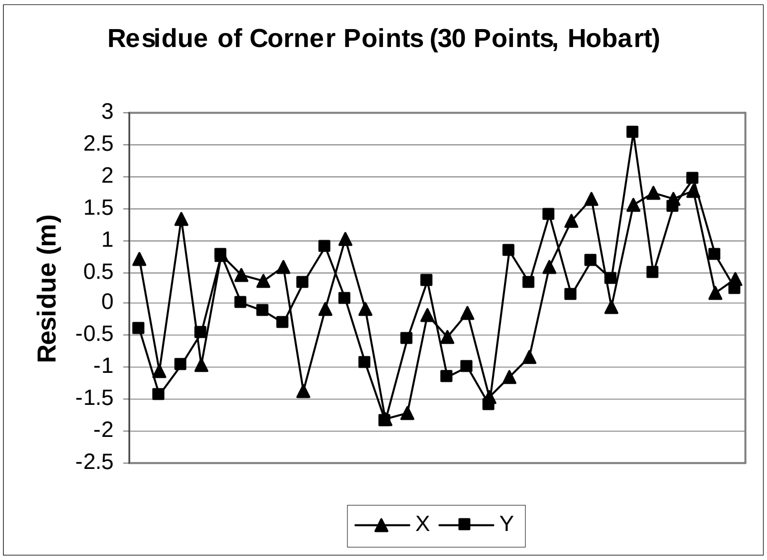


**Figure 2.19 Residuals of Corner Points after Image Registration by Using 30 Corner Points and 30 Center Points.**

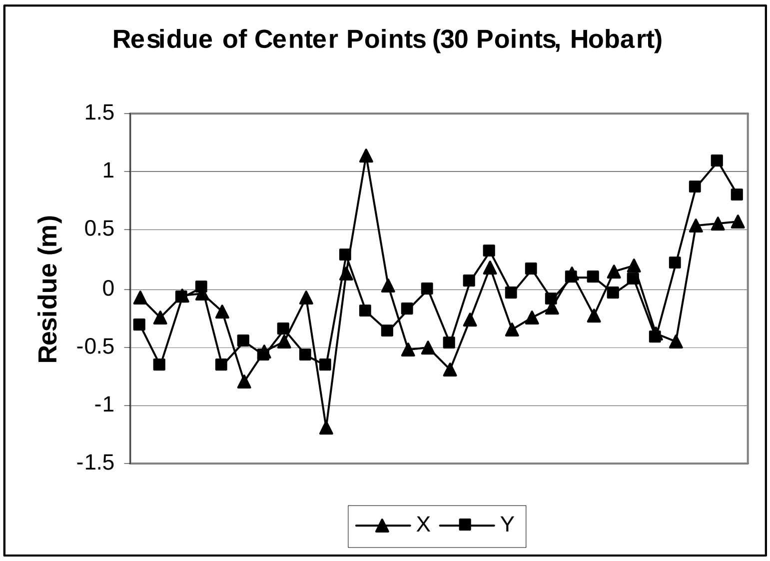


**Figure 2.20 Residuals of Center Points after Image Registration by Using 30 Corner Points and 30 Center Points.**

**Summary of Experiments**

In summary, the above experiments have tested the performance of corners and centers in three cases. The standard deviations resulting from the above three experiments are listed in **Table 2.7** and summarized in **Figure 2.21**. Obviously, the standard deviation of the centers is much smaller than that of the corners. For the registration images of different resolutions, the standard deviation of centers is only 33.6% of the deviation of corners. For registration of images having the same resolution, the standard deviation of centers is about 40% of that of the corners.

**Table 2.7 Average Distance Error of Centers and Corners.**

| | Different Resolution | Same Resolution | |
|---|---|---|---|
| | Experiment 1 | Experiment 2 | Experiment 3 |
| Corner Error (m) | 3.72 | 1.48 | 1.51 |
| Center Error (m) | 1.25 | 0.55 | 0.64 |
| Center Error / Corner Error | 33.6% | 37.2% | 42.4% |

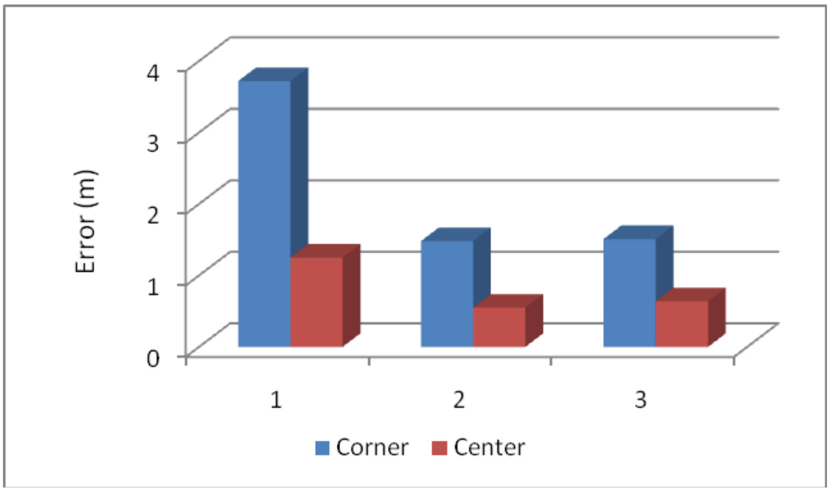


**Figure 2.21 Standard Deviation of Corners and Centers in 3 Cases. The SD of centers is much smaller than that of corners in all 3 cases.**

By comparing **Tables 2.3** and **2.7**, and **Figures 2.7** and **2.21**, it can be seen that for the registration of images having different resolutions, use of center points can improve registration accuracy by at least 60%. For registration of images having the same resolution, quantitative analysis shows that the center points can improve accuracy by at most 40% (**Table 2.3**). This is contrary to the results of our experiments which show that center points can improve accuracy by about 60% (**Table 2.7**). The reasons for the discrepancy may be:

1) Many corner features in the experiments are blurred (**Figure 2.22**, No. 1 Corner) and small (**Figure 2.22**, No. 3 Corner). Sometimes only three edge points could be selected for edge fitting, thus the accuracy of linear intersection for locating corners was not satisfactory. In contrast to this, most of the round-about features in the experiments were very regular and clear (**Figure 2.22**, No. 1, No. 3 Center), and six or more points could be used to fit the ellipse. The center features therefore had a much higher geometric accuracy than the corner features.

2) Most of the center points are roundabout on the ground, while many corners are on the building roof (**Figure 2.22**, No. 1, No. 3 Corner). The author does not exactly know whether the field surveyor measured the roof corner or the ground corner. On the image, the author always recognized that the roof corner position was the feature position. So the corner position on the image was determined by the intersection of two edges on the roof, although sometimes there wasn't definite intersection. Therefore, in these experiments, the centers may have higher accuracy than corners.

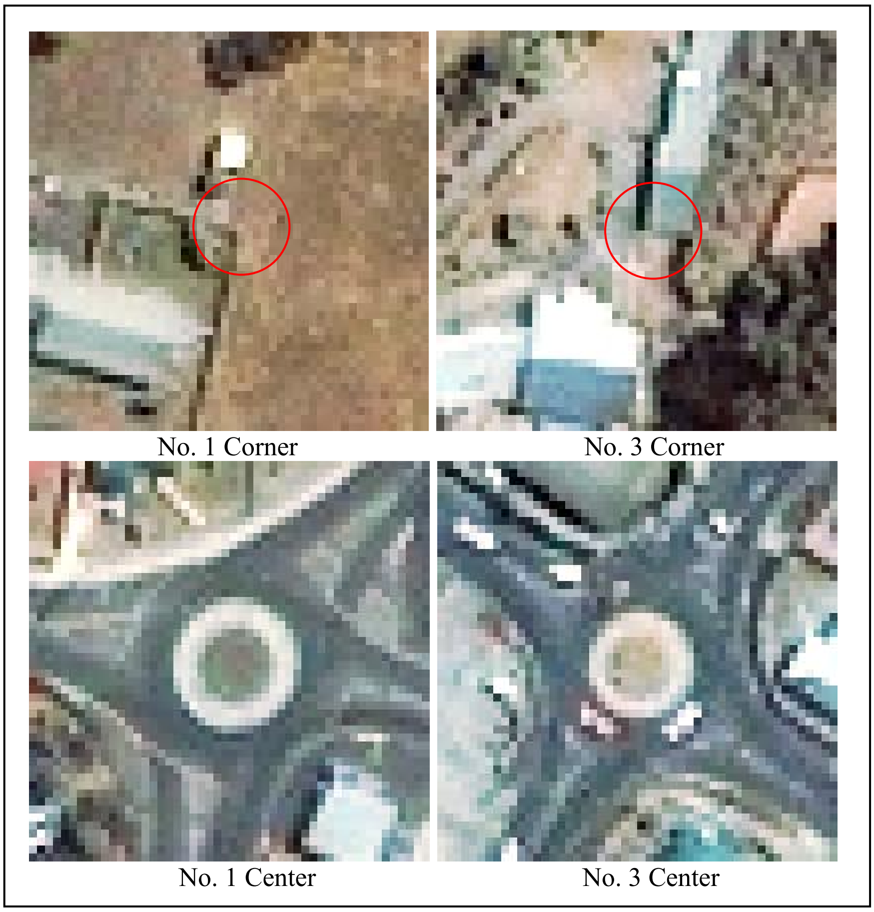


**Figure 2.22 Samples of Corners and Centers. The corner is very blurry, while the center is clear.**

## 2.4. Analysis and Conclusions

The experiments and quantitative error analysis support the same conclusion; i.e. that centers are superior to corners for image registration. Center points can improve the accuracy of image registration by at least 40%. For registration of images having different resolutions, the center points can improve accuracy much more that 40%. The problem is that most of the automatic interest point extraction algorithms can extract corners but not centers and the gravity center sometimes is difficult to find in some places. Our future work will therefore focus on how to extract gravity center points from images of different resolutions or from different modal images.

## ACKNOWLEDGMENTS

This research is sponsored by the Natural Sciences and Engineering Research Council of Canada through the Discovery Grant (NSERC Discovery Grant) awarded to Dr. Yun Zhang, the second author of the paper. We would like to acknowledge that Professor Clive Fraser, Department of Geomatics Engineering, University of Melbourne, Australia, provided us with satellite images for the tests. Thanks also go to Mr. David C. Whyte, Department of Environment, NB, Canada, who reviewed the manuscript of this paper. We appreciated the reviewer's comments and suggestions.

## REFERENCES

Auer, Matin, Peter Regitnig, and Gerhard A. Holzapfel. (2005). "An Automatic Nonrigid Registration for Stained Histological Sections." *IEEE Transactions on Image Processing*, Vol. 14( 4): 475-486.

Belongie, Serge, Jitendra Malik, and Jan Puzicha. (2002). "Shape matching and object recognition using shape contexts." *IEEE transactions on pattern analysis and machine intelligence*, Vol. 24(24) 509-522.

Besl, Paul J., and Neil D. McKay. (1992). "A Method for Registration of 3-D Shapes." *IEEE Transactions on Pattern Analysis and Machine Intelligence*, Vol. (14)2: 239-256.

Beus H.L. and Tiu S.S.H. (1987). "An improved corner detection algorithm based on chain-coded plane curves." *Pattern Recognition*, 20(3):291-296.

Boffy, Aurelien, Yanghai Tsin, and Yakup Genc. (2008). "Real-Time Feature Matching Using Adaptive and Spatially Distributed Classification Trees." http://www.macs.hw.ac.uk/bmvc2006/papers/397.pdf. Accessed: August, 14, 2008.

Chui, Haili and Anand Rangarajan. (2003). "A New Point Matching Algorithm for Non-Rigid Registration." *Computer Vision and Image Understanding*, 89 (2) 114-141.

Dmitry Chetverikov and Zsolt Szabó. (1999). "Detection of High Curvature Points in Planar Curves." http://visual.ipan.sztaki.hu/corner/. Accessed: August, 14, 2008.

Förstner, W. (1994). “A framework for low level feature extraction.” *Proceedings of the 3rd European Conference on Computer Vision*, Stockholm, Sweden, pp. 383–394.

Förstner, W. and Gülch, E. (1987). “A fast operator for detection and precise location of distinct points, corners and centres of circular features.” *Intercommission Conference on Fast Processing of Photogrammetric Data*, Interlaken, Switzerland, pp. 281–305.

Fraser Clive S. and Harry B. Hanley. (2005). “Bias-compensated RPCs for Sensor Orientation of High-resolution Satellite Imagery.” *Photogrammetric Engineering & Remote Sensing,* Vol. 71, No. 8, pp. 909–915.

Freeman H. and Davis L.S. (1977). “A corner finding algorithm for chain-coded curves.” *IEEE Trans. Computers*, 26:297-303.

Gold, Steven, Anand Rangarajan, Chien-Ping Lu, Suguna Pappu, and Eric Mjolsness. (1997). “New Algorithms for 2D and 3D Point Matching: Pose Estimation and Correspondence.” URL: http://citeseerx.ist.psu.edu/legacymapper?did=88372, Accessed: August, 14, 2008.

Harris C. and Stephens M. (1988). “A combined corner and edge detector.” *Alvey Vision Conference*, pages 147-151.

Kaplan, Alexander, Ehud Rivlin, and Ilan Shimshoni. (2004). “Robust Feature Matching Across Widely Separated Color Images.” *Proceedings of the 17th International Conference on Pattern Recognition* (ICPR’04), pp. 136-139.

Lepetit, Vincent, Julien Pilet, and Pascal Fua. (2004). “Point Matching as a Classification Problem for Fast and Robust Object Pose Estimation.” http://cvlab.epfl.ch/~vlepetit/papers/lepetit_cvpr04.pdf. Accessed: August 14, 2008.

Lepetit, Vincent, Pascal Lagger, and Pascal Fua. (2005). “Randomized Trees for Real-Time Keypoint Recognition.” *Computer Vision and Pattern Recognition*, Volume: 2, 775- 781.

Lowe, David G. (2004). “Distinctive Image Features from Scale-Invariant Keypoints.” *International Journal of Computer Vision* 60(2), 91–110.

Moravec, H.P. (1977). “Towards automatic visual obstacle avoidance.” *Proceedings of the 5th International Joint Conference on Artificial Intelligence*, Cambridge, Massachusetts, USA, p. 584.

Rosenfeld and E. Johnston. (1973). “Angle detection on digital curves.” *IEEE Trans. Computers*, 22:875-878.

Rosenfeld and J.S. Weszka. (1975). “An improved method of angle detection on digital curves.” *IEEE Trans. Computers*, 24:940-941.

Terasawa, Kengo, Takeshi Nagasaki, and Toshio Kawashima. (2005). "Robust Matching Method for Scale and Rotation Invariant Local Descriptors and Its Application to Image Indexing." *G.G. Lee et al. (Eds.): AIRS 2005*, LNCS 3689, pp. 601-615.

Xiong, Z., Y. Zhang. (2009). "A Generic Method for RPC Refinement Using Ground Control Information." *Journal of Photogrammetric Engineering & Remote Sensing,* Nov, 2008 (In press).

Zhao, Wanlei, Yugang Jiang, and Chong-Wah Ngo. (2006). "Keyframe Retrieval by Keypoints: Can Point-to-Point Matching Help?" H. Sundaram et al. (Eds.): CIVR 2006, LNCS 4071, pp. 72-81.

# Chapter 3 A NOVEL INTEREST POINT MATCHING ALGORITHM FOR HIGH RESOLUTION SATELLITE IMAGES[3]


## ABSTRACT

Interest point matching is a key technique for image registration. It is widely used for 3D shape reconstruction, change detection, medical image processing, computerized visioning systems and pattern recognition. Although numerous algorithms have been developed for different applications, processing local distortion inherent in images that are captured from different viewpoints remains problematic. High resolution satellite images are normally acquired at widely spaced intervals and typically contain local distortion due to ground relief variation. Interest point matching algorithms can be grouped into two broad categories: area-based and feature based. Although each type has its own particular advantages in specific applications, they all face the common problem of dealing with ambiguity in smooth (low texture) areas, such as grass, water, highway surfaces, building roofs, etc. In this paper, a new algorithm for interest point matching of high resolution satellite images is proposed. The conceptual basis of this algorithm is the detection of "super points"; those points which have the greatest interest strength (i.e. which represent the most prominent features) and the subsequent construction of a control network. Sufficient spatial information is then available to reduce the ambiguity and avoid false matches. We commence our paper with a brief review of current research on interest point


[3] The original paper of this chapter has been accepted by the *IEEE Transaction on Remote Sensing and Geosciences* for publication. To demonstrate the robustness of the research outcome, additional testing results (i.e. results of Test Data 4) are added into the experiment of this chapter.
Xiong Z. and Y. Zhang, "A Novel Interest Point Matching Algorithm for High Resolution Satellite Images", *IEEE Transaction on Remote Sensing and Geosciences*, 2009.

matching. We then introduce the proposed algorithm in detail and describe experiments with three sets of high resolution satellite images. The experiment results show that the proposed algorithm can successfully process local distortion in high resolution satellite images and can avoid ambiguity in matching the smooth areas.

## 3.1 Introduction

Interest point matching refers to the process of matching two sets of features and finding correspondences between them. Matching interest points (sometimes called feature points or key points) is a key requirement for image registration. Image registration is widely used in photogrammetry, remote sensing, computer vision, pattern recognition and medical image processing [Brown, 1992; Zitova and Flusser, 2003]. Unfortunately, there are still many challenges with interest point matching. The main interest point matching algorithms currently in use are area-based or feature-based. Neither type of algorithm, can avoid the problem of dealing with ambiguity in smooth (low texture) areas. Feature-based algorithms face the additional problem of the effect of outliers (points with no correspondences) on the results [Zitova and Flusser, 2003].

In this paper, we propose a novel interest point matching algorithm, in which “super points”; those points which have the greatest interest strength (i.e. which represent the most prominent features) are extracted first. A control network is then constructed using these super points. Next, each remaining interest point is assigned a unique position with regard to the closest control network point. Finally an iterative “closest point” algorithm is applied to search for correspondences (conjugate point) based on the position that has been assigned to each interest point. After each iteration, the new correspondences are added to the control network as new leaves. The control network therefore gradually becomes larger and denser. The iterations continue until no more correspondences are found. Because every point is located in a unique position relative to the control network, this method avoids the problem of how to deal with local minimums.

The first section of the paper contains a brief review of previous relevant work by others. In the second section the new algorithm is introduced in detail. Next, we present some experiments using high resolution satellite images. Finally some concluding remarks are provided.

## 3.2 Literature Review

Interest point matching is problematic and remains the subject of much research within the communities of photogrammetry, remote sensing, computer vision systems, pattern recognition, and medical image processing. Interest point matching algorithms can be grouped into two main categories: area-based algorithms and feature based algorithms. In remote sensing, area-based algorithms are normally suitable for open terrain areas but the feature-based approaches can provide more accurate results in urban areas. No single technique performs well in both circumstances [Hsieh, etc., 1992]. Both algorithms have their own unique strengths and weaknesses.

Our review of previous research in interest point matching revealed that about 90% of the papers are from the fields of computer vision, pattern recognition and medical image processing. Such applications have a number of common characteristics: a) the images they deal with have no baseline or a short baseline; b) the images are normally processed in a short time and; c) feature-based algorithms are widely used.

Because of the large number of feature based algorithms used in interest point matching, there are many classification methods for describing these algorithms. Normally feature-based algorithms can be categorized into rigid and non-rigid (according to the transformation between images), and global and local (according to the image distortions), or corrected and uncorrected (according to the image variations). In addition, most of the feature-based algorithms search for correspondences and also address the refinement of a transformation function. Therefore, feature-based algorithms can also be grouped into three additional categories [Chui and Rangarajan, 2003]. They either: solve the correspondence only, solve the transformation only, or solve both the correspondence and the transformation.

Although numerous feature based algorithms have been developed, there is no general algorithm which is suitable for a variety of different applications. Every method must take into account the specific geometric image deformation [Zitova and Flusser, 2003]. The first category of algorithms processes the global distortions. The ICP (Iterative Closest Point) algorithm is a classical global algorithm [Besl and McKay, 1992; Yang, etc., 2007]. Because this algorithm requires the assumption that one surface is a subset of the other, it is only suitable for global distortion image registration [Williams and Bennamoun, 2001]. For medical image registration and pattern recognition, many rigid global transformations are used [Besl and McKay, 1992; Mount, etc., 1997; Tu, etc., 2008]. The B-Spline and TPS (Thin Plate Spline) deformation model is a common model for global distortion in medical image registration [Booksten, 1989, Kybic and Unser, 2003].

The second category of algorithms deals with the local distortions. For non-rigid local distortions, more complicated transformations are developed. TPS was proposed initially for global transformations, but it was improved for smooth local distortions for medical image registration [Gold, etc., 1997; Chui and Rangarajan, 2003; Auer, etc., 2005]. Another common local distortion model is the elastic deformation model [Auer, etc., 2005; Rexilius, etc., 2001].

Some algorithms do not need a transformation function. In computer vision systems and pattern recognition, feature descriptors extracted from an image's gray values are usually used [Belongie, etc., 2002; Kaplan, etc., 2004; Terasawa, etc., 2005; Lepetit, etc., 2005; Zhao, etc., 2006]. SIFT (Scale Invariant Feature Transform) is one of the best descriptors for interest point matching [Lowe, 2004]. In graph matching algorithms, the topological relationship is the key feature and is widely used in pattern recognition [Gold and Rangarajan, 1996; Cross and Hancock, 1998; Demirci, etc., 2004; Caetano, etc., 2004; Shokoufandeh, etc., 2006]. Another idea is to consider interest point matching as a classification problem. The features from the reference image are used to train the classifier [Lepetit, etc., 2008; Boffy, etc., 2008].

Although many of the feature based algorithms described above are useful in solving problems for specific applications, they have four common drawbacks: 1) The features cannot be exactly matched, because of the variations of features between different images; 2) Outliers are difficult to reject [Chui and Rangarajan, 2003]; 3) For local image distortion, high dimensional non-rigid transformations are required, and a large number of correspondences are needed for the refinement of mapping functions [Brown, 1992], but too many features will make the feature matching more difficult; and 4) The feature description should fulfill several conditions, the most important ones being invariance (the descriptions of the corresponding features from the reference and sensed image have to be the same), uniqueness (two different features should have different descriptions), stability (the description of a feature which is slightly deformed in an unknown manner should be close to the description of the original feature), and independence (if the feature description is a vector, its elements should be functionally independent). Usually these conditions cannot be satisfied simultaneously and it is necessary to find an appropriate trade-off [Zitova and Flusser, 2003].

Images in photogrammetry and remote sensing contain local distortions caused by ground relief variations and differing imaging viewpoints. Because of their stability and reliability, area-based methods are usually used in remote sensing for interest point matching. Photogrammetric scientists are always attempting to improve the stability and reliability of interest point matching techniques. Hierarchical matching and relaxation algorithms are typical examples of such attempts. At the same time, great efforts are also being made to reduce the search area and increase the matching speed. The use of epipolar geometry is one of the most important achievements of such work [Masry, 1972; Helava, et al., 1973; Dowman, 1977; Gupta, 1997; Kim, 2000]. Despite the progress that has been made, area-based methods still have many drawbacks. The main limitations can be summarized as follows: 1) The rectangular image window is only suitable for image distortion caused by translation (in theory); 2) These methods cannot process smooth areas (areas without prominent texture); and 3) The methods are sensitive to image intensity changes which are caused by noise, varying illumination and the use of different sensors [Zitova and Flusser, 2003].

In summary, **Table 3.1** shows the characteristics and limitations of area-based algorithms and feature-based algorithms.

**Table 3.1 Limitations of Area-Based Algorithms and Feature-Based Algorithms**

| | Area-Based | Feature-Based |
|---|---|---|
| Typical Algorithms | ▪ Correlation-like<br>▪ Sum of squared differences<br>▪ Hierarchical<br>▪ Relaxation | ▪ ICP<br>▪ SIFT<br>▪ Rigid<br>▪ Non-rigid<br>▪ TPS<br>▪ B-spline<br>▪ Classification<br>▪ Segmentation |
| Applications | ▪ Remote sensing<br>▪ Photogrammetry | ▪ Computer vision<br>▪ Pattern recognition<br>▪ Medical image registration |
| Limitations | ▪ Slow<br>▪ Suitable only for images with little distortion<br>▪ Cannot deal with smooth areas<br>▪ High computational complexity<br>▪ Sensitive to image intensity changes which are caused by noise, varying illumination and different sensors [Zitova and Flusser, 2003]. | ▪ Suits only images with short baselines.<br>▪ The feature description must fulfill several conditions involving invariance, uniqueness, stability, and independence [Zitova and Flusser, 2003].<br>▪ Need high dimensional non-rigid mapping [Chui and Rangarajan, 2003]<br>▪ A large number of correspondences are needed for the refinement of mapping functions.<br>▪ The features cannot be exactly matched because of noise [Chui and Rangarajan, 2003].<br>▪ Affected by the existence of outliers. |

## 3.3 Methodology

The proposed algorithm first detects and extracts super points, which have the greatest interest strength (i.e. those points which represent the most prominent features). A control network can then be constructed based on these super points. This control network, like a sketch, can then control the entire image, and ambiguities in the smooth areas can be avoided. Next, every point in the image is assigned a unique position and angle relative to the closest super point in the control network. Finally, for interest point matching, those points with the smallest position and angle differences are the correspondences. The correspondences are then added to the control network to construct a bigger and stronger control network. The process is continued until no more correspondences are found. The algorithm proposed in this paper includes three parts: 1) super point detection; 2) super point matching; and 3) interest point matching.

### 3.3.1 Super Point Detection

The Harris detector is a well-known interest point detection algorithm and was used in this research to detect and extract the super points and interest points. The Harris algorithm determines whether or not a point is a corner based on the Harris matrix A at the point P(x, y).

$$A = \begin{bmatrix} \langle I_x^2 \rangle & \langle I_x I_y \rangle \\ \langle I_x I_y \rangle & \langle I_y^2 \rangle \end{bmatrix} \tag{3.1}$$

where $I$ is the image function; $I_x$, $I_y$ are the partial derivatives in x and y respectively; the angle brackets denote averaging (summation over the image patch around the point P(x, y)).

The interest strength is determined based on the magnitudes of the eigenvalues ($\lambda_1$ and $\lambda_2$) of $A$. Because the exact computation of the eigenvalues is computationally expensive, the following function $M_c$ was suggested by Harris and Stephens [1988] as the interest strength.

$$M_C = \det(A) - \kappa trace^2(A) \tag{3.2}$$

The value of κ has to be determined empirically, and in the literature values in the range 0.04 - 0.06 have been reported as feasible [Schmid, etc., 2000]. If $M_c > 0$, it is a corner, otherwise, it is not a corner. Obviously, the corner should be the point with the local maximum value of $M_c$. By calculating the interest strength $M_c$ over whole image, an image which shows the interest strength can be obtained (**Figure 3.1**). Two thresholds TA and TB can be set, with TA> TB for the interest point detection and super point detection. The point with an interest strength greater than the threshold TB and also representing the local maximum, can be extracted as an interest point. If the interest strength of such point is greater than the threshold TA and its interest strength is a local maximum, then a super point is detected (**Figure 3.2**). Like most other interest point matching processes, super point matching is an exhaustive search process, so the number of super points should be limited to an acceptable range.

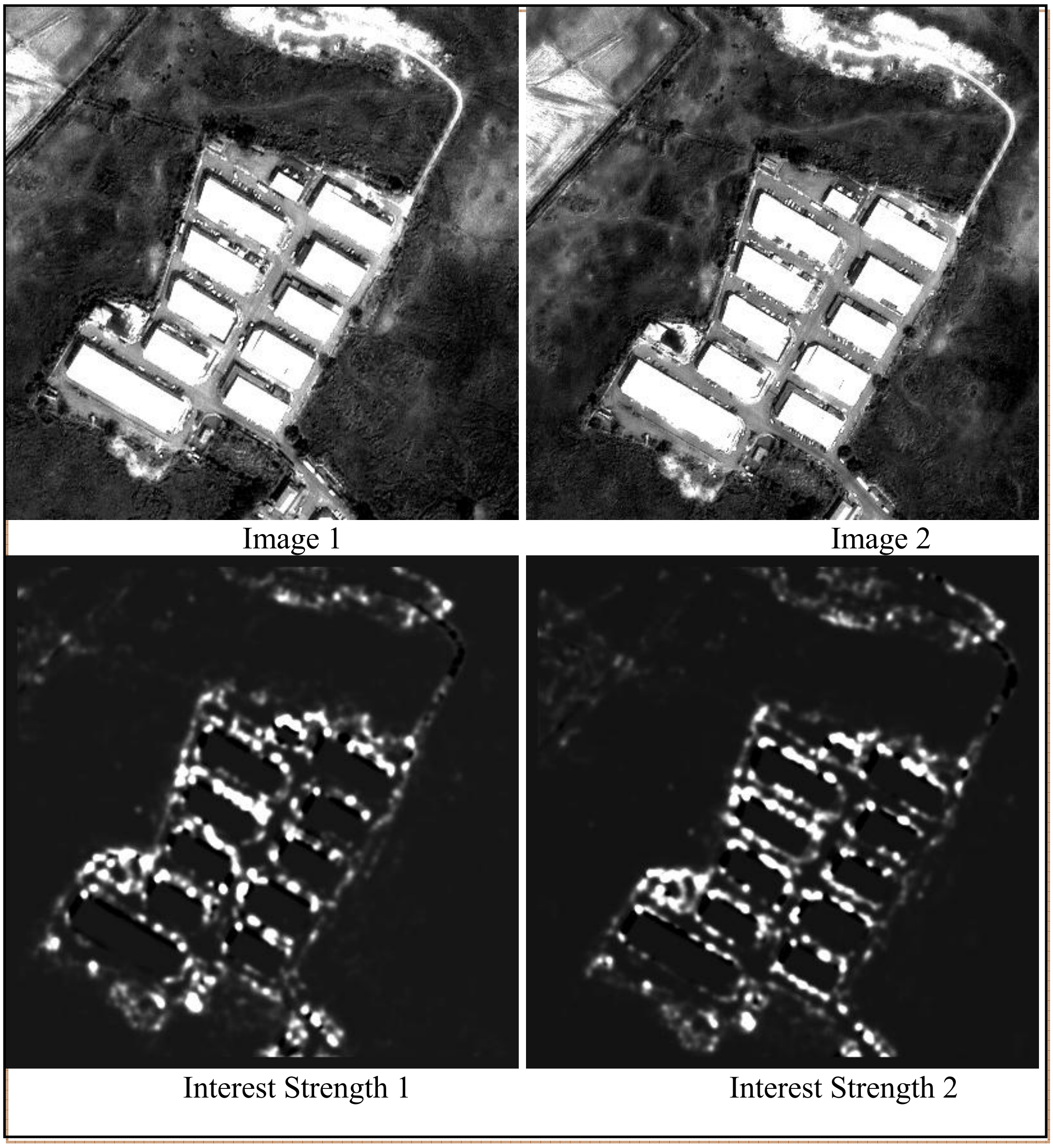


**Figure 3.1 Original image (above) and corresponding interest strength (below). The brightness is directly proportional to the interest strength.**

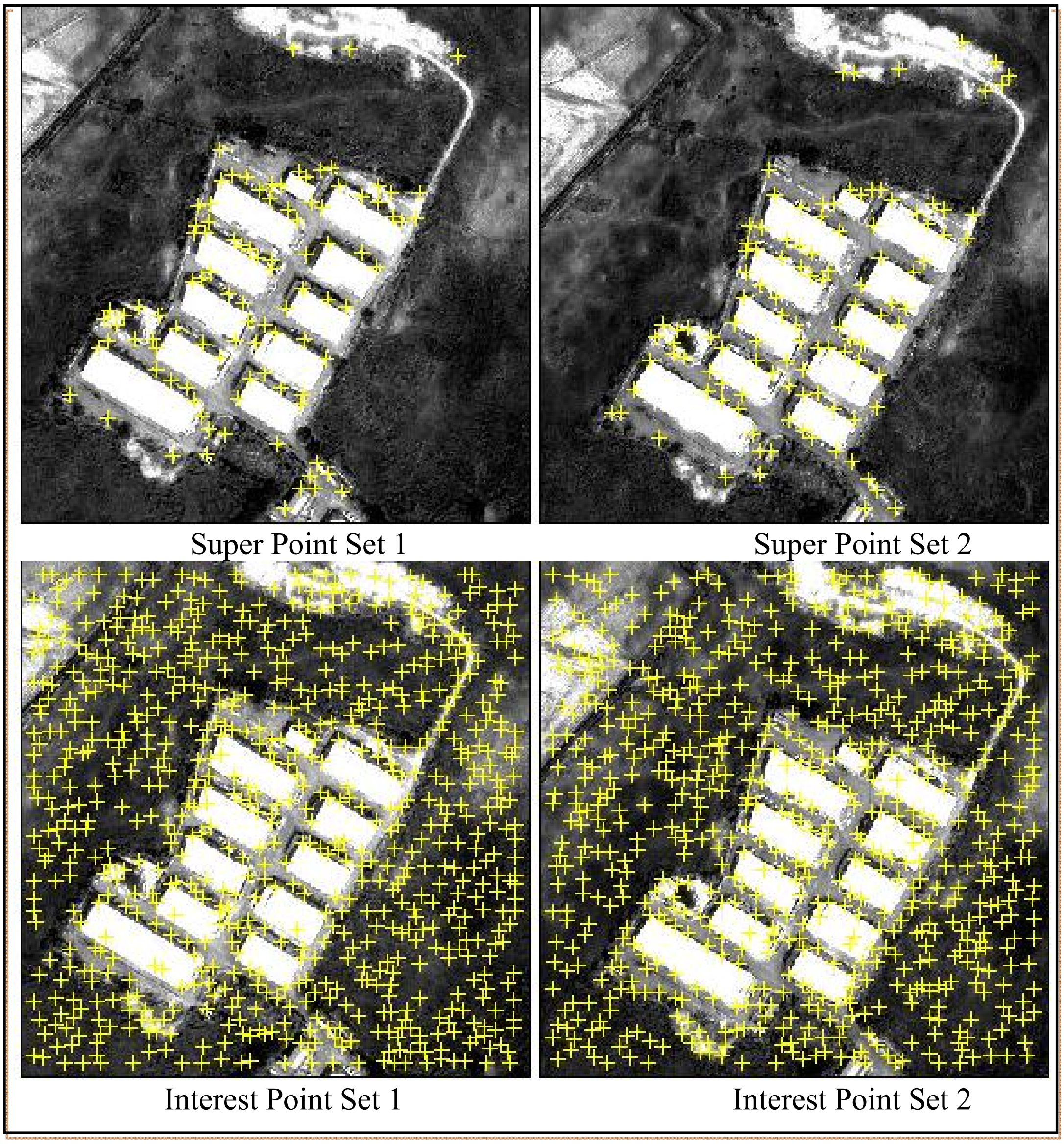


**Figure 3.2 Extracted super points (above: 99 super points in super point set 1, 111 super points in super point set 2) and interest points (below: 737 interest points in set 1, 707 interest points in set 2)**

### 3.3.2 Super Point Matching

The goal of the super point matching is to find a root from each super point set and identify the first group of correspondences (tie points). The super point matching consists of three steps (**Figure 3.3**): 1) Control network construction; 2) Assignment of relative positions and angles; and (3) Correspondence searching. A more detailed description of each step follows.

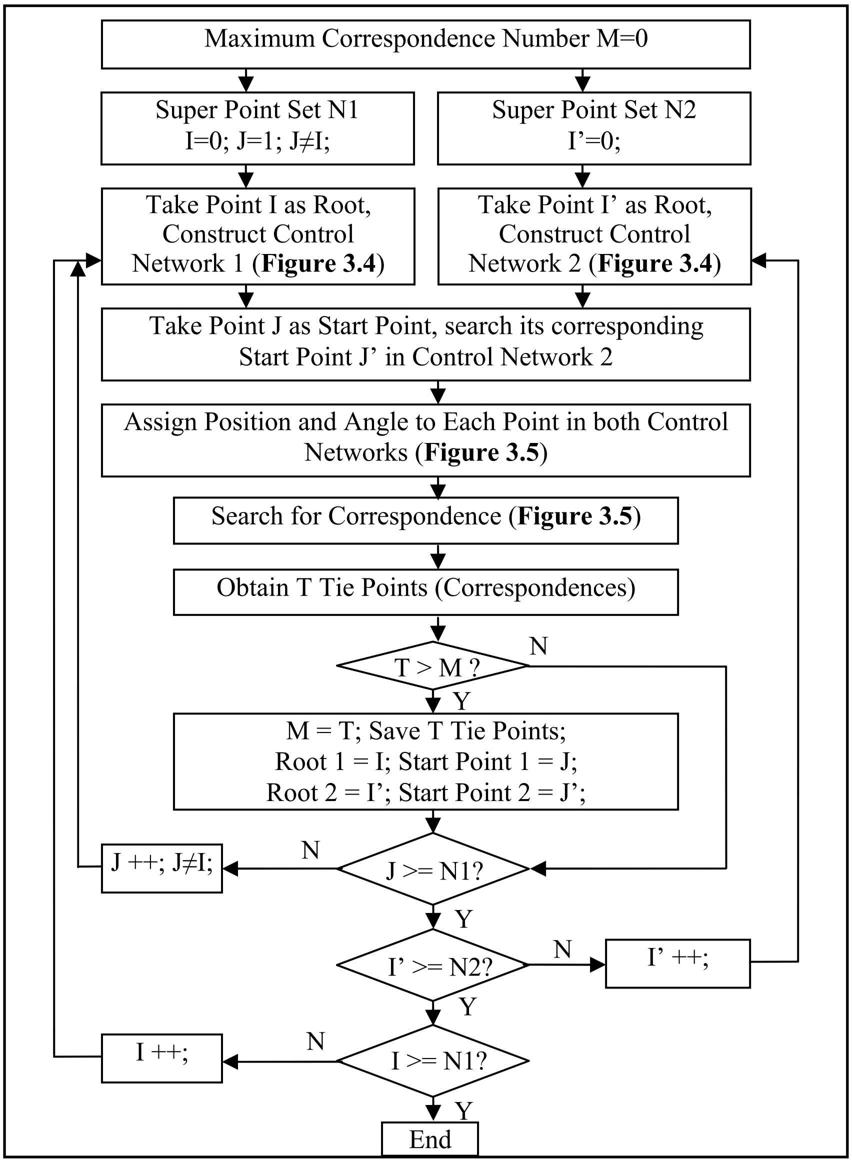


**Figure 3.3 Flow Chart of Super Point Matching Procedure**

In Step 1 a super point from each super point set is selected as a Root, and a control network is constructed. One control network is constructed for each super point set (**Figure 3.4**).

In Step 2 includes three stages:

(1) A leaf from control network 1 is selected randomly as the starting point. The distance between the starting point and the root is denoted as **S**.

(2) The corresponding starting point in control network 2 is determined according to the distance between the root and the leaf. The leaf point of control network 2 with the closest distance to **S** is selected as the corresponding starting point in control network 2.

(3) After the two starting points for both control networks have been determined, the relative positions (distance between root and leaf) and angles (clockwise from the starting point) are assigned to every point in both control networks (**Figure 3.5**).

Correspondence searching commences in Step 3. After each point in both control networks has been assigned a relative distance and angle, a corresponding point in control network 2 may be found for every leaf point in control network 1 according to their positions and angles based on the following function:

$$correspondence = Min(\sum_{i=1}^{m-1}\sum_{j=1}^{n-1} abs(Pi - P'j) Min(\sum_{i=1}^{m-1}\sum_{j=1}^{n-1} abs(\theta_{Pi} - \theta_{P'j})) \quad (3.3)$$

Where, $m$ and $n$ denote the number of leaves in control network 1 and control network 2 respectively; $P_i$ and $P'_j$ are relative distances between root and leaf in the two control networks; and $\theta_{Pi}$ and $\theta_{P'j}$ are relative angles between starting point and leaf in the two control networks.

The closest points with the smallest position differences and smallest angle differences, where both differences are less than their corresponding thresholds, will be selected as tie points (correspondences). Otherwise, if a point does not have a correspondence, it is an outlier (**Figure 3.4**). The outlier will be processed as an interest point in the next iteration.

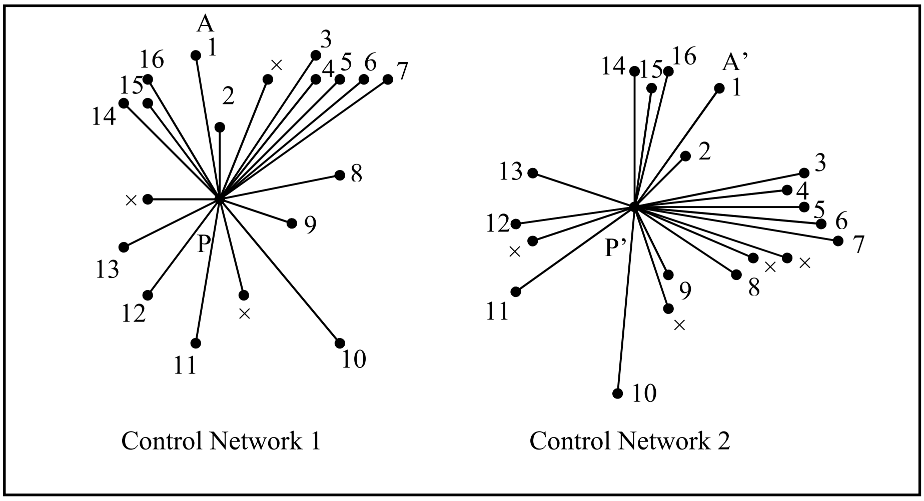


**Figure 3.4 Control Network Constructed with Super Points. P and P' are roots, and the others are leaves. A and A' are start points. Sixteen tie points (correspondences) are obtained after super point matching. "×" denotes an outlier.**

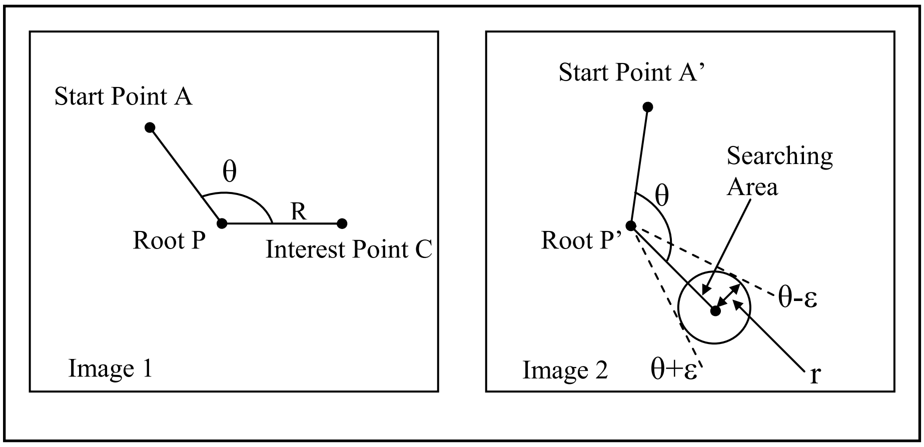


**Figure 3.5 Relative Position and Angle Assignment and Correspondence Search. After the root and start points are determined, every point (e.g. C) can be assigned a relative distance (R) and angle (θ) (Image 1). The closest candidate in the searching area is the correspondence (Image 2).**

Every super point can be either the root or the starting point. After super point matching, a number of correspondences are obtained. When the maximum possible number of correspondences is obtained, the corresponding root and starting points will be the final root and starting points of the super point control network.

Only image translation, image rotation and scale are considered when interest points are matched by determining the root and the starting point. This is acceptable because for high resolution satellite images with narrow fields of view, affine transformations can accurately simulate the geometric distortion between two images [Habib and Ai-Ruzouq, 2005].

The process of super point matching is an iterative and exhaustive search process. Every point can be either a root or a starting point. For example (**Figure 3.4**), there are 20 super points in super point set 1 and 21 super points in super point set 2. Therefore, there are $C_{20}^{1}C_{21}^{1}$ combinations for root selection, $C_{19}^{1}C_{20}^{1}$ combinations for starting point selection, and $C_{18}^{1}C_{19}^{1}$ combinations for the correspondence search. So there will be $C_{20}^{1}C_{21}^{1}C_{19}^{1}C_{20}^{1}C_{18}^{1}C_{19}^{1} = 54583200$ combinations in total. Therefore, in order to avoid combination explosion and reduce the matching time, the number of super points should be limited to an acceptable range.

After super point matching, a control network which consists of all the extracted correspondences is obtained (**Figure 3.6**).

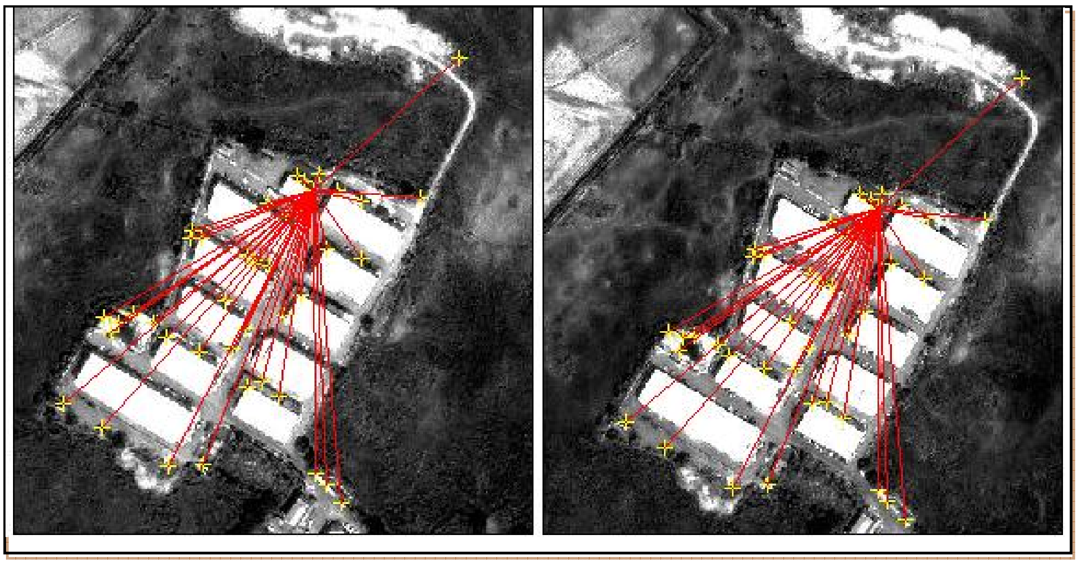

**Figure 3.6 The Result of Super Point Matching – Control Networks (41 correspondences)**

### 3.3.3 Interest Point Matching

After the super point matching, two control networks corresponding to the two interest point sets are obtained (**Figure 3.6**). Under the control of the super point network, interest point matching becomes simple. **Figure 3.7** shows a flowchart of the interest point matching process, which includes four steps. First, through a process of K-Means clustering, every interest point can be grouped with the closest node of the control network. For example (**Figure 3.8**), the interest points in the circle are grouped with the closest control point “10”. Then, taking node “10” as the root, together with all the interest points grouped with it (17, 18, 19, 20), a sub-control network is constructed. In this sub-control network, the father node “P” of node “10” is the Starting Point. Next, every point in this sub-control network is assigned a position and angle with respect to node “10” and the starting point “P”. In this way, every interest point is assigned a relative position and angle with respect to its closest control network point. Finally, interest point matching is performed between the two sub-control networks whose root nodes are correspondences. Correspondences are defined as those interest points with the minimum difference in position and angle. The new correspondences are added to the control network to construct a bigger network. This is an iterative process that continues until no new correspondence is added to the control network. The final control network is the result of interest point matching.

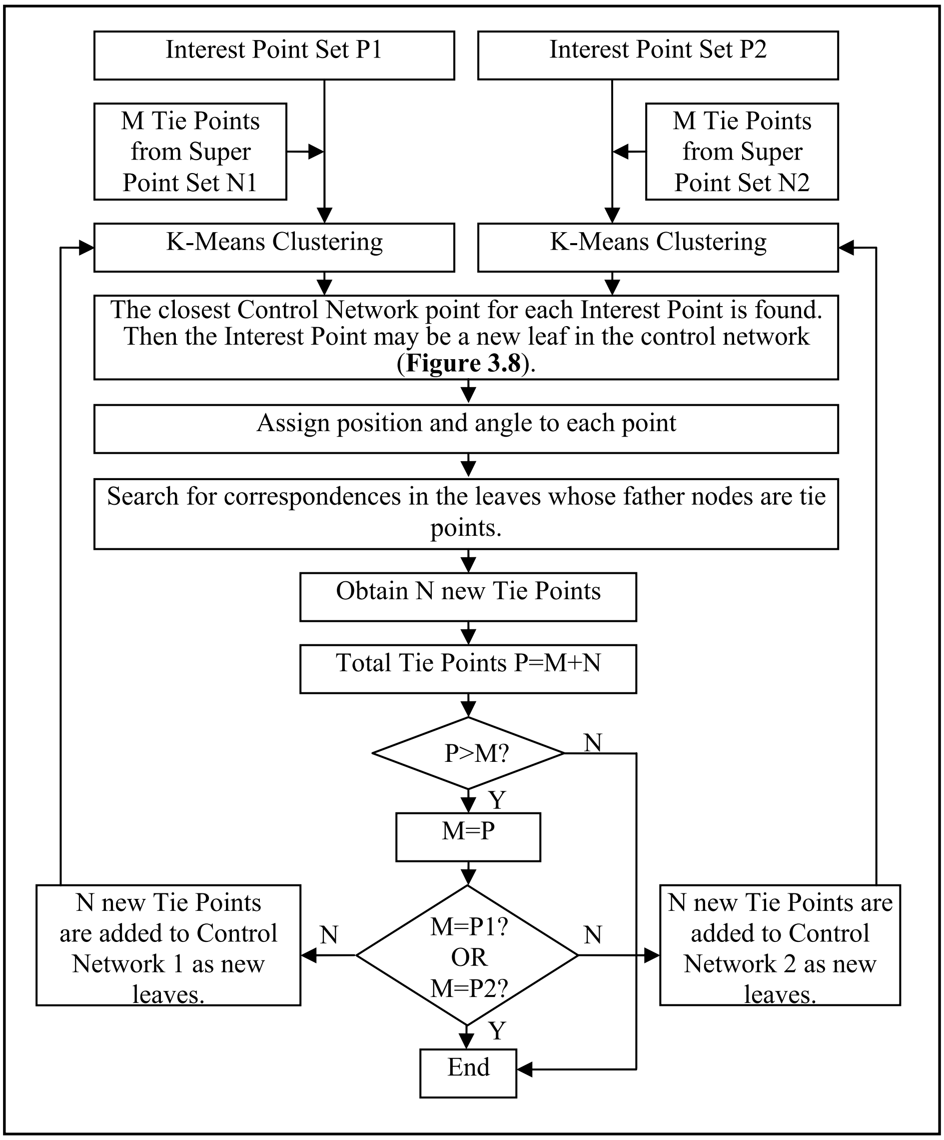


**Figure 3.7 Flow Chart of Interest Point Matching Procedure**

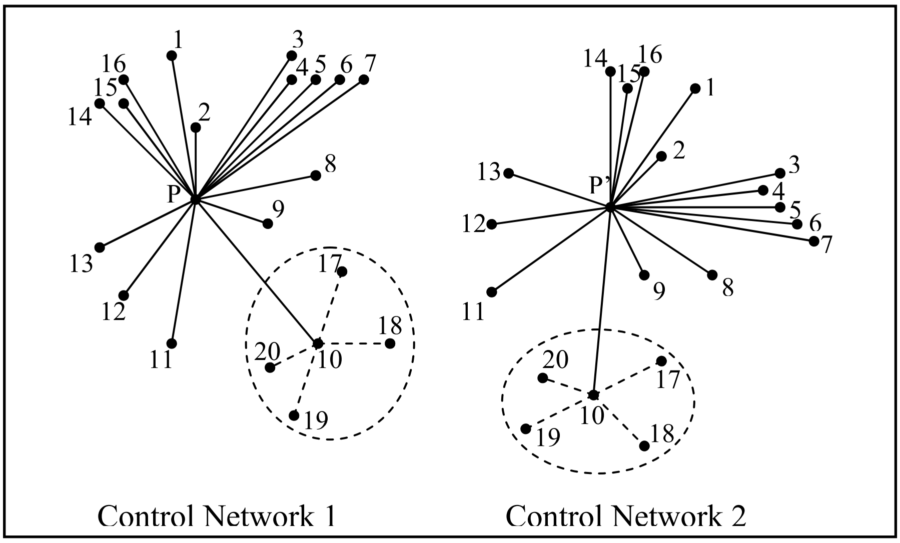


**Figure 3.8 Sub-Control Network. Interest points 17, 18, 19, and 20 are grouped with their closest control network point 10. A sub-control network is constructed with interest points 17, 18, 19, 20, 10, and node 10's father node P. The father node P will be the starting point in the sub-control network. Interest point matching is performed between two sub-control networks whose roots are correspondences (Tie Points).**

## 3.3.4 Threshold Selection

In the process of interest point matching, it is crucial to set a suitable threshold for the distance and angle differences. In remote sensing and photogrammetry, the images always contain complicated local distortions because of the long baselines (long distance between images), perspective geometry differences and ground relief variations. In such a situation, the effective ground distance for different sensors will vary with changes in ground relief, incidence angle and sensor position (**Figure 3.9**).

For example, a distance **S** on the ground with a slope β is acquired by two sensors S1 and S2 with incidence angles θ1 and θ2 respectively (**Figure 3.9**). In this case, the effective distance for sensor S1 and the effective distance for sensor S2 can be calculated as following.

$$S_e^1 = s \cdot \cos(\theta_1 - \beta) \tag{3.4}$$

$$S_e^2 = s \cdot \cos(\theta_2 + \beta) \tag{3.5}$$

Where $S_e^1$ and $S_e^2$ are effective distances for sensor S1 and sensor S2. θ1, θ2 are the incidence angles of sensor S1 and sensor S2 respectively; β is the slope of the ground; and S is the ground distance.

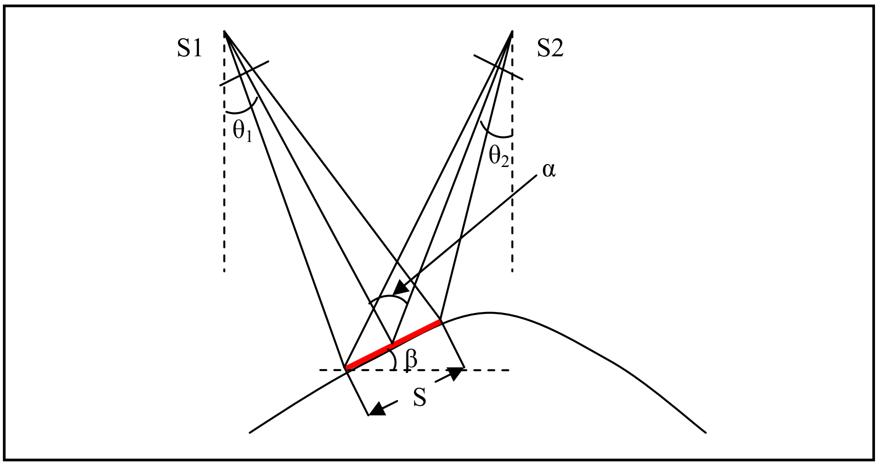


**Figure 3.9 Image Distance Difference Caused by Ground Relief Variation.**

Therefore, the difference between two effective distances caused by ground relief variation and incidence angle in such a case can be defined as follows:

$$ds = s[\cos(\theta_1 - \beta) - \cos(\theta_2 + \beta)] \tag{3.6}$$

Where *ds* is the difference between two effective distances caused by the ground relief variation and incidence angle;

Obviously, the difference between two effective distances can vary with ground slope and incidence angle. **Figure 3.10** shows the situation.

Actually, satellite elevation and pixel size can also affect the distance of two effective distances. However, the satellite elevation affects the effective distance in the form of incidence angle. As the same, the pixel size changes with the incidence angle and slope. Therefore, the effective distance could be affected mainly by incidence angle and slope. That's why we set a threshold for the correspondence search. That's also a tolerance for the difference of effective distance.

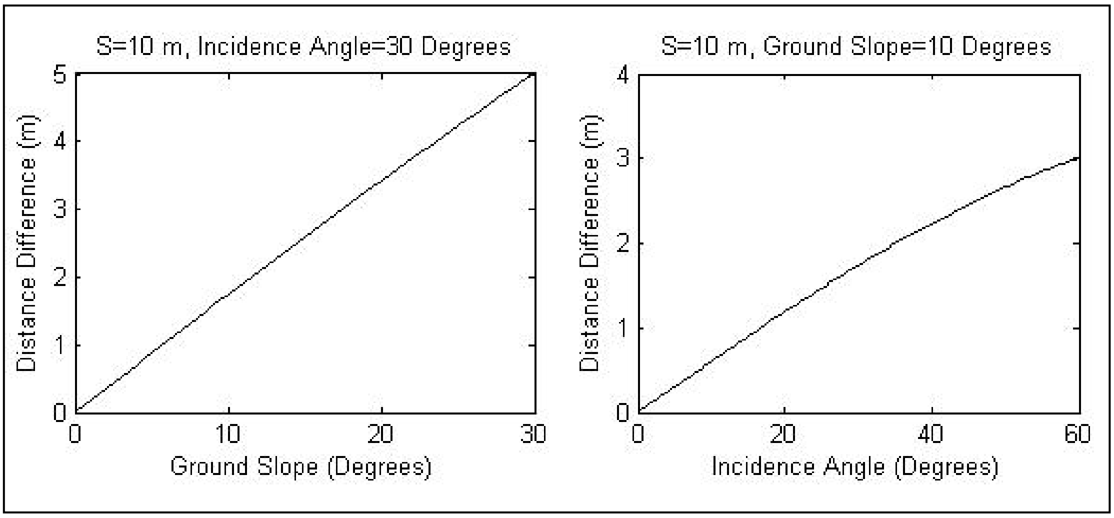


**Figure 3.10 Image Distance Difference. The distance difference changes with the incidence angle and ground slope (assuming that the forward incidence angle θ1 equals the backward incidence angle θ1).**

The difference between two effective distances is proportional to the ground slope and the incidence angle. For an image pair, the incidence angles are constants, so the ground slope is the only variable. In an image, the slope varies with the ground relief variation. Therefore, the only way to limit the distance difference between two images is to limit the ground distance. A small ground distance will lead to a small distance difference and vice-versa. That is why in the proposed interest point matching algorithm, all interest points should be grouped with their closest control network points.

It is important to determine the best way to select the threshold for the distance difference and angle difference. Obviously a large threshold will increase the number of false matches, so in order to reduce false matches, the threshold should be set as small as possible, but when the distance difference between two images is large, a small threshold may mean that correspondences are over-looked and more iterations may be needed to find matches. Another concern may be that a small threshold may lead to false matches and exclude the correct correspondence. This is possible, but because the interest point is a local maximum, there is only a small probability that in the small search area there is another local maximum and the correct one is farther away from the search area. The threshold can therefore be set by considering the radius of the local maximum. For example, if the local maximum is contained in a 5 by 5 pixel window, a threshold of 2 pixels or less can be considered as a safe threshold.

## 3.4 Experiments

Four sets of high resolution satellite images were used for our experiments:

### (1) Test Data 1:

A stereo pair of level 1A IKONOS images acquired on June 25, 2004 over Penang, Malaysia was used for this experiment (**Figure 3.11**). The incidence angles are 30° and 3.5° respectively.

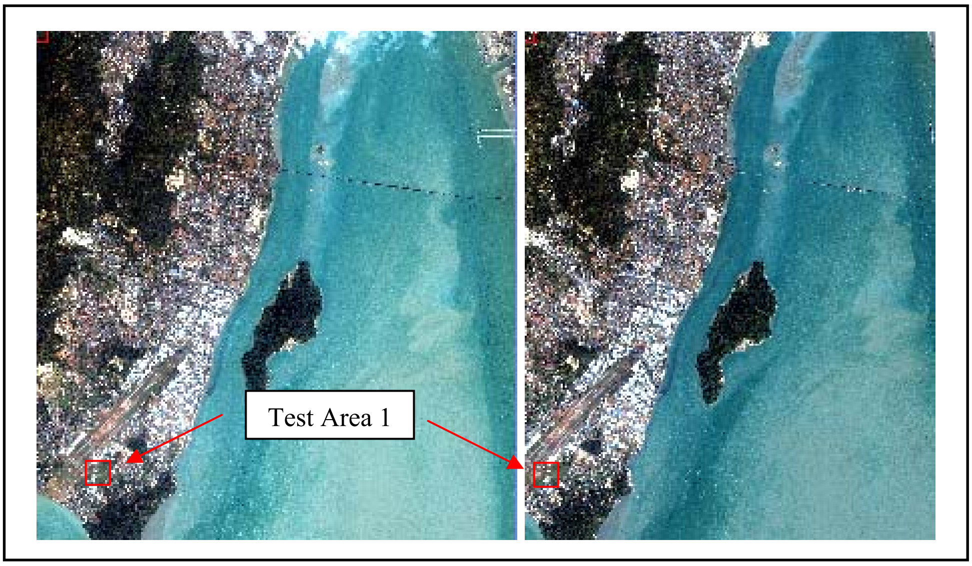


**Figure 3.11 Test Data 1 From Stereo Pair of IKONOS Images of Penang, Malaysia (From CRISP, National University of Singapore)**

A rectangular area (400 by 400 pixels) was selected as the test area. **Figure 3.12** shows two pairs of images. The pair (a) and (a') were taken directly from the original images. A second pair (b) and (b') is comprised of (b) which was taken from the original left image and (b') which was taken from the right image which has been rotated 45°. In this test area, there is large area of grass which was used to test the algorithm's capability of reducing ambiguity and avoiding false matching in a smooth area.


**Figure 3.12 Test Images From the Penang Stereo Pair: (a) and (a’) are a pair (400 by 400 pixels) without rotation, while (b) and (b’) are a pair (400 by 400 pixels) with (b’) rotated 45°.**

**Figure 3.13** shows the results of interest point matching corresponding to the image pairs from **Figure 3.12** (a), (a’) and **Figure 3.12** (b), (b’) respectively.

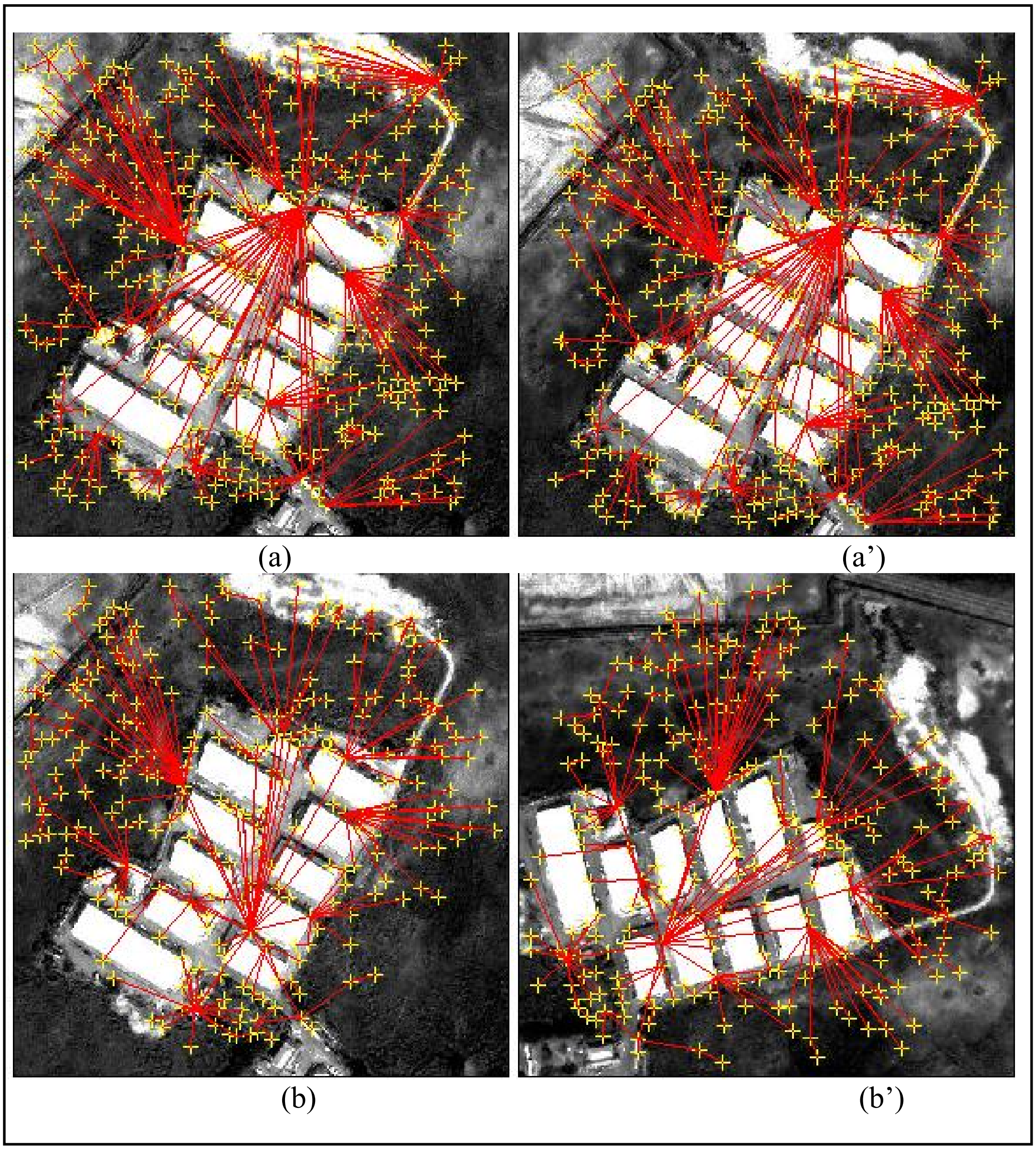


**Figure 3.13 Results of Interest Point Matching Corresponding to the Image Pair from Figure 3.12 (a), (a') (410 correspondences) and the Figure 3.12 (b), (b') (264 correspondences).**

## (2) Test Data 2:

A stereo pair of IKONOS images which was acquired on February, 2003 in Hobart, Australia was used for this experiment (**Figure 3.14**). The incidence angles are forward 75° and backward 69° respectively (Fraser and Hanley, 2005).

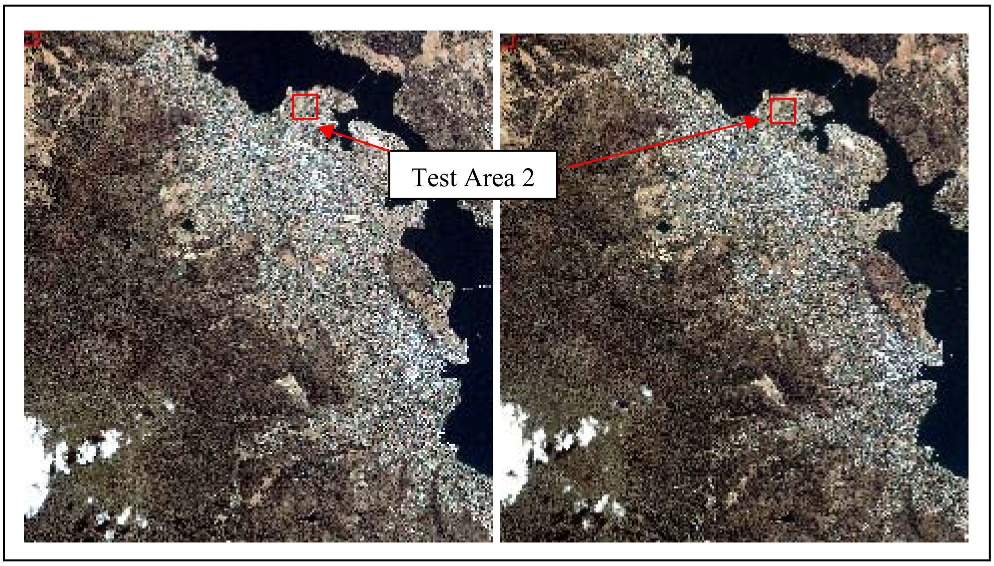


**Figure 3.14 Test Area 2 From Stereo Pair of IKONOS Images in Hobart (From the University of Melbourne)**

A rectangular area (400 by 400 pixels) was selected as the test area. **Figure 3.15** shows two pairs of images: (c) and (c') is an image pair taken directly from the original images, while (d) and (d') is another image pair where (d) was taken directly from the original left image and (d') was taken from the right image which has been rotated 315°. This is an urban area with a large area of grass where the algorithm's capability of reducing ambiguity and avoiding false matching in smooth areas could be tested.


**Figure 3.15 Test Images From the Hobart Stereo Pair: (c) and (c’) are a test image pair (400 by 400 pixels) without rotation, and (d) and (d’) are a test image pair (400 by 400 pixels) with (d’) rotated 315°.**

**Figure 3.16** shows the results of interest point matching corresponding to the image pairs from **Figure 3.15** (c), (c’) and **Figure 3.15** (d), (d’) respectively.

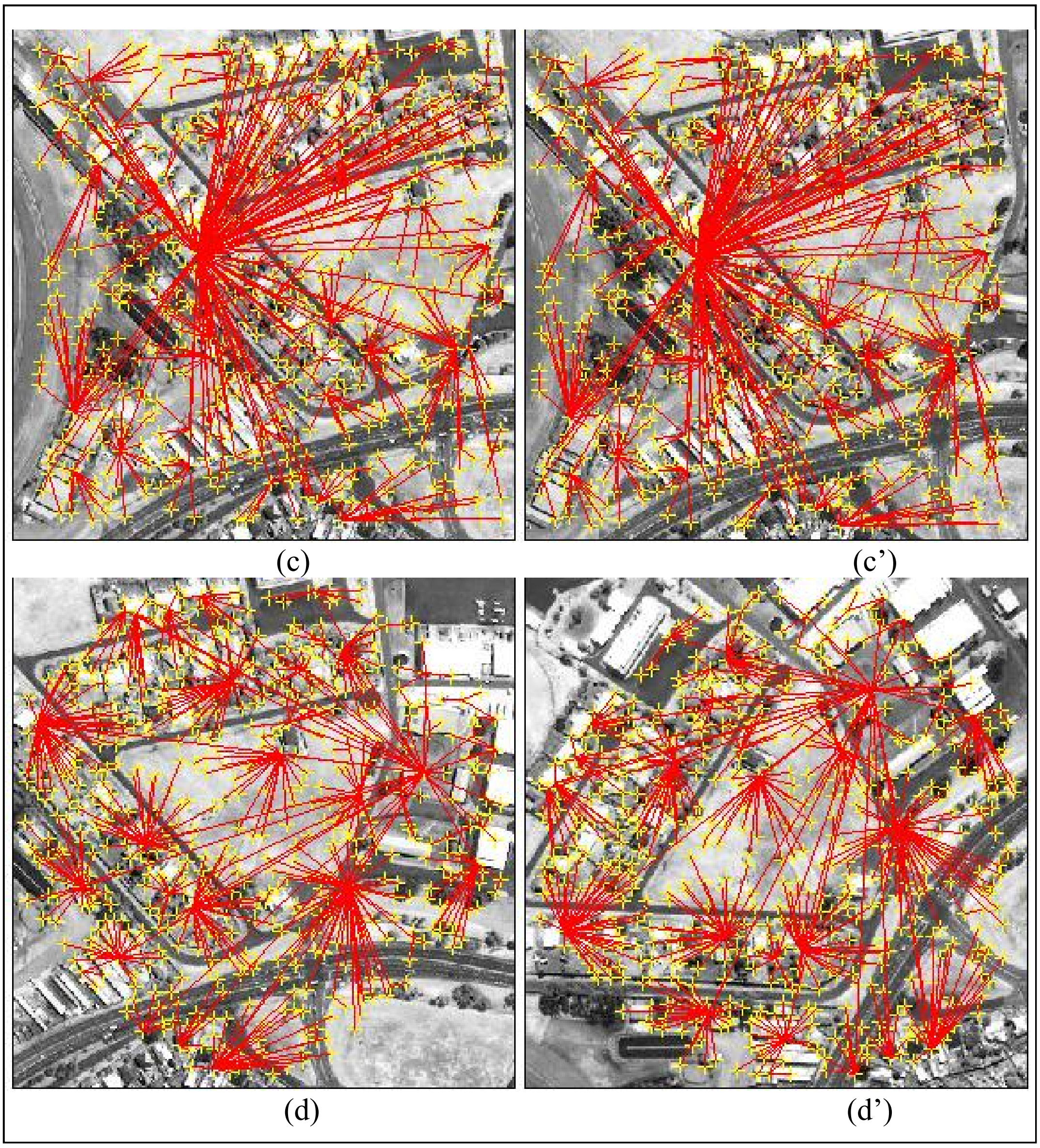

**Figure 3.16 Results of Interest Point Matching Corresponding to the Image Pair from Figure 3.15 (c), (c') (641 correspondences) and Figure 3.15 (d), (d') (561 correspondences) respectively.**

## (3) Test Data 3:

Test area 3 is also from the stereo image pair in Penang. Because the above two test areas are relatively flat and somewhat small, a larger test area from a mountainous area was selected as test area 3 (**Figure 3.17**) in order to test the algorithm under a different set of conditions.

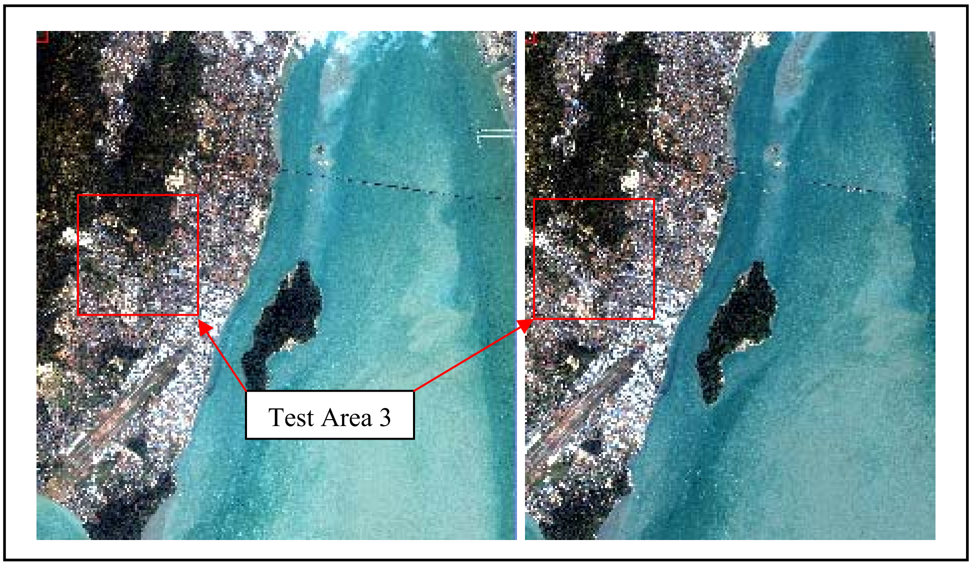


**Figure 3.17 Test Data 3 from Stereo Pair of IKONOS Images in Penang, Malaysia (From CRISP, National University of Singapore)**

A rectangular area (2000 by 2000 pixels) was selected as test area 3. **Figure 3.18** shows image pair (e) and (e'), taken directly from the original images. This is a mixed area of mountain and urban land cover. In this test area, there is large area of forest which was used to test the algorithm's capability of reducing ambiguity and avoiding false matching in a smooth area. The mountainous area was used to test the algorithm's capability of processing large distortions.

**Figure 3.19** shows the results of interest point matching corresponding to the image pair from **Figure 3.18** (e) and (e').

(e)

(e’)

**Figure 3.18 Test Area 3 in Mountainous Area (2000 by 2000 pixels).**

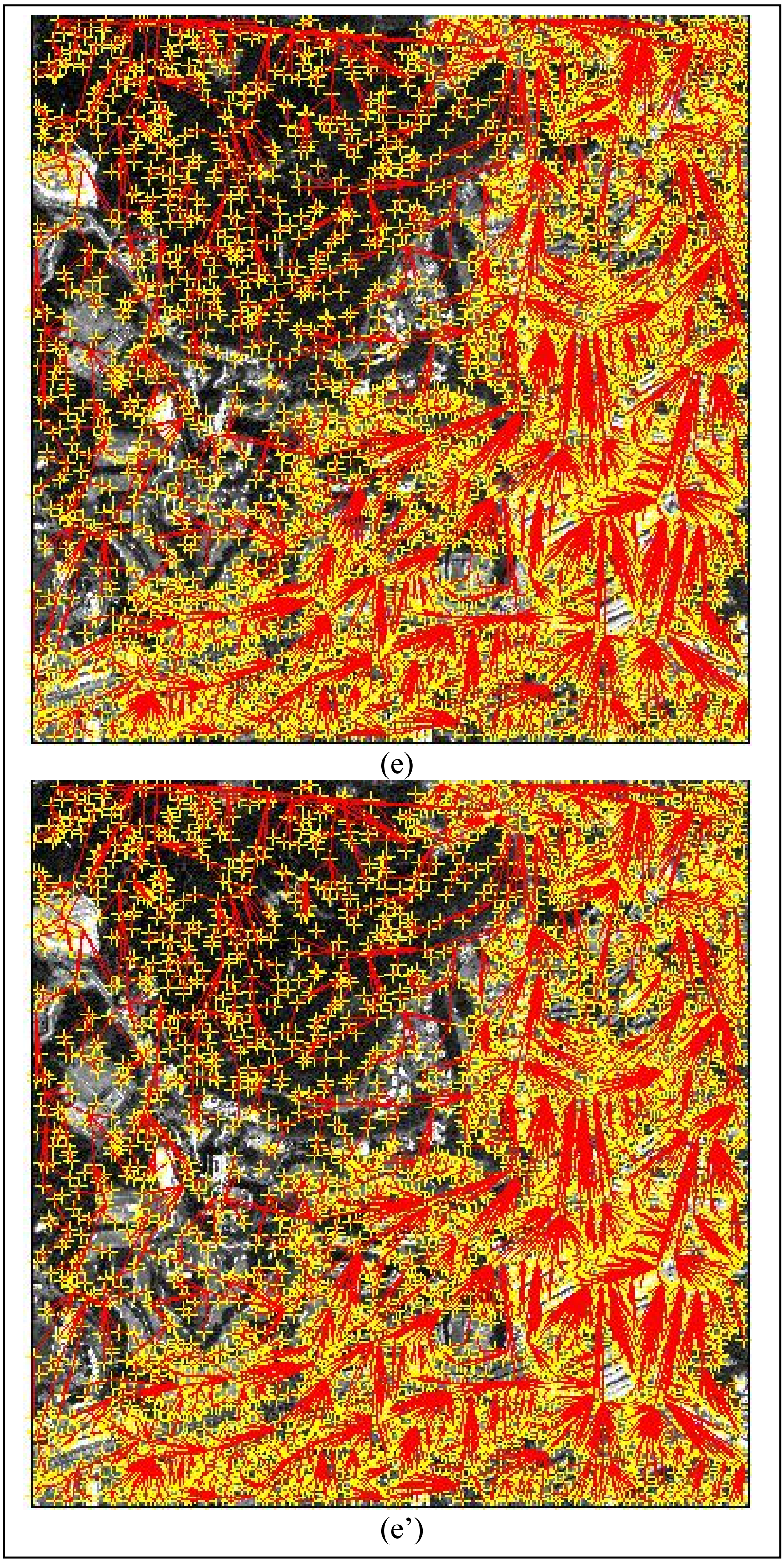
(e)
(e’)

**Figure 3.19 Result of Interest Point Matching Corresponding to the Image Pair (e) and (e’). There are 5674 correspondences in total.**

## (4) Test Data 4:

In order to test the proposed algorithm, five test areas, which are located in the densest forestry region of Fredericton (**Figure 3.20**), are chosen to challenge the capability of dealing with the ambiguity problem in the homogeneous area. Six scenes of QuickBird images cover the test field. All test image pairs are selected in the overlapping area. The corresponding results of interest point matching are illustrated in **Figure 3.21 ~ Figure 3.25** respectively.

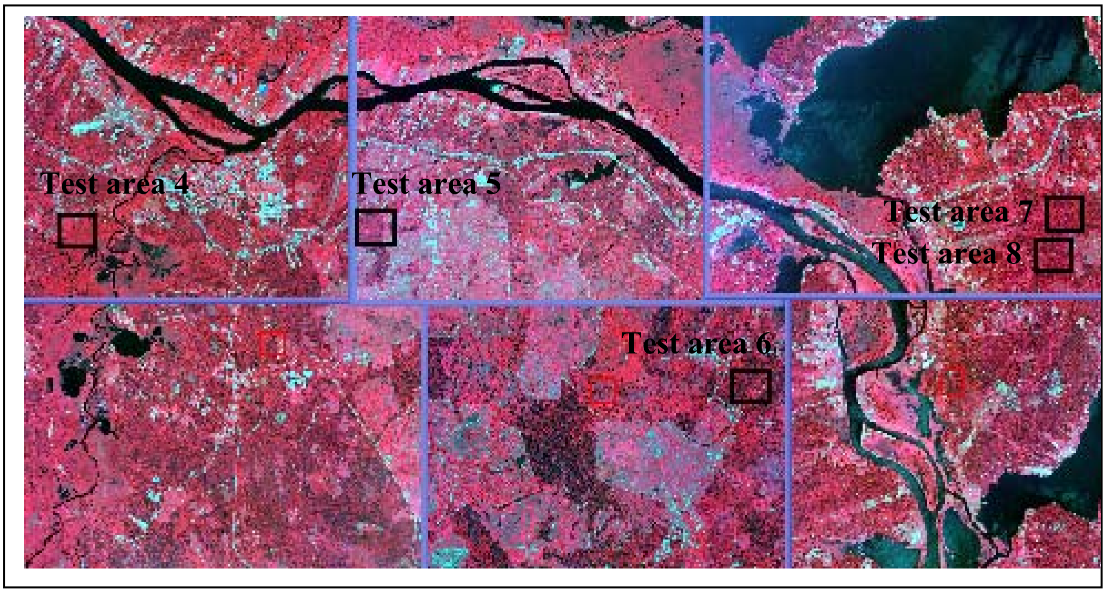


**Figure 3.20 Five test areas from QuickBird images in Fredericton.**

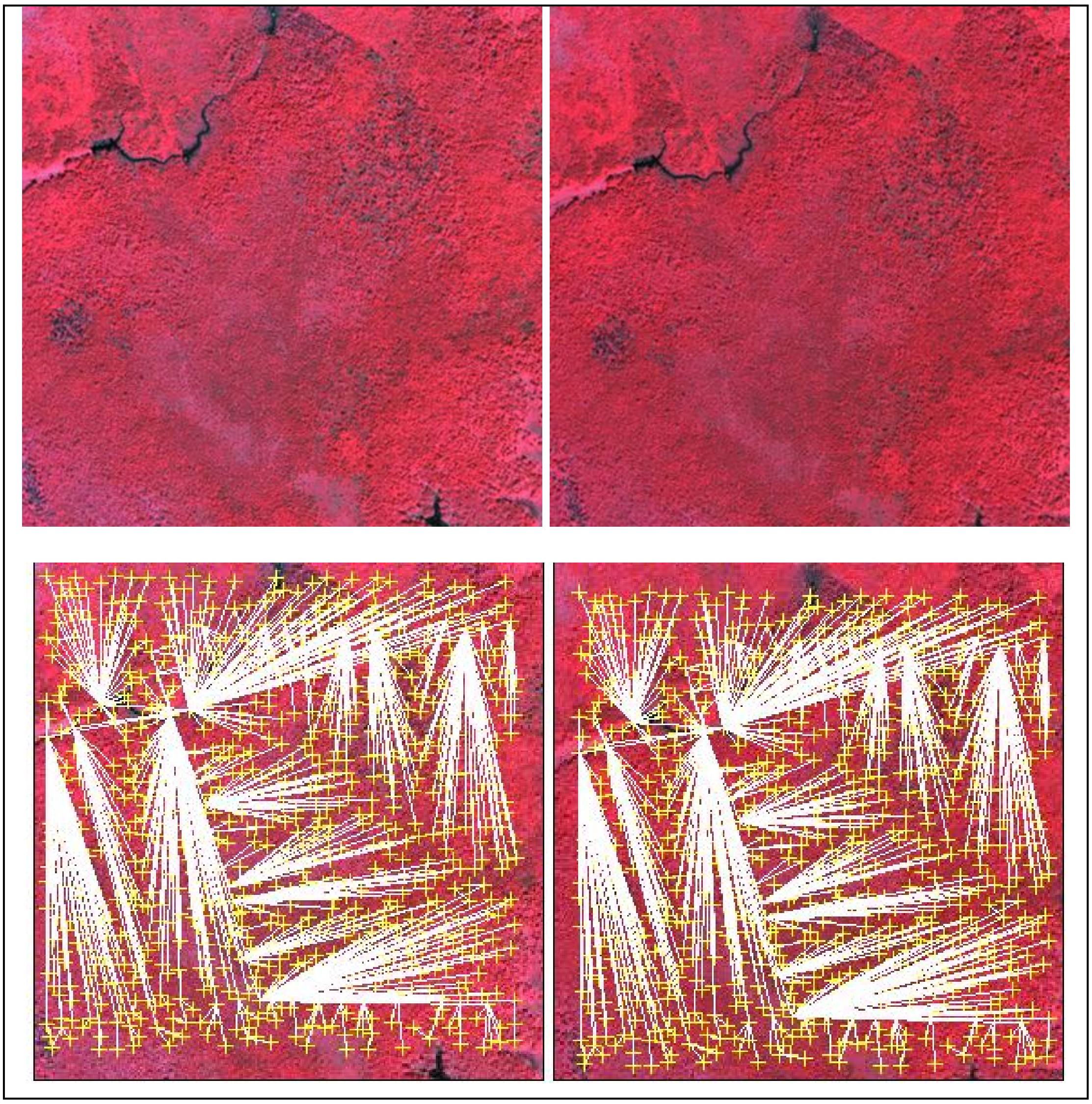

**Figure 3.21 Result of Interest Point Matching in Test Area 4 (813 correspondences are obtained).**

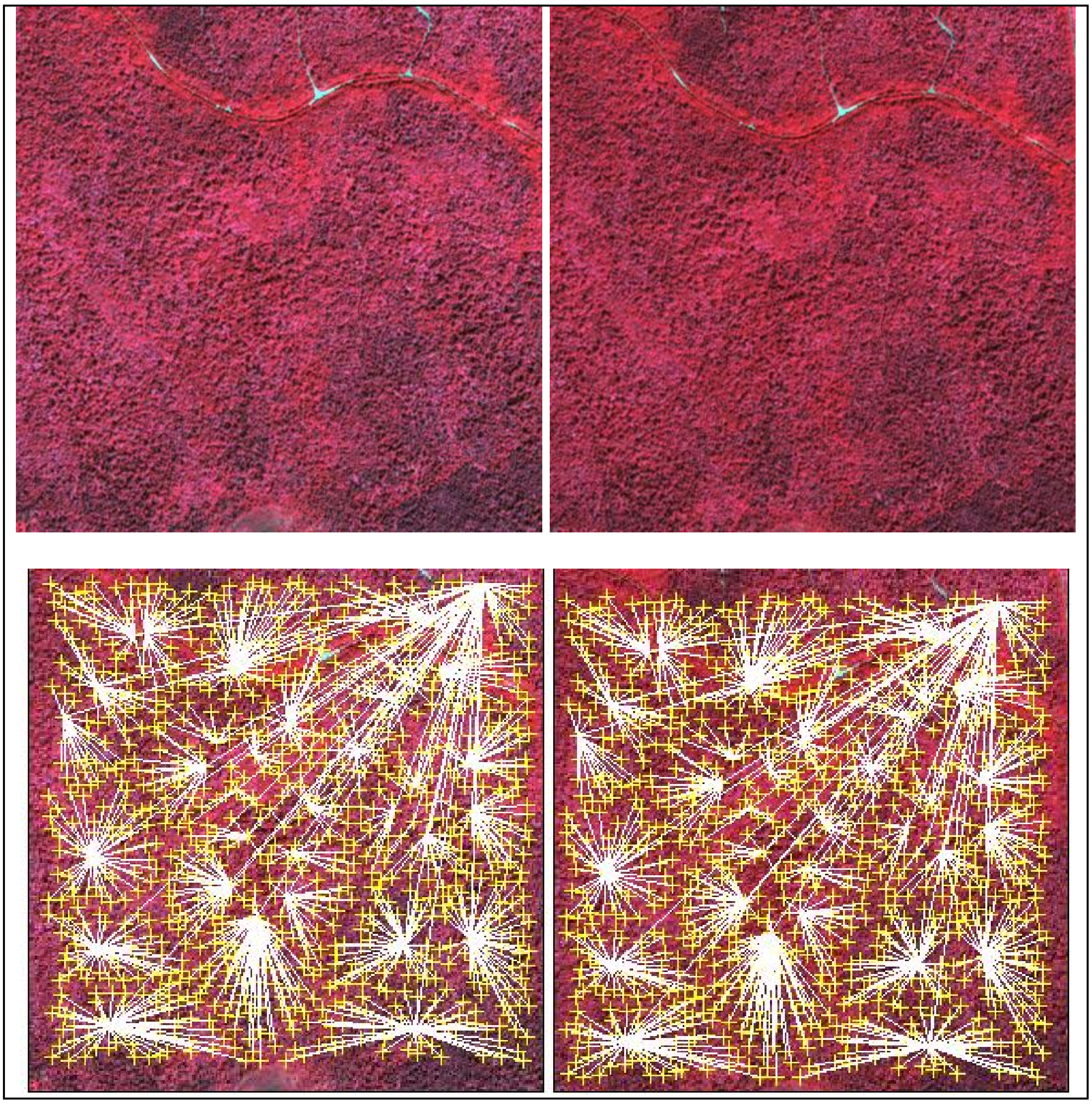

**Figure 3.22 Result of Interest Point Matching in Test Area 5 (929 correspondences are obtained).**

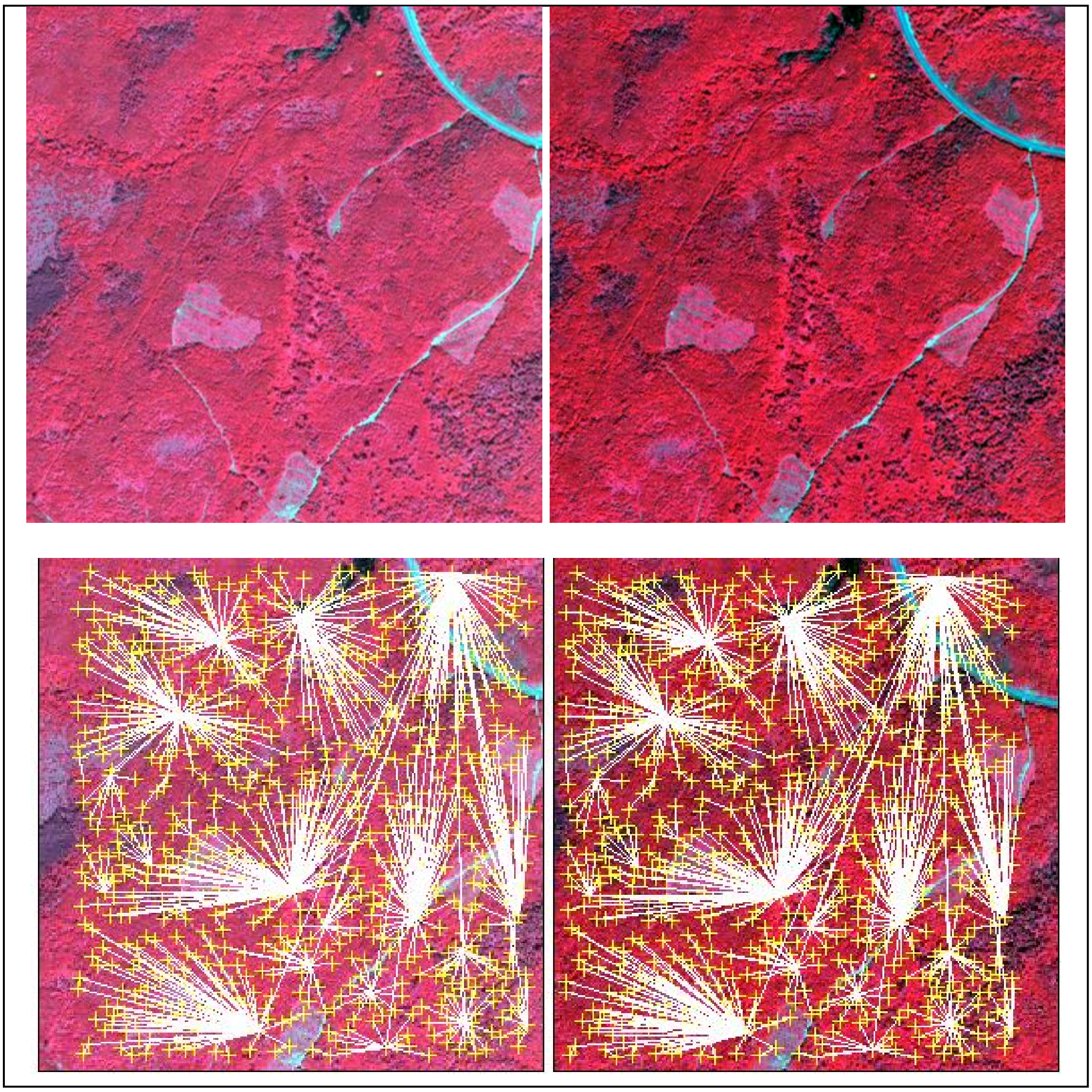

**Figure 3.23 Result of Interest Point Matching in Test Area 6 (759 correspondences are obtained).**

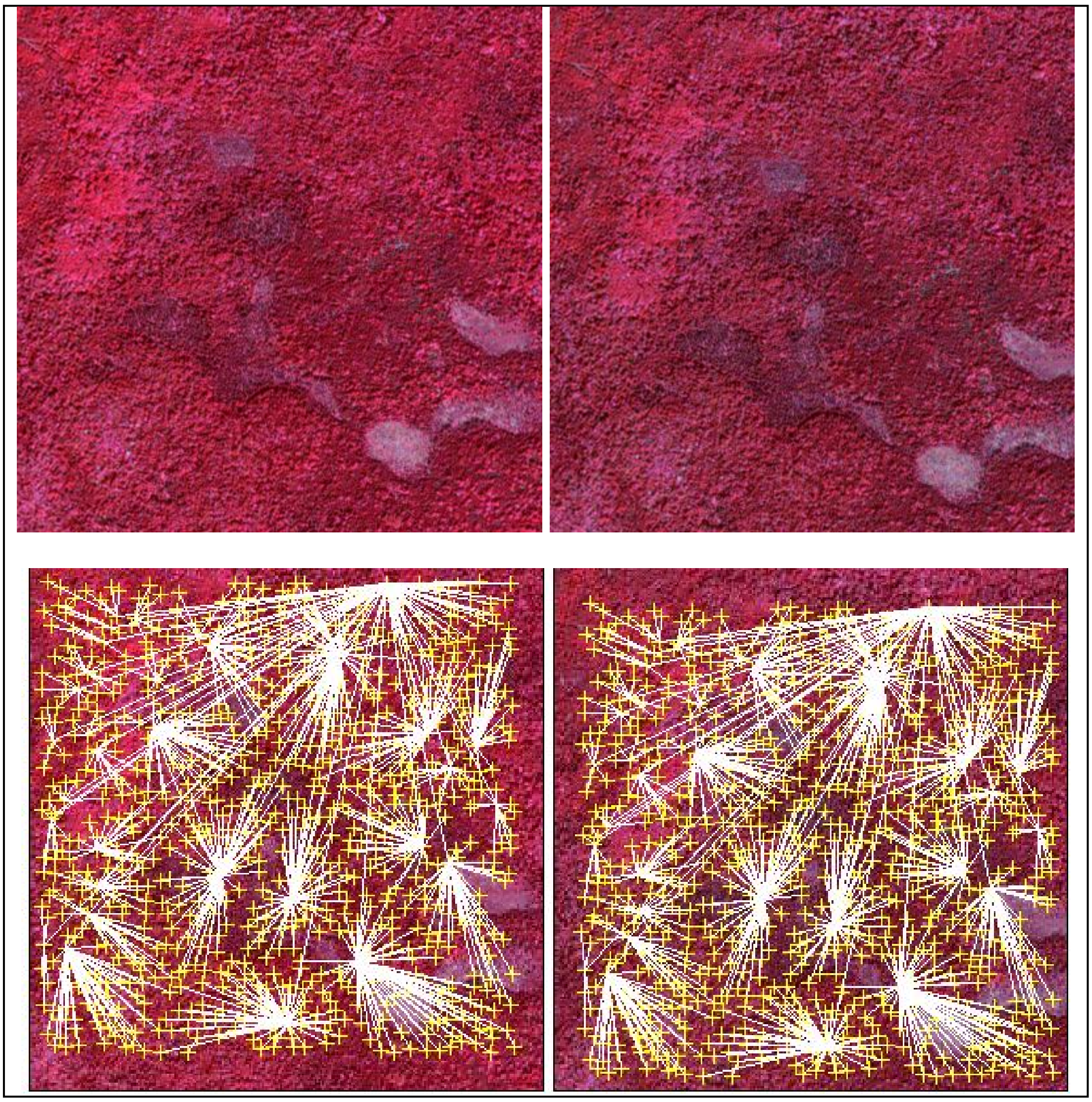

**Figure 3.24 Result of Interest Point Matching in Test Area 7 (857 correspondences are obtained).**

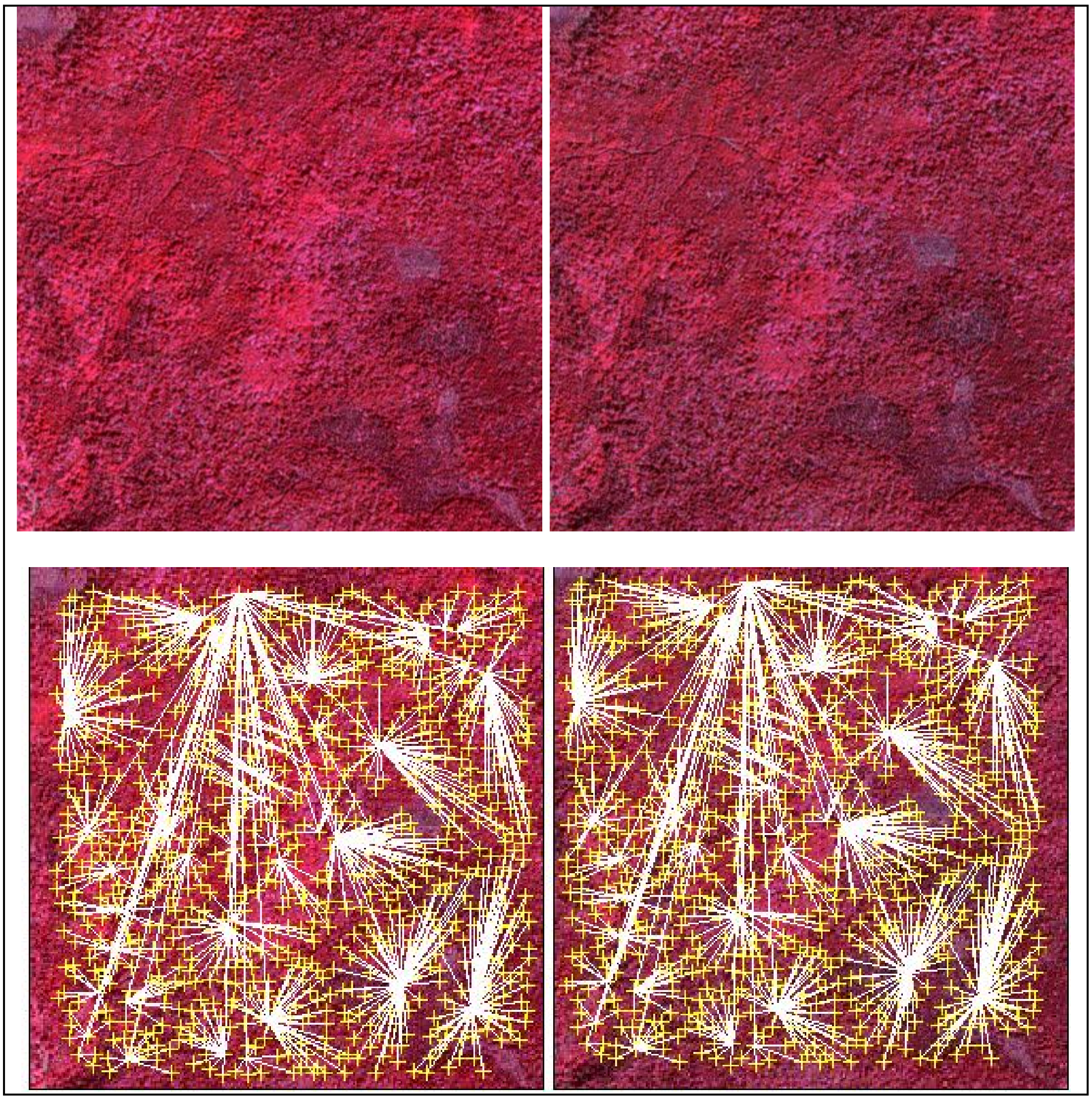

**Figure 3.25 Result of Interest Point Matching in Test Area 8 (875 correspondences are obtained).**

All the experiments illustrated satisfactory results. We carefully checked every correspondence in each of the test areas, and did not find any false matches. Even in the smooth areas (e.g. a large area of grassland), this algorithm avoided false matches efficiently. In addition, because each interest point is assigned a unique distance and angle with regard to its closest control point, its correspondence is searched only within the corresponding sub-control network, thus the process of interest point matching is very fast. By using IBM (processor 1.70 GHz, 1.69 GHz, 768 MB of RAM), each experiment took only a few seconds.

The success of this algorithm completely depends on the control network. On one hand, the control network incorporates the spatial information and easily overcomes the problem of ambiguity in the homogeneous area. On the other hand, if the first group of correspondences from the super point matching is wrong, then all the other correspondences extracted based on this control network later on will also be false. This may be the main concern for this algorithm. However, for every different image, the control network of super points is almost always unique, except where there is not any prominent texture in the image and the whole image is homogeneous or filled with man-made texture. Under those circumstances, this algorithm does not work in a complete homogeneous area, such as an area covered by snow, water, or sand. Fortunately, complete homogeneous images are extremely rare.

## 3.5 Conclusions

We have presented and successfully tested a novel algorithm for interest point matching of high resolution satellite images. This algorithm has the following characteristics:

1) It can avoid local minimum problems and can process areas without prominent details, because the proposed algorithm uses spatial information by first constructing a super point control network;
2) It can remove outliers easily, because every interest point is assigned a unique position and angle with regard to its closest control point; and

3) Because of the super point control network, the algorithm does not require an exhaustive search during the interest point matching, so it is a relatively simple, fast, and accurate algorithm.

Of course, like other algorithms, the proposed algorithm cannot solve every interest point matching problem. Because only shift and rotation are considered in the algorithm, we think this algorithm can be only used for high resolution satellite images that were captured with a narrow field of view camera, or other images that were captured with a short baseline.

## ACKNOWLEDGEMENTS

This research is sponsored by the Natural Sciences and Engineering Research Council of Canada through the Discovery Grant (NSERC Discovery Grant) awarded to Dr. Yun Zhang, the second author of the paper. We would like to acknowledge that Prof. Clive Fraser, Department of Geomatic Engineering, University of Melbourne, Australia, provided me satellite images for the tests. Special thanks go to Mr. David C. Whyte, Department of Environment, NB, Canada, who reviewed the manuscript of this report.

## REFERENCES

Auer, Matin, Peter Regitnig, and Gerhard A. Holzapfel. (2005). "An Automatic Nonrigid Registration for Stained Histological Sections." *IEEE Transactions on Image Processing*, Vol. 14, No. 4, April 2005.

Belongie, Serge, Jitendra Malik, and Jan Puzicha. (2002). "Shape matching and object recognition using shape contexts." *IEEE transactions on pattern analysis and machine intelligence*, Vol. 24.

Besl, Paul J., and Neil D. McKay. (1992). "A Method for Registration of 3-D Shapes." *IEEE Transactions on Pattern Analysis and Machine Intelligence*, Vol. 14, No. 2.

Boffy, Aurelien, Yanghai Tsin, and Yakup Genc. (2008). "Real-Time Feature Matching Using Adaptive and Spatially Distributed Classification Trees." http://www.macs.hw.ac.uk/bmvc2006/papers/397.pdf. Last date accessed: August, 14, 2008.

Booksten, Fred L. (1989). "Principal Warps: Thin-Plate Splines and the Decomposition of Deformations." *IEEE Transactions on Pattern Analysis and Machine Intelligence*, Vol. 11, No. 6.

Brown, Lisa Gottesfeld. (1992). "A survey of image registration techniques." *ACM Computing Surveys.* Vol. 24, No. 4.

Caetano, Tiberio S., Terry Caelli, and Dante A.C. Barone. (2004). "A Comparison of Junction Tree and Relaxation Algorithms for Point Matching Using Different Distance Metrics." *Technical Report TR 04-04*, February 2004, Department of Computer Science, University of Alberta.

Chui, Haili and Anand Rangarajan. (2003). "A New Point Matching Algorithm for Non-Rigid Registration." *Computer Vision and Image Understanding* 89 (2003) 114-141.

Croitoru, Arie, and Vincent Tao. (2003). "An Alternative Approach to the Point Correspondence Problem." *ASPRS 2003 Annual Conference Proceedings*, May 2003, Anchorage, Alaska.

Cross, Andrew D.J. and Edwin R. Hancock. (1998). "Graph Matching With a Dual-Step EM Algorithm." *IEEE Transactions on Pattern Analysis and Machine Intelligence*, Vol. 20, No. 11, November 1998.

Demirci, M. Fatih, Ali Shokoufandeh, Sven Dickinson, Yakov Keselman, and Lars Bretzner. (2004). "Many-to-Many Feature Matching Using Spherical Coding of Directed Graphs." T. Pajdla and J. Matas (Eds.): ECCV 2004, LNCS 3021, pp. 322-335.

Dowman I. J. (1977). "Developments in Online Techniques for Photogrammetry and Digital Mapping." *Photogrammetric Record*, 9(49): 41-54.

Gold, Steven and Anand Rangarajan. (1996). "A Graduated Assignment Algorithm for Graph Matching." *IEEE Transactions on Pattern Analysis and Machine Intelligence*, Vol. 18, No. 4.

Gold, Steven, Anand Rangarajan, Chien-Ping Lu, Suguna Pappu, and Eric Mjolsness. (1997). "New Algorithms for 2D and 3D Point Matching: Pose Estimation and Correspondence." URL:

http://citeseerx.ist.psu.edu/legacymapper?did=88372, Accessed: August, 14, 2008.

Gupta, Rajiv. (1997). “Linear Pushbroom Cameras.” *IEEE Transactions on Pattern Analysis and Intelligence, VOL. 19, NO. 9, 1997*.

Habib, Ayman and Rami Ai-Ruzouq. (2005). “Semi-Automatic Registration of Multi-Source Satellite Imagery with Varying Geometric Resolutions.” *Photogrammetric Engineering & Remote Sensing*, Vol. 71, No. 3, pp.325-332.

Harris C. and Stephens M. (1988). “A combined corner and edge detector.” *Alvey Vision Conference*, pages 147-151.

Helava, Uuno V., Chapelle, Walter E., Hornbuckle, John A. (1973). “Stereoplotting apparatus for correlating image points disposed along epipolar lines.” U.S.Patent No. 3726591, Apr. 10, 1973.

Hsieh, Yuan C., David M. McKeown, and Frederic P. Perlant. (1992). “Performance Evaluation of Scene Registration and Stereo Matching for Cartographic Feature Extraction.” *IEEE Transactions on Pattern Analysis and Machine Intelligence*, Vol. 14, No. 2.

Kaplan, Alexander, Ehud Rivlin, and Ilan Shimshoni. (2004). “Robust Feature Matching Across Widely Separated Color Images.” *Proceedings of the 17th International Conference on Pattern Recognition* (ICPR’04).

Kim, Taejung. (2000). “A Study on the Epipolarity of Linear Pushbroom Images.” *Photogrammetric Engineering & Remote Sensing*, VOL. 66, NO. 8, August 2000, 961-966.

Kybic, Jan, and Michael Unser. (2003). “Fast Parametric Elastic Image Registration.” *IEEE Transactions on Image Processing*, Vol. 12, No. 11, November 2003.

Lepetit, Vincent, Julien Pilet, and Pascal Fua. (2004). “Point Matching as a Classification Problem for Fast and Robust Object Pose Estimation.” http://cvlab.epfl.ch/~vlepetit/papers/lepetit_cvpr04.pdf. Last date accessed: August 14, 2008.

Lepetit, Vincent, Pascal Lagger, and Pascal Fua. (2005). “Randomized Trees for Real-Time Keypoint Recognition.” *Computer Vision and Pattern Recognition*, 2005. Volume: 2, 775- 781 vol. 2.

Lowe, David G. (2004). “Distinctive Image Features from Scale-Invariant Keypoints.” *International Journal of Computer Vision* 60(2), 91–110.

Masry, S. E. (1972). “An Automatic Method for Height Profile Determination.” *The Photogrammetric Record*, Volume 7 Issue 42, Pages 728 – 730.

Mount, David M., Nathan S. Netanyahu, and Jacqueline Le Moigne. (1997). “Efficient Algorithms for Robust Feature Matching.” *Proceedings of the CESDIS*

*Image Registration Workshop*, NASA Goddard Space Flight Center, Greenbelt, MD, 1997.

Rexilius, J., S.K. Warfield, C.R.G. Guttmann, X. Wei, R. Benson, L. Wolfson, M. Shenton, H. Handels, and R. Kikinis. (2001). "A Novel Nonrigid Registration Algorithm and Applications." W. Niessen and M. Viergever (Eds.): MICCAI 2001, LNCS 2208, pp. 923-931.

Schmid, Cordelia, Roger Mohr and Christian Bauckhage. (2000). "Evaluation of Interest Point Detectors." *International Journal of Computer Vision* 37(2), 151–172.

Shokoufandeh, Ali, Yakov Keselman, Faith Demirci, Diego Macrini, and Sven Dickinson. (2006). "Many-to-Many Feature Matching in Object Recognition." H.I. Christensen and H.-H. Nagel (Eds.): Cognitive Vision Systems, LNCS 3948, pp. 107-125.

Terasawa, Kengo, Takeshi Nagasaki, and Toshio Kawashima. (2005). "Robust Matching Method for Scale and Rotation Invariant Local Descriptors and Its Application to Image Indexing." G.G. Lee et al. (Eds.): AIRS 2005, LNCS 3689, pp. 601-615.

Tu, Zhuowen, Songfeng Zheng, and Alan Yuille. (2008). "Shape Matching and Registration by Data-Driven EM." *Computer Vision and Image Understanding,*109 (2008) 290-304.

Williams, John and Mohammed Bennamoun. (2001). "Simultaneous Registration of Multiple Corresponding Point Sets." *Computer Vision and Image Understanding* 81, 117-142 (2001).

Yang, Gehua, Charles V. Steward, Michal Sofka, and Chia-Ling Tsai. (2007). "Registration of Challenging Image Pairs: Initialization, Estimation, and Decision." *IEEE Transactions on Pattern Analysis and Machine Intelligence*, Vol. 29, No. 11.

Zhao, Wanlei, Yugang Jiang, and Chong-Wah Ngo. (2006). "Keyframe Retrieval by Keypoints: Can Point-to-Point Matching Help?" H. Sundaram et al. (Eds.): CIVR 2006, LNCS 4071, pp. 72-81.

Zitova, Barbara, Jan Flusser. (2003). "Image Registration Methods: a Survey." *Image and Vision Computing* 21 (2003)977-1000.

# Chapter 4 A GENERIC METHOD FOR RPC REFINEMENT USING GROUND CONTROL INFORMATION[4]


## ABSTRACT

Geometric sensor models are used in image processing to model the relationship between object space and image space and transform image data to conform to a map projection. An RPC (Rational Polynomial Coefficient) is a generic sensor model that can be used to transform images from a variety of different high-resolution satellite and airborne remote sensing systems. To date, numerous researchers have published papers about RPC refinement, aimed at improving the accuracy of the results. So far, the Bias Compensation method is the one that is the most accepted and widely used, but this method has rigorous conditions that limit its use; namely, it can only be used to improve the RPC of images obtained from cameras with a narrow field of view and small attitude errors, such as those used on IKONOS or QuickBird satellites. In many cases, these rigorous conditions may not be satisfied (e.g. cameras with wide fields of view and some satellites with large ephemeris and/or attitude errors). Therefore, a more robust method that can be used to refine the RPC under a wider range of conditions is desirable. In this paper, a generic method for RPC refinement is proposed. The method first restores the sensor's pseudo position and attitude, then adjusts these parameters using ground control points. Finally a new RPC is generated based on the sensor's adjusted position and attitude. We commence our paper with a



[4] The paper in this chapter has been accepted by *Journal of Photogrammetric Engineering & Remote Sensing* for publication (see APPENDIX II). Reprinted with permission from the American Society for Photogrammetry and Remote Sensing (see APPENDIX I). But additional material has been added to the experiment section for the comparison of the developed algorithm and previous algorithm and illustration of the robustness of such novel algorithm.
Xiong Z. and Y. Zhang, "A Generic Method for RPC Refinement Using Ground Control Information", *Journal of Photogrammetric Engineering & Remote Sensing*, 2009 (In press)

review of the previous ten years' research directed toward RPC refinement, and compare the characteristics of different refinement methods that have been proposed to date. We then present a methodology for a proposed generic method for RPC refinement and describe the results of two sets of experiments that compare the proposed Generic method with the Bias Compensation method. The results confirm that the Bias Compensation method works well only when the aforementioned rigorous conditions are met. The accuracy of the RPC refined by the Bias Compensation method decreased rapidly with the sensor's position error and attitude error. In contrast to this, the Generic method proposed in this paper was found to yield highly accurate results under a variety of different sensor positions and attitudes.

**Key Words:** RPC, Sensor Model, Refinement, Ground Control

## 4.1 Introduction

The term RPC typically refers to the Rational Polynomial Coefficient, or Rational Polynomial Camera coefficient [Chen et al., 2006]. It sometimes has been more generically defined as Rapid Positioning Capability [Dowman and Tao, 2002]. RPCs are sometimes also referred to as Rational Function Coefficients (RFCs), or Rational Functional Models (RFM) [Tao and Hu, 2001]. RPCs are recommended by the OGC (Open GIS Consortium) and are widely used in the processing of high-resolution satellite images. A RPC model is a mathematical function that relates object space coordinates (latitude, longitude, and height) to image space coordinates (line and sample). It is expressed in the form of a ratio of two cubic functions of object space coordinates. Separate rational functions are used to express the object space to line, and the object space to sample, coordinate relationships [Dial and Grodecki, 2002[a]].

Because of ephemeris and attitude error, all satellite geometric sensor models, including physical and RPC models, have a definite value of absolute positioning error. For example, the ephemeris and attitude accuracy for IKONOS is about one meter for ephemeris and about one or two arc-seconds for attitude [Grodecki and Dial, 2003]. The accuracy for a single stereo pair of IKONOS images, without ground control, is 25.0 m (CE90), and 22.0 m (LE90) [Grodecki, 2001]. If the satellite positioning accuracy does not meet the needs of users, the sensor model should be refined by using Ground Control Points (GCPs) or other auxiliary data. Before the advent of IKONOS, users of satellite imagery typically made use of physical sensor models. Nowadays, instead of physical parameters, sometimes only a rational polynomial function which consists of 80 coefficients is available. This represents a completely new challenge, because the RPC has a high number of coefficients and there is no physical interpretation for the order and terms of these coefficients. Many researchers have attempted to address this challenge. Directly calculating a new RPC based on a large number of GCPs [Di et al., 2003] has been proven unfeasible [Grodecki et al., 2003; Hu et al., 2004]. The Batch Iterative Least-Squares (BILS) method and the Incremental Discrete Kalman Filtering (IDKF) method each requires a significant number of GCPs and also the covariance matrices of the RFCs which are not available to most users [Hu and Tao, 2002]. The Pseudo GCP (PG) method, the Using Parameters Observation Equation (UPOE) method, and the Sequential Least Square Solution (SLSS) method [Bang et al., 2003] all face the problem of how to define the weightings of the coefficients for different observation equations.

In terms of accuracy and computational stability, the Bias Compensation method [Fraser and Hanley, 2003] so far appears to be the best method and has been widely used [Fraser, 2003, 2005; Hu et al., 2002], but this method is effective only when the camera Field Of View (FOV) is narrow and the position and attitude errors are small [Grodecki and Dial, 2003]. Some satellites do meet these rigid conditions. For example as noted above, IKONOS imagery has an accuracy of about one meter for ephemeris and about one or two arc-seconds for attitude, and its FOV is less than one degree [Grodecki and Dial, 2003]. But many other satellites including some of those launched from China, India, and other developing countries probably do not satisfy this condition. As a Generic Sensor Model (GSM), an RPC can accommodate an extremely wide range of images without a need for the satellite ephemeris [Samadzadegan et al., 2005]. Therefore, an RPC can be used in a number of different sensors, such as linear push-broom scanners, RADAR, airborne and space borne sensors. In these cases, the issue becomes one of how to effectively refine RPC using as few GCPs as possible.

This paper begins with a review of the latest research on RPC refinement. Next, the newly developed Generic method for RPC refinement is presented. We then present a series of experiments that focus on a comparison between the Bias Compensation method, arguably the best technique for sensor refinement currently in use, and the Generic method proposed in this paper. We conclude with some recommendations for future work.

## 4.2 Outline of RPC Refinement Methods

On September 24, 1999, IKONOS was launched. Since then, the mapping community has begun to recognize the importance of RPC; a mathematical function which relates the object space and image space (Equation 4.1).

$$x = \frac{P_1(X,Y,Z)}{P_2(X,Y,Z)} \tag{4.1a}$$

$$y = \frac{P_3(X,Y,Z)}{P_4(X,Y,Z)} \tag{4.1b}$$

$$P(X,Y,Z) = \sum_{i=0}^{m1}\sum_{j=0}^{m2}\sum_{k=0}^{m3} a_{ijk} X^i Y^j Z^k \tag{4.1c}$$

$$0 \le m_1 \le 3\,;0 \le m_2 \le 3\,;0 \le m_3 \le 3\,; m_1 + m_2 + m_3 \le 3 \tag{4.1d}$$

Here (*x, y*) are the image coordinates, (*X, Y, Z*) are the ground coordinates, and $a_{ijk}$ is the polynomial coefficient. One of the coefficients in the denominator is a constant 1. In some cases (e.g., IKONOS), the two denominators $P_2$ and $P_4$ have the same coefficients.

The RPC may be refined directly or indirectly. Direct refining methods modify the original RPCs themselves, while indirect refining methods introduce complementary or concatenated transformations in image or object space, and do not change the original RPCs directly [Hu, Tao, Croitoru, 2004].

### 4.2.1 Indirect methods

At least 3 different types of indirect methods have been proposed:

(1) The Bias Compensation method proposes a polynomial model defined in image space to correct the RPC (equation 4.2), in which *Δp* and *Δr* are added to the rational functions to capture the discrepancies between the nominal and the measured image space coordinates [Fraser and Hanley, 2003; Grodecki and Dial 2003].

$$Line = \Delta p + p(\phi, \lambda, h) \tag{4.2a}$$

$$Sample = \Delta r + r(\phi, \lambda, h) \tag{4.2b}$$

$$\Delta p = a_0 + a_s \cdot Sample + a_L \cdot Line + a_{SL} \cdot Sample \cdot Line + a_{L2} \cdot Line^2 + a_{s2} \cdot Samples + ... \tag{4.2c}$$

$$\Delta r = b_0 + b_s \cdot Sample + b_L \cdot Line + b_{LS} \cdot Sample \cdot Line + b_{L2} \cdot Line^2 + b_{s2} \cdot Sample^2 + ... \tag{4.2d}$$

Where: *Δp*, *Δr* are the adjustable functions expressing the differences between the measured and the nominal line and sample coordinates of ground control; and ($a_i$, $b_i$) are correction coefficients.

For IKONOS, an affine transformation or a translation for the simplest case is often used [Hu, Tao, Croitoru, 2004; Grodecki and Dial 2003; Fraser. and Hanley, 2003].

$$\Delta p = a_0 + a_s \cdot Sample + a_L \cdot Line \tag{4.3a}$$

$$\Delta r = b_0 + b_s \cdot Sample + b_L \cdot Line \tag{4.3b}$$

By using an affine transformation to correct the RPC of IKONOS imagery, sub-pixel accuracy is obtained [Fraser. and. Hanley, 2003; Dial and Grodecki, 2002[b], Grodecki and Lutes, 2005], but the Bias Compensation method is effective only when the camera Field Of View (FOV) is narrow and the position and attitude errors are small [Grodecki and Dial, 2003].

(2) A polynomial model defined in the domain of object coordinates to correct RPC is also proposed by Grodecki and Dial [2003] as follows:

$$\begin{aligned} \Delta p = {} & a_0 + a_P \cdot \phi + a_L \cdot \lambda + a_H \cdot h + a_{P2} \cdot \phi^2 + a_{L2} \cdot \lambda^2 \\ & + a_{H2} \cdot h^2 + a_{PL} \cdot \phi \cdot \lambda + a_{PH} \cdot \phi \cdot h + a_{LH} \cdot \lambda \cdot h + \ldots \end{aligned} \tag{4.4a}$$

$$\begin{aligned} \Delta r = {} & b_0 + b_P \cdot \phi + b_L \cdot \lambda + b_H \cdot h + b_{P2} \cdot \phi^2 + b_{L2} \cdot \lambda^2 \\ & + b_{H2} \cdot h^2 + b_{PL} \cdot \phi \cdot \lambda + b_{PH} \cdot \phi \cdot h + b_{LH} \cdot \lambda \cdot h + \ldots \end{aligned} \tag{4.4b}$$

Where: ($\phi$, $\lambda$, $h$) are ground coordinates; and ($a_i$, $b_i$) are correction coefficients.

(3) A polynomial model defined in the domain of object coordinates to correct the ground coordinates derived from the vendor-provided RPCs, has been proposed by Di et al. [2003]. In this method, the polynomial correction parameters are determined by the GCPs:

$$X = a_0 + a_1 X_{RF} + a_2 Y_{RF} + a_3 Z_{RF} \tag{4.5a}$$

$$Y = b_0 + b_1 X_{RF} + b_2 Y_{RF} + b_3 Z_{RF} \tag{4.5b}$$

$$Z = c_0 + c_1 X_{RF} + c_2 Y_{RF} + c_3 Z_{RF} \tag{4.5c}$$

Where: ($X$, $Y$, $Z$) are the ground coordinates after correction; ($X_{RF}$, $Y_{RF}$, $Z_{RF}$) are ground coordinates derived from the RPC; and ($a_i$, $b_i$, $c_i$) are correction coefficients.

In object space, the ground coordinates do not reflect the satellite sensor's imaging geometry. Therefore the method (1) is superior to methods (2) and (3) [Grodecki and Dial, 2003; Gong, et al., 2005].

### 4.2.2 Direct Methods

Sometimes, ground control information may not be available at the time of data processing or cannot be supplied due to some reasons (e.g., politics or confidentiality) [Hu and Tao, 2002]; Sometimes, it is necessary to avoid changing the existing image transfer format. Therefore, in many cases, a modified RPC is the first choice. Methods that modify the original RPCs are referred to as direct refining methods [Hu, Tao, Croitoru, 2004]. Three such methods are described below.

(1) The first method is to compute the new rational polynomial coefficients (RPCs) using the vendor-provided RPC coefficients as initial values. This method is not stable enough to provide a sufficient accuracy in operational environments, unless a large number of densely distributed GCPs (about twice the number of unknowns) are available [Toutin, 2004; Tao and Hu, 2001; Di, Ma, and Li, 2003]. Therefore, this method is not feasible for RPC refinement [Grodecki et al., 2003; Hu, Tao, Croitoru, 2004].

(2) A Batch Iterative Least-Squares (BILS) method and an Incremental Discrete Kalman Filtering (IDKF) method have been proposed to update RPC [Hu and Tao, 2002]. It has been found that the prerequisite for obtaining good results by using these methods is that the covariance matrices for the RFCs and the image measurements (provided by the data vendor who calculated the RPC initially) are available. Moreover, a significant number of new GCPs are also required [Hu and Tao, 2002]. Experiments have shown that these methods can yield good result for aerial photography (see **Table 4.1, Table 4.2**), but the accuracy obtained for IKONOS image is not sufficient for many users (see **Table 4.3**) [Hu and Tao, 2002].

**Table 4.1 Aerial photo line and sample residuals at 40 checkpoints (unit: pixels), 9 GCPs were used [Hu and Tao, 2002].**

| GCP | BILS | | | | IDKF | | | |
|---|---|---|---|---|---|---|---|---|
| | Line | | Sample | | Line | | Sample | |
| | RMSE | MAX | RMSE | MAX | RMSE | MAX | RMSE | MAX |
| 0 | 1.134 | 3.175 | 0.909 | 2.700 | 1.134 | 3.175 | 0.909 | 2.700 |
| 9 | 0.912 | 3.054 | 0.824 | 2.092 | 1.112 | 2.827 | 0.880 | 2.464 |

**Table 4.2 Aerial photo line and sample residuals at 9 checkpoints (unit: pixels), 40 GCPs were used [Hu and Tao, 2002].**

| GCP | BILS | | | | IDKF | | | |
|---|---|---|---|---|---|---|---|---|
| | Line | | Sample | | Line | | Sample | |
| | RMSE | MAX | RMSE | MAX | RMSE | MAX | RMSE | MAX |
| 0 | 0.894 | 1.428 | 1.151 | 3.253 | 0.894 | 1.428 | 1.151 | 3.253 |
| 9 | 0.423 | 0.788 | 0.579 | 1.362 | 0.609 | 1.098 | 0.677 | 1.668 |

**Table 4.3 IKONOS image line and sample residuals at 8 checkpoints (unit: pixels), 20 GCP were used [Hu and Tao, 2002].**

| Image | GCP | BILS | | | | IDKF | | | |
|---|---|---|---|---|---|---|---|---|---|
| | | Line | | Sample | | Line | | Sample | |
| | | RMSE | MAX | RMSE | MAX | RMSE | MAX | RMSE | MAX |
| Left | 0 | 2.391 | 4.418 | 6.387 | 9.839 | 2.391 | 4.418 | 6.387 | 9.839 |
| | 20 | 2.283 | 4.764 | 3.611 | 6.856 | 2.038 | 4.456 | 3.204 | 7.195 |
| Right | 0 | 2.339 | 5.038 | 8.140 | 10.722 | 2.339 | 5.038 | 8.140 | 10.722 |
| | 20 | 2.761 | 6.058 | 4.533 | 6.543 | 2.780 | 6.105 | 3.389 | 5.999 |

(3) Bang et al., proposed 3 methods to modify the RPC [2003]: the Pseudo GCP (PG) Method, the Using Parameters Observation Equation (UPOE) method, and the Sequential Least Square Solution (SLSS) method [Bang, Jeong, Kim, 2003]. For the PG method, the RPC is imported as initial values. The additional GCPs are assigned sufficiently greater weight (compared with the Pseudo GCPs) to modify the original RPC. This method is similar to the method (1) proposed by Di et al. [2003]. For the UPOE method, 59 RPC parameter observations are used instead of the pseudo GCPs. All these three methods involve a question of how to properly assign the weightings for so many different observations, since the order and terms of the RPC coefficients have no physical meaning [Farhad, All, and Ahmad, 2005]. With regard to their accuracy, an experiment comparing these three methods proposed by Bang et al. with the Bias Compensation method showed that the accuracy of SLSS is the best among

these three methods, but is still slightly poorer than that of the Bias Compensation method (see **Table 4.4**) [Bang, Jeong, Kim, 2003].

**Table 4.4 Accuracy comparison between the PG method, the UPOE method, the SLSS method, and Bias Compensation method [Bang, Jeong, Kim, 2003].**

| Method | Num. of GCP | RMSE (Unit: pixels), case 1 | | RMSE (Unit: pixels), case 2 | |
|---|---|---|---|---|---|
| | | Column | Row | Column | Row |
| PG | 5 | 1.55 | 2.29 | 1.85 | 3.71 |
| UPOE | 5 | 1.65 | 2.62 | 1.99 | 4.16 |
| SLSS | 5 | 1.54 | 2.30 | 1.79 | 3.66 |
| Bias | 5 | 1.58 | 1.74 | 1.72 | 2.33 |

### 4.2.3 Limitation of Traditional Methods

The drawbacks, limitations and relative accuracies of the direct and indirect methods described above are summarized in the **Table 4.5**, along with a comparison of their accuracies with that of the Bias Compensation method.

**Table 4.5 Accuracies, Limitations and Drawbacks of Traditional RPC Refinement Methods**

| Method | | Accuracy, Limitations and Drawbacks |
|---|---|---|
| Indirect Methods | (1) Bias Compensation method | ▪ Accuracy appears to be the best so far.<br>▪ Effective only when the camera Field Of View (FOV) is narrow and the position and attitude errors are small [Grodecki and Dial, 2003] |
| | (2) Polynomial model defined in object space to correct the image coordinates | ▪ Accuracy is poorer than Bias Compensation method.<br>▪ Effective only when the camera Field Of View (FOV) is narrow and the position and attitude errors are small [Grodecki and Dial, 2003] |
| | (3) Polynomial model defined in object space to correct the object coordinates | ▪ Accuracy is poorer than Bias Compensation method.<br>▪ Because the ground coordinates do not reflect the satellite sensor's imaging geometry, this method is not feasible for RPC refinement [Grodecki and Dial, 2003; Gong et al., 2005]. |
| Direct Methods | (1) Directly compute the new RPCs with a large number of GCPs | ▪ This method is not stable enough and may not provide a sufficient accuracy in operational environments. It is therefore not feasible for RPC refinement [Grodecki et al., 2003; Hu et al., 2004] |
| | (2) BILS method and IDKF method | ▪ Accuracy is poorer than Bias Compensation method.<br>▪ Requires a significant number of GCPs<br>▪ Requires the covariance matrices of RPC [Hu and Tao, 2002] |
| | (3) PG Method, UPOE method, and SLSS method | ▪ Accuracy is poorer than Bias Compensation method [Bang et al., 2003].<br>▪ Difficult to assign weightings for the different observation equations. |

**Table 4.5** illustrates that, in terms of accuracy and computation stability, the Bias Compensation method is undoubtedly the best method in current use. But unfortunately, the Bias Compensation method is effective only when the camera field of view is narrow and the attitude errors are small [Grodecki and Dial, 2003]. Under these rigorous conditions, the in-track and cross-track errors are equivalent to pitch and roll attitude errors (see **Fig. 4.1**). Thus, it is only necessary to estimate roll and pitch for RPC correction [Grodecki and Dial, 2003]. But with increasing camera field of view, attitude error and off-nadir angle, the in-track and cross-track errors are no longer equivalent to pitch and roll attitude errors, and the difference (X1-X1') at the

edge of field (see **Figure 4.1**) increases according following equations [Grodecki and Dial, 2003; Dial and Grodecki, 2005].

$$d = h * (\tan(c + r) - \tan(c)) \tag{4.6}$$

$$X1 = -h * \tan(c + a) \tag{4.7}$$

$$X1' = d - h * \tan(c + a + r) \tag{4.8}$$

$$difference = X1 - X1' \tag{4.9}$$

*h*: flying height;

*c*: off-nadir angle;

*r*: attitude error; and

*a*: half-angle of the camera field of view;

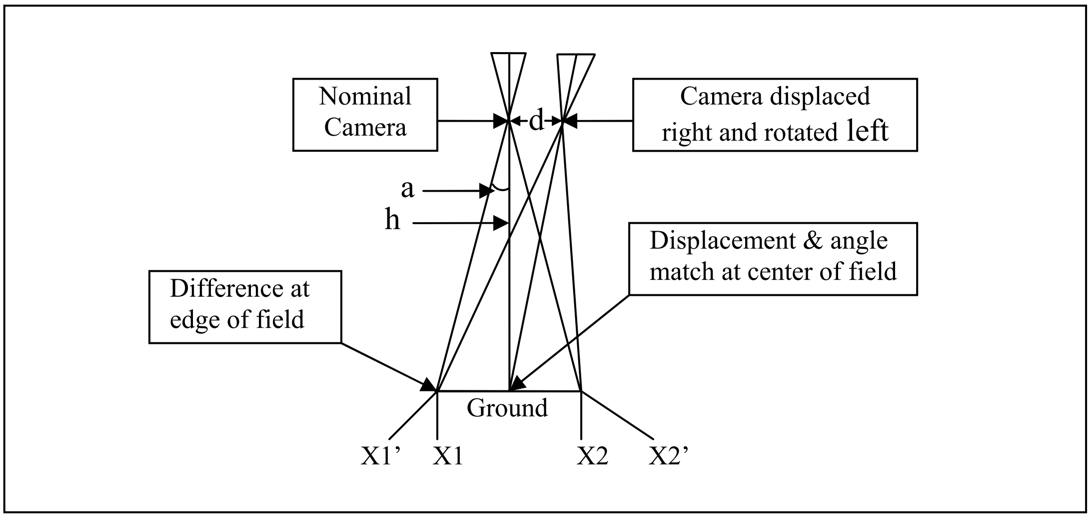


**Figure 4.1 Effect of roll and cross-track errors [Grodecki and Dial, 2003].**

**Figure 4.2, 4.3, 4.4, 4.5** show how the difference (X1-X1') at the edge of field changes with the camera field of view (FOV), the off-nadir angle, and the attitude error.

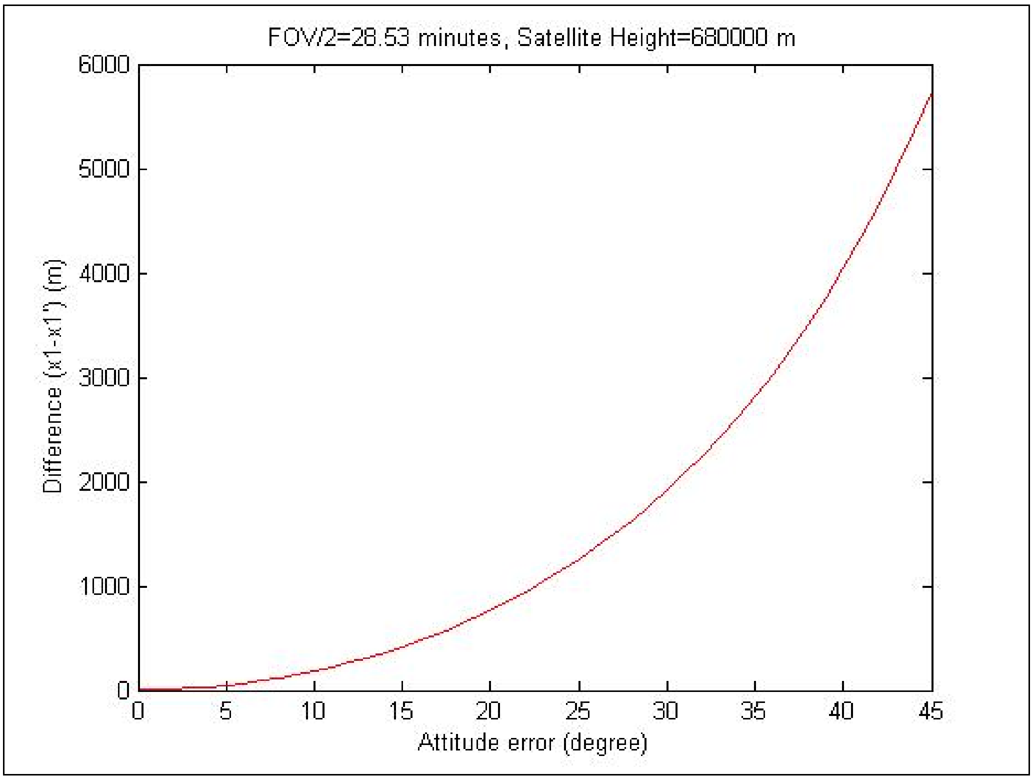


**Figure 4.2 The difference at the edge of field changes with the attitude error.**

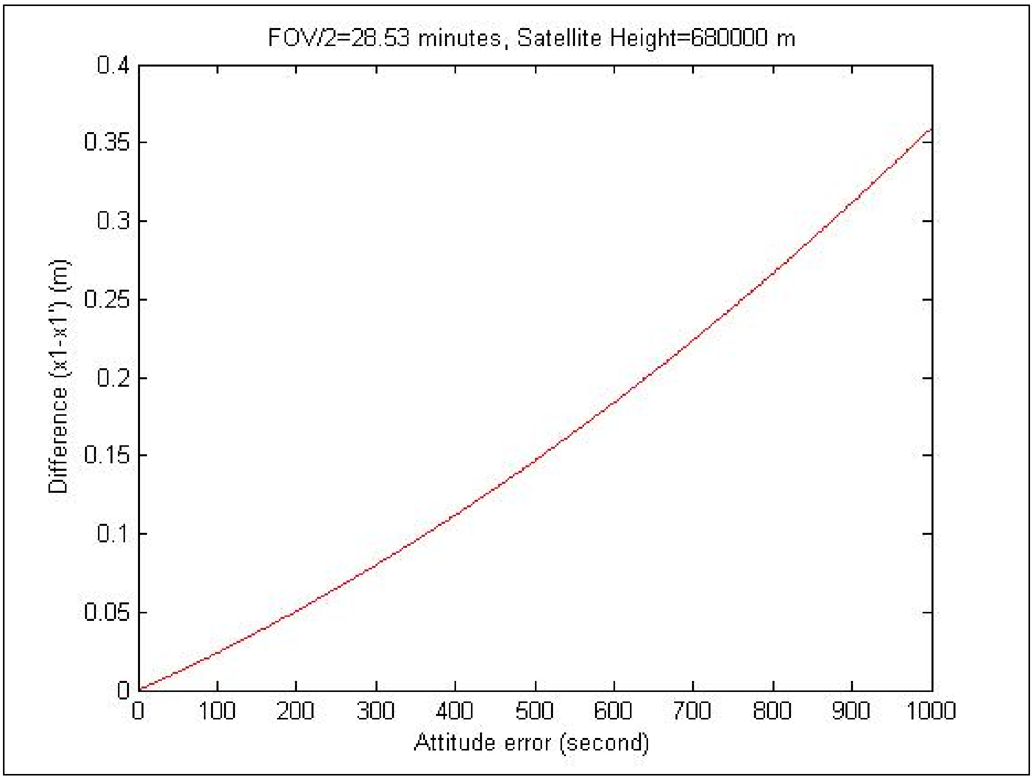


**Figure 4.3 The difference at the edge of field changes with the attitude error.**

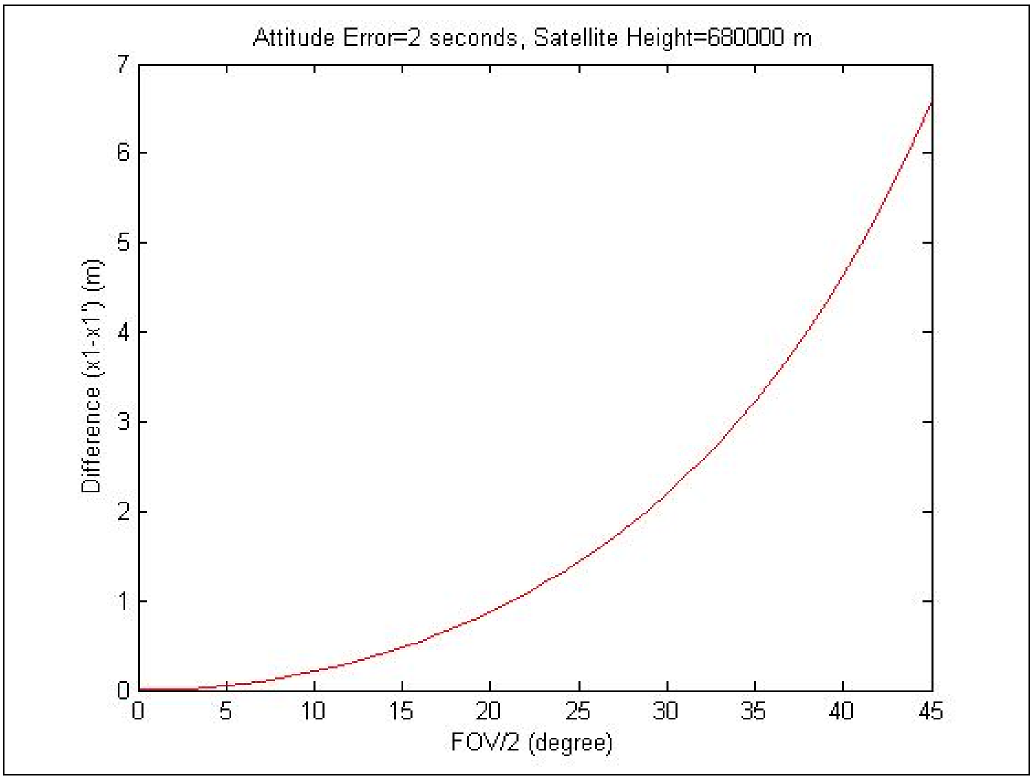


**Figure 4.4 The difference at the edge of field changes with FOV.**

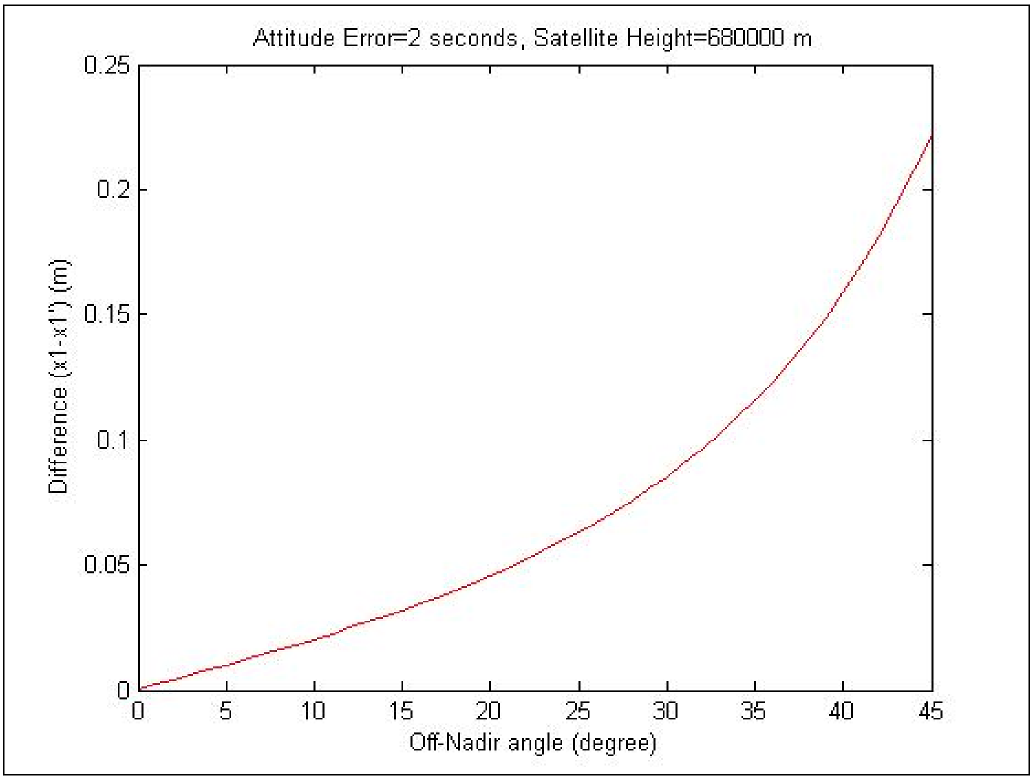


**Figure 4.5 The difference at the edge of field changes with the off-nadir angle.**

Based on **Figure 4.1, 4.2, 4.3, 4.4** and **4.5**, it is evident that the difference (X1-X1') at the edge of field increases as the width of the camera field of view, the sensor's attitude error, and the off-nadir angle increase. The attitude error is the most important factor affecting the difference (x1-x1') at the edge of the field.

For IKONOS imagery, with a roll error of 2-seconds, the difference (X1-X1') is negligible (only 0.000454 m) [Grodecki and Dial, 2003]. As a result, only a few parameters are required to effectively model the sensor errors [Grodecki and Dial, 2003]. That is why the Bias Compensation method can achieve success in RPC refinement for IKONOS and QuickBird images. It is the desire to obtain a RPC refinement method that will be effective under a wider variety of image conditions and sensor platforms that led the authors to develop the Generic Method for RPC refinement.

## 4.3 The Proposed Method

The generic method proposed in this report consists of three components (see **Fig. 4.6**). (1) Reconstruct the sensor's position and attitude. This involves restoring the pseudo light ray that existed when the image was acquired. The sensor's pseudo position and attitude (equivalent to camera Exterior Parameters (EPs)) are obtained. (2) Adjust the sensor's position and attitude. The GCPs are used to refine the EPs. (3) Generate a new RPC. The new RPC is generated using a grid of image points.

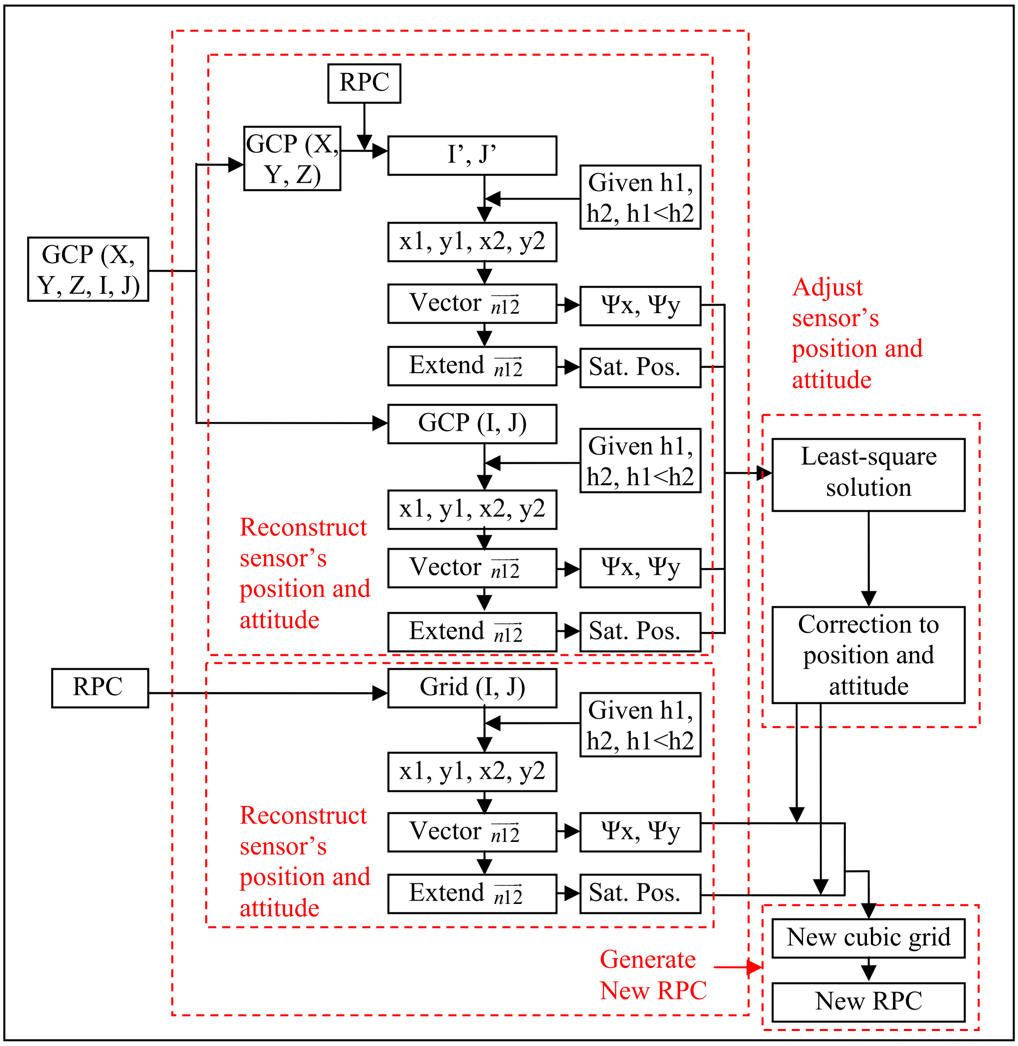


**Figure 4.6 Flowchart of RPC refinement.**

<u>Reconstructing the Sensor's Position and Attitude</u>

**Step 1.** From a point on the image P(I, J), given an elevation value (h1), the corresponding ground position P1(x1, y1) of the point P(I, J) can be obtained by an iterative process (see **Figure 4.7**). For the same image point P(I, J), given another elevation value (h2), h2>h1, another ground point P2(x2, y2) is obtained. Then for the point P(I, J) on the image, two corresponding ground points P1(x1, y1, h1) and P2(x2, y2, h2) are obtained. A vector $\overrightarrow{n12}$ from point P1(x1, y1, h1) to point P2(x2, y2, h2) can be calculated (see **Figure 4.8**). If this vector were the light ray of the

sensor in acquiring the image point P(I, J), the sensor position Ps1(Xs1, Ys1, Hs1) can be obtained from the extension of this vector. The sensor height Hs is a fixed value. For a satellite, Hs will be large, e.g., 600km. If the height is low, a small discrepancies with the x and y ($\varepsilon_x$, $\varepsilon_y$) will lead to a large correction to the two rotation angles $\psi_x$ and $\psi_y$. For an airborne remote sensing system, this height may be several thousand meters.

Of course, this vector is not the actual light ray by which the image point P(I, J) was acquired. Instead it is a pseudo light ray and sensor position Ps1(Xs1, Ys1, Hs1) is a pseudo sensor position. Fortunately, it does not matter whether the light ray is the actual one or not. Even a pseudo light ray and pseudo sensor position are effective for the RPC refinement in the proposed Generic method.

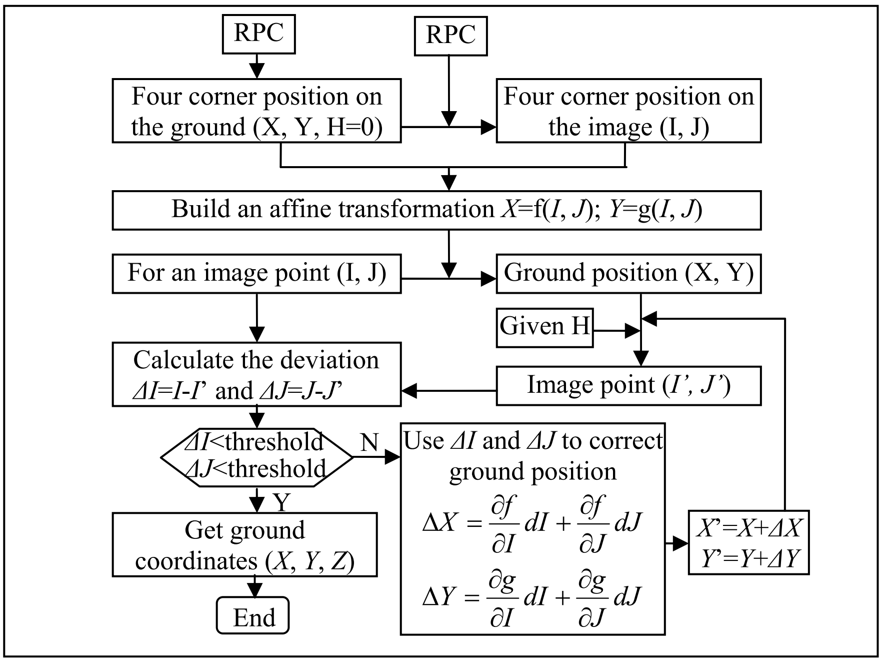


**Figure 4.7 Flow chart of ground position (X, Y, H) calculation from image position (i, j) based on RPC.**

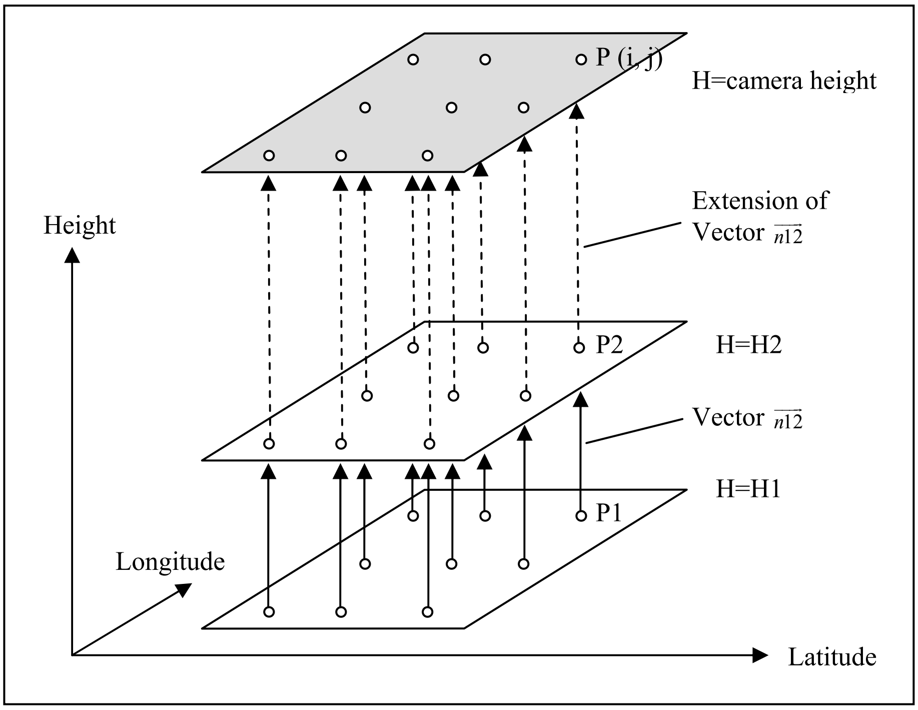


**Figure 4.8 Restoration of sensor's attitude and light ray.**

From vector $\overrightarrow{n12}$, vector $\overrightarrow{n21}$ can be obtained. From vector $\overrightarrow{n21}$, two tilted angles in x and y directions $\Psi x$ and $\Psi y$ can be obtained (see **Figure 4.9**). For high-resolution satellite images, the azimuth accuracy is very high, so the rotation angle $\Psi z$ is very small. Therefore its initial value can be set '0'. For an airborne sensor, the azimuth angle should be estimated according to GCPs and other supplemental information.

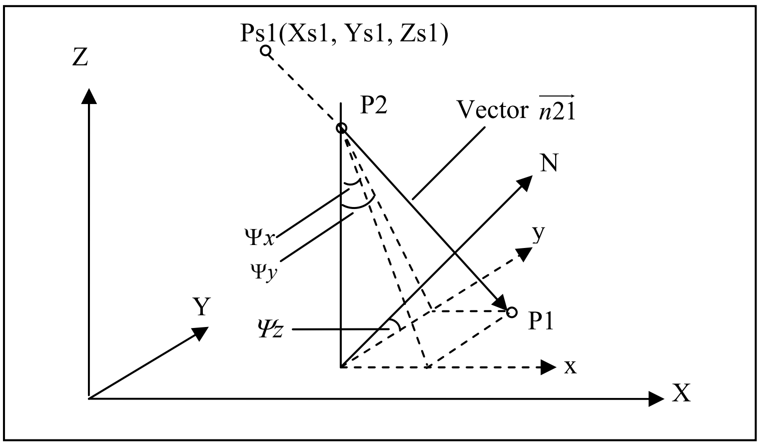


**Figure 4.9 Restoration of sensor's position and attitude.**

Up to now, for an image point P(I, J), the preceding calculations have provided corresponding pseudo sensor position Ps1(Xs1, Ys1, Hs1) and three rotation angles around the x, y, and z axis $\Psi y$ , $\Psi x$ and $\Psi z$.

<u>Adjusting the Sensor's Position and Attitude</u>

**Step 2.** For every GCP, its corresponding pseudo sensor position (*Xs, Ys, Hs*) and three rotation angles $\Psi y$ , $\Psi x$ and $\Psi z$ are calculated.

**Step 3.** The RPC adjustment observation equations for each GCP are constructed as follows.

$$(\hat{X}s + (\hat{H}s - h_i) * \tan(\hat{\psi}_x)) * \cos(\hat{\psi}_z) + (\hat{Y}s + (\hat{H}s - h_i) * \tan(\hat{\psi}_y)) * \sin(\hat{\psi}_z) - x_i + \varepsilon x_i = 0 \tag{4.10}$$

$$-(\hat{X}s + (\hat{H}s - h_i) * \tan(\hat{\psi}_x)) * \sin(\hat{\psi}_z) + (\hat{Y}s + (\hat{H}s - h_i) * \tan(\hat{\psi}_y)) * \cos(\hat{\psi}_z) - y_i + \varepsilon y_i = 0 \tag{4.11}$$

$$\hat{X}s = Xs + \Delta Xs \tag{4.12}$$

$$\hat{Y}s = Ys + \Delta Ys \tag{4.13}$$

$$\hat{H}s = Hs + \Delta Hs \tag{4.14}$$

$$\hat{\psi}_x = \psi_x + \Delta\psi_x \tag{4.15}$$

$$\hat{\psi}_y = \psi_y + \Delta\psi_y \tag{4.16}$$

$$\hat{\psi}_z = \psi_z + \Delta\psi_z \tag{4.17}$$

*Xs, Ys, Hs* are pseudo sensor position;

$x_i$, $y_i$, $h_i$ are ground coordinates of i$^{th}$ GCP; and

$\psi_x$, $\psi_y$, and $\psi_z$ are rotation angles of the vector corresponding to the i$^{th}$ GCP.

In these observation equations, the satellite position (*Xs, Ys, Hs*) and three rotation angles ($\psi_x$, $\psi_y$, $\psi_z$) are adjustable parameters.

Because the sensor's position and attitude changes with time in a pushbroom remote sensing system, we are proposing to use a polynomial model defined in the domain of image coordinates to represent the adjustable function *ΔXs, ΔYs, ΔHs,* $\Delta\psi_x$, $\Delta\psi_y$, and $\Delta\psi_z$. Although a higher order polynomial may achieve higher internal accuracy, this higher internal accuracy normally may not lead to a more accurate RPC, because the RPC is a mathematical function that is only an approximation of a rigorous physical model. Experiments by the authors have shown that the higher the order of the polynomial model, the greater the amount of the accuracy that will be lost after the approximation of the new RPC generation. Therefore, we are proposing to use a linear polynomial model for RPC refinement:

$$\Delta Xs = a_0 + a_S * Sample + a_L * Line \qquad (4.18)$$

$$\Delta Ys = b_0 + b_S * Sample + b_L * Line \qquad (4.19)$$

$$\Delta Hs = c_0 + c_S * Sample + c_L * Line \qquad (4.20)$$

$$\Delta\psi_x = d_0 + d_S * Sample + d_L * Line \qquad (4.21)$$

$$\Delta\psi_y = e_0 + e_S * Sample + e_L * Line \qquad (4.22)$$

$$\Delta\psi_z = f_0 + f_S * Sample + f_L * Line \qquad (4.23)$$

For high-resolution images obtained from satellites such as IKONOS and QuickBird, the errors in satellite height and yaw angle are very small [Grodecki and Dial, 2003]. Therefore, *ΔXs, ΔYs,* $\Delta\psi_x$, and $\Delta\psi_y$ can provide enough information to accurately correct the satellite's position and attitude. In this research, when fewer than 3 GCPs are used for RPC refinement, only the translations $a_0$, $b_0$,, $d_0$, $e_0$ are considered. When 3 to 9 GCPs are used, $a_i$, $b_i$, $d_i$, and $e_i$, are considered. According to our experiments, for IKONOS and QuickBird, all 12 parameters are considered only when: a) the number of GCPs is large enough (50 or more); b) the GCPs are distributed uniformly; and c) the GCP's accuracy is good enough (at least sub-pixel). Otherwise, too many parameters may be generated with a resultant loss of accuracy. We solve these parameters in the following order: ($d_i$, $e_i$, $f_i$) for $\Delta\psi_x$, $\Delta\psi_y$ and $\Delta\psi_z$; ($a_i$, $b_i$, $c_i$) for $\Delta Xs$, $\Delta Ys$ and $\Delta Hs$.

Generating the New RPC

**Step 4.** In order to generate a new RPC, a grid of image points is used to calculate corresponding pseudo sensor positions and attitude angles. These are adjusted according to equations (4.18) through (4.23).

**Step 5.** After the sensor positions and attitude angles corresponding to a grid of image points have been adjusted with equations (4.18~4.23), a set of cubic points is generated with these new vectors. The new RPC is generated using these cubic points.

## 4.4 Experiment

In order to evaluate the Generic method, we designed two sets of experiments. First, we used SPOT5 and IKONOS image data to test the Generic method and compare the results with that of the Bias Compensation method under the condition of narrow field view and small ephemeris and attitude errors. We then designed another set of experiments using simulated SPOT5 data generated by adding errors to the ephemeris and the attitude data. We used this simulated data to compare the Generic method and the Bias Compensation method, and to determine the Generic method's capability under a variety of different conditions.

### 4.4.1 Experiment Set 1

In this set of experiments, SPOT5 and IKONOS image data were used to test the capability of the Generic method under the condition of narrow field of view and small position and attitude errors.

#### (1) SPOT5 Data

In the SPOT5 image, there are total of 37 GCPs. We used 1, 3, and 7 GCPs to refine the RPC respectively. The other 36, 34, and 30 ground control points were used as check points. **Figure 4.10, 4.11,** and **4.12** show the distributions of GCPs and check points on the SPOT5 image in 3 of the test cases.

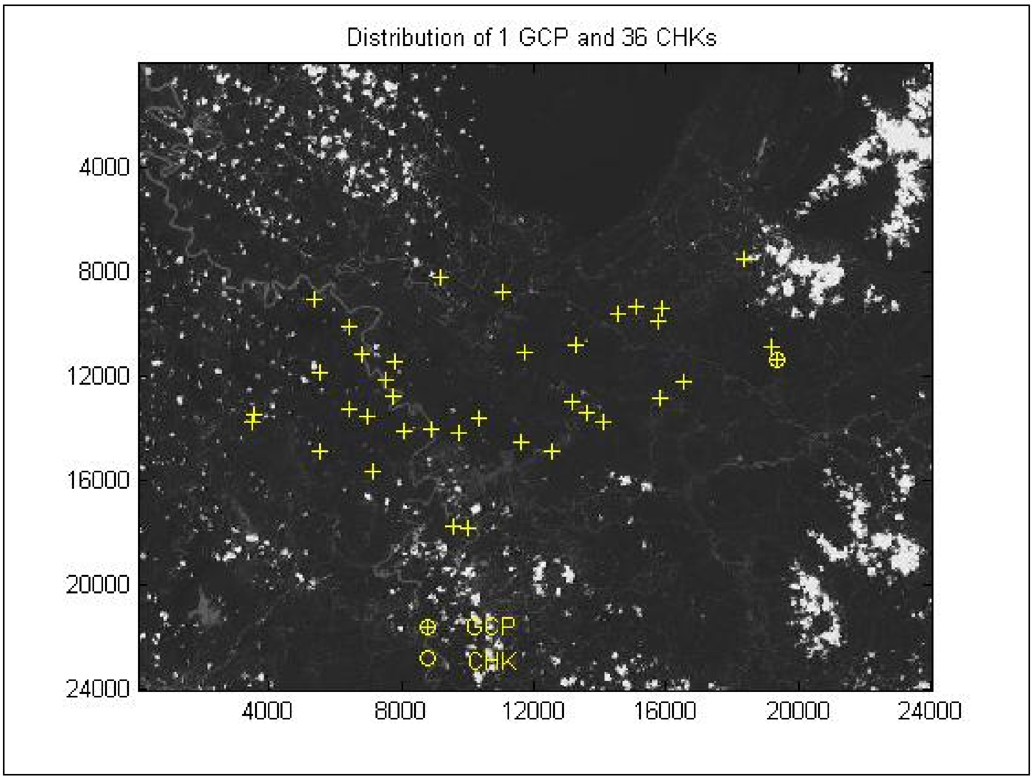


**Figure 4.10 Distribution of 1 GCP and 36 CHK points on SPOT5 image.**

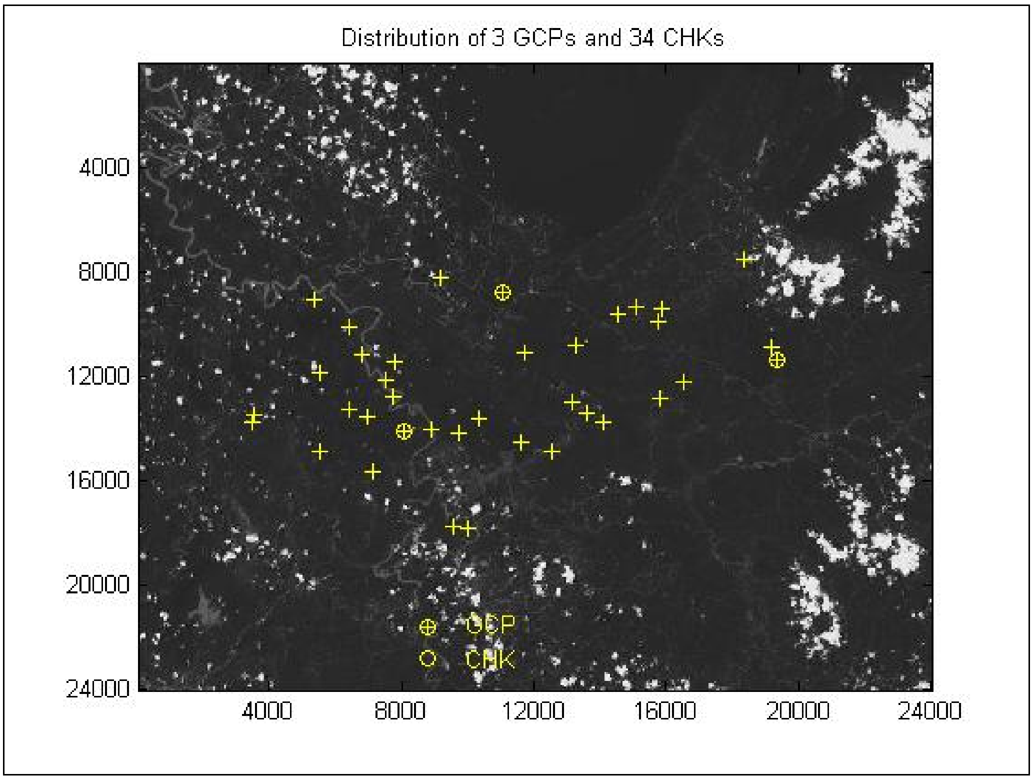


**Figure 4.11 Distribution of 3 GCPs and 34 CHK points on SPOT5 image.**

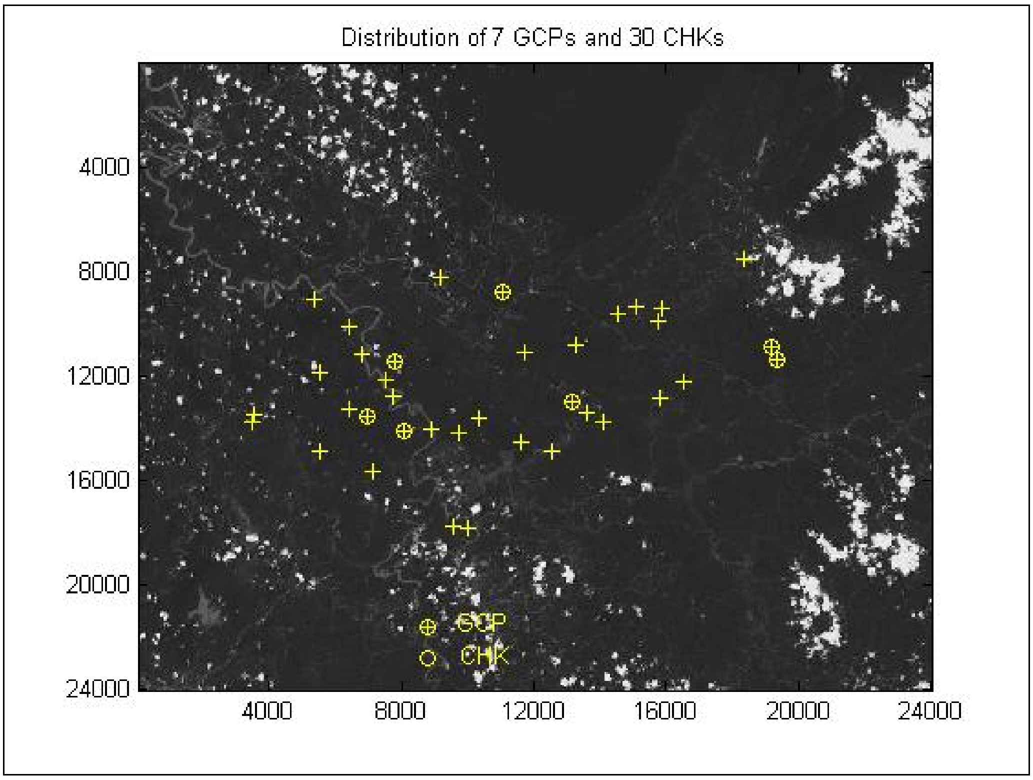


**Figure 4.12 Distribution of 7 GCP and 30 CHK points on SPOT5 image.**

The coordinates and image coordinate residue of ground control points before RPC Refinement are listed in **Appendix VII-Table 1**.

**Appendix VII-Table 2,** and **Table 3** list the image coordinate residue of 36, 34, and 30 CHK points after RPC refinement with 1, 3, and 7 GCPs by the Bias Compensation method and the Generic method respectively.

**FIG. 4.13** shows the image coordinate residue of 37 control points before RPC refinement.

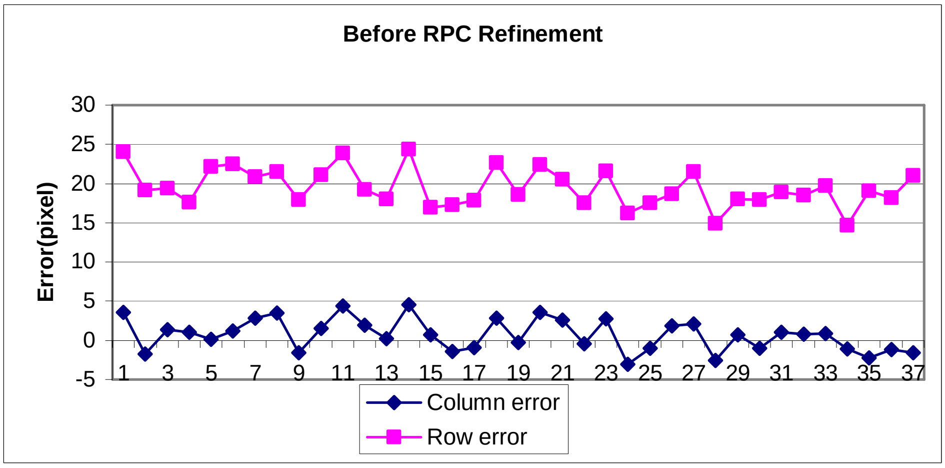


**Figure 4.13 Image Coordinate Residuals of 37 control points before RPC refinement.**

**FIG. 4.14 ~ 4.19** show the image coordinate residue of CHK points after RPC refinement with 1, 3, 7 GCPs by the Bias method and the Generic method respectively.

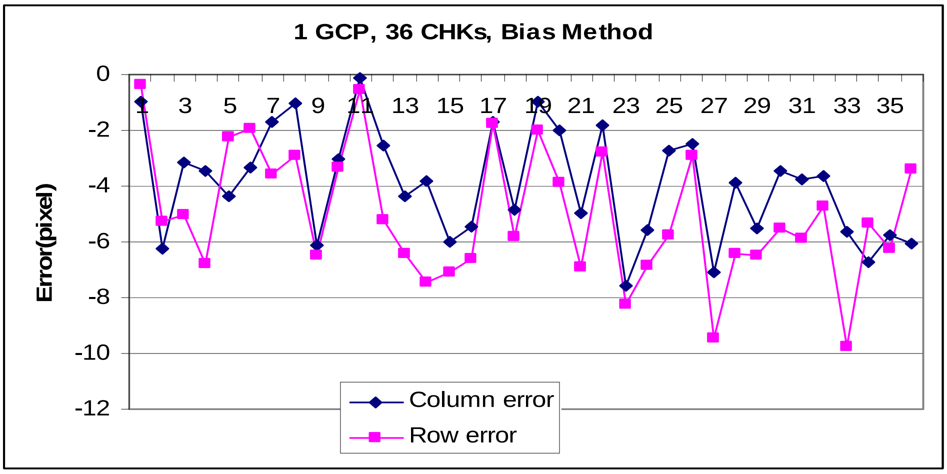


**Figure 4.14 Image Coordinate Residuals of 36 CHK points after RPC refinement with 1 GCP by the Bias method.**

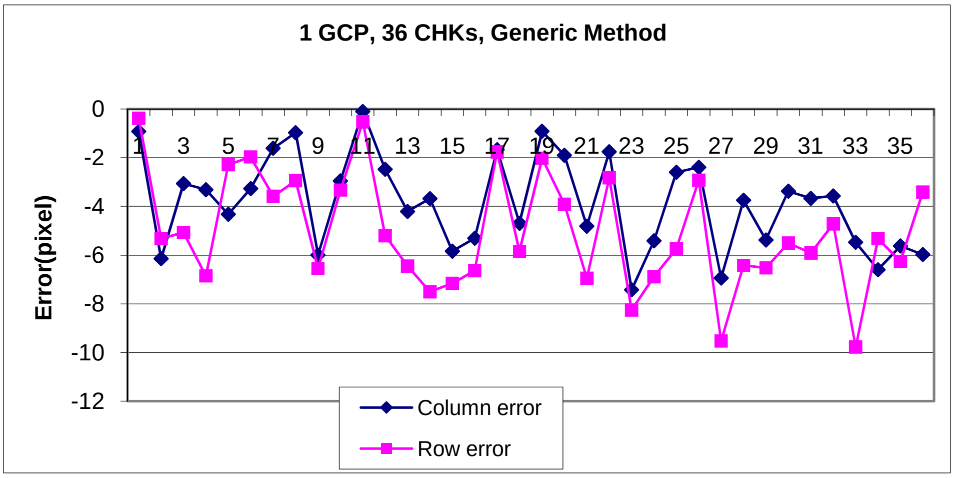


**Figure 4.15 Image Coordinate Residuals of 36 CHK points after RPC refinement with 1 GCP by the Generic method.**

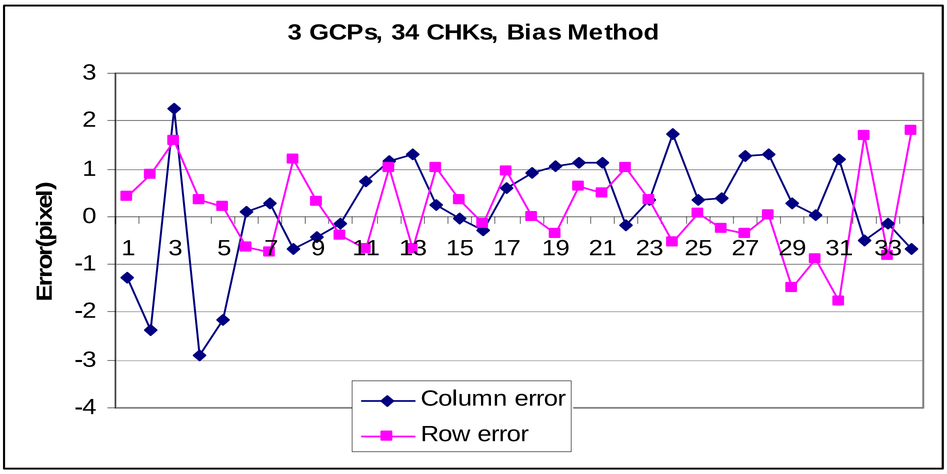


**Figure 4.16 Image Coordinate Residuals of 34 CHK points after RPC refinement with 3 GCPs by the Bias method.**

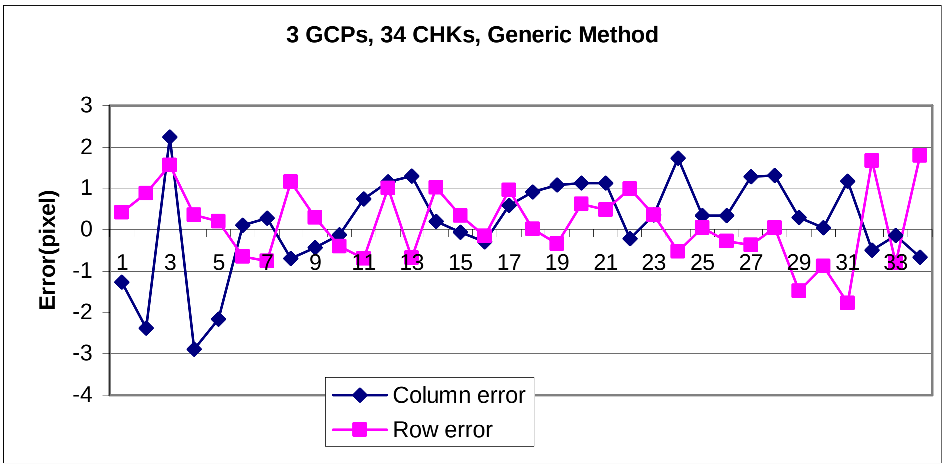


**Figure 4.17 Image Coordinate Residuals of 34 CHK points after RPC refinement with 3 GCPs by the Generic method.**

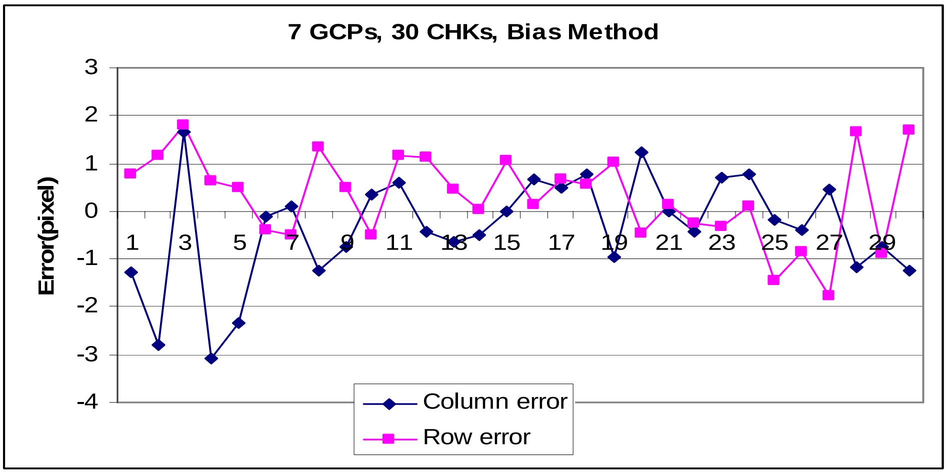


**Figure 4.18 Image Coordinate Residuals of 30 CHK points after RPC refinement with 7 GCPs by the Bias method.**

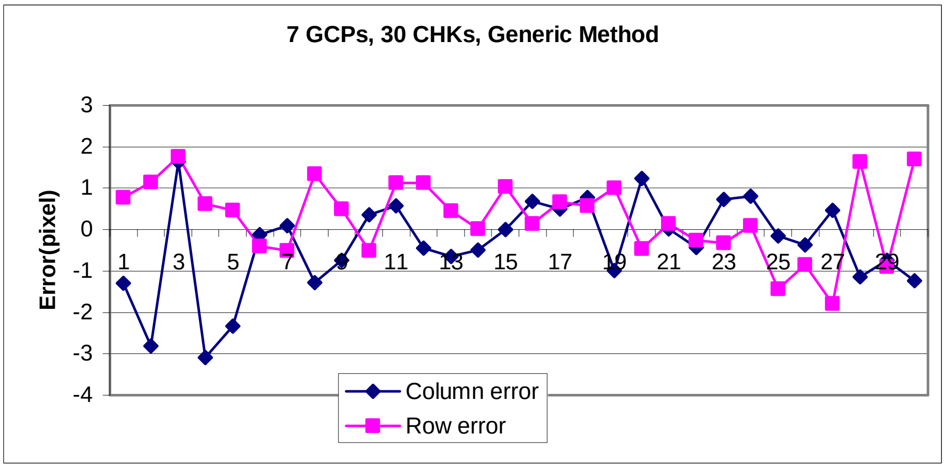


**Figure 4.19 Image Coordinate Residuals of 30 CHK points after RPC refinement with 7 GCP by the Generic method.**

**FIG. 4.20** plots the positions of the 37 GCPs within the image and shows their respective horizontal errors before RPC refinement.

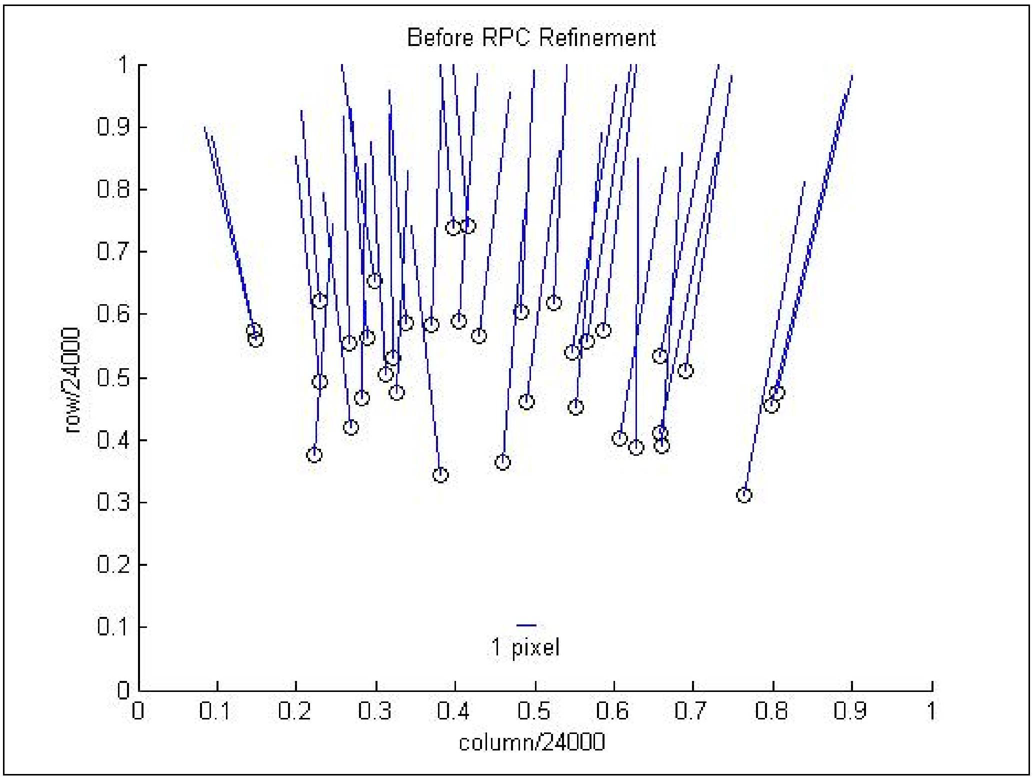


**Figure 4.20 Horizontal errors of 37 GCPs before RPC refinement.**

**FIG. 4.21 ~ 4.26** are also plots of the 37 GCPs within the image and illustrate the horizontal errors of 36, 34, 30 CHK points after RPC refinement with 1, 3, 7 GCPs by the Bias method and the Generic method respectively.

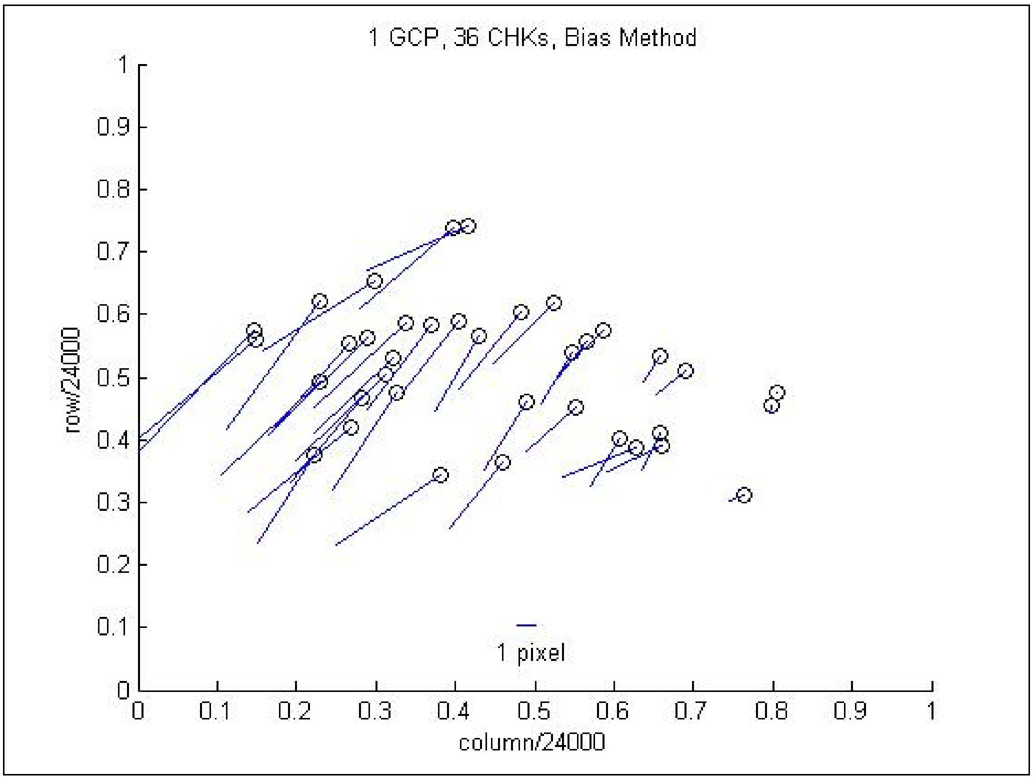


**Figure 4.21 Horizontal errors of 36 CHKs after RPC refinement with 1 GCP by the Bias method.**

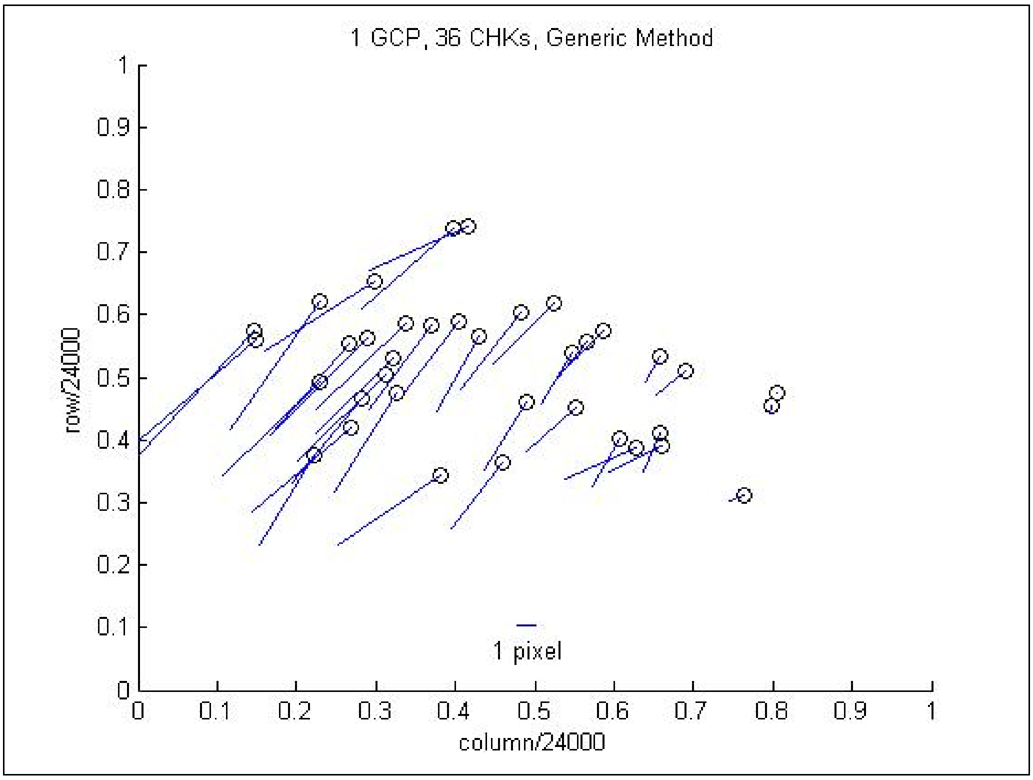


**Figure 4.22 Horizontal errors of 36 CHKs after RPC refinement with 1 GCP by the Generic method.**

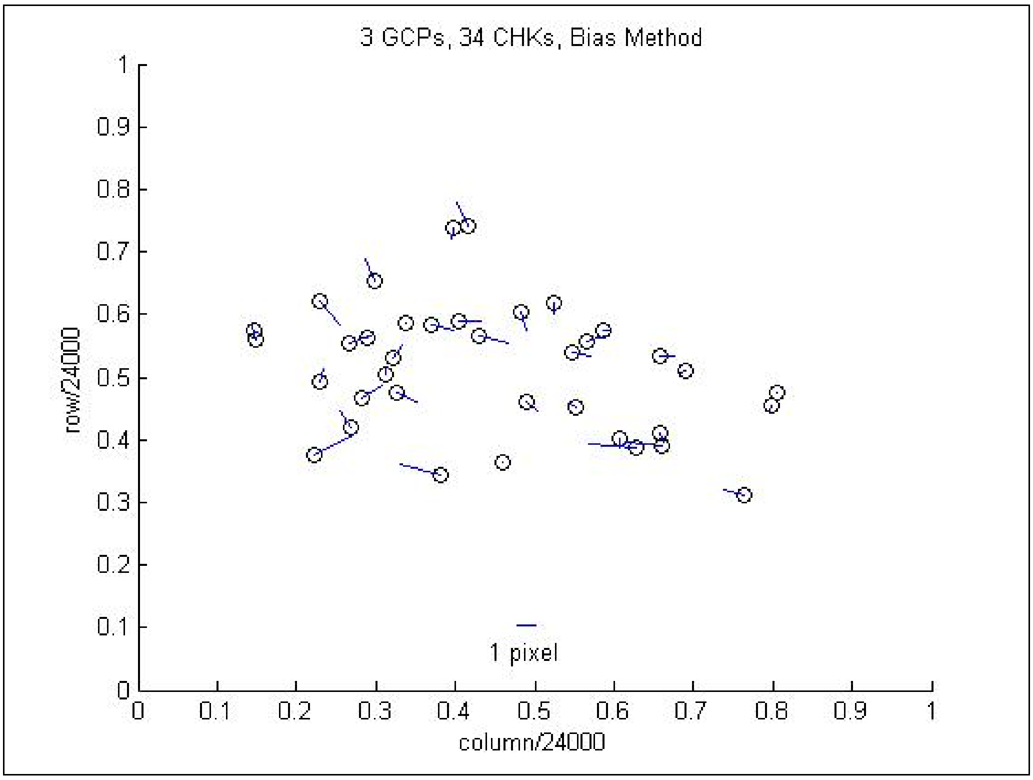


**Figure 4.23 Horizontal errors of 34 CHKs after RPC refinement with 3 GCPs by the Bias method.**

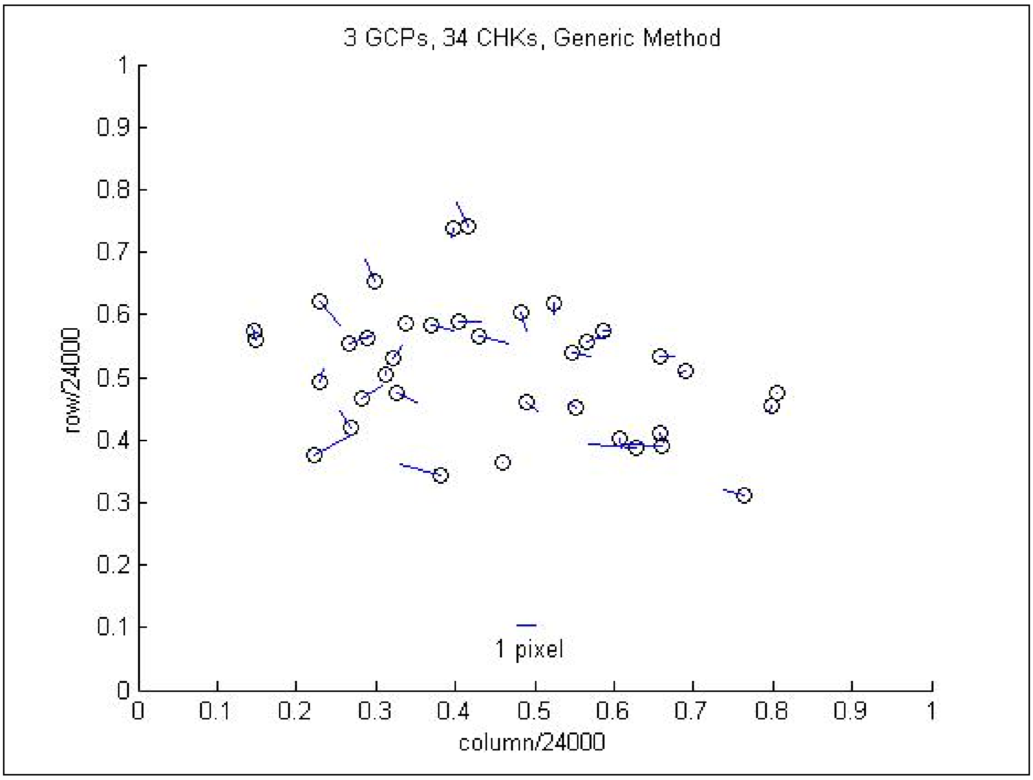


**Figure 4.24 Horizontal errors of 34 CHKs after RPC refinement with 3 GCPs by the Generic method.**

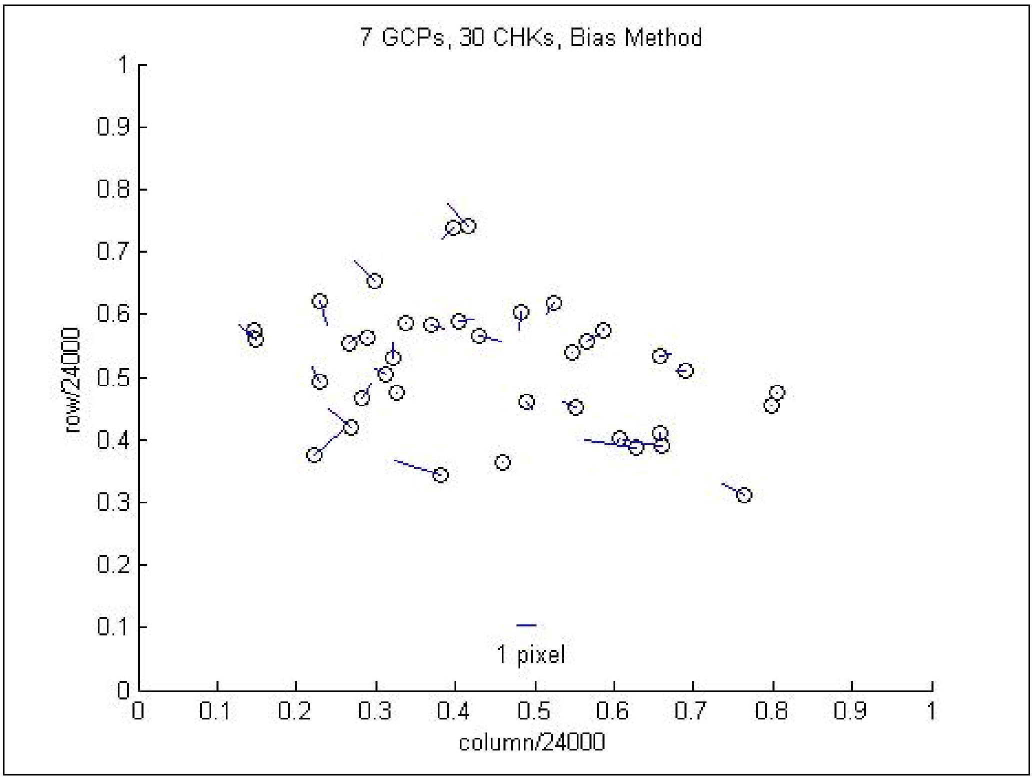


**Figure 4.25 Horizontal errors of 30 CHKs after RPC refinement with 7 GCPs by the Bias method.**

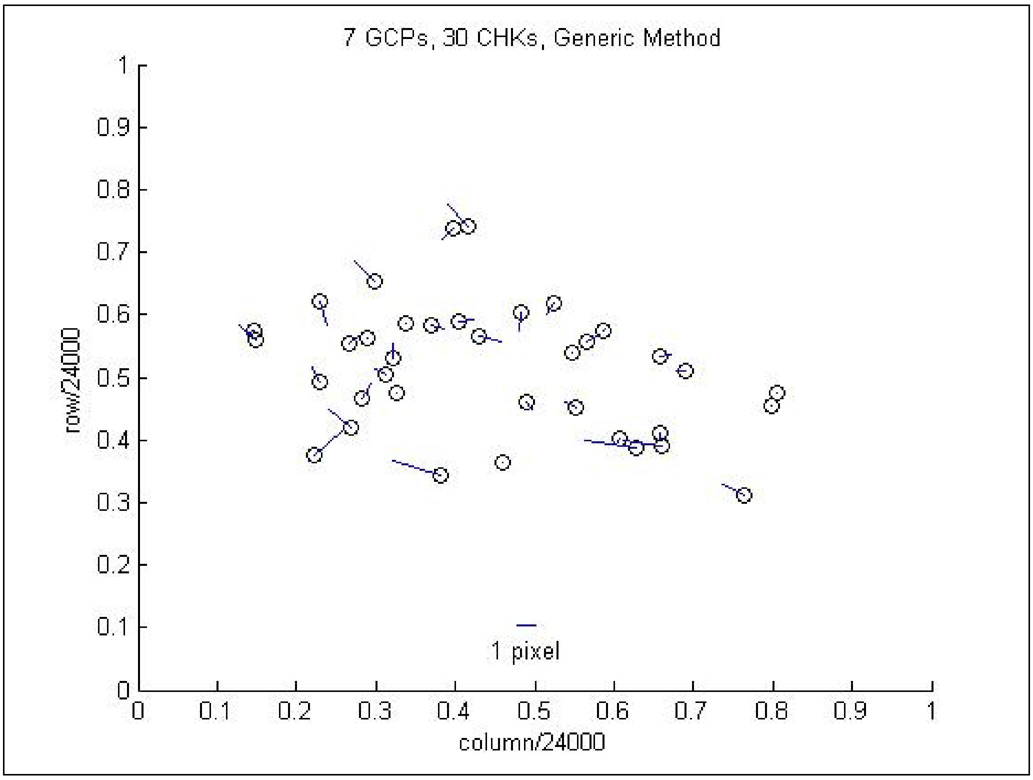


**Figure 4.26 Horizontal errors of 30 CHKs after RPC refinement with 7 GCPs by the Generic method.**

**Table 4.6** lists the accuracy comparison between the Bias method and Generic method using SPOT5 image data in 5 cases. **Figure 4.27**shows the accuracy comparison between the Bias method and Generic method using SPOT5 image data in case 1, 2, 3, and 4

**Table 4.6 Accuracy comparison between the Bias method and Generic method by using SPOT5 image data in 5 cases**

| Case | No. of GCPs (No. of CHKs) | Generic method | | Bias method | |
|---|---|---|---|---|---|
| | | Col. RMSE (pixel) | Row RMSE (pixel) | Col. RMSE (pixel) | Row RMSE (pixel) |
| 0 | 0 (37) | 2.12 | 19.65 | 2.12 | 19.65 |
| 1 | 1 (36) | 4.28 | 5.57 | 4.38 | 5.54 |
| 2 | 3 (34) | 1.13 | 0.86 | 1.13 | 0.87 |
| 3 | 7 (30) | 1.15 | 0.95 | 1.15 | 0.95 |
| 4 | 37 (0) | 0.91 | 0.70 | 0.99 | 0.76 |

Note: Col. – Column; RMSE – Root Mean Square Error

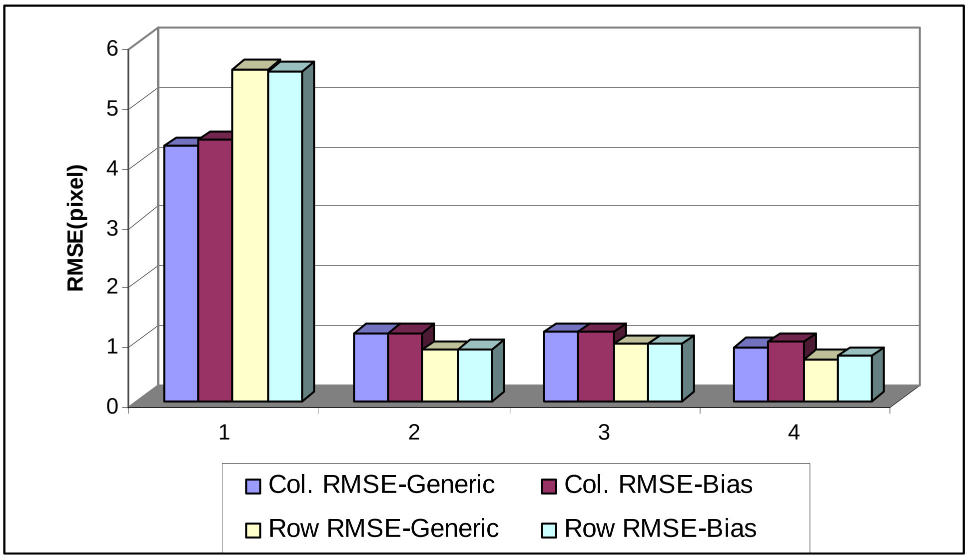


**Figure 4.27 Accuracy comparison between the Bias method and Generic method by using SPOT5 image data in case 1, 2, 3, and 4**

**Table 4.6** and **Figure 4.27** illustrate that the accuracy of the Generic method and the Bias Compensation method are quite similar when the field of view is narrow and the ephemeris and attitude errors are small. The largest difference between the accuracy of the Generic method and the accuracy of the Bias Compensation method is less than 0.1 pixels.

### (2) IKONOS Data

An IKONOS image was also used in this research. There were at total of 113 GCPs in this test field. Initially we used only 1 GCP to refine the RPC. The other 112 ground control points were used as check points. In the second test, 9 GCPs were used to refine RPC, and the other 104 ground control points were used as check points. **Figure 4.28 and 4.29** show the distributions of GCPs and check points on IKONOS image in 2 cases.

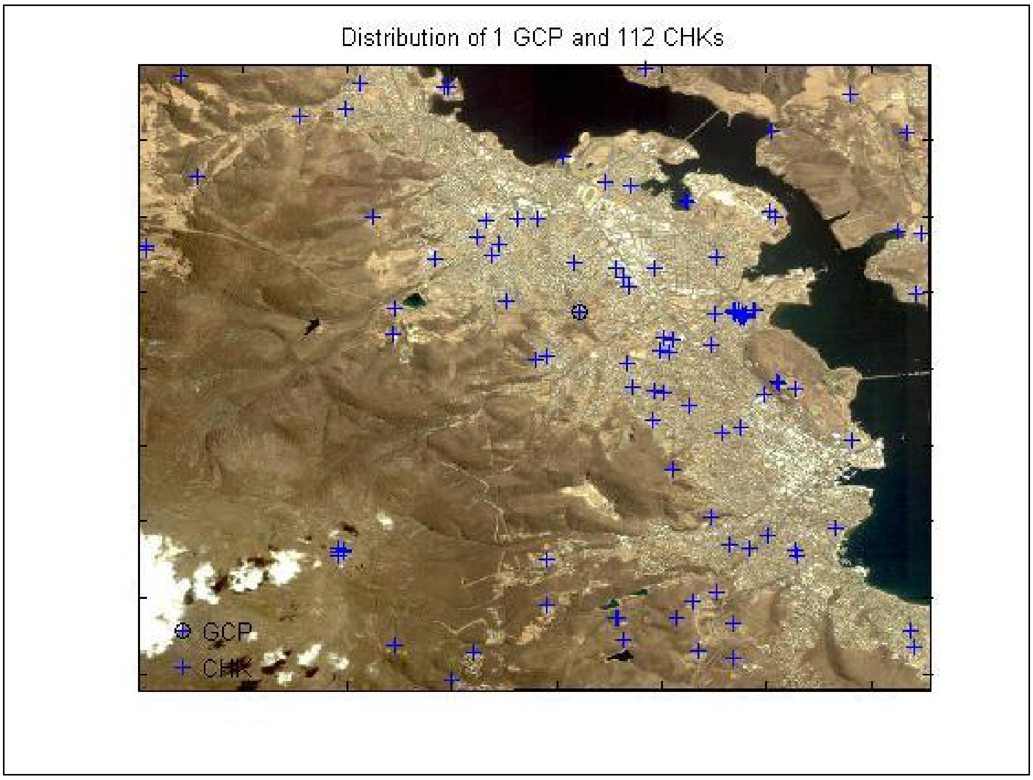


**Figure 4.28 Distribution of 1 GCP and 112 CHK points on IKONOS image.**

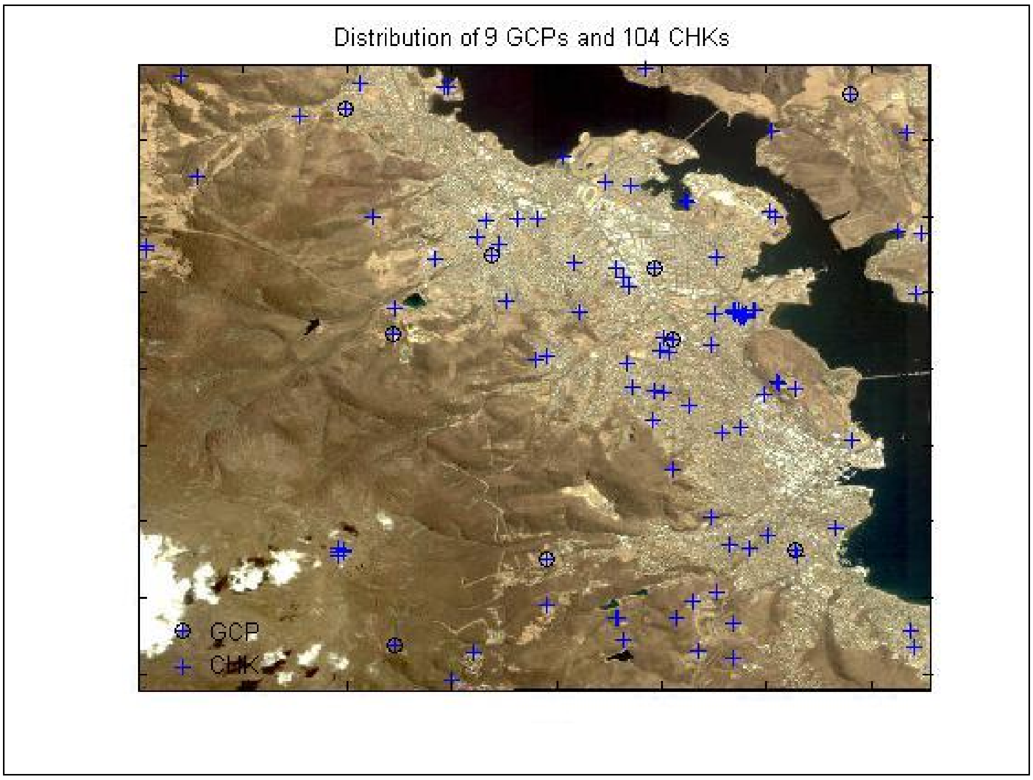


**Figure 4.29 Distribution of 9 GCPs and 104 CHK points on IKONOS image.**

**Appendix VII Table 4** lists the coordinates of 113 Ground Control Points on the IKONOS image.

**Appendix VII Table 5** and **Table 6** list the coordinate residue of 112, 104 CHK points after RPC refinement with 1 and 9 GCPs by the Bias method and the Generic method respectively.

**FIG. 4.30** and **FIG. 4.31** show the image coordinate residuals of 112 CHK points after RPC refinement with 1 GCP by the Bias method and the Generic method respectively. **FIG. 4.32** and **FIG. 4.33** illustrate the image coordinate residue of 104 CHK points after RPC refinement with 9 GCPs by the Bias method and the Generic method respectively.

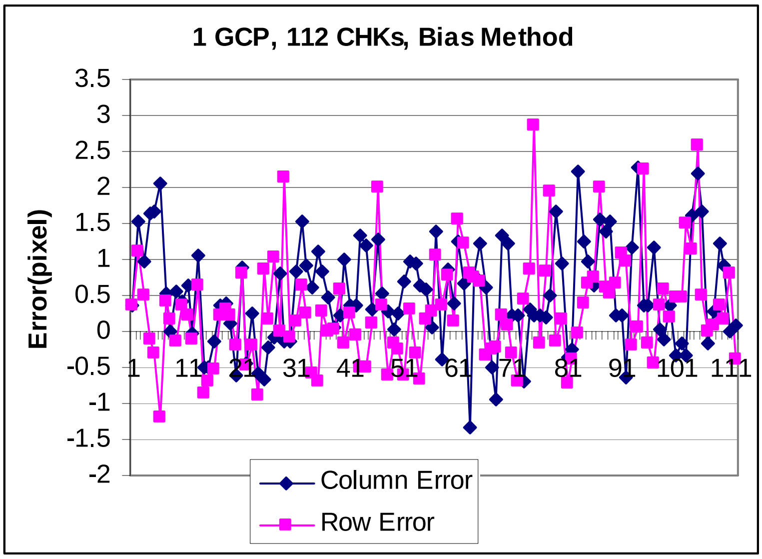


**Figure 4.30 Image Coordinate Residuals of 112 CHK points after RPC refinement with 1 GCP by the Bias method.**

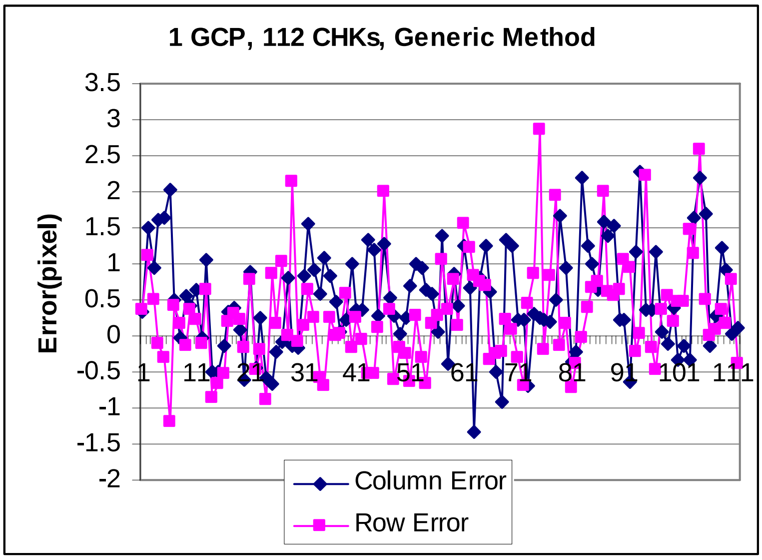


**Figure 4.31 Image Coordinate Residuals of 112 CHK points after RPC refinement with 1 GCP by the Generic method.**

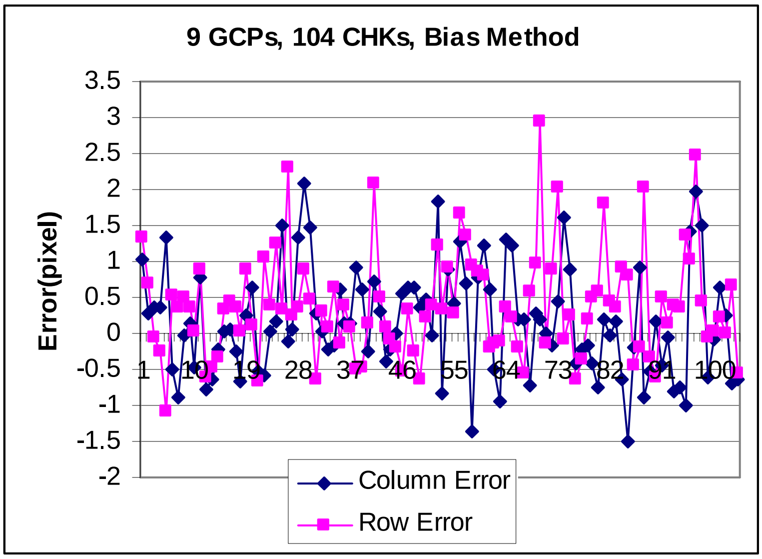


**Figure 4.32 Image Coordinate Residuals of 104 CHK points after RPC refinement with 9 GCPs by the Bias method.**

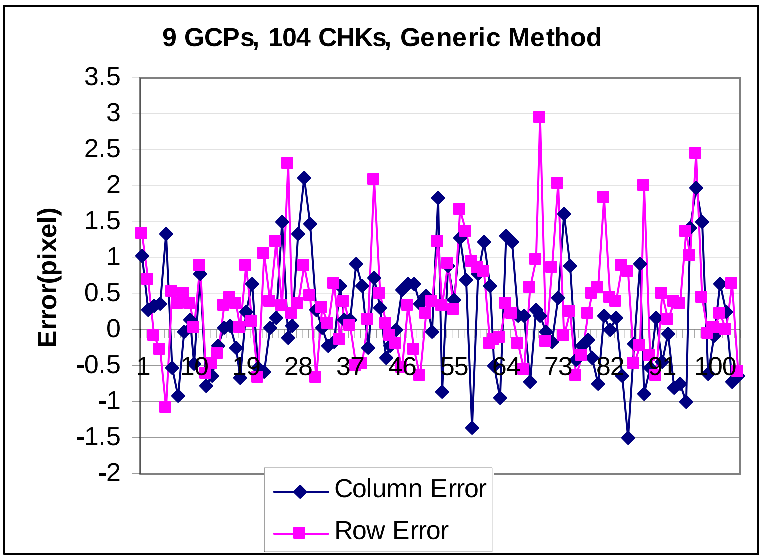


**Figure 4.33 Image Coordinate Residuals of 104 CHK points after RPC refinement with 9 GCPs by the Generic method.**

**FIG. 4.34** and **FIG. 4.35** illustrate the horizontal errors of 112 CHK points after RPC refinement with 1 GCP by the Bias method and the Generic method respectively. **FIG. 4.36** and **FIG. 4.37** show the horizontal errors of 104 CHK points after RPC refinement with 9 GCPs by the Bias method and the Generic method respectively.

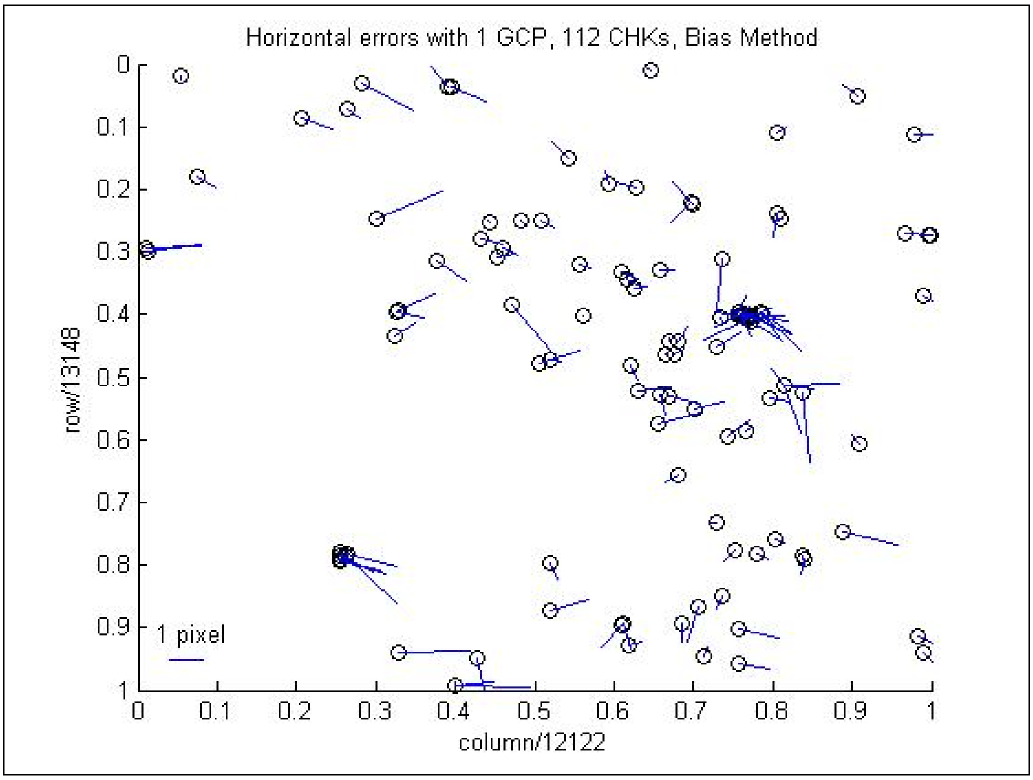

**Figure 4.34 Horizontal errors of 112 CHK points after RPC refinement with 1 GCP by the Bias method.**

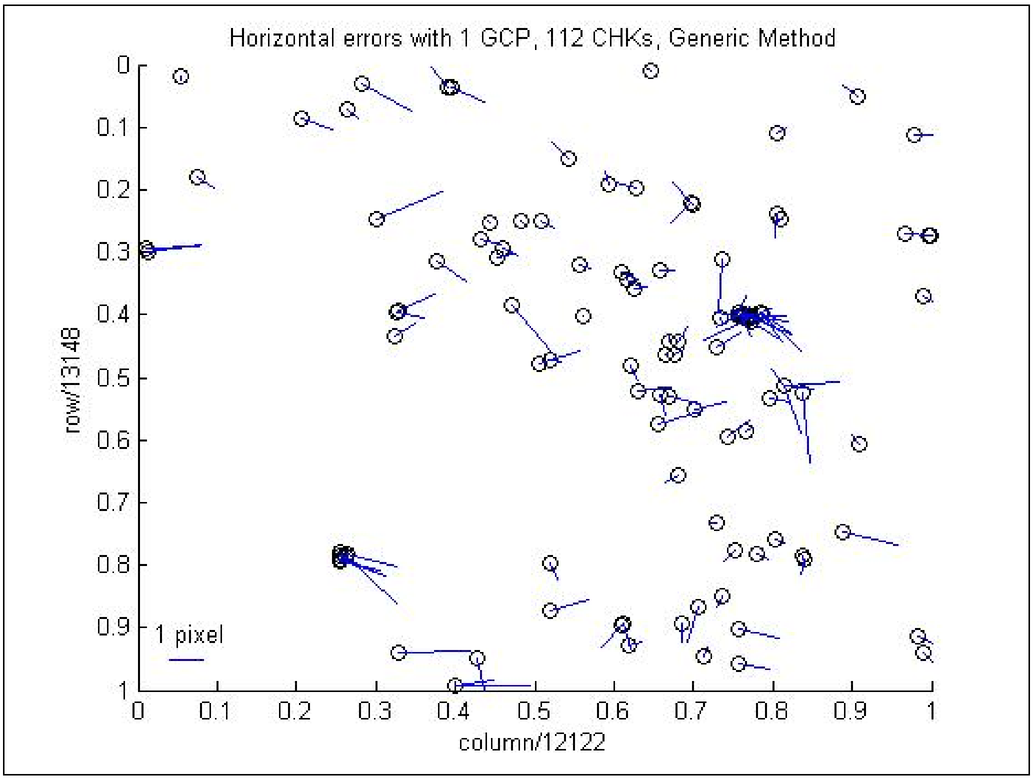

**Figure 4.35 Horizontal errors of 112 CHK points after RPC refinement with 1 GCP by the Generic method.**

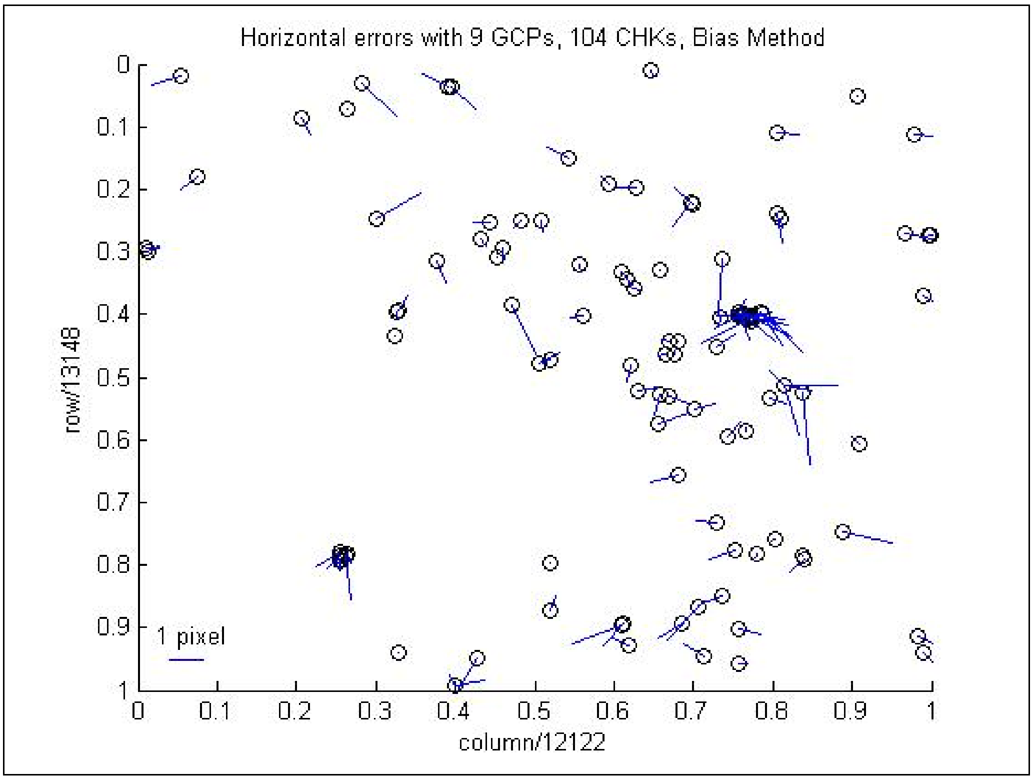


**Figure 4.36 Horizontal errors of 104 CHK points after RPC refinement with 9 GCPs by the Bias method.**

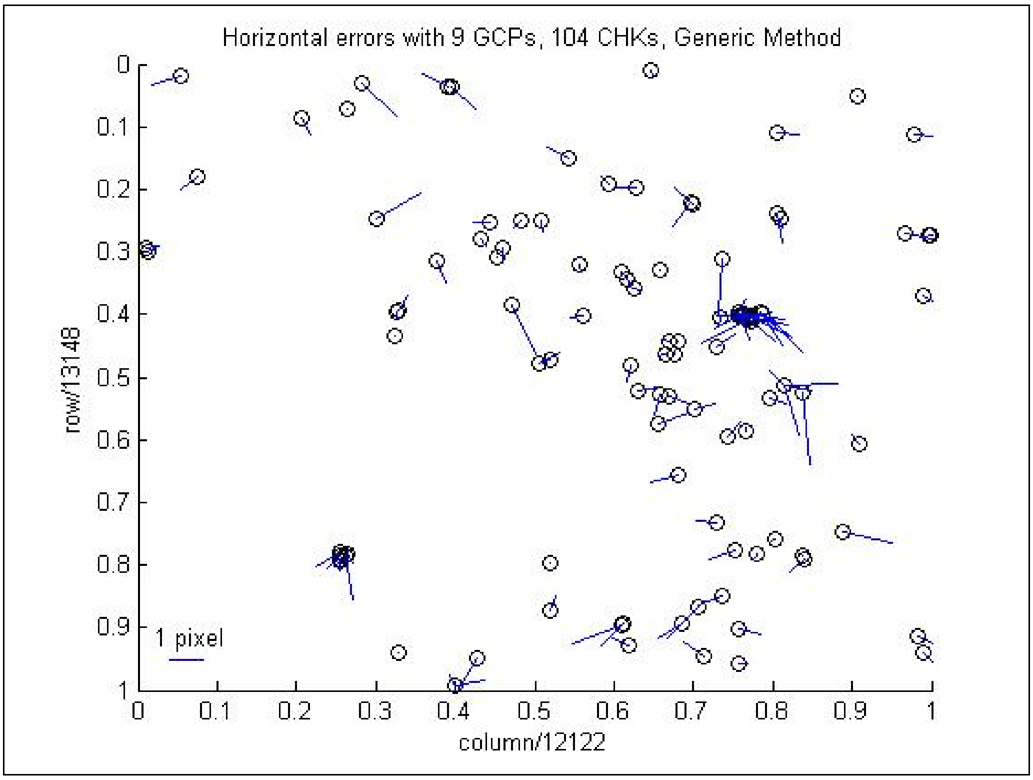


**Figure 4.37 Horizontal errors of 104 CHK points after RPC refinement with 9 GCPs by the Generic method.**

**Table 4.7** lists the accuracy comparison between the Bias method and the Generic method by using IKONOS image data in 3 cases. **Figure 4.38** shows the accuracy comparison between the Bias method and Generic method by using IKONOS image data in 3 cases.

**Table 4.7 Accuracy comparison between the Bias method and the Generic method by using IKONOS image data in 4 cases**

| Case | No. of GCPs (No. of CHKs) | Generic method | | Bias method | |
|---|---|---|---|---|---|
| | | Col. RMSE (pixel) | Row RMSE (pixel) | Col. RMSE (pixel) | Row RMSE (pixel) |
| 0 | 0 (113) | 5.09 | 3.41 | 5.09 | 3.41 |
| 1 | 1 (112) | 0.90 | 0.79 | 0.90 | 0.79 |
| 2 | 9 (104) | 0.76 | 0.83 | 0.76 | 0.83 |
| 3 | 114 (0) | 0.62 | 0.70 | 0.68 | 0.71 |

Note: Col. – column; RMSE – Root Mean Square Error

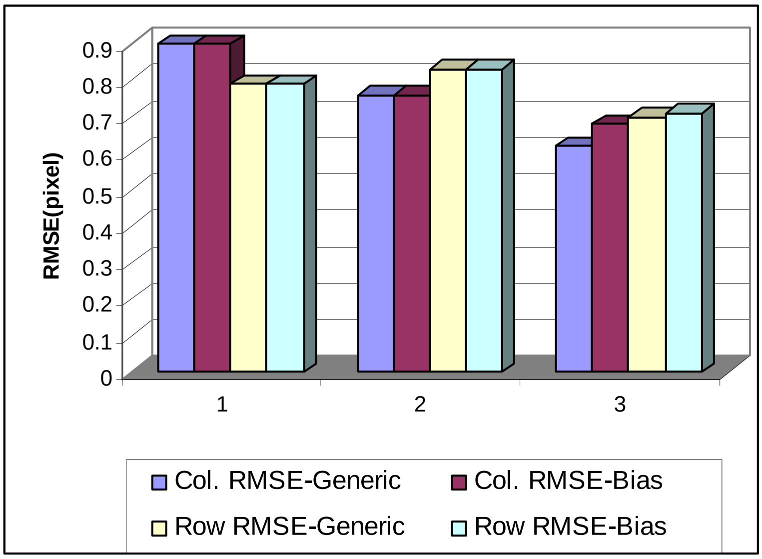


**Figure 4.38 Accuracy comparison between the Bias method and Generic method by using IKONOS image data in 3 cases.**

**Table 4.7** and **Figure 4.38** show that the accuracy of the Generic method and the accuracy of the Bias Compensation method are again similar. Once again, the largest difference in accuracy between the two methods is less than 0.1 pixels.

This experiment set showed that the Generic method has the same capability as the Bias Compensation method to process images having a narrow field of view and small position and attitude errors.

## 4.4.2 Experiment Set 2

In this set of experiments, SPOT5 image data was used to produce simulated data in 9 cases (**Table 4.8**) to test the capability of processing images under a variety of different ephemeris and attitude errors.

**Table 4.8 9 cases of simulated SPOT5 data by adding different error to satellite position and attitude data**

| Case | Δx (m) | Δy (m) | Δz (m) | ΔΨx (rad) | ΔΨy (rad) | ΔΨz (rad) |
|---|---|---|---|---|---|---|
| 1 | 1000 | 1000 | 1000 | 0.1 | 0.1 | 0.1 |
| 2 | 100 | 100 | 100 | 0.01 | 0.01 | 0.01 |
| 3 | 10 | 10 | 10 | 0.001 | 0.001 | 0.001 |
| 4 | 1000 | 1000 | 1000 | 0 | 0 | 0 |
| 5 | 100 | 100 | 100 | 0 | 0 | 0 |
| 6 | 10 | 10 | 10 | 0 | 0 | 0 |
| 7 | 0 | 0 | 0 | 0.1 | 0.1 | 0.1 |
| 8 | 0 | 0 | 0 | 0.01 | 0.01 | 0.01 |
| 9 | 0 | 0 | 0 | 0.001 | 0.001 | 0.001 |

**Appendix VII Tables 7** through **9** list the image coordinate residuals of the control points after the error is added into the ephemeris and attitude data. 1, 3, and 7 GCPs are used to refine the RPC sensor model in 9 cases (**Table 4.8**) by using the Bias method and the Generic method respectively, and 36, 34, 30 GCPs are used to check the accuracy of the refined RPC sensor mode. The corresponding results are presented in tables and figures.

**Appendix VII Tables 10** through **14** present the image coordinate residuals of 36 CHKs after RPC refinement by using the Bias method and the Generic method, 1 GCP from case 1 to case 9. **Appendix VII Tables 15** through **19** present the image coordinate residuals of 34 CHKs after RPC refinement by using the Bias method and the Generic method, 3 GCPs from case 1 to case 9. **Appendix VII Tables 20** through

**24** present the image coordinate residuals of 30 CHKs after RPC refinement by using the Bias method and the Generic method, 7 GCP from case 1 to case 9.

**Figures 4.39** through **4.47** present the image coordinate residuals of 36 CHKs after RPC refinement by using the Bias method and the Generic method, 1 GCP from case 1 to case 9. **Figures 4.48** through **4.56** present the image coordinate residuals of 34 CHKs after RPC refinement by using the Bias method and the Generic method, 3 GCPs from case 1 to case 9. **Figures 4.57** through **4.65** present the image coordinate residuals of 30 CHKs after RPC refinement by using the Bias method and the Generic method, 7 GCP from case 1 to case 9.

**Figures 4.66** through **4.83** illustrate the horizontal errors of 36 CHKs after RPC refinement by using the Bias method and the Generic method, 1 GCP from case 1 to case 9. **Figures 4.84** through **4.101** illustrate the horizontal errors of 34 CHKs after RPC refinement by using the Bias method and the Generic method, 3 GCPs from case 1 to case 9. **Figures 4.102** through **4.119** illustrate the horizontal errors of 30 CHKs after RPC refinement by using the Bias method and the Generic method, 7 GCP from case 1 to case 9.

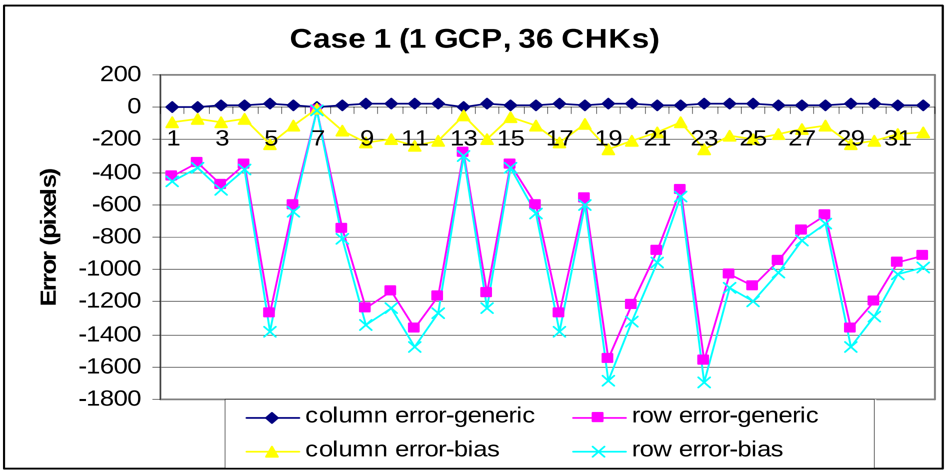


**Figure 4.39 Image Coordinate Residuals of Case 1 (1 GCP).**

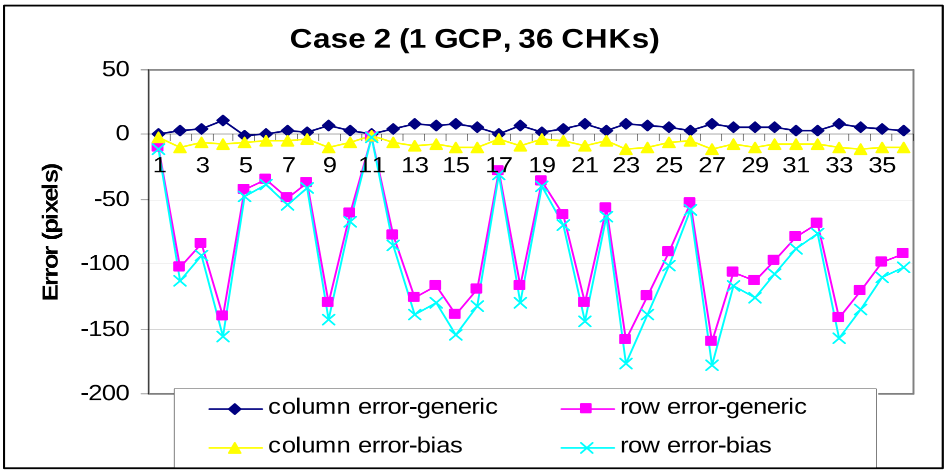


**Figure 4.40 Image Coordinate Residuals of Case 2 (1 GCP).**

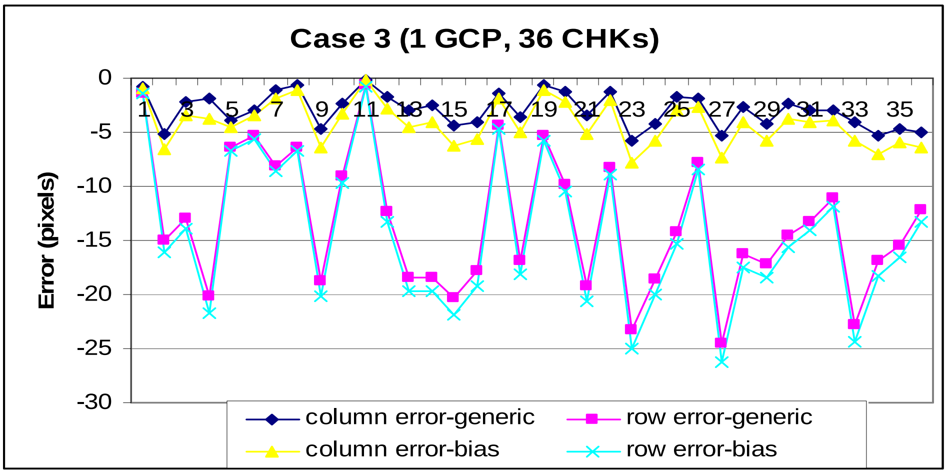


**Figure 4.41 Image Coordinate Residuals of Case 3 (1 GCP).**

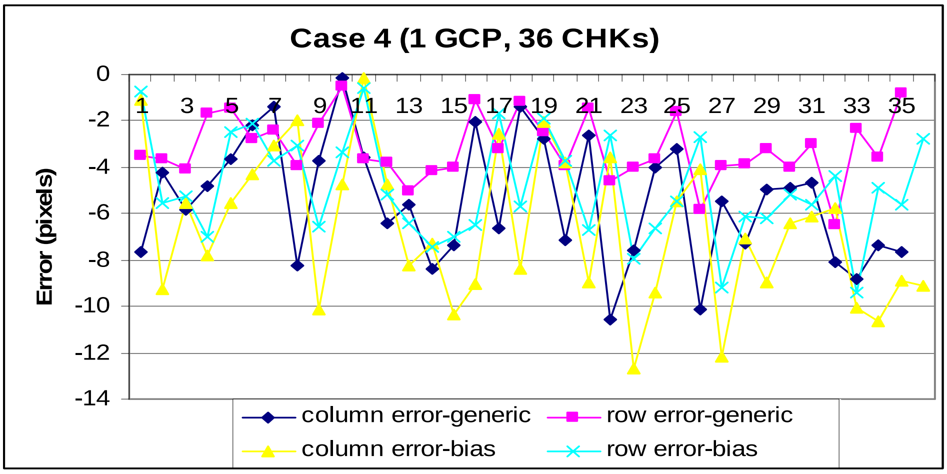

**Figure 4.42 Image Coordinate Residuals of Case 4 (1 GCP).**

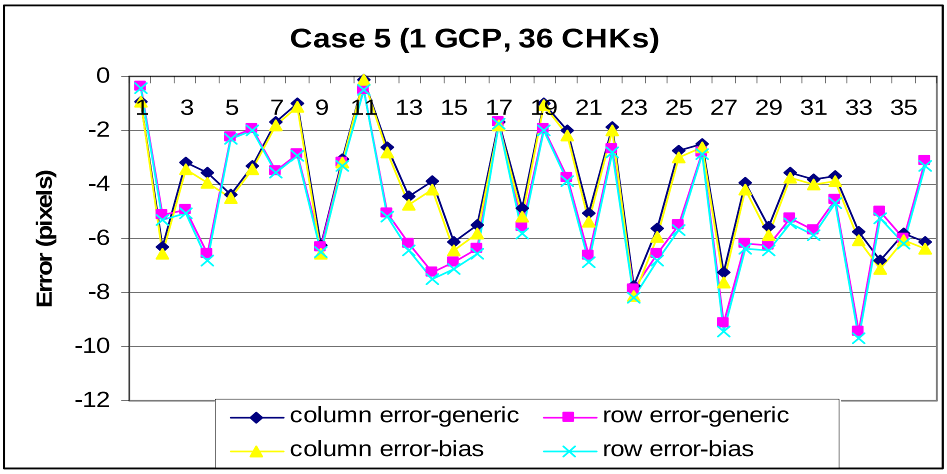

**Figure 4.43 Image Coordinate Residuals of Case 5 (1 GCP).**

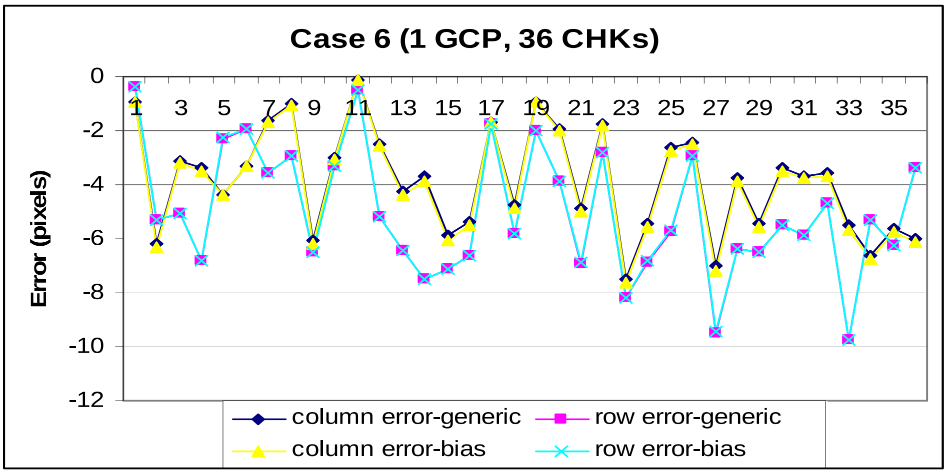

**Figure 4.44 Image Coordinate Residuals of Case 6 (1 GCP).**

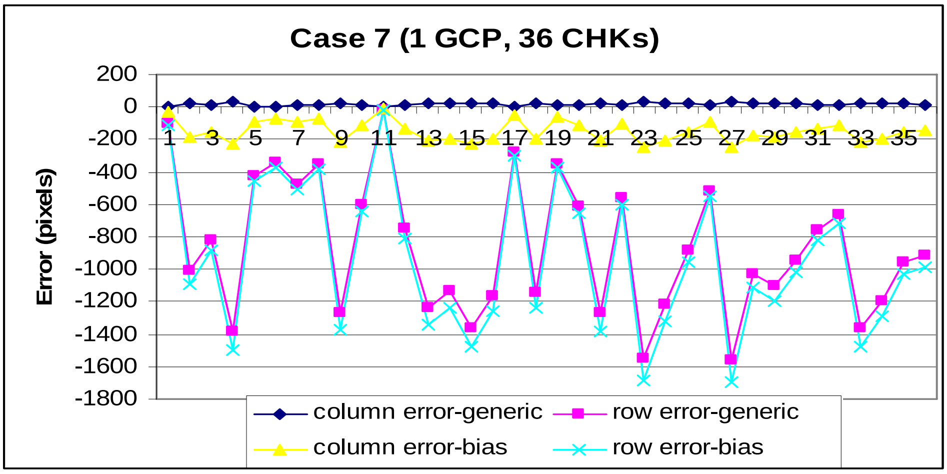


**Figure 4.45 Image Coordinate Residuals of Case 7 (1 GCP).**

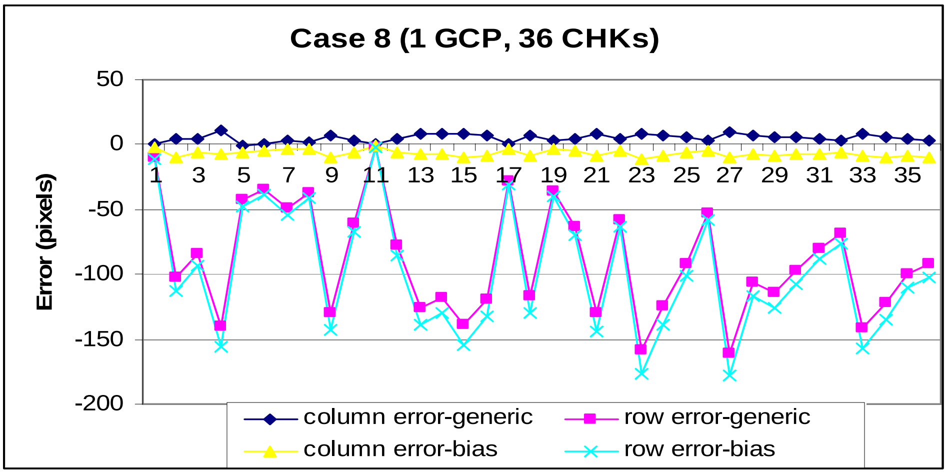


**Figure 4.46 Image Coordinate Residuals of Case 8 (1 GCP).**

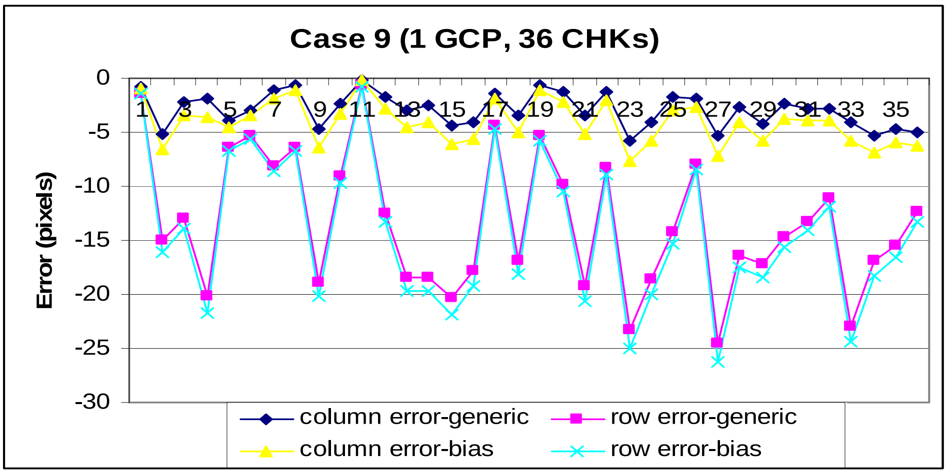


**Figure 4.47 Image Coordinate Residuals of Case 9 (1 GCP).**

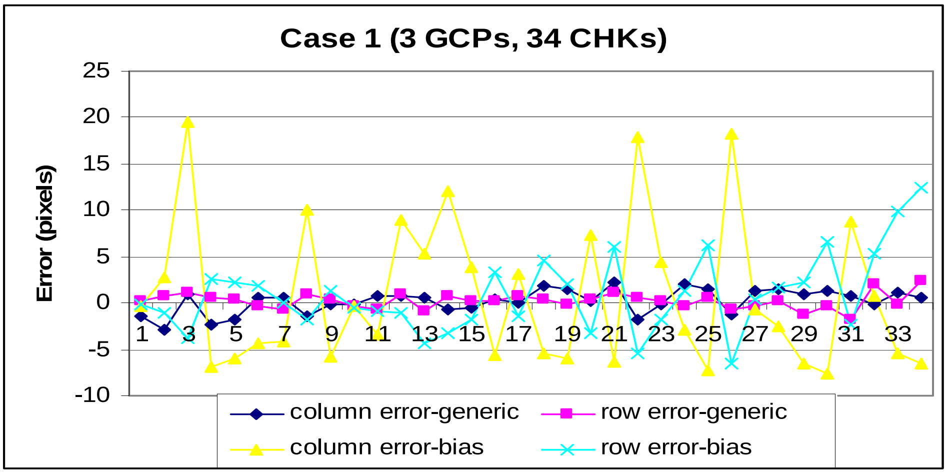


**Figure 4.48 Image Coordinate Residuals of Case 1 (3 GCP).**

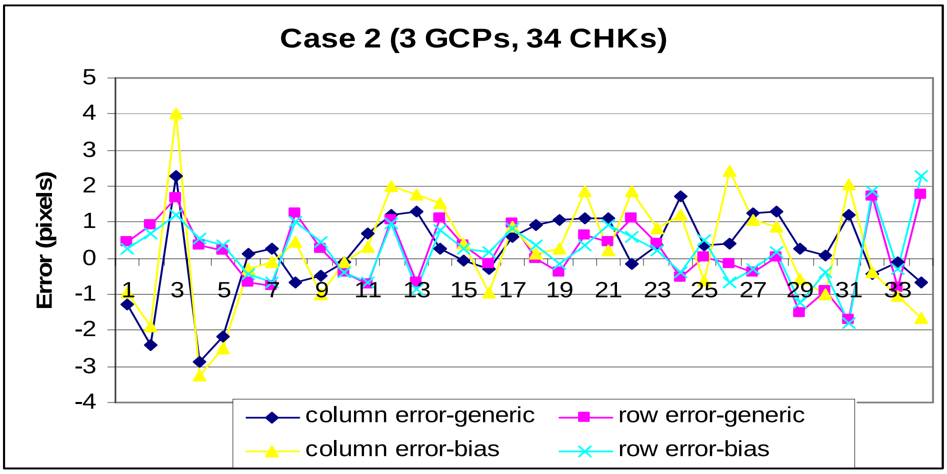


**Figure 4.49 Image Coordinate Residuals of Case 2 (3 GCP).**

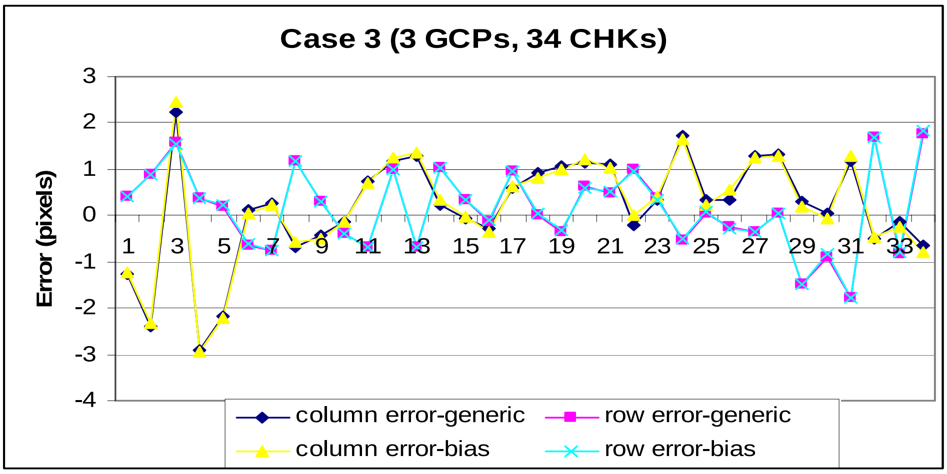


**Figure 4.50 Image Coordinate Residuals of Case 3 (3 GCP).**

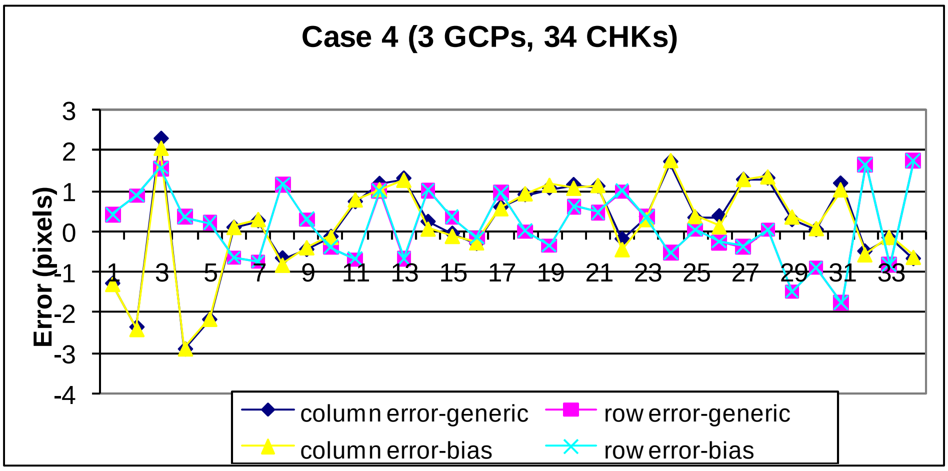


**Figure 4.51 Image Coordinate Residuals of Case 4 (3 GCP).**

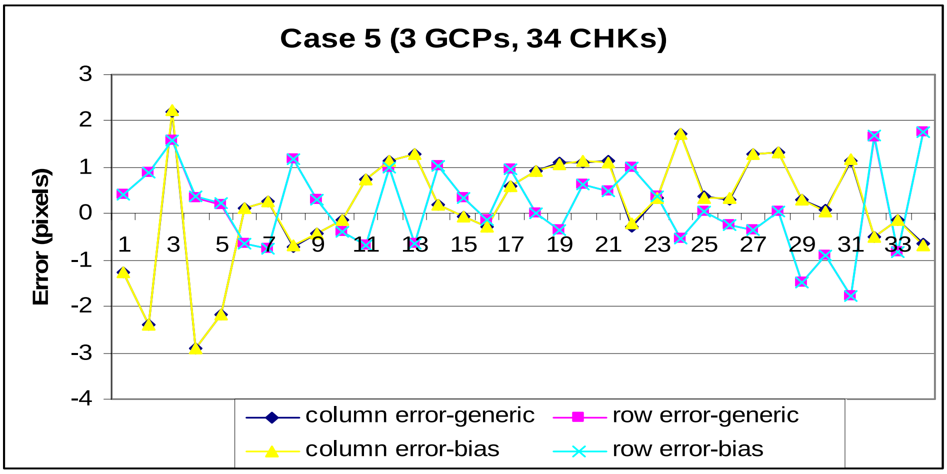


**Figure 4.52 Image Coordinate Residuals of Case 5 (3 GCP).**

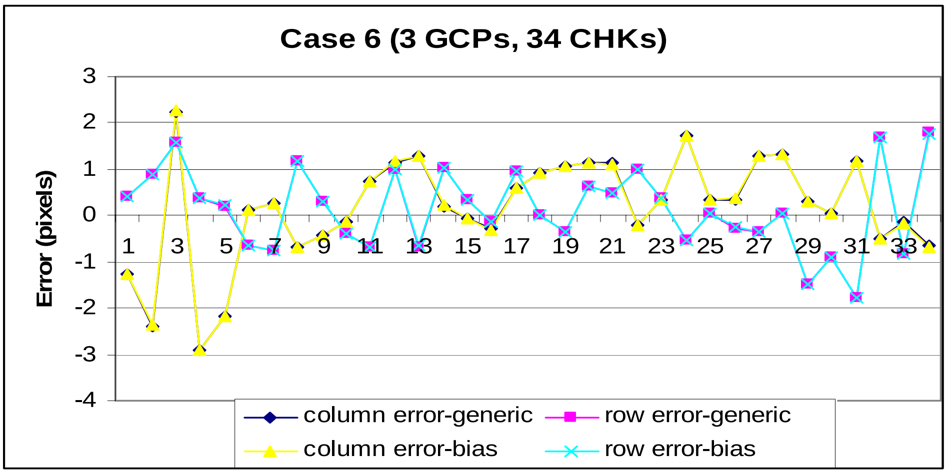


**Figure 4.53 Image Coordinate Residuals of Case 3 (3 GCP).**

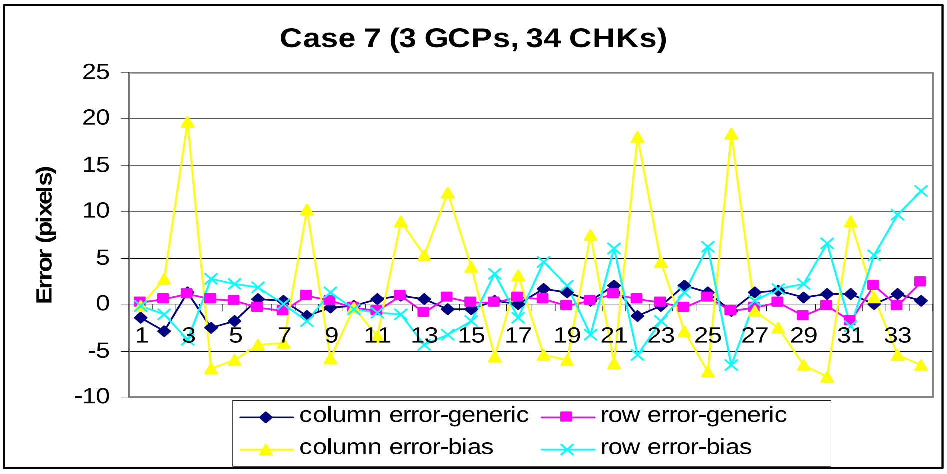


**Figure 4.54 Image Coordinate Residuals of Case 7 (3 GCP).**

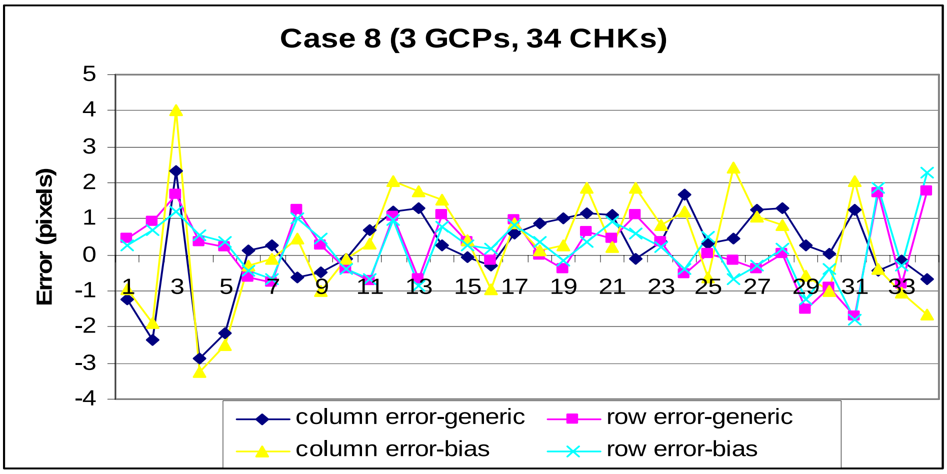


**Figure 4.55 Image Coordinate Residuals of Case 8 (3 GCP).**

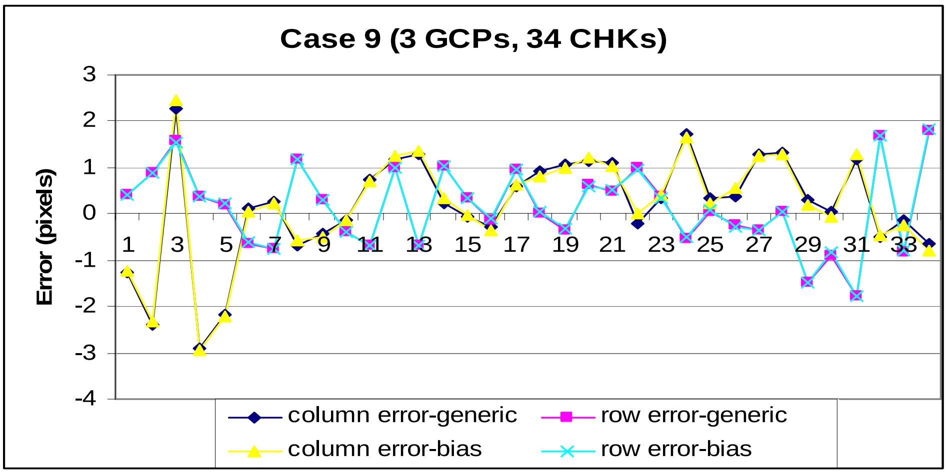


**Figure 4.56 Image Coordinate Residuals of Case 9 (3 GCP).**

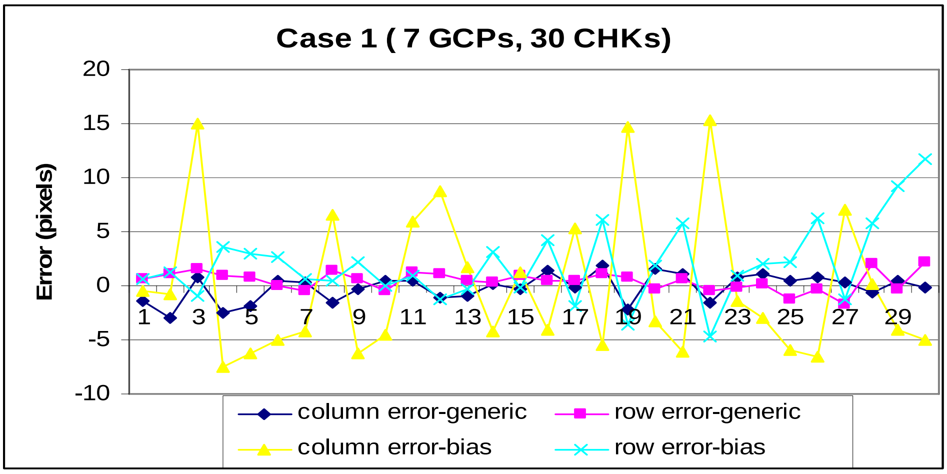

**Figure 4.57 Image Coordinate Residuals of Case 1 (7 GCP).**

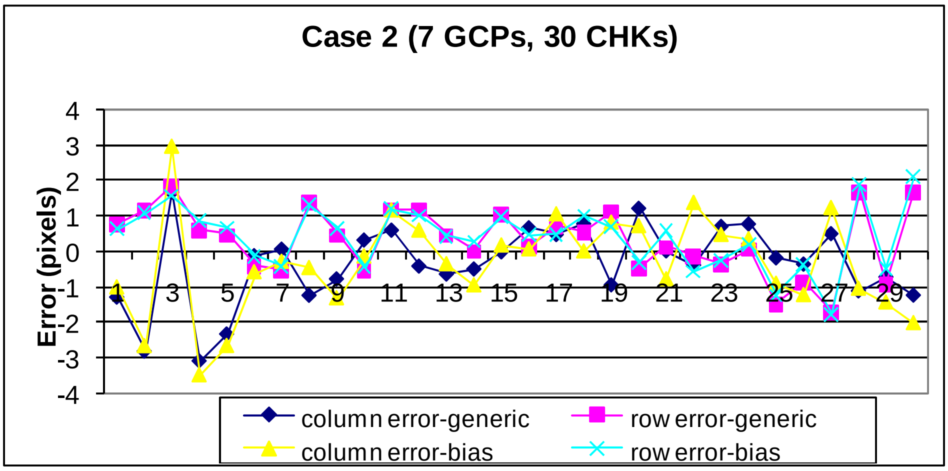

**Figure 4.58 Image Coordinate Residuals of Case 2 (7 GCP).**

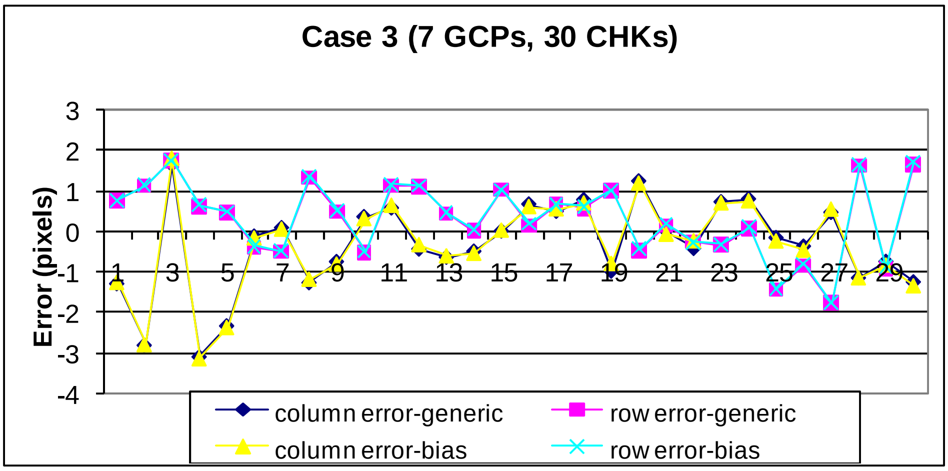

**Figure 4.59 Image Coordinate Residuals of Case 3 (7 GCP).**

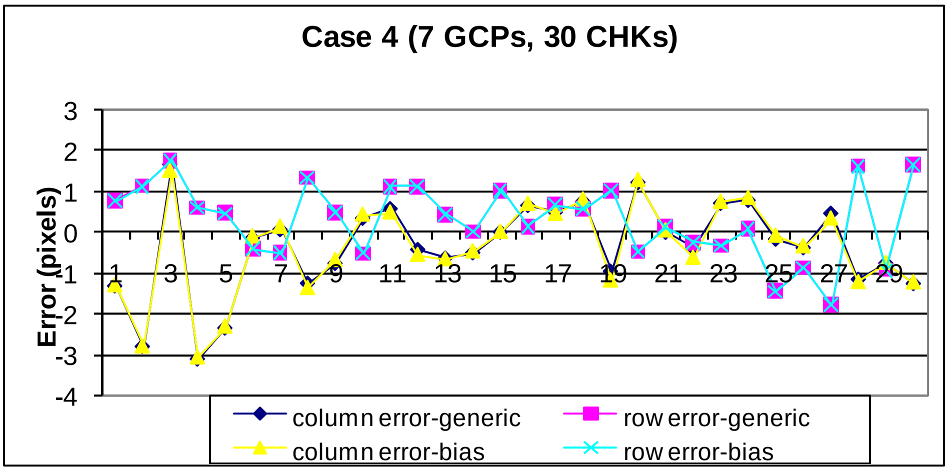


**Figure 4.60 Image Coordinate Residuals of Case 4 (7 GCP).**

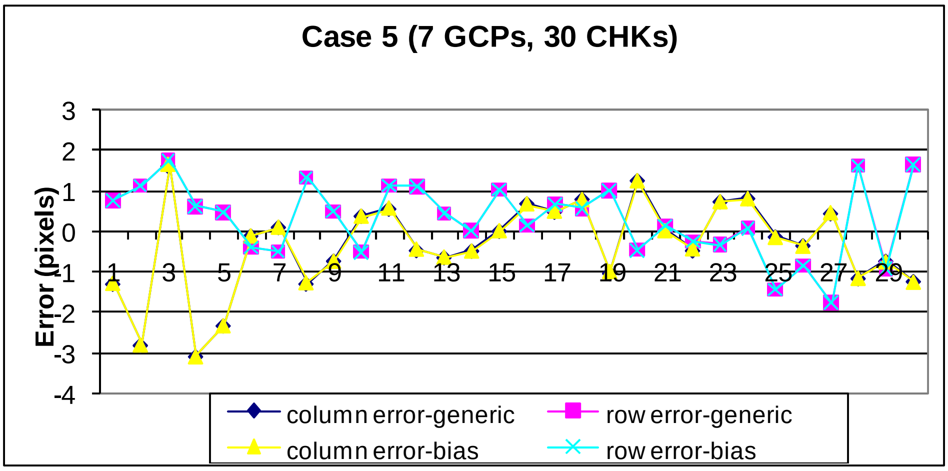


**Figure 4.61 Image Coordinate Residuals of Case 5 (7 GCP).**

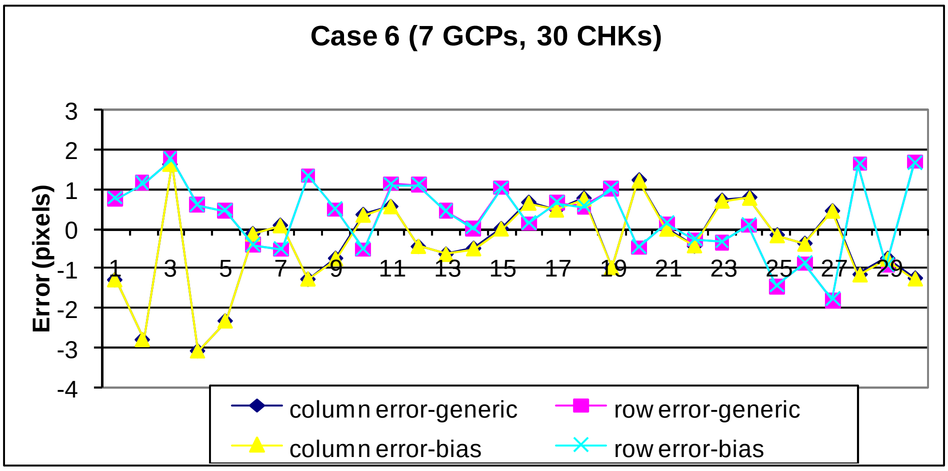


**Figure 4.62 Image Coordinate Residuals of Case 6 (7 GCP).**

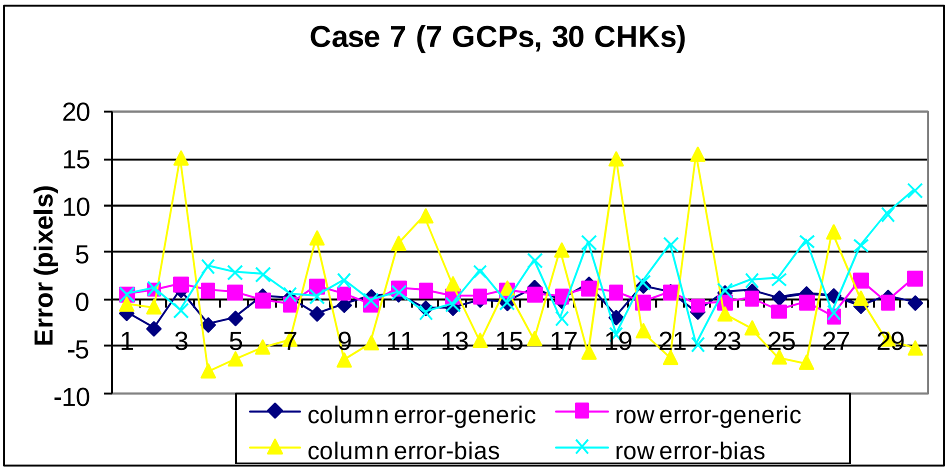


**Figure 4.63 Image Coordinate Residuals of Case 7 (7 GCP).**

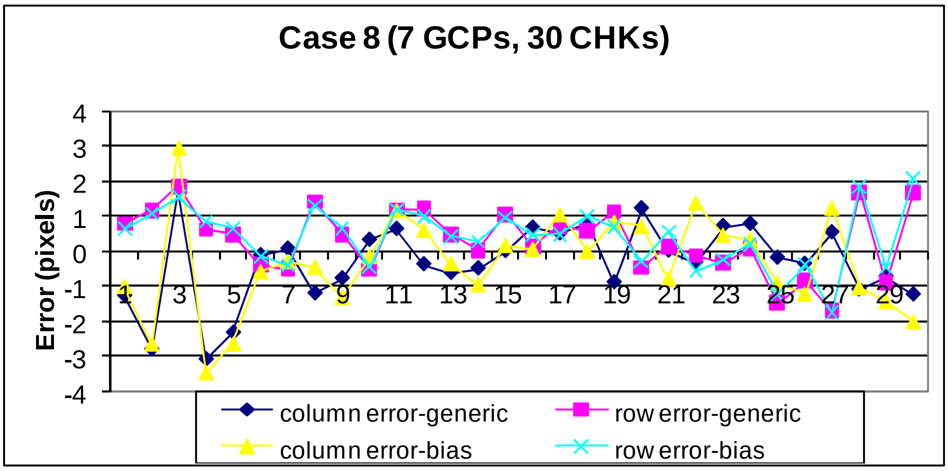


**Figure 4.64 Image Coordinate Residuals of Case 8 (7 GCP).**

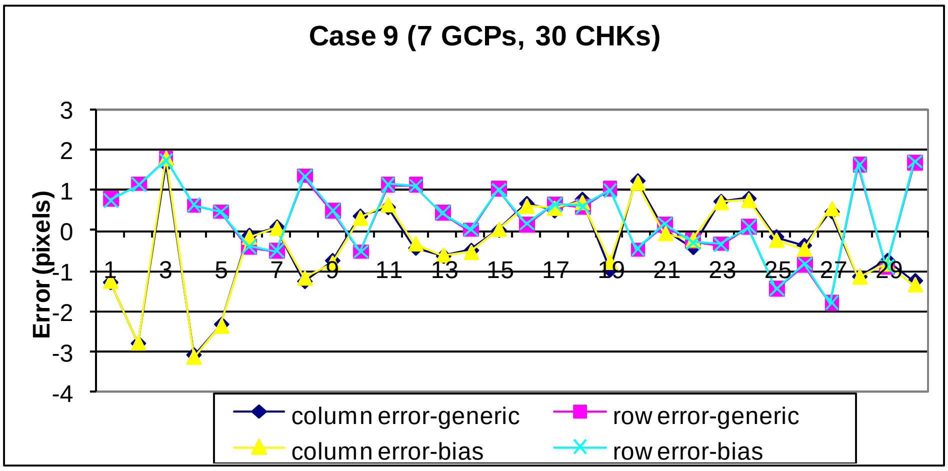


**Figure 4.65 Image Coordinate Residuals of Case 9 (7 GCP).**

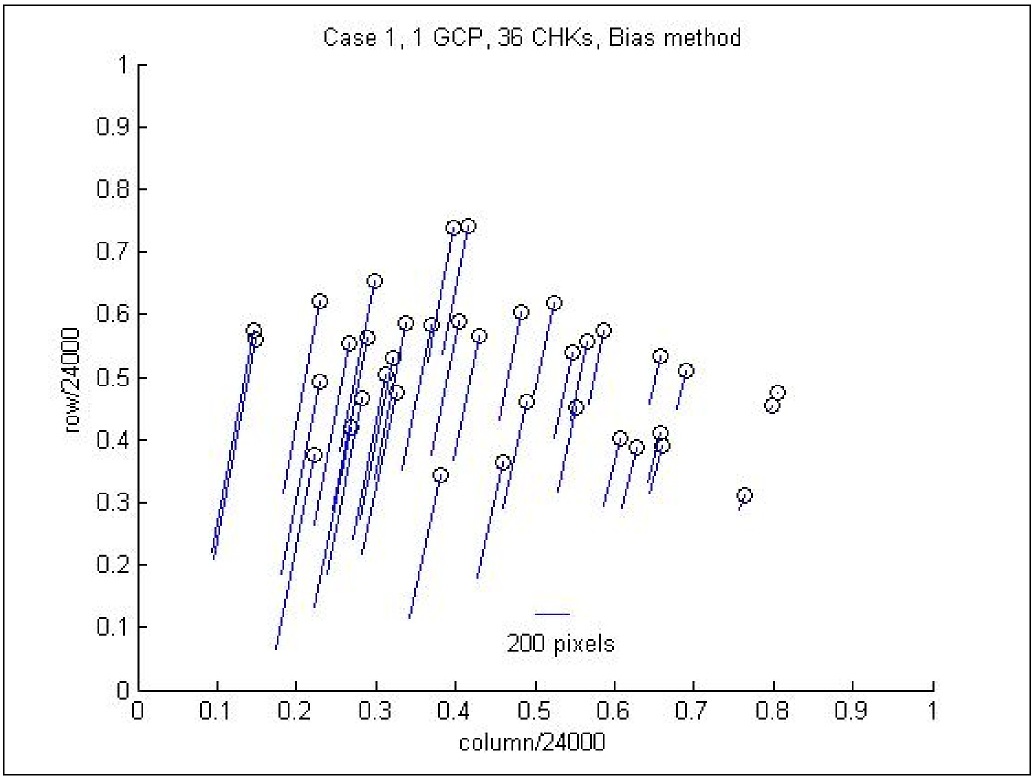


**Figure 4.66 Horizontal errors of Case 1 by the Bias method (1 GCP).**

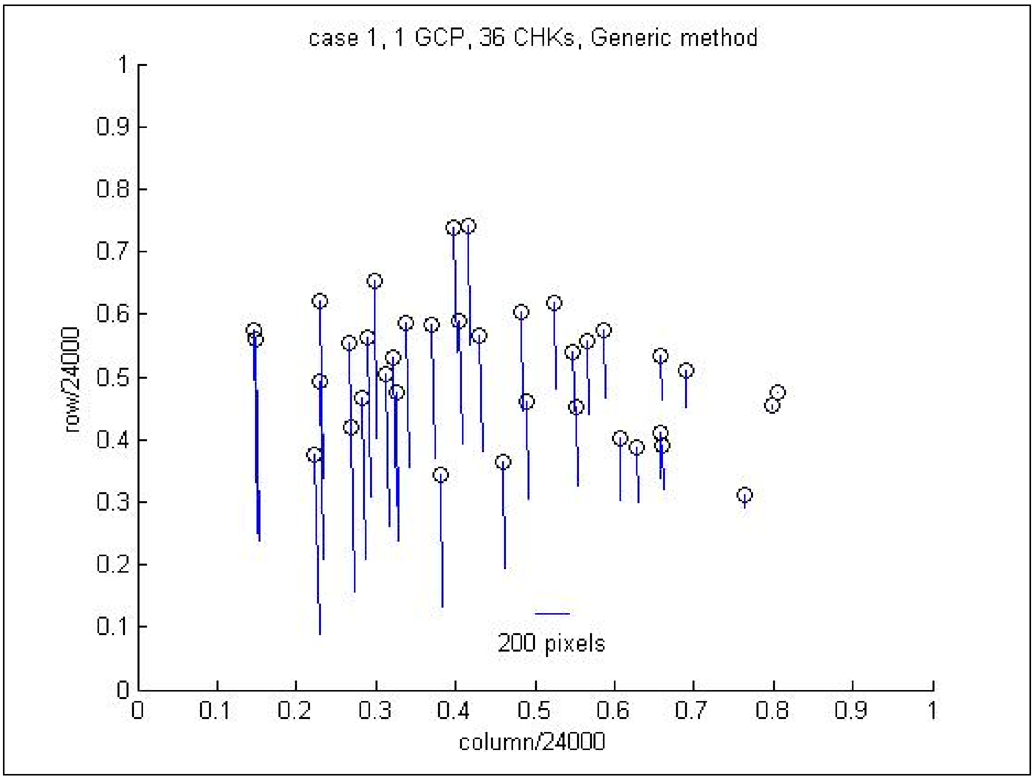


**Figure 4.67 Horizontal errors of Case 1 by the Generic method (1 GCP).**

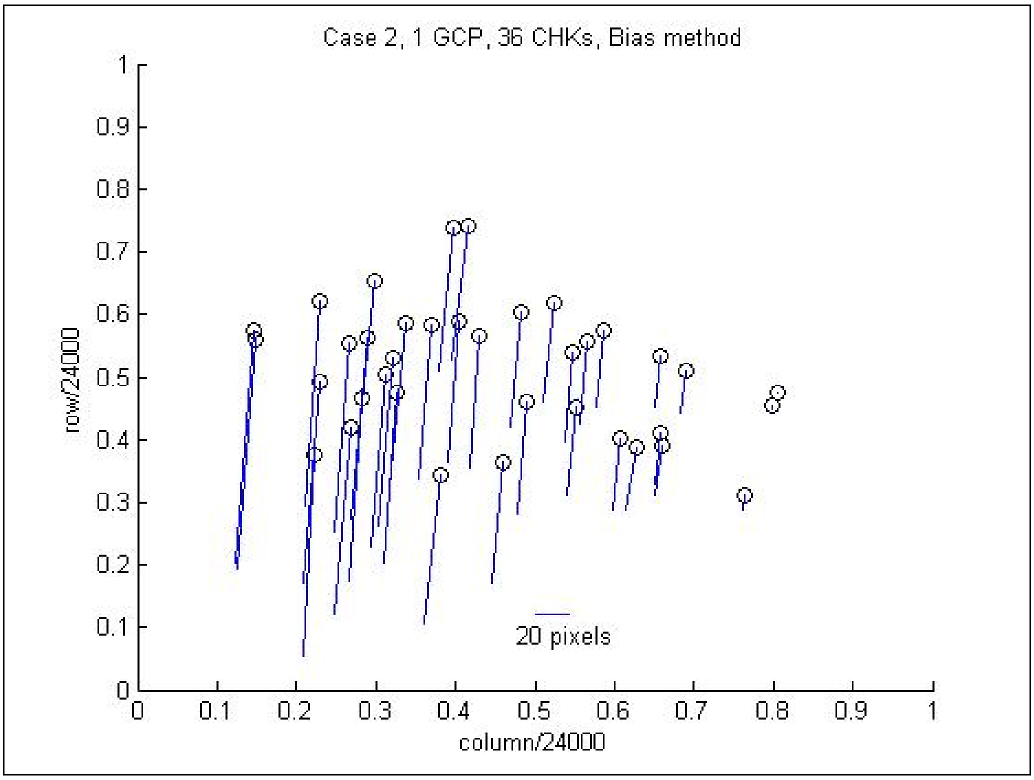


**Figure 4.68 Horizontal errors of Case 2 by the Bias method (1 GCP).**

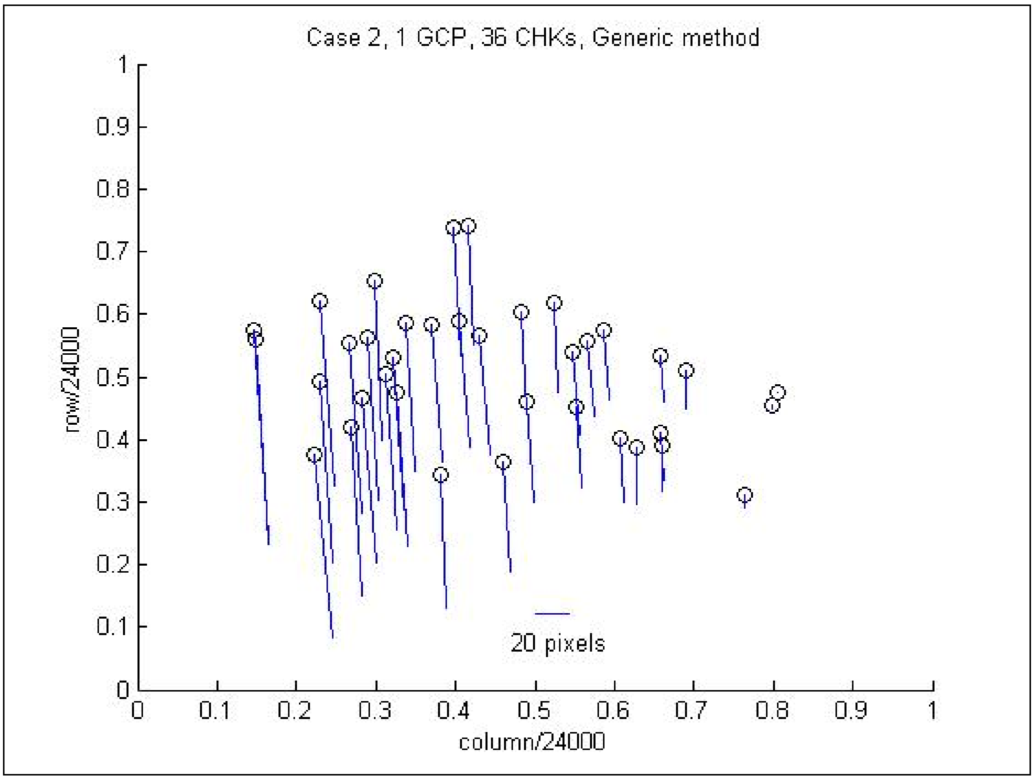


**Figure 4.69 Horizontal errors of Case 2 by the Generic method (1 GCP).**

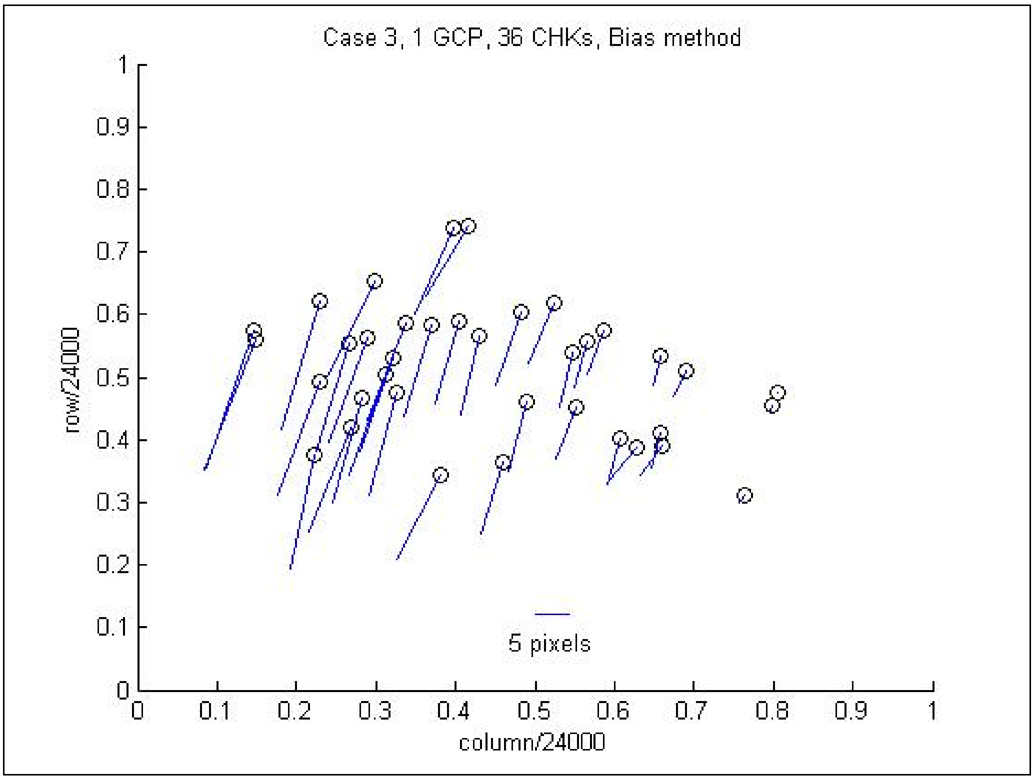


**Figure 4.70 Horizontal errors of Case 3 by the Bias method (1 GCP).**

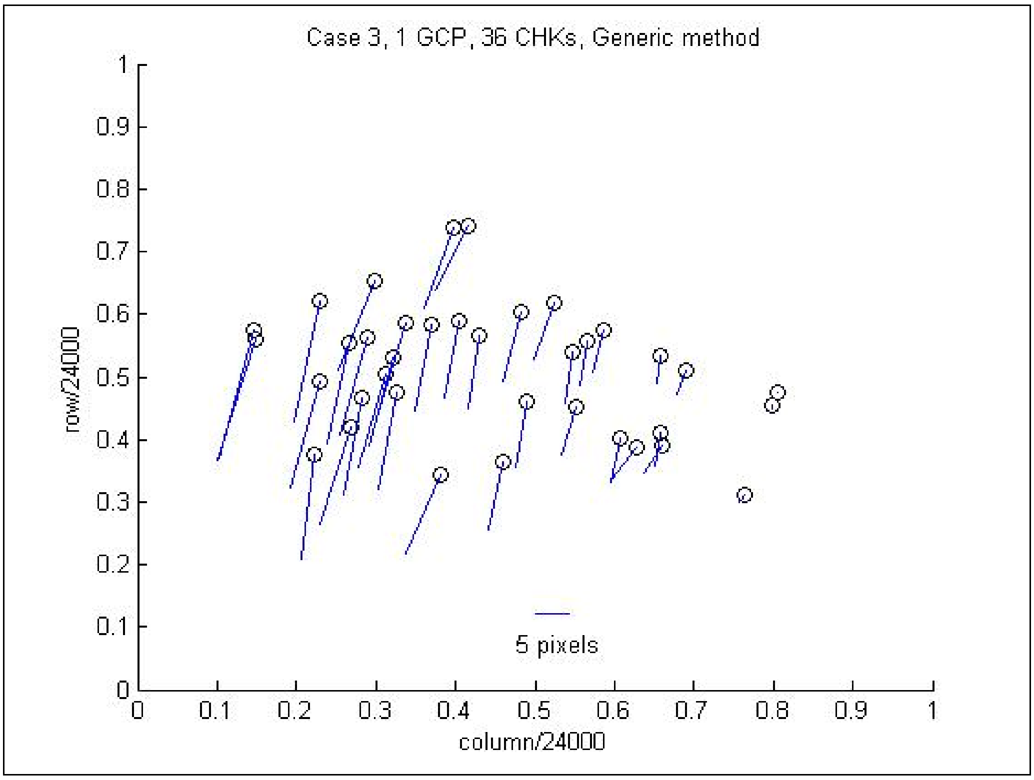


**Figure 4.71 Horizontal errors of Case 3 by the Generic method (1 GCP).**

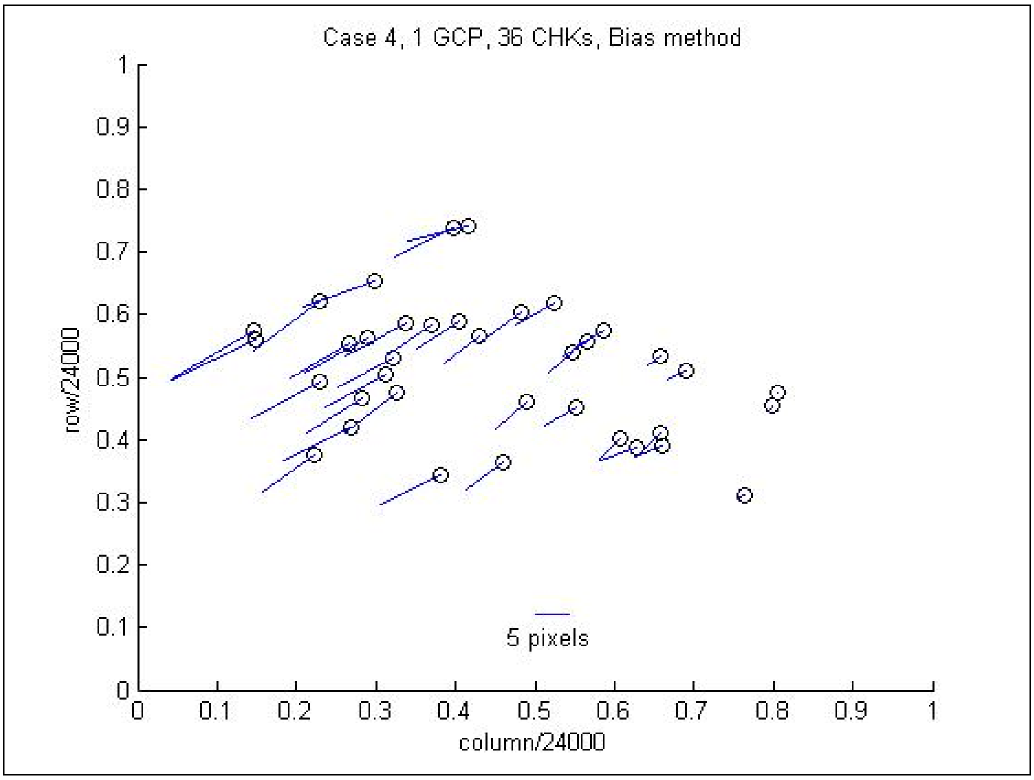


**Figure 4.72 Horizontal errors of Case 4 by the Bias method (1 GCP).**

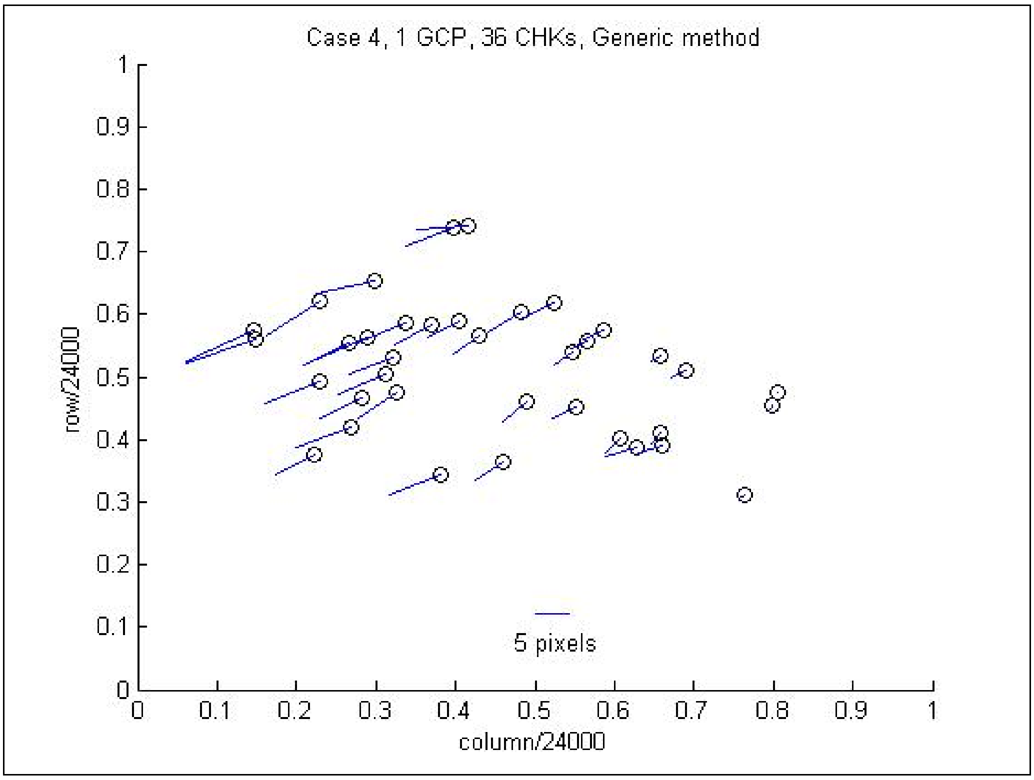


**Figure 4.73 Horizontal errors of Case 4 by the Generic method (1 GCP).**

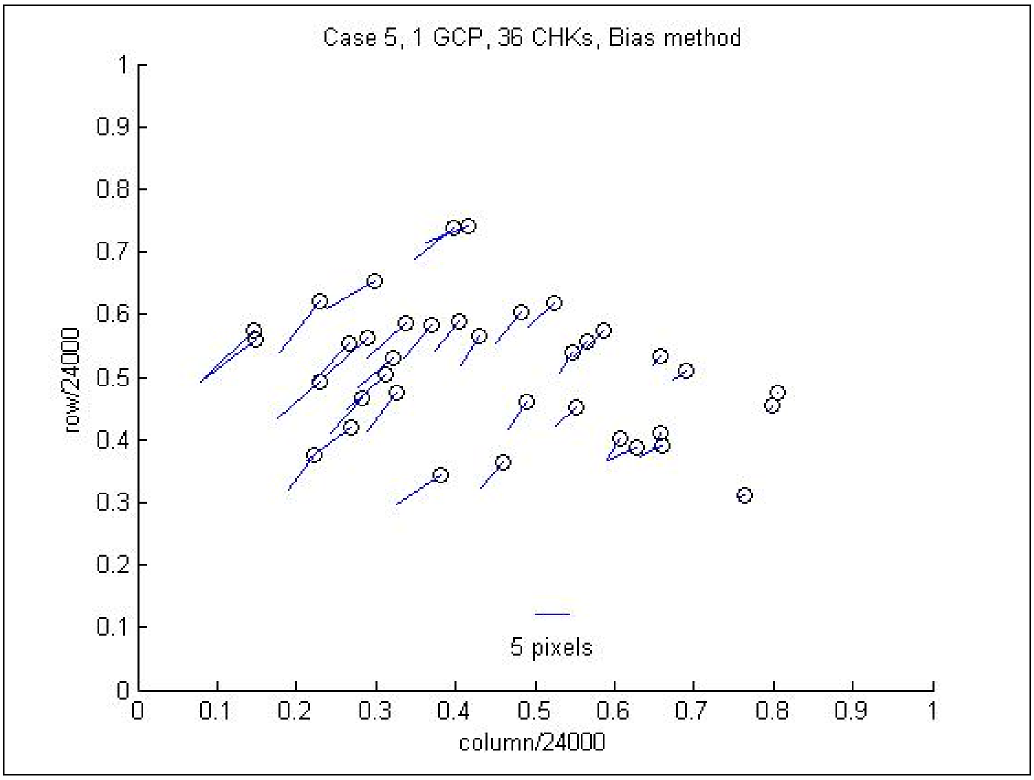

**Figure 4.74 Horizontal errors of Case 5 by the Bias method (1 GCP).**

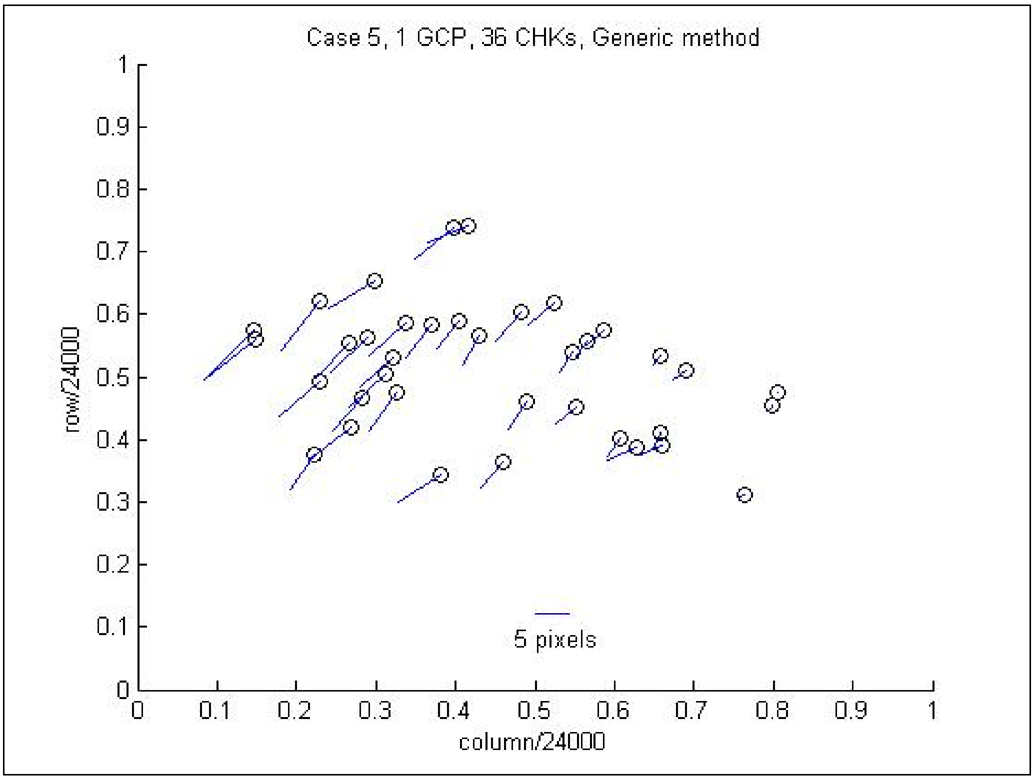

**Figure 4.75 Horizontal errors of Case 5 by the Generic method (1 GCP).**

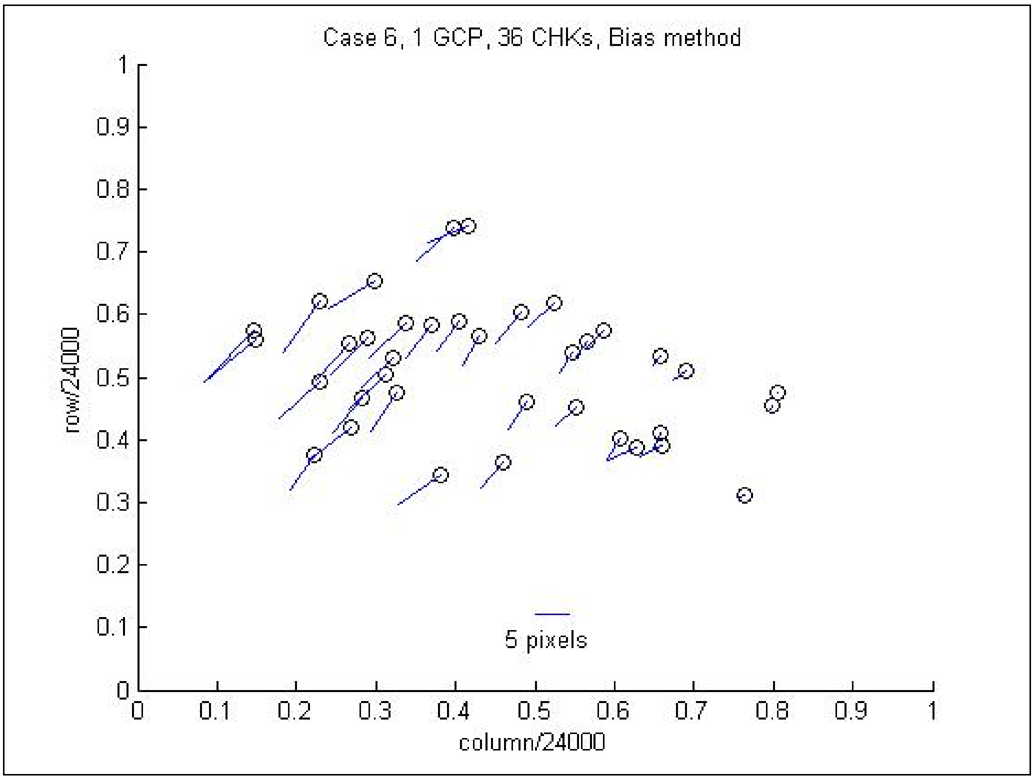

**Figure 4.76 Horizontal errors of Case 6 by the Bias method (1 GCP).**

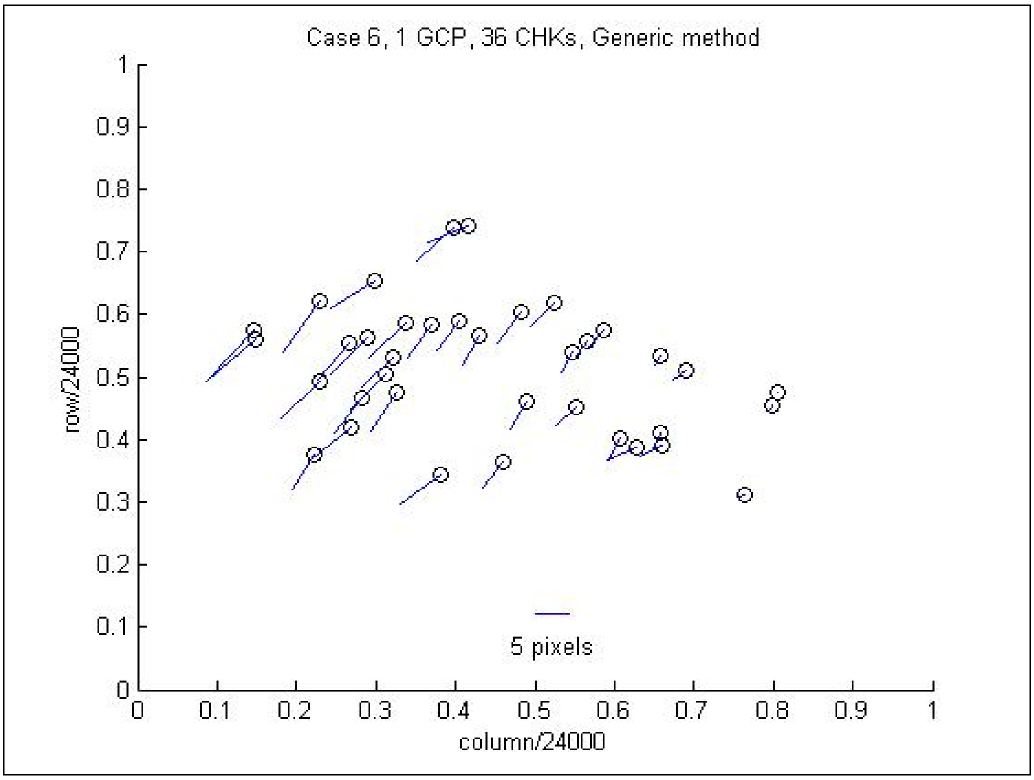

**Figure 4.77 Horizontal errors of Case 6 by the Generic method (1 GCP).**

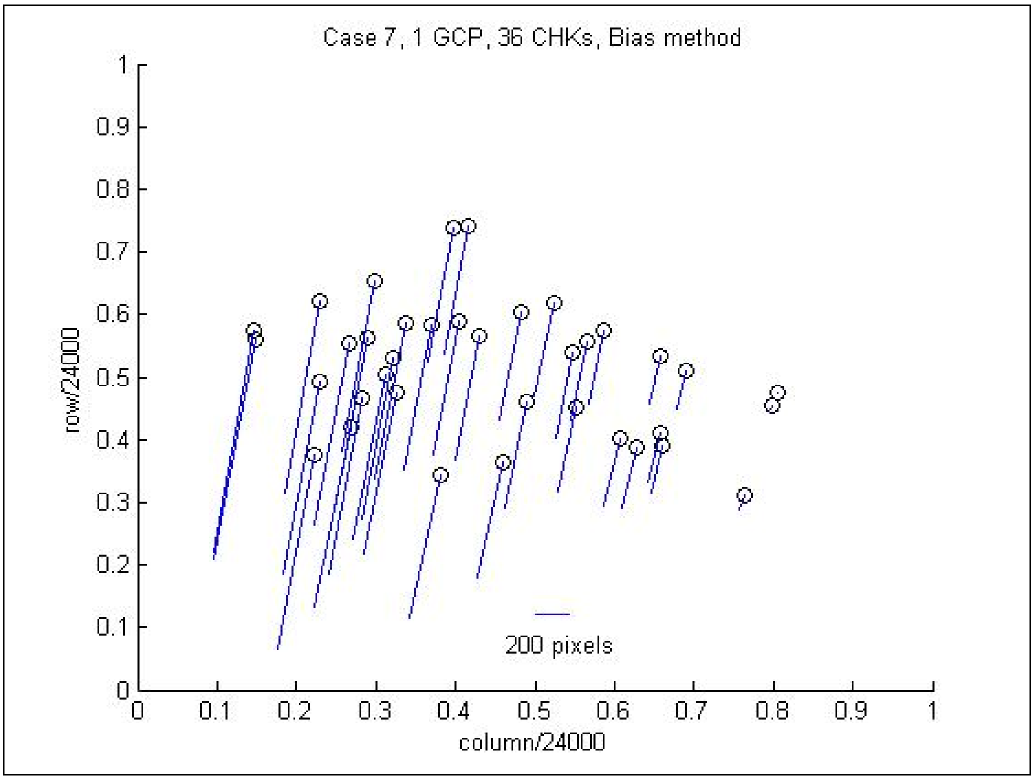


**Figure 4.78 Horizontal errors of Case 7 by the Bias method (1 GCP).**

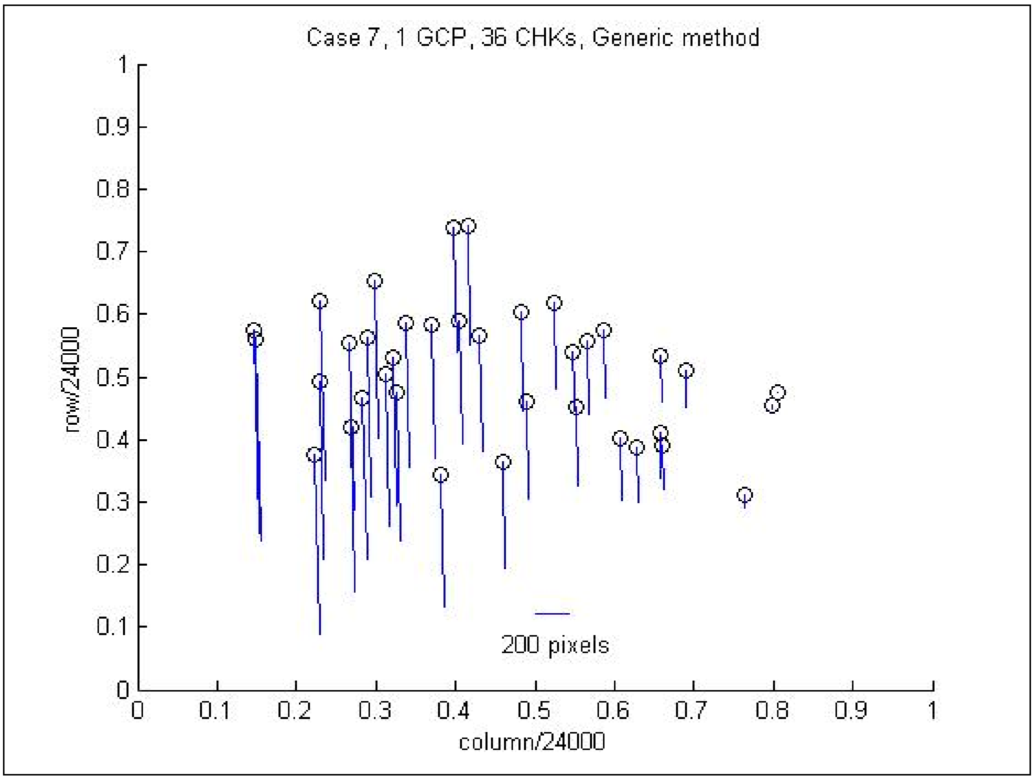


**Figure 4.79 Horizontal errors of Case 7 by the Generic method (1 GCP).**

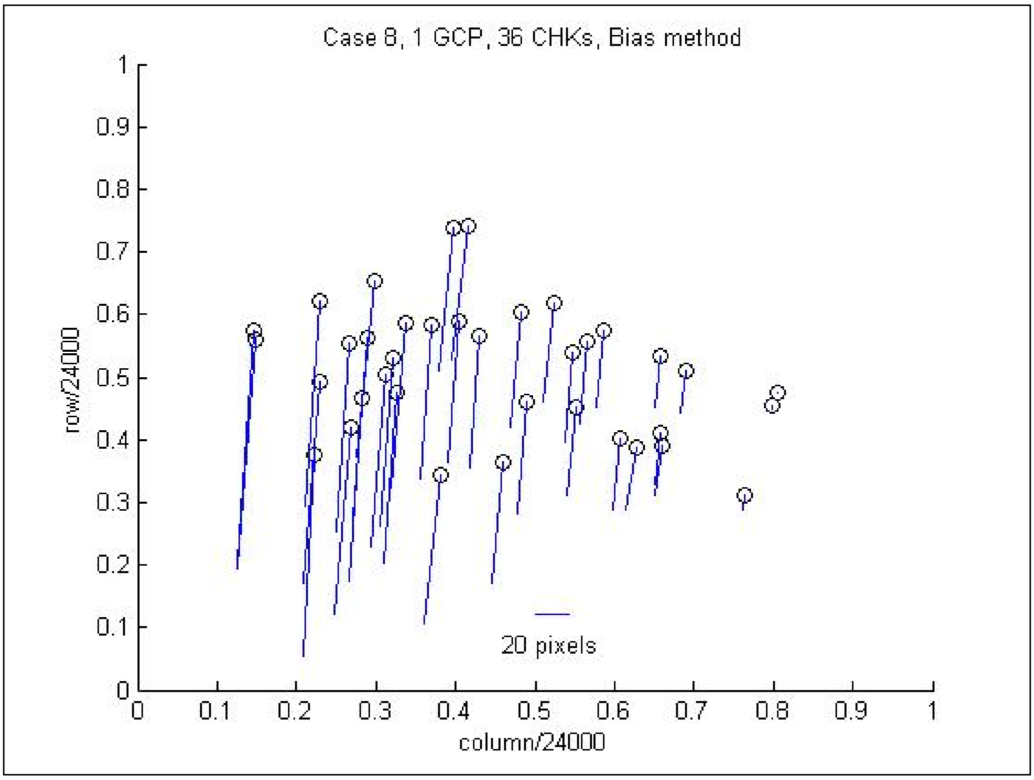

**Figure 4.80 Horizontal errors of Case 8 by the Bias method (1 GCP).**

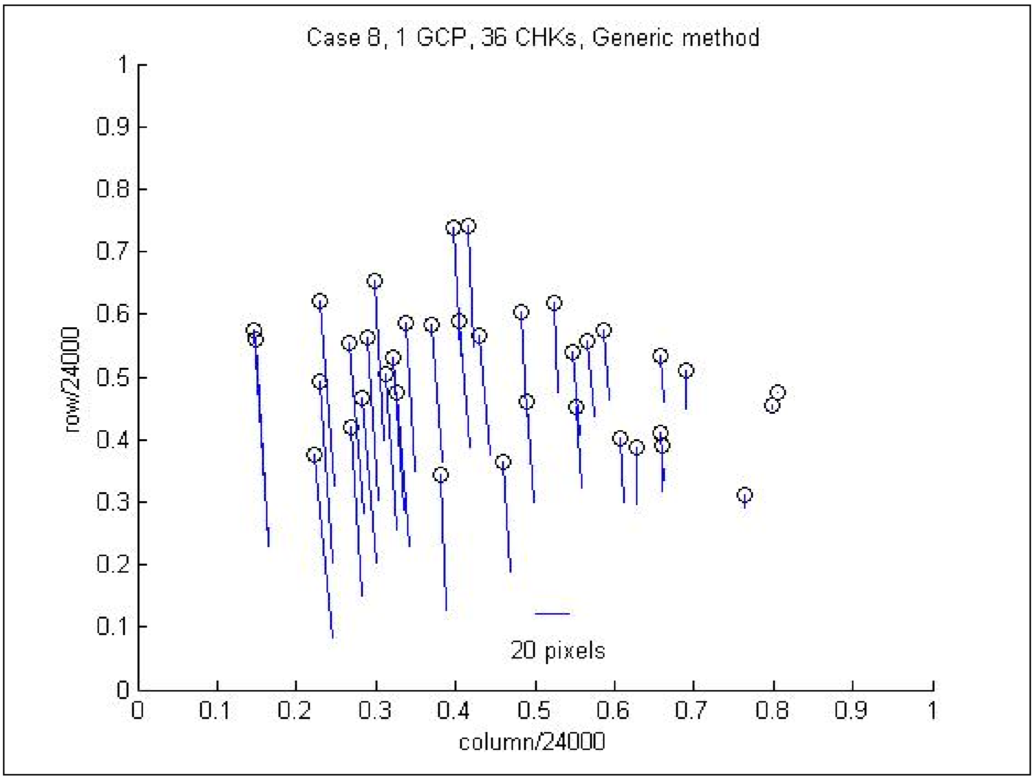

**Figure 4.81 Horizontal errors of Case 8 by the Generic method (1 GCP).**

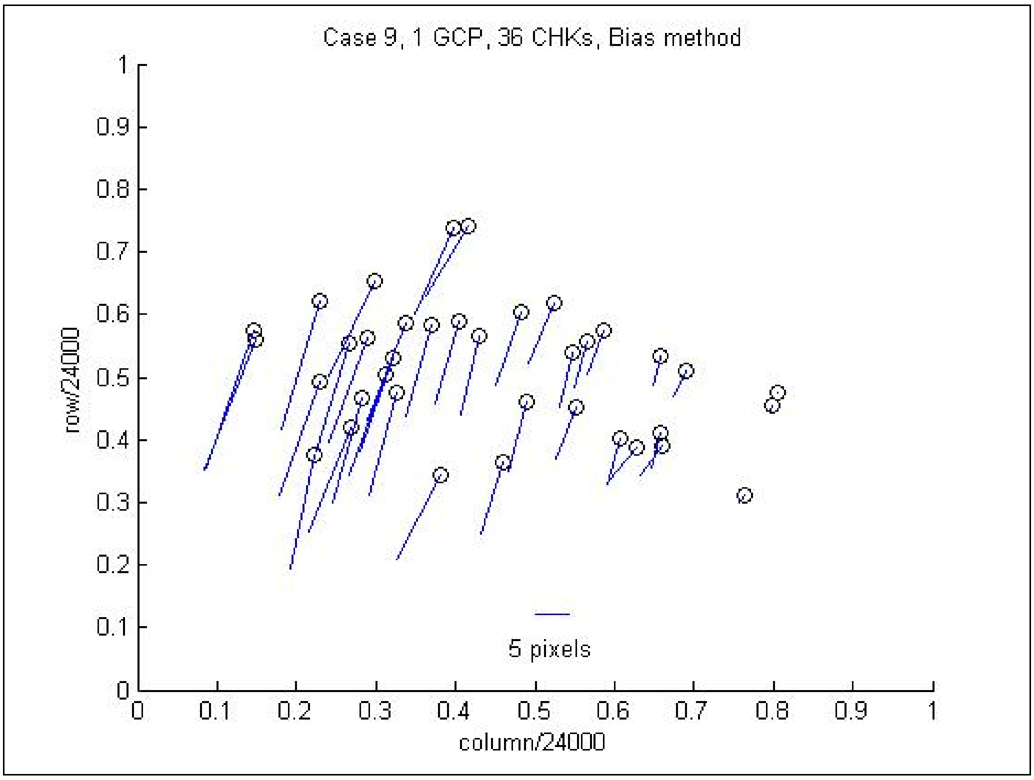


**Figure 4.82 Horizontal errors of Case 9 by the Bias method (1 GCP).**

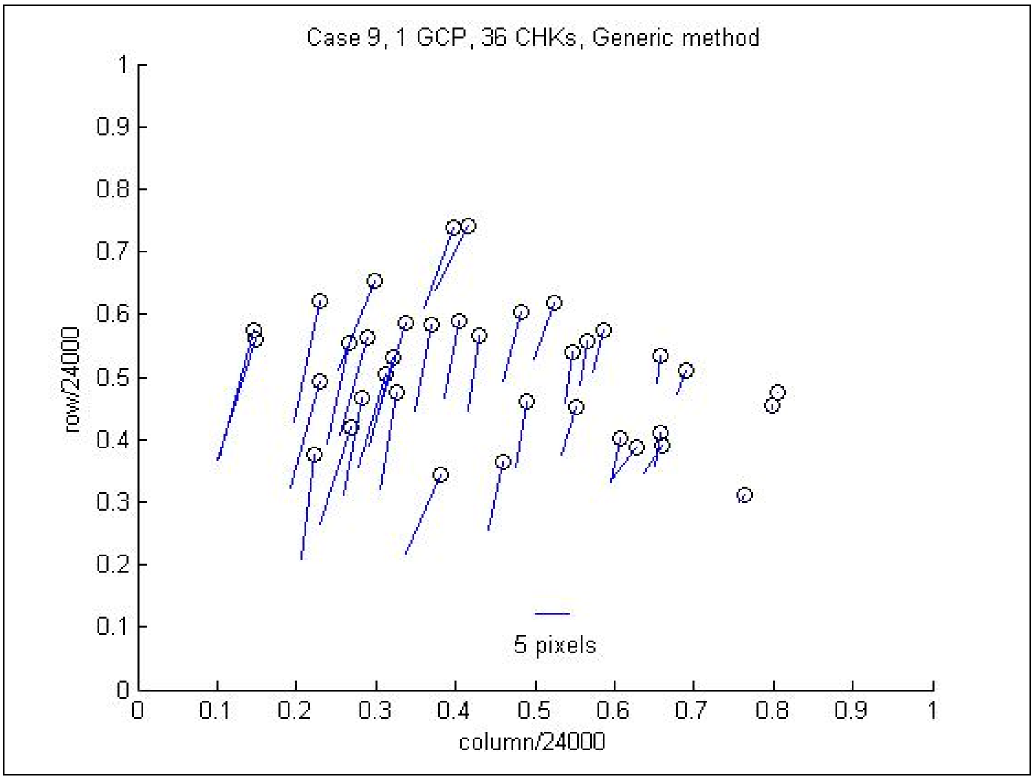


**Figure 4.83 Horizontal errors of Case 9 by the Generic method (1 GCP).**

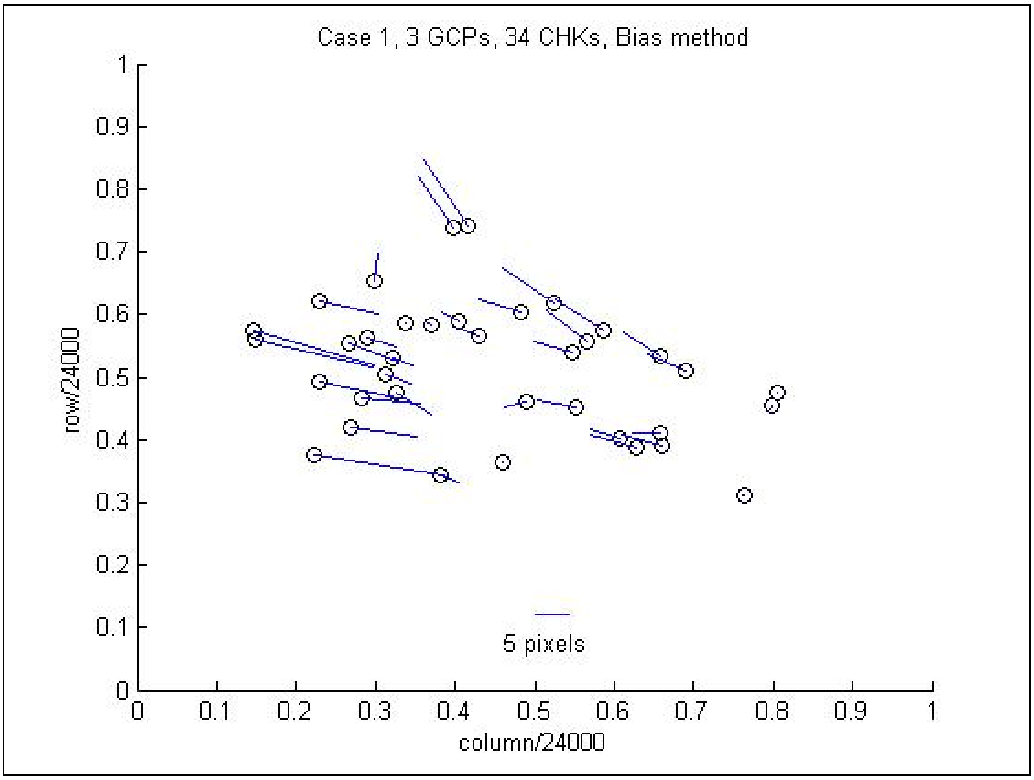


**Figure 4.84 Horizontal errors of Case 1 by the Bias method (3 GCP).**

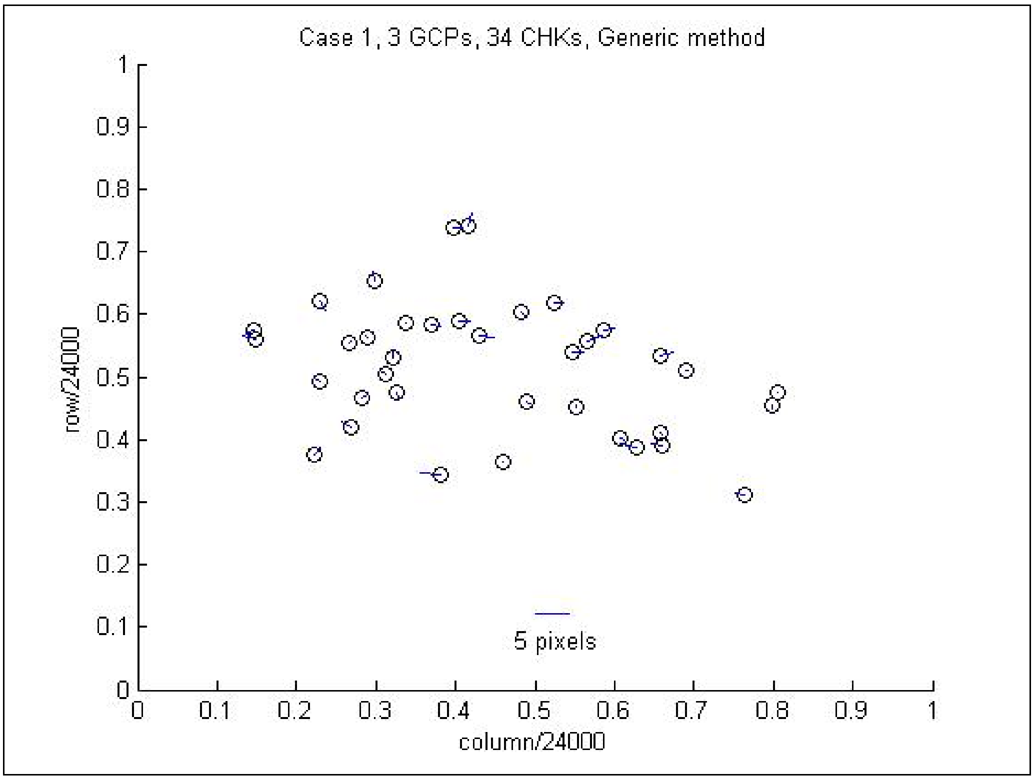


**Figure 4.85 Horizontal errors of Case 1 by the Generic method (3 GCP).**

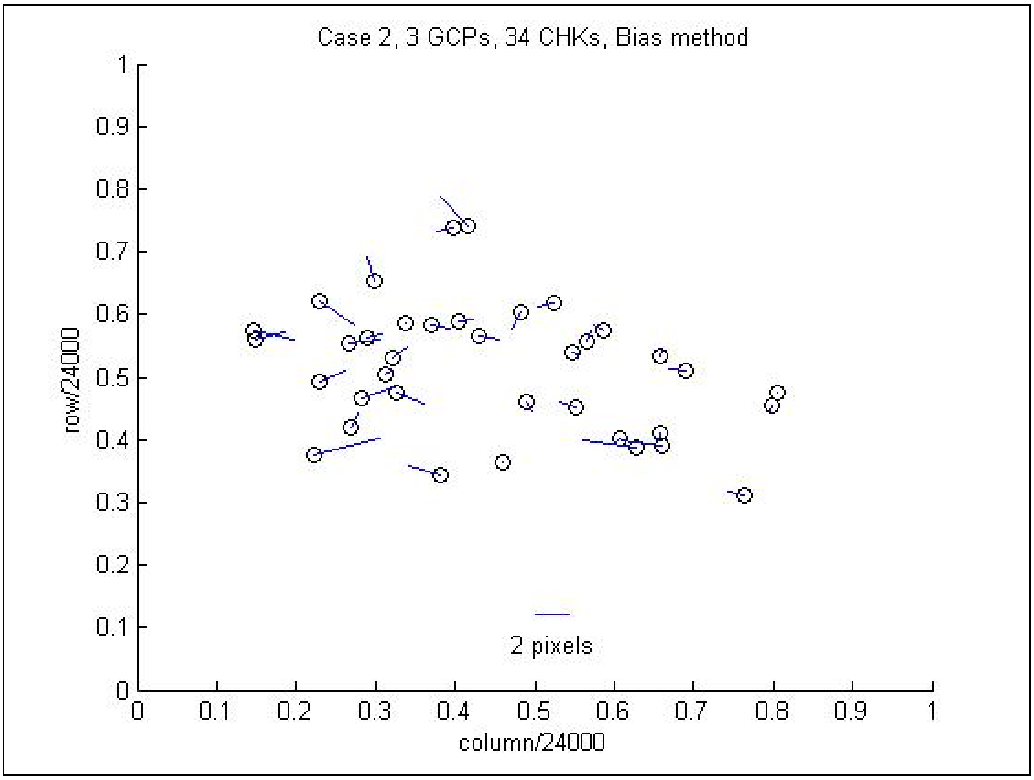


**Figure 4.86 Horizontal errors of Case 2 by the Bias method (3 GCP).**

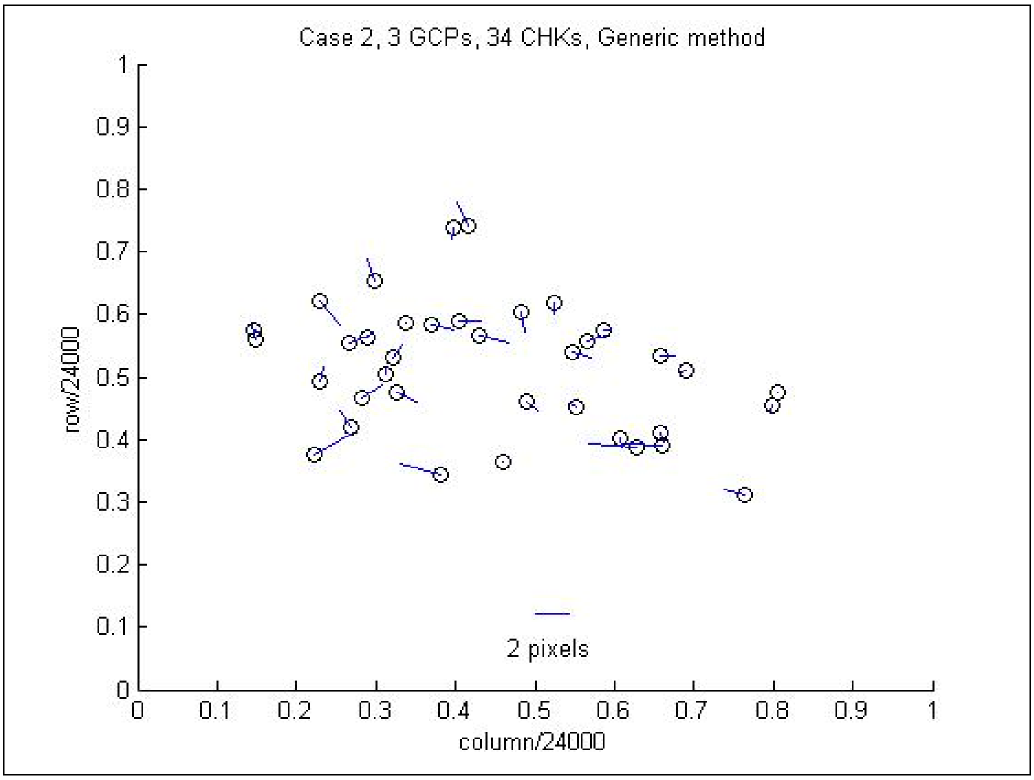


**Figure 4.87 Horizontal errors of Case 2 by the Generic method (3 GCP).**

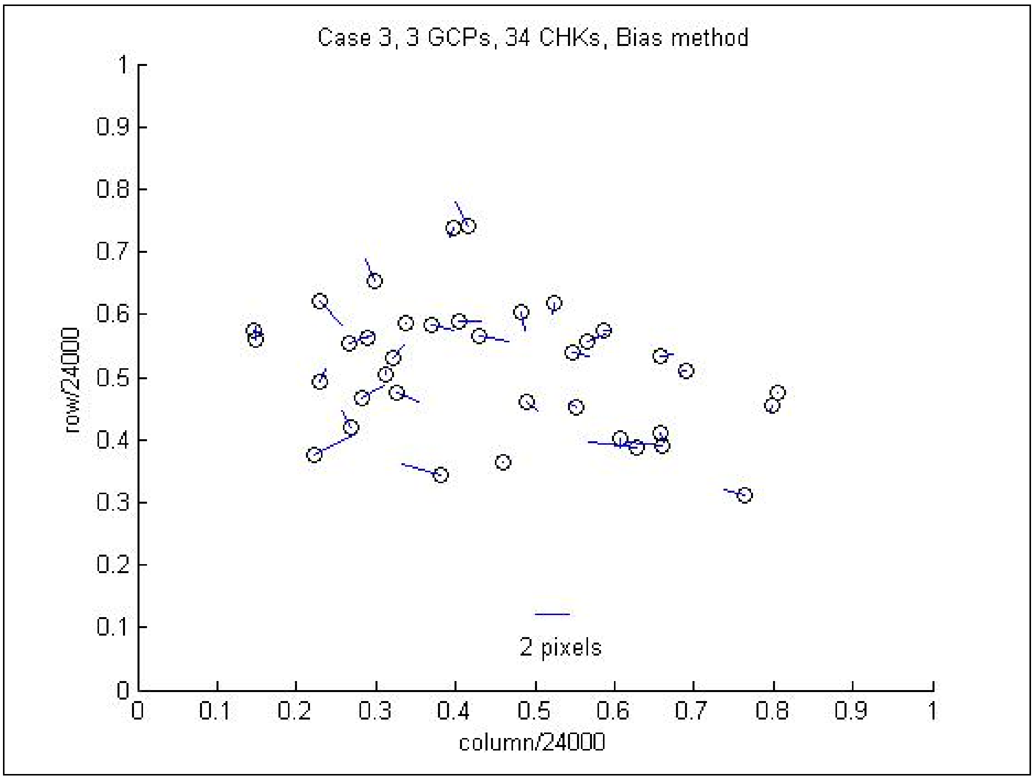


**Figure 4.88 Horizontal errors of Case 3 by the Bias method (3 GCP).**

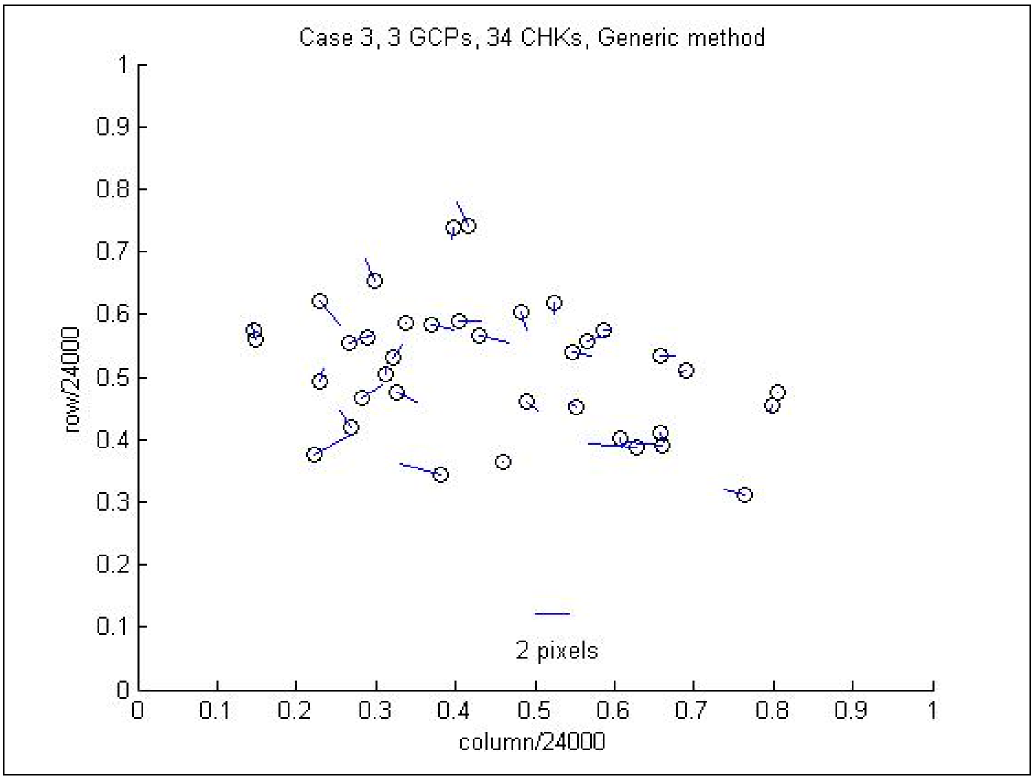


**Figure 4.89 Horizontal errors of Case 3 by the Generic method (3 GCP).**

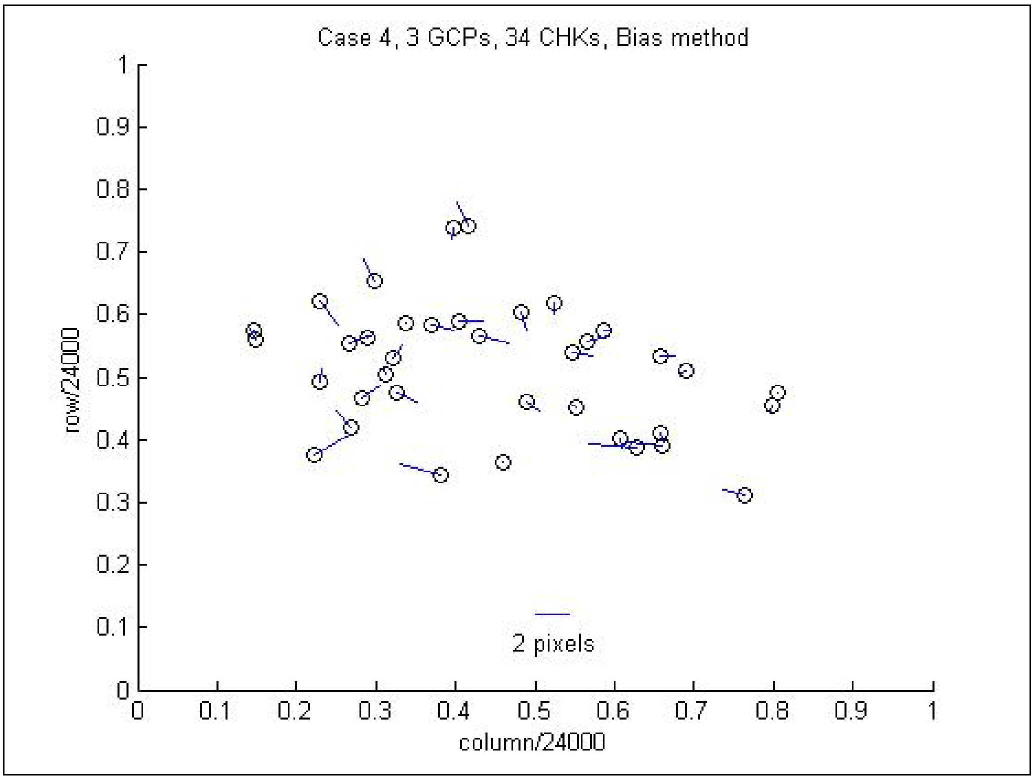


**Figure 4.90 Horizontal errors of Case 4 by the Bias method (3 GCP).**

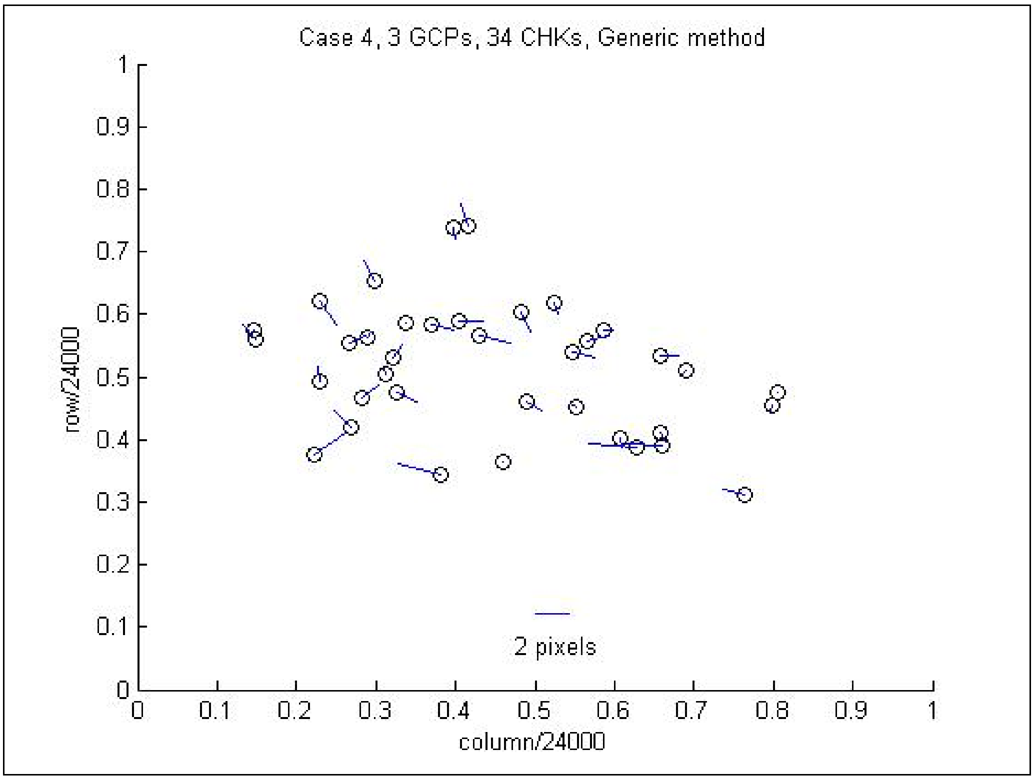


**Figure 4.91 Horizontal errors of Case 4 by the Generic method (3 GCP).**

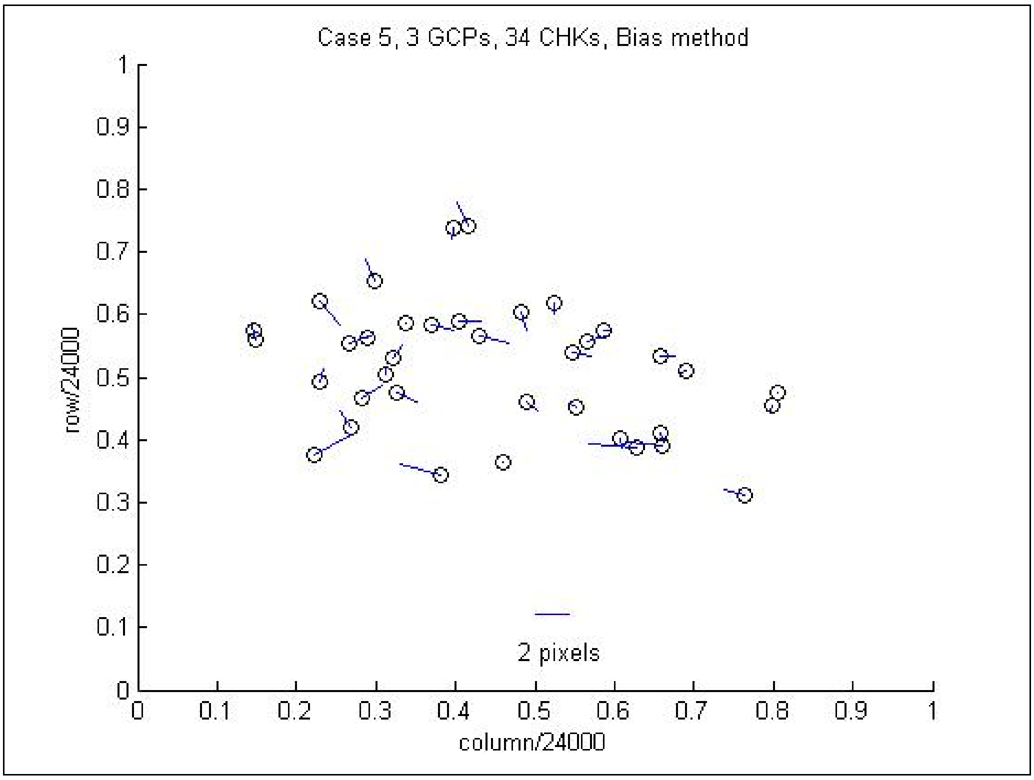


**Figure 4.92 Horizontal errors of Case 5 by the Bias method (3 GCP).**

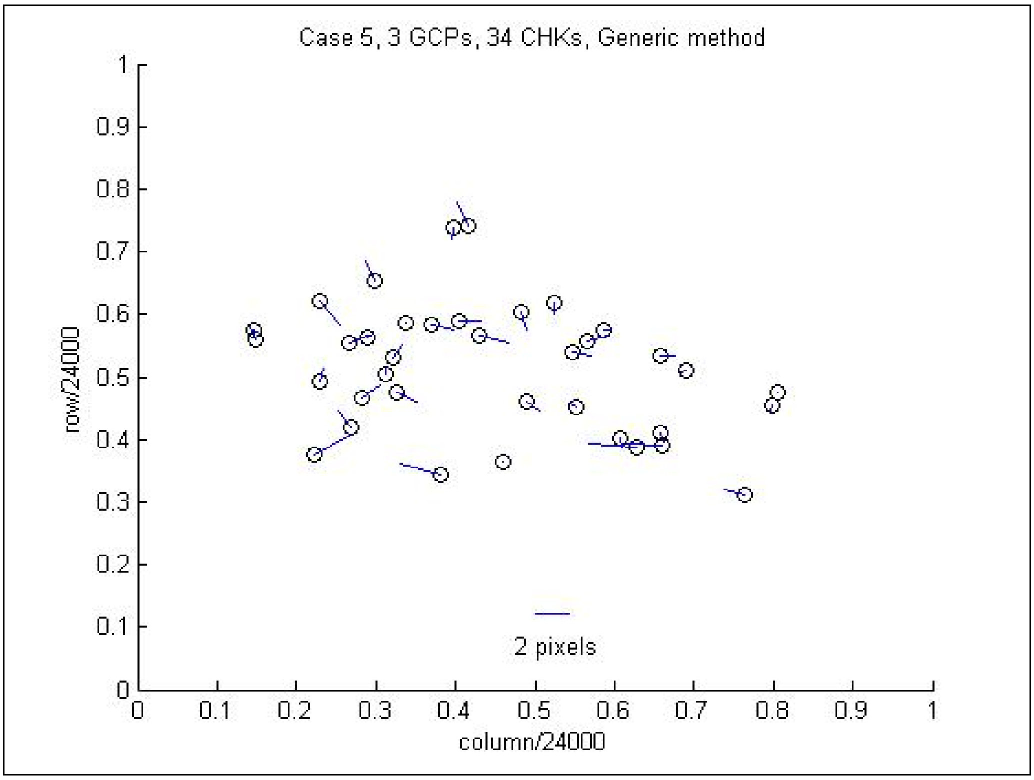


**Figure 4.93 Horizontal errors of Case 5 by the Generic method (3 GCP).**

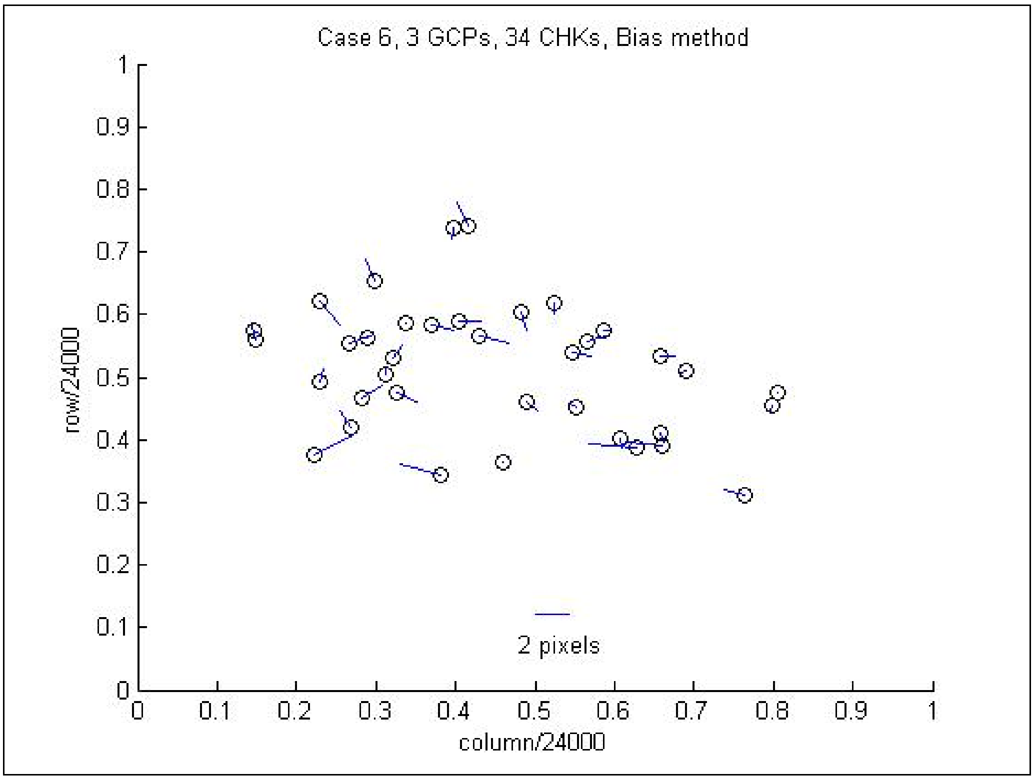


**Figure 4.94 Horizontal errors of Case 6 by the Bias method (3 GCP).**

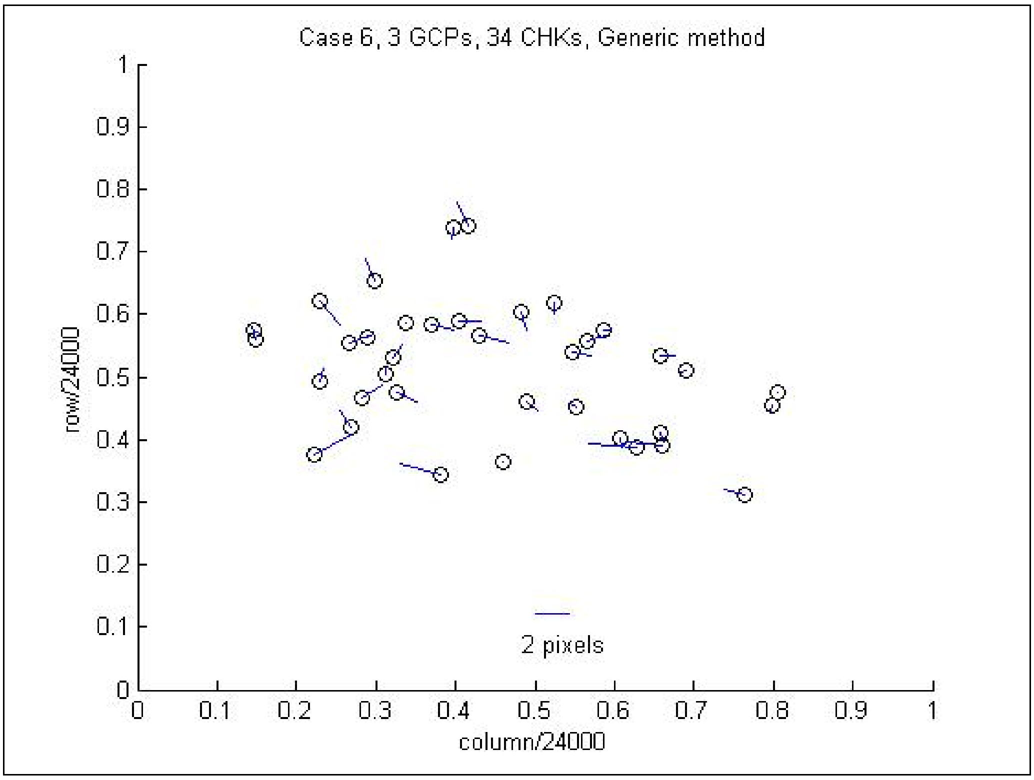


**Figure 4.95 Horizontal errors of Case 6 by the Generic method (3 GCP).**

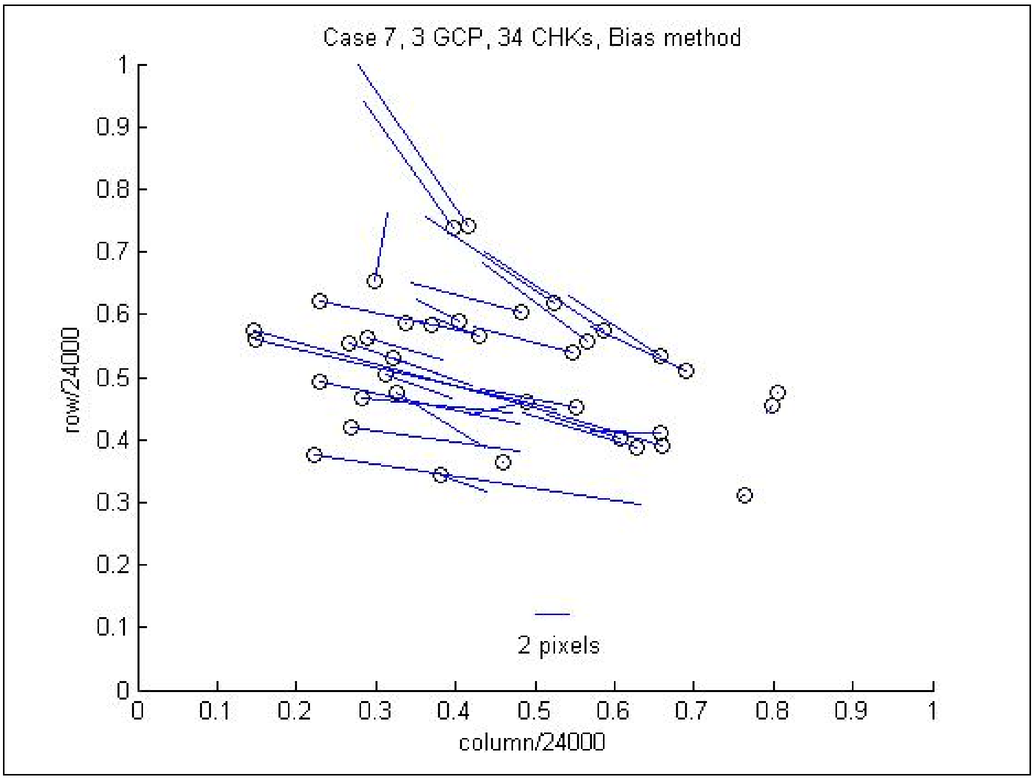


**Figure 4.96 Horizontal errors of Case 7 by the Bias method (3 GCP).**

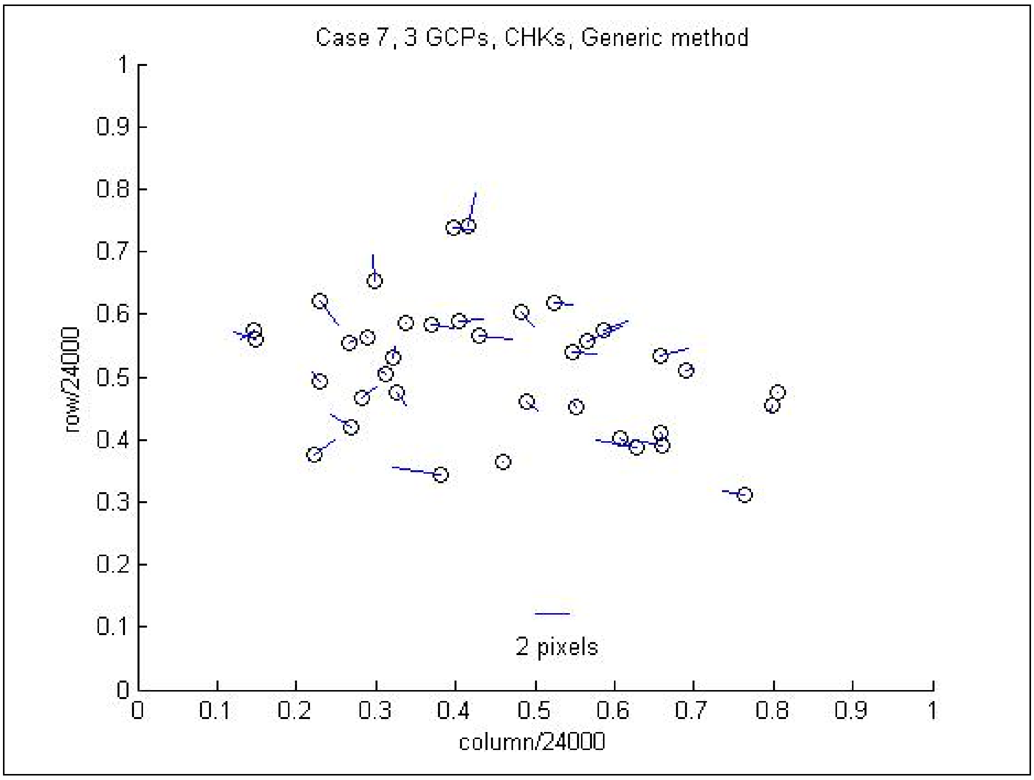


**Figure 4.97 Horizontal errors of Case 7 by the Generic method (3 GCP).**

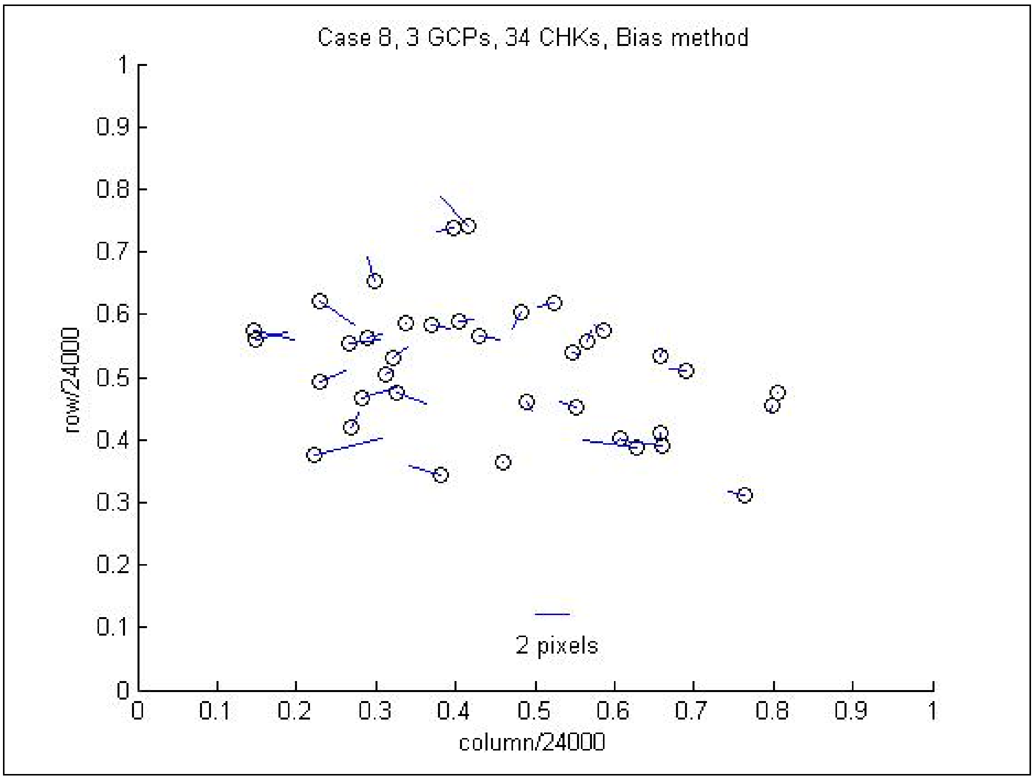


**Figure 4.98 Horizontal errors of Case 8 by the Bias method (3 GCP).**

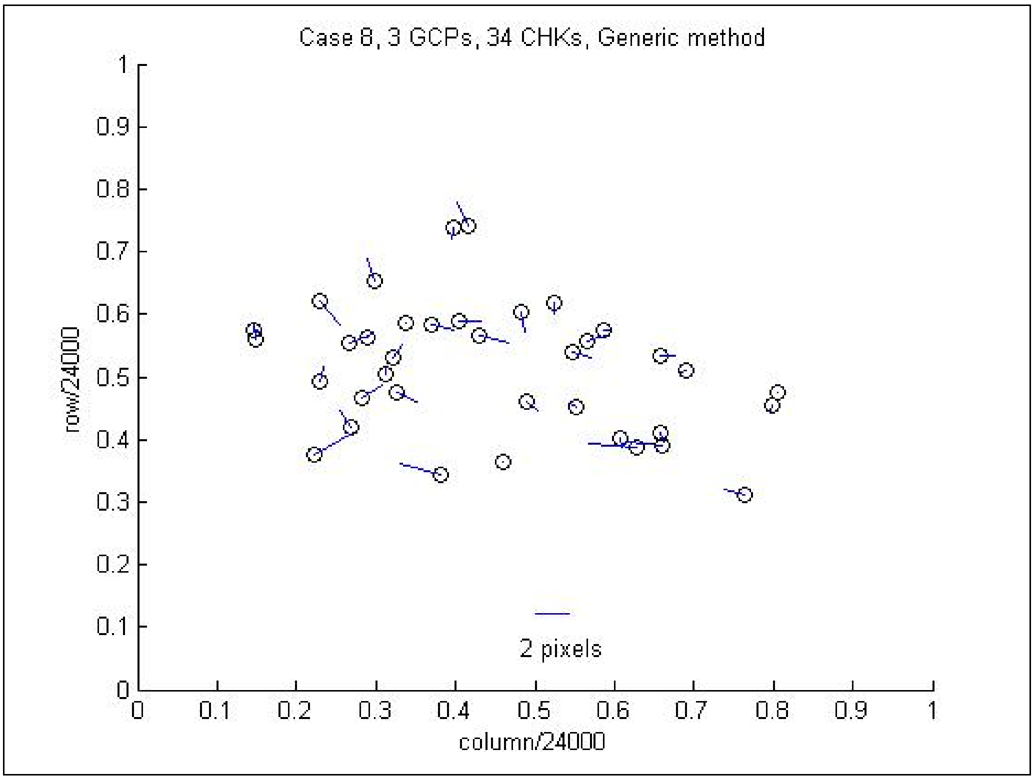


**Figure 4.99 Horizontal errors of Case 8 by the Generic method (3 GCP).**

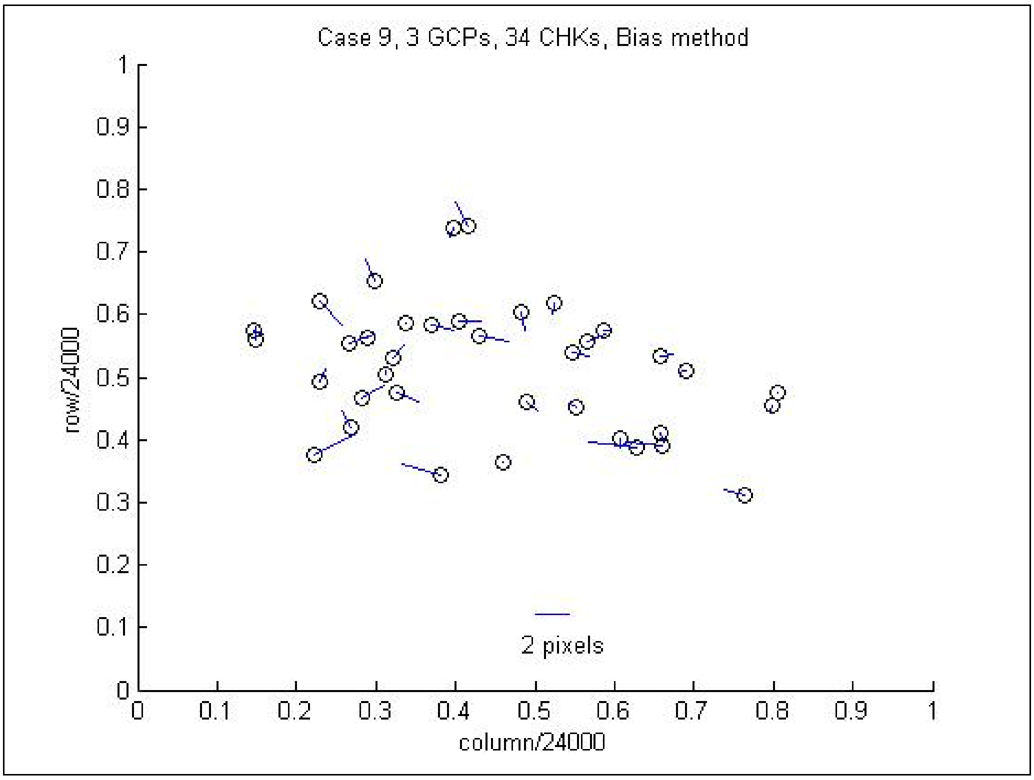

**Figure 4.100 Horizontal errors of Case 9 by the Bias method (3 GCP).**

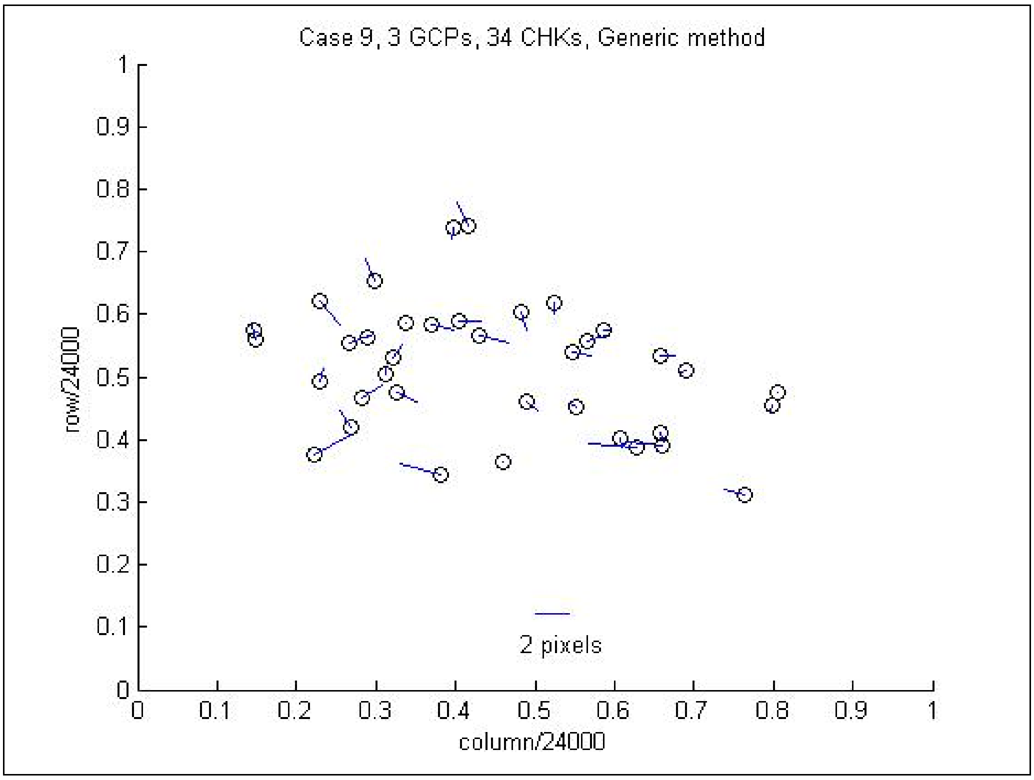

**Figure 4.101 Horizontal errors of Case 9 by the Generic method (3 GCP).**

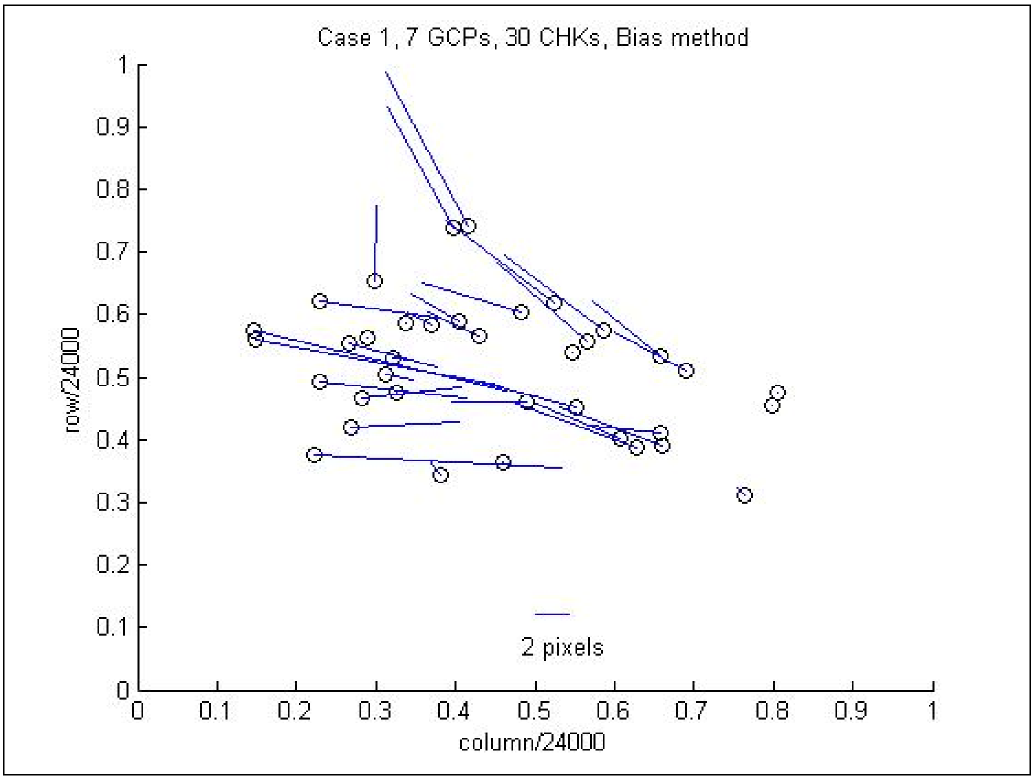


**Figure 4.102 Horizontal errors of Case 1 by the Bias method (7 GCP).**

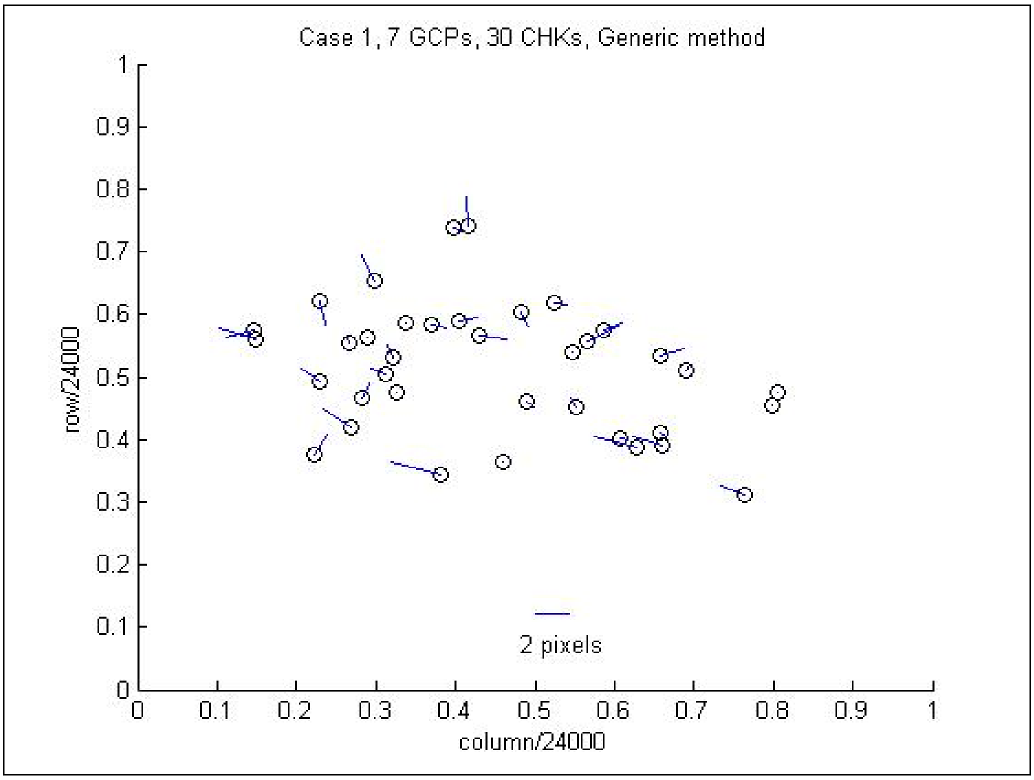


**Figure 4.103 Horizontal errors of Case 1 by the Generic method (7 GCP).**

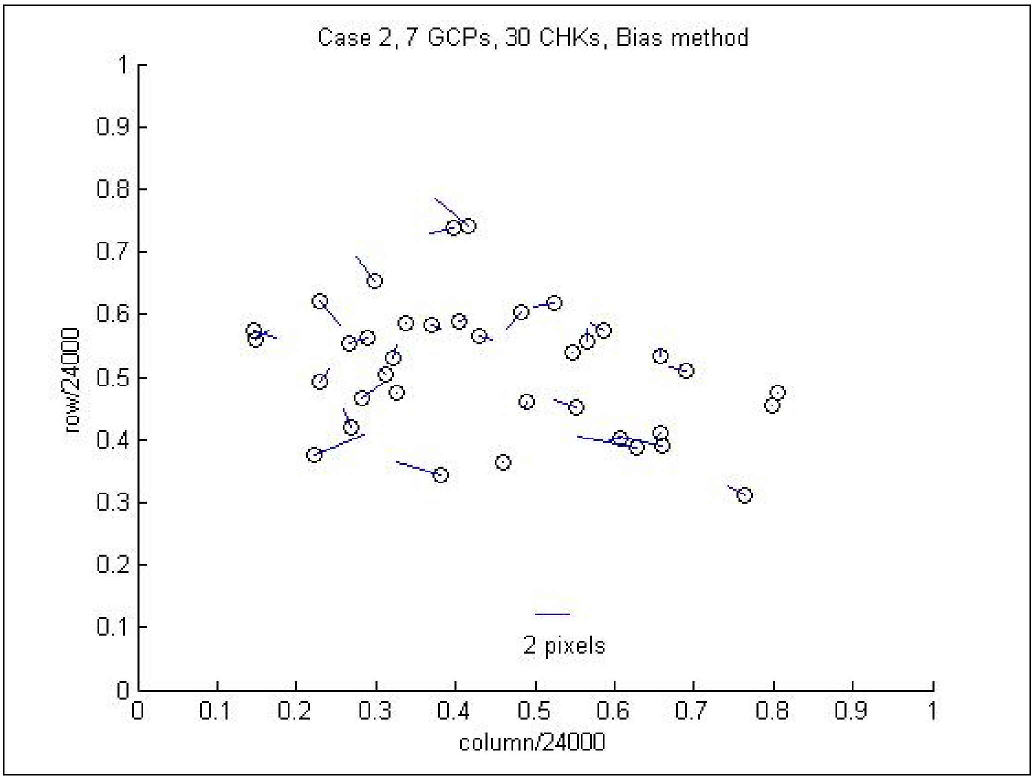

**Figure 4.104 Horizontal errors of Case 2 by the Bias method (7 GCP).**

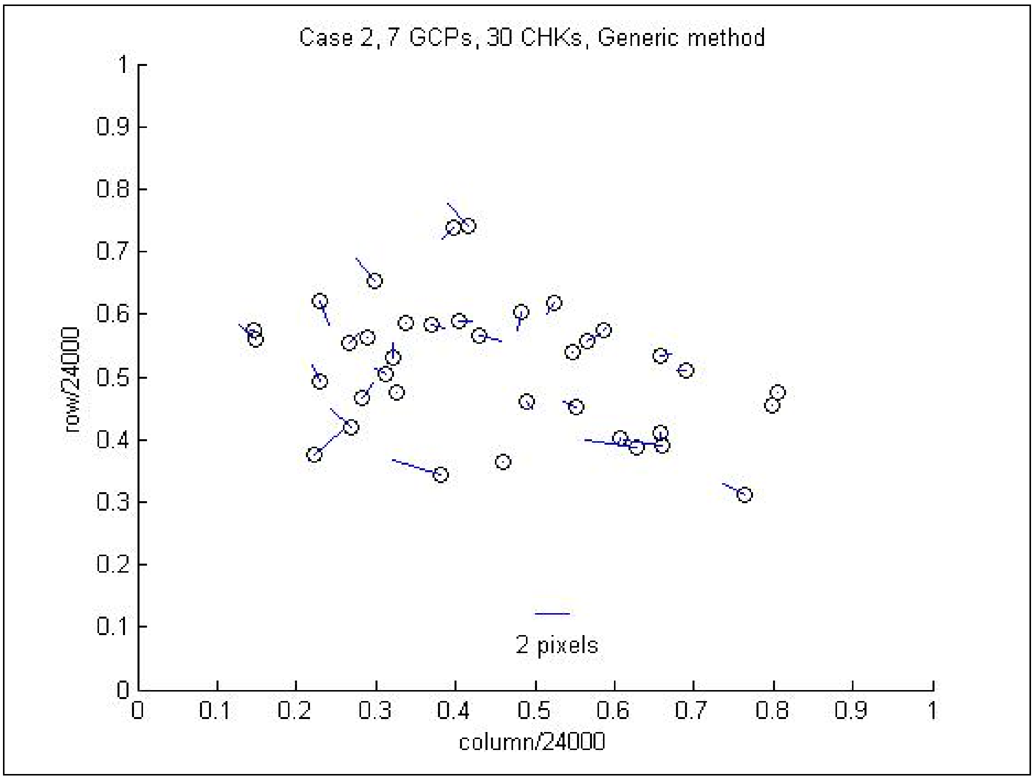

**Figure 4.105 Horizontal errors of Case 2 by the Generic method (7 GCP).**

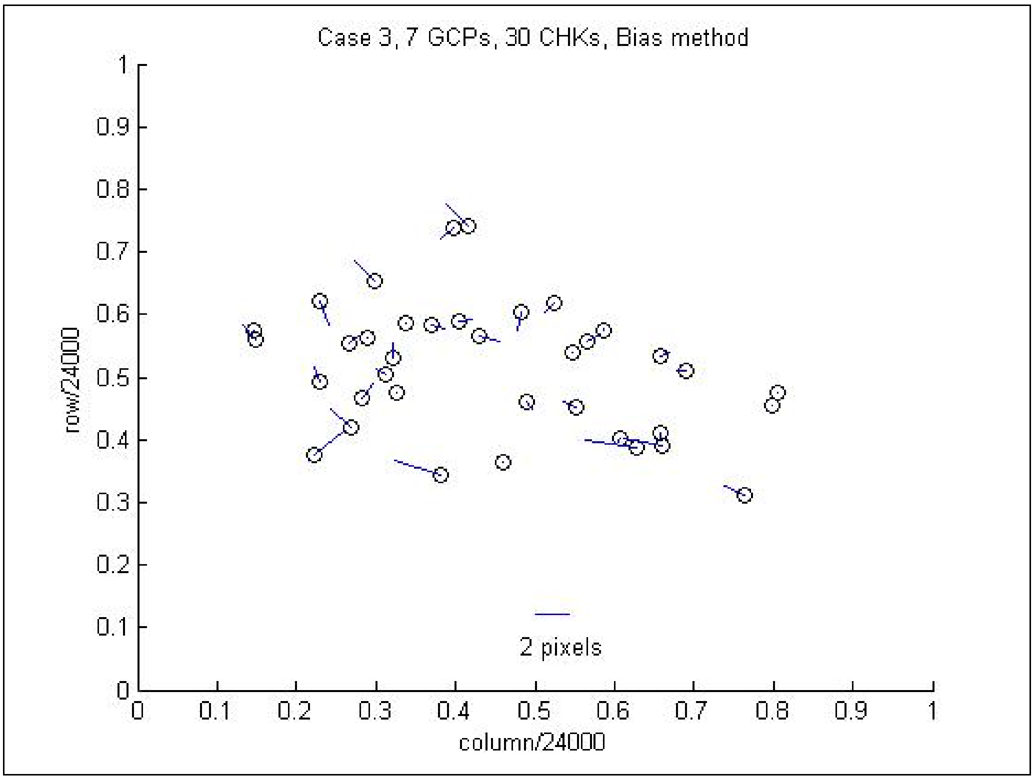


**Figure 4.106 Horizontal errors of Case 3 by the Bias method (7 GCP).**

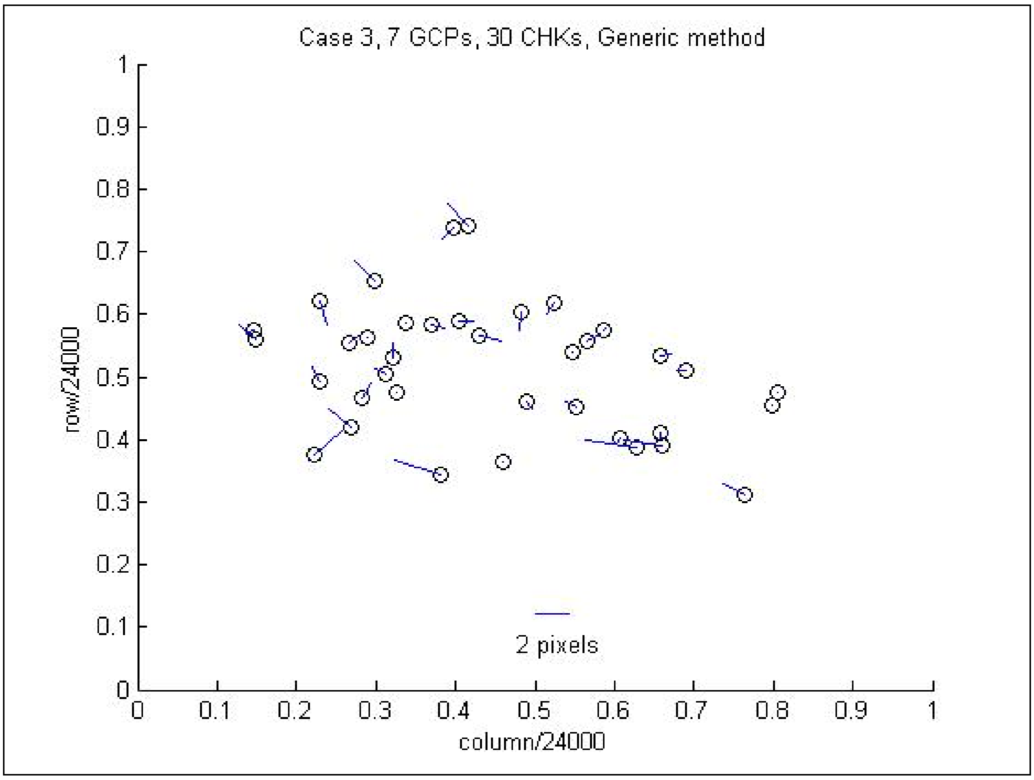


**Figure 4.107 Horizontal errors of Case 3 by the Generic method (7 GCP).**

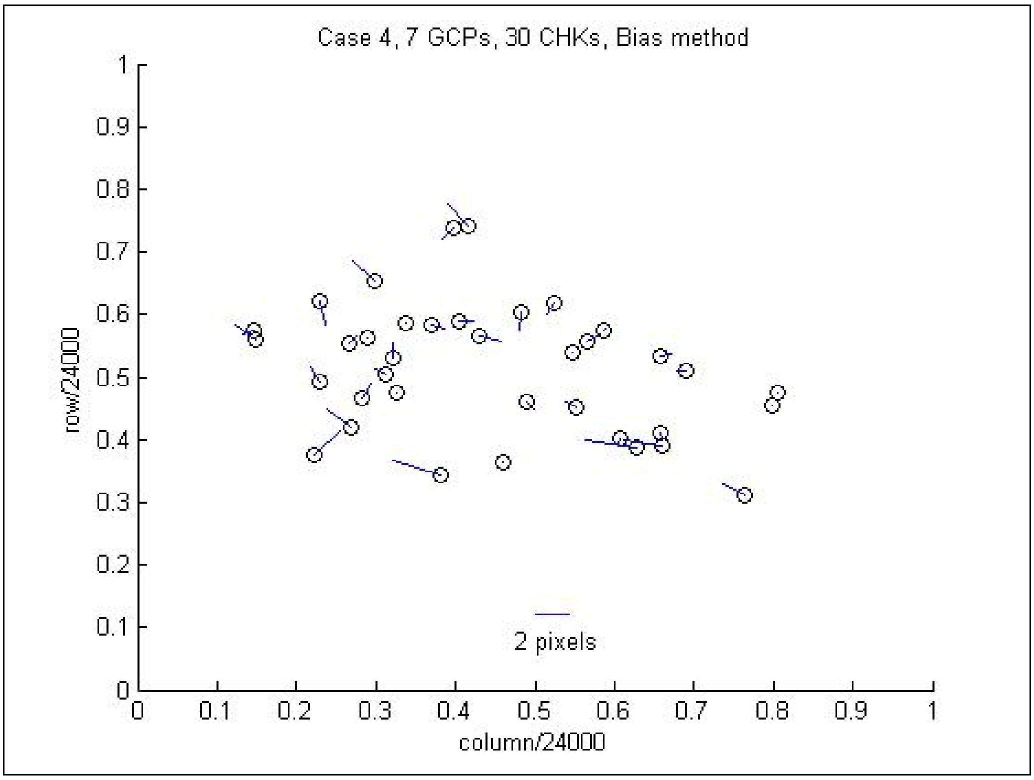

**Figure 4.108 Horizontal errors of Case 4 by the Bias method (7 GCP).**

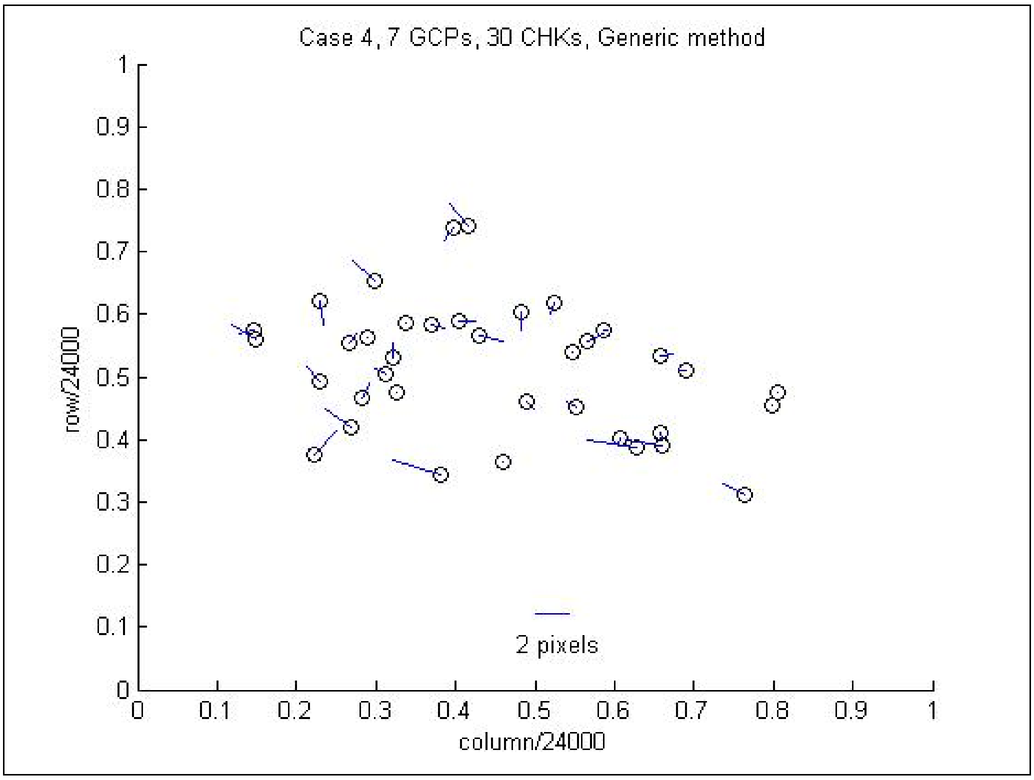

**Figure 4.109 Horizontal errors of Case 4 by the Generic method (7 GCP).**

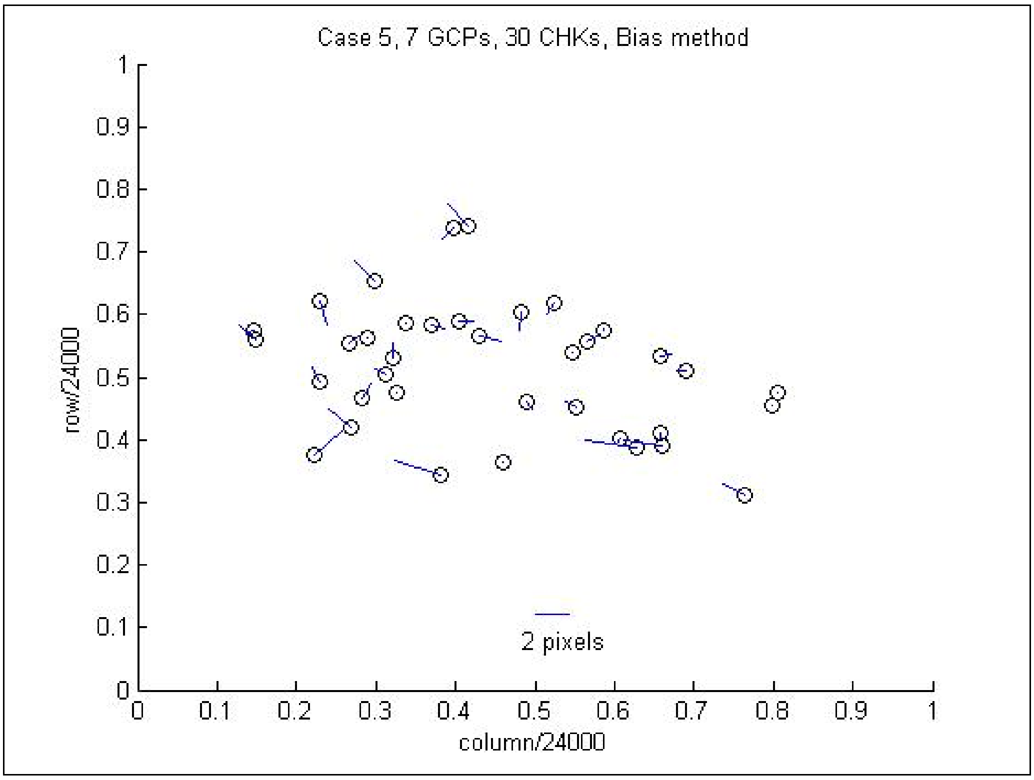


**Figure 4.110 Horizontal errors of Case 5 by the Bias method (7 GCP).**

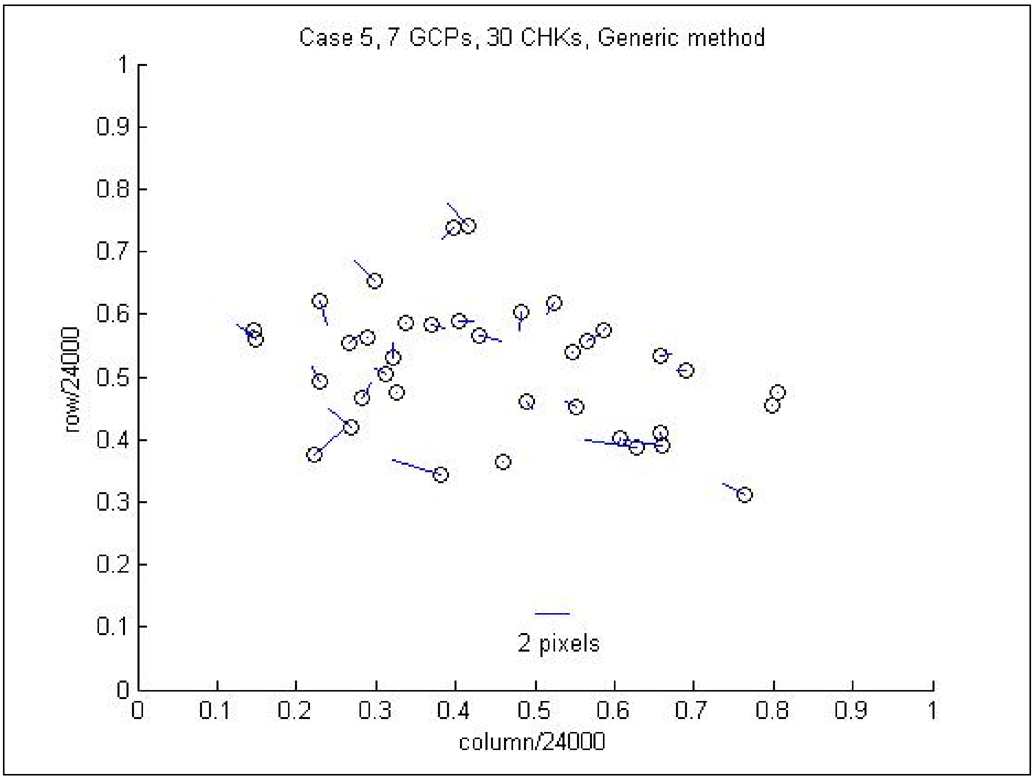


**Figure 4.111 Horizontal errors of Case 5 by the Generic method (7 GCP).**

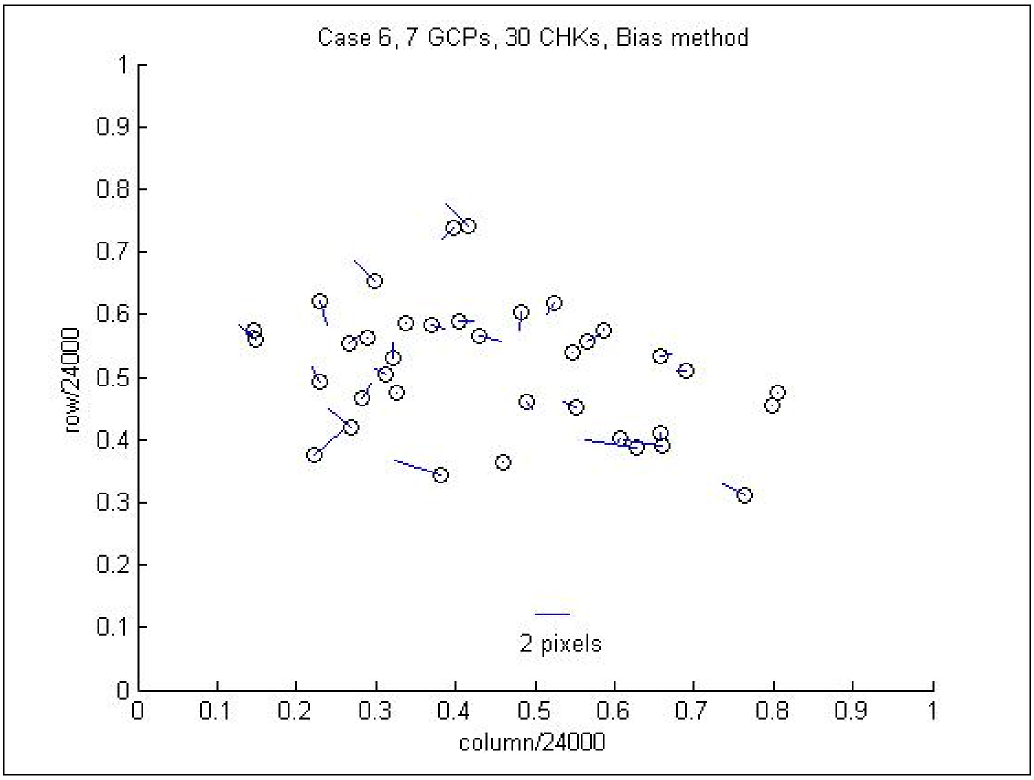


**Figure 4.112 Horizontal errors of Case 6 by the Bias method (7 GCP).**

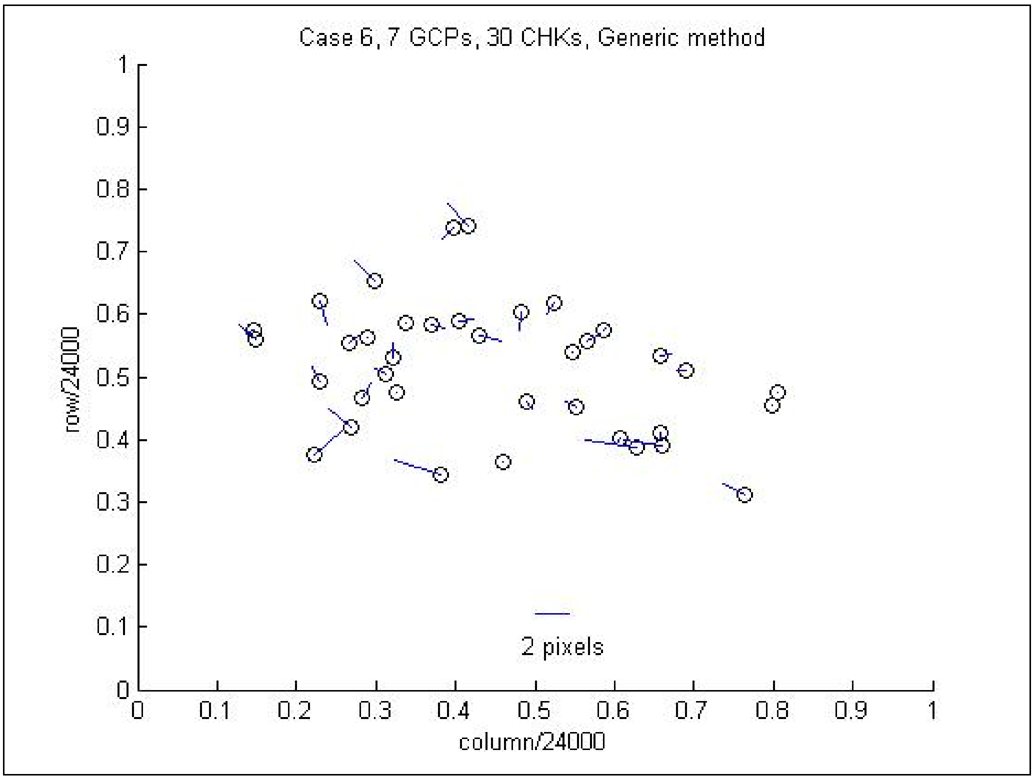


**Figure 4.113 Horizontal errors of Case 6 by the Generic method (7 GCP).**

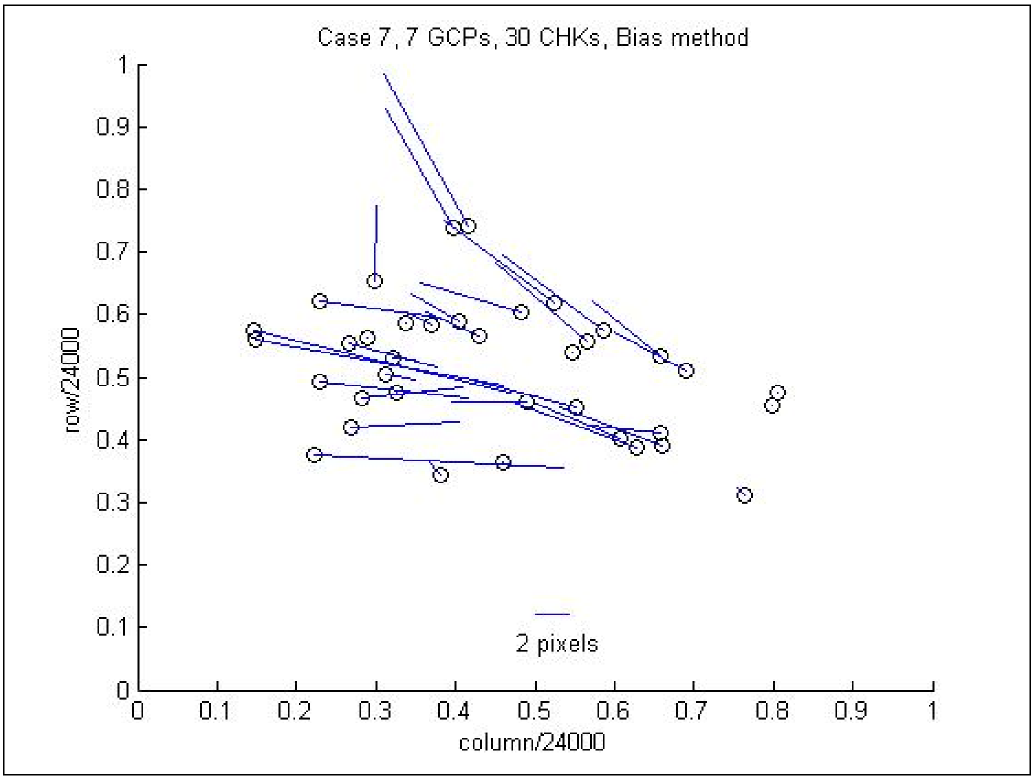


**Figure 4.114 Horizontal errors of Case 7 by the Bias method (7 GCP).**

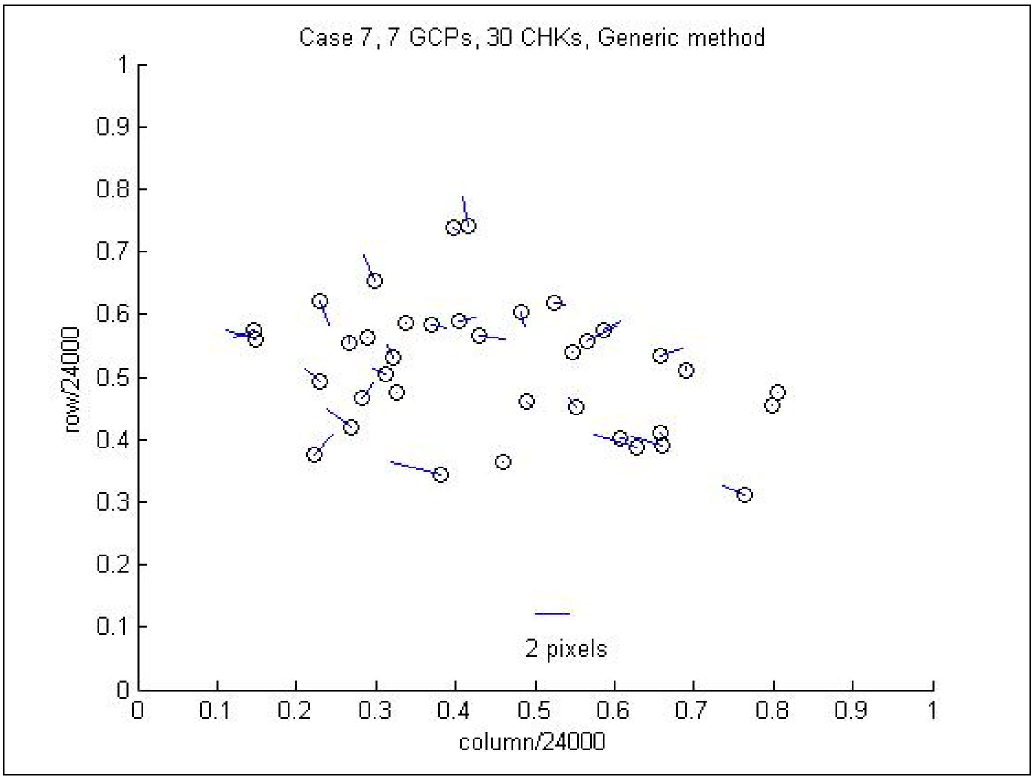


**Figure 4.115 Horizontal errors of Case 7 by the Generic method (7 GCP).**

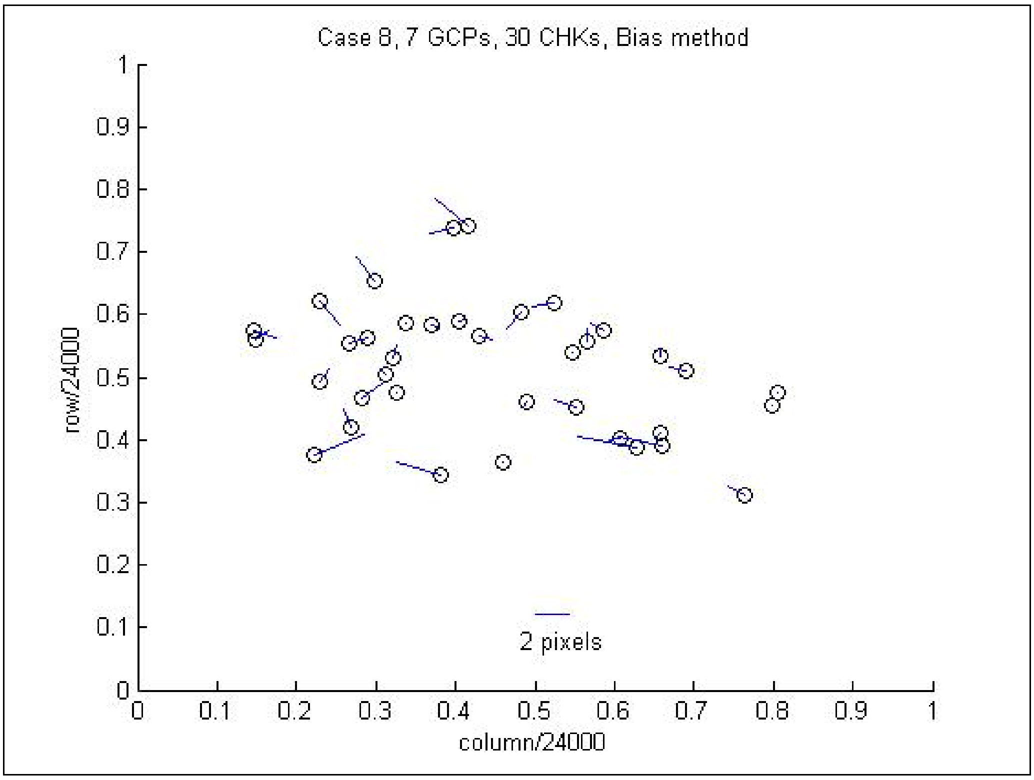

**Figure 4.116 Horizontal errors of Case 8 by the Bias method (7 GCP).**

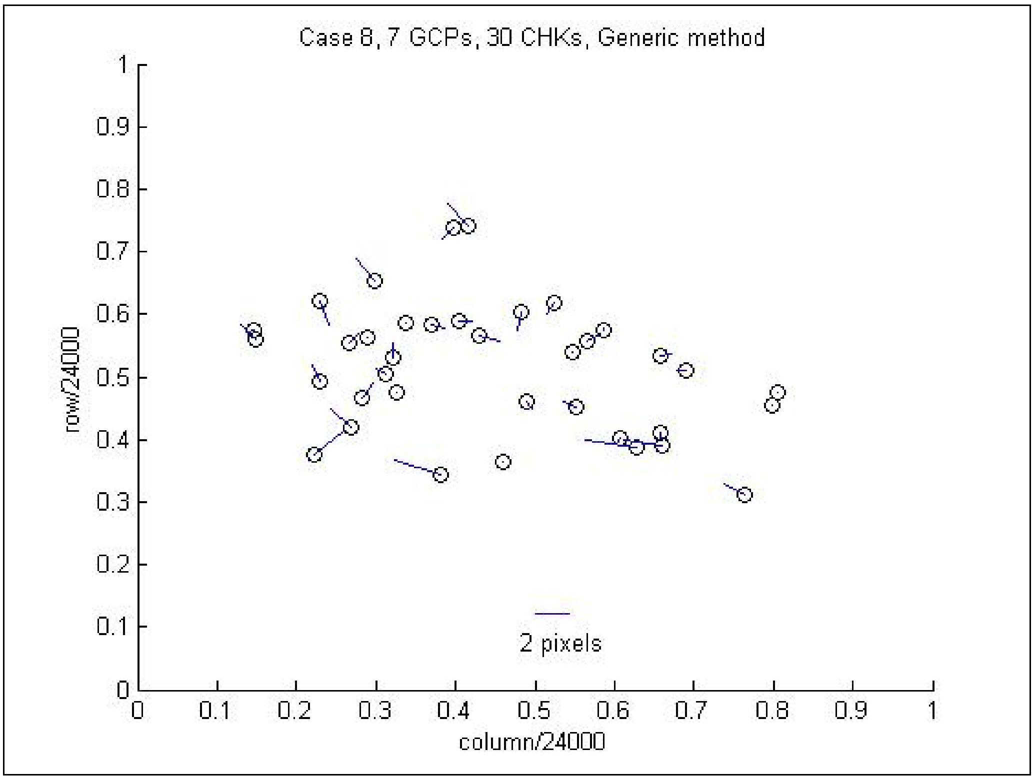

**Figure 4.117 Horizontal errors of Case 8 by the Generic method (7 GCP).**

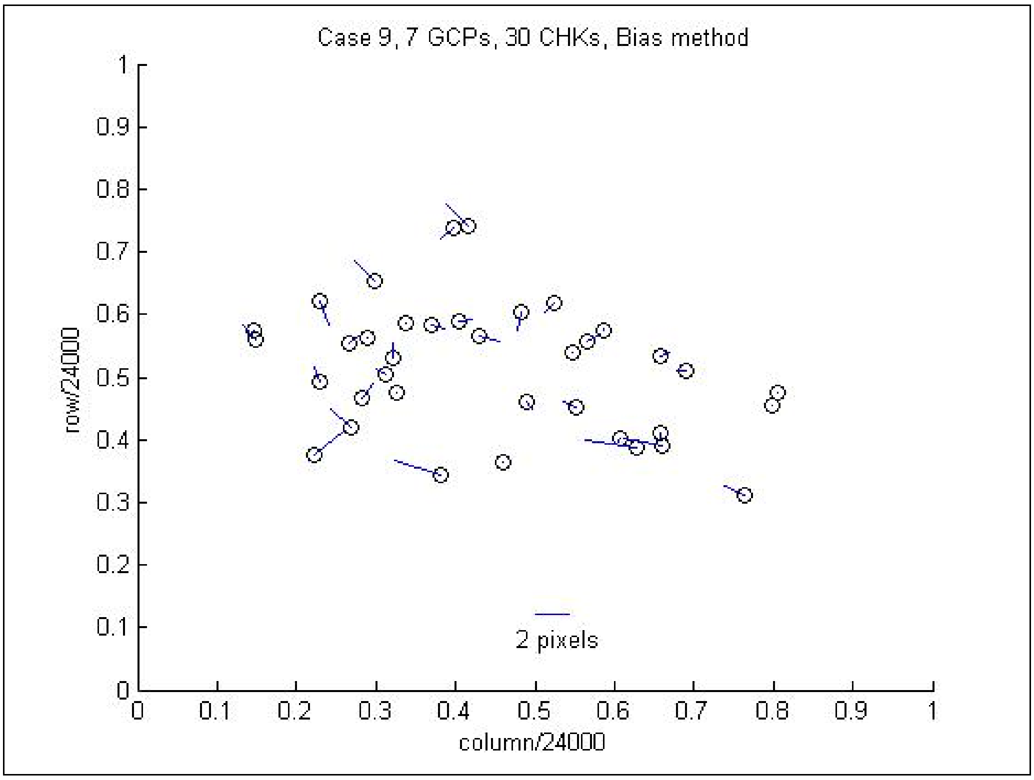


**Figure 4.118 Horizontal errors of Case 9 by the Bias method (7 GCP).**

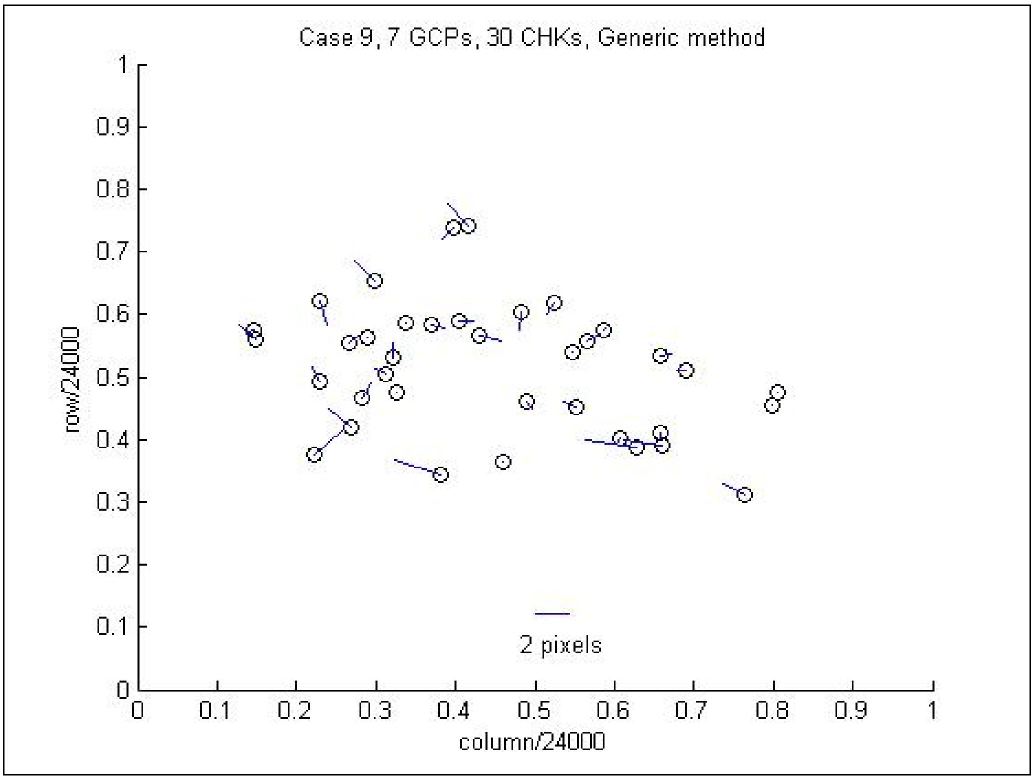


**Figure 4.119 Horizontal errors of Case 9 by the Generic method (7 GCP).**

**Table 4.9** lists the accuracy comparison between the Bias method and Generic method by using 1 GCP and 36 CHK points in 9 cases. **Table 4.10** lists the accuracy comparison between the Bias method and Generic method by using 3 GCP and 34 CHK points in 9 cases. **Table 4.11** lists the accuracy comparison between the Bias method and Generic method by using 7 GCP and 30 CHK points in 9 cases.

**Table 4.9 Accuracy comparison between the Bias method and Generic method by using 1 GCP and 36 CHK points in 9 cases.**

| No. of case | 1 GCP, 36 CHKs | | | |
|---|---|---|---|---|
| | Bias method | | Generic method | |
| | Column Std. Dev. (pixel) | Row Std. Dev. (pixel) | Column Std. Dev. (pixel) | Row Std. Dev. (pixel) |
| 1 | 1040.90 | 166.77 | 959.91 | 17.22 |
| 2 | 109.06 | 7.59 | 98.33 | 5.45 |
| 3 | 15.86 | 4.58 | 14.79 | 3.32 |
| 4 | 5.40 | 7.36 | 3.41 | 5.94 |
| 5 | 5.52 | 4.68 | 5.34 | 4.45 |
| 6 | 5.53 | 4.42 | 5.54 | 4.30 |
| 7 | 1040.75 | 160.96 | 961.33 | 19.70 |
| 8 | 109.07 | 7.27 | 98.55 | 5.62 |
| 9 | 15.86 | 4.55 | 14.81 | 3.31 |

**Table 4.10 Accuracy comparison between the Bias method and Generic method by using 3 GCP and 34 CHK points in 9 cases.**

| No. of case | 3 GCP, 34 CHKs | | | |
|---|---|---|---|---|
| | Bias method | | Generic method | |
| | Column Std. Dev. (pixel) | Row Std. Dev. (pixel) | Column Std. Dev. (pixel) | Row Std. Dev. (pixel) |
| 1 | 4.22 | 7.88 | 0.86 | 1.29 |
| 2 | 0.85 | 1.50 | 0.88 | 1.13 |
| 3 | 0.86 | 1.15 | 0.87 | 1.13 |
| 4 | 0.87 | 1.13 | 0.87 | 1.14 |
| 5 | 0.87 | 1.13 | 0.87 | 1.13 |
| 6 | 0.87 | 1.137 | 0.86 | 1.13 |
| 7 | 4.20 | 7.97 | 0.86 | 1.21 |
| 8 | 0.85 | 1.51 | 0.88 | 1.13 |
| 9 | 0.86 | 1.15 | 0.87 | 1.13 |

**Table 4.11 Accuracy comparison between the Bias method and Generic method by using 7 GCP and 30 CHK points in 9 cases.**

| No. of case | 7 GCP, 30 CHKs | | | |
|---|---|---|---|---|
| | Bias method | | Generic method | |
| | Column Std. Dev. (pixel) | Row Std. Dev. (pixel) | Column Std. Dev. (pixel) | Row Std. Dev. (pixel) |
| 1 | 4.02 | 6.71 | 0.97 | 1.25 |
| 2 | 0.95 | 1.39 | 0.97 | 1.15 |
| 3 | 0.95 | 1.15 | 0.95 | 1.15 |
| 4 | 0.95 | 1.16 | 0.95 | 1.15 |
| 5 | 0.95 | 1.15 | 0.95 | 1.15 |
| 6 | 0.95 | 1.15 | 0.95 | 1.15 |
| 7 | 3.99 | 6.79 | 0.98 | 1.18 |
| 8 | 0.95 | 1.39 | 0.97 | 1.15 |
| 9 | 0.95 | 1.15 | 0.95 | 1.15 |

**FIG. 4.120 ~ 4.122** illustrate the RMSE of 36 CHK points after RPC refinement with 1 GCP in 9 cases. **FIG. 4.123 ~ 4.125** show the RMSE of 34 CHK points after RPC refinement with 3 GCPs in 9 cases. **FIG. 4.126 ~ 4.128** illustrate the RMSE of 30 CHK points after RPC refinement with 7 GCPs in 9 cases.

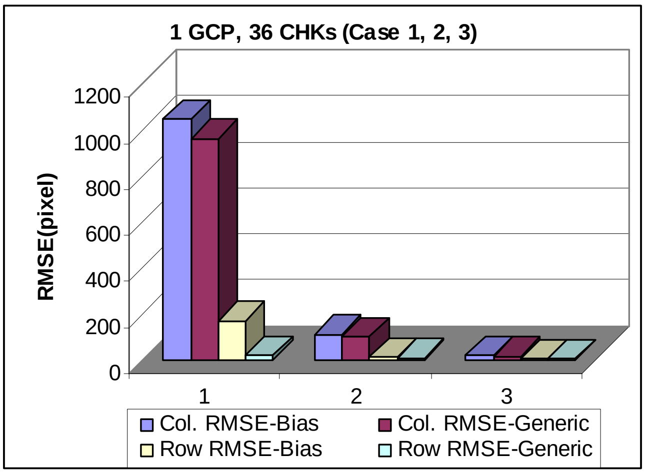


**Figure 4.120 RMSE of 36 CHK points after RPC refinement with 1 GCP in case 1, 2, 3.**

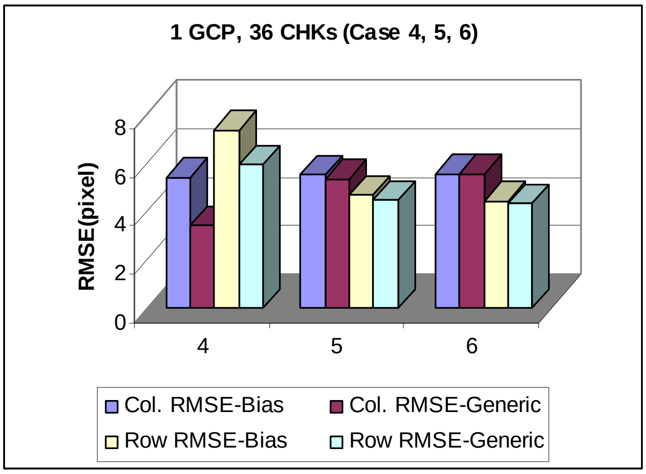


**Figure 4.121 RMSE of 36 CHK points after RPC refinement with 1 GCP in case 4, 5, 6.**

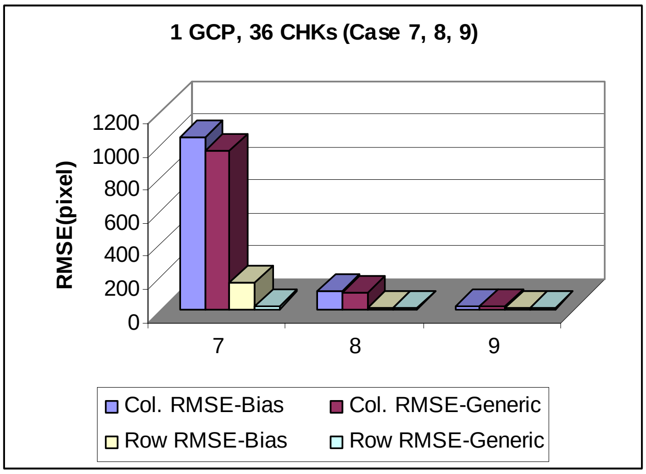


**Figure 4.122 RMSE of 36 CHK points after RPC refinement with 1 GCP in case 7, 8, 9.**

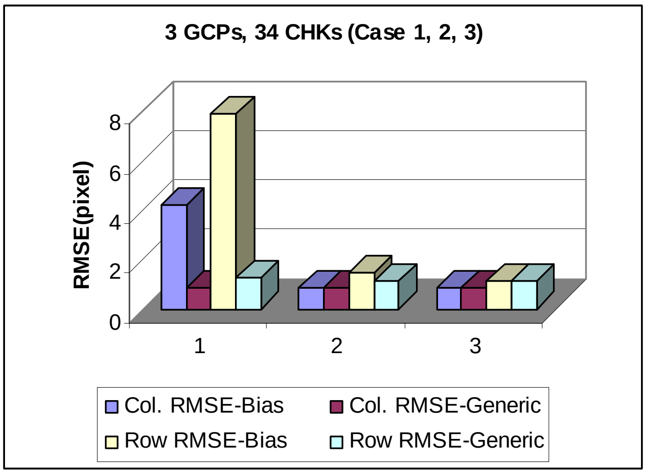


**Figure 4.123 RMSE of 34 CHK points after RPC refinement with 3 GCPs in case 1, 2, 3.**

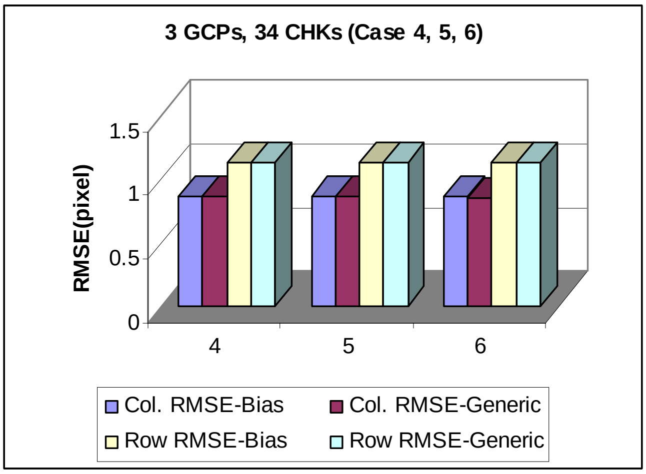


**Figure 4.124 RMSE of 34 CHK points after RPC refinement with 3 GCPs in case 4, 5, 6.**

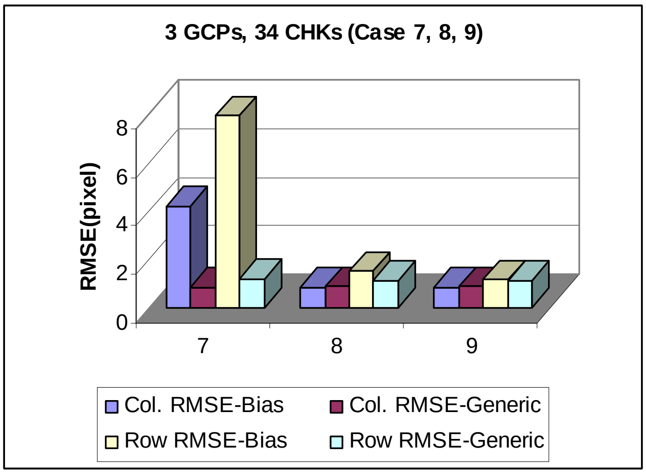


**Figure 4.125 RMSE of 34 CHK points after RPC refinement with 3 GCPs in case 7, 8, 9.**

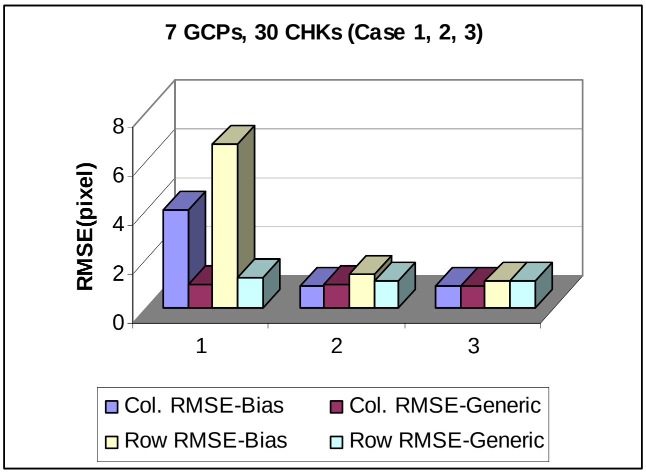


**Figure 4.126 RMSE of 30 CHK points after RPC refinement with 7 GCPs in case 1, 2, 3.**

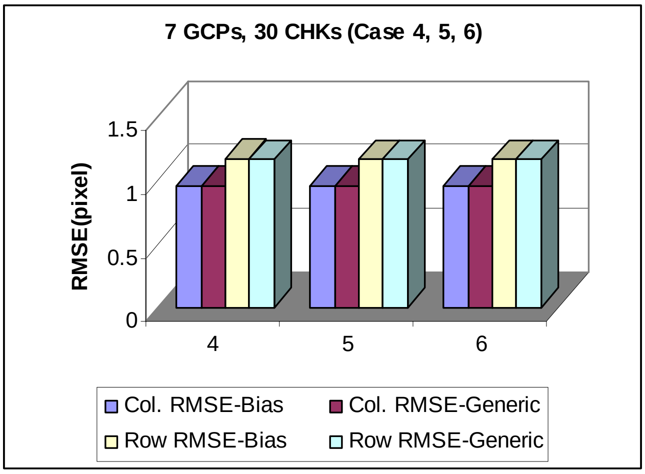


**Figure 4.127 RMSE of 30 CHK points after RPC refinement with 7 GCPs in case 4, 5, 6.**

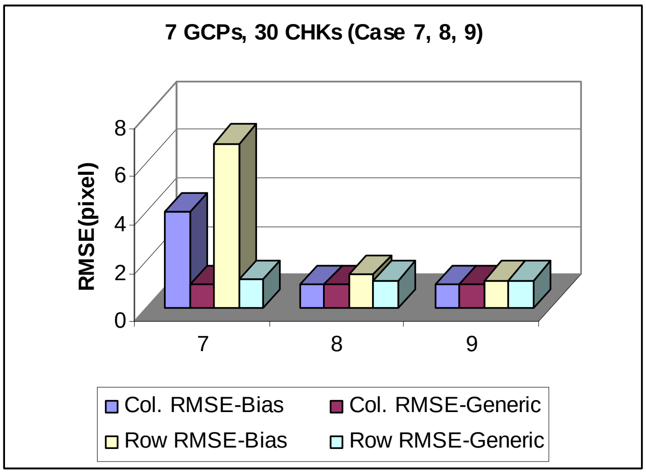


**Figure 4.128 RMSE of 30 CHK points after RPC refinement with 7 GCPs in case 7, 8, 9.**

From **Table 4.9~4.11** and **Figure 4.120~4.128**, it is evident that the Bias Compensation method is very good at detecting ephemeris data error and can work well under a variety of different ephemeris error, but with increasing attitude error, use of the Bias Compensation method becomes progressively less feasible. This is particularly obvious in case 1 and case 7 when the attitude error is greater than 0.01 radians (**Table 4.10, 4.11** and **Figure 4.123, 4.125, 4.126, 4.128)** where the RMSE of column and row for the Bias Compensation method ranges from about 4 to 7 pixels. In contrast to this, the Generic method is very stable in that the RMSE remains about 1 pixel under a variety of different cases.

From the experiments, we can at least recognize that,

1) The main geometric error with the high resolution satellite sensors is verified again to be a drift error (Grodeki and Gene, 2003). The experiment results (**Figures 4.66** through **4.83**) when only 1 GCP was used obviously illustrated this point. That is the reason why the Bias method works well with IKONOS and QuickBird images.
2) With the increasing of the sensor's position error and attitude error (from case 3 to case 1, case 9 to case 7), especially the attitude error, the Bias method gradually becomes less effective (case 1 and 7, **Figure 4.84, 4.85, 4.96, 4.97, 4.102, 4.103, 4.114, 4.115** ). The error of the sensor model refined by the Bias method rapidly increases with the error of the sensor's attitude. On the other hand, Bias method can handle the sensor's position error perfectly. The reason is that the Bias method simulates the error in the image space with a linear function.
3) The experiments clearly illustrate the robust of the proposed Generic method. No matter what kind of combination of the sensor's position and attitude errors, the Generic can always adjust the sensor model to pixel level accuracy.

## 4.5 Conclusion

Unlike the Bias Compensation method which is defined in image space, the proposed Generic method is defined in object space. It directly modifies the RPC coefficients, but it does not require any supplemental information about RPC, such as the covariance matrices, like other direct methods.

The Generic method simulates the sensor’s imaging geometry and can be used to adjust the camera’s position and attitude. Therefore, it can effectively refine the RPC under a variety of different conditions. As position and attitude errors increase, the Bias Compensation method becomes less effective. Especially when the attitude error is greater than 0.01 radians, the RMSE of column and row error for the Bias Compensation method ranges from about 4 to 7 pixels. In contrast to this, the Generic method described in this paper is very stable under a variety of different conditions. Even when the attitude error is greater than 0.01 radians, the RMSE always remains about 1 pixel. In fact, it appears that the Generic method completely overcomes the drawbacks and limitations of the Bias Compensation method. It can be used regardless of the sensor’s field of view, attitude error or position error.

We hope this Generic method can be used to refine not only the RPCs of high-resolution satellite images, but also other generic sensor models. In future, we plan to test this method under a wider variety of different conditions and sensors, such as airborne wide-angle cameras, large off-nadir angles, and different satellite data.

## ACKNOWLEDGEMENTS

This research is sponsored by the Natural Sciences and Engineering Research Council of Canada through the Discovery Grant (NSERC Discovery Grant) awarded to Dr. Yun Zhang, the second author of the paper. We would like to acknowledge that Prof. Clive Fraser, Department of Geomatic Engineering, University of Melborne, Australia, provided us satellite image and ground control data for the tests.

Special thanks go to Mr. David C. Whyte, Department of Environment, NB, Canada, who reviewed the manuscript of this report.

This research was made possible through a scholarship indirectly from NSERC Discovery Grant which was granted to my supervisor Dr. Yun Zhang.

# REFERENCES

Bang Ki In, Soo Jeong, Kyung-Ok Kim. (2003). "Modification of sensor model parameters with a few GCP." *ASPRS 2003 annual conference proceedings*, May 2003, Anchorage, Alaska.

Bang Ki In, Soo Jeong, Kyung-Ok Kim, and Woosug Cho. (2003). "Automatic DEM generation using Ikonos stereo imagery." URL: http://www.ieeexplore.ieee.org/iel5/9010/28607/01295492.pdf?arnumber=1295492, last date accessed 6 January 2008.

Chen Liang-Chien, Tee-Ann Teo, and Chien-Liang Liu. (2006). "The geometrical comparisons of RSM and RFM for FORMOSAT-2 satellite images." *Photogrammetric Engineering & Remote Sensing,* Vol. 72, No. 5, pp. 573-579.

Cheng, P., T. Toutin, and Y. Zhang. (2003a). "QuickBird-Geometric correction, data fusion, and automatic DEM extraction." *Proceedings of the 24th Asia Conference on Remote Sensing (ACRS 2003) and 2003 International Symposium on Remote Sensing*, 03-07 November, Busan, Korea, unpaginated CD_ROM.

Cheng, P., T. Toutin, Y. Zhang, and M. Wood. (2003b). "QuickBird-Geometric correction, path and block processing and data fusion." *Earth Observation Magazine*, 12(3):24-30.

Di Kaichang, Ruijin Ma, and Rong Xing Li. (2003). "Rational functions and potential for rigorous sensor model recovery." *Photogrammetric Engineering & Remote Sensing,* Vol. 69, No. 1, pp. 33-41.

Dial Gene and Grodecki Jacek. (2002[a]). "Block adjustment with rational polynomial camera models." *ACSM-ASPRS 2002 annual conference proceedings.*

Dial Gene and Grodecki Jacek. (2002[b]). "IKONOS accuracy without ground control." *Pecora 15/Land Satellite Information IV/ISPRS Commission I/FIEOS 2002 Conference Proceedings*.

Dial Gene and Grodecki Jacek. (2005). "RPC Replacement Camera Models." A*SPRS 2005 annual conference proceedings,* Baltimore, Maryland, March 7-11, 2005.

Dowman Ian and Vincent Tao. (2002). "An Update on the use of rational functions for photogrammetric restitution." *ISPRS Article, Vol. 7, No., 3, September 2002*. URL: http://www.isprs.org/publications/highlights/highlights0703/22_HL_09_02_Article_Dowman.pdf, last date accessed 6 January 2008.

Farhad Samadzadegan, All Azizi, and Ahmad Abootalebi. (2005). "Automatic determination of the optimum generic sensor model based on genetic algorithm concepts." *Photogrammetric Engineering & Remote Sensing,* Vol. 71, No. 3, pp. 277-288.

Fraser Clive S., G. Dial, J. Grodecki. (2006). "Sensor orientation via RPCs." *ISPRS Journal of Photogrammetry & Remote Sensing*, 60(2006) 182-194.

Fraser Clive S. and Harry B. Hanley. (2003). "Bias Compensation in Rational Functions for Ikonos Satellite Imagery." *Photogrammetric Engineering & Remote Sensing,* Vol. 69, No. 1, pp. 53 – 57.

Fraser Clive S. and Harry B. Hanley. (2005). "Bias-compensated RPCs for Sensor Orientation of High-resolution Satellite Imagery." *Photogrammetric Engineering & Remote Sensing,* Vol. 71, No. 8, pp. 909–915.

Gong Jianming, Yang Xiaomei, Zhou Chenghu, Sun Xiaoyu, and Xue Cunjin. (2005). "Refinement and evaluation of Beijing-1 orthorectification based on RFM." *ISPRS conference 2005, Commission VI, WG VI/4*.

Grodecki Jacek and Gene Dial. (2003). "Block adjustment of high resolution satellite images described by rational polynomials." *Photogrammetric Engineering & Remote Sensing,* Vol. 69, No. 1, pp. 59-68.

Grodecki Jacek and Gene Dial. (2002). "IKONOS geometric accuracy validation." *Pecora 15/Land Satellite Information IV/ISPRS Commission I/FIEOS 2002 Conference Proceedings*.

Grodecki Jacek. (2001). "IKONOS stereo feature extraction-RPC approach." *Proceedings of ASPRS 2001 Conference*, St. Louis, April 23-27, 2001. URL: http://www.geoeye.com/whitepapers_pdfs/2005/IKONOS%20Geometric%20Calibrations%20-%20ASPRS%202005%20_final.pdf, last date accessed 31 December 2007.

Grodecki Jacek and James Lutes. (2005). "IKONOS Geometric Calibrations." *ASPRS 2005, Baltimore, Marylan*d, March 7-11, 2005.

Hu Yong and C. Vincent Tao. (2002). "Updating solutions of the rational function model using additional control information." *Photogrammetric Engineering & Remote Sensing,* Vol. 68, No. 7, pp. 715-723.

Hu Yong, Tao Vincent, Arie Croitoru. (2004). "Understanding the rational function model: methods and applications." URL:

http://www.geoict.net/Resources/Publications/IAPRS2004_RFM2394.pdf, last date accessed 31 December 2007.

Manual A. Aguilar, Fernando J. Aguilar, Francisco Aguera, and Jaime A. Sanchez. (2007). "Geometric accuracy assessment of QuickBird basic imagery using different operational approaches." *Photogrammetric Engineering & Remote Sensing,* Vol. 73, No. 12, pp. 1321-1332.

Tao C. Vincent and Yong Hu. (2002). "3D reconstruction methods based on the rational function model." *Photogrammetric Engineering & Remote Sensing,* Vol. 68, No. 7, pp. 705-714.

Tao C. Vincent and Yong Hu. (2001). "A comprehensive study of the rational function model for photogrammetric processing." *Photogrammetric Engineering & Remote Sensing,* Vol. 67, No. 12, pp. 1347-1357.

Toutin, T., and P. Cheng. (2000). "Demystification of IKONOS." *Earth Observation Magazine*, 9(7):17-21.

# Chapter 5 BUNDLE ADJUSTMENT WITH RATIONAL POLYNOMIAL CAMERA MODEL BASED ON GENERIC METHOD[5]


## ABSTRACT

A Rational Polynomial Camera (RPC) model is a kind of generic sensor model that can be used in different remote sensing systems to model the relationship between object space and image space and transform image data to conform to a map projection. Unlike traditional physical camera models, a RPC model has many coefficients (a total of 80) and these coefficients do not have a physical interpretation. This represents a difficult challenge for the mapping community. For RPC refinement, many solutions, including direct and indirect methods, have been developed. One of them, the recently developed Generic Method has been shown to be a robust method. Because the Generic Method can simulate the camera's exterior parameters, it can be used in any geometric situation. Even so, the performance of bundle adjustment with the Generic Method is still unknown. In this paper, through experiments with a stereo pair and a stereo triplet, the capability of high accuracy geopositioning based on the Generic Method is demonstrated. We first give a brief review of previous bundle adjustment methods based on RPC. Then the bundle adjustment algorithm based on the Generic Method is introduced in detail. We finally present the experiments with the IKONOS and QuickBird imagery. Experiments


[5] This chapter has been submitted to *ISPRS Journal of Photogrammetry and Remote Sensing* as a research paper for peer review and publication. Comments from one reviewer have been received with the recommendation of acceptance with minor revision.
Xiong Z. and Y. Zhang, "Bundle Adjustment with Rational Polynomial Camera Model Based on Generic Method", *ISPRS Journal of Photogrammetry and Remote Sensing*, 2009.

show that the bundle adjustment based on the Generic Method can reach sub-pixel accuracy in the image space and sub-meter accuracy in the object space.

**Key Words:** Bundle Adjustment, Rational Polynomial Model, Generic Method

## 5.1 Introduction

A Rational Polynomial Camera (RPC) model (sometimes referred to as a Rational Polynomial Coefficient, or a Rational Polynomial Camera Coefficient [Chen et al., 2006]) is a kind of generic sensor model that is widely used in the processing of high resolution satellite images. It is a mathematical function that relates object space coordinates (latitude, longitude, and height) to image space coordinates (line and sample), and is expressed in the form of a ratio of two cubic functions of object space coordinates. Separate rational functions are used to express the coordinate relationships for the object space to line, and the object space to sample [Dial and Grodecki, 2002[a]].

With the application of RPC in the photogrammetric industry, numerous researchers have attempted to conduct sensor orientation and block adjustments based on the RPC model. Toutin [2003] reported a block bundle adjustment result for IKONOS in-track images. He achieved a planimetric accuracy of ±5 to ±7 m. Rose and Fradkin [2005] published block adjustment results obtained using IKONOS and QuickBird images. For IKONOS, they achieved an accuracy of 0.6 meters in latitude, 1.9 meters in longitude, and 3.9 meters in height. For QuickBird, they obtained an accuracy of 7.8 meters in latitude, 15 meters in longitude, and 6.3 meters in height.

Perhaps the most critical advance in block adjustment of high resolution satellite images described with a RPC was made by Fraser and Hanley in 2003. They proposed an Image-Space Bias Compensation model for sensor orientation [Fraser et al., 2006]. Grodecki and Dial [2003] analysed the characteristics of IKONOS and proposed several block adjustment models including the Bias Compensation model [Dial and Grodecki, 2002[a]]. Their analysis and experiments confirmed that the Image-Space Bias Compensation model is the most accurate block adjustment model; however, this model only approximates the photogrammetric errors in image space, so it can yield an accurate compensation only under a limited set of conditions, over a very small range of error. Research shows that success with the Bias Compensation model depends on three factors: (1) narrow field-of-view (FOV) of the satellite line scanner [Fraser and Hanley, 2005]; (2) absence of higher-order error sources such as perturbations in scan velocity [Fraser and Hanley, 2005]; and (3) small satellite position and attitude errors [Grodecki and Dial, 2003].

The recently-developed Generic Method can simulate the camera's exterior parameters and therefore can overcome the limitations of the Bias Compensation method [Xiong and Zhang, 2008]. But what is the performance when it is used for aerotriangulation? What accuracy can be achieved when it is used for geopositioning? These questions are addressed in this paper.

In this paper, a Generic Method based block adjustment model is introduced. We begin our paper with a brief review of the latest research on RPC based block adjustment models. We then present our newly developed Generic method based bundle block adjustment algorithm in detail. In the experiment section, we test the new algorithm by using IKONOS and QuickBird images. Finally, some concluding remarks and recommendations for the future work are presented.

## 5.2 Review of RPC Based Block Adjustment Models

An RPC is a mathematical function that relates object space to image space (Equation 5.1).

$$p = \frac{P_1(\phi,\lambda,h)}{P_2(\phi,\lambda,h)} \tag{5.1a}$$

$$r = \frac{P_3(\phi,\lambda,h)}{P_4(\phi,\lambda,h)} \tag{5.1b}$$

$$P(\phi,\lambda,h) = \sum_{i=0}^{m1}\sum_{j=0}^{m2}\sum_{k=0}^{m3} a_{ijk}\phi^i\lambda^j h^k \tag{5.1c}$$

$$0 \le m_1 \le 3\,;0 \le m_2 \le 3\,;0 \le m_3 \le 3\,;m_1 + m_2 + m_3 \le 3 \tag{5.1d}$$

Here ($p, r$) are the image coordinates, ($\phi, \lambda, h$) are the ground coordinates, and $a_{ijk}$ is the polynomial coefficient.

To date, several RPC-based block adjustment models defined in both image and object space have been proposed:

(1) Image-Space Adjustment Models Defined in the Domain of Image Coordinates. An example of this type of model is presented as Equation 5.2. It is well known as the Image-Space Bias Compensation Adjustment Model. In this model, $\Delta p$ and $\Delta r$ are added to the rational functions to capture the discrepancies between the nominal and the measured image space coordinates [Fraser and Hanley, 2003; Fraser and Hanley, 2005; Grodecki and Dial, 2003; Fraser et al., 2006].

$$Line_i^{(j)} = \Delta p^{(j)} + p^{(j)}(\phi_k, \lambda_k, h_k) + \varepsilon_{Li} \tag{5.2a}$$

$$Sample_i^{(j)} = \Delta r^{(j)} + r^{(j)}(\phi_k, \lambda_k, h_k) + \varepsilon_{Si} \tag{5.2b}$$

Where $Line_i^{(j)}$ and $Sample_i^{(j)}$ are the measured line and sample coordinates on image $j$ of $i^{th}$ image point, corresponding to the $k^{th}$ ground control or tie point with object space coordinates ($\phi_k$, $\lambda_k$, $h_k$); $\Delta p^{(j)}$, $\Delta r^{(j)}$ are the adjustable functions expressing the differences between the measured and the nominal line and sample coordinates of ground control and /or tie points, for image $j$;

$\varepsilon_{Li}$ and $\varepsilon_{Si}$ are random unobservable errors;

$p^{(j)}$ and $r^{(j)}$ are the given line and sample; and

$$\Delta p^{(j)} = a_0^{(j)} + a_S^{(j)} \cdot Sample_i + a_L^{(j)} \cdot Line_i + a_{SL}^{(j)} \cdot Sample_i \cdot Line_i + a_{L2}^{(j)} \cdot Line_i^2 + a_{S2}^{(j)} \cdot Sample_i^2 + \ldots \tag{5.3a}$$

$$\Delta r^{(j)} = b_0^{(j)} + b_S^{(j)} \cdot Sample_i + b_L^{(j)} \cdot Line_i + b_{SL}^{(j)} \cdot Sample_i \cdot Line_i + b_{L2}^{(j)} \cdot Line_i^2 + b_{S2}^{(j)} \cdot Sample_i^2 + \ldots \tag{5.3b}$$

Where $a_i^{(j)}$, $b_i^{(j)}$ are correction coefficients for the $j^{th}$ image.

For IKONOS imagery, the affine transformation or a translation for the simplest case is often used [Hu et al., 2004; Grodecki and Dial, 2003; Fraser and Hanley, 2003]:

$$\Delta p^{(j)} = a_0^{(j)} + a_S^{(j)} \cdot Sample_i + a_L^{(j)} \cdot Line_i \tag{5.4a}$$

$$\Delta r^{(j)} = b_0^{(j)} + b_S^{(j)} \cdot Sample_i + b_L^{(j)} \cdot Line_i \tag{5.4b}$$

(2) Image-Space Adjustment Models Defined in the Domain of Object Space Coordinates. This type of model presented by Grodecki and Dial [2003]

accomplishes image-space compensation using a polynomial function that is defined in object space. It is represented by Equation 5.5:

$$\begin{aligned}\Delta p^{(j)} &= a_i^{(j)} + a_P^{(j)} \cdot \phi_k + a_L^{(j)} \cdot \lambda_k + a_H^{(j)} \cdot h_k + a_{P2}^{(j)} \cdot \phi_k^2 + a_{L2}^{(j)} \cdot \lambda_k^2 \\ &+ a_{H2}^{(j)} \cdot h_k^2 + a_{PL}^{(j)} \cdot \phi_k \cdot \lambda_k + a_{PH}^{(j)} \cdot \phi_k \cdot h_k + a_{LH}^{(j)} \cdot \lambda_k \cdot h_k + \dots\end{aligned} \tag{5.5a}$$

$$\begin{aligned}\Delta r^{(j)} &= b_0^{(j)} + b_P^{(j)} \cdot \phi_k + b_L^{(j)} \cdot \lambda_k + b_H^{(j)} \cdot h_k + b_{P2}^{(j)} \cdot \phi_k^2 + b_{L2}^{(j)} \cdot \lambda_k^2 \\ &+ b_{H2}^{(j)} \cdot h_k^2 + b_{PL}^{(j)} \cdot \phi_k \cdot \lambda_k + b_{PH}^{(j)} \cdot \phi_k \cdot h_k + b_{LH}^{(j)} \cdot \lambda_k \cdot h_k + \dots\end{aligned} \tag{5.5b}$$

Where ($\phi_k$, $\lambda_k$, $h_k$) are ground coordinates, and ($a_i^{(j)}$, $b_i^{(j)}$) are correction coefficients for the $j^{th}$ image.

It has been noted that sensor adjustment models defined in the domain of object coordinates are in general less accurate than models defined in the domain of image-space coordinates [Grodecki and Dial, 2003].

(3) Object-Space Adjustment Models. The object-space RPC block adjustment model, for the $k^{th}$ ground control or tie point being the $i^{th}$ image point on the $j^{th}$ image, is defined as follows:

$$Line_i^{(j)} = p^{(j)}(\phi_k + \Delta\phi^{(j)}, \lambda_k + \Delta\lambda^{(j)}, h_k + \Delta h^{(j)}) + \varepsilon_{Li} \tag{5.6a}$$

$$Sample_i^{(j)} = r^{(j)}(\phi_k + \Delta\phi^{(j)}, \lambda_k + \Delta\lambda^{(j)}, h_k + \Delta h^{(j)}) + \varepsilon_{Si} \tag{5.6b}$$

Where $\Delta\phi^{(j)}$, $\Delta\lambda^{(j)}$, and $\Delta h^{(j)}$ are adjustable functions expressing the differences between the measured and the nominal object-space coordinates of a ground control or tie point, for the $j^{th}$ image.

As is the case for the image space adjustment models, the object-space adjustment model can be represented by a polynomial model defined in either image space or object space coordinates. In both cases, the object-space RPC block adjustment model is nonlinear in the adjustment parameters and is unrelated to imaging geometry [Grodecki and Dial, 2003], therefore this model is rarely used.

In summary, the use of image space models is preferable to the use of object-space models. It is also apparent that among the image-space adjustment models, the model defined in the image space (i.e. the Image-Space Bias Compensation Adjustment Model) is more accurate than the model defined in the object space. But as previously noted this model is effective only when the camera Field Of View (FOV) is narrow and the position and attitude errors of the camera are small [Grodecki and Dial, 2003].

## 5.3 Generic Method Based Bundle Block Adjustment

The Generic Method based Bundle Block Adjustment Model proposed in this paper (**Figure. 5.1**) is defined in the domain of object coordinates. It can simulate the camera's six exterior parameters by restoring the camera's position and attitude from the rational polynomial camera model. This model can therefore be used regardless of the camera field of view, position error and attitude error [Xiong and Zhang, 2008]. The model is comprised of three steps. The first step is to reconstruct the pseudo light ray that existed when the image was acquired and obtain the sensor's pseudo position and attitude (equivalent to camera Exterior Parameters (EPs)). The second step is to use Ground Control Points (GCPs) and tie points to build observation equations. The third step is to conduct the block adjustment and export the image and object coordinates of the GCPs and tie points, the corrected parameters for the sensor model and new RPCs. Each of these steps is described in more detail below.

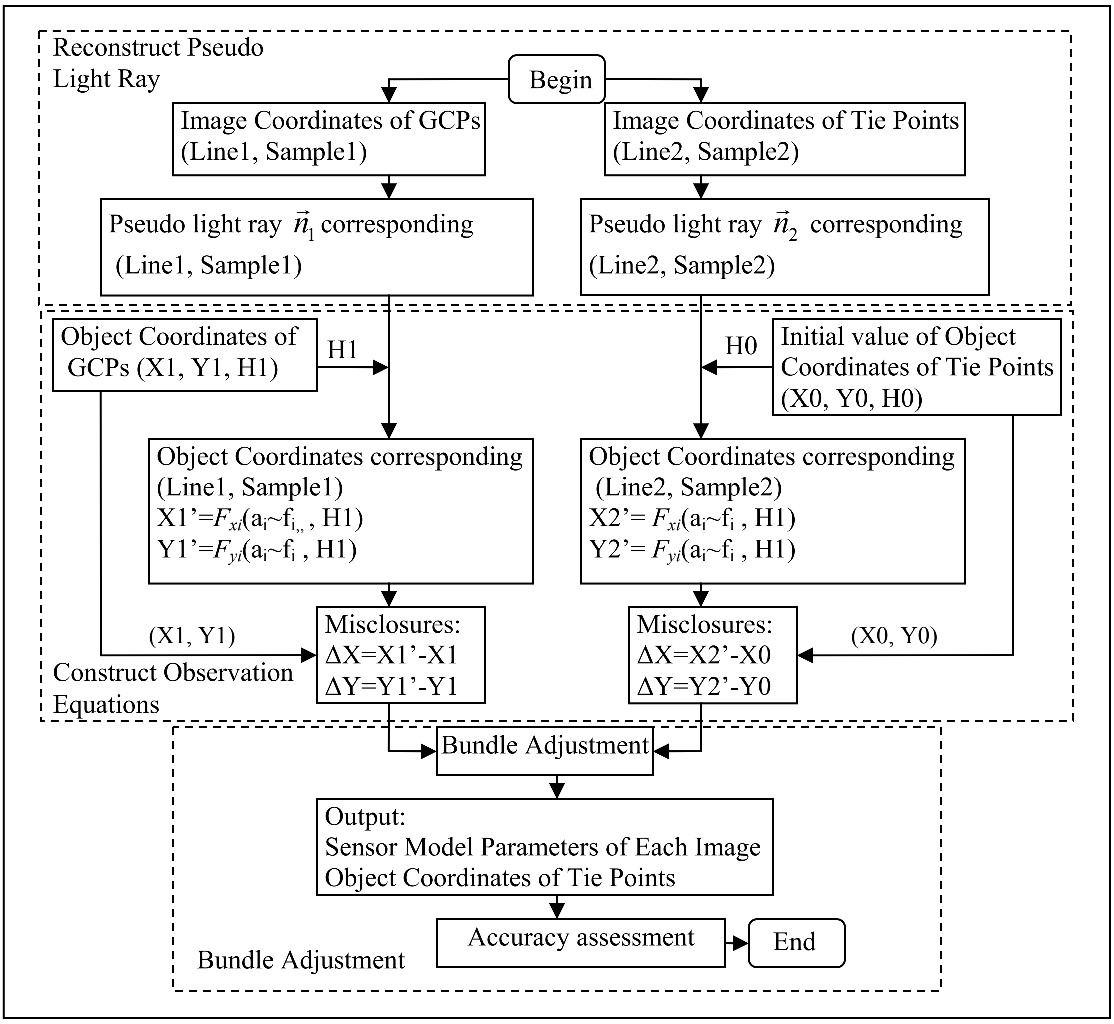


**Figure 5.1 Flowchart of Generic Method Based Bundle Adjustment**

## Reconstructing the Pseudo Light Ray

From a point on the image P(I, J), a pseudo light ray can be restored and the corresponding sensor position Ps1(Xs1, Ys1, Hs1) and pseudo attitude ( $\Psi y$ , $\Psi x$ and $\Psi z$) can be obtained [Xiong and Zhang, 2008] **(Figure 5.2, 5.3)**.

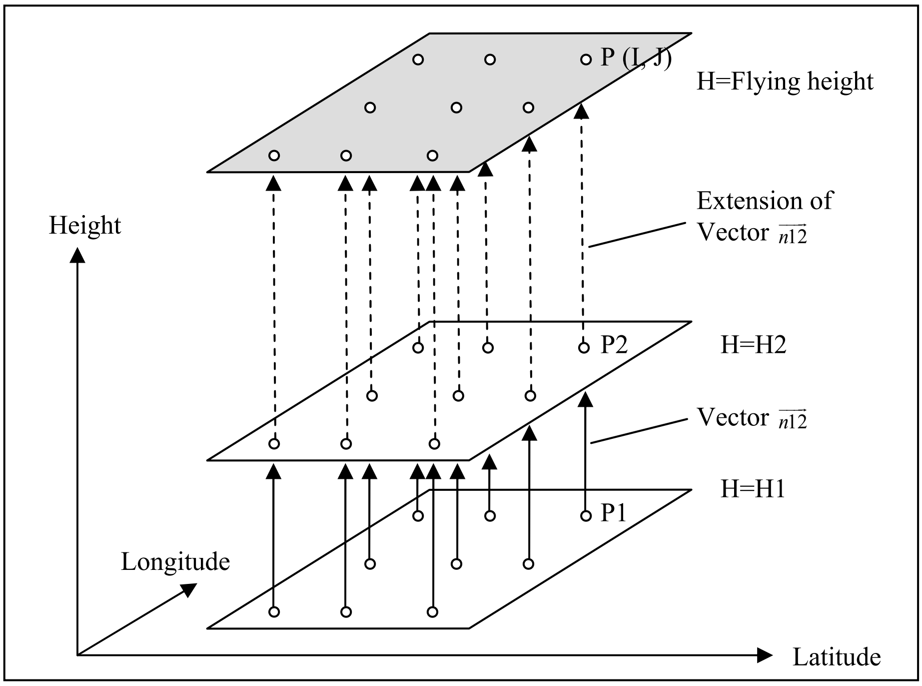


**Figure 5.2 Reconstructing Pseudo Light Ray [Xiong and Zhang, 2008].**

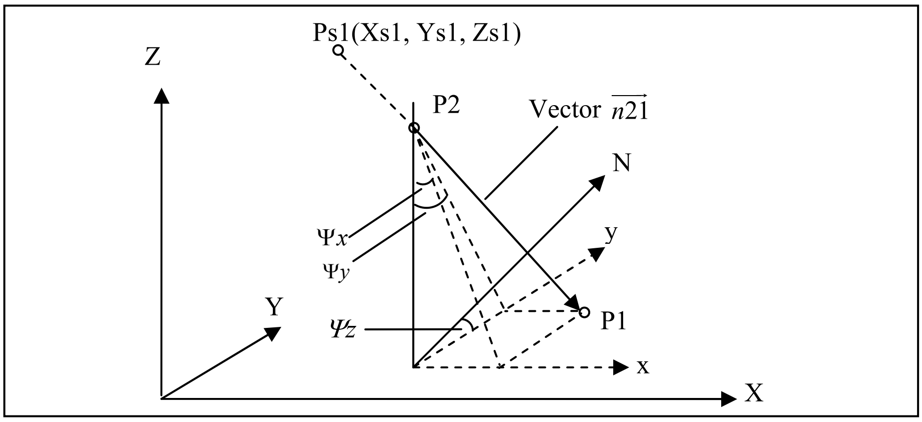


**Figure 5.3 Reconstructing the Sensor's Attitude [Xiong and Zhang, 2008].**

## Construct Observation Equation

For a GCP, its coordinates (X, Y, H) are known. For a tie point, its initial coordinates (X0, Y0, H0) need to be estimated. Then for GCP i on image j, two observation equations can be constructed.

$$F_{xi} = (\hat{X}^j_{si} + (\hat{H}^j_{si} - h_i) * \tan(\hat{\psi}^j_{xi})) * \cos(\hat{\psi}^j_{zi}) + (\hat{Y}^j_{si} + (\hat{H}^j_{si} - h_i) * \tan(\hat{\psi}^j_{yi})) * \sin(\hat{\psi}^j_{zi}) - x_i + \varepsilon x_i \tag{5.7}$$

$$F_{yi} = -(\hat{X}_{si}^{j} + (\hat{H}_{si}^{j} - h_i) * \tan(\hat{\psi}_{xi}^{j})) * \sin(\hat{\psi}_{zi}^{j}) + (\hat{Y}_{si}^{j} + (\hat{H}_{si}^{j} - h_i) * \tan(\hat{\psi}_{yi}^{j})) * \cos(\hat{\psi}_{zi}^{j}) - y_i + \varepsilon y_i \tag{5.8}$$

$\hat{X}_{si}^{j}$, $\hat{Y}_{si}^{j}$, $\hat{H}_{si}^{j}$; $\hat{\psi}_{xi}^{j}$, $\hat{\psi}_{yi}^{j}$, $\hat{\psi}_{zi}^{j}$ are the sensor position and attitude corresponding to the $i^{th}$ GCP or tie point on $j^{th}$ image; and $x_i$, $y_i$, $h_i$ are ground coordinates of $i^{th}$ GCP or tie point.

In these observation equations, the satellite position ($\hat{X}_{si}^{j}$, $\hat{Y}_{si}^{j}$, $\hat{H}_{si}^{j}$) and three rotation angles ($\hat{\psi}_{xi}^{j}$, $\hat{\psi}_{yi}^{j}$, $\hat{\psi}_{zi}^{j}$) are adjustable parameters.

$$\hat{X}_{si}^{j} = X_{si0}^{j} + \Delta X_{si}^{j} \tag{5.9}$$

$$\hat{Y}_{si}^{j} = Y_{si0}^{j} + \Delta Y_{si}^{j} \tag{5.10}$$

$$\hat{H}_{si}^{j} = H_{si0}^{j} + \Delta H_{si}^{j} \tag{5.11}$$

$$\hat{\psi}_{xi}^{j} = \psi_{xi0}^{j} + \Delta\psi_{xi}^{j} \tag{5.12}$$

$$\hat{\psi}_{yi}^{j} = \psi_{yi0}^{j} + \Delta\psi_{yi}^{j} \tag{5.13}$$

$$\hat{\psi}_{zi}^{j} = \psi_{zi0}^{j} + \Delta\psi_{zi}^{j} \tag{5.14}$$

$X_{si0}^{j}$, $Y_{si0}^{j}$, $H_{si0}^{j}$; $\psi_{xi0}^{j}$, $\psi_{yi0}^{j}$, $\psi_{zi0}^{j}$ are the initial values of the sensor position and attitude corresponding to the $i^{th}$ GCP or tie point on $j^{th}$ image; $\Delta X_{si}^{j}$, $\Delta Y_{si}^{j}$, $\Delta H_{si}^{j}$, $\Delta\psi_{xi}^{j}$, $\Delta\psi_{yi}^{j}$, $\Delta\psi_{zi}^{j}$ are unknowns and need to be estimated. Because the position and attitude of the sensor change over time in a pushbroom remote sensing system, a polynomial model defined in the domain of image coordinates is proposed to represent the adjustable functions $\Delta X_{si}^{j}$, $\Delta Y_{si}^{j}$, $\Delta H_{si}^{j}$, $\Delta\psi_{xi}^{j}$, $\Delta\psi_{yi}^{j}$, $\Delta\psi_{zi}^{j}$, also a linear polynomial model for block adjustment [Xiong and Zhang, 2008] is proposed.

$$\Delta X_{si}^{j} = a_0^{j} + a_S^{j} \cdot Sample_i + a_L^{j} \cdot Line_i \tag{5.15}$$

$$\Delta Y_{si}^{j} = b_0^j + b_S^j \cdot Sample_i + b_L^j \cdot Line_i \tag{5.16}$$

$$\Delta H_{si}^{j} = c_0^j + c_S^j \cdot Sample_i + c_L^j \cdot Line_i \tag{5.17}$$

$$\Delta \psi_{xi}^{j} = d_0^j + d_S^j \cdot Sample_i + d_L^j \cdot Line_i \tag{5.18}$$

$$\Delta \psi_{yi}^{j} = e_0^j + e_S^j \cdot Sample_i + e_L^j \cdot Line_i \tag{5.19}$$

$$\Delta \psi_{zi}^{j} = f_0^j + f_S^j \cdot Sample_i + f_L^j \cdot Line_i \tag{5.20}$$

Where, *a, b, c, d, e, f* are polynomial coefficients; *Sample, Line* are image coordinates.

**<u>Generic Method Based Bundle Adjustment Algorithm</u>**

After linearization of the above observation equations 5.7 and 5.8, using a Taylor series expansion, the following linearized model can be obtained:

$$F_i = F_{i_0} + dF_i + \varepsilon = 0 \tag{5.21}$$

Where

$$F_{i_0} = \begin{bmatrix} F_{xi_0} \\ F_{yi_0} \end{bmatrix} = W_{Pi} \tag{5.22}$$

$$dF_i = \begin{bmatrix} dF_{xi} \\ dF_{yi} \end{bmatrix} = \begin{bmatrix} \dfrac{\partial F_{xi}}{\partial X^T} \\ \dfrac{\partial F_{yi}}{\partial X^T} \end{bmatrix} dX = \begin{bmatrix} \left.\dfrac{\partial F_{xi}}{\partial X_A^T}\right|_{X0} & \left.\dfrac{\partial F_{xi}}{\partial X_G^T}\right|_{X0} \\ \left.\dfrac{\partial F_{yi}}{\partial X_A^T}\right|_{X0} & \left.\dfrac{\partial F_{yi}}{\partial X_A^T}\right|_{X0} \end{bmatrix} \begin{bmatrix} dX_A \\ dX_G \end{bmatrix} = \begin{bmatrix} B_{Ai} & B_{Gi} \end{bmatrix} \begin{bmatrix} dX_A \\ dX_G \end{bmatrix}$$

(5.23)

$dX = X - X_0$ is the vector of unknown corrections to the approximate model parameters, $X_0$,

$$dX = \begin{bmatrix} dX_A \\ dX_G \end{bmatrix} \tag{5.24}$$

$dX_A$ is the sub-vector of the corrections to the approximate adjustment parameters for n images,

$$\begin{aligned} dX_A = [da_0^{(1)} \quad da_S^{(1)} \quad da_L^{(1)} \quad \cdots \quad df_0^{(1)} \quad df_S^{(1)} \quad df_L^{(1)} \\ \ldots \quad da_0^{(n)} \quad da_S^{(n)} \quad da_L^{(n)} \quad \cdots \quad df_0^{(n)} \quad df_S^{(n)} \quad df_L^{(n)}]^T \end{aligned} \tag{5.25}$$

$dX_G$ is the sub-vector of the corrections to the approximate object space coordinates for $m$ ground control and $p$ tie points,

$$dX_G = [dx_1 \quad dy_1 \quad dh_1 \quad \cdots \quad dx_{m+p} \quad dy_{m+p} \quad dh_{m+p}]^T \tag{5.26}$$

$X_0$ is the vector of the approximate model parameters,

$$X_0 = \begin{bmatrix} X_{A0} \\ X_{G0} \end{bmatrix} \tag{5.27}$$

and $\varepsilon$ is the vector of unobservable random errors.

For the $k^{th}$ ground control or tie point, being the $i^{th}$ image point on the $j^{th}$ image, we can obtain:

$$B_{Gi} dX_G = \begin{bmatrix} \dfrac{\partial F_{xi}}{\partial X_G^T} \\ \dfrac{\partial F_{yi}}{\partial X_G^T} \end{bmatrix} dX_G = \begin{bmatrix} 0 & \cdots & 0 & \left.\dfrac{\partial F_{xi}}{\partial x_k}\right|_{X0} & \left.\dfrac{\partial F_{xi}}{\partial y_k}\right|_{X0} & \left.\dfrac{\partial F_{xi}}{\partial h_k}\right|_{X0} & 0 & \cdots & 0 \\ 0 & \cdots & 0 & \left.\dfrac{\partial F_{yi}}{\partial x_k}\right|_{X0} & \left.\dfrac{\partial F_{yi}}{\partial y_k}\right|_{X0} & \left.\dfrac{\partial F_{yi}}{\partial h_k}\right|_{X0} & 0 & \cdots & 0 \end{bmatrix} \begin{bmatrix} \vdots \\ dx_k \\ dy_k \\ dh_k \\ \vdots \end{bmatrix} \tag{5.28}$$

Where

$$\begin{bmatrix} \dfrac{\partial F_{xi}}{\partial x_k} & \dfrac{\partial F_{xi}}{\partial y_k} & \dfrac{\partial F_{xi}}{\partial h_k} \end{bmatrix} = \begin{bmatrix} -1 & 0 & -(tg(\psi_{xi0}^j) \cdot \cos(\psi_{zi0}^j) + tg(\psi_{yi0}^j) \cdot \sin(\psi_{zi0}^j)) \end{bmatrix} \tag{5.29}$$

$$\begin{bmatrix} \dfrac{\partial F_{yi}}{\partial x_k} & \dfrac{\partial F_{yi}}{\partial y_k} & \dfrac{\partial F_{yi}}{\partial h_k} \end{bmatrix} = \begin{bmatrix} 0 & 1 & (tg(\psi_{xi0}^j) \cdot \sin(\psi_{zi0}^j) + tg(\psi_{yi0}^j) \cdot \cos(\psi_{zi0}^j)) \end{bmatrix} \tag{5.30}$$

Likewise,

$$B_{Ai}dX_A = \begin{bmatrix} \left.\dfrac{\partial F_{xi}}{\partial X_A^T}\right|_{X0} \\ \left.\dfrac{\partial F_{yi}}{\partial X_A^T}\right|_{X0} \end{bmatrix} dX_A$$

$$= \begin{bmatrix} 0 & \cdots & 0 & \left.\dfrac{\partial F_{xi}}{\partial a_0^j}\right|_{X0} & \left.\dfrac{\partial F_{xi}}{\partial a_S^j}\right|_{X0} & \left.\dfrac{\partial F_{xi}}{\partial a_L^j}\right|_{X0} & \cdots & \left.\dfrac{\partial F_{xi}}{\partial f_0^j}\right|_{X0} & \left.\dfrac{\partial F_{xi}}{\partial f_S^j}\right|_{X0} & \left.\dfrac{\partial F_{xi}}{\partial f_L^j}\right|_{X0} & 0 & \cdots & 0 \\ 0 & \cdots & 0 & \left.\dfrac{\partial F_{yi}}{\partial a_0^j}\right|_{X0} & \left.\dfrac{\partial F_{yi}}{\partial a_S^j}\right|_{X0} & \left.\dfrac{\partial F_{yi}}{\partial a_L^j}\right|_{X0} & \cdots & \left.\dfrac{\partial F_{yi}}{\partial f_0^j}\right|_{X0} & \left.\dfrac{\partial F_{yi}}{\partial f_S^j}\right|_{X0} & \left.\dfrac{\partial F_{yi}}{\partial f_L^j}\right|_{X0} & 0 & \cdots & 0 \end{bmatrix}$$

$$\cdot \begin{bmatrix} \cdots & da_0^j & da_S^j & da_L^j & \cdots & df_0^j & df_S^j & df_L^j & \cdots \end{bmatrix}^T \tag{5.31}$$

Where

$$\begin{bmatrix} \dfrac{\partial F_{xi}}{\partial a_0^j} & \dfrac{\partial F_{xi}}{\partial a_S^j} & \dfrac{\partial F_{xi}}{\partial a_L^j} \end{bmatrix} = \begin{bmatrix} \cos(\psi_{zi0}^j) & \cos(\psi_{zi0}^j) \cdot Sample_i & \cos(\psi_{zi0}^j) \cdot Line_i \end{bmatrix} \tag{5.32}$$

$$\begin{bmatrix} \dfrac{\partial F_{xi}}{\partial b_0^j} & \dfrac{\partial F_{xi}}{\partial b_S^j} & \dfrac{\partial F_{xi}}{\partial b_L^j} \end{bmatrix} = \begin{bmatrix} \sin(\psi_{zi0}^j) & \sin(\psi_{zi0}^j) \cdot Sample_i & \sin(\psi_{zi0}^j) \cdot Line_i \end{bmatrix} \tag{5.33}$$

$$\begin{bmatrix} \dfrac{\partial F_{xi}}{\partial c_0^j} \\ \dfrac{\partial F_{xi}}{\partial c_S^j} \\ \dfrac{\partial F_{xi}}{\partial c_L^j} \end{bmatrix} = \begin{bmatrix} \cos(\psi_{zi0}^j) \cdot tg(\psi_{xi0}^j) + \sin(\psi_{zi0}^j) \cdot tg(\psi_{yi0}^j) \\ (\cos(\psi_{zi0}^j) \cdot tg(\psi_{xi0}^j) + \sin(\psi_{zi0}^j) \cdot tg(\psi_{yi0}^j)) \cdot Sample_i \\ (\cos(\psi_{zi0}^j) \cdot tg(\psi_{xi0}^j) + \sin(\psi_{zi0}^j) \cdot tg(\psi_{yi0}^j)) \cdot Line_i \end{bmatrix} \tag{5.34}$$

$$\begin{bmatrix} \dfrac{\partial F_{xi}}{\partial d_0^j} \\ \dfrac{\partial F_{xi}}{\partial d_S^j} \\ \dfrac{\partial F_{xi}}{\partial d_L^j} \end{bmatrix} = \begin{bmatrix} (H_{si0}^j - h_i) \cdot \cos(\psi_{zi0}^j) \cdot (1 + tg^2(\psi_{xi0}^j)) \\ (H_{si0}^j - h_i) \cdot \cos(\psi_{zi0}^j) \cdot (1 + tg^2(\psi_{xi0}^j)) \cdot Sample_i \\ (H_{si0}^j - h_i) \cdot \cos(\psi_{zi0}^j) \cdot (1 + tg^2(\psi_{xi0}^j)) \cdot Line_i \end{bmatrix} \tag{5.35}$$

$$\begin{bmatrix} \dfrac{\partial F_{xi}}{\partial e_0^j} \\ \dfrac{\partial F_{xi}}{\partial e_S^j} \\ \dfrac{\partial F_{xi}}{\partial e_L^j} \end{bmatrix} = \begin{bmatrix} (H_{si0}^j - h_i)\cdot \sin(\psi_{zi0}^j)\cdot(1+tg^2(\psi_{yi0}^j)) \\ (H_{si0}^j - h_i)\cdot \sin(\psi_{zi0}^j)\cdot(1+tg^2(\psi_{yi0}^j))\cdot Sample_i \\ (H_{si0}^j - h_i)\cdot \sin(\psi_{zi0}^j)\cdot(1+tg^2(\psi_{yi0}^j))\cdot Line_i \end{bmatrix} \tag{5.36}$$

$$\begin{bmatrix} \dfrac{\partial F_{xi}}{\partial f_0^j} \\ \dfrac{\partial F_{xi}}{\partial f_S^j} \\ \dfrac{\partial F_{xi}}{\partial f_L^j} \end{bmatrix} = \begin{bmatrix} [X_{si0}^j + (H_{si0}^j - h_i)\cdot tg(\psi_{xi0}^j)]\cdot(-\sin(\psi_{zi0}^j) \\ +[Y_{si0}^j + (H_{si0}^j - h_i)\cdot tg(\psi_{yi0}^j)]\cdot\cos(\psi_{zi0}^j) \\ \{[X_{si0}^j + (H_{si0}^j - h_i)\cdot tg(\psi_{xi0}^j)]\cdot(-\sin(\psi_{zi0}^j) \\ +[Y_{si0}^j + (H_{si0}^j - h_i)\cdot tg(\psi_{yi0}^j)]\cdot\cos(\psi_{zi0}^j)\}\cdot Sample_i \\ \{[X_{si0}^j + (H_{si0}^j - h_i)\cdot tg(\psi_{xi0}^j)]\cdot(-\sin(\psi_{zi0}^j) \\ +[Y_{si0}^j + (H_{si0}^j - h_i)\cdot tg(\psi_{yi0}^j)]\cdot\cos(\psi_{zi0}^j)\}\cdot Line_i \end{bmatrix} \tag{5.37}$$

$$\begin{bmatrix} \dfrac{\partial F_{yi}}{\partial a_0^j} & \dfrac{\partial F_{yi}}{\partial a_S^j} & \dfrac{\partial F_{yi}}{\partial a_L^j} \end{bmatrix} = \begin{bmatrix} -\sin(\psi_{zi0}^j) & -\sin(\psi_{zi0}^j)\cdot Sample_i & -\sin(\psi_{zi0}^j)\cdot Line_i \end{bmatrix} \tag{5.38}$$

$$\begin{bmatrix} \dfrac{\partial F_{yi}}{\partial b_0^j} & \dfrac{\partial F_{yi}}{\partial b_S^j} & \dfrac{\partial F_{yi}}{\partial b_L^j} \end{bmatrix} = \begin{bmatrix} \cos(\psi_{zi0}^j) & \cos(\psi_{zi0}^j)\cdot Sample_i & \cos(\psi_{zi0}^j)\cdot Line_i \end{bmatrix} \tag{5.39}$$

$$\begin{bmatrix} \dfrac{\partial F_{yi}}{\partial c_0^j} \\ \dfrac{\partial F_{yi}}{\partial c_S^j} \\ \dfrac{\partial F_{yi}}{\partial c_L^j} \end{bmatrix} = \begin{bmatrix} -\sin(\psi_{zi0}^j)\cdot tg(\psi_{xi0}^j) + \cos(\psi_{zi0}^j)\cdot tg(\psi_{yi0}^j) \\ (-\sin(\psi_{zi0}^j)\cdot tg(\psi_{xi0}^j) + \cos(\psi_{zi0}^j)\cdot tg(\psi_{yi0}^j))\cdot Sample_i \\ (-\sin(\psi_{zi0}^j)\cdot tg(\psi_{xi0}^j) + \cos(\psi_{zi0}^j)\cdot tg(\psi_{yi0}^j))\cdot Line_i \end{bmatrix} \tag{5.40}$$

$$\begin{bmatrix} \dfrac{\partial F_{yi}}{\partial d_0^j} \\ \dfrac{\partial F_{yi}}{\partial d_S^j} \\ \dfrac{\partial F_{yi}}{\partial d_L^j} \end{bmatrix} = \begin{bmatrix} -(H_{si0}^j - h_i)\cdot \sin(\psi_{zi0}^j)\cdot(1+tg^2(\psi_{xi0}^j)) \\ -(H_{si0}^j - h_i)\cdot \sin(\psi_{zi0}^j)\cdot(1+tg^2(\psi_{xi0}^j))\cdot Sample_i \\ -(H_{si0}^j - h_i)\cdot \sin(\psi_{zi0}^j)\cdot(1+tg^2(\psi_{xi0}^j))\cdot Line_i \end{bmatrix} \tag{5.41}$$

$$\begin{bmatrix} \frac{\partial F_{yi}}{\partial e_0^j} \\ \frac{\partial F_{yi}}{\partial e_S^j} \\ \frac{\partial F_{yi}}{\partial e_L^j} \end{bmatrix} = \begin{bmatrix} (H_{si0}^j - h_i) \cdot \cos(\psi_{zi0}^j) \cdot (1 + tg^2(\psi_{yi0}^j)) \\ (H_{si0}^j - h_i) \cdot \cos(\psi_{zi0}^j) \cdot (1 + tg^2(\psi_{yi0}^j)) \cdot Sample_i \\ (H_{si0}^j - h_i) \cdot \cos(\psi_{zi0}^j) \cdot (1 + tg^2(\psi_{yi0}^j)) \cdot Line_i \end{bmatrix} \tag{5.42}$$

$$\begin{bmatrix} \frac{\partial F_{yi}}{\partial f_0^j} \\ \frac{\partial F_{yi}}{\partial f_S^j} \\ \frac{\partial F_{yi}}{\partial f_L^j} \end{bmatrix} = \begin{bmatrix} -[X_{si0}^j + (H_{si0}^j - h_i) \cdot tg(\psi_{xi0}^j)] \cdot \cos(\psi_{zi0}^j) \\ +[Y_{si0}^j + (H_{si0}^j - h_i) \cdot tg(\psi_{yi0}^j)] \cdot (-\sin(\psi_{zi0}^j) \\ \{-[X_{si0}^j + (H_{si0}^j - h_i) \cdot tg(\psi_{xi0}^j)] \cdot \cos(\psi_{zi0}^j) \\ +[Y_{si0}^j + (H_{si0}^j - h_i) \cdot tg(\psi_{yi0}^j)] \cdot (-\sin(\psi_{zi0}^j)\} \cdot Sample_i \\ \{-[X_{si0}^j + (H_{si0}^j - h_i) \cdot tg(\psi_{xi0}^j)] \cdot \cos(\psi_{zi0}^j) \\ +[Y_{si0}^j + (H_{si0}^j - h_i) \cdot tg(\psi_{yi0}^j)] \cdot (-\sin(\psi_{zi0}^j)\} \cdot Line_i \end{bmatrix} \tag{5.43}$$

Then, the RPC block adjustment model in matrix form can be expressed as

$$\begin{bmatrix} B_A & B_G \\ I & 0 \\ 0 & I \end{bmatrix} \begin{bmatrix} dX_A \\ dX_G \end{bmatrix} + \varepsilon = \begin{bmatrix} W_p \\ W_A \\ W_G \end{bmatrix} \tag{5.44}$$

or

$$BdX + \varepsilon = W \tag{5.45}$$

with *a priori* covariance matrix of the vector of misclosures , *W*,

$$C_W = \begin{bmatrix} C_P & 0 & 0 \\ 0 & C_A & 0 \\ 0 & 0 & C_G \end{bmatrix} \tag{5.46}$$

Where $B_A$ is the first-order design matrix for the adjustment parameters, and $B_G$ is the first-order design matrix for the object-space coordinates. $W_P$ is the vector of misclosures of the observation equations in object space,

$$W_P = \begin{bmatrix} W_P \\ \vdots \\ W_{Pi} \\ \vdots \end{bmatrix} \tag{5.47}$$

$W_{Pi}$ is the sub-vector of misclosures in the object-space coordinates for the $i^{th}$ GCP or tie point on the $j^{th}$ image.

$$W_{Pi} = \begin{bmatrix} [X^j_{si0} + (H^j_{si0} - h_i)\cdot tg(\psi^j_{xi0})]\cdot\cos(\psi^j_{zi0}) + [Y^j_{si0} + (H^j_{si0} - h_i)\cdot tg(\psi^j_{yi0})]\cdot\sin(\psi^j_{zi0}) - x_i \\ -[X^j_{si0} + (H^j_{si0} - h_i)\cdot tg(\psi^j_{xi0})]\cdot\sin(\psi^j_{zi0}) + [Y^j_{si0} + (H^j_{si0} - h_i)\cdot tg(\psi^j_{yi0})]\cdot\cos(\psi^j_{zi0}) - y_i \end{bmatrix} \tag{5.48}$$

$W_A = 0$ is the vector of misclosures for the adjustment parameters.

$W_G = 0$ is the vector of misclosures for the object-space coordinates.

$C_P$ is the *a priori* covariance matrix* of image-space coordinates.

$C_A$ is the *a priori* covariance matrix* of the adjustment parameters.

$C_G$ is the *a priori* covariance matrix* of the object-space coordinates.

For a tie point, without any prior knowledge, $C_G$ can be made large enough; e.g.100,0000 m$^{2,}$ so that the object coordinates of tie points will be solved as other unknowns in the least squares solutions.

Next, the estimated corrections to the adjustment parameters and the approximate values of the object coordinates can be obtained by least squares solutions:

$$d\hat{X} = -(B^T C_W^{-1} B)^{-1}(B^T C_W^{-1} W) \tag{5.49}$$

Unlike the rational polynomial functions (Equation 5.1), the observation equations (Equation 5.7, 5.8) are linear, so the least squares solutions converge quickly.

---

* If the *a priori* covariance is not available, a unit matrix can be used here.

**Accuracy Estimation**

*a-posteriori* variance factor can be calculated as following.

$$\sigma_0 = \pm\sqrt{\frac{[pvv]}{n-t}} \tag{5.50}$$

n: observation number
t: unknown number

$$[pvv] = V^T PV = (B\delta X + l)^T PV = \delta X^T B^T PV + l^T PV \tag{5.51}$$

Because,

$$B^T PV = 0 \tag{5.52}$$

So,

$$[pvv] = l^T PV = l^T P(B\delta X + l) = l^T Pl + (B^T Pl)^T \delta X \tag{5.53}$$

Therefore, the covariance of the object coordinates can be calculated as follows:

$$C_{XX} = Q_{XX} \cdot \sigma_0^2 \tag{5.54}$$

$$Q_{XX} = N^{-1} = (B^T PB)^{-1} \tag{5.55}$$

## 5.4 Experiment

We used two sets of high-resolution satellite images (HRSIs) to test the Generic Method based bundle adjustment algorithm. One is a stereo triplet of IKONOS Geo-imagery, whereas the other is a QuickBird Basic stereo pair. These HRSIs were previously used by Fraser and Hanley [2005] in their Bias-compensated RPC research. **Table 5.1** shows the essential characteristics of the two HRSI data sets.

**Table 5.1 Characteristics of the Two HRSI Imagery Test Fields [Fraser and Hanley, 2005]**

| | IKONOS, Hobart | QuickBird, Melbourne |
|---|---|---|
| Area | 120 km2 (11×11 km) | 300 km2 (17.5×17.5 km) |
| Elevation Range | Sea level to 1280 m | Sea level to 50 m |
| Image Coverage (elevation angles) | Stereo triplet (69˚, 75˚, 69˚) | Stereo pair (approx. 63˚ each) |
| Number of GCPs | 113 | 81 |
| Notable Features | Full scene; mountainous terrain | Full scene, low relief area |
| Base-to-height ratio | 0.8 | 1.0 |
| Date of acquisition | February, 2003 | July, 2003 |
| GCP measurement on image | Sub-pixel accuracy for roundabout features (traffic circles); pixel accuracy for other features. | Sub-pixel accuracy for all features. |
| Scan model | Reverse model for 69˚ images; Forward model for 75˚ image | N/A |

For the Hobart test field, "in order to insure high-accuracy GCPs and image coordinate data, multiple GPS and image measurements were made for each GCP with the centroids of roundabouts being determined by a best-fitting ellipse to six or more edge points around the circumference of the feature, in both object and image space. The estimated accuracy of this procedure is 0.2 pixels" [Fraser and Hanley, 2005]. The corner points were measured manually. Therefore, the corner GCPs have lower accuracy than the roundabout GCPs. In the Hobart test field, there are 65 roundabout GCPs and 48 corner GCPs.

For the Melbourne test field, "the majority of the 81 GCPs used were also road roundabouts, with the remaining points being corners and other distinct features conducive to high precision measurement in both the imagery and on the ground. Roundabouts were measured as described above, and in the case of corners, the feature point was defined in image space by the intersection of best-fitting lines to edge points" [Fraser and Hanley, 2005].

**Figure 5.4** shows the distribution of GCPs in the Hobart test field and the Melbourne test field respectively.

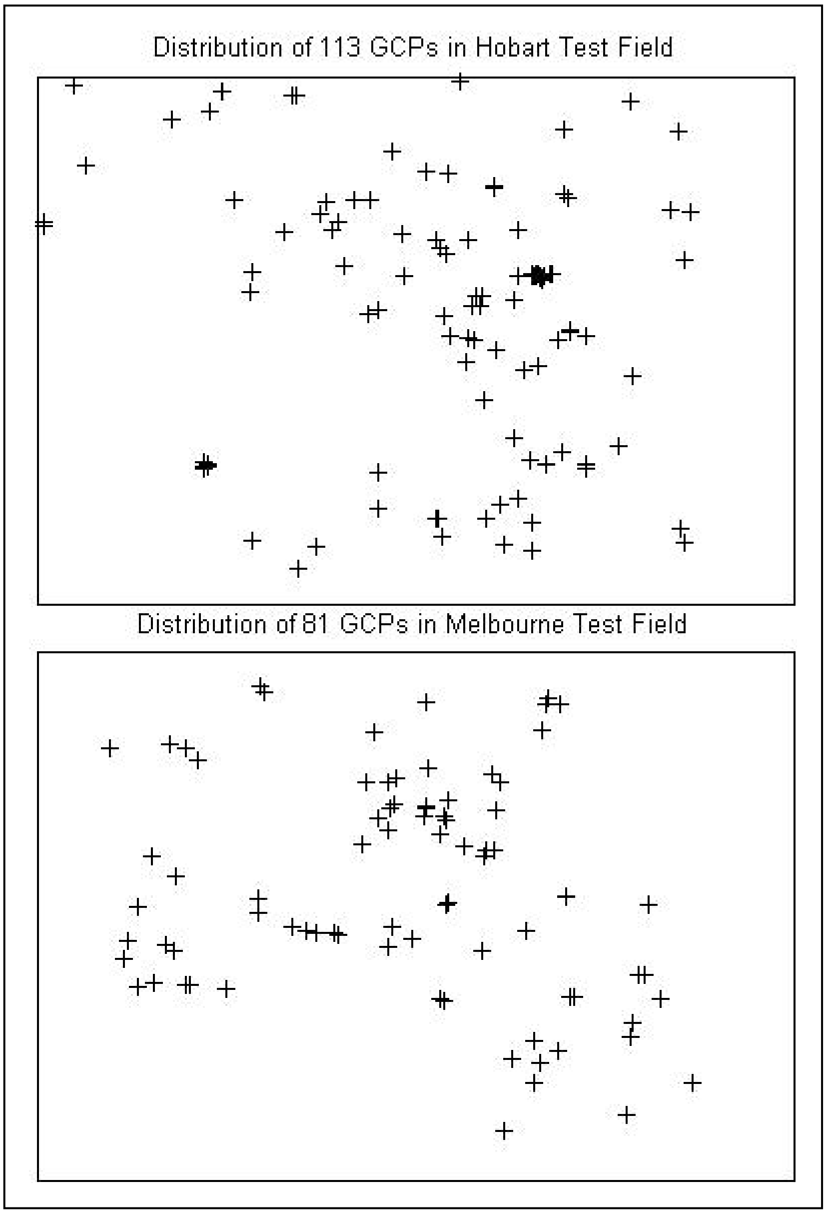


**Figure 5.4 Distribution of GCPs in Hobart and Melbourne Test Fields.**

For IKONOS and QuickBird images, yaw and radial errors are negligible [Grodecki and Dial, 2003; Dial and Grodecki, 2005], so in our experiments, we only considered

$\Delta X_{si}^{j}$, $\Delta Y_{si}^{j}$, $\Delta \psi_{xi}^{j}$, $\Delta \psi_{yi}^{j}$ (Equation 5.15, 5.16, 5.18, 5.19). The Shift model and Affine Model were both used to test the bundle adjustment algorithm. In the Shift model, only the terms $a_0$, $b_0$, $d_0$, $e_0$ are adjustable parameters; in the Affine model, the terms $a_0$, $a_L$, $a_S$, $b_0$, $b_L$, $b_S$, $d_0$, $d_L$, $d_S$, $e_0$, $e_L$, $e_S$ are adjustable parameters.

We designed 10 cases for both sets of test data. Each of these cases has 1 to 10 GCPs respectively. **Table 5.2** and **Table 5.3** show the accuracy estimation for ground coordinates for two test fields in case 10 (10 GCPs were used).

**Table 5.2 Accuracy Estimation for 103 points (IKONOS data, Hobart Test Field, 10 GCPs)**

| NO | σx (m) | σy (m) | σh (m) | NO | σx (m) | σy (m) | σh (m) |
|---|---|---|---|---|---|---|---|
| 1 | 0.341321 | 0.242218 | 1.023640 | 53 | 0.346373 | 0.244625 | 1.014724 |
| 2 | 0.340272 | 0.242432 | 1.023657 | 54 | 0.348070 | 0.243588 | 1.017357 |
| 3 | 0.337543 | 0.243280 | 1.022822 | 55 | 0.348073 | 0.243588 | 1.017357 |
| 4 | 0.337553 | 0.243298 | 1.022768 | 56 | 0.348051 | 0.243583 | 1.017382 |
| 5 | 0.341500 | 0.243061 | 1.021660 | 57 | 0.348050 | 0.243583 | 1.017381 |
| 6 | 0.338483 | 0.242814 | 1.023604 | 58 | 0.347811 | 0.243630 | 1.017345 |
| 7 | 0.338240 | 0.242175 | 1.025105 | 59 | 0.347871 | 0.243632 | 1.017314 |
| 8 | 0.343668 | 0.243217 | 1.020305 | 60 | 0.347882 | 0.243618 | 1.017349 |
| 9 | 0.343285 | 0.243166 | 1.020604 | 61 | 0.347893 | 0.243605 | 1.017385 |
| 10 | 0.343440 | 0.243066 | 1.020798 | 62 | 0.347834 | 0.243603 | 1.017416 |
| 11 | 0.342843 | 0.242226 | 1.022975 | 63 | 0.347822 | 0.243617 | 1.017382 |
| 12 | 0.342798 | 0.242229 | 1.022988 | 64 | 0.347764 | 0.243606 | 1.017436 |
| 13 | 0.344855 | 0.242647 | 1.021224 | 65 | 0.347777 | 0.243590 | 1.017478 |
| 14 | 0.345560 | 0.242801 | 1.020562 | 66 | 0.347727 | 0.243589 | 1.017506 |
| 15 | 0.344969 | 0.243309 | 1.019501 | 67 | 0.347677 | 0.243587 | 1.017530 |
| 16 | 0.344349 | 0.243046 | 1.020464 | 68 | 0.347664 | 0.243603 | 1.017488 |
| 17 | 0.344006 | 0.243041 | 1.020621 | 69 | 0.347714 | 0.243605 | 1.017461 |
| 18 | 0.346020 | 0.242811 | 1.020340 | 70 | 0.348669 | 0.244081 | 1.015570 |
| 19 | 0.342520 | 0.243318 | 1.020532 | 71 | 0.347612 | 0.244341 | 1.015141 |
| 20 | 0.348527 | 0.242443 | 1.020141 | 72 | 0.346180 | 0.244119 | 1.016531 |
| 21 | 0.346987 | 0.242904 | 1.019702 | 73 | 0.348374 | 0.244040 | 1.015832 |
| 22 | 0.346980 | 0.242894 | 1.019731 | 74 | 0.348376 | 0.244039 | 1.015834 |
| 23 | 0.348525 | 0.242980 | 1.018857 | 75 | 0.348352 | 0.244034 | 1.015860 |
| 24 | 0.348457 | 0.242948 | 1.018972 | 76 | 0.348350 | 0.244035 | 1.015859 |
| 25 | 0.350933 | 0.242419 | 1.019207 | 77 | 0.349552 | 0.244398 | 1.014083 |
| 26 | 0.347450 | 0.243244 | 1.018621 | 78 | 0.340435 | 0.245211 | 1.015390 |
| 27 | 0.346343 | 0.242077 | 1.021820 | 79 | 0.340454 | 0.245183 | 1.015494 |
| 28 | 0.350680 | 0.243045 | 1.017768 | 80 | 0.340469 | 0.245158 | 1.015584 |
| 29 | 0.351093 | 0.243050 | 1.017579 | 81 | 0.340549 | 0.245182 | 1.015453 |
| 30 | 0.351117 | 0.243049 | 1.017575 | 82 | 0.340448 | 0.245208 | 1.015400 |
| 31 | 0.341787 | 0.243639 | 1.019935 | 83 | 0.340567 | 0.245169 | 1.015495 |
| 32 | 0.341767 | 0.243646 | 1.019924 | 84 | 0.345031 | 0.245613 | 1.011449 |
| 33 | 0.346351 | 0.243860 | 1.017278 | 85 | 0.344998 | 0.245616 | 1.011449 |
| 34 | 0.345738 | 0.243946 | 1.017274 | 86 | 0.341984 | 0.246055 | 1.010949 |
| 35 | 0.345811 | 0.244106 | 1.016735 | 87 | 0.341978 | 0.246053 | 1.010960 |
| 36 | 0.345787 | 0.243399 | 1.018893 | 88 | 0.342438 | 0.245864 | 1.011586 |
| 37 | 0.345889 | 0.243450 | 1.018705 | 89 | 0.345072 | 0.245756 | 1.010828 |
| 38 | 0.346114 | 0.244308 | 1.015945 | 90 | 0.343818 | 0.245545 | 1.012285 |
| 39 | 0.344163 | 0.243944 | 1.017987 | 91 | 0.347502 | 0.245133 | 1.012251 |
| 40 | 0.344359 | 0.243920 | 1.017976 | 92 | 0.347150 | 0.245110 | 1.012509 |
| 41 | 0.343742 | 0.243576 | 1.019280 | 93 | 0.346811 | 0.245410 | 1.011487 |
| 42 | 0.345679 | 0.243345 | 1.019092 | 94 | 0.346397 | 0.245479 | 1.011403 |
| 43 | 0.344985 | 0.243625 | 1.018614 | 95 | 0.350089 | 0.245626 | 1.009057 |
| 44 | 0.346426 | 0.243780 | 1.017493 | 96 | 0.350112 | 0.245733 | 1.008596 |
| 45 | 0.346515 | 0.243867 | 1.017185 | 97 | 0.349053 | 0.244973 | 1.012172 |
| 46 | 0.347253 | 0.243810 | 1.017049 | 98 | 0.346897 | 0.244937 | 1.013282 |
| 47 | 0.346329 | 0.244131 | 1.016424 | 99 | 0.347863 | 0.245036 | 1.012467 |
| 48 | 0.346758 | 0.244207 | 1.015992 | 100 | 0.347024 | 0.245617 | 1.010532 |
| 49 | 0.347280 | 0.244378 | 1.015165 | 101 | 0.346914 | 0.245848 | 1.009590 |
| 50 | 0.348088 | 0.244122 | 1.015673 | 102 | 0.346065 | 0.245585 | 1.011128 |
| 51 | 0.347342 | 0.243618 | 1.017585 | 103 | 0.346343 | 0.245804 | 1.010035 |
| 52 | 0.350918 | 0.243439 | 1.016572 | | | | |

**Table 5.3 Accuracy Estimation for 71 points (QuickBird data, Melbourne Test Field, 10 GCPs)**

| NO | σx (m) | σy (m) | σh (m) | NO | σx (m) | σy (m) | σh (m) |
|---|---|---|---|---|---|---|---|
| 1 | 0.162342 | 0.152985 | 0.267337 | 37 | 0.162787 | 0.153149 | 0.267244 |
| 2 | 0.162462 | 0.152986 | 0.267261 | 38 | 0.163546 | 0.152856 | 0.266401 |
| 3 | 0.161709 | 0.153023 | 0.267791 | 39 | 0.160989 | 0.153041 | 0.268293 |
| 4 | 0.161709 | 0.153023 | 0.267791 | 40 | 0.164222 | 0.152813 | 0.265910 |
| 5 | 0.162068 | 0.153095 | 0.267639 | 41 | 0.162674 | 0.153086 | 0.267234 |
| 6 | 0.161796 | 0.153016 | 0.267727 | 42 | 0.160753 | 0.153076 | 0.268495 |
| 7 | 0.162410 | 0.153071 | 0.267388 | 43 | 0.161005 | 0.153014 | 0.268250 |
| 8 | 0.161477 | 0.153041 | 0.267965 | 44 | 0.163637 | 0.152872 | 0.266380 |
| 9 | 0.161992 | 0.153088 | 0.267676 | 45 | 0.161053 | 0.153034 | 0.268243 |
| 10 | 0.162279 | 0.153078 | 0.267483 | 46 | 0.161786 | 0.153164 | 0.267916 |
| 11 | 0.162600 | 0.153042 | 0.267234 | 47 | 0.162202 | 0.153116 | 0.267577 |
| 12 | 0.162717 | 0.153064 | 0.267180 | 48 | 0.162017 | 0.153117 | 0.267701 |
| 13 | 0.162737 | 0.153035 | 0.267138 | 49 | 0.161214 | 0.153004 | 0.268099 |
| 14 | 0.162088 | 0.153075 | 0.267603 | 50 | 0.162794 | 0.153143 | 0.267232 |
| 15 | 0.162270 | 0.153085 | 0.267497 | 51 | 0.160263 | 0.153222 | 0.269032 |
| 16 | 0.162054 | 0.153093 | 0.267645 | 52 | 0.163549 | 0.152868 | 0.266423 |
| 17 | 0.162425 | 0.153069 | 0.267376 | 53 | 0.160919 | 0.153015 | 0.268309 |
| 18 | 0.162395 | 0.153084 | 0.267411 | 54 | 0.163468 | 0.152884 | 0.266501 |
| 19 | 0.162273 | 0.153084 | 0.267494 | 55 | 0.162781 | 0.152934 | 0.266996 |
| 20 | 0.162743 | 0.153030 | 0.267130 | 56 | 0.162807 | 0.152932 | 0.266977 |
| 21 | 0.162940 | 0.152960 | 0.266929 | 57 | 0.161442 | 0.152993 | 0.267933 |
| 22 | 0.163364 | 0.152877 | 0.266549 | 58 | 0.164000 | 0.152907 | 0.266214 |
| 23 | 0.160912 | 0.153091 | 0.268403 | 59 | 0.161038 | 0.153234 | 0.268524 |
| 24 | 0.164086 | 0.152866 | 0.266103 | 60 | 0.160999 | 0.153242 | 0.268564 |
| 25 | 0.162035 | 0.153179 | 0.267774 | 61 | 0.163355 | 0.152980 | 0.266688 |
| 26 | 0.163453 | 0.152829 | 0.266396 | 62 | 0.161187 | 0.153006 | 0.268118 |
| 27 | 0.160726 | 0.153115 | 0.268558 | 63 | 0.160794 | 0.153186 | 0.268611 |
| 28 | 0.162617 | 0.153095 | 0.267281 | 64 | 0.161977 | 0.153116 | 0.267725 |
| 29 | 0.164198 | 0.152885 | 0.266065 | 65 | 0.162611 | 0.153003 | 0.267187 |
| 30 | 0.162876 | 0.153141 | 0.267174 | 66 | 0.162615 | 0.153003 | 0.267184 |
| 31 | 0.161847 | 0.153121 | 0.267816 | 67 | 0.162788 | 0.153032 | 0.267102 |
| 32 | 0.160696 | 0.153201 | 0.268701 | 68 | 0.161977 | 0.153008 | 0.267598 |
| 33 | 0.164043 | 0.152905 | 0.266185 | 69 | 0.161869 | 0.153012 | 0.267674 |
| 34 | 0.160780 | 0.153040 | 0.268433 | 70 | 0.161437 | 0.153053 | 0.268005 |
| 35 | 0.163914 | 0.152954 | 0.266319 | 71 | 0.162314 | 0.152999 | 0.267371 |
| 36 | 0.164596 | 0.152820 | 0.265714 | | | | |

**Tables 5.4, 5.5** show the accuracies of ground coordinates for both test fields by comparing the ground coordinates calculated by bundle block adjustment and the ground coordinates surveyed by GPS. **Figure 5.5** and **Figure 5.6** show the same situation corresponding with **Table 5.4** and **Table 5.5**.

**Table 5.4 RMSE of CHKs in Object Space (Hobart Test Field)**

| GCP/ CHK | Shift | | | Affine | | |
|---|---|---|---|---|---|---|
| | X (m) | Y (m) | Z (m) | X (m) | Y (m) | Z (m) |
| 1/112 | 0.564 | 0.643 | 0.943 | 0.564 | 0.643 | 0.943 |
| 2/111 | 0.570 | 0.668 | 0.928 | 0.573 | 0.658 | 1.152 |
| 3/110 | 0.761 | 0.556 | 0.938 | 0.837 | 0.628 | 1.002 |
| 4/109 | 0.601 | 0.510 | 0.934 | 0.908 | 0.512 | 1.052 |
| 5/108 | 0.558 | 0.510 | 0.958 | 0.896 | 0.511 | 0.958 |
| 6/107 | 0.551 | 0.501 | 0.936 | 0.861 | 0.514 | 0.984 |
| 7/106 | 0.562 | 0.500 | 0.929 | 0.591 | 0.512 | 0.963 |
| 8/105 | 0.558 | 0.502 | 0.940 | 0.599 | 0.512 | 1.016 |
| 9/104 | 0.564 | 0.504 | 0.951 | 0.584 | 0.500 | 0.989 |
| 10/103 | 0.566 | 0.507 | 0.943 | 0.588 | 0.503 | 0.994 |

**Table 5.5 RMSE of CHKs in Object Space (Melbourne Test Field)**

| GCP/ CHK | Shift | | | Affine | | |
|---|---|---|---|---|---|---|
| | X (m) | Y (m) | Z (m) | X (m) | Y (m) | Z (m) |
| 1/80 | 0.578 | 0.473 | 0.468 | 0.578 | 0.473 | 0.468 |
| 2/79 | 0.588 | 0.473 | 0.441 | 0.592 | 0.466 | 0.440 |
| 3/78 | 0.587 | 0.486 | 0.410 | 0.639 | 0.552 | 0.370 |
| 4/77 | 0.599 | 0.485 | 0.434 | 0.660 | 0.545 | 0.407 |
| 5/76 | 0.617 | 0.511 | 0.440 | 0.699 | 0.602 | 0.423 |
| 6/75 | 0.615 | 0.509 | 0.444 | 0.672 | 0.573 | 0.421 |
| 7/74 | 0.589 | 0.491 | 0.449 | 0.587 | 0.492 | 0.419 |
| 8/73 | 0.592 | 0.490 | 0.440 | 0.596 | 0.506 | 0.408 |
| 9/72 | 0.598 | 0.485 | 0.418 | 0.624 | 0.530 | 0.394 |
| 10/71 | 0.611 | 0.481 | 0.424 | 0.617 | 0.457 | 0.407 |

Notes: RMSE – Root Mean Square Error; CHK – Check Point; GCP – Ground Control Point

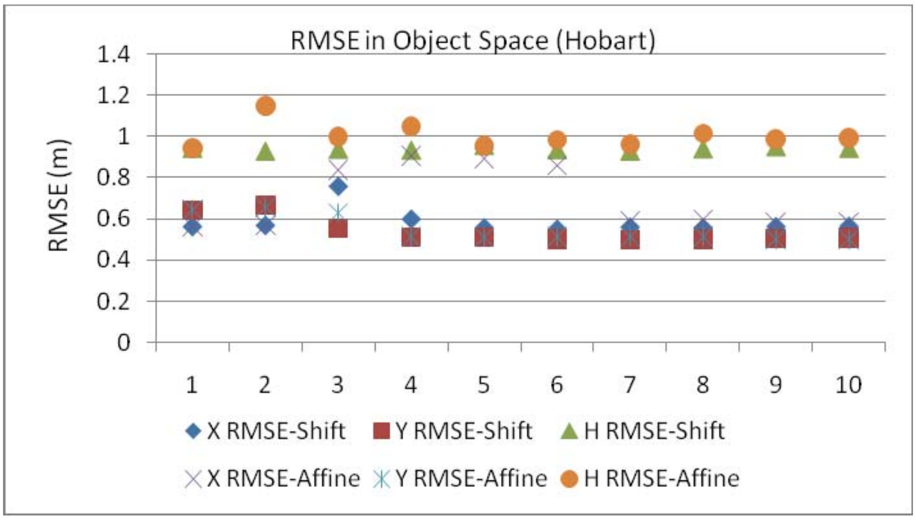


**Figure 5.5 RMSE of CHKs in Object Space in Hobart Test Field.**

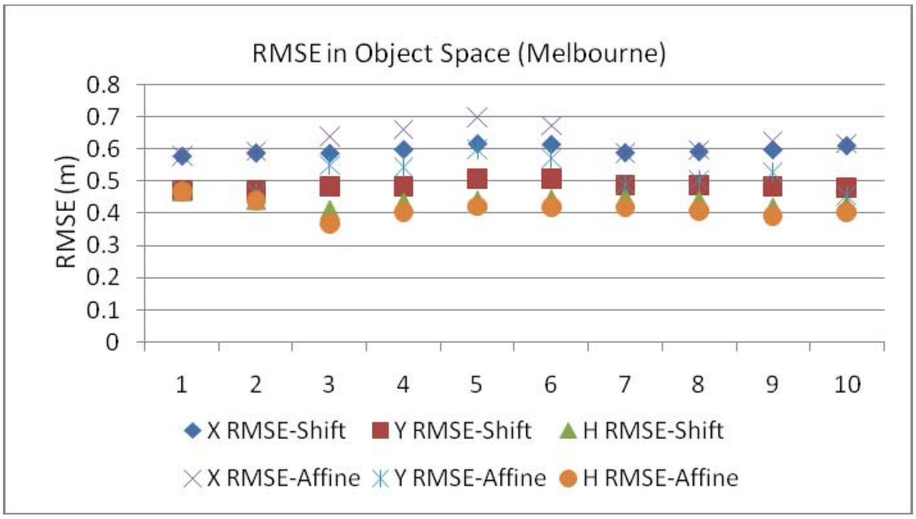


**Figure 5.6 RMSE of CHKs in Object Space in Melbourne Test Field.**

By comparison of **Table 5.2**, **Table 5.3** and **Table 5.4** (Case 10, the red row) and **Table 5.5** (Case 10, the red row), we can find that the estimated accuracy is a little bit better than the real accuracy. The reason is that we did not consider the GCPs' error during the error estimation.

**Tables 5.4, 5.5** and **Figures 5.5, 5.6** illustrate that the planimetric and height accuracies are all less than one meter in both test fields except the height accuracy in the Hobart field (about 1 meter).

The experiment results also show that there are no obvious differences between the Shift model and Affine model. In terms of accuracy, sometimes the Shift model is slightly better, and sometimes the Affine model is slightly better. But the Shift model is always more stable than the Affine model. The reason is that we used a small number (1 to 10) of GCPs in the experiments, so the Affine model may become over-parameterized.

With the increasing of GCPs, the Affine model shows better accuracy than the Shift model. We compared the case of 10 GCPs and found that, in terms of accuracy in object space, the Affine model is a little bit better in Melbourne test field (**Table 5.5, Figure 5.6**), but the Shift model is a little bit better in the Hobart test field (**Table 5.4, Figure 5.5**). This seems unreasonable. In fact, this is caused by low accuracy GCPs. In Hobart test field, we used 48 low accuracy GCPs (corner points only with pixel accuracy whose image coordinates were measured once manually) (**Table 5.1**). Because the Affine model has more parameters than the Shift model, the Affine model is more sensitive to the low accuracy GCPs, especially when a small number of GCPs was used.

## 5.5 Conclusion

This paper has proposed a Generic Method based bundle adjustment algorithm with RPC. We compared the Affine Model and Shift Model for 10 cases. The following conclusions are drawn:

(1) Experiments using IKONOS and QuickBird imagery show that this algorithm is effective and can readily achieve sub-meter accuracy in the object space.

(2) When using a small number of GCPs, the accuracy of the Shift model is quite similar to the accuracy of the Affine model, but the Shift model is more stable.

(3) With the increasing of GCPs, the Affine model can achieve better results than the Shift model.

(4) Because there are not high-order error sources from IKONOS and QuickBird, the Shift model is good enough (in terms of accuracy) to process those kind of imagery.

(5) In this paper, only the affine model and shift model are proposed and compared. Because the RPC model is a generic sensor model and can be used in a wide variety of different remote sensing systems, therefore, for different sensors, using different models should be considered.

## ACKNOWLEDGEMENTS

This research is sponsored by the Natural Sciences and Engineering Research Council of Canada through the Discovery Grant (NSERC Discovery Grant) awarded to Dr. Yun Zhang, the second author of the paper. We would like to thank Dr. Marcelo C. Santos for arranging time from his busy schedule to discuss the research topic and give me good suggestion. We are grateful to Prof. Clive Fraser, Department of Geomatic Engineering, University of Melborne, Australia, provided us satellite image and ground control data for the tests. Special thanks go to Mr. David C. Whyte, Department of Environment, NB, Canada, who reviewed the manuscript of this report.

## REFERENCES

Chen, Liang-Chien, Tee-Ann Teo, and Chien-Liang Liu. (2006). "The geometrical comparisons of RSM and RFM for FORMOSAT-2 satellite images." *Photogrammetric Engineering & Remote Sensing,* Vol. 72, No. 5, pp. 573-579.

Dial, Gene and Jacek Grodecki. (2002[a]). "Block adjustment with rational polynomial camera models." *ACSM-ASPRS 2002 annual conference proceedings.*

Dial, Gene and Jacek Grodecki. (2002[b]). "IKONOS accuracy without ground control." *Pecora 15/Land Satellite Information IV/ISPRS Commission I/FIEOS 2002 Conference Proceedings*.

Dial, Gene and Jacek Grodecki. (2005). "RPC Replacement Camera Models." A*SPRS 2005 annual conference proceedings,* Baltimore, Maryland, March 7-11, 2005.

Dowman, Ian and Vincent Tao. (2002). "An Update on the use of rational functions for photogrammetric restitution." *ISPRS Article, Vol. 7, No., 3, September 2002*. URL: http://www.isprs.org/publications/highlights/highlights0703/22_HL_09_02_Article_Dowman.pdf, last date accessed 6 January 2008.

Fraser, Clive S., G. Dial, J. Grodecki. (2006). "Sensor orientation via RPCs." *ISPRS Journal of Photogrammetry & Remote Sensing*, 60(2006) 182-194.

Fraser, Clive S. and Harry B. Hanley. (2003). "Bias Compensation in Rational Functions for Ikonos Satellite Imagery." *Photogrammetric Engineering & Remote Sensing,* Vol. 69, No. 1, pp. 53 – 57.

Fraser, Clive S. and Harry B. Hanley. (2005). "Bias-compensated RPCs for Sensor Orientation of High-resolution Satellite Imagery." *Photogrammetric Engineering & Remote Sensing,* Vol. 71, No. 8, pp. 909–915.

Grodecki, Jacek and Gene Dial. (2003). "Block adjustment of high resolution satellite images described by rational polynomials." *Photogrammetric Engineering & Remote Sensing,* Vol. 69, No. 1, pp. 59-68.

Grodecki, Jacek and James Lutes. (2005). "IKONOS Geometric Calibrations." *ASPRS 2005, Baltimore, Marylan*d, March 7-11, 2005.

Hu, Yong, Vincent Tao, Arie Croitoru. (2004). "Understanding the rational function model: methods and applications." URL: http://www.geoict.net/Resources/Publications/IAPRS2004_RFM2394.pdf, last date accessed 31 December 2007.

Rose, Eugene and Kiril Fradkin. (2005). "Multi-Sensor Triangulation." *ASPRS 2005, Baltimore, Marylan*d, March 7-11, 2005.

Tao, C. Vincent and Yong Hu. (2001). "A comprehensive study of the rational function model for photogrammetric processing." *Photogrammetric Engineering & Remote Sensing,* Vol. 67, No. 12, pp. 1347-1357.

Toutin, T. (2003). "Block Adjustment of IKONOS In-Track Images, International Journal of Remote Sensing." 24(4): 851-857.

Xiong, Z., Y. Zhang. (2008). "A Generic Method for RPC Refinement Using Ground Control Information." Journal of *Photogrammetric Engineering & Remote Sensing,* 2008 (In press).

# Chapter 6

# SUMMARY AND CONCLUSIONS

This chapter summarizes the research conducted for this dissertation. It begins with the outline of the research drawn from Chapters 2 to 5. The contributions of this research are then presented. Finally, some suggestions for future work are provided.

## 6.1 Summary of Research

Aerial triangulation is at the technical core of photogrammetry. Automated aerial triangulation has, therefore, been the subject of extensive research. Any improvement to the process may offer huge commercial potential. This research has touched on the main components of aerial triangulation and has attempted to solve existing problems inherent in the four major steps of aerial triangulation: interest point extraction, interest point matching, sensor model refinement, and bundle block adjustment.

For interest point extraction, two typical feature points: corners and centers were studied to characterize their utility for image registration. Using quantitative analysis, the research was able to identify which of the two types of points is most suitable for use as tie points and which type provides more accurate control for bundle block adjustment.

For interest point matching, the most recent area-based and feature-based methods were examined. In order to overcome the problem of ambiguity in smooth areas, a new algorithm was developed and investigated.

With respect to the topic of sensor model refinement, various RPC refinement methods were studied. The research indicated that direct refinement methods require a lot of supplementary information which is unavailable to public, while indirect methods are subject to prerequisites that seriously influence their applicability. A generic method for sensor model refinement was developed that avoids the above noted issues.

Various RPC-based bundle block adjustment methods were studied. Because the current methods are based on indirect sensor model refinement methods, they share the same limitations as the indirect methods, e.g. the feasibility is limited by rigorous conditions. A more robust bundle block adjustment method based on a generic method of sensor model refinement was developed and investigated.

## 6.2 Achievements of This Research

**Interest point extraction**

Two typical interest point types: corners and centers were studied. The research clearly shows that when used as tie points, centers can provide more accurate control than corners. Center points can improve the accuracy of image registration by at least 40%. For registration of images having different resolutions, center points can improve accuracy much more that 40%. This finding will have an important impact on the accuracy improvement of aerial triangulation.

**Interest point matching**

A novel algorithm for interest point matching of high resolution satellite images was developed. This algorithm has following characteristics:

1) It can avoid local minimum problems and can process areas without prominent details;
2) It can remove outliers easily; and
3) It does not require an exhaustive search during the interest point matching.

This new development has demonstrated the potential to improve the robustness of automatic image matching for a variety of remote sensing images.

**Sensor model refinement**

A Generic method which is defined in object space was developed. It directly modifies the RPC coefficients, but unlike other direct methods, it does not require any supplementary, proprietary information about RPC, such as the covariance matrices. The Generic method simulates the sensor's imaging geometry and can be used to adjust the camera's position and attitude. It can be used to effectively refine the RPC regardless of the sensor's field of view, attitude error or position error. This development widens the suitability of RPCs to a wide range of remote sensing sensors.

**Bundle block adjustment**

A bundle adjustment algorithm with RPC based on the Generic Method has been developed. This algorithm is effective and can readily achieve sub-meter accuracy in object space for IKONOS and QuickBird images. This algorithm can successfully process IKONOS and QuickBird images, regardless of the number of GCPs that are used.

## 6.3 Suggestions for Future Work

Based on this research, the following suggestions for further research are presented.

Most of the existing automatic interest point extraction algorithms can only extract corners; however this research has shown that centers are more suitable for use as tie points for bundle block adjustment and image registration. Methods of extracting gravity center points from images of different resolutions or from different modal images are therefore of great significance and should be the focus of further research.

The interest point matching algorithm proposed in this research has been shown to be effective in processing high resolution images including images with large almost homogeneous areas. Further tests should be conducted using other types of images, including aerial images and other images captured with wide field of view cameras.

The proposed generic sensor model should be tested under a wider variety of conditions and sensors, such as airborne wide angle cameras, large off-nadir angles, and different satellite data.

# APPENDIX I

**Permission from the American Society for Photogrammetry and Remote Sensing**

Tue, 23 Dec 2008 14:30:26 -0500

Zhen Xiong
Remote Sensing/GIS
Department of Geodesy and Geomatics Engineering
University of New Brunswick PO Box 4400, 15 Dineen Dr.
Fredericton, NB E3B 5A3
Canada
(506) 453 5058
(506) 453 4943 (Fax)
Email: z.xiong@unb.ca

ASPRS grants you permission to use the following paper in your PhD dissertation:

Xiong, Zhen and Yun Zhang. A Generic Method for RPC Refinement using Ground Control Information. *Photogrammetric Engineering and Remote Sensing.* The American Society for Photogrammetry and Remote Sensing, Bethesda, MD. In press.

Please include acknowledgments, in the following format, with the reprinted material:

"Reprinted with permission from the American Society for Photogrammetry and Remote Sensing. "

If this information is to be reprinted in any other format, please contact ASPRS.

Thank you,
Matthew Austin
ASPRS Publications Production Assistant
maustin@asprs.org
301-493-0290, ext. 108
301-493-0208 (fax)

# APPENDIX II

**An Email from the ASPRS regarding the acception for publication of the paper "*A Generic Method for RPC Refinement using Ground Control Information*"**
Mon, 8 Sep 2008 13:14:02 -0400

Mr. Xiong,

I have reviewed the revisions to your manuscript, ***A Generic Method for RPC Refinement using Ground Control Information*** (08-023) and am pleased to inform you that your revised paper has been accepted for publication in *PE&RS*.. Instructions for preparing the final manuscript are attached. Please follow these instructions very carefully. Also, the payment form for color plates is attached.

<u>Please send everything to:</u>

Dr. Russell G. Congalton
Editor-in-Chief, *Photogrammetric Engineering and Remote Sensing*
4 Ryan Way
Durham, NH 03824
E-mail:russ.congalton@unh.edu

# APPENDIX III Melbourne GCPs (from University of Melbourne)

| Name | Lat. | Lon. | H | Column | Row | Column | Row |
|---|---|---|---|---|---|---|---|
| ADD | -37.8085 | 144.9454 | 20.28849 | 12369.44 | 10083.61 | 12877.03 | 9095.001 |
| ALB | -37.8459 | 144.955 | 7.170011 | 13486.02 | 15515.15 | 13964.03 | 13899.03 |
| AQUA | -37.8431 | 144.9622 | 8.93653 | 14333.15 | 15237.87 | 14841.59 | 13501.94 |
| BASA | -37.8376 | 144.9233 | 7.468966 | 9752.803 | 13837.11 | 10142.41 | 12971.25 |
| BASB | -37.8376 | 144.9233 | 7.492172 | 9753.247 | 13834.29 | 10142.74 | 12969.65 |
| BAY | -37.7941 | 144.9559 | 40.35642 | 13621.09 | 8200.519 | 14175.78 | 7184.96 |
| BEACON | -37.8395 | 144.9275 | 6.610494 | 10243.66 | 14164.32 | 10642.42 | 13190.9 |
| CAN | -37.7993 | 144.9726 | 36.33333 | 15586.97 | 9202.913 | 16190.13 | 7772.138 |
| COOK | -37.8324 | 144.9121 | 8.266415 | 8430.682 | 12922.29 | 8797.904 | 12347.67 |
| ERROL | -37.799 | 144.9504 | 18.80163 | 12958.06 | 8816.108 | 13495.87 | 7829.754 |
| EXB | -37.8055 | 144.9714 | 46.21848 | 15443.74 | 10052.04 | 16031.43 | 8587.81 |
| FAR | -37.7985 | 144.9658 | 49.50392 | 14792.7 | 8980.23 | 15369.96 | 7717.203 |
| FITZ | -37.8107 | 144.9791 | 35.82659 | 16350.1 | 10917.91 | 16961.02 | 9218.985 |
| GOLD | -37.7974 | 144.9894 | 24.18482 | 17561.04 | 9214.918 | 18226.81 | 7437.553 |
| GREY | -37.8119 | 144.986 | 30.72621 | 17149.24 | 11204.1 | 17784.05 | 9341.405 |
| HOWARD | -37.8035 | 144.9541 | 40.50427 | 13400.94 | 9506.123 | 13936.49 | 8419.621 |
| KEP | -37.7953 | 144.9664 | 53.36097 | 14858.6 | 8528.351 | 15441.01 | 7295.363 |
| MOR | -37.7954 | 144.9548 | 35.93759 | 13484.81 | 8368.798 | 14035.78 | 7355.43 |
| MUR | -37.8002 | 144.9731 | 37.51961 | 15642.09 | 9344.378 | 16244.69 | 7893.75 |
| NEILL | -37.7935 | 144.9736 | 31.59272 | 15700.98 | 8408.65 | 16315.87 | 7018.228 |
| NOT | -37.8413 | 144.9381 | 8.002017 | 11496.14 | 14592.12 | 11925.95 | 13379.57 |
| PALM | -37.7958 | 144.9663 | 51.61476 | 14850.98 | 8607.913 | 15432.77 | 7367.854 |
| POW | -37.8141 | 144.9856 | 34.65663 | 17105.1 | 11513.83 | 17734.23 | 9639.059 |
| QALF | -37.8485 | 144.9856 | 19.01539 | 17089.64 | 16369.84 | 17673.18 | 14097.12 |
| QBENT | -37.8886 | 144.9962 | 8.64464 | 18304.77 | 22183.33 | 18866.3 | 19259.47 |
| QBLCK | -37.818 | 144.8849 | 15.54912 | 5197.87 | 10442.61 | 5519.656 | 10603.29 |
| QBOORAN | -37.8814 | 145.0346 | 53.20531 | 22807.7 | 21779.45 | 23539.87 | 18172.8 |
| QBURT | -37.7689 | 145.0039 | 53.21381 | 19301.15 | 5407.217 | 20032.34 | 3698.875 |
| QCARL | -37.7567 | 144.9658 | 59.16075 | 14817.97 | 3054.905 | 15435.97 | 2302.878 |
| QCARP | -37.9149 | 144.9937 | 13.1469 | 18008.56 | 25834.14 | 18506.36 | 22707.52 |
| QCHAT | -37.81 | 144.8768 | 22.66126 | 4233.153 | 9182.974 | 4551.16 | 9609.71 |
| QCROM | -37.8421 | 144.9996 | 12.76794 | 18721.74 | 15700.82 | 19371.61 | 13195.02 |
| QFALC | -37.7844 | 144.9881 | 40.69321 | 17424.04 | 7348.355 | 18093.99 | 5770.98 |
| QFINCH | -37.8683 | 145.0439 | 52.59964 | 23892.64 | 20085.67 | 24686.64 | 16417.66 |
| QGOO | -37.7589 | 145.0097 | 59.441 | 19985.89 | 4076.447 | 20740.52 | 2378.601 |
| QHOCK | -37.7856 | 144.9466 | 43.33672 | 12529.73 | 6850.254 | 13066.19 | 6130.106 |
| QHSC | -37.7708 | 144.8872 | 38.14063 | 5474.987 | 3803.153 | 5884.176 | 4488.431 |
| QJOR | -37.8593 | 145.0388 | 49.73879 | 23299.65 | 18735.46 | 24081.79 | 15267.62 |
| QJUBI | -37.8472 | 144.8686 | 10.85747 | 3278.322 | 14296.79 | 3490.492 | 14472.01 |
| QKEMB | -37.8336 | 145.0398 | 46.36842 | 23437.44 | 15137.04 | 24254.39 | 11919.05 |
| QKOO | -37.8994 | 145.0551 | 48.43921 | 25167.42 | 24645.42 | 25974.38 | 20417.2 |
| QMADD | -37.8411 | 144.8697 | 15.5079 | 3399.664 | 13453.29 | 3628.459 | 13677.93 |
| QMANS | -37.7569 | 145.0056 | 65.97615 | 19513.98 | 3718.031 | 20253.75 | 2138.822 |
| QMART | -37.8973 | 145.0031 | 12.82944 | 19115.55 | 23516.48 | 19690.14 | 20363.34 |
| QMASN | -37.8424 | 144.8819 | 19.93966 | 4853.975 | 13835.99 | 5110.075 | 13798 |
| QMCK | -37.9105 | 145.0337 | 29.7934 | 22670.88 | 25863.7 | 23360.02 | 21955.56 |
| QMICH | -37.7875 | 144.9902 | 41.1009 | 17661.35 | 7814.718 | 18334.86 | 6158.656 |
| QMORE | -37.8286 | 144.8726 | 19.09895 | 3743.379 | 11749.13 | 4009.459 | 12051.37 |
| QMYRT | -37.8568 | 144.8785 | 9.802156 | 4458.68 | 15814.73 | 4672.89 | 15681.14 |
| QNEWHOPE | -37.8861 | 145.0107 | 32.8613 | 20014.54 | 22057.22 | 20636.75 | 18882.19 |
| QNRTH | -37.8448 | 144.8847 | 19.02184 | 5193.386 | 14220.54 | 5451.822 | 14096.65 |
| QORRONA | -37.8661 | 145.0147 | 39.51191 | 20493.77 | 19304.35 | 21162.96 | 16259.23 |
| QORRONB | -37.8661 | 145.0158 | 40.12594 | 20618.58 | 19330.13 | 21291.89 | 16262.59 |
| QPEAR | -37.7673 | 144.949 | 55.74847 | 12823.88 | 4287.765 | 13384.94 | 3752.721 |

| | | | | | | | |
|---|---|---|---|---|---|---|---|
| QPGDN | -37.7814 | 144.9671 | 42.96298 | 14944.52 | 6585.435 | 15548.34 | 5487.624 |
| QPOP | -37.7845 | 144.9561 | 53.61974 | 13653.61 | 6835.168 | 14216.94 | 5943.704 |
| QRAIL | -37.858 | 144.8899 | 14.60521 | 5810.997 | 16154.51 | 6052.737 | 15778.6 |
| QRAL | -37.7593 | 145.0052 | 67.44128 | 19465.9 | 4047.016 | 20202.86 | 2448.929 |
| QRGLN | -37.7703 | 144.8624 | 44.36752 | 2506.481 | 3337.702 | 2865.042 | 4550.923 |
| QRIDD | -37.8903 | 145.0052 | 22.71995 | 19358.25 | 22556.2 | 19951.08 | 19443.94 |
| QSALT | -37.8579 | 144.8734 | 6.703014 | 3844.82 | 15884.39 | 4042.641 | 15843.33 |
| QSAND | -37.8821 | 145.0033 | 23.80487 | 19144.32 | 21375.57 | 19742.8 | 18386.96 |
| QSTAT | -37.8769 | 145.0355 | 49.32136 | 22905.59 | 21155.21 | 23648.82 | 17572.92 |
| QSTKDB | -37.8661 | 144.9723 | 6.640094 | 15518.74 | 18629.99 | 16024.02 | 16436.63 |
| QSTKDC | -37.8669 | 144.9734 | 6.742439 | 15648.66 | 18762.07 | 16156.28 | 16537.08 |
| QSTRAND | -37.8595 | 144.9022 | 7.143365 | 7259.742 | 16568.54 | 7536.482 | 15912.14 |
| QTHANET | -37.859 | 145.0366 | 51.02087 | 23055.23 | 18661.28 | 23826.98 | 15242.2 |
| QTHIS | -37.7511 | 144.9128 | 47.94392 | 8530.776 | 1416.81 | 9020.788 | 1823.423 |
| QTHRN | -37.7489 | 144.9114 | 53.5884 | 8355.822 | 1073.009 | 8843.332 | 1545.627 |
| QTWICK | -37.8297 | 145.0127 | 15.73713 | 20261.75 | 14161.72 | 20979.72 | 11519.52 |
| QVICT | -37.8577 | 144.8885 | 13.9448 | 5643.326 | 16090.63 | 5882.745 | 15746.5 |
| QWARR | -37.7754 | 144.8914 | 36.96345 | 5969.041 | 4525.57 | 6380.529 | 5067.699 |
| QWEST | -37.7696 | 144.8821 | 29.60833 | 4855.19 | 3557.21 | 5258.351 | 4352.077 |
| QZOO | -37.7857 | 144.9536 | 50.0165 | 13354.43 | 6965.511 | 13909.27 | 6108.843 |
| SHRINEA | -37.831 | 144.9735 | 32.10924 | 15684.77 | 13704.41 | 16247.32 | 11890.87 |
| SHRINEB | -37.831 | 144.9738 | 32.08407 | 15710.47 | 13699.2 | 16273.62 | 11881.5 |
| SIM | -37.8122 | 144.9886 | 22.56295 | 17452.43 | 11291.51 | 18098.61 | 9360.326 |
| STO | -37.8407 | 144.9369 | 8.205102 | 11364.43 | 14482.52 | 11791.39 | 13300.57 |
| SWA | -37.8403 | 144.9312 | 6.702513 | 10687.33 | 14334.99 | 11097.3 | 13274.93 |
| TODD | -37.8268 | 144.9116 | 7.568104 | 8367.492 | 12126.82 | 8744.845 | 11623.2 |
| VIN | -37.8389 | 144.9555 | 12.87691 | 13556.33 | 14526.65 | 14048.69 | 12981.59 |

## APPENDIX IV Hobart GCPs (from University of Melbourne)


Feature:
Roundabout

Location:
Allunga Rd/ Berriedale Rd

Coordinates:

| UTM | | |
|---|---|---|
| X | Y | Z |
| 519653.5615 | 5259759.2209 | 94.4649 |
| WGS84 geographic | | |
| Lat | Long | Height |
| -42.81447376 | 147.24040121 | 94.4649 |


Feature:
Roundabout

Location:
Boondar ST/ Allunga Rd

Coordinates:

| UTM | | |
|---|---|---|
| X | Y | Z |
| 519885.3591 | 5260271.7756 | 59.0294 |
| WGS84 geographic | | |
| Lat | Long | Height |
| -42.80985206 | 147.24321843 | 59.0294 |

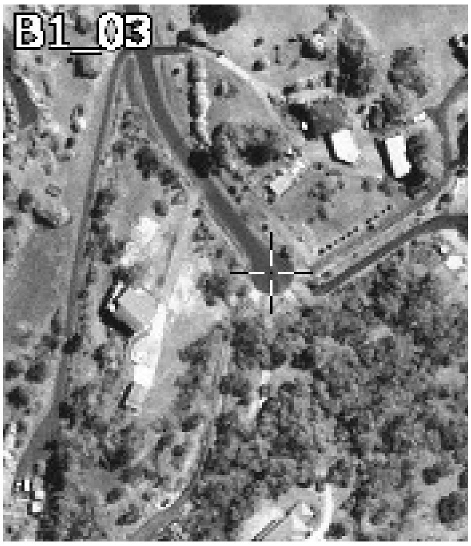


Feature:
Turnaround Point

Location:
Greenvale Ct

Coordinates:

| UTM | | |
|---|---|---|
| X | Y | Z |
| 518944.5098 | 5259596.6710 | 129.6879 |
| WGS84 geographic | | |
| Lat | Long | Height |
| -42.81595545 | 147.23173367 | 129.6879 |


Feature:
Corner of a Fence

Location:
45 Church Rd

Coordinates:

| UTM | | |
|---|---|---|
| X | Y | Z |
| 516531.5817 | 5256907.7950 | 356.3429 |
| WGS84 geographic | | |
| Lat | Long | Height |
| -42.84022552 | 147.20229730 | 356.3429 |

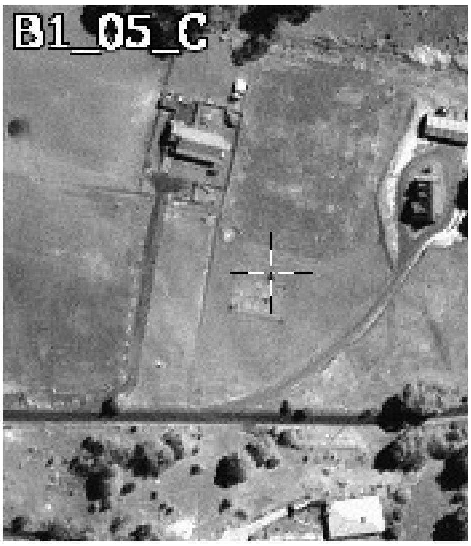


Feature:
Shelter

Location:
45 Church Rd

Coordinates:

| UTM | | |
|---|---|---|
| X | Y | Z |
| 516542.0633 | 5256846.9530 | 359.2805 |
| WGS84 geographic | | |
| Lat | Long | Height |
| -42.84077320 | 147.20242736 | 359.2805 |


Feature:
Street Corner

Location:
Nelson Dr/ Beneve Ct

Coordinates:

| UTM | | |
|---|---|---|
| X | Y | Z |
| 520082.3401 | 5257453.3629 | 132.5842 |
| WGS84 geographic | | |
| Lat | Long | Height |
| -42.83522753 | 147.24572818 | 132.5842 |


Feature:
Corner of building

Location:
Collinsvale Rd

Coordinates:

| UTM | | |
|---|---|---|
| X | Y | Z |
| 517316.4191 | 5258409.8570 | 367.1250 |
| WGS84 geographic | | |
| Lat | Long | Height |
| -42.82668165 | 147.21185511 | 367.125 |


Feature:
Water Tank

Location:
Furlleners Rd

Coordinates:

| UTM | | |
|---|---|---|
| X | Y | Z |
| 517048.9390 | 5260565.5134 | 450.2904 |
| WGS84 geographic | | |
| Lat | Long | Height |
| -42.80727528 | 147.20851745 | 450.2904 |


Feature:
Roundabout

Location:
Barossa Rd/ Tolosa Rd - Glenorchi

Coordinates:

| UTM | | |
|---|---|---|
| X | Y | Z |
| 521934.7996 | 5256622.6768 | 45.5947 |
| WGS84 geographic | | |
| Lat | Long | Height |
| -42.84265718 | 147.26842709 | 45.5947 |


Feature:
Roundabout

Location:
Vieste Dr/ Tolosa Rd - Glenorchi

Coordinates:

| UTM | | |
|---|---|---|
| X | Y | Z |
| 522043.8188 | 5256839.1842 | 39.6236 |
| WGS84 geographic | | |
| Lat | Long | Height |
| -42.84070434 | 147.26975271 | 39.6236 |


Feature:
Roundabout

Location:
Brent St/ Chapel St - Glenorchi

Coordinates:

| UTM | | |
|---|---|---|
| X | Y | Z |
| 521697.9850 | 5257023.2127 | 39.2630 |
| WGS84 geographic | | |
| Lat | Long | Height |
| -42.83905701 | 147.26551365 | 39.263 |


Feature:
Roundabout

Location:
Pitcarin St/ Chapel St - Glenorchi

Coordinates:

| UTM | | |
|---|---|---|
| X | Y | Z |
| 521825.5608 | 5257347.6785 | 27.5097 |
| WGS84 geographic | | |
| Lat | Long | Height |
| -42.83613149 | 147.26706217 | 27.5097 |


Feature:
Sewage Basin

Location:
Sewage Treatment off Main Rd - Cameron

Coordinates:

| UTM | | |
|---|---|---|
| X | Y | Z |
| 521244.2592 | 5260185.9910 | 0.7069 |
| WGS84 geographic | | |
| Lat | Long | Height |
| -42.81058806 | 147.25984225 | 0.7069 |


Feature:
Sewage Basin

Location:
Sewage Treatment off Main Rd - Cameron

Coordinates:

| UTM | | |
|---|---|---|
| X | Y | Z |
| 521244.2592 | 5260185.9910 | 0.7069 |
| WGS84 geographic | | |
| Lat | Long | Height |
| -42.81066606 | 147.25935884 | 0.6069 |


Feature:
Roundabout

Location:
Derwent Entertainment Center Loyd La - Glenorchi

Coordinates:

| UTM | | |
|---|---|---|
| X | Y | Z |
| 523037.6283 | 5258693.1430 | 0.1624 |
| WGS84 geographic | | |
| Lat | Long | Height |
| -42.82397969 | 147.28183806 | 0.1624 |


Feature:
Roundabout

Location:
Acton Cr/ Renfrew Cir -Glenorchi

Coordinates:

| UTM | | |
|---|---|---|
| X | Y | Z |
| 523668.8882 | 5258150.3804 | 7.3790 |
| WGS84 geographic | | |
| Lat | Long | Height |
| -42.82884813 | 147.28958350 | 7.379 |


Feature:
Roundabout

Location:
Springfield Av/ Forth Av - Glenorchi

Coordinates:

| UTM | | |
|---|---|---|
| X | Y | Z |
| 523203.7541 | 5256484.9902 | 41.6249 |
| WGS84 geographic | | |
| Lat | Long | Height |
| -42.84385962 | 147.28396141 | 41.6249 |


Feature:
Roundabout

Location:
Barry ST/ Eady St - Glenorchi

Coordinates:

| UTM | | |
|---|---|---|
| X | Y | Z |
| 522628.1784 | 5257380.9040 | 17.3837 |
| WGS84 geographic | | |
| Lat | Long | Height |
| -42.83580895 | 147.27688172 | 17.3837 |


Feature:
Roundabout

Location:
Bowden St/ Tolosa St - Glenorchi

Coordinates:

| UTM | | |
|---|---|---|
| X | Y | Z |
| 522324.0339 | 5257408.2912 | 21.3512 |
| WGS84 geographic | | |
| Lat | Long | Height |
| -42.83557126 | 147.27315912 | 21.3512 |


Feature:
Roundabout

Location:
Howard Rd/ Gepp Prd -Glenorchi

Coordinates:

| UTM | | |
|---|---|---|
| X | Y | Z |
| 524076.9939 | 5258096.5692 | -0.0502 |
| WGS84 geographic | | |
| Lat | Long | Height |
| -42.82931998 | 147.29457881 | -0.0502 |


Feature:
Turnaround point

Location:
Dimboola Pl/ Illawarra Pl

Coordinates:

| UTM | | |
|---|---|---|
| X | Y | Z |
| 521030.8770 | 5256557.8932 | 82.4803 |
| WGS84 geographic | | |
| Lat | Long | Height |
| -42.84326597 | 147.25736787 | 82.4803 |


Feature:
Roundabout

Location:
East Derwent HYW/ Grasstree Hill Rd

Coordinates:

| UTM | | |
|---|---|---|
| X | Y | Z |
| 527445.4790 | 5260012.6563 | 8.9504 |
| WGS84 geographic | | |
| Lat | Long | Height |
| -42.81195176 | 147.33569777 | 8.9504 |


Feature:
Tank

Location:
Sandersons Rd/ East Derwent Rd

Coordinates:

| UTM | | |
|---|---|---|
| X | Y | Z |
| 526240.7649 | 5259239.4720 | 9.0741 |
| WGS84 geographic | | |
| Lat | Long | Height |
| -42.81895672 | 147.32099862 | 9.0741 |


Feature:
Sewage Basin

Location:
Sewage Treatment plant Derwent Park Rd - Lutana

Coordinates:

| UTM | | |
|---|---|---|
| X | Y | Z |
| 524934.1553 | 5257747.3290 | 6.2341 |
| WGS84 geographic | | |
| Lat | Long | Height |
| -42.83243751 | 147.30508139 | 6.2341 |


Feature:
Sewage Basin

Location:
Sewage Treatment plant Derwent Park Rd - Lutana

Coordinates:

| UTM | | |
|---|---|---|
| X | Y | Z |
| 524927.0803 | 5257782.5930 | 6.2267 |
| WGS84 geographic | | |
| Lat | Long | Height |
| -42.83212018 | 147.30499327 | 6.2267 |


Feature:
Roundabout

Location:
End of Risdon Rd - Lutana

Coordinates:

| UTM | | |
|---|---|---|
| X | Y | Z |
| 526289.6107 | 5257431.6615 | 13.5590 |
| WGS84 geographic | | |
| Lat | Long | Height |
| -42.83523477 | 147.32168054 | 13.559 |


Feature:
Roundabout

Location:
End of Risdon Rd - Lutana

Coordinates:

| UTM | | |
|---|---|---|
| X | Y | Z |
| 526224.2370 | 5257545.2777 | 21.0215 |
| WGS84 geographic | | |
| Lat | Long | Height |
| -42.83421388 | 147.32087534 | 21.0215 |


Feature:
Tank

Location:

Coordinates:

| UTM | | |
|---|---|---|
| X | Y | Z |
| 528311.9161 | 5259239.8820 | 104.9297 |
| WGS84 geographic | | |
| Lat | Long | Height |
| -42.81887920 | 147.34633419 | 104.9297 |


Feature:
Street Corner

Location:
Lime Rd/ Anear Ct - New Town

Coordinates:

| UTM | | |
|---|---|---|
| X | Y | Z |
| 525376.5568 | 5256599.6491 | 43.5848 |
| WGS84 geographic | | |
| Lat | Long | Height |
| -42.84275806 | 147.31054606 | 43.5848 |


Feature:
Roundabout

Location:
Lagoon Rd - Otago

Coordinates:

| UTM | | |
|---|---|---|
| X | Y | Z |
| 524301.3349 | 5260570.4091 | 51.6418 |
| WGS84 geographic | | |
| Lat | Long | Height |
| -42.80703532 | 147.29721685 | 51.6418 |


Feature:
Corner of pier

Location:
Penenju Rd Otago

Coordinates:

| UTM | | |
|---|---|---|
| X | Y | Z |
| 523539.9911 | 5260765.5712 | -2.1197 |
| WGS84 geographic | | |
| Lat | Long | Height |
| -42.80530162 | 147.28789722 | -2.1197 |

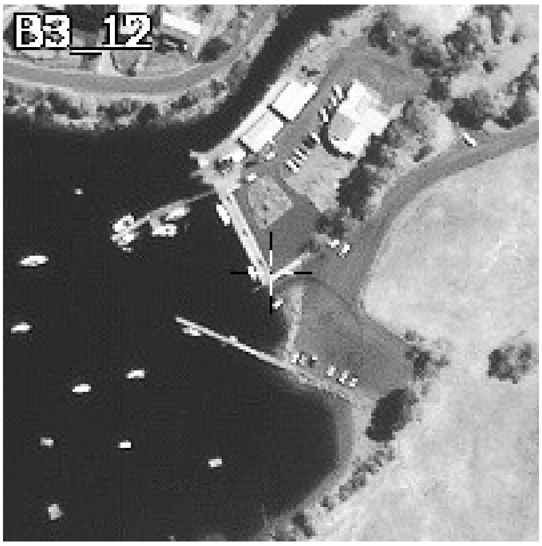


Feature:
Corner of car park

Location:
De Bomfort La -Geilston Bay

Coordinates:

| UTM | | |
|---|---|---|
| X | Y | Z |
| 528188.5573 | 5257126.4120 | -2.3928 |
| WGS84 geographic | | |
| Lat | Long | Height |
| -42.83791597 | 147.34493100 | -2.3928 |


Feature:
Corner of car park

Location:
Highschool De Bomfort La - Geilston Bay

Coordinates:

| UTM | | |
|---|---|---|
| X | Y | Z |
| 528546.8730 | 5257092.0440 | 10.2284 |
| WGS84 geographic | | |
| Lat | Long | Height |
| -42.83821217 | 147.34931722 | 10.2284 |


Feature:
Corner of car park

Location:
Highschool De Bomfort La - Geilston Bay

Coordinates:

| UTM | | |
|---|---|---|
| X | Y | Z |
| 528567.1831 | 5257096.5720 | 10.5894 |
| WGS84 geographic | | |
| Lat | Long | Height |
| -42.83817063 | 147.34956551 | 10.5894 |


Feature:
Tank

Location:
NW of Limeklin Gully Reservoir

Coordinates:

| UTM | | |
|---|---|---|
| X | Y | Z |
| 520370.4584 | 5255001.2574 | 167.4864 |
| WGS84 geographic | | |
| Lat | Long | Height |
| -42.85730173 | 147.24934237 | 167.4864 |


Feature:
Shelter

Location:
Tolosa Park

Coordinates:

| UTM | | |
|---|---|---|
| X | Y | Z |
| 520425.2441 | 5255532.4433 | 112.9719 |
| WGS84 geographic | | |
| Lat | Long | Height |
| -42.85251681 | 147.24999367 | 112.9719 |


Feature:
Shelter

Location:
Tolosa

Coordinates:

| UTM | | |
|---|---|---|
| X | Y | Z |
| 520408.7392 | 5255510.8926 | 114.2219 |
| WGS84 geographic | | |
| Lat | Long | Height |
| -42.85271132 | 147.24979244 | 114.2219 |


Feature:
Roundabout

Location:
Hopkins St/ Gormanston Rd - Moonah

Coordinates:

| UTM | | |
|---|---|---|
| X | Y | Z |
| 524435.5264 | 5256336.9994 | 19.8141 |
| WGS84 geographic | | |
| Lat | Long | Height |
| -42.84515393 | 147.29904175 | 19.8141 |


Feature:
Roundabout

Location:
Carlton St/ Pedder St - New Town

Coordinates:

| UTM | | |
|---|---|---|
| X | Y | Z |
| 524524.0475 | 5254609.1743 | 41.5025 |
| WGS84 geographic | | |
| Lat | Long | Height |
| -42.86071051 | 147.30020040 | 41.5025 |


Feature:
Roundabout

Location:
Wellwood St/Pickard St - Lenah Valley

Coordinates:

| UTM | | |
|---|---|---|
| X | Y | Z |
| 523996.6945 | 5254353.3171 | 58.7682 |
| WGS84 geographic | | |
| Lat | Long | Height |
| -42.86303129 | 147.29375605 | 58.7682 |


Feature:
Roundabout

Location:
Giblin St/ Doyle Av - Mt Stuart

Coordinates:

| UTM | | |
|---|---|---|
| X | Y | Z |
| 524088.4528 | 5253833.0172 | 95.0857 |
| WGS84 geographic | | |
| Lat | Long | Height |
| -42.86771380 | 147.29490160 | 95.0857 |


Feature:
Roundabout

Location:
Hopkins St/Charles St - West Moonah

Coordinates:

| UTM | | |
|---|---|---|
| X | Y | Z |
| 523943.2595 | 5256150.4757 | 25.0198 |
| WGS84 geographic | | |
| Lat | Long | Height |
| -42.84684919 | 147.29302541 | 25.0198 |


Feature:
Roundabout

Location:
Albert Rd/ Charles St - West Moonah

Coordinates:

| UTM | | |
|---|---|---|
| X | Y | Z |
| 524040.4751 | 5255977.1916 | 29.3035 |
| WGS84 geographic | | |
| Lat | Long | Height |
| -42.84840660 | 147.29422255 | 29.3035 |


Feature:
Roundabout

Location:
Mt Stuart Rd/ Dale Cr - Mt Stuart

Coordinates:

| UTM | | |
|---|---|---|
| X | Y | Z |
| 524381.5024 | 5253170.5181 | 183.7533 |
| WGS84 geographic | | |
| Lat | Long | Height |
| -42.87367042 | 147.29851794 | 183.7533 |

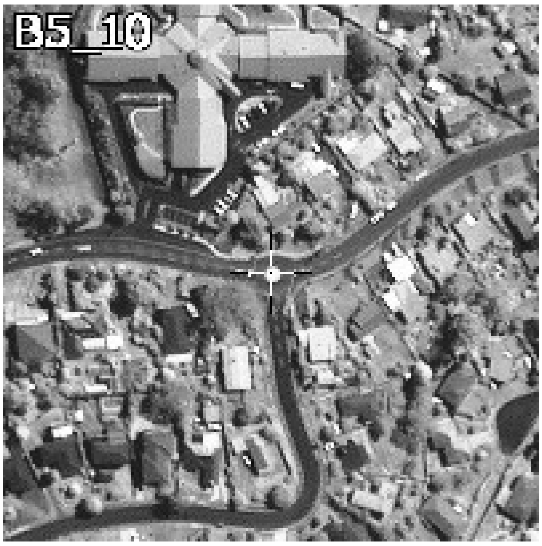


Feature:
Roundabout

Location:
Kalang Av/ Lumeah Av - Lenah Valley

Coordinates:

| UTM | | |
|---|---|---|
| X | Y | Z |
| 522577.1765 | 5254438.9760 | 157.7802 |
| WGS84 geographic | | |
| Lat | Long | Height |
| -42.86230318 | 147.27637575 | 157.7802 |


Feature:
Roundabout

Location:
Kalang Av/ Alcides Av - Lenah Valley

Coordinates:

| UTM | | |
|---|---|---|
| X | Y | Z |
| 522751.1700 | 5254509.7654 | 137.7189 |
| WGS84 geographic | | |
| Lat | Long | Height |
| -42.86166055 | 147.27850278 | 137.7189 |


Feature:
Street Corner

Location:
Loftus St - West Moonah

Coordinates:

| UTM | | |
|---|---|---|
| X | Y | Z |
| 522150.8433 | 5255659.3960 | 96.8164 |
| WGS84 geographic | | |
| Lat | Long | Height |
| -42.85132552 | 147.27110882 | 96.8164 |


Feature:
Roundabout

Location:
Amy St/ Charles St - West Moonah

Coordinates:

| UTM | | |
|---|---|---|
| X | Y | Z |
| 523839.7101 | 5256333.7687 | 23.2047 |
| WGS84 geographic | | |
| Lat | Long | Height |
| -42.84520184 | 147.29175038 | 23.2047 |


Feature:
Tank

Location:

Coordinates:

| UTM | | |
|---|---|---|
| X | Y | Z |
| 523239.5673 | 5255453.5440 | 155.0340 |
| WGS84 geographic | | |
| Lat | Long | Height |
| -42.85314693 | 147.28444230 | 155.034 |


Feature:
Roundabout

Location:
Valentine St/Montagu St - New Town

Coordinates:

| UTM | | |
|---|---|---|
| X | Y | Z |
| 524721.5468 | 5254838.3610 | 24.9900 |
| WGS84 geographic | | |
| Lat | Long | Height |
| -42.85864027 | 147.30260789 | 24.99 |


Feature:
Roundabout

Location:
Valentine St/Carlton St - New Town

Coordinates:

| UTM | | |
|---|---|---|
| X | Y | Z |
| 524576.4623 | 5254867.2196 | 28.9348 |
| WGS84 geographic | | |
| Lat | Long | Height |
| -42.85838508 | 147.30083073 | 28.9348 |


Feature:
Roundabout

Location:
Montagu St/ Pedder St - New Town

Coordinates:

| UTM | | |
|---|---|---|
| X | Y | Z |
| 524671.2421 | 5254578.8350 | 36.5935 |
| WGS84 geographic | | |
| Lat | Long | Height |
| -42.86097898 | 147.30200353 | 36.5935 |


Feature:
Roundabout

Location:
Side road off Bay Rd/ Pirie St - New Town

Coordinates:

| UTM | | |
|---|---|---|
| X | Y | Z |
| 525304.6625 | 5254737.5752 | 52.9904 |
| WGS84 geographic | | |
| Lat | Long | Height |
| -42.85952878 | 147.30975005 | 52.9904 |


Feature:
Roundabout

Location:
Doyle Av/ Montagu St - North Hobart

Coordinates:

| UTM | | |
|---|---|---|
| X | Y | Z |
| 524552.7865 | 5253726.1477 | 93.8594 |
| WGS84 geographic | | |
| Lat | Long | Height |
| -42.86866140 | 147.30059077 | 93.8594 |


Feature:
Roundabout

Location:
Toorak Av/ Elphinstone Rd - Mt Stuart

Coordinates:

| UTM | | |
|---|---|---|
| X | Y | Z |
| 524942.0197 | 5253464.4495 | 123.4042 |
| WGS84 geographic | | |
| Lat | Long | Height |
| -42.87100543 | 147.30536756 | 123.4042 |


Feature:
Roundabout

Location:
Arthur St/ Lochner St - North Hobart

Coordinates:

| UTM | | |
|---|---|---|
| X | Y | Z |
| 525460.7668 | 5252874.0144 | 78.3815 |
| WGS84 geographic | | |
| Lat | Long | Height |
| -42.87630527 | 147.31174530 | 78.3815 |


Feature:
Roundabout

Location:
Federal St/ Letitia St - North Hobart

Coordinates:

| UTM | | |
|---|---|---|
| X | Y | Z |
| 526119.5120 | 5253671.0913 | 29.5483 |
| WGS84 geographic | | |
| Lat | Long | Height |
| -42.86910523 | 147.31977390 | 29.5483 |


Feature:
Roundabout

Location:
Bell St/ Bay Rd - New Town

Coordinates:

| UTM | | |
|---|---|---|
| X | Y | Z |
| 525354.7392 | 5255359.6527 | 13.5233 |
| WGS84 geographic | | |
| Lat | Long | Height |
| -42.85392520 | 147.31033497 | 13.5233 |

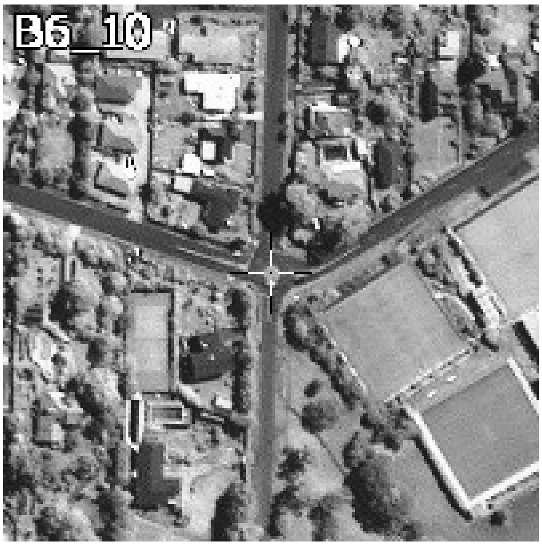


Feature:
Roundabout

Location:
Talune St/ Natone St - Lindisfarne

Coordinates:

| UTM | | |
|---|---|---|
| X | Y | Z |
| 528461.5954 | 5255801.7806 | 1.3629 |
| WGS84 geographic | | |
| Lat | Long | Height |
| -42.84983439 | 147.34833900 | 1.3629 |

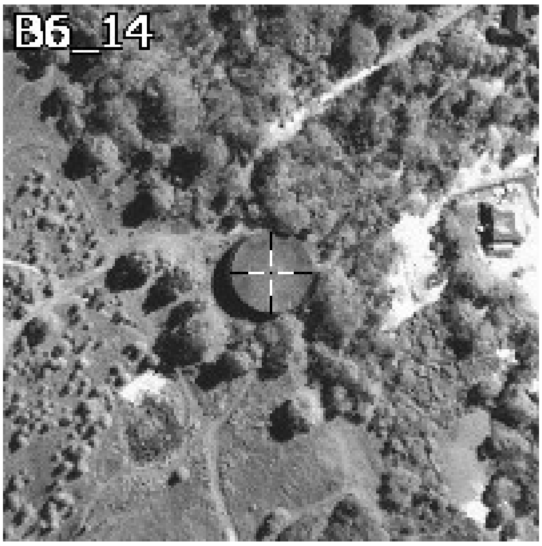


Feature:
Tank

Location:
Fielding Dr - West Hobart

Coordinates:

| UTM | | |
|---|---|---|
| X | Y | Z |
| 524687.0220 | 5252131.3134 | 228.3833 |
| WGS84 geographic | | |
| Lat | Long | Height |
| -42.88301881 | 147.30230424 | 228.3833 |


Feature:
Cricket pitch

Location:
Brooker Av/ Cornelian Bay, Sports ground - Moonah

Coordinates:

| UTM | | |
|---|---|---|
| X | Y | Z |
| 525993.4555 | 5255425.6770 | -0.0184 |
| WGS84 geographic | | |
| Lat | Long | Height |
| -42.85330918 | 147.31814951 | -0.0184 |


Feature:
Cricket pitch

Location:
Brooker Av/ Cornelian Bay, Sports ground - Moonah

Coordinates:

| UTM | | |
|---|---|---|
| X | Y | Z |
| 525994.9922 | 5255427.3060 | -0.0231 |
| WGS84 geographic | | |
| Lat | Long | Height |
| -42.85329446 | 147.31816824 | -0.0231 |


Feature:
Cricket pitch

Location:
Brooker Av/ Cornelian Bay, Sports ground - Moonah

Coordinates:

| UTM | | |
|---|---|---|
| X | Y | Z |
| 525975.8259 | 5255445.9100 | -0.0126 |
| WGS84 geographic | | |
| Lat | Long | Height |
| -42.85312758 | 147.31793280 | -0.0126 |


Feature:
Cricket pitch

Location:
Brooker Av/ Cornelian Bay, Sports ground - Moonah

Coordinates:

| UTM | | |
|---|---|---|
| X | Y | Z |
| 525974.2441 | 5255444.2290 | -0.0035 |
| WGS84 geographic | | |
| Lat | Long | Height |
| -42.85314277 | 147.31791352 | -0.0035 |


Feature:
Hockeyfield

Location:
Bell St/ Cornelia Bay - Moonah

Coordinates:

| UTM | | |
|---|---|---|
| X | Y | Z |
| 525771.1967 | 5255299.2950 | 4.9848 |
| WGS84 geographic | | |
| Lat | Long | Height |
| -42.85445480 | 147.31543498 | 4.9848 |


Feature:
Hockeyfield

Location:
Bell St/ Cornelia Bay - Moonah

Coordinates:

| UTM | | |
|---|---|---|
| X | Y | Z |
| 525782.0572 | 5255297.4890 | 4.9737 |
| WGS84 geographic | | |
| Lat | Long | Height |
| -42.85447070 | 147.31556799 | 4.9737 |

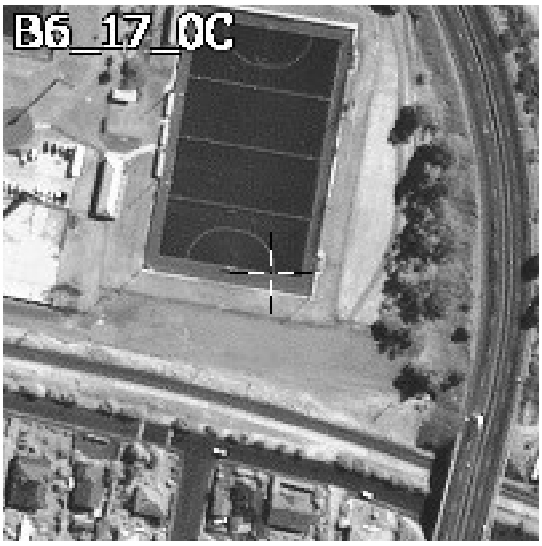


Feature:
Hockeyfield

Location:
Bell St/ Cornelia Bay - Moonah

Coordinates:

| UTM | | |
|---|---|---|
| X | Y | Z |
| 525814.4605 | 5255292.1530 | 4.9910 |
| WGS84 geographic | | |
| Lat | Long | Height |
| -42.85451766 | 147.31596484 | 4.9910 |


Feature:
Hockeyfield

Location:
Bell St/ Cornelia Bay - Moonah

Coordinates:

| UTM | | |
|---|---|---|
| X | Y | Z |
| 525825.3478 | 5255290.3550 | 4.9406 |
| WGS84 geographic | | |
| Lat | Long | Height |
| -42.85453348 | 147.31609818 | 4.9406 |


Feature:
Hockeyfield

Location:
Bell St/ Cornelia Bay - Moonah

Coordinates:

| UTM | | |
|---|---|---|
| X | Y | Z |
| 525832.7879 | 5255335.4070 | 4.9516 |
| WGS84 geographic | | |
| Lat | Long | Height |
| -42.85412753 | 147.31618718 | 4.9516 |

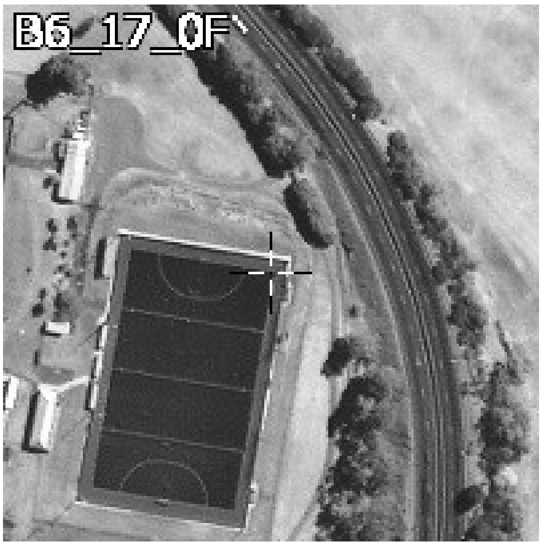


Feature:
Hockeyfield

Location:
Bell St/ Cornelia Bay - Moonah

Coordinates:

| UTM | | |
|---|---|---|
| X | Y | Z |
| 525840.1708 | 5255380.4310 | 4.9526 |
| WGS84 geographic | | |
| Lat | Long | Height |
| -42.85372183 | 147.31627547 | 4.9526 |

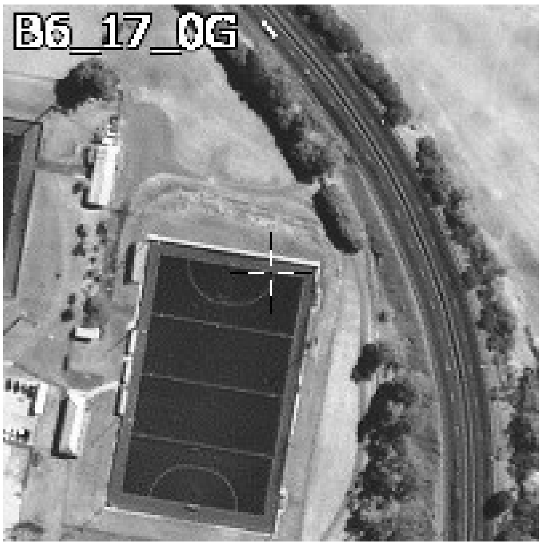


Feature:
Hockeyfield

Location:
Bell St/ Cornelia Bay - Moonah

Coordinates:

| UTM | | |
|---|---|---|
| X | Y | Z |
| 525829.2958 | 5255382.2400 | 4.9694 |
| WGS84 geographic | | |
| Lat | Long | Height |
| -42.85370591 | 147.31614228 | 4.9694 |


Feature:
Hockeyfield

Location:
Bell St/ Cornelia Bay - Moonah

Coordinates:

| UTM | | |
|---|---|---|
| X | Y | Z |
| 525796.9123 | 5255387.5720 | 4.9734 |
| WGS84 geographic | | |
| Lat | Long | Height |
| -42.85365898 | 147.31574568 | 4.9734 |


Feature:
Hockeyfield

Location:
Bell St/ Cornelia Bay - Moonah

Coordinates:

| UTM | | |
|---|---|---|
| X | Y | Z |
| 525786.0395 | 5255389.3510 | 4.9230 |
| WGS84 geographic | | |
| Lat | Long | Height |
| -42.85364333 | 147.31561252 | 4.9230 |


Feature:
Hockeyfield

Location:
Bell St/ Cornelia Bay - Moonah

Coordinates:

| UTM | | |
|---|---|---|
| X | Y | Z |
| 525778.6079 | 5255344.3260 | 4.9383 |
| WGS84 geographic | | |
| Lat | Long | Height |
| -42.85404904 | 147.31552363 | 4.9383 |

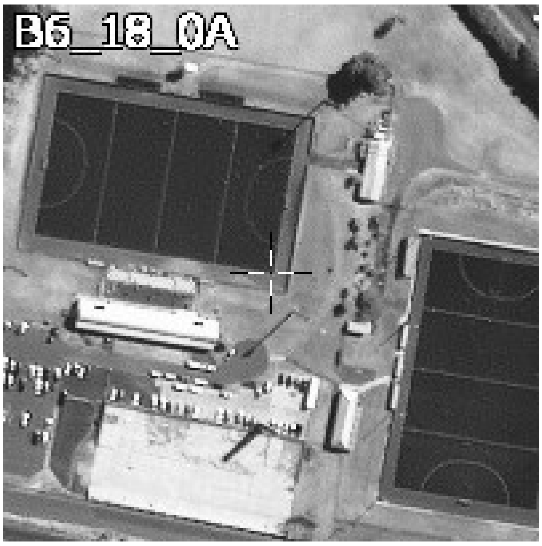


Feature:
Hockeyfield

Location:
Bell St/ Cornelia Bay - Moonah

Coordinates:

| UTM | | |
|---|---|---|
| X | Y | Z |
| 525727.1947 | 5255379.2970 | 3.2137 |
| WGS84 geographic | | |
| Lat | Long | Height |
| -42.85373585 | 147.31489275 | 3.2137 |


Feature:
Hockeyfield

Location:
Bell St/ Cornelia Bay - Moonah

Coordinates:

| UTM | | |
|---|---|---|
| X | Y | Z |
| 525728.9922 | 5255390.1920 | 3.2378 |
| WGS84 geographic | | |
| Lat | Long | Height |
| -42.85363768 | 147.31491425 | 3.2378 |


Feature:
Hockeyfield

Location:
Bell St/ Cornelia Bay - Moonah

Coordinates:

| UTM | | |
|---|---|---|
| X | Y | Z |
| 525734.3181 | 5255422.5670 | 3.2269 |
| WGS84 geographic | | |
| Lat | Long | Height |
| -42.85334596 | 147.31497796 | 3.2269 |


Feature:
Hockeyfield

Location:
Bell St/ Cornelia Bay - Moonah

Coordinates:

| UTM | | |
|---|---|---|
| X | Y | Z |
| 525736.0904 | 5255433.4370 | 3.2066 |
| WGS84 geographic | | |
| Lat | Long | Height |
| -42.85324801 | 147.31499915 | 3.2066 |


Feature:
Hockeyfield

Location:
Bell St/ Cornelia Bay - Moonah

Coordinates:

| UTM | | |
|---|---|---|
| X | Y | Z |
| 525691.0545 | 5255440.8310 | 3.1983 |
| WGS84 geographic | | |
| Lat | Long | Height |
| -42.85318294 | 147.31444760 | 3.1983 |

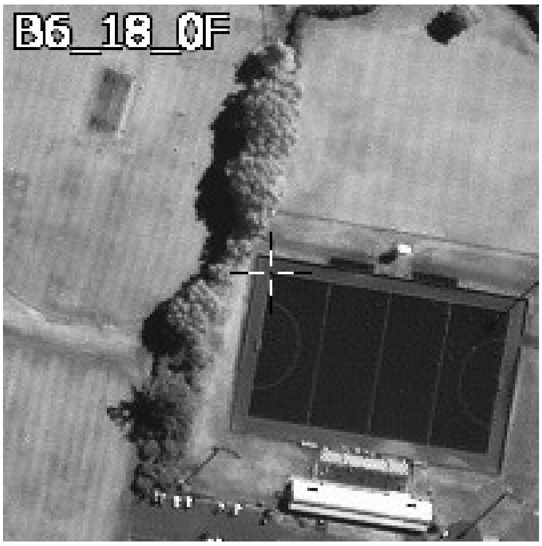


Feature:
Hockeyfield

Location:
Bell St/ Cornelia Bay - Moonah

Coordinates:

| UTM | | |
|---|---|---|
| X | Y | Z |
| 525646.0415 | 5255448.2150 | 3.2057 |
| WGS84 geographic | | |
| Lat | Long | Height |
| -42.85311796 | 147.31389633 | 3.2057 |


Feature:
Hockeyfield

Location:
Bell St/ Cornelia Bay - Moonah

Coordinates:

| UTM | | |
|---|---|---|
| X | Y | Z |
| 525644.2173 | 5255437.3630 | 3.2005 |
| WGS84 geographic | | |
| Lat | Long | Height |
| -42.85321575 | 147.31387450 | 3.2005 |


Feature:
Hockeyfield

Location:
Bell St/ Cornelia Bay - Moonah

Coordinates:

| UTM | | |
|---|---|---|
| X | Y | Z |
| 525638.9095 | 5255404.9600 | 3.2227 |
| WGS84 geographic | | |
| Lat | Long | Height |
| -42.85350772 | 147.31381102 | 3.2227 |


Feature:
Hockeyfield

Location:
Bell St/ Cornelia Bay - Moonah

Location:

Coordinates:

| UTM | | |
|---|---|---|
| X | Y | Z |
| 525637.1335 | 5255394.0810 | 3.2117 |
| WGS84 geographic | | |
| Lat | Long | Height |
| -42.85360575 | 147.31378977 | 3.2117 |


Feature:
Hockeyfield

Location:
Bell St/ Cornelia Bay - Moonah

Coordinates:

| UTM | | |
|---|---|---|
| X | Y | Z |
| 525682.1462 | 5255386.6800 | 3.2223 |
| WGS84 geographic | | |
| Lat | Long | Height |
| -42.85367088 | 147.31434104 | 3.2223 |


Feature:
Corner at Sportsground

Location:
Athletic Centre at Domain - Glebe

Coordinates:

| UTM | | |
|---|---|---|
| X | Y | Z |
| 526605.5934 | 5253786.0660 | 83.3369 |
| WGS84 geographic | | |
| Lat | Long | Height |
| -42.86805309 | 147.32571932 | 83.3369 |


Feature:
Roundabout

Location:
Burnett ST/ Murray St - North Hobart

Coordinates:

| UTM | | |
|---|---|---|
| X | Y | Z |
| 525750.5145 | 5252976.0444 | 52.5855 |
| WGS84 geographic | | |
| Lat | Long | Height |
| -42.87537676 | 147.31528829 | 52.5855 |


Feature:
Roundabout

Location:
Doyle Av/ Waverley Av - Mt Stuart

Coordinates:

| UTM | | |
|---|---|---|
| X | Y | Z |
| 524415.2052 | 5253773.5635 | 102.8670 |
| WGS84 geographic | | |
| Lat | Long | Height |
| -42.86823882 | 147.29890438 | 102.8670 |


Feature:
Corner of Cricket Pitch

Location:

Coordinates:

| UTM | | |
|---|---|---|
| X | Y | Z |
| 526335.4458 | 5253934.5450 | 85.0177 |
| WGS84 geographic | | |
| Lat | Long | Height |
| -42.86672537 | 147.32240512 | 85.0177 |


Feature:
Corner of Cricket Pitch

Location:

Coordinates:

| UTM | | |
|---|---|---|
| X | Y | Z |
| 526337.6132 | 5253937.6420 | 85.0253 |
| WGS84 geographic | | |
| Lat | Long | Height |
| -42.86669741 | 147.32243151 | 85.0253 |

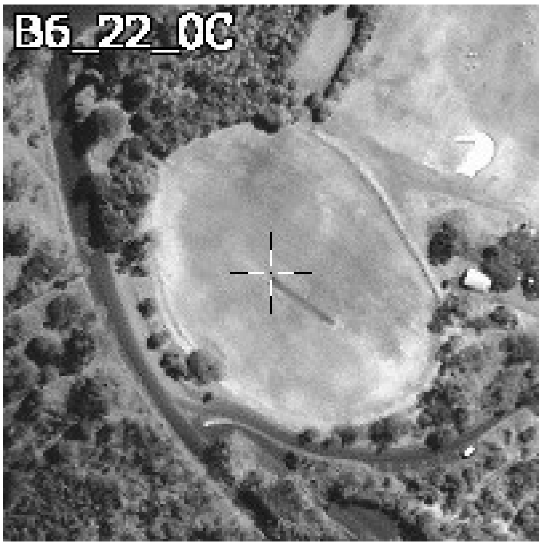


Feature:
Corner of Cricket Pitch

Location:

Coordinates:

| UTM | | |
|---|---|---|
| X | Y | Z |
| 526313.9306 | 5253954.2500 | 84.7857 |
| WGS84 geographic | | |
| Lat | Long | Height |
| -42.86654867 | 147.32214081 | 84.7857 |


Feature:
Corner of Cricket Pitch

Location:

Coordinates:

| UTM | | |
|---|---|---|
| X | Y | Z |
| 526311.6155 | 5253951.1450 | 84.8301 |
| WGS84 geographic | | |
| Lat | Long | Height |
| -42.86657671 | 147.32211262 | 84.8301 |


Feature:
Round featured lawn

Location:
War memorial - Hobart

Coordinates:

| UTM | | |
|---|---|---|
| X | Y | Z |
| 527486.2915 | 5252698.2747 | 19.2781 |
| WGS84 geographic | | |
| Lat | Long | Height |
| -42.87781762 | 147.33655432 | 19.2781 |


Feature:
Corner of car park

Location:
Pinnacle Rd - The Springs

Coordinates:

| UTM | | |
|---|---|---|
| X | Y | Z |
| 520303.0523 | 5248555.7440 | 689.8207 |
| WGS84 geographic | | |
| Lat | Long | Height |
| -42.91534657 | 147.24875041 | 689.8207 |


Feature:
Corner of car park

Location:
Mt Wellington

Coordinates:

| UTM | | |
|---|---|---|
| X | Y | Z |
| 519309.5615 | 5250656.0970 | 1256.7574 |
| WGS84 geographic | | |
| Lat | Long | Height |
| -42.89645835 | 147.23650607 | 1256.7574 |

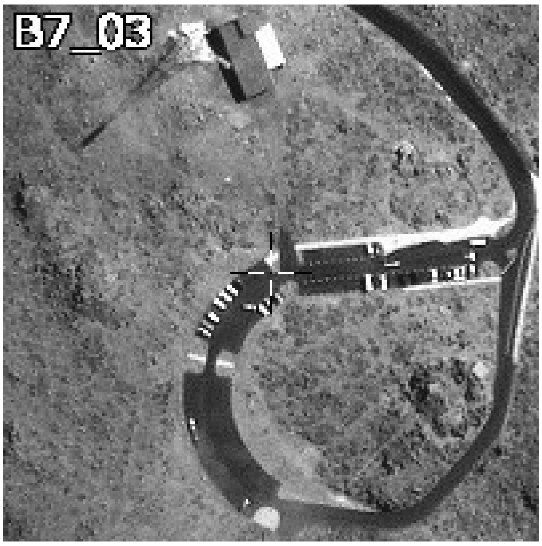


Feature:
Corner of car park

Location:
Mt Wellington

Coordinates:

| UTM | | |
|---|---|---|
| X | Y | Z |
| 519316.5863 | 5250748.1190 | 1260.6792 |
| WGS84 geographic | | |
| Lat | Long | Height |
| -42.89562949 | 147.23658894 | 1260.6792 |


Feature:
Corner of building

Location:
Mt Wellington

Coordinates:

| UTM | | |
|---|---|---|
| X | Y | Z |
| 519393.1104 | 5250715.8130 | 1261.7064 |
| WGS84 geographic | | |
| Lat | Long | Height |
| -42.89591848 | 147.23752732 | 1261.7064 |


Feature:
Corner of building

Location:
Mt Wellington

Coordinates:

| UTM | | |
|---|---|---|
| X | Y | Z |
| 519397.4131 | 5250712.0090 | 1261.6884 |
| WGS84 geographic | | |
| Lat | Long | Height |
| -42.89595262 | 147.23758015 | 1261.6884 |


Feature:
Corner of building

Location:
Mt Wellington

Coordinates:

| UTM | | |
|---|---|---|
| X | Y | Z |
| 519394.0340 | 5250708.7230 | 1262.5262 |
| WGS84 geographic | | |
| Lat | Long | Height |
| -42.89598230 | 147.23753887 | 1262.5262 |


<u>Feature:</u>
Corner of building

<u>Location:</u>
Mt Wellington

<u>Coordinates:</u>

| UTM | | |
|---|---|---|
| X | Y | Z |
| 519390.1514 | 5250712.2040 | 1262.6425 |
| WGS84 geographic | | |
| Lat | Long | Height |
| -42.89595105 | 147.23749120 | 1262.6425 |


<u>Feature:</u>
Corner of building

<u>Location:</u>
Mt Wellington

<u>Coordinates:</u>

| UTM | | |
|---|---|---|
| X | Y | Z |
| 519321.5788 | 5250826.5130 | 1259.0221 |
| WGS84 geographic | | |
| Lat | Long | Height |
| -42.89492342 | 147.23664739 | 1259.0221 |


<u>Feature:</u>
Corner of foot path with street

<u>Location:</u>
Mt Wellington

<u>Coordinates:</u>

| UTM | | |
|---|---|---|
| X | Y | Z |
| 519402.4983 | 5250745.0000 | 1258.2201 |
| WGS84 geographic | | |
| Lat | Long | Height |
| -42.89565540 | 147.23764129 | 1258.2201 |


Feature:
Corner of car park

Location:
Mt Wellington

Coordinates:

| UTM | | |
|---|---|---|
| X | Y | Z |
| 519320.5868 | 5250669.0580 | 1257.3182 |
| WGS84 geographic | | |
| Lat | Long | Height |
| -42.89634135 | 147.23664066 | 1257.3182 |

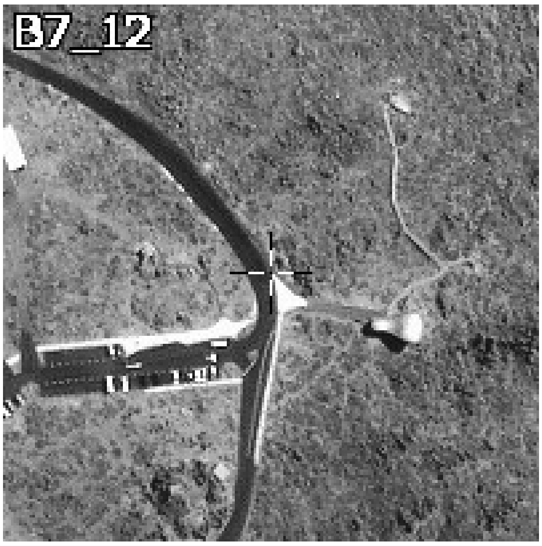


Feature:
Corner of car park

Location:
Mt Wellington

Coordinates:

| UTM | | |
|---|---|---|
| X | Y | Z |
| 519413.7240 | 5250786.0160 | 1256.8439 |
| WGS84 geographic | | |
| Lat | Long | Height |
| -42.89528576 | 147.23777736 | 1256.8439 |


Feature:
Roundabout

Location:
Saunder Cr/ Moree Cl - Cascades

Coordinates:

| UTM | | |
|---|---|---|
| X | Y | Z |
| 522733.0340 | 5250245.5237 | 190.2642 |
| WGS84 geographic | | |
| Lat | Long | Height |
| -42.90006132 | 147.27845341 | 190.2642 |


Feature:
Tank

Location:
In Ridgeway park, South of Upper Reservior - Ridgeway

Coordinates:

| UTM | | |
|---|---|---|
| X | Y | Z |
| 523828.0043 | 5249000.3219 | 251.9132 |
| WGS84 geographic | | |
| Lat | Long | Height |
| -42.91124111 | 147.29191826 | 251.9132 |


Feature:
Tank

Location:
In Ridgeway park, South of Upper Reservior - Ridgeway

Coordinates:

| UTM | | |
|---|---|---|
| X | Y | Z |
| 523800.1500 | 5248990.4192 | 251.8862 |
| WGS84 geographic | | |
| Lat | Long | Height |
| -42.91133115 | 147.29157744 | 251.8862 |


Feature:
Corner of car park

Location:
Stephenson Pl - Fern Tree

Coordinates:

| UTM | | |
|---|---|---|
| X | Y | Z |
| 521230.9450 | 5247763.4150 | 423.2605 |
| WGS84 geographic | | |
| Lat | Long | Height |
| -42.92245632 | 147.26014873 | 423.2605 |


Feature:
Corner of car park

Location:
Stephenson Pl - Fern Tree

Coordinates:

| UTM | | |
|---|---|---|
| X | Y | Z |
| 521236.8777 | 5247756.5860 | 423.0093 |
| WGS84 geographic | | |
| Lat | Long | Height |
| -42.92251765 | 147.26022168 | 423.0093 |


Feature:
Corner of Street

Location:
Bracken La - Fern Tree

Coordinates:

| UTM | | |
|---|---|---|
| X | Y | Z |
| 521561.9281 | 5248345.7113 | 433.8235 |
| WGS84 geographic | | |
| Lat | Long | Height |
| -42.91720339 | 147.26418191 | 433.8235 |


Feature:
Shelter

Location:
Bridgeway Rd/ Bridgeway Reservior - Ridgeway

Coordinates:

| UTM | | |
|---|---|---|
| X | Y | Z |
| 523912.6526 | 5248541.3177 | 284.7487 |
| WGS84 geographic | | |
| Lat | Long | Height |
| -42.91537184 | 147.29297486 | 284.7487 |


Feature:
Round feature

Location:
Property in Turnip Field Rd - Turnip Fields

Coordinates:

| UTM | | |
|---|---|---|
| X | Y | Z |
| 522712.1234 | 5249281.3582 | 287.0207 |
| WGS84 geographic | | |
| Lat | Long | Height |
| -42.90874438 | 147.27823632 | 287.0207 |


Feature:
Roundabout

Location:
Grosvener St/ Lord St -Dynnyrne

Coordinates:

| UTM | | |
|---|---|---|
| X | Y | Z |
| 526619.1199 | 5250362.5848 | 16.1257 |
| WGS84 geographic | | |
| Lat | Long | Height |
| -42.89888150 | 147.32604722 | 16.1257 |


Feature:
Roundabout

Location:
Grosvener St/ York St - Dynnyrne

Coordinates:

| UTM | | |
|---|---|---|
| X | Y | Z |
| 526644.5885 | 5250260.4015 | 13.1207 |
| WGS84 geographic | | |
| Lat | Long | Height |
| -42.89980079 | 147.32636402 | 13.1207 |

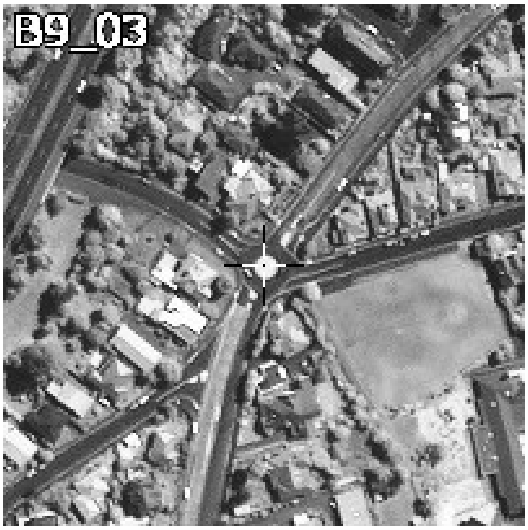


Feature:
Roundabout

Location:
Princes St/ Proctors Rd - Dynnyrne

Coordinates:

| UTM | | |
|---|---|---|
| X | Y | Z |
| 525901.4316 | 5250400.8987 | 50.0069 |
| WGS84 geographic | | |
| Lat | Long | Height |
| -42.89856118 | 147.31725490 | 50.0069 |


Feature:
Roundabout

Location:
Davey St/ Lynton Av - Dynnyrne

Coordinates:

| UTM | | |
|---|---|---|
| X | Y | Z |
| 525572.0960 | 5250498.3862 | 82.7498 |
| WGS84 geographic | | |
| Lat | Long | Height |
| -42.89769440 | 147.31321663 | 82.7498 |

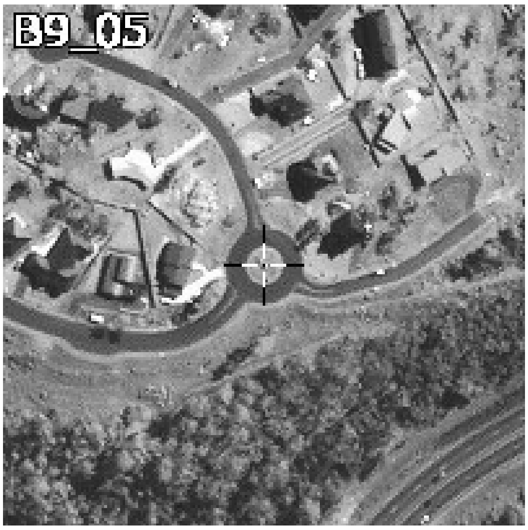


Feature:
Roundabout

Location:
Woodcutters Rd

Coordinates:

| UTM | | |
|---|---|---|
| X | Y | Z |
| 525340.9723 | 5249563.0495 | 224.8773 |
| WGS84 geographic | | |
| Lat | Long | Height |
| -42.90612492 | 147.31042804 | 224.8773 |


Feature:
Roundabout

Location:
Woodcuters Rd

Coordinates:

| UTM | | |
|---|---|---|
| X | Y | Z |
| 524985.1346 | 5249369.9588 | 273.4112 |
| WGS84 geographic | | |
| Lat | Long | Height |
| -42.90787546 | 147.30607767 | 273.4112 |


Feature:
Roundabout

Location:
Plaster Ct/ Lipscomp Av - Sandy Bay

Coordinates:

| UTM | | |
|---|---|---|
| X | Y | Z |
| 528381.2208 | 5248675.1035 | 56.5304 |
| WGS84 geographic | | |
| Lat | Long | Height |
| -42.91401389 | 147.34771552 | 56.5304 |


Feature:
Street corner

Location:
Lipscomp Av/ Churchil Av - Sandy Bay

Coordinates:

| UTM | | |
|---|---|---|
| X | Y | Z |
| 528435.6921 | 5248332.7390 | 96.3145 |
| WGS84 geographic | | |
| Lat | Long | Height |
| -42.91709488 | 147.34840024 | 96.3145 |


Feature:
Corner of car park

Location:
Marieville Esplanade - Sandy Bay

Coordinates:

| UTM | | |
|---|---|---|
| X | Y | Z |
| 527233.6784 | 5250839.3120 | -2.4923 |
| WGS84 geographic | | |
| Lat | Long | Height |
| -42.89456684 | 147.33355144 | -2.4923 |


Feature:
Centre of Hockeyfield

Location:
Anglesea St - South Hobart

Coordinates:

| UTM | | |
|---|---|---|
| X | Y | Z |
| 525299.2432 | 5251065.1480 | 47.1107 |
| WGS84 geographic | | |
| Lat | Long | Height |
| -42.89259974 | 147.30984912 | 47.1107 |


Feature:
Roundabout

Location:
King St/ Parliament St - Dynnyrne

Coordinates:

| UTM | | |
|---|---|---|
| X | Y | Z |
| 526190.8319 | 5250696.9773 | 37.7947 |
| WGS84 geographic | | |
| Lat | Long | Height |
| -42.89588508 | 147.32078576 | 37.7947 |


Feature:
Corner of building

Location:
Sports ground off Olinda Grove -
Mt Nelson

Coordinates:

| UTM | | |
|---|---|---|
| X | Y | Z |
| 525602.4682 | 5248887.8400 | 254.3795 |
| WGS84 geographic | | |
| Lat | Long | Height |
| -42.91219652 | 147.31366215 | 254.3795 |


Feature:
Centre of tennis court

Location:
Matric College - Mt Nelson

Coordinates:

| UTM | | |
|---|---|---|
| X | Y | Z |
| 525598.7020 | 5248150.7630 | 256.6078 |
| WGS84 geographic | | |
| Lat | Long | Height |
| -42.91883409 | 147.31364967 | 256.6078 |

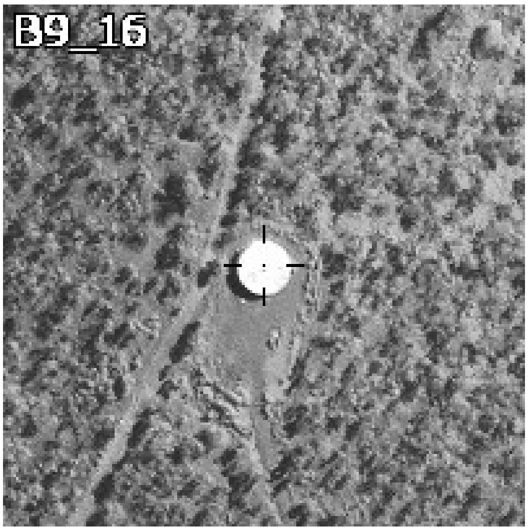


Feature:
Tank

Location:
Tolmans Hill - West of Mt Nelson

Coordinates:

| UTM | | |
|---|---|---|
| X | Y | Z |
| 524709.9635 | 5249055.3151 | 351.6752 |
| WGS84 geographic | | |
| Lat | Long | Height |
| -42.91071783 | 147.30272063 | 351.6752 |


Feature:
Centre of tennis court

Location:

Coordinates:

| UTM | | |
|---|---|---|
| X | Y | Z |
| 525078.7652 | 5248317.3220 | 232.1978 |
| WGS84 geographic | | |
| Lat | Long | Height |
| -42.91735149 | 147.30727175 | 232.1978 |

# APPENDIX V Measurements on Images for Corners in Hobart Test Field

edge 1: 131 3882; 130 3888; 128 3896; 126 3905;
edge 2: 131 3882; 129 3881; 124 3880; 122 3879; 118 3878; 113 3877;
edge 1: 137 3855; 136 3859; 135 3863; 134 3866; 133 3870; 133 3873; 132 3877;
edge 2: 137 3855; 134 3855; 133 3854; 129 3853; 126 3852; 124 3852; 120 3851;
edge 1: 3637 3258; 3635 3256; 3632 3253; 3629 3250; 3625 3247; 3621 3243; 3618 3240;
edge 2: 3637 3268; 3634 3271; 3630 3275; 3627 3279; 3623 3284; 3620 3287; 3618 3289;
edge 1: 3632 3285; 3629 3282; 3625 3279; 3624 3277; 3622 3274; 3620 3273; 3617 3271; 3614 3267;
edge 2: 3632 3291; 3629 3295; 3626 3299; 3623 3302; 3619 3305; 3616 3308; 3614 3311; 3612 3314;
edge 1: 918 2383; 918 2381; 919 2379; 919 2376; 919 2374;
edge 2: 919 2384; 920 2384; 922 2384; 925 2384;
edge 1: 924 2354; 924 2351; 925 2349; 925 2347; 925 2345; 925 2343;
edge 2: 924 2354; 926 2354; 927 2354; 929 2354;
edge 1: 8914 4085; 8911 4085; 8907 4084; 8903 4083; 8899 4082; 8895 4081;
edge 2: 8924 4060; 8923 4064; 8922 4069; 8921 4073; 8920 4077; 8919 4082;
edge 1: 8882 4126; 8887 4126; 8891 4128; 8895 4129; 8899 4130;
edge 2: 8908 4128; 8909 4123; 8911 4119; 8911 4115; 8913 4111; 8914 4107; 8915 4103;
edge 1: 11718 3543; 11716 3539; 11715 3536; 11713 3532; 11711 3528;
edge 2: 11721 3544; 11723 3542; 11725 3541; 11727 3539; 11730 3537;
edge 1: 11706 3599; 11704 3595; 11702 3591; 11700 3588; 11699 3585; 11697 3581;
edge 2: 11707 3600; 11710 3599; 11712 3597; 11714 3595; 11717 3593;
edge 1: 12079 3583; 12078 3579; 12077 3576; 12076 3572;
edge 2: 12079 3583; 12083 3582; 12088 3581; 12093 3581; 12097 3580;
edge 1: 12067 3636; 12066 3632; 12065 3628; 12064 3625;
edge 2: 12068 3636; 12072 3636; 12076 3635; 12079 3634;
edge 1: 12100 3579; 12099 3576; 12099 3574; 12099 3570; 12098 3566;
edge 2: 12097 3580; 12092 3580; 12089 3582; 12084 3582;
edge 1: 12088 3631; 12087 3628; 12086 3625; 12086 3622;
edge 2: 12087 3633; 12082 3633; 12077 3635; 12072 3636;
edge 1: 5700 5038; 5699 5035; 5698 5032; 5697 5028; 5696 5024; 5694 5020;
edge 2: 5697 5046; 5692 5047; 5687 5048; 5681 5050; 5677 5051;
edge 1: 5692 5071; 5691 5068; 5690 5064; 5689 5062; 5688 5058; 5687 5054;
edge 2: 5690 5078; 5685 5079; 5682 5080; 5679 5081; 5675 5082; 5670 5083;
edge 1: 9306 5372; 9307 5367; 9307 5365; 9308 5361; 9309 5356;
edge 2: 9307 5374; 9311 5375; 9315 5375; 9320 5376; 9326 5377;
edge 1: 9293 5425; 9294 5420; 9295 5416; 9296 5411; 9297 5406; 9298 5400;
edge 2: 9296 5427; 9300 5428; 9305 5429; 9310 5429; 9315 5430;
edge 1: 9359 5381; 9359 5378; 9359 5374; 9360 5370; 9361 5364; 9362 5359;
edge 2: 9357 5382; 9351 5381; 9346 5380; 9340 5379; 9335 5379; 9328 5378;
edge 1: 9346 5434; 9346 5429; 9347 5425; 9348 5421; 9349 5416;
edge 2: 9345 5435; 9339 5434; 9333 5433; 9327 5433; 9321 5431;
edge 1: 9364 5338; 9360 5338; 9355 5337; 9351 5336; 9345 5335;
edge 2: 9363 5348; 9364 5342; 9365 5338; 9365 5334; 9366 5331;
edge 1: 9351 5391; 9347 5390; 9342 5390; 9337 5389; 9333 5388;
edge 2: 9351 5401; 9352 5396; 9353 5391; 9353 5387; 9355 5380;
edge 1: 9371 5294; 9367 5293; 9362 5292; 9355 5291; 9350 5290;
edge 2: 9373 5296; 9372 5300; 9371 5305; 9370 5310; 9369 5316;
edge 1: 9360 5347; 9355 5346; 9350 5345; 9345 5344; 9339 5343;
edge 2: 9360 5350; 9359 5354; 9359 5359; 9357 5364; 9356 5371;
edge 1: 9320 5287; 9319 5290; 9318 5296; 9317 5302; 9316 5311;
edge 2: 9323 5286; 9327 5286; 9332 5287; 9334 5288; 9338 5288;
edge 1: 9308 5341; 9306 5346; 9306 5352; 9305 5357; 9304 5364;
edge 2: 9310 5339; 9314 5340; 9320 5341; 9324 5341; 9328 5342;

edge 1: 9315 5317; 9314 5323; 9313 5328; 9312 5335; 9311 5341;
edge 2: 9315 5330; 9319 5331; 9324 5332; 9329 5333; 9336 5334;
edge 1: 9304 5369; 9302 5373; 9302 5378; 9301 5385; 9300 5390; 9299 5397;
edge 2: 9302 5383; 9307 5384; 9311 5384; 9316 5385; 9321 5386;
edge 1: 9260 5291; 9260 5285; 9262 5281; 9262 5274; 9264 5269;
edge 2: 9256 5292; 9251 5291; 9245 5291; 9238 5289; 9232 5288;
edge 1: 9248 5345; 9248 5340; 9249 5335; 9249 5330; 9250 5325;
edge 2: 9243 5346; 9239 5345; 9235 5345; 9229 5344; 9226 5343;
edge 1: 9265 5239; 9260 5239; 9254 5238; 9246 5237; 9238 5235;
edge 2: 9268 5243; 9267 5249; 9266 5255; 9265 5260; 9264 5267;
edge 1: 9254 5294; 9250 5293; 9245 5292; 9241 5291; 9236 5291; 9229 5290;
edge 2: 9256 5296; 9255 5300; 9254 5304; 9254 5308; 9252 5313; 9251 5321;
edge 1: 9206 5230; 9212 5231; 9217 5232; 9226 5234; 9235 5235;
edge 2: 9223 5234; 9222 5241; 9222 5249; 9221 5254; 9219 5267;
edge 1: 9193 5284; 9201 5285; 9209 5286; 9219 5288; 9226 5289;
edge 2: 9211 5289; 9210 5299; 9209 5304; 9208 5310; 9206 5320; 9205 5328;
edge 1: 9180 5227; 9179 5233; 9177 5238; 9177 5245; 9176 5251; 9174 5262;
edge 2: 9182 5227; 9188 5227; 9195 5228; 9203 5230; 9210 5231;
edge 1: 9167 5281; 9166 5288; 9165 5295; 9164 5303; 9162 5311; 9161 5321;
edge 2: 9169 5280; 9174 5281; 9182 5282; 9188 5283; 9196 5284; 9204 5286;
edge 1: 9177 5246; 9176 5250; 9174 5259; 9173 5265; 9172 5270; 9171 5277;
edge 2: 9173 5279; 9178 5279; 9183 5281; 9191 5282; 9200 5283; 9209 5285;
edge 1: 9165 5295; 9164 5302; 9163 5309; 9162 5315; 9161 5321; 9160 5327;
edge 2: 9161 5332; 9167 5333; 9174 5334; 9184 5336; 9192 5337; 9199 5338;
edge 1: 9196 5282; 9203 5284; 9220 5287; 9228 5287; 9237 5289;
edge 2: 9215 5286; 9216 5278; 9218 5269; 9219 5262; 9221 5250;
edge 1: 9183 5336; 9192 5338; 9201 5339; 9208 5340; 9216 5341; 9225 5343;
edge 2: 9203 5338; 9205 5330; 9206 5323; 9207 5317; 9208 5309; 9210 5298;
edge 1: 10138 6895; 10141 6898; 10145 6902; 10147 6905; 10150 6909;
edge 2: 10156 6910; 10158 6908; 10163 6905; 10166 6902; 10170 6897;
edge 1: 10144 6945; 10140 6941; 10137 6936; 10133 6932;
edge 2: 10147 6945; 10151 6942; 10155 6938; 10160 6935; 10164 6931;
edge 1: 3959 12332; 3962 12335; 3964 12338; 3965 12340;
edge 2: 3957 12351; 3960 12349; 3963 12347; 3966 12345;
edge 1: 3978 12242; 3981 12245; 3983 12247; 3984 12250;
edge 2: 3985 12255; 3983 12257; 3980 12258; 3977 12261;
edge 1: 3081 10428; 3077 10426; 3074 10424; 3071 10421;
edge 2: 3081 10428; 3083 10425; 3088 10421; 3092 10416;
edge 1: 3127 10217; 3132 10213; 3135 10209; 3138 10206;
edge 2: 3126 10217; 3122 10215; 3119 10211; 3116 10209;
edge 1: 3093 10258; 3091 10259; 3089 10260; 3087 10261;
edge 2: 3094 10258; 3093 10255; 3091 10252; 3090 10248;
edge 1: 3140 10047; 3139 10043; 3137 10038; 3135 10033;
edge 2: 3140 10047; 3138 10048; 3135 10049; 3136 10049;
edge 1: 3174 10339; 3170 10339; 3163 10340; 3156 10340; 3149 10342;
edge 2: 3174 10340; 3174 10347; 3174 10352; 3174 10359;
edge 1: 3220 10128; 3213 10128; 3207 10129; 3199 10130; 3195 10131;
edge 2: 3221 10128; 3221 10136; 3221 10141; 3220 10147;
edge 1: 3091 10416; 3089 10419; 3084 10424; 3081 10427;
edge 2: 3091 10416; 3089 10413; 3086 10410; 3084 10409;
edge 1: 3139 10205; 3136 10208; 3131 10213; 3127 10217;
edge 2: 3138 10205; 3135 10202; 3133 10201; 3130 10198;
edge 1: 4851 13055; 4848 13055; 4845 13056;
edge 2: 4851 13055; 4852 13058; 4853 13061;
edge 1: 4859 13018; 4856 13018; 4853 13019;
edge 2: 4859 13018; 4860 13020; 4861 13024;

edge 1: 11983 12369; 11983 12362; 11982 12354;
edge 2: 11984 12369; 11986 12369; 11991 12369;
edge 1: 11977 12398; 11981 12398; 11984 12398;
edge 2: 11977 12397; 11977 12390; 11976 12382;
edge 1: 10748 9831; 10752 9831; 10758 9832; 10762 9832;
edge 2: 10763 9835; 10761 9839; 10757 9847; 10751 9859;
edge 1: 10737 9880; 10741 9881; 10745 9881; 10750 9882;
edge 2: 10752 9884; 10747 9894; 10743 9899; 10740 9905;
edge 1: 9184 11868; 9181 11872; 9178 11875; 9176 11877;
edge 2: 9185 11869; 9187 11870; 9189 11873;
edge 1: 9185 11865; 9187 11867; 9189 11868;
edge 2: 9185 11865; 9181 11868; 9179 11871; 9177 11873;

## APPENDIX VI Measurements on Images for Roundabout Features in Hobart Test Field

Point 1: 3204 936; 3199 938; 3198 942; 3198 946; 3200 950; 3205 952; 3209 951; 3213 948; 3213 943; 3211 938;
Point 2: 3185 1012; 3182 1012; 3179 1015; 3178 1018; 3178 1023; 3181 1025; 3185 1027; 3189 1026; 3192 1022; 3194 1018; 3191 1014;
Point 3: 3198 971; 3193 973; 3191 975; 3190 978; 3190 982; 3192 985; 3196 987; 3200 987; 3203 984; 3205 980; 3204 975; 3202 972;
Point 4: 3429 412; 3425 414; 3423 416; 3422 419; 3424 425; 3429 428; 3437 426; 3439 419; 3437 414; 3432 411;
Point 5: 3411 509; 3406 506; 3402 507; 3398 512; 3398 515; 3400 520; 3405 522; 3410 521; 3414 517; 3414 514;
Point 6: 3421 456; 3416 457; 3413 460; 3412 464; 3413 468; 3416 471; 3421 473; 3426 470; 3429 465; 3429 461; 3425 457;
Point 7: 2505 1110; 2509 1113; 2511 1118; 2509 1123; 2506 1125; 2503 1126; 2498 1124; 2495 1119; 2496 1114;
Point 8: 2480 1172; 2481 1176; 2482 1179; 2485 1181; 2489 1181; 2493 1179; 2495 1174; 2494 1169; 2489 1166; 2485 1165;
Point 9: 2490 1141; 2488 1146; 2490 1149; 2493 1152; 2497 1153; 2501 1152; 2504 1149; 2505 1145; 2504 1141; 2499 1137;
Point 10: 5477 4057; 5473 4059; 5472 4062; 5471 4065; 5472 4068; 5477 4071; 5481 4069; 5483 4066; 5483 4063; 5481 4059;
Point 11: 5452 4160; 5449 4161; 5446 4163; 5446 4166; 5446 4169; 5449 4172; 5452 4172; 5456 4171; 5457 4168; 5457 4165; 5456 4162; 5454 4161;
Point 12: 5466 4103; 5463 4104; 5461 4107; 5460 4110; 5460 4114; 5465 4115; 5468 4115; 5472 4112; 5472 4109; 5472 4106; 5470 4104;
Point 13: 5584 3839; 5579 3843; 5579 3845; 5579 3849; 5582 3852; 5585 3852; 5590 3851; 5591 3847; 5591 3844; 5588 3840;
Point 14: 5559 3945; 5555 3946; 5553 3948; 5552 3951; 5553 3954; 5555 3956; 5559 3957; 5563 3955; 5565 3951; 5564 3947; 5561 3945;
Point 15: 5573 3885; 5569 3887; 5568 3890; 5568 3894; 5570 3898; 5574 3899; 5578 3897; 5580 3894; 5580 3890; 5578 3887;
Point 16: 5236 3657; 5233 3660; 5233 3662; 5234 3666; 5238 3668; 5243 3667; 5246 3663; 5244 3658; 5240 3656;
Point 17: 5213 3761; 5209 3761; 5208 3764; 5207 3767; 5207 3771; 5211 3773; 5215 3773; 5219 3770; 5219 3767; 5218 3764; 5215 3762;
Point 18: 5228 3702; 5224 3703; 5222 3706; 5222 3709; 5224 3713; 5227 3714; 5231 3714; 5234 3711; 5234 3707; 5233 3704; 5230 3702;
Point 19: 5364 3326; 5360 3329; 5358 3333; 5359 3338; 5363 3340; 5367 3341; 5370 3338; 5372 3334; 5370 3330; 5367 3328;
Point 20: 5337 3438; 5334 3439; 5331 3441; 5330 3446; 5331 3449; 5335 3452; 5338 3451; 5342 3449; 5343 3445; 5342 3442; 5340 3439;
Point 21: 5352 3376; 5349 3377; 5347 3380; 5346 3382; 5347 3385; 5349 3388; 5353 3390; 5357 3388; 5360 3385; 5360 3382; 5358 3379; 5355 3376;
Point 22: 4778 477; 4772 480; 4769 486; 4771 494; 4778 497; 4782 496; 4787 492; 4788 487; 4787 481; 4782 477;
Point 23: 4746 602; 4742 604; 4739 608; 4738 612; 4738 617; 4741 621; 4745 623; 4751 622; 4756 618; 4757 612; 4754 606; 4751 603;
Point 24: 4764 535; 4758 538; 4756 541; 4756 544; 4756 548; 4758 552; 4764 554; 4768 554; 4774 550; 4775 545; 4774 541; 4774 537; 4766 535;
Point 25: 4740 487; 4733 488; 4730 494; 4731 499; 4735 502; 4740 503; 4747 500; 4748 495; 4745 489;
Point 26: 4709 612; 4703 613; 4698 618; 4698 622; 4699 627; 4704 630; 4710 630; 4714 627; 4716 622; 4715 617; 4712 613;

Point 27: 4726 544; 4721 546; 4716 550; 4716 554; 4718 559; 4722 561; 4727 562; 4731 560; 4734 554; 4734 550; 4730 546;
Point 28: 6571 1971; 6566 1973; 6564 1976; 6563 1980; 6565 1984; 6569 1987; 6574 1988; 6578 1985; 6580 1980; 6579 1977; 6575 1972;
Point 29: 6540 2097; 6535 2099; 6532 2102; 6531 2106; 6533 2110; 6536 2113; 6540 2113; 6545 2111; 6548 2107; 6547 2101; 6544 2098;
Point 30: 6558 2028; 6554 2030; 6551 2033; 6551 2038; 6553 2042; 6556 2044; 6559 2044; 6564 2042; 6567 2038; 6567 2035; 6565 2031;
Point 31: 7204 2520; 7202 2522; 7200 2524; 7201 2526; 7203 2528; 7205 2528; 7208 2526; 7207 2524; 7206 2522;
Point 32: 7174 2643; 7171 2644; 7170 2646; 7170 2648; 7172 2650; 7175 2650; 7177 2647; 7177 2645; 7175 2644;
Point 33: 7192 2575; 7189 2576; 7188 2578; 7188 2581; 7191 2583; 7194 2582; 7195 2580; 7194 2577;
Point 34: 6745 4193; 6741 4195; 6739 4198; 6738 4201; 6739 4204; 6743 4208; 6745 4208; 6750 4206; 6752 4201; 6750 4196; 6746 4194;
Point 35: 6719 4298; 6715 4299; 6713 4302; 6713 4305; 6714 4310; 6718 4311; 6723 4310; 6726 4307; 6726 4303; 6725 4300; 6722 4298;
Point 36: 6735 4239; 6731 4241; 6728 4243; 6727 4245; 6728 4250; 6731 4253; 6735 4253; 6739 4251; 6742 4248; 6742 4245; 6740 4241;
Point 37: 6163 3290; 6160 3293; 6158 3296; 6158 3299; 6160 3302; 6163 3304; 6167 3304; 6171 3302; 6172 3299; 6172 3295; 6170 3292;
Point 38: 6135 3407; 6131 3409; 6129 3412; 6129 3415; 6130 3418; 6132 3420; 6136 3421; 6140 3419; 6142 3417; 6142 3410; 6141 3410; 6138 3408;
Point 39: 6153 3342; 6149 3344; 6146 3347; 6146 3351; 6148 3354; 6153 3356; 6158 3354; 6160 3350; 6160 3346; 6157 3343;
Point 40: 5860 3264; 5856 3266; 5855 3270; 5855 3273; 5856 3275; 5857 3277; 5860 3278; 5862 3279; 5866 3277; 5869 3273; 5869 3270; 5867 3267; 5865 3265;
Point 41: 5833 3379; 5829 3380; 5826 3386; 5828 3390; 5830 3392; 5834 3393; 5839 3390; 5839 3386; 5839 3382; 5836 3379;
Point 42: 5850 3315; 5845 3317; 5843 3319; 5843 3323; 5845 3326; 5848 3329; 5852 3328; 5856 3325; 5857 3320; 5853 3316;
Point 43: 7611 2566; 7606 2567; 7602 2570; 7601 2575; 7601 2580; 7604 2584; 7609 2586; 7615 2585; 7620 2580; 7620 2575; 7619 2571; 7614 2566;
Point 44: 7579 2692; 7573 2694; 7569 2698; 7569 2703; 7572 2709; 7577 2712; 7583 2711; 7589 2706; 7589 2700; 7584 2694;
Point 45: 7598 2622; 7594 2623; 7591 2625; 7588 2628; 7587 2632; 7588 2636; 7591 2640; 7596 2642; 7603 2641; 7606 2637; 7607 2632; 7606 2627; 7604 2624;
Point 46: 4587 4138; 4583 4135; 4579 4135; 4575 4137; 4573 4139; 4573 4142; 4574 4146; 4578 4149; 4582 4149; 4588 4144; 4587 4139; 4586 4136;
Point 47: 4566 4224; 4565 4218; 4561 4216; 4555 4217; 4552 4219; 4551 4223; 4552 4226; 4555 4229; 4559 4231; 4566 4226;
Point 48: 4571 4170; 4566 4172; 4565 4176; 4564 4181; 4568 4184; 4571 4185; 4578 4178; 4578 4174; 4575 4171;
Point 49: 10977 641; 10969 643; 10963 647; 10958 656; 10957 661; 10957 667; 10960 673; 10965 680; 10973 684; 10979 684; 10988 683; 10996 677; 10998 672; 11001 665; 11001 658; 10996 648; 10988 643;
Point 50: 10949 762; 10937 765; 10929 774; 10926 781; 10927 790; 10932 799; 10938 803; 10947 806; 10956 805; 10964 799; 10969 789; 10970 778; 10961 766;
Point 51: 10967 697; 10967 699; 10948 706; 10945 712; 10944 721; 10948 730; 10952 735; 10960 740; 10967 740; 10974 739; 10980 735; 10985 729; 10988 721; 10988 716; 10985 707; 10979 701; 10971 697;
Point 52: 9773 1426; 9767 1428; 9764 1431; 9763 1435; 9765 1440; 9768 1444; 9775 1445; 9778 1445; 9782 1444; 9784 1440; 9784 1435; 9783 1431; 9779 1427;
Point 53: 9744 1548; 9735 1550; 9736 1553; 9736 1560; 9740 1564; 9745 1566; 9750 1565; 9753 1559; 9753 1554; 9750 1548;

Point 54: 9762 1482; 9757 1484; 9754 1488; 9754 1493; 9755 1497; 9761 1500; 9766 1500; 9771 1497; 9772 1492; 9771 1487; 9768 1484;
Point 55: 8467 2916; 8463 2918; 8458 2923; 8458 2928; 8459 2933; 8463 2937; 8469 2938; 8473 2937; 8478 2934; 8480 2928; 8479 2922; 8476 2918; 8470 2916;
Point 56: 8437 3040; 8431 3042; 8428 3046; 8427 3050; 8427 3054; 8431 3058; 8437 3061; 8444 3059; 8448 3055; 8448 3049; 8446 3043; 8440 3039;
Point 57: 8455 2971; 8448 2974; 8446 2979; 8446 2984; 8449 2991; 8454 2993; 8460 2992; 8465 2987; 8467 2982; 8465 2975; 8462 2973;
Point 58: 8461 2881; 8456 2881; 8453 2885; 8451 2889; 8451 2893; 8453 2898; 8455 2901; 8461 2903; 8465 2902; 8471 2899; 8472 2892; 8472 2888; 8469 2883; 8464 2881;
Point 59: 8431 3004; 8425 3005; 8421 3009; 8420 3013; 8421 3019; 8423 3023; 8427 3025; 8433 3026; 8438 3023; 8441 3018; 8441 3012; 8438 3007; 8434 3004;
Point 60: 8450 2936; 8445 2936; 8440 2940; 8438 2945; 8439 2951; 8441 2954; 8446 2957; 8452 2957; 8457 2953; 8460 2947; 8459 2942; 8455 2938;
Point 61: 9825 3231; 9819 3232; 9814 3236; 9811 3242; 9811 3247; 9812 3252; 9817 3257; 9824 3260; 9830 3258; 9836 3254; 9838 3249; 9838 3243; 9835 3236; 9829 3231;
Point 62: 9794 3350; 9785 3354; 9781 3360; 9781 3365; 9783 3371; 9787 3376; 9795 3378; 9802 3376; 9807 3371; 9808 3365; 9808 3360; 9803 3353;
Point 63: 9813 3283; 9806 3285; 9800 3290; 9799 3296; 9799 3301; 9802 3307; 9809 3311; 9815 3311; 9823 3307; 9826 3300; 9826 3295; 9822 3288;
Point 64: 9761 3130; 9759 3130; 9757 3132; 9756 3134; 9758 3137; 9760 3138; 9764 3137; 9765 3134; 9764 3132; 9763 3130;
Point 65: 9731 3244; 9729 3245; 9727 3248; 9728 3251; 9731 3253; 9734 3253; 9736 3250; 9736 3247; 9735 3245;
Point 66: 9749 3180; 9747 3181; 9744 3183; 9745 3187; 9748 3189; 9751 3188; 9753 3186; 9753 3182; 9751 3181;
Point 67: 11863 1451; 11855 1453; 11850 1457; 11848 1462; 11848 1466; 11848 1473; 11852 1478; 11855 1481; 11862 1483; 11868 1482; 11873 1479; 11877 1474; 11878 1468; 11878 1462; 11874 1456; 11869 1452;
Point 68: 11845 1521; 11836 1523; 11831 1528; 11829 1533; 11829 1540; 11831 1545; 11837 1551; 11846 1553; 11855 1550; 11859 1544; 11861 1538; 11859 1529; 11853 1523;
Point 69: 11857 1483; 11849 1485; 11843 1491; 11840 1497; 11840 1503; 11842 1508; 11847 1512; 11853 1515; 11862 1514; 11869 1508; 11872 1500; 11870 1492; 11865 1486;
Point 70: 3929 5711; 3925 5715; 3922 5719; 3920 5722; 3920 5725; 3920 5730; 3922 5735; 3926 5739; 3933 5742; 3939 5742; 3946 5739; 3950 5734; 3951 5728; 3950 5722; 3949 5715; 3945 5711;
Point 71: 3925 5747; 3917 5749; 3912 5754; 3909 5759; 3909 5766; 3913 5773; 3920 5777; 3929 5778; 3935 5775; 3939 5769; 3940 5760; 3936 5752; 3932 5747;
Point 72: 3931 5726; 3923 5729; 3918 5734; 3916 5739; 3916 5744; 3918 5750; 3922 5755; 3930 5758; 3939 5756; 3945 5751;
Point 73: 3979 5172; 3976 5174; 3975 5177; 3976 5180; 3978 5182; 3982 5182; 3986 5179; 3986 5176; 3985 5174;
Point 74: 3962 5237; 3958 5239; 3957 5242; 3958 5245; 3960 5247; 3963 5247; 3967 5247; 3968 5244; 3968 5241; 3966 5239;
Point 75: 3972 5200; 3969 5202; 3968 5205; 3969 5209; 3971 5211; 3976 5211; 3978 5208; 3978 5203;
Point 76: 3964 5194; 3962 5195; 3959 5197; 3959 5199; 3960 5202; 3964 5204; 3966 5203; 3969 5200; 3969 5198; 3967 5195;
Point 77: 3947 5259; 3943 5260; 3942 5262; 3942 5266; 3944 5268; 3947 5269; 3950 5267; 3951 5265; 3951 5262; 3949 5259;
Point 78: 3958 5222; 3954 5224; 3952 5226; 3952 5229; 3955 5232; 3958 5232; 3962 5230; 3962 5226; 3960 5222;
Point 79: 7971 4337; 7969 4338; 7967 4340; 7967 4342; 7969 4345; 7971 4346; 7975 4346; 7977 4343; 7977 4340; 7974 4338;
Point 80: 7944 4452; 7941 4453; 7939 4455; 7939 4457; 7940 4460; 7942 4461; 7945 4462; 7949 4460; 7948 4457; 7947 4454;
Point 81: 7961 4387; 7958 4388; 7956 4389; 7956 4392; 7957 4394; 7959 4397; 7963 4397; 7966 4395; 7965 4390;

Point 82: 8065 6072; 8063 6073; 8060 6075; 8060 6076; 8060 6079; 8062 6082; 8065 6082; 8069 6080; 8070 6077; 8068 6073;
Point 83: 8038 6176; 8035 6177; 8034 6179; 8033 6181; 8034 6184; 8037 6185; 8039 6186; 8042 6185; 8044 6182; 8043 6178; 8041 6176;
Point 84: 8055 6116; 8051 6117; 8050 6120; 8051 6123; 8053 6126; 8056 6126; 8059 6124; 8060 6121; 8058 6118;
Point 85: 7541 6336; 7539 6337; 7538 6338; 7539 6340; 7541 6341; 7543 6341; 7543 6339; 7543 6336;
Point 86: 7516 6431; 7514 6431; 7514 6434; 7516 6435; 7518 6436; 7520 6433; 7518 6431;
Point 87: 7532 6375; 7530 6377; 7529 6378; 7530 6381; 7532 6381; 7535 6380; 7535 6378; 7534 6376;
Point 88: 7639 6866; 7636 6868; 7635 6870; 7636 6874; 7639 6875; 7641 6874; 7643 6872; 7643 6870; 7642 6867;
Point 89: 7620 6941; 7617 6942; 7616 6943; 7616 6946; 7617 6949; 7619 6950; 7622 6949; 7624 6947; 7624 6945; 7622 6942;
Point 90: 7632 6898; 7629 6899; 7628 6902; 7629 6905; 7631 6906; 7633 6907; 7636 6904; 7637 6901; 7636 6899;
Point 91: 7480 4523; 7476 4525; 7474 4528; 7475 4532; 7478 4536; 7481 4537; 7485 4536; 7487 4533; 7488 4529; 7487 4526; 7484 4524;
Point 92: 7453 4636; 7449 4637; 7447 4640; 7447 4643; 7448 4647; 7450 4649; 7455 4649; 7459 4647; 7461 4644; 7460 4639; 7457 4637;
Point 93: 7469 4572; 7466 4574; 7463 4577; 7463 4580; 7465 4585; 7470 4586; 7474 4585; 7477 4581; 7477 4577; 7474 4573;
Point 94: 7579 4701; 7576 4702; 7576 4704; 7576 4707; 7578 4708; 7582 4707; 7583 4705; 7582 4702;
Point 95: 7552 4812; 7549 4813; 7548 4815; 7549 4818; 7552 4818; 7555 4817; 7555 4814; 7554 4813;
Point 96: 7568 4749; 7566 4751; 7564 4752; 7566 4755; 7569 4756; 7571 4755; 7572 4753; 7571 4750;
Point 97: 7948 7549; 7942 7550; 7937 7558; 7936 7562; 7938 7567; 7939 7572; 7946 7576; 7955 7576; 7961 7571; 7964 7564; 7963 7557; 7959 7552; 7954 7548;
Point 98: 7942 7576; 7935 7577; 7930 7581; 7928 7587; 7928 7591; 7929 7594; 7931 7598; 7938 7602; 7943 7604; 7950 7601; 7954 7596; 7955 7591; 7954 7583; 7949 7578;
Point 99: 7946 7560; 7937 7564; 7934 7573; 7935 7579; 7937 7584; 7943 7588; 7950 7588; 7958 7584; 7961 7578; 7960 7571; 7956 7564; 7952 7561;
Point 100: 6141 6283; 6139 6283; 6137 6285; 6139 6288; 6140 6289; 6143 6288; 6143 6286; 6143 6284; 6142 6283;
Point 101: 6128 6324; 6126 6324; 6125 6327; 6126 6329; 6128 6329; 6131 6328; 6132 6325; 6130 6324;
Point 102: 6137 6301; 6134 6301; 6134 6303; 6134 6305; 6136 6306; 6139 6305; 6140 6303; 6139 6301;
Point 103: 6311 6205; 6309 6206; 6308 6207; 6308 6209; 6311 6212; 6313 6210; 6314 6208; 6314 6206;
Point 104: 6296 6257; 6294 6258; 6293 6260; 6294 6262; 6296 6263; 6299 6261; 6299 6260; 6298 6257;
Point 105: 6306 6227; 6303 6228; 6303 6231; 6304 6233; 6306 6234; 6308 6232; 6309 6230; 6308 6229;
Point 106: 7377 4343; 7374 4343; 7374 4346; 7375 4349; 7377 4350; 7380 4349; 7382 4346; 7380 4343;
Point 107: 7349 4455; 7347 4457; 7345 4458; 7345 4460; 7346 4462; 7348 4463; 7352 4463; 7353 4460; 7352 4457;
Point 108: 7366 4392; 7363 4393; 7362 4395; 7362 4397; 7364 4399; 7368 4399; 7369 4397; 7369 4394; 7369 4392;
Point 109: 6803 5255; 6797 5257; 6791 5262; 6788 5269; 6789 5274; 6793 5281; 6800 5284; 6805 5284; 6812 5281; 6816 5275; 6818 5270; 6815 5263; 6810 5257;
Point 110: 6791 5298; 6786 5298; 6781 5301; 6777 5306; 6776 5311; 6776 5317; 6780 5323; 6788 5326; 6792 5326; 6798 5324; 6802 5319; 6804 5313; 6803 5306; 6800 5301; 6795 5298;
Point 111: 6799 5274; 6792 5276; 6787 5280; 6785 5286; 6785 5293; 6788 5299; 6795 5303; 6802 5302; 6809 5299; 6812 5292; 6812 5287; 6810 5281; 6806 5277;
Point 112: 8259 5836; 8254 5840; 8253 5843; 8255 5842; 8259 5849; 8263 5847; 8265 5843; 8265 5840; 8263 5837;
Point 113: 8230 5950; 8228 5950; 8226 5953; 8224 5955; 8226 5959; 8229 5961; 8231 5961; 8235 5959; 8236 5955; 8236 5952; 8233 5950;
Point 114: 8248 5884; 8244 5886; 8243 5888; 8243 5891; 8244 5894; 8247 5896; 8250 5896; 8253 5893; 8254 5890; 8252 5886;
Point 115: 8114 5808; 8110 5811; 8109 5814; 8110 5819; 8114 5821; 8118 5821; 8121 5818; 8121 5815; 8121 5821; 8118 5809;

Point 116: 8087 5919; 8083 5920; 8081 5922; 8081 5926; 8082 5930; 8087 5932; 8091 5930; 8094 5926; 8092 5923; 8090 5920;
Point 117: 8104 5855; 8100 5857; 8098 5859; 8098 5863; 8100 5867; 8104 5868; 8107 5867; 8110 5864; 8110 5860; 8109 5857;
Point 118: 8210 6097; 8207 6098; 8203 6103; 8203 6107; 8205 6111; 8207 6114; 8212 6114; 8218 6111; 8219 6106; 8218 6100; 8214 6097;
Point 119: 8184 6204; 8179 6205; 8177 6207; 8175 6210; 8175 6213; 8177 6217; 8180 6220; 8184 6222; 8190 6219; 8192 6215; 8193 6210; 8189 6206; 8186 6204;
Point 120: 8201 6142; 8195 6144; 8193 6148; 8193 6153; 8196 6157; 8201 6159; 8207 6157; 8208 6153; 8209 6149; 8206 6144;
Point 121: 8846 5944; 8841 5947; 8839 5951; 8839 5956; 8842 5959; 8847 5961; 8852 5960; 8856 5956; 8856 5952; 8855 5947; 8850 5944;
Point 122: 8823 6042; 8819 6042; 8816 6044; 8814 6047; 8814 6050; 8815 6055; 8819 6058; 8824 6058; 8828 6056; 8830 6052; 8831 6049; 8829 6045; 8825 6042;
Point 123: 8838 5985; 8832 5987; 8830 5989; 8829 5993; 8832 6000; 8837 6003; 8843 6001; 8846 5996; 8846 5991; 8842 5986;
Point 124: 8104 6972; 8100 6974; 8099 6976; 8099 6979; 8101 6981; 8104 6982; 8107 6981; 8108 6978; 8108 6975; 8105 6972;
Point 125: 8084 7048; 8081 7049; 8079 7052; 8080 7055; 8083 7058; 8087 7057; 8088 7055; 8088 7052; 8087 7049;
Point 126: 8097 7004; 8093 7005; 8091 7008; 8091 7010; 8094 7013; 8096 7014; 8100 7012; 8100 7008; 8099 7005;
Point 127: 8498 7245; 8496 7246; 8495 7248; 8495 7250; 8497 7252; 8500 7252; 8502 7250; 8502 7247; 8501 7246;
Point 128: 8483 7305; 8481 7305; 8479 7307; 8479 7309; 8481 7311; 8484 7311; 8486 7309; 8486 7307; 8485 7305;
Point 129: 8493 7270; 8490 7271; 8489 7273; 8489 7275; 8491 7277; 8494 7277; 8496 7274; 8495 7272;
Point 130: 9008 7819; 9004 7821; 9003 7823; 9003 7825; 9005 7828; 9008 7830; 9012 7827; 9013 7823; 9011 7820;
Point 131: 8987 7903; 8984 7904; 8982 7906; 8982 7909; 8983 7912; 8987 7914; 8991 7912; 8993 7909; 8992 7906; 8990 7904;
Point 132: 9000 7854; 8996 7854; 8995 7856; 8995 7859; 8996 7862; 8999 7864; 9003 7864; 9005 7861; 9005 7858; 9003 7854;
Point 133: 9656 7005; 9653 7007; 9651 7009; 9651 7012; 9653 7015; 9657 7017; 9661 7016; 9663 7012; 9663 7008; 9660 7005;
Point 134: 9630 7116; 9625 7117; 9624 7120; 9624 7124; 9626 7126; 9629 7127; 9633 7126; 9636 7122; 9635 7119; 9633 7116;
Point 135: 9646 7051; 9644 7052; 9642 7054; 9641 7055; 9641 7058; 9643 7061; 9646 7063; 9650 7061; 9652 7058; 9652 7054; 9650 7052;
Point 136: 8890 5314; 8888 5315; 8887 5316; 8887 5318; 8889 5320; 8891 5320; 8893 5318; 8893 5315; 8891 5314;
Point 137: 8860 5433; 8858 5434; 8857 5436; 8858 5438; 8861 5439; 8863 5438; 8863 5435; 8862 5434;
Point 138: 8878 5365; 8876 5366; 8875 5368; 8875 5370; 8877 5371; 8879 5370; 8881 5368; 8881 5366;
Point 139: 11992 4867; 11990 4868; 11989 4870; 11990 4872; 11992 4873; 11994 4873; 11995 4871; 11995 4869; 11994 4868;
Point 140: 11961 4993; 11959 4994; 11958 4996; 11959 4998; 11960 4999; 11962 4999; 11963 4998; 11964 4996; 11963 4994;
Point 141: 11980 4922; 11978 4923; 11977 4924; 11978 4927; 11980 4927; 11982 4927; 11983 4925; 11982 4923;
Point 142: 8260 8602; 8254 8604; 8250 8609; 8248 8613; 8249 8618; 8250 8623; 8253 8627; 8259 8630; 8265 8632; 8272 8630; 8277 8625; 8279 8620; 8279 8613; 8277 8608; 8273 8604;
Point 143: 8259 8604; 8253 8606; 8247 8611; 8246 8617; 8246 8623; 8251 8630; 8259 8634; 8266 8634; 8272 8629; 8275 8625; 8276 8618; 8276 8612; 8272 8608;
Point 144: 8263 8603; 8255 8605; 8249 8612; 8248 8619; 8251 8627; 8255 8631; 8261 8633; 8269 8633; 8274 8629; 8278 8623; 8278 8617; 8275 8609; 8272 8605;

Point 145: 9293 7706; 9288 7709; 9286 7712; 9286 7715; 9288 7719; 9292 7721; 9297 7719; 9299 7716; 9299 7713; 9297 7708;
Point 146: 9269 7805; 9264 7806; 9262 7810; 9262 7814; 9263 7817; 9267 7819; 9272 7818; 9275 7815; 9275 7810; 9274 7808; 9271 7805;
Point 147: 9283 7747; 9278 7750; 9277 7754; 9277 7756; 9279 7759; 9284 7761; 9288 7759; 9289 7755; 9289 7752; 9287 7748;
Point 148: 7968 6928; 7963 6930; 7963 6932; 7963 6935; 7966 6938; 7969 6938; 7972 6936; 7973 6933; 7973 6930; 7970 6927;
Point 149: 7950 6999; 7946 6999; 7944 7002; 7944 7005; 7946 7007; 7949 7008; 7952 7008; 7955 7005; 7954 7002; 7952 6999;
Point 150: 7960 6957; 7957 6959; 7956 6961; 7956 6964; 7958 6967; 7961 6968; 7965 6966; 7966 6962; 7965 6958;
Point 151: 11059 7976; 11056 7961; 11044 7946; 11026 7941; 11004 7944; 10982 7971; 10984 7993; 10989 8002; 11001 8015; 11018 8019; 11037 8014; 11050 8005; 11060 7985; 11058 7966;
Point 152: 10995 8056; 10974 8059; 10953 8085; 10956 8110; 10962 8125; 10986 8136; 11013 8131; 11022 8123; 11030 8105; 11030 8088; 11015 8064;
Point 153: 11032 7994; 11014 7989; 10993 7994; 10973 8014; 10973 8041; 10977 8051; 10990 8063; 11008 8067; 11027 8063; 11039 8052; 11048 8034; 11048 8021; 11045 8010; 11030 7993;
Point 154: 6309 10489; 6305 10486; 6301 10485; 6299 10489; 6300 10491; 6301 10493; 6305 10493; 6306 10491; 6307 10489; 6305 10486;
Point 155: 6294 10508; 6291 10510; 6291 10514; 6294 10516; 6297 10516; 6299 10513; 6298 10511;
Point 156: 6299 10495; 6296 10497; 6296 10499; 6297 10502; 6301 10502; 6304 10501; 6304 10498; 6302 10496;
Point 157: 7407 11743; 7404 11744; 7400 11748; 7398 11753; 7398 11756; 7399 11760; 7403 11765; 7409 11766; 7415 11765; 7419 11762; 7421 11757; 7421 11752; 7420 11748; 7419 11745; 7415 11742;
Point 158: 7410 11734; 7403 11736; 7399 11741; 7399 11747; 7401 11752; 7405 11755; 7410 11757; 7416 11756; 7420 11751; 7421 11745; 7420 11740; 7416 11735;
Point 159: 7411 11740; 7404 11742; 7400 11747; 7398 11752; 7400 11758; 7405 11763; 7411 11764; 7417 11761; 7421 11756; 7421 11751; 7421 11747; 7417 11742;
Point 160: 7382 11754; 7379 11754; 7375 11756; 7371 11759; 7370 11764; 7371 11768; 7373 11772; 7379 11776; 7385 11776; 7394 11766; 7392 11761; 7390 11757; 7387 11754;
Point 161: 7382 11744; 7377 11745; 7374 11748; 7371 11753; 7371 11758; 7374 11764; 7379 11766; 7383 11767; 7389 11764; 7394 11756; 7393 11751; 7390 11746;
Point 162: 7383 11751; 7375 11754; 7371 11758; 7371 11763; 7372 11768; 7377 11773; 7384 11773; 7389 11771; 7392 11767; 7393 11761; 7392 11755; 7389 11753;
Point 163: 7500 12215; 7495 12216; 7492 12221; 7492 12225; 7492 12229; 7497 12234; 7505 12234; 7509 12231; 7510 12227; 7510 12221; 7507 12217;
Point 164: 7504 12187; 7498 12190; 7496 12193; 7496 12199; 7502 12206; 7510 12206; 7514 12200; 7514 12195; 7510 12190;
Point 165: 7501 12206; 7497 12208; 7494 12211; 7494 12219; 7498 12224; 7505 12224; 7509 12221; 7512 12217; 7512 12211;
Point 166: 6300 11483; 6298 11484; 6297 11486; 6297 11488; 6300 11489; 6303 11488; 6303 11485; 6302 11483;
Point 167: 6305 11453; 6302 11454; 6302 11457; 6302 11459; 6304 11460; 6307 11459; 6308 11457; 6308 11455; 6306 11453;
Point 168: 6302 11473; 6299 11473; 6299 11476; 6299 11478; 6302 11479; 6305 11478; 6305 11474;
Point 169: 10154 10309; 10150 10311; 10148 10313; 10148 10315; 10149 10318; 10151 10320; 10154 10320; 10157 10319; 10158 10316; 10159 10313; 10157 10311;
Point 170: 10125 10427; 10121 10429; 10119 10431; 10119 10434; 10121 10437; 10124 10438; 10127 10438; 10129 10436; 10129 10432; 10129 10430; 10127 10428;
Point 171: 10143 10355; 10139 10359; 10137 10360; 10138 10363; 10140 10365; 10143 10366; 10147 10364; 10148 10361; 10147 10357;
Point 172: 10178 10411; 10175 10412; 10173 10414; 10173 10417; 10175 10421; 10178 10422; 10182 10420; 10183 10417; 10182 10414; 10181 10411;

Point 173: 10148 10531; 10146 10532; 10144 10535; 10144 10538; 10147 10540; 10148 10541; 10152 10540; 10154 10538; 10154 10534; 10152 10531;
Point 174: 10168 10458; 10164 10459; 10162 10461; 10163 10464; 10165 10467; 10168 10468; 10172 10465; 10172 10461; 10170 10458;
Point 175: 9443 10284; 9441 10284; 9439 10286; 9439 10288; 9440 10291; 9442 10292; 9445 10292; 9447 10290; 9447 10287; 9446 10285;
Point 176: 9418 10383; 9416 10384; 9414 10386; 9414 10389; 9416 10391; 9418 10392; 9421 10391; 9422 10389; 9422 10386; 9420 10384;
Point 177: 9434 10322; 9430 10323; 9429 10325; 9429 10328; 9432 10331; 9435 10331; 9438 10329; 9438 10325; 9436 10323;
Point 178: 9120 10197; 9117 10199; 9116 10200; 9116 10202; 9118 10205; 9121 10205; 9123 10204; 9125 10201; 9123 10198;
Point 179: 9100 10279; 9097 10280; 9096 10282; 9096 10284; 9097 10286; 9100 10287; 9103 10286; 9103 10283; 9103 10281; 9101 10279;
Point 180: 9113 10229; 9109 10231; 9109 10234; 9109 10236; 9112 10237; 9115 10236; 9116 10234; 9116 10230;
Point 181: 8917 11176; 8913 11178; 8911 11180; 8910 11183; 8911 11186; 8912 11188; 8914 11189; 8918 11191; 8923 11189; 8925 11185; 8924 11181; 8921 11177;
Point 182: 8914 11181; 8910 11182; 8907 11185; 8907 11187; 8908 11192; 8911 11194; 8915 11195; 8919 11194; 8921 11190; 8921 11186; 8919 11183; 8917 11181;
Point 183: 8916 11179; 8911 11180; 8909 11184; 8909 11188; 8911 11191; 8915 11194; 8921 11191; 8923 11187; 8923 11182; 8920 11179;
Point 184: 8571 11385; 8567 11387; 8565 11389; 8564 11392; 8567 11398; 8572 11400; 8576 11398; 8578 11394; 8577 11391; 8577 11389; 8576 11387;
Point 185: 8575 11364; 8570 11365; 8568 11369; 8568 11372; 8570 11378; 8573 11378; 8578 11376; 8580 11372; 8580 11368; 8577 11365;
Point 186: 8572 11378; 8567 11381; 8566 11385; 8567 11390; 8571 11391; 8577 11391; 8579 11387; 8579 11383; 8577 11380;
Point 187: 11921 12012; 11919 12013; 11919 12015; 11919 12017; 11920 12019; 11922 12019; 11925 12018; 11925 12016; 11925 12015; 11924 12013;
Point 188: 11899 12109; 11896 12110; 11896 12111; 11895 12113; 11897 12115; 11900 12115; 11901 12114; 11902 12111; 11901 12109;
Point 189: 11914 12049; 11911 12050; 11911 12052; 11912 12054; 11914 12056; 11916 12055; 11917 12052; 11916 12050;
Point 190: 9730 9984; 9728 9985; 9726 9986; 9726 9988; 9728 9991; 9730 9991; 9732 9991; 9733 9989; 9733 9987; 9732 9985;
Point 191: 9704 10091; 9702 10091; 9700 10092; 9700 10095; 9701 10097; 9703 10098; 9707 10097; 9707 10094; 9706 10092; 9705 10091;
Point 192: 9720 10026; 9718 10027; 9716 10029; 9717 10031; 9718 10033; 9722 10033; 9723 10031; 9723 10028; 9722 10026;
Point 193: 8312 11722; 8306 11724; 8302 11727; 8301 11731; 8302 11735; 8304 11740; 8308 11742; 8315 11743; 8319 11740; 8321 11736; 8321 11732; 8321 11728; 8319 11724; 8315 11721;
Point 194: 8323 11658; 8318 11660; 8315 11663; 8314 11668; 8314 11671; 8317 11676; 8321 11678; 8327 11678; 8331 11676; 8333 11672;
Point 195: 8316 11699; 8310 11702; 8306 11706; 8305 11711; 8307 11715; 8311 11719; 8316 11721; 8321 11719; 8325 11714; 8326 11709; 8325 11704; 8322 11701;

# APPENDIX VII: Data and Results of Chapter 4

**Table 1 Coordinates of Ground Control Points and Image Coordinate Residue before RPC Refinement**

| No | X (m) | Y (m) | H (m) | Column (pixel) | Row (pixel) |
|---|---|---|---|---|---|
| 1 | 392036.6277 | 155877.5606 | 3.5041 | 3.595864 | 24.03925 |
| 2 | 366967.8819 | 159509.6738 | 58.8329 | -1.72234 | 19.11356 |
| 3 | 371764.358 | 157086.8601 | 47.763 | 1.379613 | 19.36164 |
| 4 | 356139.6847 | 159783.5595 | 5.6422 | 1.077857 | 17.59935 |
| 5 | 382326.7206 | 153376.2986 | 2.852 | 0.15996 | 22.13981 |
| 6 | 384377.4289 | 152709.9586 | 2.753 | 1.220399 | 22.45898 |
| 7 | 380746.9801 | 152862.0239 | 5.3869 | 2.86517 | 20.84356 |
| 8 | 383878.6158 | 151486.1033 | 43.272 | 3.51649 | 21.47576 |
| 9 | 358524.9995 | 156528.1055 | 4.1755 | -1.59599 | 17.89804 |
| 10 | 376641.673 | 150672.406 | 64.089 | 1.508824 | 21.09634 |
| 11 | 392344.1561 | 147087.2497 | 4.1697 | 4.422933 | 23.89347 |
| 12 | 372448.3874 | 151041.2767 | 93.226 | 1.97344 | 19.22113 |
| 13 | 358914.527 | 153698.255 | 7.7727 | 0.195417 | 17.99683 |
| 14 | 392560.0307 | 145779.1242 | 4.1686 | 4.535597 | 24.41091 |
| 15 | 361579.578 | 152522.034 | 96.711 | 0.731811 | 16.93213 |
| 16 | 355030.59 | 152852.15 | 19.6852 | -1.44726 | 17.29342 |
| 17 | 360370.1 | 150966.47 | 61.7264 | -0.90008 | 17.80824 |
| 18 | 384642.509 | 145338.739 | 2.4403 | 2.82828 | 22.65799 |
| 19 | 360615.8612 | 149246.3082 | 91.31 | -0.28365 | 18.58585 |
| 20 | 382288.196 | 144291.54 | 2.895 | 3.580121 | 22.39936 |
| 21 | 375217.8526 | 145543.8963 | 77.585 | 2.563183 | 20.50194 |
| 22 | 356750.252 | 148781.729 | 88.598 | -0.41518 | 17.4938 |
| 23 | 376128.104 | 144301.694 | 1.9293 | 2.715756 | 21.59622 |
| 24 | 348791.57 | 150028.1484 | 4.8572 | -3.05707 | 16.19862 |
| 25 | 358060.4458 | 147898.8017 | 71.439 | -1.01157 | 17.55684 |
| 26 | 367261.889 | 145645.561 | 75.072 | 1.83767 | 18.68183 |
| 27 | 377255.4163 | 142995.1709 | 2.8321 | 2.080628 | 21.49094 |
| 28 | 348488.342 | 149315.701 | 3.984 | -2.57301 | 14.92662 |
| 29 | 363118.302 | 145512.918 | 83.64 | 0.674627 | 18.0105 |
| 30 | 360901.288 | 145835.575 | 78.217 | -0.96903 | 17.90765 |
| 31 | 365305.802 | 144691.909 | 87.062 | 1.055944 | 18.92246 |
| 32 | 370120.6596 | 142684.4332 | 78.841 | 0.777252 | 18.50515 |
| 33 | 372521.923 | 141194.164 | 3.1089 | 0.887035 | 19.69875 |
| 34 | 353398.1688 | 145389.3206 | 6.8632 | -1.08737 | 14.66035 |
| 35 | 357396.9564 | 142514.9403 | 4.6579 | -2.19854 | 19.10547 |
| 36 | 362849.4785 | 135985.1405 | 12.644 | -1.19665 | 18.15925 |
| 37 | 363935.9508 | 135562.4915 | 28.7268 | -1.5459 | 21.00786 |

**Table 2 Image Coordinate Residuals of CHK points after RPC refinement with 1 GCP and 3 GCPs by the Bias Compensation method and the Generic method**

| No | 1 GCP, 36 CHKs | | | | No | 3 GCPs, 34 CHKs | | | |
|---|---|---|---|---|---|---|---|---|---|
| | Bias-Compensation | | Generic method | | | Bias-Compensation | | Generic method | |
| | Column error (pixel) | Row error (pixel) | Column error (pixel) | Row error (pixel) | | Column error (pixel) | Row error (pixel) | Column error (pixel) | Row error (pixel) |
| 1 | -0.93973 | -0.37166 | -0.92631 | -0.38105 | 1 | -1.26633 | 0.424825 | -1.26612 | 0.414457 |
| 2 | -6.25793 | -5.29735 | -6.15294 | -5.33117 | 2 | -2.37558 | 0.891606 | -2.38025 | 0.885944 |
| 3 | -3.15598 | -5.04927 | -3.06886 | -5.07842 | 3 | 2.267838 | 1.580485 | 2.245135 | 1.564904 |
| 4 | -3.45774 | -6.81156 | -3.31952 | -6.86278 | 4 | -2.90035 | 0.36075 | -2.89345 | 0.353001 |
| 5 | -4.37564 | -2.2711 | -4.32859 | -2.29129 | 5 | -2.16984 | 0.212412 | -2.16305 | 0.203894 |
| 6 | -3.3152 | -1.95193 | -3.27599 | -1.97036 | 6 | 0.101664 | -0.64528 | 0.108929 | -0.65245 |
| 7 | -1.67043 | -3.56735 | -1.61825 | -3.58884 | 7 | 0.266499 | -0.74814 | 0.274671 | -0.75513 |
| 8 | -1.01911 | -2.93515 | -0.97845 | -2.95264 | 8 | -0.67606 | 1.180962 | -0.69186 | 1.167177 |
| 9 | -6.13159 | -6.51287 | -6.00378 | -6.56019 | 9 | -0.446 | 0.306193 | -0.43737 | 0.302463 |
| 10 | -3.02677 | -3.31458 | -2.96133 | -3.33681 | 10 | -0.12889 | -0.38344 | -0.12526 | -0.39485 |
| 11 | -0.11266 | -0.51744 | -0.10699 | -0.52857 | 11 | 0.731973 | -0.68406 | 0.738905 | -0.68711 |
| 12 | -2.56216 | -5.18978 | -2.48166 | -5.21513 | 12 | 1.168738 | 1.012149 | 1.156651 | 0.999886 |
| 13 | -4.34018 | -6.41408 | -4.21535 | -6.4589 | 13 | 1.302751 | -0.6633 | 1.297456 | -0.67108 |
| 14 | -3.80379 | -7.47879 | -3.68649 | -7.51672 | 14 | 0.227532 | 1.036171 | 0.210811 | 1.021428 |
| 15 | -5.98285 | -7.11749 | -5.8454 | -7.16606 | 15 | -0.05767 | 0.350666 | -0.0634 | 0.342796 |
| 16 | -5.43567 | -6.60267 | -5.31584 | -6.64126 | 16 | -0.30136 | -0.14348 | -0.29303 | -0.14657 |
| 17 | -1.70732 | -1.75292 | -1.67691 | -1.76606 | 17 | 0.591019 | 0.965573 | 0.588249 | 0.960344 |
| 18 | -4.81924 | -5.82506 | -4.7004 | -5.86027 | 18 | 0.905322 | 0.012473 | 0.914484 | 0.012365 |
| 19 | -0.95548 | -2.01155 | -0.91804 | -2.02449 | 19 | 1.071046 | -0.34194 | 1.081724 | -0.33931 |
| 20 | -1.97241 | -3.90897 | -1.90685 | -3.92601 | 20 | 1.142051 | 0.623322 | 1.135051 | 0.615764 |
| 21 | -4.95077 | -6.91711 | -4.81886 | -6.95612 | 21 | 1.11331 | 0.476337 | 1.123154 | 0.47868 |
| 22 | -1.81984 | -2.8147 | -1.76029 | -2.83147 | 22 | -0.19857 | 1.005054 | -0.22026 | 0.986306 |
| 23 | -7.59267 | -8.21229 | -7.43398 | -8.26546 | 23 | 0.357513 | 0.36149 | 0.353144 | 0.355728 |
| 24 | -5.54716 | -6.85407 | -5.42031 | -6.89074 | 24 | 1.718758 | -0.53043 | 1.725855 | -0.52842 |
| 25 | -2.69793 | -5.72908 | -2.60417 | -5.75288 | 25 | 0.336853 | 0.051459 | 0.347029 | 0.055506 |
| 26 | -2.45497 | -2.91997 | -2.40099 | -2.93399 | 26 | 0.367425 | -0.25368 | 0.34667 | -0.27193 |
| 27 | -7.10861 | -9.4843 | -6.94873 | -9.53674 | 27 | 1.276209 | -0.36784 | 1.280411 | -0.36708 |
| 28 | -3.86097 | -6.40042 | -3.75247 | -6.42777 | 28 | 1.315403 | 0.044935 | 1.322248 | 0.047859 |
| 29 | -5.50462 | -6.50327 | -5.38821 | -6.53355 | 29 | 0.288764 | -1.48905 | 0.299549 | -1.4822 |
| 30 | -3.47965 | -5.48845 | -3.37931 | -5.51232 | 30 | 0.040787 | -0.89227 | 0.051441 | -0.88489 |
| 31 | -3.75835 | -5.90576 | -3.67708 | -5.92251 | 31 | 1.182589 | -1.76755 | 1.175522 | -1.77548 |
| 32 | -3.64856 | -4.71216 | -3.57907 | -4.7269 | 32 | -0.49164 | 1.678732 | -0.48996 | 1.677736 |
| 33 | -5.62297 | -9.75056 | -5.48084 | -9.79066 | 33 | -0.15116 | -0.80966 | -0.13837 | -0.80069 |
| 34 | -6.73414 | -5.30544 | -6.60714 | -5.33688 | 34 | -0.66906 | 1.790866 | -0.65536 | 1.801244 |
| 35 | -5.73225 | -6.25166 | -5.62902 | -6.27009 | | | | | |
| 36 | -6.0815 | -3.40305 | -5.98264 | -3.41948 | | | | | |

**Table 3 Image Coordinate Residuals of 30 CHK points after RPC refinement with 7 GCPs by the Bias Compensation method and the Generic method.**

| No. | Bias-Compensation | | Generic method | |
|---|---|---|---|---|
| | Column | Row | Column | Row |
| 1 | -1.286026 | 0.776871 | -1.29503 | 0.768402 |
| 2 | -2.803578 | 1.15122 | -2.812543 | 1.148228 |
| 3 | 1.660251 | 1.782666 | 1.636296 | 1.770831 |
| 4 | -3.097172 | 0.622585 | -3.095424 | 0.615621 |
| 5 | -2.334874 | 0.476697 | -2.333441 | 0.468856 |
| 6 | -0.124389 | -0.399604 | -0.121534 | -0.406158 |
| 7 | 0.08709 | -0.503735 | 0.090735 | -0.510394 |
| 8 | -1.259181 | 1.351378 | -1.274891 | 1.340142 |
| 9 | -0.752162 | 0.498008 | -0.745456 | 0.494269 |
| 10 | 0.35647 | -0.511016 | 0.362539 | -0.513923 |
| 11 | 0.57879 | 1.145433 | 0.568434 | 1.134879 |
| 12 | -0.431305 | 1.135719 | -0.444556 | 1.122874 |
| 13 | -0.636415 | 0.454166 | -0.639182 | 0.447097 |
| 14 | -0.496041 | 0.019971 | -0.488995 | 0.015667 |
| 15 | 0.008141 | 1.046528 | 0.009312 | 1.041599 |
| 16 | 0.665696 | 0.147932 | 0.67486 | 0.146252 |
| 17 | 0.492346 | 0.675943 | 0.490816 | 0.668932 |
| 18 | 0.769131 | 0.576808 | 0.780886 | 0.577473 |
| 19 | -0.974459 | 1.030139 | -0.988924 | 1.013336 |
| 20 | 1.230699 | -0.461791 | 1.241768 | -0.460916 |
| 21 | 0.005705 | 0.140208 | 0.018182 | 0.142241 |
| 22 | -0.416864 | -0.240209 | -0.429844 | -0.256675 |
| 23 | 0.717818 | -0.324567 | 0.727424 | -0.324731 |
| 24 | 0.789902 | 0.089203 | 0.801926 | 0.090842 |
| 25 | -0.164958 | -1.44531 | -0.149386 | -1.440488 |
| 26 | -0.378909 | -0.855494 | -0.363389 | -0.850588 |
| 27 | 0.461433 | -1.780943 | 0.463044 | -1.788901 |
| 28 | -1.159539 | 1.648013 | -1.148727 | 1.645742 |
| 29 | -0.758303 | -0.900212 | -0.734317 | -0.894743 |
| 30 | -1.259999 | 1.700593 | -1.235235 | 1.707296 |

## Table 4 Coordinates of 113 Ground Control Points on the IKONOS image

| No | X | Y | H | Column | Row | No | X | Y | H | Column | Row |
|---|---|---|---|---|---|---|---|---|---|---|---|
| 1 | 519653.6 | 5259759 | 94.4649 | 3206 | 944 | 58 | 528461.6 | 5255802 | 1.3629 | 11992 | 4870 |
| 2 | 519885.4 | 5260272 | 59.0294 | 3430 | 419 | 59 | 524687 | 5252131 | 228.3833 | 8265 | 8616 |
| 3 | 518944.5 | 5259597 | 129.6879 | 2503 | 1118 | 60 | 525993.5 | 5255426 | -0.0184 | 9525 | 5246 |
| 4 | 516531.6 | 5256908 | 356.3429 | 131 | 3882 | 61 | 525995 | 5255427 | -0.0231 | 9527 | 5245 |
| 5 | 516542.1 | 5256847 | 359.2805 | 142 | 3944 | 62 | 525975.8 | 5255446 | -0.0126 | 9507 | 5225 |
| 6 | 520082.3 | 5257453 | 132.5842 | 3640 | 3264 | 63 | 525974.2 | 5255444 | -0.0035 | 9506 | 5227 |
| 7 | 517316.4 | 5258410 | 367.125 | 919 | 2383 | 64 | 525771.2 | 5255299 | 4.9848 | 9306 | 5374 |
| 8 | 517048.9 | 5260566 | 450.2904 | 667 | 255 | 65 | 525825.3 | 5255290 | 4.9406 | 9358 | 5383 |
| 9 | 521934.8 | 5256623 | 45.5947 | 5477 | 4065 | 66 | 525832.8 | 5255335 | 4.9516 | 9365 | 5338 |
| 10 | 522043.8 | 5256839 | 39.6236 | 5585 | 3846 | 67 | 525840.2 | 5255380 | 4.9526 | 9373 | 5294 |
| 11 | 521698 | 5257023 | 39.263 | 5239 | 3662 | 68 | 525786 | 5255389 | 4.923 | 9320 | 5285 |
| 12 | 521825.6 | 5257348 | 27.5097 | 5365 | 3334 | 69 | 525778.6 | 5255344 | 4.9383 | 9313 | 5330 |
| 13 | 521244.3 | 5260186 | 0.7069 | 4778 | 486 | 70 | 525727.2 | 5255379 | 3.2137 | 9259 | 5294 |
| 14 | 521204.7 | 5260177 | 0.6069 | 4740 | 496 | 71 | 525736.1 | 5255433 | 3.2066 | 9268 | 5240 |
| 15 | 523037.6 | 5258693 | 0.1624 | 6572 | 1980 | 72 | 525691.1 | 5255441 | 3.1983 | 9224 | 5233 |
| 16 | 523668.9 | 5258150 | 7.379 | 7204 | 2525 | 73 | 525646 | 5255448 | 3.2057 | 9179 | 5226 |
| 17 | 523203.8 | 5256485 | 41.6249 | 6745 | 4201 | 74 | 525637.1 | 5255394 | 3.2117 | 9171 | 5279 |
| 18 | 522628.2 | 5257381 | 17.3837 | 6165 | 3297 | 75 | 525682.1 | 5255387 | 3.2223 | 9215 | 5286 |
| 19 | 522324 | 5257408 | 21.3512 | 5862 | 3271 | 76 | 526605.6 | 5253786 | 83.3369 | 10154 | 6911 |
| 20 | 524077 | 5258097 | -0.0502 | 7611 | 2576 | 77 | 525750.5 | 5252976 | 52.5855 | 9293 | 7714 |
| 21 | 521030.9 | 5256558 | 82.4803 | 4580 | 4141 | 78 | 524415.2 | 5253774 | 102.867 | 7968 | 6932 |
| 22 | 527445.5 | 5260013 | 8.9504 | 10980 | 663 | 79 | 526335.4 | 5253935 | 85.0177 | 9884 | 6764 |
| 23 | 526240.8 | 5259239 | 9.0741 | 9775 | 1436 | 80 | 526337.6 | 5253938 | 85.0253 | 9885 | 6763 |
| 24 | 524934.2 | 5257747 | 6.2341 | 8469 | 2928 | 81 | 526313.9 | 5253954 | 84.7857 | 9862 | 6746 |
| 25 | 524927.1 | 5257783 | 6.2267 | 8462 | 2891 | 82 | 526311.6 | 5253951 | 84.8301 | 9861 | 6750 |
| 26 | 526289.6 | 5257432 | 13.559 | 9825 | 3245 | 83 | 527486.3 | 5252698 | 19.2781 | 11022 | 7981 |
| 27 | 526224.2 | 5257545 | 21.0215 | 9761 | 3133 | 84 | 520303.1 | 5248556 | 689.8207 | 3967 | 12343 |
| 28 | 528311.9 | 5259240 | 104.9297 | 11864 | 1467 | 85 | 519309.6 | 5250656 | 1256.757 | 3081 | 10428 |
| 29 | 525376.6 | 5256600 | 43.5848 | 8918 | 4085 | 86 | 519316.6 | 5250748 | 1260.679 | 3089 | 10337 |
| 30 | 524301.3 | 5260570 | 51.6418 | 7845 | 119 | 87 | 519321.6 | 5250827 | 1259.022 | 3094 | 10258 |
| 31 | 528188.6 | 5257126 | -2.3928 | 11719 | 3545 | 88 | 519402.5 | 5250745 | 1258.22 | 3174 | 10338 |
| 32 | 528546.9 | 5257092 | 10.2284 | 12079 | 3583 | 89 | 519320.6 | 5250669 | 1257.318 | 3092 | 10415 |
| 33 | 528567.2 | 5257097 | 10.5894 | 12100 | 3579 | 90 | 519413.7 | 5250786 | 1256.844 | 3185 | 10298 |
| 34 | 520370.5 | 5255001 | 167.4864 | 3936 | 5727 | 91 | 522733 | 5250246 | 190.2642 | 6303 | 10489 |
| 35 | 520425.2 | 5255532 | 112.9719 | 3980 | 5178 | 92 | 523828 | 5249000 | 251.9132 | 7410 | 11754 |
| 36 | 520408.7 | 5255511 | 114.2219 | 3964 | 5199 | 93 | 523800.2 | 5248990 | 251.8862 | 7383 | 11764 |
| 37 | 524435.5 | 5256337 | 19.8141 | 7972 | 4342 | 94 | 521236.9 | 5247757 | 423.0093 | 4851 | 13055 |
| 38 | 524524 | 5254609 | 41.5025 | 8065 | 6077 | 95 | 521230.9 | 5247763 | 423.2605 | 4844 | 13048 |
| 39 | 523996.7 | 5254353 | 58.7682 | 7541 | 6338 | 96 | 521561.9 | 5248346 | 433.8235 | 5179 | 12467 |
| 40 | 524088.5 | 5253833 | 95.0857 | 7639 | 6871 | 97 | 523912.7 | 5248541 | 284.7487 | 7501 | 12225 |
| 41 | 523943.3 | 5256150 | 25.0198 | 7481 | 4530 | 98 | 522712.1 | 5249281 | 287.0207 | 6300 | 11486 |
| 42 | 524040.5 | 5255977 | 29.3035 | 7579 | 4705 | 99 | 526619.1 | 5250363 | 16.1257 | 10154 | 10315 |
| 43 | 524381.5 | 5253171 | 183.7533 | 7949 | 7563 | 100 | 526644.6 | 5250260 | 13.1207 | 10179 | 10416 |
| 44 | 522577.2 | 5254439 | 157.7802 | 6140 | 6286 | 101 | 525901.4 | 5250401 | 50.0069 | 9443 | 10288 |
| 45 | 522751.2 | 5254510 | 137.7189 | 6311 | 6208 | 102 | 525572.1 | 5250498 | 82.7498 | 9121 | 10201 |
| 46 | 522150.8 | 5255659 | 96.8164 | 5702 | 5043 | 103 | 525341 | 5249563 | 224.8773 | 8918 | 11183 |
| 47 | 523839.7 | 5256334 | 23.2047 | 7377 | 4346 | 104 | 524985.1 | 5249370 | 273.4112 | 8572 | 11391 |
| 48 | 523239.6 | 5255454 | 155.034 | 6803 | 5270 | 105 | 528381.2 | 5248675 | 56.5304 | 11922 | 12015 |
| 49 | 524721.5 | 5254838 | 24.99 | 8259 | 5843 | 106 | 528435.7 | 5248333 | 96.3145 | 11984 | 12369 |
| 50 | 524576.5 | 5254867 | 28.9348 | 8115 | 5815 | 107 | 527233.7 | 5250839 | -2.4923 | 10763 | 9832 |
| 51 | 524671.2 | 5254579 | 36.5935 | 8211 | 6106 | 108 | 525299.2 | 5251065 | 47.1107 | 8841 | 9623 |
| 52 | 525304.7 | 5254738 | 52.9904 | 8847 | 5953 | 109 | 526190.8 | 5250697 | 37.7947 | 9730 | 9988 |
| 53 | 524552.8 | 5253726 | 93.8594 | 8103 | 6977 | 110 | 525602.5 | 5248888 | 254.3795 | 9184 | 11868 |
| 54 | 524942 | 5253464 | 123.4042 | 8498 | 7249 | 111 | 525598.7 | 5248151 | 256.6078 | 9181 | 12606 |
| 55 | 525460.8 | 5252874 | 78.3815 | 9008 | 7825 | 112 | 524710 | 5249055 | 351.6752 | 8312 | 11732 |
| 56 | 526119.5 | 5253671 | 29.5483 | 9657 | 7011 | 113 | 525078.8 | 5248317 | 232.1978 | 8657 | 12432 |
| 57 | 525354.7 | 5255360 | 13.5233 | 8890 | 5317 | | | | | | |

**Table 5 Residue of 112 CHK points after RPC refinement with 1 GCP.**

| No | Generic (112 CHKs, 1 GCP) | | Bias (112 CHKs, 1 GCP) | | No | Generic (112 CHKs, 1 GCP) | | Bias (112 CHKs, 1 GCP) | |
|---|---|---|---|---|---|---|---|---|---|
| | Column (pixel) | Row (pixel) | Column (pixel) | Row (pixel) | | Column (pixel) | Row (pixel) | Column (pixel) | Row (pixel) |
| 1 | 0.329788 | 0.348275 | 0.347896 | 0.351736 | 57 | 1.40152 | 1.046512 | 1.384934 | 1.044002 |
| 2 | 1.511749 | 1.104575 | 1.52875 | 1.105962 | 58 | -0.388 | 0.353816 | -0.39021 | 0.364439 |
| 3 | 0.939715 | 0.508268 | 0.960616 | 0.513649 | 59 | 0.871773 | 0.779768 | 0.863226 | 0.777951 |
| 4 | 1.612974 | -0.11567 | 1.641792 | -0.10117 | 60 | 0.407125 | 0.149108 | 0.398575 | 0.14729 |
| 5 | 1.63539 | -0.3104 | 1.664141 | -0.29582 | 61 | 1.251867 | 1.548325 | 1.243398 | 1.546506 |
| 6 | 2.028573 | -1.20603 | 2.044237 | -1.20004 | 62 | 0.672296 | 1.232437 | 0.663831 | 1.23062 |
| 7 | 0.499236 | 0.411361 | 0.526872 | 0.425294 | 63 | -1.32854 | 0.820554 | -1.33631 | 0.819145 |
| 8 | -0.03776 | 0.165516 | -0.00749 | 0.179886 | 64 | 0.793142 | 0.744866 | 0.785185 | 0.743443 |
| 9 | 0.550926 | -0.14688 | 0.55808 | -0.14544 | 65 | 1.236929 | 0.694425 | 1.228987 | 0.692983 |
| 10 | 0.414426 | 0.371429 | 0.421257 | 0.372438 | 66 | 0.62156 | -0.33131 | 0.613633 | -0.33277 |
| 11 | 0.634417 | 0.225875 | 0.642516 | 0.226889 | 67 | -0.4949 | -0.25992 | -0.50264 | -0.26137 |
| 12 | -0.0401 | -0.12271 | -0.03244 | -0.12251 | 68 | -0.925 | -0.22782 | -0.93275 | -0.22925 |
| 13 | 1.047569 | 0.64238 | 1.058703 | 0.640146 | 69 | 1.343758 | 0.23338 | 1.336162 | 0.231846 |
| 14 | -0.50672 | -0.85004 | -0.49546 | -0.85226 | 70 | 1.239909 | 0.088546 | 1.23233 | 0.086989 |
| 15 | -0.49988 | -0.67913 | -0.49579 | -0.68134 | 71 | 0.219707 | -0.30723 | 0.212286 | -0.30878 |
| 16 | -0.13645 | -0.53399 | -0.13468 | -0.53573 | 72 | 0.225491 | -0.68784 | 0.218229 | -0.68938 |
| 17 | 0.346165 | 0.208082 | 0.348955 | 0.209021 | 73 | -0.68317 | 0.450633 | -0.69045 | 0.449118 |
| 18 | 0.375507 | 0.296518 | 0.380311 | 0.29591 | 74 | 0.314291 | 0.854168 | 0.306854 | 0.852644 |
| 19 | 0.096831 | 0.222757 | 0.102756 | 0.222451 | 75 | 0.238161 | 2.87053 | 0.22826 | 2.873812 |
| 20 | -0.62151 | -0.18028 | -0.62133 | -0.18256 | 76 | 0.217044 | -0.18082 | 0.208578 | -0.1786 |
| 21 | 0.881553 | 0.791166 | 0.892439 | 0.794826 | 77 | 0.205709 | 0.834394 | 0.203603 | 0.839227 |
| 22 | -0.43075 | -0.47042 | -0.43995 | -0.47373 | 78 | 0.49951 | 1.945467 | 0.490695 | 1.948845 |
| 23 | 0.242065 | -0.18212 | 0.236271 | -0.18484 | 79 | 1.668093 | -0.14916 | 1.659273 | -0.14578 |
| 24 | -0.58901 | -0.87919 | -0.5918 | -0.8812 | 80 | 0.944545 | 0.163988 | 0.935815 | 0.167352 |
| 25 | -0.65957 | 0.853125 | -0.66231 | 0.851103 | 81 | -0.36136 | -0.71628 | -0.37009 | -0.71291 |
| 26 | -0.21197 | 0.17806 | -0.21936 | 0.176233 | 82 | -0.23227 | -0.39758 | -0.2478 | -0.39756 |
| 27 | -0.08089 | 1.019504 | -0.08776 | 1.018089 | 83 | 2.204674 | -0.04017 | 2.213014 | -0.02294 |
| 28 | 0.80231 | 0.006145 | 0.791923 | 0.008067 | 84 | 1.243444 | 0.398114 | 1.237081 | 0.387626 |
| 29 | -0.12728 | 2.139037 | -0.13154 | 2.139461 | 85 | 0.986686 | 0.678371 | 0.98017 | 0.66753 |
| 30 | -0.15518 | -0.07334 | -0.15233 | -0.07362 | 86 | 0.639563 | 0.756742 | 0.633183 | 0.745998 |
| 31 | 0.838945 | 0.128946 | 0.824389 | 0.125792 | 87 | 1.571968 | 2.002901 | 1.565291 | 1.992234 |
| 32 | 1.552965 | 0.651837 | 1.537514 | 0.649364 | 88 | 1.387816 | 0.624625 | 1.381398 | 0.614084 |
| 33 | 0.928787 | 0.242209 | 0.913281 | 0.239751 | 89 | 1.536987 | 0.545193 | 1.53038 | 0.534614 |
| 34 | 0.59429 | -0.59357 | 0.607664 | -0.58524 | 90 | 0.216636 | 0.646811 | 0.21876 | 0.657306 |
| 35 | 1.090727 | -0.69946 | 1.103362 | -0.69376 | 91 | 0.231564 | 1.063951 | 0.229888 | 1.076779 |
| 36 | 0.824046 | 0.262009 | 0.836742 | 0.267782 | 92 | -0.6287 | 0.958016 | -0.63029 | 0.970854 |
| 37 | 0.477435 | -0.00632 | 0.47546 | -0.00689 | 93 | 1.160908 | -0.21178 | 1.167737 | -0.19407 |
| 38 | 0.060008 | 0.017328 | 0.05681 | 0.018618 | 94 | 2.27456 | 0.041516 | 2.281414 | 0.059237 |
| 39 | 0.215677 | 0.573356 | 0.214448 | 0.575828 | 95 | 0.359593 | 2.231636 | 0.365862 | 2.249224 |
| 40 | 1.005275 | -0.17277 | 1.004138 | -0.16826 | 96 | 0.366759 | -0.17077 | 0.36478 | -0.15682 |
| 41 | 0.373447 | 0.250377 | 0.373083 | 0.250306 | 97 | 1.173359 | -0.46699 | 1.175974 | -0.45292 |
| 42 | 0.374183 | -0.05172 | 0.373461 | -0.05151 | 98 | 0.055267 | 0.36978 | 0.040599 | 0.37079 |
| 43 | 1.342784 | -0.52035 | 1.341811 | -0.51171 | 99 | -0.0976 | 0.569204 | -0.11253 | 0.570071 |
| 44 | 1.185889 | -0.51494 | 1.191493 | -0.50738 | 100 | 0.383017 | 0.198529 | 0.371751 | 0.201616 |
| 45 | 0.287896 | 0.099209 | 0.292623 | 0.105816 | 101 | -0.33038 | 0.466381 | -0.33964 | 0.471233 |
| 46 | 1.265098 | 2.005305 | 1.271924 | 2.009716 | 102 | -0.15187 | 0.469273 | -0.15848 | 0.480608 |
| 47 | 0.522526 | 0.355683 | 0.522615 | 0.355468 | 103 | -0.3382 | 1.482677 | -0.34318 | 1.495733 |
| 48 | 0.281641 | -0.61512 | 0.27755 | -0.6149 | 104 | 1.641923 | 1.137911 | 1.62085 | 1.141341 |
| 49 | 0.020016 | -0.17363 | 0.01654 | -0.17316 | 105 | 2.208233 | 2.573475 | 2.187668 | 2.579049 |
| 50 | 0.244937 | -0.26097 | 0.241094 | -0.25998 | 106 | 1.690564 | 0.490038 | 1.673649 | 0.489597 |
| 51 | 0.706169 | -0.62637 | 0.700761 | -0.62471 | 107 | -0.1519 | -0.01011 | -0.16062 | -0.00728 |
| 52 | 0.988543 | 0.287697 | 0.98574 | 0.292072 | 108 | 0.278721 | 0.093115 | 0.266398 | 0.095338 |
| 53 | 0.93574 | -0.30047 | 0.932041 | -0.29468 | 109 | 1.234376 | 0.358158 | 1.226706 | 0.370644 |
| 54 | 0.651285 | -0.66069 | 0.64434 | -0.65699 | 110 | 0.919759 | 0.163409 | 0.911527 | 0.176203 |
| 55 | 0.583767 | 0.162702 | 0.574059 | 0.163269 | 111 | 0.014263 | 0.790403 | 0.010559 | 0.805607 |
| 56 | 0.051599 | 0.282398 | 0.045528 | 0.281581 | 112 | 0.099009 | -0.39968 | 0.092354 | -0.3876 |

## Table 6 Residue of 104 CHK points after RPC refinement with 9 GCPs.

| No | Generic (104 CHKs, 9 GCPs) | | Bias (104 CHKs, 9 GCPs) | | No | Generic (104 CHKs, 9 GCPs) | | Bias (104 CHKs, 9 GCPs) | |
|---|---|---|---|---|---|---|---|---|---|
| | Column (pixel) | Row (pixel) | Column (pixel) | Row (pixel) | | Column (pixel) | Row (pixel) | Column (pixel) | Row (pixel) |
| 1 | 1.038921 | 1.330294 | 1.041529 | 1.33377 | 57 | 0.688975 | 1.361301 | 0.68865 | 1.361593 |
| 2 | 0.267473 | 0.692008 | 0.271625 | 0.698697 | 58 | -1.35483 | 0.940448 | -1.35495 | 0.941027 |
| 3 | 0.34558 | -0.07799 | 0.352612 | -0.06472 | 59 | 0.774175 | 0.865249 | 0.774025 | 0.865825 |
| 4 | 0.364271 | -0.275 | 0.371311 | -0.26168 | 60 | 1.223005 | 0.816718 | 1.22285 | 0.817293 |
| 5 | 1.339836 | -1.0899 | 1.343882 | -1.08309 | 61 | 0.612667 | -0.2071 | 0.612507 | -0.20653 |
| 6 | -0.51946 | 0.521021 | -0.51298 | 0.534414 | 62 | -0.51111 | -0.1362 | -0.51125 | -0.13563 |
| 7 | -0.90825 | 0.35633 | -0.90225 | 0.370494 | 63 | -0.94624 | -0.10601 | -0.94638 | -0.10544 |
| 8 | -0.03479 | 0.494255 | -0.03295 | 0.496758 | 64 | 1.317864 | 0.355782 | 1.317705 | 0.356263 |
| 9 | 0.149504 | 0.350635 | 0.15144 | 0.353125 | 65 | 1.220068 | 0.213243 | 1.219902 | 0.213721 |
| 10 | -0.47769 | 0.017025 | -0.47607 | 0.018899 | 66 | 0.193778 | -0.18294 | 0.193628 | -0.18246 |
| 11 | 0.770356 | 0.886229 | 0.771328 | 0.886643 | 67 | 0.193477 | -0.56396 | 0.193342 | -0.56348 |
| 12 | -0.79059 | -0.60715 | -0.78961 | -0.60674 | 68 | -0.72124 | 0.572217 | -0.72137 | 0.572701 |
| 13 | -0.63895 | -0.46674 | -0.63848 | -0.46638 | 69 | 0.282306 | 0.97616 | 0.282163 | 0.976643 |
| 14 | -0.22838 | -0.3334 | -0.22792 | -0.33266 | 70 | 0.205191 | 2.942754 | 0.206447 | 2.947338 |
| 15 | 0.039614 | 0.334896 | 0.041098 | 0.337475 | 71 | -0.01467 | -0.15404 | -0.01361 | -0.15086 |
| 16 | 0.06084 | 0.450164 | 0.061955 | 0.451481 | 72 | -0.15576 | 0.8718 | -0.15336 | 0.877338 |
| 17 | -0.26093 | 0.372725 | -0.25962 | 0.374261 | 73 | 0.43912 | 2.019374 | 0.440491 | 2.024038 |
| 18 | -0.65714 | 0.024577 | -0.65699 | 0.024895 | 74 | 1.608297 | -0.07509 | 1.609668 | -0.07043 |
| 19 | 0.256459 | 0.886735 | 0.259486 | 0.891355 | 75 | 0.882656 | 0.238345 | 0.884029 | 0.242997 |
| 20 | 0.629763 | 0.101981 | 0.629252 | 0.10273 | 76 | -0.42387 | -0.64208 | -0.42249 | -0.63743 |
| 21 | -0.52688 | -0.67489 | -0.52686 | -0.67425 | 77 | -0.22903 | -0.35455 | -0.22929 | -0.35313 |
| 22 | -0.59542 | 1.058718 | -0.5954 | 1.059356 | 78 | -0.14906 | 0.224935 | -0.16689 | 0.207868 |
| 23 | 0.025349 | 0.390913 | 0.025075 | 0.391907 | 79 | -0.39671 | 0.508942 | -0.41479 | 0.491539 |
| 24 | 0.156627 | 1.235818 | 0.156525 | 1.237216 | 80 | -0.73625 | 0.590522 | -0.75426 | 0.573252 |
| 25 | 1.500515 | 0.322082 | 1.501006 | 0.327508 | 81 | 0.201192 | 1.834707 | 0.18319 | 1.817507 |
| 26 | -0.09883 | 2.304329 | -0.0981 | 2.306937 | 82 | -0.0019 | 0.452131 | -0.01977 | 0.435016 |
| 27 | 0.058894 | 0.233237 | 0.05975 | 0.236247 | 83 | 0.171473 | 0.378815 | 0.153529 | 0.361726 |
| 28 | 1.33334 | 0.359398 | 1.332067 | 0.359459 | 84 | -0.63326 | 0.901273 | -0.62823 | 0.912338 |
| 29 | 2.098019 | 0.886448 | 2.096901 | 0.887201 | 85 | -1.49855 | 0.794509 | -1.49352 | 0.805574 |
| 30 | 1.477274 | 0.477315 | 1.476157 | 0.478087 | 86 | -0.19939 | -0.46543 | -0.19279 | -0.45127 |
| 31 | 0.285702 | -0.65435 | 0.289564 | -0.64833 | 87 | 0.913973 | -0.21195 | 0.920571 | -0.19779 |
| 32 | 0.014677 | 0.305994 | 0.018568 | 0.312067 | 88 | -0.90056 | 2.006461 | -0.89423 | 2.02073 |
| 33 | -0.2127 | 0.090058 | -0.21154 | 0.092642 | 89 | -0.52525 | -0.35059 | -0.51997 | -0.33869 |
| 34 | -0.1581 | 0.627567 | -0.15639 | 0.631041 | 90 | 0.166273 | -0.63611 | 0.171901 | -0.62412 |
| 35 | 0.600072 | -0.13806 | 0.602455 | -0.13286 | 91 | -0.43292 | 0.502037 | -0.43277 | 0.503287 |
| 36 | 0.148224 | 0.37551 | 0.14913 | 0.377211 | 92 | -0.05085 | 0.125144 | -0.04963 | 0.128329 |
| 37 | 0.148414 | 0.068009 | 0.149388 | 0.069935 | 93 | -0.80474 | 0.391551 | -0.80278 | 0.396314 |
| 38 | 0.924209 | -0.50794 | 0.927802 | -0.49918 | 94 | -0.74142 | 0.352786 | -0.73728 | 0.363026 |
| 39 | 0.60783 | -0.48005 | 0.611643 | -0.47223 | 95 | -0.9975 | 1.352669 | -0.99283 | 1.364268 |
| 40 | -0.25807 | 0.139751 | -0.2546 | 0.146774 | 96 | 1.428097 | 1.034503 | 1.428792 | 1.037961 |
| 41 | 0.729334 | 2.08249 | 0.732283 | 2.087756 | 97 | 1.972991 | 2.457065 | 1.97449 | 2.462383 |
| 42 | 0.297793 | 0.486509 | 0.298683 | 0.488113 | 98 | 1.493671 | 0.455212 | 1.493168 | 0.455561 |
| 43 | -0.39469 | 0.078776 | -0.39127 | 0.086435 | 99 | -0.61785 | -0.06643 | -0.61654 | -0.0634 |
| 44 | -0.22243 | -0.08973 | -0.22157 | -0.08781 | 100 | -0.08614 | 0.036108 | -0.08532 | 0.038653 |
| 45 | -0.00844 | -0.18712 | -0.00743 | -0.18479 | 101 | 0.625217 | 0.218704 | 0.629612 | 0.229789 |
| 46 | 0.56148 | -0.5364 | 0.562569 | -0.53327 | 102 | 0.245725 | -0.00547 | 0.250274 | 0.005659 |
| 47 | 0.643459 | 0.325415 | 0.645659 | 0.330549 | 103 | -0.71315 | 0.643126 | -0.70806 | 0.656355 |
| 48 | 0.626243 | -0.26726 | 0.6288 | -0.26085 | 104 | -0.63842 | -0.5699 | -0.63391 | -0.55945 |
| 49 | 0.36753 | -0.64263 | 0.3692 | -0.63819 | 57 | 0.688975 | 1.361301 | 0.68865 | 1.361593 |
| 50 | 0.467686 | 0.223059 | 0.46808 | 0.225014 | 58 | -1.35483 | 0.940448 | -1.35495 | 0.941027 |
| 51 | -0.03162 | 0.398143 | -0.03141 | 0.399202 | 59 | 0.774175 | 0.865249 | 0.774025 | 0.865825 |
| 52 | 1.821164 | 1.22846 | 1.819956 | 1.228743 | 60 | 1.223005 | 0.816718 | 1.22285 | 0.817293 |

**Table 7 Image Coordinate Residuals of 37 control points after the error is added into the ephemeris and attitude data in case 1, case 2, case 3, and case 4.**

| No | Case 1 | | Case 2 | | No | Case 3 | | Case 4 | |
|---|---|---|---|---|---|---|---|---|---|
| | Column error (pixel) | Row error (pixel) | Column error (pixel) | Row error (pixel) | | Column error (pixel) | Row error (pixel) | Column error (pixel) | Row error (pixel) |
| 1 | 33682.57 | 27779.47 | 3349.419 | 2483.732 | 1 | 338.2855 | 266.9507 | 539.3641 | 268.1397 |
| 2 | 33524.56 | 26798.64 | 3340.916 | 2381.335 | 2 | 332.7604 | 252.2784 | 531.2433 | 263.3146 |
| 3 | 33556.81 | 27000.22 | 3344.31 | 2401.65 | 3 | 335.8709 | 254.5348 | 534.9265 | 263.6085 |
| 4 | 33476.5 | 26392.03 | 3343.658 | 2339.287 | 4 | 335.5999 | 246.7129 | 532.7105 | 261.8934 |
| 5 | 33623.39 | 27434.11 | 3344.333 | 2447.408 | 5 | 334.7292 | 261.6128 | 534.9114 | 266.4263 |
| 6 | 33638.52 | 27517.35 | 3345.732 | 2455.997 | 6 | 335.8143 | 262.7594 | 536.2046 | 266.7513 |
| 7 | 33617.76 | 27377.84 | 3346.826 | 2440.591 | 7 | 337.4203 | 259.7657 | 537.4506 | 265.1645 |
| 8 | 33640.51 | 27506.33 | 3347.986 | 2453.974 | 8 | 338.1085 | 261.6745 | 538.4895 | 265.8191 |
| 9 | 33489.61 | 26509.84 | 3340.915 | 2351.23 | 9 | 332.909 | 248.1799 | 530.3704 | 262.292 |
| 10 | 33597.14 | 27240.27 | 3345.007 | 2426.971 | 10 | 336.0358 | 258.6363 | 535.7051 | 265.5387 |
| 11 | 33707.6 | 27868.06 | 3350.695 | 2492.109 | 11 | 339.1565 | 267.6683 | 540.3294 | 268.3222 |
| 12 | 33573.2 | 27076.36 | 3345.046 | 2408.906 | 12 | 336.4763 | 255.1431 | 535.7102 | 263.6894 |
| 13 | 33498.01 | 26549.09 | 3342.689 | 2355.118 | 13 | 334.6979 | 248.6618 | 532.2515 | 262.4931 |
| 14 | 33712.77 | 27888.39 | 3350.919 | 2494.528 | 14 | 339.2786 | 268.378 | 540.4798 | 268.8865 |
| 15 | 33513.12 | 26653.64 | 3343.245 | 2364.605 | 15 | 335.2254 | 248.6539 | 533.1839 | 261.4475 |
| 16 | 33480.26 | 26410.01 | 3341.097 | 2340.517 | 16 | 333.0775 | 246.5711 | 530.16 | 261.8576 |
| 17 | 33508.63 | 26624.78 | 3341.593 | 2362.395 | 17 | 333.5973 | 249.2238 | 531.406 | 262.3924 |
| 18 | 33659.9 | 27592.95 | 3347.634 | 2463.328 | 18 | 337.4486 | 263.6833 | 537.9308 | 267.2238 |
| 19 | 33513.65 | 26648.59 | 3342.211 | 2365.378 | 19 | 334.2136 | 250.2244 | 532.0964 | 263.2311 |
| 20 | 33648.54 | 27513.68 | 3348.028 | 2455.075 | 20 | 338.1746 | 262.6273 | 538.4392 | 267.0257 |
| 21 | 33601.8 | 27231.39 | 3346.012 | 2425.214 | 21 | 337.0908 | 257.9339 | 536.6743 | 265.1479 |
| 22 | 33496.21 | 26507.25 | 3342.068 | 2350.199 | 22 | 334.0984 | 247.725 | 531.5066 | 262.1916 |
| 23 | 33610.38 | 27281.65 | 3346.297 | 2431.102 | 23 | 337.2519 | 259.5083 | 536.8924 | 266.2789 |
| 24 | 33456.79 | 26201.74 | 3339.709 | 2318.474 | 24 | 331.5202 | 243.3864 | 527.8172 | 260.9241 |
| 25 | 33503.39 | 26565.08 | 3341.459 | 2355.976 | 25 | 333.4953 | 248.3599 | 531.0687 | 262.2746 |
| 26 | 33556.82 | 26930.63 | 3344.596 | 2393.444 | 26 | 336.3323 | 253.12 | 535.0371 | 263.3971 |
| 27 | 33619.67 | 27335.68 | 3345.837 | 2436.309 | 27 | 336.6282 | 259.9356 | 536.4001 | 266.2108 |
| 28 | 33457.21 | 26195.58 | 3340.197 | 2316.658 | 28 | 332.0066 | 242.0607 | 528.2739 | 259.6807 |
| 29 | 33534.52 | 26775.64 | 3343.234 | 2377.298 | 29 | 335.1683 | 250.9019 | 533.3978 | 262.7683 |
| 30 | 33521.17 | 26689.95 | 3341.527 | 2368.641 | 30 | 333.5283 | 249.9436 | 531.484 | 262.6739 |
| 31 | 33547.87 | 26865.7 | 3343.714 | 2387.076 | 31 | 335.5495 | 252.7009 | 534.049 | 263.6899 |
| 32 | 33578.03 | 27064.31 | 3343.782 | 2406.424 | 32 | 335.2828 | 254.2612 | 534.3476 | 263.3011 |
| 33 | 33595.4 | 27172.95 | 3344.14 | 2418.212 | 33 | 335.4051 | 256.5144 | 534.6977 | 264.5259 |
| 34 | 33486.79 | 26413.96 | 3341.414 | 2337.979 | 34 | 333.4449 | 243.955 | 530.4218 | 259.51 |
| 35 | 33509.95 | 26594.25 | 3340.241 | 2359.776 | 35 | 332.3095 | 250.1355 | 529.8327 | 264.0203 |
| 36 | 33553.28 | 26857.9 | 3341.408 | 2384.616 | 36 | 333.2974 | 251.7635 | 531.573 | 263.2504 |
| 37 | 33559.72 | 26904.58 | 3341.122 | 2391.816 | 37 | 332.9487 | 255.0472 | 531.3672 | 266.1041 |

**Table 8 Image Coordinate Residuals of 37 control points after the error is added into the ephemeris and attitude data in case 5, case 6, case 7, and case 8.**

| No | Case 5 | | Case 6 | | No | Case 7 | | Case 8 | |
|---|---|---|---|---|---|---|---|---|---|
| | Column error (pixel) | Row error (pixel) | Column error (pixel) | Row error (pixel) | | Column error (pixel) | Row error (pixel) | Column error (pixel) | Row error (pixel) |
| 1 | 57.18682 | 48.43465 | 8.952097 | 26.46434 | 1 | 33137.09 | 27452.94 | 3295.803 | 2458.525 |
| 2 | 51.58138 | 43.52222 | 3.599472 | 21.54313 | 2 | 32984.48 | 26472.33 | 3287.606 | 2356.121 |
| 3 | 54.74511 | 43.77494 | 6.710986 | 21.79173 | 3 | 33015.57 | 26673.78 | 3290.937 | 2376.431 |
| 4 | 54.24285 | 42.02027 | 6.380902 | 20.03307 | 4 | 32938.77 | 26065.74 | 3290.491 | 2314.066 |
| 5 | 53.65191 | 46.55664 | 5.50944 | 24.56983 | 5 | 33079.72 | 27107.46 | 3290.828 | 2422.185 |
| 6 | 54.73653 | 46.87637 | 6.573098 | 24.88905 | 6 | 33094.38 | 27190.65 | 3292.201 | 2430.772 |
| 7 | 56.3408 | 45.26483 | 8.213379 | 23.27502 | 7 | 33074.37 | 27051.15 | 3293.34 | 2415.365 |
| 8 | 57.03265 | 45.89977 | 8.870354 | 23.908 | 8 | 33096.36 | 27179.57 | 3294.458 | 2428.746 |
| 9 | 51.60601 | 42.33117 | 3.714247 | 20.33519 | 9 | 32951.16 | 26183.37 | 3287.713 | 2325.999 |
| 10 | 54.94691 | 45.53399 | 6.854839 | 23.53366 | 10 | 33054.42 | 26913.46 | 3291.563 | 2401.734 |
| 11 | 58.03745 | 48.32809 | 9.791216 | 26.32885 | 11 | 33161.39 | 27541.04 | 3297.064 | 2466.871 |
| 12 | 55.36415 | 43.66272 | 7.31351 | 21.66019 | 12 | 33031.36 | 26749.57 | 3291.652 | 2383.667 |
| 13 | 53.40994 | 42.44323 | 5.51043 | 20.43835 | 13 | 32959.29 | 26222.45 | 3289.478 | 2329.878 |
| 14 | 58.15484 | 48.85176 | 9.90529 | 26.84846 | 14 | 33166.41 | 27561.29 | 3297.283 | 2469.286 |
| 15 | 53.98854 | 41.38106 | 6.053512 | 19.37453 | 15 | 32973.68 | 26326.95 | 3289.991 | 2339.362 |
| 16 | 51.72226 | 41.74918 | 3.863314 | 19.73844 | 16 | 32942.31 | 26083.33 | 3287.934 | 2315.271 |
| 17 | 52.34382 | 42.26623 | 4.422164 | 20.25371 | 17 | 32969.37 | 26297.99 | 3288.355 | 2337.146 |
| 18 | 56.36251 | 47.11136 | 8.189023 | 25.10027 | 18 | 33115.14 | 27265.81 | 3294.091 | 2438.079 |
| 19 | 52.97024 | 43.05181 | 5.042164 | 21.03399 | 19 | 32974.19 | 26321.69 | 3288.965 | 2340.124 |
| 20 | 57.09041 | 46.86093 | 8.938996 | 24.8446 | 20 | 33104.18 | 27186.48 | 3294.511 | 2429.82 |
| 21 | 55.99733 | 44.96677 | 7.913443 | 22.94879 | 21 | 33058.97 | 26904.26 | 3292.578 | 2399.958 |
| 22 | 52.79268 | 41.96677 | 4.906021 | 19.94438 | 22 | 32957.54 | 26180.32 | 3288.872 | 2324.94 |
| 23 | 56.15751 | 46.06542 | 8.067783 | 24.04422 | 23 | 33067.31 | 26954.44 | 3292.855 | 2405.842 |
| 24 | 50.04289 | 40.67572 | 2.25059 | 18.65096 | 24 | 32919.99 | 25874.88 | 3286.626 | 2293.213 |
| 25 | 52.21381 | 42.03207 | 4.31298 | 20.00792 | 25 | 32964.39 | 26238.1 | 3288.246 | 2330.715 |
| 26 | 55.17962 | 43.15593 | 7.178086 | 21.13194 | 26 | 33015.68 | 26603.5 | 3291.261 | 2368.182 |
| 27 | 55.53751 | 45.96475 | 7.434964 | 23.94029 | 27 | 33076.26 | 27008.38 | 3292.379 | 2411.046 |
| 28 | 50.5255 | 39.40724 | 2.735802 | 17.37998 | 28 | 32920.43 | 25868.68 | 3287.116 | 2291.394 |
| 29 | 53.96853 | 42.49007 | 6.010017 | 20.46236 | 29 | 32994.25 | 26448.5 | 3289.951 | 2352.032 |
| 30 | 52.29712 | 42.3884 | 4.362959 | 20.35996 | 30 | 32981.4 | 26362.84 | 3288.273 | 2343.375 |
| 31 | 54.37809 | 43.403 | 6.395301 | 21.37442 | 31 | 33007.06 | 26538.51 | 3290.401 | 2361.809 |
| 32 | 54.15935 | 42.98862 | 6.124592 | 20.9575 | 32 | 33036.04 | 26736.99 | 3290.406 | 2381.154 |
| 33 | 54.29414 | 44.18535 | 6.237739 | 22.15143 | 33 | 33052.83 | 26845.53 | 3290.737 | 2392.939 |
| 34 | 52.08423 | 39.15109 | 4.235369 | 17.1153 | 34 | 32948.65 | 26086.81 | 3288.261 | 2312.706 |
| 35 | 51.02937 | 43.60214 | 3.133735 | 21.56043 | 35 | 32970.73 | 26266.9 | 3287.032 | 2334.495 |
| 36 | 52.10868 | 42.66859 | 4.14669 | 20.61055 | 36 | 33012.33 | 26530.08 | 3288.118 | 2359.317 |
| 37 | 51.77367 | 45.51745 | 3.798706 | 23.45892 | 37 | 33018.49 | 26576.73 | 3287.817 | 2366.516 |

**Table 9 Image Coordinate Residuals of 37 control points after the error is added into the ephemeris and attitude data in case 9.**

| No | Case 9 | |
|---|---|---|
| | Column error (pixel) | Row error (pixel) |
| 1 | 332.9255 | 264.5016 |
| 2 | 327.4286 | 249.8284 |
| 3 | 330.5334 | 252.0843 |
| 4 | 330.2816 | 244.262 |
| 5 | 329.3796 | 259.1619 |
| 6 | 330.4623 | 260.3084 |
| 7 | 332.0723 | 257.3144 |
| 8 | 332.7566 | 259.223 |
| 9 | 327.5873 | 245.728 |
| 10 | 330.6918 | 256.1838 |
| 11 | 333.7952 | 265.2159 |
| 12 | 331.1369 | 252.6904 |
| 13 | 329.3753 | 246.2089 |
| 14 | 333.917 | 265.9251 |
| 15 | 329.8988 | 246.2008 |
| 16 | 327.7595 | 244.1175 |
| 17 | 328.2723 | 246.77 |
| 18 | 332.0954 | 261.2296 |
| 19 | 328.8879 | 247.7701 |
| 20 | 332.8239 | 260.173 |
| 21 | 331.7477 | 255.4795 |
| 22 | 328.7773 | 245.2701 |
| 23 | 331.9081 | 257.0535 |
| 24 | 326.2096 | 240.9313 |
| 25 | 328.1726 | 245.9049 |
| 26 | 330.9984 | 250.665 |
| 27 | 331.283 | 257.4804 |
| 28 | 326.6963 | 239.6054 |
| 29 | 329.8391 | 248.4464 |
| 30 | 328.2019 | 247.4881 |
| 31 | 330.2176 | 250.2454 |
| 32 | 329.9451 | 251.8053 |
| 33 | 330.065 | 254.0582 |
| 34 | 328.128 | 241.4987 |
| 35 | 326.9874 | 247.6785 |
| 36 | 327.9678 | 249.3046 |
| 37 | 327.6177 | 252.5882 |

**Table 10 Image Coordinate Residuals of CHK points after RPC refinement by using 1 GCP in Case 1 and Case 2.**

| No | Case 1 (1 GCP, 36 CHKs) | | | | No | Case 2 (1 GCP, 36 CHKs) | | | |
|---|---|---|---|---|---|---|---|---|---|
| | Generic method | | Bias method | | | Generic method | | Bias method | |
| | Column error (pixel) | Row error (pixel) | Column error (pixel) | Row error (pixel) | | Column error (pixel) | Row error (pixel) | Column error (pixel) | Row error (pixel) |
| 1 | 1.858994 | -100.139 | -30.1998 | -108.921 | 1 | 0.025416 | -10.104 | -1.49921 | -10.7962 |
| 2 | 16.64064 | -1003.71 | -188.205 | -1089.74 | 2 | 3.704729 | -102.457 | -10.003 | -113.193 |
| 3 | 15.8582 | -818.792 | -155.953 | -888.164 | 3 | 4.907959 | -84.256 | -6.60824 | -92.8783 |
| 4 | 27.1682 | -1377.69 | -236.265 | -1496.36 | 4 | 10.45396 | -140.16 | -7.26102 | -155.241 |
| 5 | 5.966169 | -420.028 | -89.3769 | -454.276 | 5 | -0.2849 | -42.9592 | -6.58604 | -47.1199 |
| 6 | 5.217178 | -343.093 | -74.2484 | -371.041 | 6 | 0.015451 | -35.1827 | -5.18718 | -38.5313 |
| 7 | 9.817793 | -472.077 | -95.0129 | -510.553 | 7 | 2.924906 | -49.1931 | -4.09256 | -53.9368 |
| 8 | 7.423445 | -352.228 | -72.2567 | -382.057 | 8 | 2.368675 | -36.954 | -2.93233 | -40.5535 |
| 9 | 22.36345 | -1270.04 | -223.159 | -1378.55 | 9 | 6.641599 | -129.431 | -10.0038 | -143.298 |
| 10 | 10.90329 | -597.499 | -115.624 | -648.116 | 10 | 2.796336 | -61.1578 | -5.91207 | -67.5571 |
| 11 | 0.437872 | -18.6307 | -5.16832 | -20.3328 | 11 | 0.062003 | -2.28749 | -0.22357 | -2.41925 |
| 12 | 14.48186 | -747.782 | -139.566 | -812.026 | 12 | 4.749241 | -77.4644 | -5.87304 | -85.6217 |
| 13 | 23.37016 | -1234.23 | -214.757 | -1339.3 | 13 | 8.055605 | -125.858 | -8.2293 | -139.41 |
| 14 | 21.33926 | -1136.02 | -199.651 | -1234.74 | 14 | 7.496355 | -117.268 | -7.67385 | -129.923 |
| 15 | 24.07391 | -1361.27 | -232.505 | -1478.38 | 15 | 7.746621 | -138.828 | -9.82152 | -154.011 |
| 16 | 20.47089 | -1163.72 | -204.139 | -1263.61 | 16 | 6.186725 | -119.169 | -9.32574 | -132.133 |
| 17 | 5.024767 | -274.408 | -52.8662 | -295.443 | 17 | 0.94685 | -28.3044 | -3.28425 | -31.1994 |
| 18 | 20.42988 | -1141.32 | -199.114 | -1239.8 | 18 | 6.56079 | -116.284 | -8.70768 | -129.15 |
| 19 | 7.49404 | -348.154 | -64.2267 | -374.705 | 19 | 2.423677 | -35.7137 | -2.8908 | -39.4528 |
| 20 | 11.94738 | -606.541 | -110.97 | -656.999 | 20 | 3.9293 | -62.5626 | -4.90637 | -69.314 |
| 21 | 22.84908 | -1271.1 | -216.562 | -1381.14 | 21 | 7.788666 | -129.877 | -8.8505 | -144.329 |
| 22 | 11.58415 | -562.788 | -102.39 | -606.736 | 22 | 3.695804 | -57.323 | -4.62128 | -63.4264 |
| 23 | 26.0391 | -1552.59 | -255.979 | -1686.65 | 23 | 8.190696 | -158.388 | -11.2093 | -176.054 |
| 24 | 21.32572 | -1218.92 | -209.377 | -1323.31 | 24 | 6.652587 | -124.751 | -9.45952 | -138.552 |
| 25 | 17.26531 | -883.868 | -155.944 | -957.759 | 25 | 6.017706 | -91.1734 | -6.32311 | -101.084 |
| 26 | 9.78557 | -513.375 | -93.0945 | -552.711 | 26 | 2.562199 | -52.6085 | -5.0815 | -58.2186 |
| 27 | 26.60113 | -1558.55 | -255.561 | -1692.81 | 27 | 8.727404 | -160.113 | -10.7215 | -177.87 |
| 28 | 19.01061 | -1026.18 | -178.251 | -1112.75 | 28 | 6.31811 | -105.611 | -7.68453 | -117.23 |
| 29 | 19.01418 | -1104.9 | -191.598 | -1198.43 | 29 | 5.498648 | -113.354 | -9.39153 | -125.887 |
| 30 | 17.6542 | -943.566 | -164.899 | -1022.69 | 30 | 5.849322 | -96.7565 | -7.2048 | -107.452 |
| 31 | 13.48867 | -761.89 | -134.739 | -824.08 | 31 | 3.702307 | -79.4688 | -7.13692 | -88.1041 |
| 32 | 11.92699 | -664.633 | -117.366 | -715.435 | 32 | 2.877555 | -68.9375 | -6.77897 | -76.3159 |
| 33 | 24.30985 | -1360.38 | -225.977 | -1474.42 | 33 | 8.089576 | -141.109 | -9.5051 | -156.549 |
| 34 | 20.05393 | -1196.33 | -202.815 | -1294.14 | 34 | 5.290994 | -121.158 | -10.6777 | -134.752 |
| 35 | 16.00119 | -958.333 | -159.491 | -1030.48 | 35 | 3.790393 | -98.8834 | -9.51065 | -109.912 |
| 36 | 14.68685 | -914.988 | -153.044 | -983.804 | 36 | 3.011523 | -92.0968 | -9.79656 | -102.712 |

**Table 11 Image Coordinate Residuals of CHK points after RPC refinement by using 1 GCP in Case 3 and Case 4.**

| No | Case 3 (1 GCP, 36 CHKs) | | | | No | Case 4 (1 GCP, 36 CHKs) | | | |
|---|---|---|---|---|---|---|---|---|---|
| | Generic method | | Bias method | | | Generic method | | Bias method | |
| | Column error (pixel) | Row error (pixel) | Column error (pixel) | Row error (pixel) | | Column error (pixel) | Row error (pixel) | Column error (pixel) | Row error (pixel) |
| 1 | -0.83874 | -1.35555 | -0.99312 | -1.42728 | 1 | -0.93468 | -0.59175 | -1.11571 | -0.74683 |
| 2 | -5.1282 | -15.0221 | -6.51826 | -16.0995 | 2 | -7.68021 | -3.51389 | -9.23654 | -5.57196 |
| 3 | -2.24119 | -12.9778 | -3.40768 | -13.8432 | 3 | -4.22659 | -3.62371 | -5.55327 | -5.27798 |
| 4 | -1.88024 | -20.1578 | -3.67871 | -21.6651 | 4 | -5.82089 | -4.09859 | -7.76932 | -6.99312 |
| 5 | -3.91277 | -6.34813 | -4.54941 | -6.76515 | 5 | -4.82237 | -1.65103 | -5.56844 | -2.46017 |
| 6 | -2.93885 | -5.28323 | -3.46431 | -5.6186 | 6 | -3.65648 | -1.48213 | -4.27521 | -2.13524 |
| 7 | -1.14925 | -8.13714 | -1.85833 | -8.61229 | 7 | -2.20062 | -2.8041 | -3.02922 | -3.72202 |
| 8 | -0.63414 | -6.34268 | -1.1701 | -6.70347 | 8 | -1.35998 | -2.37985 | -1.99027 | -3.0674 |
| 9 | -4.68163 | -18.8126 | -6.36967 | -20.1981 | 9 | -8.25965 | -3.93756 | -10.1094 | -6.59447 |
| 10 | -2.36178 | -9.1004 | -3.24281 | -9.74168 | 10 | -3.75415 | -2.13602 | -4.7747 | -3.34777 |
| 11 | -0.09348 | -0.6998 | -0.12215 | -0.70968 | 11 | -0.11626 | -0.53875 | -0.15043 | -0.56428 |
| 12 | -1.72674 | -12.4171 | -2.80231 | -13.2349 | 12 | -3.53794 | -3.65812 | -4.76961 | -5.1971 |
| 13 | -2.93002 | -18.3626 | -4.58075 | -19.7162 | 13 | -6.41185 | -3.80479 | -8.22834 | -6.39345 |
| 14 | -2.51485 | -18.4577 | -4.05328 | -19.7241 | 14 | -5.58981 | -5.04507 | -7.29594 | -7.43902 |
| 15 | -4.41898 | -20.2911 | -6.2011 | -21.8069 | 15 | -8.38238 | -4.13728 | -10.3198 | -7.02894 |
| 16 | -4.10873 | -17.8579 | -5.68133 | -19.1542 | 16 | -7.33216 | -4.03741 | -9.07376 | -6.4941 |
| 17 | -1.40303 | -4.40702 | -1.83003 | -4.69473 | 17 | -2.04041 | -1.11628 | -2.54896 | -1.66269 |
| 18 | -3.51686 | -16.8663 | -5.06501 | -18.1536 | 18 | -6.66553 | -3.22962 | -8.38339 | -5.6554 |
| 19 | -0.56749 | -5.37806 | -1.10403 | -5.75069 | 19 | -1.40428 | -1.15717 | -2.04062 | -1.86083 |
| 20 | -1.29374 | -9.76758 | -2.18781 | -10.4441 | 20 | -2.76793 | -2.47799 | -3.8055 | -3.73859 |
| 21 | -3.49217 | -19.2079 | -5.18024 | -20.653 | 21 | -7.12201 | -3.96971 | -8.9732 | -6.69487 |
| 22 | -1.18647 | -8.25963 | -2.02676 | -8.86968 | 22 | -2.60624 | -1.45492 | -3.58734 | -2.60765 |
| 23 | -5.78919 | -23.2292 | -7.75842 | -24.9916 | 23 | -10.5616 | -4.60585 | -12.6626 | -7.9624 |
| 24 | -4.14942 | -18.6379 | -5.78335 | -20.0181 | 24 | -7.60934 | -4.00811 | -9.41105 | -6.6119 |
| 25 | -1.69649 | -14.2653 | -2.9463 | -15.258 | 25 | -4.02271 | -3.62907 | -5.4427 | -5.48944 |
| 26 | -1.87814 | -7.88156 | -2.65038 | -8.44238 | 26 | -3.17401 | -1.6205 | -4.0797 | -2.67572 |
| 27 | -5.29783 | -24.5457 | -7.27199 | -26.3172 | 27 | -10.1004 | -5.83398 | -12.2059 | -9.20585 |
| 28 | -2.69126 | -16.3125 | -4.11036 | -17.4761 | 28 | -5.48903 | -3.93687 | -7.08201 | -6.11824 |
| 29 | -4.24089 | -17.1798 | -5.75034 | -18.4343 | 29 | -7.3131 | -3.85607 | -8.99579 | -6.21259 |
| 30 | -2.40648 | -14.6054 | -3.72914 | -15.677 | 30 | -4.93541 | -3.19322 | -6.43082 | -5.19659 |
| 31 | -2.89829 | -13.2509 | -3.99587 | -14.1168 | 31 | -4.87149 | -3.97591 | -6.13217 | -5.58545 |
| 32 | -2.89706 | -11.1247 | -3.8735 | -11.8636 | 32 | -4.64912 | -2.97482 | -5.78211 | -4.36057 |
| 33 | -4.04938 | -22.8801 | -5.83374 | -24.423 | 33 | -8.11319 | -6.45369 | -10.0579 | -9.37651 |
| 34 | -5.35053 | -16.8822 | -6.96912 | -18.2425 | 34 | -8.85408 | -2.29944 | -10.6471 | -4.86616 |
| 35 | -4.63269 | -15.5065 | -5.98124 | -16.6145 | 35 | -7.37819 | -3.57245 | -8.90681 | -5.6361 |
| 36 | -5.03116 | -12.2636 | -6.32994 | -13.3308 | 36 | -7.63551 | -0.802 | -9.1126 | -2.78241 |

**Table 12 Image Coordinate Residuals of CHK points after RPC refinement by using 1 GCP in Case 5 and Case 6.**

| No | Case 5 (1 GCP, 36 CHKs) | | | | No | Case 6 (1 GCP, 36 CHKs) | | | |
|---|---|---|---|---|---|---|---|---|---|
| | Generic method | | Bias method | | | Generic method | | Bias method | |
| | Column error (pixel) | Row error (pixel) | Column error (pixel) | Row error (pixel) | | Column error (pixel) | Row error (pixel) | Column error (pixel) | Row error (pixel) |
| 1 | -0.93962 | -0.40618 | -0.96802 | -0.41711 | 1 | -0.94018 | -0.38774 | -0.95319 | -0.38412 |
| 2 | -6.32376 | -5.15029 | -6.57346 | -5.32953 | 2 | -6.18573 | -5.31428 | -6.30582 | -5.30533 |
| 3 | -3.20031 | -4.93277 | -3.40974 | -5.07682 | 3 | -3.09579 | -5.06398 | -3.19431 | -5.05673 |
| 4 | -3.58893 | -6.58303 | -3.91199 | -6.83149 | 4 | -3.36234 | -6.83192 | -3.52439 | -6.81539 |
| 5 | -4.38893 | -2.2264 | -4.50294 | -2.29512 | 5 | -4.34476 | -2.28413 | -4.39585 | -2.27862 |
| 6 | -3.32415 | -1.92053 | -3.41831 | -1.97539 | 6 | -3.2903 | -1.96453 | -3.33219 | -1.95941 |
| 7 | -1.68712 | -3.5085 | -1.81404 | -3.58693 | 7 | -1.63481 | -3.57914 | -1.69191 | -3.57343 |
| 8 | -1.0256 | -2.89284 | -1.12219 | -2.95199 | 8 | -0.99151 | -2.9443 | -1.03494 | -2.94046 |
| 9 | -6.24591 | -6.29213 | -6.54884 | -6.52059 | 9 | -6.04141 | -6.528 | -6.19104 | -6.51327 |
| 10 | -3.04948 | -3.21143 | -3.20794 | -3.31777 | 10 | -2.97769 | -3.31919 | -3.05045 | -3.3148 |
| 11 | -0.112 | -0.52505 | -0.11739 | -0.52367 | 11 | -0.11182 | -0.52374 | -0.11408 | -0.51961 |
| 12 | -2.59693 | -5.05316 | -2.79069 | -5.18904 | 12 | -2.5011 | -5.19293 | -2.59178 | -5.18827 |
| 13 | -4.44863 | -6.18532 | -4.74491 | -6.40853 | 13 | -4.24927 | -6.42376 | -4.39486 | -6.4101 |
| 14 | -3.88895 | -7.26111 | -4.16631 | -7.4707 | 14 | -3.71609 | -7.48307 | -3.85178 | -7.47393 |
| 15 | -6.11211 | -6.85312 | -6.43258 | -7.10258 | 15 | -5.88169 | -7.12512 | -6.04198 | -7.11002 |
| 16 | -5.52796 | -6.37122 | -5.81102 | -6.58553 | 16 | -5.34468 | -6.60496 | -5.48313 | -6.59474 |
| 17 | -1.71618 | -1.69407 | -1.79233 | -1.74039 | 17 | -1.68329 | -1.75197 | -1.71627 | -1.74818 |
| 18 | -4.90548 | -5.58679 | -5.18461 | -5.79994 | 18 | -4.72667 | -5.82286 | -4.86313 | -5.81447 |
| 19 | -0.96881 | -1.92997 | -1.06443 | -1.99083 | 19 | -0.92459 | -2.00738 | -0.9663 | -2.00386 |
| 20 | -1.99671 | -3.77257 | -2.15751 | -3.88499 | 20 | -1.91821 | -3.90223 | -1.99185 | -3.89967 |
| 21 | -5.05761 | -6.64609 | -5.36216 | -6.88499 | 21 | -4.848 | -6.91411 | -4.99927 | -6.90408 |
| 22 | -1.84742 | -2.68527 | -1.99733 | -2.78634 | 22 | -1.77027 | -2.80849 | -1.83751 | -2.80424 |
| 23 | -7.75757 | -7.88674 | -8.11195 | -8.17604 | 23 | -7.47325 | -8.21528 | -7.6547 | -8.1975 |
| 24 | -5.64659 | -6.59132 | -5.94104 | -6.81969 | 24 | -5.44728 | -6.85 | -5.59231 | -6.84054 |
| 25 | -2.75036 | -5.53072 | -2.97522 | -5.69583 | 25 | -2.62099 | -5.72115 | -2.72721 | -5.71652 |
| 26 | -2.47966 | -2.79408 | -2.61733 | -2.88701 | 26 | -2.40909 | -2.91161 | -2.47033 | -2.90816 |
| 27 | -7.2741 | -9.1536 | -7.62935 | -9.44452 | 27 | -6.98754 | -9.486 | -7.16949 | -9.46848 |
| 28 | -3.93065 | -6.16831 | -4.18631 | -6.36169 | 28 | -3.77229 | -6.39176 | -3.89527 | -6.38609 |
| 29 | -5.58573 | -6.25512 | -5.85772 | -6.46336 | 29 | -5.41027 | -6.49535 | -5.54233 | -6.4885 |
| 30 | -3.53852 | -5.27039 | -3.77676 | -5.44876 | 30 | -3.39653 | -5.47838 | -3.50999 | -5.47403 |
| 31 | -3.79809 | -5.71862 | -3.99549 | -5.86314 | 31 | -3.68894 | -5.89312 | -3.7807 | -5.89096 |
| 32 | -3.68641 | -4.54321 | -3.8607 | -4.66641 | 32 | -3.58858 | -4.70025 | -3.66755 | -4.69703 |
| 33 | -5.74979 | -9.44566 | -6.07061 | -9.70067 | 33 | -5.51003 | -9.74524 | -5.66992 | -9.73316 |
| 34 | -6.83472 | -5.02367 | -7.12547 | -5.24962 | 34 | -6.62978 | -5.29643 | -6.77156 | -5.28803 |
| 35 | -5.80412 | -5.99712 | -6.04616 | -6.18316 | 35 | -5.64433 | -6.23984 | -5.7586 | -6.2379 |
| 36 | -6.14793 | -3.15488 | -6.38117 | -3.33431 | 36 | -5.9969 | -3.3904 | -6.10659 | -3.38953 |

**Table 13 Image Coordinate Residuals of CHK points after RPC refinement by using 1 GCP in Case 7 and Case 8.**

| No | Case 7 (1 GCP, 36 CHKs) | | | | No | Case 8 (1 GCP, 36 CHKs) | | | |
|---|---|---|---|---|---|---|---|---|---|
| | Generic method | | Bias method | | | Generic method | | Bias method | |
| | Column error (pixel) | Row error (pixel) | Column error (pixel) | Row error (pixel) | | Column error (pixel) | Row error (pixel) | Column error (pixel) | Row error (pixel) |
| 1 | 1.880203 | -99.9007 | -29.321 | -108.346 | 1 | 0.025263 | -10.0834 | -1.47978 | -10.7607 |
| 2 | 18.93418 | -1004.78 | -181.927 | -1088.96 | 2 | 3.864816 | -102.632 | -9.67731 | -113.164 |
| 3 | 17.62814 | -819.642 | -150.836 | -887.512 | 3 | 5.02954 | -84.396 | -6.3456 | -92.8543 |
| 4 | 30.78795 | -1379.38 | -227.636 | -1495.55 | 4 | 10.71531 | -140.427 | -6.79159 | -155.219 |
| 5 | 6.749784 | -420.368 | -86.6879 | -453.831 | 5 | -0.23306 | -43.0205 | -6.45493 | -47.101 |
| 6 | 5.826861 | -343.34 | -72.0311 | -370.634 | 6 | 0.055311 | -35.2294 | -5.08155 | -38.5131 |
| 7 | 10.73593 | -472.517 | -92.036 | -510.137 | 7 | 2.986171 | -49.2684 | -3.94328 | -53.9209 |
| 8 | 8.046782 | -352.549 | -70.054 | -381.72 | 8 | 2.408891 | -37.0088 | -2.8252 | -40.54 |
| 9 | 25.65231 | -1271.66 | -215.249 | -1377.92 | 9 | 6.877685 | -129.684 | -9.57032 | -143.286 |
| 10 | 12.15087 | -598.243 | -111.993 | -647.826 | 10 | 2.880205 | -61.2732 | -5.71992 | -67.552 |
| 11 | 0.444431 | -18.6076 | -5.01812 | -20.2528 | 11 | 0.062472 | -2.2861 | -0.2193 | -2.41484 |
| 12 | 16.12028 | -748.763 | -135.048 | -811.713 | 12 | 4.860872 | -77.6143 | -5.63065 | -85.6185 |
| 13 | 26.58187 | -1235.9 | -207.124 | -1338.83 | 13 | 8.285821 | -126.114 | -7.80531 | -139.408 |
| 14 | 24.16844 | -1137.59 | -192.727 | -1234.34 | 14 | 7.696394 | -117.507 | -7.29211 | -129.923 |
| 15 | 27.75211 | -1363.2 | -224.104 | -1477.96 | 15 | 8.012349 | -139.12 | -9.34892 | -154.015 |
| 16 | 23.45009 | -1165.39 | -197.044 | -1263.3 | 16 | 6.398628 | -119.419 | -8.92832 | -132.139 |
| 17 | 5.602553 | -274.831 | -51.2724 | -295.476 | 17 | 0.985461 | -28.3668 | -3.1919 | -31.2069 |
| 18 | 23.34687 | -1143.03 | -192.216 | -1239.59 | 18 | 6.767627 | -116.538 | -8.31799 | -129.162 |
| 19 | 8.261689 | -348.729 | -62.23 | -374.807 | 19 | 2.475428 | -35.797 | -2.77187 | -39.4657 |
| 20 | 13.29981 | -607.499 | -107.443 | -657.025 | 20 | 4.020879 | -62.7022 | -4.705 | -69.328 |
| 21 | 26.22889 | -1273.06 | -208.866 | -1380.97 | 21 | 8.030718 | -130.165 | -8.41118 | -144.346 |
| 22 | 12.89361 | -563.697 | -99.1043 | -606.843 | 22 | 3.785643 | -57.4556 | -4.42767 | -63.444 |
| 23 | 30.51139 | -1554.97 | -246.415 | -1686.41 | 23 | 8.517935 | -158.741 | -10.6573 | -176.073 |
| 24 | 24.54736 | -1220.8 | -202.017 | -1323.19 | 24 | 6.88283 | -125.029 | -9.03742 | -138.571 |
| 25 | 19.41954 | -885.271 | -150.725 | -957.785 | 25 | 6.167808 | -91.3782 | -6.0224 | -101.104 |
| 26 | 10.98668 | -514.255 | -90.1527 | -552.904 | 26 | 2.64443 | -52.7351 | -4.90363 | -58.2399 |
| 27 | 31.10619 | -1560.96 | -245.981 | -1692.61 | 27 | 9.057198 | -160.471 | -10.1664 | -177.891 |
| 28 | 21.61304 | -1027.83 | -172.164 | -1112.78 | 28 | 6.501484 | -105.851 | -7.33201 | -117.253 |
| 29 | 21.87631 | -1106.67 | -185.008 | -1198.45 | 29 | 5.701616 | -113.612 | -9.00972 | -125.91 |
| 30 | 20.00562 | -945.11 | -159.346 | -1022.78 | 30 | 6.013929 | -96.9803 | -6.8816 | -107.476 |
| 31 | 15.32554 | -763.206 | -130.366 | -824.301 | 31 | 3.829167 | -79.6567 | -6.87674 | -88.1319 |
| 32 | 13.5648 | -665.821 | -113.576 | -715.757 | 32 | 2.99121 | -69.1068 | -6.54567 | -76.347 |
| 33 | 28.1235 | -1362.59 | -217.755 | -1474.48 | 33 | 8.365952 | -141.431 | -9.02143 | -156.58 |
| 34 | 23.34549 | -1198.36 | -195.681 | -1294.39 | 34 | 5.527558 | -121.451 | -10.2506 | -134.79 |
| 35 | 18.60511 | -960.205 | -154.084 | -1031.21 | 35 | 3.975243 | -99.1452 | -9.16457 | -109.969 |
| 36 | 17.15911 | -916.814 | -147.919 | -984.559 | 36 | 3.186354 | -92.351 | -9.46609 | -102.77 |

**Table 14 Image Coordinate Residuals of CHK points after RPC refinement by using 1 GCP in Case 9.**

| No | Case 9 (1 GCP, 36 CHKs) | | | |
|---|---|---|---|---|
| | Generic method | | Bias method | |
| | Column error | Row error | Column error | Row error |
| 1 | -0.83839 | -1.35324 | -0.99144 | -1.42358 |
| 2 | -5.1125 | -15.0399 | -6.48835 | -16.0967 |
| 3 | -2.2292 | -12.992 | -3.3836 | -13.8409 |
| 4 | -1.85472 | -20.185 | -3.63542 | -21.6631 |
| 5 | -3.90747 | -6.35426 | -4.53744 | -6.76326 |
| 6 | -2.93469 | -5.28785 | -3.45468 | -5.61678 |
| 7 | -1.14306 | -8.14471 | -1.84467 | -8.61073 |
| 8 | -0.62996 | -6.34814 | -1.16034 | -6.70215 |
| 9 | -4.65857 | -18.8384 | -6.3297 | -20.1971 |
| 10 | -2.35343 | -9.11209 | -3.22522 | -9.74129 |
| 11 | -0.09306 | -0.69945 | -0.12178 | -0.70923 |
| 12 | -1.71573 | -12.4324 | -2.78009 | -13.2347 |
| 13 | -2.90753 | -18.3887 | -4.54166 | -19.7163 |
| 14 | -2.4953 | -18.482 | -4.01815 | -19.7243 |
| 15 | -4.39305 | -20.321 | -6.15748 | -21.8076 |
| 16 | -4.08803 | -17.8836 | -5.64472 | -19.1551 |
| 17 | -1.39899 | -4.41323 | -1.82154 | -4.69557 |
| 18 | -3.49666 | -16.8922 | -5.02912 | -18.1551 |
| 19 | -0.5622 | -5.38644 | -1.09308 | -5.75212 |
| 20 | -1.28466 | -9.78173 | -2.16931 | -10.4457 |
| 21 | -3.46855 | -19.2373 | -5.13973 | -20.655 |
| 22 | -1.17754 | -8.27307 | -2.00892 | -8.87163 |
| 23 | -5.75728 | -23.2653 | -7.70737 | -24.9938 |
| 24 | -4.12695 | -18.6663 | -5.74441 | -20.0203 |
| 25 | -1.68177 | -14.2861 | -2.91861 | -15.2602 |
| 26 | -1.86994 | -7.89438 | -2.63398 | -8.4447 |
| 27 | -5.26568 | -24.5823 | -7.22065 | -26.3198 |
| 28 | -2.67333 | -16.337 | -4.07787 | -17.4787 |
| 29 | -4.22107 | -17.2062 | -5.71514 | -18.4371 |
| 30 | -2.39037 | -14.6282 | -3.69936 | -15.6798 |
| 31 | -2.88581 | -13.27 | -3.9719 | -14.1199 |
| 32 | -2.88584 | -11.1419 | -3.85195 | -11.8669 |
| 33 | -4.02242 | -22.913 | -5.78902 | -24.4265 |
| 34 | -5.32744 | -16.9122 | -6.92963 | -18.2467 |
| 35 | -4.61461 | -15.5333 | -5.94917 | -16.6205 |
| 36 | -5.01406 | -12.2895 | -6.29932 | -13.3369 |

**Table 15 Image Coordinate Residuals of CHK points after RPC refinement by using 3 GCPs in Case 1 and Case 2.**

| No | Case 1 (3 GCP, 34 CHKs) | | | | No | Case 2 (3 GCP, 34 CHKs) | | | |
|---|---|---|---|---|---|---|---|---|---|
| | Generic method | | Bias method | | | Generic method | | Bias method | |
| | Column error (pixel) | Row error (pixel) | Column error (pixel) | Row error (pixel) | | Column error (pixel) | Row error (pixel) | Column error (pixel) | Row error (pixel) |
| 1 | -1.43679 | 0.29226 | -0.31039 | -0.13474 | 1 | -1.26272 | 0.435184 | -0.96116 | 0.26526 |
| 2 | -2.96953 | 0.685485 | 2.773123 | -1.12844 | 2 | -2.38365 | 0.909666 | -1.89507 | 0.704529 |
| 3 | 0.858407 | 1.176612 | 19.55323 | -3.85995 | 3 | 2.286206 | 1.67264 | 4.014252 | 1.19511 |
| 4 | -2.39188 | 0.609109 | -6.93251 | 2.668204 | 4 | -2.89076 | 0.357011 | -3.24509 | 0.557004 |
| 5 | -1.71291 | 0.428727 | -6.00341 | 2.219808 | 5 | -2.16233 | 0.207973 | -2.48116 | 0.381707 |
| 6 | 0.662725 | -0.36732 | -4.34039 | 1.854045 | 6 | 0.111265 | -0.65054 | -0.30117 | -0.41882 |
| 7 | 0.503944 | -0.65843 | -4.10911 | 0.023428 | 7 | 0.251697 | -0.76879 | -0.1195 | -0.6742 |
| 8 | -1.43532 | 1.01831 | 10.13231 | -1.87915 | 8 | -0.65295 | 1.248299 | 0.459901 | 1.025153 |
| 9 | -0.14315 | 0.442937 | -5.74505 | 1.36603 | 9 | -0.46492 | 0.279952 | -0.97872 | 0.432476 |
| 10 | -0.07514 | -0.39881 | -0.38136 | -0.52044 | 10 | -0.12843 | -0.38659 | -0.10934 | -0.3895 |
| 11 | 0.752617 | -0.6768 | -3.40103 | -0.93855 | 11 | 0.70153 | -0.71326 | 0.316363 | -0.65834 |
| 12 | 0.691499 | 0.957939 | 8.900665 | -1.02294 | 12 | 1.19283 | 1.068032 | 2.019357 | 0.953683 |
| 13 | 0.5304 | -0.93254 | 5.346594 | -4.28054 | 13 | 1.27742 | -0.65446 | 1.76317 | -0.87918 |
| 14 | -0.76171 | 0.799266 | 11.968 | -3.22645 | 14 | 0.244798 | 1.108815 | 1.529669 | 0.801806 |
| 15 | -0.54529 | 0.235165 | 3.920714 | -1.87632 | 15 | -0.06106 | 0.373329 | 0.405005 | 0.252652 |
| 16 | 0.451589 | 0.217649 | -5.64571 | 3.370238 | 16 | -0.29766 | -0.15679 | -0.93278 | 0.152328 |
| 17 | 0.051828 | 0.800805 | 3.085421 | -1.45246 | 17 | 0.572801 | 0.972433 | 0.89217 | 0.827848 |
| 18 | 1.829861 | 0.460621 | -5.44604 | 4.548286 | 18 | 0.910576 | -0.00326 | 0.123045 | 0.377808 |
| 19 | 1.573389 | -0.12108 | -5.91711 | 1.999576 | 19 | 1.045663 | -0.37926 | 0.260337 | -0.15115 |
| 20 | 0.241046 | 0.342163 | 7.358087 | -3.20084 | 20 | 1.127066 | 0.649864 | 1.861093 | 0.366333 |
| 21 | 2.238702 | 1.029715 | -6.26551 | 6.109161 | 21 | 1.12809 | 0.46231 | 0.222327 | 0.931078 |
| 22 | -1.77609 | 0.616084 | 17.90276 | -5.43287 | 22 | -0.1725 | 1.119139 | 1.850613 | 0.572965 |
| 23 | -0.17466 | 0.231934 | 4.444864 | -1.72667 | 23 | 0.353437 | 0.384035 | 0.836217 | 0.234779 |
| 24 | 2.067576 | -0.34946 | -2.81222 | 1.359232 | 24 | 1.706494 | -0.55168 | 1.194827 | -0.37471 |
| 25 | 1.506129 | 0.621009 | -7.21556 | 6.147837 | 25 | 0.348604 | 0.034175 | -0.62039 | 0.514969 |
| 26 | -1.17854 | -0.62741 | 18.25967 | -6.4472 | 26 | 0.395326 | -0.13945 | 2.400885 | -0.67845 |
| 27 | 1.32342 | -0.30432 | -0.68672 | 0.329682 | 27 | 1.264291 | -0.37905 | 1.046394 | -0.31759 |
| 28 | 1.54363 | 0.170499 | -2.5282 | 1.6417 | 28 | 1.299474 | 0.022819 | 0.854587 | 0.149881 |
| 29 | 0.912865 | -1.20662 | -6.49114 | 2.245715 | 29 | 0.27049 | -1.52541 | -0.56921 | -1.25584 |
| 30 | 1.355689 | -0.25572 | -7.6459 | 6.583039 | 30 | 0.059945 | -0.90977 | -0.98285 | -0.37747 |
| 31 | 0.810428 | -1.7478 | 8.772001 | -2.27744 | 31 | 1.220183 | -1.70478 | 2.052258 | -1.81739 |
| 32 | -0.08943 | 1.97382 | 0.788269 | 5.298132 | 32 | -0.45038 | 1.708601 | -0.38945 | 1.881072 |
| 33 | 1.167793 | -0.1911 | -5.37139 | 9.832916 | 33 | -0.12062 | -0.83271 | -1.05493 | -0.319 |
| 34 | 0.615772 | 2.37814 | -6.48886 | 12.42552 | 34 | -0.64997 | 1.757469 | -1.67375 | 2.259509 |

**Table 16 Image Coordinate Residuals of CHK points after RPC refinement by using 3 GCPs in Case 3 and Case 4.**

| No | Case 3 (3 GCP, 34 CHKs) | | | | No | Case 4 (3 GCP, 34 CHKs) | | | |
|---|---|---|---|---|---|---|---|---|---|
| | Generic method | | Bias method | | | Generic method | | Bias method | |
| | Column error (pixel) | Row error (pixel) | Column error (pixel) | Row error (pixel) | | Column error (pixel) | Row error (pixel) | Column error (pixel) | Row error (pixel) |
| 1 | -1.26747 | 0.423103 | -1.23511 | 0.410016 | 1 | -1.28819 | 0.42678 | -1.2952 | 0.420846 |
| 2 | -2.37976 | 0.893152 | -2.32819 | 0.874074 | 2 | -2.36664 | 0.89244 | -2.41185 | 0.891646 |
| 3 | 2.252055 | 1.582075 | 2.43894 | 1.54422 | 3 | 2.291004 | 1.578985 | 2.075355 | 1.583957 |
| 4 | -2.89494 | 0.358361 | -2.93367 | 0.379155 | 4 | -2.90841 | 0.359001 | -2.89119 | 0.359868 |
| 5 | -2.16487 | 0.20947 | -2.19975 | 0.228128 | 5 | -2.17876 | 0.210346 | -2.16042 | 0.211441 |
| 6 | 0.107409 | -0.64744 | 0.062405 | -0.62381 | 6 | 0.09523 | -0.64714 | 0.114971 | -0.64553 |
| 7 | 0.270405 | -0.75133 | 0.228974 | -0.74161 | 7 | 0.259354 | -0.75039 | 0.31085 | -0.74828 |
| 8 | -0.68672 | 1.181135 | -0.5659 | 1.166943 | 8 | -0.66304 | 1.179057 | -0.81971 | 1.185119 |
| 9 | -0.44171 | 0.304627 | -0.49884 | 0.31863 | 9 | -0.44863 | 0.304761 | -0.38588 | 0.307846 |
| 10 | -0.1282 | -0.38818 | -0.12625 | -0.38431 | 10 | -0.13144 | -0.38753 | -0.13106 | -0.38357 |
| 11 | 0.734043 | -0.68536 | 0.690399 | -0.68107 | 11 | 0.731322 | -0.68506 | 0.797633 | -0.68158 |
| 12 | 1.161198 | 1.011886 | 1.251055 | 1.007912 | 12 | 1.177321 | 1.010367 | 1.049553 | 1.016712 |
| 13 | 1.296005 | -0.66453 | 1.346846 | -0.68303 | 13 | 1.30878 | -0.66443 | 1.283744 | -0.65894 |
| 14 | 0.215973 | 1.03532 | 0.354966 | 1.015143 | 14 | 0.238161 | 1.034056 | 0.074166 | 1.041307 |
| 15 | -0.06242 | 0.349891 | -0.01297 | 0.342634 | 15 | -0.05234 | 0.349545 | -0.10521 | 0.354777 |
| 16 | -0.29612 | -0.1443 | -0.36561 | -0.1141 | 16 | -0.30159 | -0.1456 | -0.26679 | -0.14295 |
| 17 | 0.58746 | 0.964516 | 0.620209 | 0.953516 | 17 | 0.595146 | 0.964715 | 0.577697 | 0.968941 |
| 18 | 0.911408 | 0.012831 | 0.825249 | 0.048784 | 18 | 0.905871 | 0.010961 | 0.948077 | 0.012709 |
| 19 | 1.076379 | -0.34164 | 0.989156 | -0.32256 | 19 | 1.070949 | -0.34247 | 1.159574 | -0.34087 |
| 20 | 1.135701 | 0.62156 | 1.213239 | 0.599499 | 20 | 1.147544 | 0.621951 | 1.086418 | 0.626313 |
| 21 | 1.121507 | 0.477574 | 1.022755 | 0.521281 | 21 | 1.113438 | 0.475479 | 1.153852 | 0.476308 |
| 22 | -0.21273 | 1.002832 | 0.006074 | 0.96453 | 22 | -0.18735 | 1.002014 | -0.43444 | 1.008862 |
| 23 | 0.354312 | 0.360088 | 0.404994 | 0.350075 | 23 | 0.361636 | 0.360164 | 0.310356 | 0.36362 |
| 24 | 1.723299 | -0.53044 | 1.665954 | -0.51474 | 24 | 1.719576 | -0.53103 | 1.769338 | -0.52982 |
| 25 | 0.344615 | 0.0529 | 0.238695 | 0.096921 | 25 | 0.337535 | 0.050437 | 0.384801 | 0.050404 |
| 26 | 0.354212 | -0.2562 | 0.57109 | -0.29382 | 26 | 0.377701 | -0.25685 | 0.131096 | -0.25065 |
| 27 | 1.278838 | -0.36877 | 1.253078 | -0.3629 | 27 | 1.277652 | -0.36895 | 1.302314 | -0.3679 |
| 28 | 1.319517 | 0.04426 | 1.268951 | 0.054927 | 28 | 1.316266 | 0.043863 | 1.365918 | 0.044172 |
| 29 | 0.29495 | -1.4891 | 0.201346 | -1.46729 | 29 | 0.289074 | -1.49038 | 0.372419 | -1.49165 |
| 30 | 0.049628 | -0.89154 | -0.06461 | -0.84384 | 30 | 0.040994 | -0.89438 | 0.085668 | -0.89681 |
| 31 | 1.18125 | -1.77073 | 1.270767 | -1.77389 | 31 | 1.185337 | -1.77116 | 1.046827 | -1.76991 |
| 32 | -0.48625 | 1.674507 | -0.48077 | 1.693977 | 32 | -0.49232 | 1.673581 | -0.56248 | 1.671413 |
| 33 | -0.14271 | -0.82212 | -0.24759 | -0.77881 | 33 | -0.15791 | -0.82483 | -0.13108 | -0.83356 |
| 34 | -0.66146 | 1.778153 | -0.77656 | 1.819039 | 34 | -0.67566 | 1.775335 | -0.62714 | 1.766319 |

**Table 17 Image Coordinate Residuals of CHK points after RPC refinement by using 3 GCPs in Case 5 and Case 6.**

| No | Case 5 (3 GCP, 34 CHKs) | | | | No | Case 6 (3 GCP, 34 CHKs) | | | |
|---|---|---|---|---|---|---|---|---|---|
| | Generic method | | Bias method | | | Generic method | | Bias method | |
| | Column error (pixel) | Row error (pixel) | Column error (pixel) | Row error (pixel) | | Column error (pixel) | Row error (pixel) | Column error (pixel) | Row error (pixel) |
| 1 | -1.27553 | 0.42328 | -1.26963 | 0.426882 | 1 | -1.26929 | 0.421704 | -1.26708 | 0.4275 |
| 2 | -2.39066 | 0.893778 | -2.37982 | 0.892448 | 2 | -2.38133 | 0.891245 | -2.37661 | 0.89253 |
| 3 | 2.203099 | 1.577947 | 2.244102 | 1.581205 | 3 | 2.241695 | 1.57137 | 2.260996 | 1.580921 |
| 4 | -2.88936 | 0.356661 | -2.89849 | 0.359971 | 4 | -2.89472 | 0.358606 | -2.89922 | 0.359982 |
| 5 | -2.15962 | 0.20806 | -2.16797 | 0.211619 | 5 | -2.16456 | 0.209733 | -2.16873 | 0.211638 |
| 6 | 0.114303 | -0.64923 | 0.103907 | -0.64608 | 6 | 0.107835 | -0.64698 | 0.102794 | -0.64613 |
| 7 | 0.282219 | -0.75015 | 0.271836 | -0.74879 | 7 | 0.27352 | -0.74915 | 0.267924 | -0.74884 |
| 8 | -0.72148 | 1.176939 | -0.69485 | 1.181366 | 8 | -0.69502 | 1.173224 | -0.68235 | 1.18098 |
| 9 | -0.42568 | 0.306106 | -0.43941 | 0.306118 | 9 | -0.43762 | 0.307676 | -0.44477 | 0.305941 |
| 10 | -0.12896 | -0.38793 | -0.12871 | -0.38371 | 10 | -0.12856 | -0.38828 | -0.12848 | -0.38372 |
| 11 | 0.749665 | -0.68244 | 0.738593 | -0.68376 | 11 | 0.738853 | -0.68192 | 0.732678 | -0.68399 |
| 12 | 1.133371 | 1.007744 | 1.153053 | 1.012817 | 12 | 1.154089 | 1.005299 | 1.163406 | 1.012416 |
| 13 | 1.288624 | -0.66256 | 1.298197 | -0.66236 | 13 | 1.296225 | -0.66562 | 1.299636 | -0.66271 |
| 14 | 0.178166 | 1.031364 | 0.207902 | 1.037241 | 14 | 0.20769 | 1.026688 | 0.221279 | 1.036823 |
| 15 | -0.07453 | 0.349286 | -0.06474 | 0.351711 | 15 | -0.06462 | 0.347217 | -0.0607 | 0.351395 |
| 16 | -0.28289 | -0.14587 | -0.2982 | -0.14311 | 16 | -0.2943 | -0.14269 | -0.30134 | -0.14313 |
| 17 | 0.582631 | 0.965775 | 0.588199 | 0.966693 | 17 | 0.587707 | 0.963702 | 0.589244 | 0.966461 |
| 18 | 0.927769 | 0.010844 | 0.908955 | 0.013037 | 18 | 0.913618 | 0.014878 | 0.905046 | 0.013071 |
| 19 | 1.1003 | -0.33968 | 1.080056 | -0.34112 | 19 | 1.082255 | -0.33703 | 1.0721 | -0.34115 |
| 20 | 1.119725 | 0.622085 | 1.134786 | 0.624343 | 20 | 1.133821 | 0.61833 | 1.139621 | 0.624139 |
| 21 | 1.138545 | 0.474558 | 1.117195 | 0.476773 | 21 | 1.123144 | 0.479522 | 1.113533 | 0.476821 |
| 22 | -0.27127 | 0.996643 | -0.22482 | 1.006102 | 22 | -0.22492 | 0.989147 | -0.20385 | 1.005817 |
| 23 | 0.342096 | 0.359603 | 0.351713 | 0.362216 | 23 | 0.352292 | 0.357372 | 0.355847 | 0.362071 |
| 24 | 1.73764 | -0.52966 | 1.724026 | -0.52993 | 24 | 1.726526 | -0.52778 | 1.719492 | -0.52994 |
| 25 | 0.363762 | 0.050064 | 0.340874 | 0.051704 | 25 | 0.346789 | 0.055266 | 0.336489 | 0.051837 |
| 26 | 0.295734 | -0.26255 | 0.341729 | -0.25289 | 26 | 0.341954 | -0.26993 | 0.3628 | -0.25312 |
| 27 | 1.285974 | -0.36794 | 1.27897 | -0.36775 | 27 | 1.280808 | -0.36741 | 1.276635 | -0.36774 |
| 28 | 1.333161 | 0.045539 | 1.320767 | 0.044836 | 28 | 1.322916 | 0.04695 | 1.316252 | 0.044904 |
| 29 | 0.318565 | -1.48786 | 0.297056 | -1.4897 | 29 | 0.300204 | -1.48464 | 0.289524 | -1.4895 |
| 30 | 0.068917 | -0.8951 | 0.044373 | -0.89384 | 30 | 0.051241 | -0.88924 | 0.040258 | -0.89353 |
| 31 | 1.150475 | -1.77633 | 1.169278 | -1.76917 | 31 | 1.1731 | -1.77844 | 1.181533 | -1.7691 |
| 32 | -0.49857 | 1.669168 | -0.49773 | 1.674375 | 32 | -0.49149 | 1.670582 | -0.49124 | 1.674683 |
| 33 | -0.12868 | -0.82655 | -0.15181 | -0.8256 | 33 | -0.14295 | -0.82072 | -0.15384 | -0.82476 |
| 34 | -0.64261 | 1.774925 | -0.66819 | 1.774529 | 34 | -0.66006 | 1.780759 | -0.67225 | 1.775392 |

**Table 18 Image Coordinate Residuals of CHK points after RPC refinement by using 3 GCPs in Case 7 and Case 8.**

| No | Case 7 (3 GCP, 34 CHKs) | | | | No | Case 8 (3 GCP, 34 CHKs) | | | |
|---|---|---|---|---|---|---|---|---|---|
| | Generic method | | Bias method | | | Generic method | | Bias method | |
| | Column error (pixel) | Row error (pixel) | Column error (pixel) | Row error (pixel) | | Column error (pixel) | Row error (pixel) | Column error (pixel) | Row error (pixel) |
| 1 | -1.37951 | 0.27874 | -0.23959 | -0.1619 | 1 | -1.25564 | 0.43376 | -0.95821 | 0.265592 |
| 2 | -2.87673 | 0.662798 | 2.781986 | -1.13692 | 2 | -2.37329 | 0.907245 | -1.89167 | 0.704566 |
| 3 | 1.244826 | 1.118308 | 19.68611 | -3.86484 | 3 | 2.328679 | 1.66583 | 4.032694 | 1.194778 |
| 4 | -2.44583 | 0.631964 | -6.91333 | 2.669661 | 4 | -2.89644 | 0.359478 | -3.24575 | 0.556993 |
| 5 | -1.76338 | 0.448711 | -5.98208 | 2.22118 | 5 | -2.16753 | 0.210133 | -2.48185 | 0.381699 |
| 6 | 0.598217 | -0.34144 | -4.32755 | 1.859153 | 6 | 0.104365 | -0.64774 | -0.30225 | -0.41886 |
| 7 | 0.413921 | -0.64706 | -4.12506 | 0.03192 | 7 | 0.242331 | -0.76741 | -0.12368 | -0.67421 |
| 8 | -1.16867 | 0.987951 | 10.24956 | -1.87078 | 8 | -0.62378 | 1.244615 | 0.473678 | 1.024797 |
| 9 | -0.26385 | 0.459843 | -5.78563 | 1.382764 | 9 | -0.47788 | 0.281977 | -0.98452 | 0.432427 |
| 10 | -0.07604 | -0.39924 | -0.3674 | -0.51887 | 10 | -0.12774 | -0.3867 | -0.10902 | -0.38952 |
| 11 | 0.642761 | -0.67133 | -3.45092 | -0.918 | 11 | 0.689772 | -0.71239 | 0.309934 | -0.6584 |
| 12 | 0.901235 | 0.939921 | 9.010687 | -1.00848 | 12 | 1.215693 | 1.065729 | 2.030861 | 0.953347 |
| 13 | 0.60515 | -0.96142 | 5.365575 | -4.25856 | 13 | 1.285836 | -0.65749 | 1.764826 | -0.87938 |
| 14 | -0.46525 | 0.759146 | 12.11014 | -3.21162 | 14 | 0.277303 | 1.104058 | 1.544507 | 0.801437 |
| 15 | -0.44551 | 0.218 | 3.970448 | -1.8582 | 15 | -0.05009 | 0.371396 | 0.40956 | 0.252444 |
| 16 | 0.33672 | 0.253294 | -5.68518 | 3.372459 | 16 | -0.30997 | -0.153 | -0.93626 | 0.152359 |
| 17 | 0.102191 | 0.782131 | 3.103304 | -1.43576 | 17 | 0.578446 | 0.970472 | 0.893395 | 0.827725 |
| 18 | 1.688658 | 0.505037 | -5.50288 | 4.546499 | 18 | 0.895247 | 0.001465 | 0.118661 | 0.377878 |
| 19 | 1.391885 | -0.09355 | -6.00771 | 2.007758 | 19 | 1.025985 | -0.37606 | 0.25153 | -0.15107 |
| 20 | 0.381297 | 0.307481 | 7.415833 | -3.18868 | 20 | 1.142599 | 0.646061 | 1.86649 | 0.366185 |
| 21 | 2.087443 | 1.083945 | -6.31789 | 6.105622 | 21 | 1.111369 | 0.468078 | 0.21823 | 0.931148 |
| 22 | -1.31244 | 0.549765 | 18.13218 | -5.42978 | 22 | -0.12155 | 1.11129 | 1.873837 | 0.572591 |
| 23 | -0.07212 | 0.21304 | 4.494897 | -1.71856 | 23 | 0.364707 | 0.38191 | 0.840837 | 0.234666 |
| 24 | 1.957326 | -0.32871 | -2.86369 | 1.363558 | 24 | 1.694402 | -0.54931 | 1.189814 | -0.37466 |
| 25 | 1.338845 | 0.677582 | -7.28766 | 6.136918 | 25 | 0.330162 | 0.040196 | -0.62537 | 0.51509 |
| 26 | -0.71603 | -0.69247 | 18.49162 | -6.44762 | 26 | 0.446139 | -0.14717 | 2.42422 | -0.6788 |
| 27 | 1.272549 | -0.29694 | -0.71399 | 0.330314 | 27 | 1.258708 | -0.37817 | 1.043801 | -0.31755 |
| 28 | 1.441824 | 0.186223 | -2.58397 | 1.639341 | 28 | 1.288321 | 0.024661 | 0.849549 | 0.149965 |
| 29 | 0.729859 | -1.17281 | -6.5963 | 2.232527 | 29 | 0.250448 | -1.52159 | -0.57769 | -1.25567 |
| 30 | 1.183057 | -0.19208 | -7.72923 | 6.553523 | 30 | 0.040716 | -0.90303 | -0.98764 | -0.37729 |
| 31 | 1.04001 | -1.76164 | 8.906624 | -2.29588 | 31 | 1.245122 | -1.70674 | 2.065798 | -1.81751 |
| 32 | -0.01368 | 1.994604 | 0.845212 | 5.259677 | 32 | -0.4425 | 1.710497 | -0.38241 | 1.881081 |
| 33 | 1.031239 | -0.12711 | -5.47929 | 9.717762 | 33 | -0.13615 | -0.82601 | -1.05786 | -0.31891 |
| 34 | 0.446541 | 2.441377 | -6.62716 | 12.30721 | 34 | -0.669 | 1.764172 | -1.67898 | 2.259622 |

**Table 19 Image Coordinate Residuals of CHK points after RPC refinement by using 3 GCPs in Case 9.**

| No | Case 9 (3 GCP, 34 CHKs) | | | |
|---|---|---|---|---|
| | Generic method | | Bias method | |
| | Column error | Row error | Column error | Row error |
| 1 | -1.26718 | 0.423236 | -1.23483 | 0.410082 |
| 2 | -2.37901 | 0.893131 | -2.32783 | 0.874082 |
| 3 | 2.256108 | 1.581593 | 2.440815 | 1.544189 |
| 4 | -2.89588 | 0.358887 | -2.93375 | 0.379156 |
| 5 | -2.16578 | 0.209971 | -2.19983 | 0.22813 |
| 6 | 0.106349 | -0.64688 | 0.062283 | -0.62382 |
| 7 | 0.269084 | -0.7509 | 0.228541 | -0.74161 |
| 8 | -0.68402 | 1.180991 | -0.56451 | 1.166901 |
| 9 | -0.44335 | 0.30512 | -0.49943 | 0.318612 |
| 10 | -0.12855 | -0.38786 | -0.12623 | -0.38431 |
| 11 | 0.732542 | -0.68499 | 0.689743 | -0.6811 |
| 12 | 1.163258 | 1.011898 | 1.252206 | 1.007869 |
| 13 | 1.296597 | -0.66458 | 1.347007 | -0.68307 |
| 14 | 0.21903 | 1.035084 | 0.356453 | 1.015098 |
| 15 | -0.06156 | 0.34996 | -0.01252 | 0.342601 |
| 16 | -0.29774 | -0.14359 | -0.36596 | -0.1141 |
| 17 | 0.58778 | 0.964594 | 0.620326 | 0.953492 |
| 18 | 0.909496 | 0.013637 | 0.824814 | 0.048788 |
| 19 | 1.074067 | -0.341 | 0.988271 | -0.32256 |
| 20 | 1.137041 | 0.62145 | 1.213777 | 0.599477 |
| 21 | 1.119486 | 0.478476 | 1.022347 | 0.521287 |
| 22 | -0.20778 | 1.002292 | 0.008405 | 0.964498 |
| 23 | 0.355214 | 0.360153 | 0.405454 | 0.350059 |
| 24 | 1.721795 | -0.5299 | 1.66545 | -0.51474 |
| 25 | 0.342416 | 0.053837 | 0.238206 | 0.096936 |
| 26 | 0.359157 | -0.25672 | 0.573432 | -0.29385 |
| 27 | 1.278013 | -0.36838 | 1.252818 | -0.3629 |
| 28 | 1.31812 | 0.044754 | 1.268449 | 0.054935 |
| 29 | 0.29263 | -1.48839 | 0.200508 | -1.46727 |
| 30 | 0.047375 | -0.89053 | -0.06507 | -0.84381 |
| 31 | 1.183557 | -1.77065 | 1.272129 | -1.77388 |
| 32 | -0.48569 | 1.675004 | -0.48005 | 1.694008 |
| 33 | -0.14454 | -0.82109 | -0.24782 | -0.77872 |
| 34 | -0.66364 | 1.779186 | -0.77702 | 1.819127 |

**Table 20 Image Coordinate Residuals of CHK points after RPC refinement by using 7 GCPs in Case 1 and Case 2.**

| No | Case 1 (7 GCP, 30 CHKs) | | | | No | Case 2 (7 GCP, 30 CHKs) | | | |
|---|---|---|---|---|---|---|---|---|---|
| | Generic method | | Bias method | | | Generic method | | Bias method | |
| | Column error (pixel) | Row error (pixel) | Column error (pixel) | Row error (pixel) | | Column error (pixel) | Row error (pixel) | Column error (pixel) | Row error (pixel) |
| 1 | -1.40789 | 0.684927 | -0.50467 | 0.617247 | 1 | -1.28441 | 0.788451 | -1.01782 | 0.643595 |
| 2 | -3.00581 | 1.111612 | -0.70535 | 1.216068 | 2 | -2.81084 | 1.158817 | -2.67417 | 1.096761 |
| 3 | 0.766523 | 1.5827 | 14.97074 | -1.01374 | 3 | 1.681594 | 1.861539 | 2.955786 | 1.563932 |
| 4 | -2.50544 | 0.919562 | -7.54366 | 3.521266 | 4 | -3.08693 | 0.618445 | -3.50078 | 0.853164 |
| 5 | -1.83079 | 0.727057 | -6.26336 | 2.893043 | 5 | -2.32678 | 0.473178 | -2.66978 | 0.668437 |
| 6 | 0.523031 | -0.0729 | -4.99486 | 2.708904 | 6 | -0.11362 | -0.40539 | -0.58682 | -0.13844 |
| 7 | 0.347306 | -0.39133 | -4.15081 | 0.557442 | 7 | 0.073484 | -0.52263 | -0.2956 | -0.41624 |
| 8 | -1.61218 | 1.351609 | 6.496198 | 0.432951 | 8 | -1.23196 | 1.408627 | -0.47015 | 1.32749 |
| 9 | -0.37547 | 0.674768 | -6.32583 | 2.113317 | 9 | -0.76812 | 0.471643 | -1.32455 | 0.652707 |
| 10 | 0.501778 | -0.44494 | -4.47809 | 0.043272 | 10 | 0.329691 | -0.54202 | -0.14516 | -0.44115 |
| 11 | 0.431545 | 1.223628 | 5.925217 | 0.897124 | 11 | 0.608311 | 1.193646 | 1.15844 | 1.193629 |
| 12 | -1.07088 | 1.035207 | 8.803953 | -1.25134 | 12 | -0.40728 | 1.200525 | 0.588303 | 1.012182 |
| 13 | -0.87832 | 0.438044 | 1.684399 | -0.37968 | 13 | -0.63337 | 0.471746 | -0.36234 | 0.435349 |
| 14 | 0.124978 | 0.334255 | -4.24926 | 3.050719 | 14 | -0.48865 | 0.01395 | -0.95899 | 0.274426 |
| 15 | -0.33119 | 0.962493 | 1.25017 | -0.19378 | 15 | -0.00286 | 1.049783 | 0.166829 | 0.972664 |
| 16 | 1.455262 | 0.546691 | -4.05264 | 4.194321 | 16 | 0.675558 | 0.139491 | 0.057955 | 0.470092 |
| 17 | -0.1807 | 0.483723 | 5.251781 | -1.83724 | 17 | 0.485746 | 0.698354 | 1.047686 | 0.49019 |
| 18 | 1.817964 | 1.103718 | -5.48533 | 6.029685 | 18 | 0.789824 | 0.567883 | -0.00192 | 1.006997 |
| 19 | -2.20865 | 0.768859 | 14.76388 | -3.56641 | 19 | -0.93867 | 1.137488 | 0.811679 | 0.70293 |
| 20 | 1.622314 | -0.2609 | -3.20516 | 1.850291 | 20 | 1.225776 | -0.48187 | 0.714335 | -0.29258 |
| 21 | 1.056064 | 0.665106 | -6.03505 | 5.844682 | 21 | 0.023695 | 0.129515 | -0.78809 | 0.564628 |
| 22 | -1.63475 | -0.49252 | 15.24876 | -4.66236 | 22 | -0.37879 | -0.13219 | 1.369262 | -0.56529 |
| 23 | 0.845705 | -0.22792 | -1.455 | 0.983791 | 23 | 0.714309 | -0.33565 | 0.463034 | -0.24969 |
| 24 | 1.056622 | 0.231594 | -2.90239 | 2.091697 | 24 | 0.782233 | 0.068501 | 0.344122 | 0.20532 |
| 25 | 0.40103 | -1.18454 | -5.95022 | 2.218085 | 25 | -0.17521 | -1.47717 | -0.91439 | -1.23237 |
| 26 | 0.818062 | -0.26541 | -6.53456 | 6.24906 | 26 | -0.35163 | -0.86647 | -1.23435 | -0.38097 |
| 27 | 0.264898 | -1.69615 | 7.096174 | -1.22314 | 27 | 0.509959 | -1.72022 | 1.226217 | -1.77881 |
| 28 | -0.69527 | 1.964707 | 0.131966 | 5.798692 | 28 | -1.10696 | 1.679088 | -1.05422 | 1.866121 |
| 29 | 0.406242 | -0.34784 | -4.05684 | 9.229276 | 29 | -0.7148 | -0.91524 | -1.4443 | -0.46551 |
| 30 | -0.15022 | 2.213261 | -4.97595 | 11.71887 | 30 | -1.22805 | 1.675873 | -2.02672 | 2.10648 |

**Table 21 Image Coordinate Residuals of CHK points after RPC refinement by using 7 GCPs in Case 3 and Case 4.**

| No | Case 3 (7 GCP, 30 CHKs) | | | | No | Case 4 (7 GCP, 30 CHKs) | | | |
|---|---|---|---|---|---|---|---|---|---|
| | Generic method | | Bias method | | | Generic method | | Bias method | |
| | Column error (pixel) | Row error (pixel) | Column error (pixel) | Row error (pixel) | | Column error (pixel) | Row error (pixel) | Column error (pixel) | Row error (pixel) |
| 1 | -1.29105 | 0.775889 | -1.25858 | 0.764789 | 1 | -1.31475 | 0.7803 | -1.31552 | 0.772745 |
| 2 | -2.80737 | 1.152777 | -2.79055 | 1.146133 | 2 | -2.80416 | 1.152784 | -2.81604 | 1.149394 |
| 3 | 1.647128 | 1.784979 | 1.787337 | 1.761878 | 3 | 1.67905 | 1.781416 | 1.499204 | 1.78359 |
| 4 | -3.09362 | 0.620116 | -3.1362 | 0.644219 | 4 | -3.11201 | 0.621608 | -3.08734 | 0.621037 |
| 5 | -2.33209 | 0.473772 | -2.36704 | 0.494535 | 5 | -2.34986 | 0.475425 | -2.32757 | 0.475215 |
| 6 | -0.12013 | -0.40194 | -0.1694 | -0.37491 | 6 | -0.13727 | -0.40082 | -0.11044 | -0.4006 |
| 7 | 0.089044 | -0.507 | 0.049986 | -0.49597 | 7 | 0.074779 | -0.50535 | 0.127098 | -0.50437 |
| 8 | -1.26704 | 1.35186 | -1.18278 | 1.34949 | 8 | -1.24933 | 1.349481 | -1.37978 | 1.353259 |
| 9 | -0.74819 | 0.49601 | -0.80867 | 0.512925 | 9 | -0.75937 | 0.496797 | -0.69323 | 0.498741 |
| 10 | 0.3591 | -0.5128 | 0.306718 | -0.50412 | 10 | 0.351544 | -0.51195 | 0.424514 | -0.50973 |
| 11 | 0.574515 | 1.145272 | 0.634881 | 1.150855 | 11 | 0.586246 | 1.143369 | 0.476447 | 1.147854 |
| 12 | -0.43851 | 1.13523 | -0.33116 | 1.124647 | 12 | -0.41873 | 1.133044 | -0.56708 | 1.138505 |
| 13 | -0.63774 | 0.453228 | -0.6098 | 0.453133 | 13 | -0.63087 | 0.452535 | -0.67378 | 0.456328 |
| 14 | -0.49225 | 0.018939 | -0.5435 | 0.045206 | 14 | -0.4965 | 0.017862 | -0.4793 | 0.020293 |
| 15 | 0.008263 | 1.045194 | 0.023822 | 1.039969 | 15 | 0.01371 | 1.044986 | 0.001225 | 1.048029 |
| 16 | 0.670951 | 0.147889 | 0.603071 | 0.179851 | 16 | 0.666615 | 0.146218 | 0.690006 | 0.147852 |
| 17 | 0.490735 | 0.674138 | 0.548005 | 0.658231 | 17 | 0.501867 | 0.673654 | 0.444663 | 0.676845 |
| 18 | 0.777937 | 0.577353 | 0.690749 | 0.61901 | 18 | 0.769764 | 0.575466 | 0.795384 | 0.576074 |
| 19 | -0.98213 | 1.028758 | -0.79503 | 0.998807 | 19 | -0.95434 | 1.025932 | -1.19465 | 1.031321 |
| 20 | 1.237855 | -0.46251 | 1.179122 | -0.44537 | 20 | 1.232933 | -0.46315 | 1.275736 | -0.4625 |
| 21 | 0.013961 | 0.140946 | -0.07599 | 0.181532 | 21 | 0.007808 | 0.138615 | 0.035858 | 0.13857 |
| 22 | -0.42336 | -0.2419 | -0.23685 | -0.27168 | 22 | -0.39686 | -0.24464 | -0.63881 | -0.2398 |
| 23 | 0.724142 | -0.3261 | 0.69278 | -0.31792 | 23 | 0.722435 | -0.32664 | 0.740835 | -0.3262 |
| 24 | 0.79728 | 0.087814 | 0.745464 | 0.099647 | 24 | 0.793648 | 0.087182 | 0.834163 | 0.08704 |
| 25 | -0.15645 | -1.44623 | -0.24119 | -1.42605 | 25 | -0.16179 | -1.44757 | -0.09497 | -1.44893 |
| 26 | -0.36817 | -0.85567 | -0.46726 | -0.81146 | 26 | -0.37521 | -0.85858 | -0.35246 | -0.86084 |
| 27 | 0.466369 | -1.7841 | 0.539992 | -1.78316 | 27 | 0.473204 | -1.78599 | 0.328636 | -1.78547 |
| 28 | -1.1484 | 1.643324 | -1.14765 | 1.663934 | 28 | -1.15158 | 1.641308 | -1.23606 | 1.638888 |
| 29 | -0.74457 | -0.91374 | -0.83255 | -0.87558 | 29 | -0.75428 | -0.91736 | -0.76121 | -0.92532 |
| 30 | -1.24736 | 1.686763 | -1.34333 | 1.721911 | 30 | -1.256 | 1.683096 | -1.24266 | 1.674914 |

**Table 22 Image Coordinate Residuals of CHK points after RPC refinement by using 7 GCPs in Case 5 and Case 6.**

| No | Case 5 (7 GCP, 30 CHKs) | | | | No | Case 6 (7 GCP, 30 CHKs) | | | |
|---|---|---|---|---|---|---|---|---|---|
| | Generic method | | Bias method | | | Generic method | | Bias method | |
| | Column error (pixel) | Row error (pixel) | Column error (pixel) | Row error (pixel) | | Column error (pixel) | Row error (pixel) | Column error (pixel) | Row error (pixel) |
| 1 | -1.29845 | 0.775307 | -1.28931 | 0.779111 | 1 | -1.29258 | 0.774599 | -1.28669 | 0.779763 |
| 2 | -2.81023 | 1.152485 | -2.80419 | 1.151762 | 2 | -2.80739 | 1.152295 | -2.80299 | 1.152004 |
| 3 | 1.608523 | 1.779843 | 1.641344 | 1.78286 | 3 | 1.638676 | 1.77611 | 1.655581 | 1.782785 |
| 4 | -3.08699 | 0.61759 | -3.0949 | 0.621746 | 4 | -3.0931 | 0.62054 | -3.09567 | 0.621819 |
| 5 | -2.32663 | 0.471547 | -2.333 | 0.475878 | 5 | -2.33162 | 0.474065 | -2.33355 | 0.475947 |
| 6 | -0.11219 | -0.40456 | -0.12171 | -0.4005 | 6 | -0.11941 | -0.40131 | -0.12285 | -0.40048 |
| 7 | 0.1004 | -0.50664 | 0.092166 | -0.50444 | 7 | 0.092187 | -0.50491 | 0.088665 | -0.50445 |
| 8 | -1.29398 | 1.346675 | -1.27424 | 1.351261 | 8 | -1.2739 | 1.345333 | -1.26367 | 1.351056 |
| 9 | -0.73167 | 0.49662 | -0.74527 | 0.497715 | 9 | -0.74395 | 0.499137 | -0.75048 | 0.49761 |
| 10 | 0.3763 | -0.51078 | 0.363931 | -0.51102 | 10 | 0.36425 | -0.5091 | 0.357864 | -0.51115 |
| 11 | 0.552639 | 1.140143 | 0.566055 | 1.145549 | 11 | 0.56849 | 1.139736 | 0.57502 | 1.145312 |
| 12 | -0.47013 | 1.130256 | -0.4478 | 1.136145 | 12 | -0.44569 | 1.12769 | -0.43587 | 1.135902 |
| 13 | -0.64591 | 0.451645 | -0.6414 | 0.454652 | 13 | -0.63923 | 0.451246 | -0.63816 | 0.454479 |
| 14 | -0.48355 | 0.016525 | -0.49483 | 0.020213 | 14 | -0.49118 | 0.01973 | -0.49638 | 0.020205 |
| 15 | 0.006238 | 1.045474 | 0.006933 | 1.04707 | 15 | 0.009004 | 1.044868 | 0.007502 | 1.046971 |
| 16 | 0.682606 | 0.145043 | 0.667349 | 0.148311 | 16 | 0.67236 | 0.149084 | 0.665088 | 0.148357 |
| 17 | 0.478033 | 0.673655 | 0.486975 | 0.676298 | 17 | 0.489412 | 0.671479 | 0.491206 | 0.676242 |
| 18 | 0.791526 | 0.573446 | 0.771697 | 0.576927 | 18 | 0.778973 | 0.578674 | 0.769334 | 0.577015 |
| 19 | -1.03505 | 1.021501 | -0.99768 | 1.030372 | 19 | -0.99338 | 1.016061 | -0.97797 | 1.030274 |
| 20 | 1.251392 | -0.46268 | 1.23594 | -0.46178 | 20 | 1.240929 | -0.46001 | 1.23196 | -0.46171 |
| 21 | 0.028601 | 0.137221 | 0.007943 | 0.140142 | 21 | 0.015338 | 0.142496 | 0.005161 | 0.140304 |
| 22 | -0.47661 | -0.24933 | -0.43968 | -0.24025 | 22 | -0.43474 | -0.25471 | -0.41976 | -0.2403 |
| 23 | 0.731219 | -0.32624 | 0.720953 | -0.32506 | 23 | 0.726074 | -0.32477 | 0.718966 | -0.32494 |
| 24 | 0.809908 | 0.08814 | 0.795195 | 0.088562 | 24 | 0.800472 | 0.090312 | 0.791301 | 0.088718 |
| 25 | -0.13609 | -1.44592 | -0.15777 | -1.44643 | 25 | -0.1518 | -1.44236 | -0.16404 | -1.44617 |
| 26 | -0.35357 | -0.86014 | -0.37708 | -0.8575 | 26 | -0.36742 | -0.85421 | -0.37952 | -0.85715 |
| 27 | 0.43737 | -1.79073 | 0.44947 | -1.78335 | 27 | 0.458465 | -1.7915 | 0.461566 | -1.78313 |
| 28 | -1.16155 | 1.636979 | -1.16545 | 1.642917 | 28 | -1.15387 | 1.639238 | -1.15837 | 1.643336 |
| 29 | -0.73659 | -0.91915 | -0.76105 | -0.91686 | 29 | -0.74599 | -0.91344 | -0.76099 | -0.91597 |
| 30 | -1.23505 | 1.682555 | -1.26145 | 1.68356 | 30 | -1.24724 | 1.688189 | -1.26328 | 1.684467 |

**Table 23 Image Coordinate Residuals of CHK points after RPC refinement by using 7 GCPs in Case 5 and Case 6.**

| No | Case 7 (7 GCP, 30 CHKs) | | | | No | Case 8 (7 GCP, 30 CHKs) | | | |
|---|---|---|---|---|---|---|---|---|---|
| | Generic method | | Bias method | | | Generic method | | Bias method | |
| | Column error (pixel) | Row error (pixel) | Column error (pixel) | Row error (pixel) | | Column error (pixel) | Row error (pixel) | Column error (pixel) | Row error (pixel) |
| 1 | -1.35458 | 0.674191 | -0.43761 | 0.587934 | 1 | -1.278 | 0.787511 | -1.01483 | 0.643951 |
| 2 | -2.97837 | 1.106637 | -0.72102 | 1.19859 | 2 | -2.80768 | 1.158456 | -2.67304 | 1.096908 |
| 3 | 1.067841 | 1.547182 | 15.07306 | -1.03035 | 3 | 1.714829 | 1.857318 | 2.971255 | 1.563739 |
| 4 | -2.56731 | 0.946464 | -7.52816 | 3.518544 | 4 | -3.09362 | 0.621525 | -3.5015 | 0.853191 |
| 5 | -1.8823 | 0.749465 | -6.24324 | 2.890859 | 5 | -2.33225 | 0.475779 | -2.67025 | 0.668457 |
| 6 | 0.450506 | -0.04289 | -4.98547 | 2.709522 | 6 | -0.12152 | -0.40198 | -0.58795 | -0.13845 |
| 7 | 0.261559 | -0.37872 | -4.16571 | 0.562455 | 7 | 0.064445 | -0.52094 | -0.29935 | -0.41623 |
| 8 | -1.40997 | 1.339166 | 6.59088 | 0.430716 | 8 | -1.20979 | 1.407015 | -0.45854 | 1.327249 |
| 9 | -0.50012 | 0.69505 | -6.36747 | 2.124894 | 9 | -0.7816 | 0.474205 | -1.33022 | 0.652696 |
| 10 | 0.378941 | -0.43389 | -4.53202 | 0.057564 | 10 | 0.316464 | -0.54038 | -0.15178 | -0.44116 |
| 11 | 0.591932 | 1.220047 | 6.018774 | 0.901526 | 11 | 0.625838 | 1.193045 | 1.168382 | 1.193392 |
| 12 | -0.82603 | 1.010223 | 8.929425 | -1.24738 | 12 | -0.38031 | 1.19754 | 0.601515 | 1.011918 |
| 13 | -0.81156 | 0.431515 | 1.724063 | -0.37081 | 13 | -0.62595 | 0.471111 | -0.35871 | 0.435222 |
| 14 | 0.0469 | 0.363849 | -4.27441 | 3.050671 | 14 | -0.49703 | 0.017271 | -0.96073 | 0.274444 |
| 15 | -0.3047 | 0.952355 | 1.261671 | -0.18599 | 15 | 0.000238 | 1.048896 | 0.167501 | 0.972612 |
| 16 | 1.352149 | 0.584842 | -4.09422 | 4.189849 | 16 | 0.66432 | 0.143728 | 0.055376 | 0.47015 |
| 17 | -0.06846 | 0.458687 | 5.302154 | -1.83487 | 17 | 0.498318 | 0.695741 | 1.05239 | 0.49012 |
| 18 | 1.694284 | 1.154239 | -5.52572 | 6.021916 | 18 | 0.776086 | 0.573428 | -0.0046 | 1.007072 |
| 19 | -1.79267 | 0.717057 | 14.9794 | -3.57527 | 19 | -0.89275 | 1.131339 | 0.83348 | 0.702662 |
| 20 | 1.517749 | -0.2386 | -3.25209 | 1.847954 | 20 | 1.214332 | -0.47917 | 0.709911 | -0.2925 |
| 21 | 0.9249 | 0.716014 | -6.09185 | 5.830035 | 21 | 0.009171 | 0.135106 | -0.79132 | 0.564743 |
| 22 | -1.21678 | -0.54377 | 15.46814 | -4.67469 | 22 | -0.33267 | -0.13829 | 1.391301 | -0.56553 |
| 23 | 0.794199 | -0.21741 | -1.4796 | 0.976753 | 23 | 0.708717 | -0.33426 | 0.460804 | -0.24961 |
| 24 | 0.96204 | 0.248588 | -2.95267 | 2.082348 | 24 | 0.771917 | 0.070645 | 0.339749 | 0.205439 |
| 25 | 0.243583 | -1.15378 | -6.0432 | 2.199441 | 25 | -0.19243 | -1.4735 | -0.9215 | -1.23219 |
| 26 | 0.682683 | -0.20755 | -6.60131 | 6.214937 | 26 | -0.36677 | -0.86016 | -1.23731 | -0.3808 |
| 27 | 0.478216 | -1.7029 | 7.228855 | -1.25162 | 27 | 0.533267 | -1.72127 | 1.239557 | -1.77887 |
| 28 | -0.61442 | 1.987531 | 0.194964 | 5.751653 | 28 | -1.0984 | 1.681362 | -1.04655 | 1.866173 |
| 29 | 0.317134 | -0.29164 | -4.14235 | 9.107997 | 29 | -0.72502 | -0.9092 | -1.44493 | -0.46543 |
| 30 | -0.26805 | 2.267787 | -5.09043 | 11.59477 | 30 | -1.24134 | 1.681811 | -2.0295 | 2.106582 |

**Table 24 Image Coordinate Residuals of CHK points after RPC refinement by using 7 GCPs in Case 9.**

| No | Case 9 (7 GCP, 30 CHKs) | | | |
|---|---|---|---|---|
| | Generic method | | Bias method | |
| | Column error | Row error | Column error | Row error |
| 1 | -1.29013 | 0.775958 | -1.25828 | 0.764858 |
| 2 | -2.80701 | 1.152986 | -2.79041 | 1.146158 |
| 3 | 1.650427 | 1.784821 | 1.788916 | 1.761869 |
| 4 | -3.09412 | 0.620592 | -3.13629 | 0.644227 |
| 5 | -2.33245 | 0.474192 | -2.3671 | 0.494542 |
| 6 | -0.12077 | -0.40143 | -0.16952 | -0.37491 |
| 7 | 0.088318 | -0.50668 | 0.049598 | -0.49597 |
| 8 | -1.26484 | 1.351937 | -1.1816 | 1.349467 |
| 9 | -0.74944 | 0.496429 | -0.80925 | 0.512915 |
| 10 | 0.357844 | -0.51246 | 0.306045 | -0.50414 |
| 11 | 0.57624 | 1.14543 | 0.635878 | 1.150829 |
| 12 | -0.43586 | 1.13515 | -0.32983 | 1.12462 |
| 13 | -0.63702 | 0.453362 | -0.60944 | 0.453114 |
| 14 | -0.49292 | 0.019376 | -0.54367 | 0.045206 |
| 15 | 0.008544 | 1.04529 | 0.023885 | 1.039958 |
| 16 | 0.669974 | 0.148416 | 0.602819 | 0.179857 |
| 17 | 0.491937 | 0.674064 | 0.548475 | 0.658224 |
| 18 | 0.776647 | 0.578025 | 0.690485 | 0.61902 |
| 19 | -0.97763 | 1.02835 | -0.79284 | 0.998794 |
| 20 | 1.23672 | -0.4621 | 1.178679 | -0.44536 |
| 21 | 0.0126 | 0.141611 | -0.0763 | 0.181549 |
| 22 | -0.41884 | -0.24231 | -0.23463 | -0.27168 |
| 23 | 0.723561 | -0.32581 | 0.692559 | -0.31791 |
| 24 | 0.79624 | 0.088173 | 0.74503 | 0.099664 |
| 25 | -0.15815 | -1.44574 | -0.24189 | -1.42603 |
| 26 | -0.36964 | -0.85494 | -0.46753 | -0.81142 |
| 27 | 0.468616 | -1.78403 | 0.541336 | -1.78314 |
| 28 | -1.14762 | 1.643693 | -1.14687 | 1.663977 |
| 29 | -0.74564 | -0.91305 | -0.83255 | -0.87549 |
| 30 | -1.24873 | 1.687438 | -1.34355 | 1.722003 |

# CURRICULUM VITAE

**Name:** ZHEN XIONG

**Address:** 610#-780 Montgomery Street, Fredericton, NB, Canada E3B 2Y1

**Universities attended:**

1993, MS., Engineering Survey, Wuhan University, Wuhan University, China

1986, Dip., Photogrammetry, Wuhan University, China

**Publications:**

1. **Xiong, Z.** and Y. Zhang, Comparison of Corner and Center for Image Registration, *Journal of Photogrammetric Engineering & Remote Sensing* (under review)
2. **Xiong, Z.** and Y. Zhang, Image Registration, Book Chapter, Encyclopedia of Geography. 2008
3. **Xiong, Z.** and Y. Zhang, A Novel Interest Point Matching Algorithm for Remote Sensing Images, *IEEE Transaction on Geoscience and Remote Sensing* (accepted)
4. **Xiong, Z.** and Y. Zhang, Generic Method Based Bundle Block Adjustment with Rational Polynomial Camera Models, *ISPRS Journal of Photogrammetry & Remote Sensing* (under review)
5. **Xiong, Z.** and Y. Zhang, A Generic Method for RPC Refinement, *Journal of Photogrammetric Engineering & Remote Sensing* (In press)
6. **Xiong, Z.** and Y. Zhang, An Initial Study of Vehicle Information Extraction from Single Pass QuickBird Satellite Images. *Journal of Photogrammetric Engineering & Remote Sensing,* Vol. 74, No 11, November 2008
7. **Xiong, Z.** and Y. Zhang, Automated Vehicle Information Extraction from One Pass of QuickBird Imagery. *Proceedings of ISPRS workshop on Image Fusion*, Sep. 25-27, 2007, Chengdu, China
8. **Xiong, Z.** and Y. Zhang, Study on Tie Point Selection for Co-Registration of Different Resolution Imagery. *Proceedings of ISPRS workshop on Image Fusion*, Sep. 25-27, 2007, Chengdu, China
9. **Xiong**, **Z.** and Y. Zhang, Automatic 3D Building Reconstruction from Stereo Ikonos images, *Proceedings of ASPRS Annual conference 2007*, Tampa, FL, May 7-11
10. **Xiong, Z.** and Y. Zhang, Semi-Automated Vehicle Information Extraction from QuickBird Imagery. *Proceedings of ASPRS Annual conference 2007*, Tampa, FL, May 7-11
11. **Xiong, Z.** and Y. Zhang, Automatic 3D Building Extraction from Stereo Ikonos Images. *Proceedings of ASPRS Annual conference 2006*, Reno, NV, May 1-6

12. **Xiong, Z.** and Y. Zhang, An Initial Study of Moving Target Detection Based on a Single Set of High Spatial Resolution Satellite Imagery. *Proceedings of ASPRS Annual conference 2006*, Reno, NV, May 1-6

13. **Xiong, Z.** and Y. Zhang, Extraction of Attitude Parameters of Moving Target from a Single Set of High Spatial Resolution Satellite Imagery. *Proceedings of MAPPS/ASPRS 2006 Fall Specialty Conference*, San Antonio, TX, Nov 6-10